

AD-A249 986



2

# PROCEEDINGS

 SPIE—The International Society for Optical Engineering

AEOSR-TR- 92 0254

## Sol-Gel Optics

John D. Mackenzie  
Donald R. Ulrich  
*Chairs/Editors*

11-13 July 1990  
San Diego, California

DTIC  
ELECTE  
APR 20 1992  
S D D

APR 20 1992  
and 19  
12

This document has been approved  
for public release and sale; its  
distribution is unlimited.

92-09734



Volume 1328

92 4 15 072

Approved for public release;  
distribution unlimited.

2025 RELEASE UNDER E.O. 14176

Standard Form 298 (Rev. 7-89)  
Prescribed by GSA Gen. Reg. No. 27  
201-100-0000

## COMPONENT PART NOTICE

THIS PAPER IS A COMPONENT PART OF THE FOLLOWING COMPILATION REPORT:

TITLE: Sol-Gel Optics: Proceedings SPIE-The International Society for Optical Engineering Held in San Diego, California on 11-13 July 1990. Volume 1328.

TO ORDER THE COMPLETE COMPILATION REPORT, USE AD-A249 986.

THE COMPONENT PART IS PROVIDED HERE TO ALLOW USERS ACCESS TO INDIVIDUALLY AUTHORED SECTIONS OF PROCEEDING, ANNALS, SYMPOSIA, ETC. HOWEVER, THE COMPONENT SHOULD BE CONSIDERED WITHIN THE CONTEXT OF THE OVERALL COMPILATION REPORT AND NOT AS A STAND-ALONE TECHNICAL REPORT.

THE FOLLOWING COMPONENT PART NUMBERS COMPRISE THE COMPILATION REPORT:

AD#: P006 406 thru AD#: P006 450  
 AD#: \_\_\_\_\_ AD#: \_\_\_\_\_  
 AD#: \_\_\_\_\_ AD#: \_\_\_\_\_



Accession For	
NTIS CRA&I	<input checked="" type="checkbox"/>
DTIC TAB	<input type="checkbox"/>
Unannounced	<input type="checkbox"/>
Justification	
By _____	
Distribution /	
Availability Codes	
Dist	Avail and/or Special
A-1	

# Sol-Gel Optics

**John D. Mackenzie**  
**Donald R. Ulrich**  
*Chairs/Editors*

**11-13 July 1990**  
**San Diego, California**

*Sponsored by*  
SPIE—The International Society for Optical Engineering

Accession For	
NTIS	CRA&I <input checked="" type="checkbox"/>
DTIC	TAB <input type="checkbox"/>
Unannounced	<input type="checkbox"/>
Justification	
By 	
Distribution/	
Availability Codes	
Dist	Avail and/or Special
A-1	

*Published by*  
**SPIE—The International Society for Optical Engineering**  
P.O. Box 10, Bellingham, Washington 98227-0010 USA



**Volume 1328**

SPIE (The Society of Photo-Optical Instrumentation Engineers) is a nonprofit society dedicated to advancing engineering and scientific applications of optical, electro-optical, and optoelectronic instrumentation, systems, and technology.





The papers appearing in this book comprise the proceedings of the meeting mentioned on the cover and title page. They reflect the authors' opinions and are published as presented and without change, in the interests of timely dissemination. Their inclusion in this publication does not necessarily constitute endorsement by the editors or by SPIE.

Please use the following format to cite material from this book:

Author(s), "Title of Paper," *Sol-Gel Optics*, John D. Mackenzie, Donald R. Ulrich, Editors, Proc. SPIE 1328, page numbers (1990).

Library of Congress Catalog Card No. 90-52822  
ISBN 0-8194-0389-X

Published by  
**SPIE—The International Society for Optical Engineering**  
P.O. Box 10, Bellingham, Washington 98227-0010 USA  
Telephone 206/676-3290 (Pacific Time) • Fax 206/647-1445

Copyright © 1990, The Society of Photo-Optical Instrumentation Engineers.

Copying of material in this book for sale or for internal or personal use beyond the fair use provisions granted by the U.S. Copyright Law is subject to payment of copying fees. The Transactional Reporting Service base fee for this volume is \$2.00 per article and should be paid directly to Copyright Clearance Center, 27 Congress Street, Salem, MA 01970. For those organizations that have been granted a photocopy license by CCC, a separate system of payment has been arranged. The fee code for users of the Transactional Reporting Service is 0-8194-0389-X/90/\$2.00.

Individual readers of this book and nonprofit libraries acting for them are permitted to make fair use of the material in it, such as to copy an article for teaching or research, without payment of a fee. Reproduction or systematic or multiple reproduction of any material in this book (including abstracts) is prohibited except with the permission of SPIE and one of the authors.

Permission is granted to quote excerpts from articles in this book in other scientific or technical works with acknowledgment of the source, including the author's name, the title of the book, SPIE volume number, page number(s), and year. Reproduction of figures and tables is likewise permitted in other articles and books provided that the same acknowledgment of the source is printed with them, permission of one of the original authors is obtained, and notification is given to SPIE.

In the case of authors who are employees of the United States government, its contractors or grantees, SPIE recognizes the right of the United States government to retain a nonexclusive, royalty-free license to use the author's copyrighted article for United States government purposes.

Printed in the United States of America

# SOL-GEL OPTICS

Volume 1328

## CONTENTS

	Conference Committee .....	vii
	Introduction .....	ix
	<b>OVERVIEW PAPER</b>	
1328-01	<b>Sol-gel optics: present status and future trends</b> J. D. Mackenzie, Univ. of California/Los Angeles; D. R. Ulrich, Airforce Office of Scientific Research. ....	2
<b>SESSION 1</b>	<b>BULK SOLIDS AND APPLICATIONS</b>	
1328-02	<b>Chemical processing of glasses</b> R. M. Laine, Univ. of Washington. ....	16
1328-04	<b>Theory and application of spectroscopically active glasses prepared by the sol-gel method</b> R. Reisfeld, Hebrew Univ. of Jerusalem (Israel). ....	29
1328-05	<b>Optical properties of transition metal oxide gels</b> C. Sanchez, Univ. Pierre et Marie Curie (France). ....	40
1328-06	<b>Silica glass monoliths from alkoxide gels: an old game with new results</b> Y. Sano, S. H. Wang, S. R. Chaudhuri, A. Sarkar, Orion Labs., Inc. ....	52
1328-07	<b>Pregrooving on glass disks by the sol-gel method (Part I): formation and evaluation of pregrooved glass disks</b> A. Matsuda, Y. Matsuno, S. Kataoka, S. Katayama, T. Tsuno, Nippon Sheet Glass Co., Ltd. (Japan); N. Tohge, T. Minami, Univ. of Osaka Prefecture (Japan). ....	62
1328-08	<b>Pregrooving on glass disks by the sol-gel method (Part II): effects of the addition of organic polymers on the formation of glass films in the SiO<sub>2</sub>-TiO<sub>2</sub> system</b> A. Matsuda, Y. Matsuno, S. Kataoka, S. Katayama, T. Tsuno, Nippon Sheet Glass Co., Ltd. (Japan); N. Tohge, T. Minami, Univ. of Osaka Prefecture (Japan). ....	71
1328-09	<b>New developments in sol-gel imaging</b> N. J. Phillips, Loughborough Univ. of Technology (UK). ....	80
1328-47	<b>New laser media based on microporous glasses</b> G. B. Altshuler, E. G. Dulneva, Institute of Fine Mechanics and Optics (USSR); V. A. Bakhanov, O. V. Mazurin, G. P. Roskova, Institute of Silicate Chemistry (USSR). ....	89
<b>SESSION 2</b>	<b>NLO AND GRIN MATERIALS</b>	
1328-10	<b>Third-order optical properties of quasi-two-dimensional conjugated discs: silicon naphthalocyanine</b> N. Wang, Y. M. Cai, J. R. Heflin, J. W. Wu, D. C. Rodenberger, A. F. Garito, Univ. of Pennsylvania. ....	100
1328-11	<b>Obtaining CdSe<sub>x</sub>S<sub>1-x</sub> precipitates in sol-gel matrices</b> C. M. Bagnall, J. Zarzycki, Univ. of Montpellier II (France). ....	108
1328-12	<b>Preparation of semiconducting sulfides microcrystalline-doped silica glasses by the sol-gel process</b> M. Nogami, M. Watabe, K. Nagasaka, Aichi Institute of Technology (Japan). ....	119

(continued)

# SOL-GEL OPTICS

Volume 1328

1328-13	<b>Preparation of CdS-doped glasses by the sol-gel method</b> N. Tohge, M. Asuka, T. Minami, Univ. of Osaka Prefecture (Japan). . . . .	125
1328-14	<b>Graded index materials by the sol-gel process</b> M. Yamane, A. Yasumori, M. Iwasaki, K. Hayashi, Tokyo Institute of Technology (Japan). . . . .	133
1328-15	<b>Sol-gel derived gradient index optical materials</b> T. M. Che, J. B. Caldwell, R. M. Mininni, Enimont America Inc. . . . .	145
1328-16	<b>Sol-gel derived r-GRIN doped-silica lenses</b> K. Shiro, Hitachi Cable Ltd. (Japan). . . . .	160
<b>SESSION 3 COMPOSITES AND LASERS I</b>		
1328-17	<b>Sol-gel processed inorganic and organically modified composites for nonlinear optics and photonics</b> P. N. Prasad, SUNY/Buffalo. . . . .	168
1328-18	<b>Solid-state tunable lasers based on dye-doped sol-gel materials</b> B. S. Dunn, J. D. Mackenzie, J. I. Zink, O. M. Stafsudd, Univ. of California/Los Angeles. . . . .	174
1328-19	<b>Sol-gel glass solid-state lasers doped with organic molecules</b> C. Whitehurst, D. J. Shaw, T. A. King, Univ. of Manchester (UK). . . . .	183
1328-20	<b>Transparent gel and xerogel of thorium phosphate: optical spectroscopy with Nd<sup>3+</sup>, Er<sup>3+</sup>, Eu<sup>3+</sup>, Cr<sup>3+</sup> and Rhodamine 6G</b> M. Genet, V. Brandel, M. P. LaHalle, E. Simoni, Univ. Paris Sud (France). . . . .	194
1328-46	<b>New technology of optical components based on local laser thermoconsolidation of porous glasses and coats</b> V. P. Veiko, E. B. Iakovlev, G. K. Kostjuk, V. A. Chuiko, P. A. Fomichov, Leningrad Institute of Precision Mechanics and Optics (USSR); V. S. Kozhukharov, Institute of Chemical Technology (Bulgaria). . . . .	201
<b>SESSION 4 COMPOSITES AND LASERS II</b>		
1328-21	<b>Interaction between host matrices and fluorescent species trapped in metal alkoxides derived gels</b> C. Guizard, J. C. Achddou, A. Larbot, L. Cot, Lab. de Physicochimie des Materiaux/CNRS (France); G. Le Flem, C. Parent, Lab. de Chimie du Solide/CNRS (France); C. L. Lurin, Kodak Pathe (France). . . . .	208
1328-22	<b>Porous optical composites</b> S. T. Reed, C. S. Ashley, C. J. Brinker, R. J. Walko, Sandia National Labs.; R. Ellefson, J. Gill, EG&G Mound Applied Technologies. . . . .	220
1328-23	<b>Gel-silica hybrid optics</b> L. L. Hench, J. K. West, B. F. Zhu, R. Ochoa, Univ. of Florida. . . . .	230
1328-24	<b>PMMA-impregnated silica gels: synthesis and characterization</b> B. L. Abramoff, L. C. Klein, Rutgers Univ. . . . .	241
1328-25	<b>Inorganic/organic composites for optical application</b> H. Schmidt, Univ. des Saarlandes (FRG); M. Popall, Fraunhofer-Institut für Silicatforschung (FRG). . . . .	249
1328-26	<b>Synthesis and properties of transparent ZrO<sub>2</sub> containing SiO<sub>2</sub> polymethacrylate polymers</b> R. Nass, H. Schmidt, Univ. des Saarlandes (FRG); E. Arpac, Inoenuc Univ. (Turkey). . . . .	258

# SOL-GEL OPTICS

Volume 1328

1328-27	<b>Preparation and optical properties of amorphous silica doped with functional organic molecules by the sol-gel process</b> A. Makishima, K. Morita, H. Inoue, Univ. of Tokyo (Japan); T. Tani, Electrotechnical Lab. (Japan). . . . .	264
<b>SESSION 5 FILMS AND COATINGS I</b>		
1328-28	<b>Sol-gel synthesis of optical thin films and coatings</b> D. R. Uhlmann, J. M. Boulton, G. Teowee, L. W. Weisenbach, B. J. Zelinski, Univ. of Arizona. . . . .	270
1328-29	<b>Process-induced variations in sol-gel derived oxide coatings</b> B. E. Yoldas, PPG Industries, Inc. . . . .	296
1328-30	<b>Al<sub>2</sub>O<sub>3</sub>-H<sub>2</sub>O-SiO<sub>2</sub> sol-gel HR coatings for high-power laser applications</b> H. G. Floch, J. J. Priotton, Commissariat a l'Energie Atomique (France); I. M. Thomas, Lawrence Livermore National Lab. . . . .	307
1328-31	<b>Laser processing of channel waveguide structures in sol-gel coatings</b> B. D. Fabes, D. J. Taylor, L. W. Weisenbach, M. M. Stuppi, D. L. Klein, L. J. Raymond, B. J. Zelinski, D. P. Birnie III, Univ. of Arizona. . . . .	319
1328-32	<b>Vibrational spectra and structure of silica gel films spun on c-Si substrates</b> R. M. Almeida, Instituto Superior Técnico (Portugal); C. G. Pantano, The Pennsylvania State Univ. . . . .	329
1328-33	<b>Optical and mechanical characterization of spin-on deposited silicon and titanium dioxide films</b> P. Shen, M. Li, S. I. Najafi, J. F. Currie, Ecole Polytechnique (Canada); R. Leonelli, Univ. of Montreal (Canada). . . . .	338
<b>SESSION 6 FILMS AND COATINGS II</b>		
1328-34	<b>Electrochromic properties of sol-gel-derived WO<sub>3</sub> coatings</b> P. Judeinstein, J. Livage, Univ. Pierre et Marie Curie (France). . . . .	344
1328-35	<b>Sol-gel nano-porous silica-titania thin films with liquid fill for optical interferometric sensors</b> A. J. Martin, M. Green, Imperial College of Science, Technology and Medicine (UK). . . . .	352
1328-36	<b>Optical switches based on semiconducting vanadium dioxide films prepared by the sol-gel process</b> R. S. Potember, K. R. Speck, Johns Hopkins Univ. . . . .	364
1328-37	<b>Characterization of an all-solid-state electrochromic window</b> J. C. Tonazzi, B. Valla, M. A. Macedo, P. Baudry, M. A. Aegerter, Univ. of São Paulo (Brazil); A. C. Martins Rodrigues, L. O. Bulhoes, Federal Univ. of São Carlos (Brazil). . . . .	375
1328-38	<b>Characterization of sol-gel thin films of TiO<sub>2</sub>-PbO, TiO<sub>2</sub>-Bi<sub>2</sub>O<sub>3</sub> and TiO<sub>2</sub>-CeO<sub>2</sub> compositions</b> M. A. Aegerter, E. R. La Serra, Univ. of São Paulo (Brazil); A. C. Martins Rodrigues, Univ. of São Carlos (Brazil); G. Kordas, G. Moore, Univ. of Illinois Urbana-Champaign. . . . .	391
<b>SESSION 7 FILMS AND COATINGS III</b>		
1328-39	<b>Preparation of Li<sub>2</sub>B<sub>4</sub>O<sub>7</sub> thin films by sol-gel method and their characterization</b> T. Yoko, H. Yamashita, S. Sakka, Kyoto Univ. (Japan). . . . .	416
1328-40	<b>Photovoltaic effect and optical properties of ferroelectric thin films made by sol-gel processing</b> Y. Xu, C. J. Chen, N. Desimone, J. D. Mackenzie, Univ. of California Los Angeles. . . . .	428

(continued)

## SOL-GEL OPTICS

Volume 1328

1328-41	<b>Properties of undoped, copper-doped strontium-barium niobate thin films by sol-gel method</b>	
	C. J. Chen, Y. Xu, J. D. Mackenzie, Univ. of California/Los Angeles. ....	441
1328-42	<b>Optical properties and densification of sol-gel-derived <math>\text{PbTiO}_3</math> thin layers</b>	
	K. D. Budd, D. A. Payne, Univ. of Illinois/Urbana-Champaign. ....	450
1328-43	<b>Sol-gel processing of lithium niobate thin layers for optical applications</b>	
	D. J. Eichorst, D. A. Payne, Univ. of Illinois/Urbana-Champaign. ....	456
1328-44	<b>Electrical and optical properties of alkoxide-derived lithium niobate thin layers</b>	
	D. S. Hagberg, D. J. Eichorst, D. A. Payne, Univ. of Illinois/Urbana-Champaign. ....	466
1328-45	<b>Densification of sol-gel silica glass by laser irradiation</b>	
	D. J. Shaw, T. A. King, Univ. of Manchester (UK). ....	474
	Addendum. ....	482
	Author Index. ....	483

SOL-GEL OPTICS

Volume 1328

CONFERENCE COMMITTEE

*Chair*

**John D. Mackenzie**, University of California/Los Angeles  
**Donald R. Ulrich**, Air Force Office of Scientific Research

*Program Committee*

**Ilhan Aksay**, University of Washington  
**C. L. Giles**, NEC Research Institute, Inc.  
**Larry L. Hench**, University of Florida  
**Shin-ichi Hirano**, Nagoya University (Japan)  
**Terence A. King**, University of Manchester (UK)  
**Jacques Livage**, Université Pierre et Marie Curie  
**Richard S. Lytel**, Lockheed Missiles & Space Company, Inc.  
**David A. Payne**, University of Illinois/Urbana-Champaign  
**Nicholas J. Phillips**, Loughborough University of Technology (UK)  
**Paras N. Prasad**, SUNY/Buffalo  
**Helmut Schmidt**, Fraunhofer-Institut für Silicatiforschung (FRG)  
**Donald R. Uhlmann**, University of Arizona  
**Masayuki Yamane**, Tokyo Institute of Technology (Japan)

*Session Chairs*

Session 1—Bulk Solids and Applications  
**J. Zarzycki**, University of Montpellier II (France)

Session 2—NLO and GRIN Materials  
**Donald R. Uhlmann**, University of Arizona

Session 3—Composites and Lasers I  
**Larry L. Hench**, University of Florida

Session 4—Composites and Lasers II  
**Leonard H. Caveny**, Innovative Science and Technology/SDIO

(continued)

## SOL-GEL OPTICS

Volume 1328

### Session 5—Films and Coatings I

**David A. Payne**, University of Illinois/Urbana-Champaign

### Session 6—Films and Coatings II

**Masayuki Yamane**, Tokyo Institute of Technology (Japan)

### Session 7—Films and Coatings III

**Jane A. Alexander**, DARPA/DSO

---

Conference 1328, *Sol-Gel Optics*, was part of a six-conference program on Optical Materials held at SPIE's International Symposium on Optical and Optoelectronic Applied Science and Engineering, 8–13 July 1990, San Diego, California. The other conferences were:

Conference 1323, *Optical Thin Films III*

Conference 1324, *Modeling of Optical Thin Films II*

Conference 1325, *Diamond Optics III*

Conference 1326, *Window and Dome Technologies and Materials II*

Conference 1327, *Properties and Characteristics of Optical Glass II*

Program Chair **Robert W. Schwartz**, Naval Weapons Center

## INTRODUCTION

The sol-gel process is a relatively new technique for the preparation and fabrication of inorganic oxides of extremely high purity and homogeneity. In recent years, it has been convincingly demonstrated that this process is ideally suited for optical materials in the forms of thin films, bulk solids, and fibers. Many of these materials are discussed in this proceedings. Examples include optically transparent thin ferroelectric films of extremely good quality, almost as good as single crystals and dense silica glasses, which have better transmission from the ultraviolet to the infrared than similar materials made by conventional methods. The exploitation of the sol-gel technique to fabricate gradient refractive index lenses has been successfully developed to the pilot plant stage. There is a good possibility that in the near future, lenses for microscopes and cameras will be fabricated by this method.

The sol-gel method also lends itself to the fabrication of new composites, especially those that are optically transparent and have high third-order nonlinear indices. This proceedings includes reports on the attempts to fabricate semiconductor-in-glass quantum-well confinement lenses. The successful preparation of organic dyes-in-oxides laser elements is discussed, as well as research on the fabrication of grooved glass discs through the mechanical patterning of the soft gels.

This proceedings is the first on sol-gel optics. From the high level of research activities and the proven successes of applications, there is little doubt that other proceedings will follow. We hope the reader will not only be impressed by the range of research and potentials of sol-gel optics, but will seriously follow its future progress. The session chairs and the participants have interacted well with the authors to make this first Sol-Gel Optics Conference a great success. We are also grateful to the Air Force Office of Scientific Research, Directorate of Chemical and Atmospheric Sciences, for the travel support for some of our invited foreign speakers.

**John D. Mackenzie**

University of California/Los Angeles

**Donald R. Ulrich**

Air Force Office of Scientific Research



SOL-GEL OPTICS

Volume 1328

**OVERVIEW PAPER**

## Overview Paper

### Sol-gel optics, present status and future trends

John D. Mackenzie  
Department of Materials Science and Engineering  
University of California, Los Angeles, CA 90024-1595

and

Donald R. Ulrich  
U.S. Air Force Office of Scientific Research  
Bolling Air Force Base, Washington, D.C. 20332-6448

### Abstract

The sol-gel process is based on the mixing of liquid reactants on a molecular scale and the subsequent solidification of the solution into a porous amorphous oxide gel. The porous gel is then heated to give glasses or polycrystalline solids. Additives can be made to the liquid mixture to give composites. Many new optical materials have been prepared by the sol-gel technique in the past five years. The present status of the scientific understanding of the process is summarized and examples presented of different types of materials successfully developed for optical applications. The enormous potentials of the process are not fully exploited at present. Sol-gel optics promises to be a growing field of science and technology.

### 1. INTRODUCTION

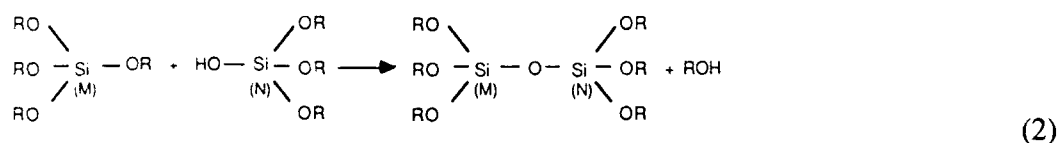
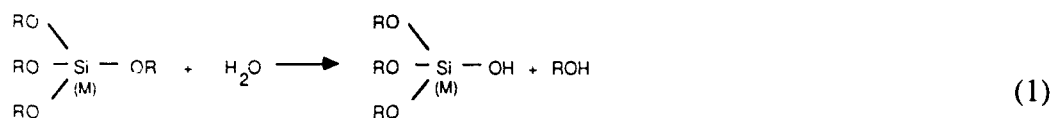
There are many factors which contribute to the successful development of devices for optical applications. For instance, the exploitation of new or old principles of physics, the innovativeness of design and the relative ease and economics of manufacturing. Of equal importance is the availability of new or improved materials and the relative ease of fabrication of such materials into the desired shapes and configurations. The sol-gel process is not only concerned with the fabrication of optical materials but it can also lead to the preparation of new and/or improved optical materials. In the past five years many advances have been made in the research and development of optical materials derived from the sol-gel process. Some of these materials have been successfully utilized in optical components and devices. The primary purpose of this paper is to present an overview of the topic of sol-gel optics, addressing in particular the present status and future trends. However, in order to enhance the future exploitation of the sol-gel process, it is essential that a critical summary be made regarding both the advantages and limitations of the process itself.

### 2. THE SOL-GEL PROCESS

The sol-gel process is by no means a new method for the preparation of materials. As early as 1864, Thomas Graham had prepared gels of silica.<sup>1</sup> The word "sol" implies a dispersion of colloidal particles in a liquid.<sup>2</sup> Colloids are in turn described as solid particles with dimensions in the range of 10 to 1000Å, each containing  $10^3$  to  $10^9$  atoms. When the viscosity of a sol increases sufficiently, usually throughout the partial loss of its liquid phase and/or polymerization of the solid particles, it becomes a porous solid body which is now termed a "gel". These definitions are obviously not rigorous. For approximately 100 years, the potentials of the sol-gel process were not well appreciated. Prior to 1979, by far the majority of materials prepared via this process were silica and silicates. Excellent reviews of these materials are available in two books.<sup>3,4</sup> At approximately 1980, the sol-gel process was "re-discovered". Since that time, a great deal of scientific knowledge have been generated and many other materials have been prepared. Scientific advances in the last decade are treated in a recent publication.<sup>5</sup>

## 2-1 Basic Principles

Because the overwhelming majority of published research has been on silica, it is convenient to use  $\text{SiO}_2$  as an example. The sol-gel process, in the most simplistic terms, is represented by the following reactions:



In (1), a silicon alkoxide such as tetraethoxy silane (TEOS), usually dissolved in an alcoholic solution, is hydrolyzed. In (2), the alkoxy group of one TEOS molecule reacts with the OH group of an adjacent molecule to form an Si-O-Si bond. If this process repeats itself, then more and more Si-O-Si bonds are formed. As polymerization continues, the viscosity of the solution increases until a solid gel is formed. One major advantage of this process is the formation of the Si-O-Si bond at room temperature in a liquid solution. The silicon can be replaced by another element M such as Ti or Zr. Thus  $\text{TiO}_2$  and  $\text{ZrO}_2$  gels can be prepared. Indeed, if two alkoxides are used such that M is Ti and N is Ba, then a  $\text{BaTiO}_3$  gel is formed. Ideally, any metal alkoxides can be employed and any number of alkoxides can be mixed to form a homogeneous solution. Thus, theoretically, any oxide glass composition or any crystalline oxide can be prepared in the gel form. However, when two or more alkoxides are in solution, frequently do not react to form ideal gels as depicted by (1) and (2) above<sup>6</sup>. For instance, one alkoxide may hydrolyse very differently from another and self polymerization may occur. Alternately, "complexes" may form in solution prior to hydrolysis and condensation. With the exception of silicon alkoxides, the knowledge needed to control the reactions of multicomponent gel systems is lacking and therefore it is not possible to predict if homogeneous ideal gels can be prepared. Indeed, even for a single component system like  $\text{SiO}_2$  there are many interdependent factors which can influence the structure and microstructure of the gel and hence the structure and properties of the final oxide product. These include the particular alkoxide used (e.g. methoxide vs ethoxide), its concentration in the solution, the catalyst used, the pH, the temperature, concentration of water, the particular solvent and other additives.<sup>7</sup>

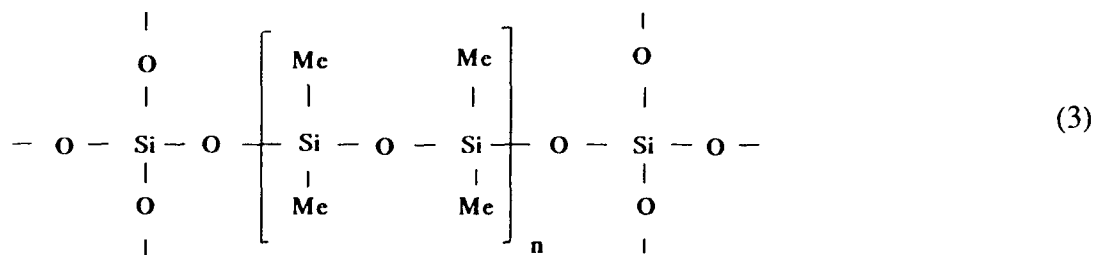
It is possible to use other starting materials than alkoxides. For instance, in the literature there are numerous examples of the use of acetates, nitrates and other precursors. However, frequently a metal oxygen bond is not formed at the solution stage and thus the ultrahomogeneity offered by alkoxides is not attained. After the gel is formed, it is usually porous and contains liquids in the interconnecting pores. The liquids must be removed and then the porous amorphous oxide (xerogel) must be heated to remove the pores. The behavior of gels during this heat-treatment is fundamentally different for two general families of materials because of the structure of the metal-oxygen polyhedra.<sup>8</sup> One family (A) is prone to crystallize at relatively low temperatures, much lower than  $0.5 T_m$ . The other family (B) will lose porosity and densify to a glass-like solid at temperatures higher than  $T_m$ . The behavior of gels is thus somewhat similar to that of molten oxides when they are cooled from the melt as described by Zachariasen rules<sup>9</sup> for glass formation. Examples of these two families are shown in Table 1.

Table 1. Crystallization Behavior of Two Types of Porous Oxide Gels

System	Crystallization Temp., $T_c$ ( $^{\circ}\text{K}$ )	$0.5T_L$
<u>Type A</u>		
$\text{Al}_2\text{O}_3$	748	1162
$\text{TiO}_2$	473	1072
$\text{ZrO}_2$	773	1497
$\text{Ta}_2\text{O}_5$	623	1062
<u>Type B</u>		
$\text{SiO}_2$	1643	1000
$\text{GeO}_2$	968	695
$20\text{B}_2\text{O}_3\text{-}80\text{SiO}_2$	1273	662
$15\text{P}_2\text{O}_5\text{-}85\text{SiO}_2$	1253	652

## 2-2 The Ormosils

The reactions between two metal alkoxides to form an oxide gel are represented by the simplified eqs. (1) and (2). This leads to the formation of a three-dimensional oxide structure which is both weak and brittle. However, if organic groups are present in the oxide network which do not contribute to cross-linking, then the brittleness of the resultant gel is decreased. Such materials are known as "ormosils" (organically modified silicates), "ormocers" (organically modified ceramics) or "ceramer" (ceramic-polymer).<sup>10,11</sup> If polydimethylsiloxane (PDMS) are reacted with TEOS, the reaction product would be:



Because the Me groups do not contribute to cross-linking, rotational motion can occur within the siloxane unit and between the siloxane unit and the silicon-oxygen network. These organic inorganic polymers are somewhat similar to the silicones but contain more inorganic constituents. They can be made into highly transparent optical lenses.<sup>12</sup> As for the oxide gels, organic dyes can also be incorporated into the ormosils to form optically active composites.<sup>13</sup> Recently, ormosils which exhibited even rubbery behavior have been reported.<sup>14</sup> As for the oxide gels, thin films and coatings can also be prepared by dipping or spinning.<sup>12</sup>

## 2-3 Exploitation of the Process

The various stages of the sol-gel process is illustrated in Figure 1. In stage (1) of the figure, the solution viscosity is low, somewhat similar to that of water. After a homogeneous solution is made, it can be applied to a substrate to form thin coatings by dipping or spinning. The film can then be dried and heat-treated to give a glass-like or polycrystalline film. A filler can also be added to the

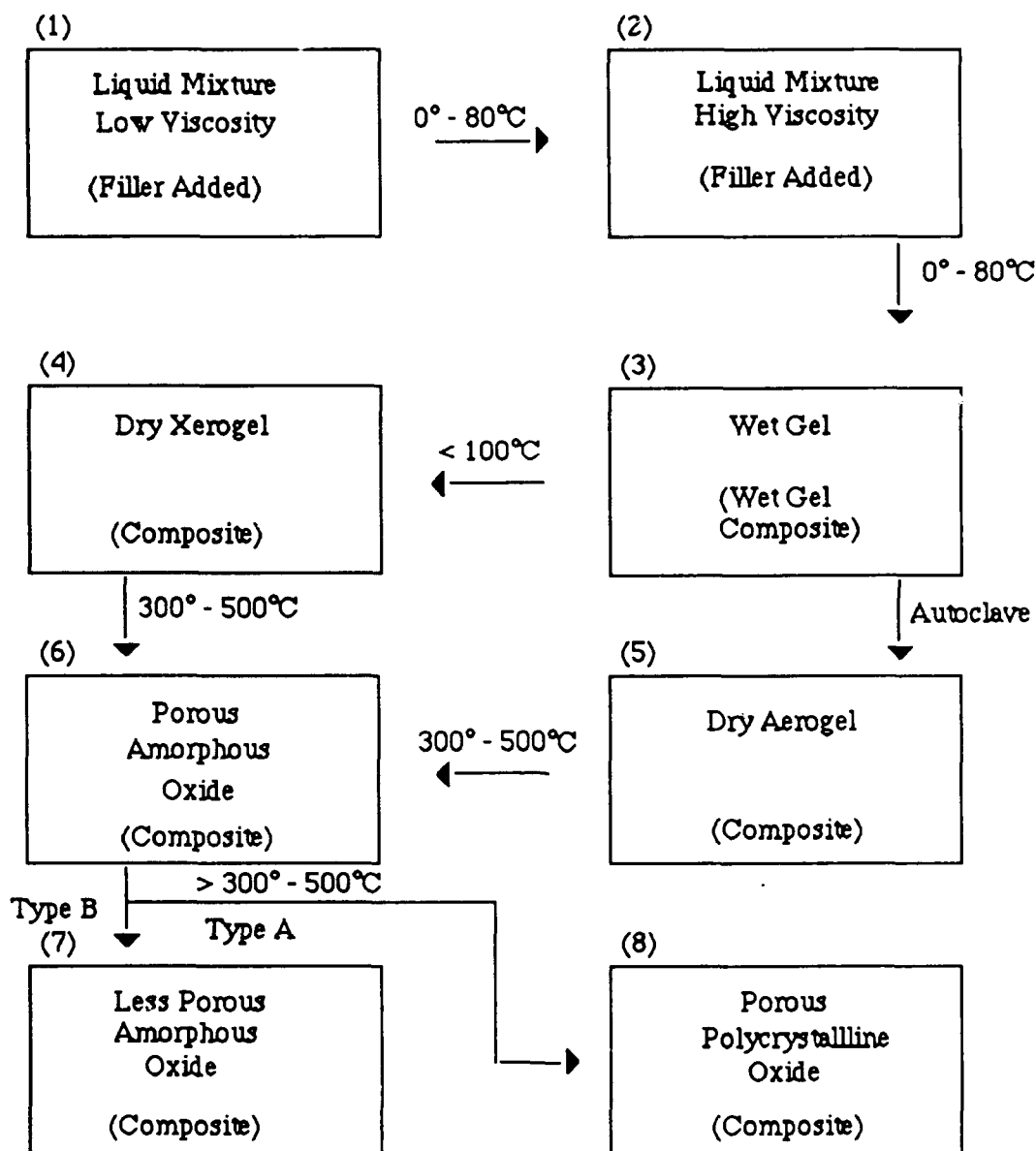


Figure 1. Various Stages of the Sol-Gel Process

liquid such that a composite film can be formed. The film thickness is governed by the concentration of the precursors in the solution and can be further controlled by multiple dipping. The technique can also be modified to prepare multilayers of different oxides. Thin films are particularly important in that if

the initial gel film were to form chemical bonds with the substrate, then subsequent shrinkage during heat-treatment would result in densification in the thickness direction rather than in the lateral directions along the substrate surface.

In stage (2) the viscosity of the starting liquid mixture has increased substantially due to the polymerization reaction. The viscosity can be controlled via the amount of water present or by other additives.<sup>15</sup> The wet gel formed at stage (3) is very porous and mechanically weak. The drying of a wet gel is usually accompanied by large shrinkages and frequently by fracture. Because when the liquid in the pores evaporates, a strong capillary pressure  $P$  is exerted on the weak pore walls for the small pore radius  $r$ :

$$P = 2g \cos \theta / r \quad (4)$$

Here,  $g$  is the vapor-liquid surface tension. The wet gel can be dried in an autoclave by a technique known as hypercritical drying to minimize cracking.<sup>16</sup> The dry aerogel and the dry xerogel are both very porous. Because the pores are usually very small ( $< 1000 \text{ \AA}$ ) and interconnecting, different materials can be impregnated into them to yield components which are now important for various optical applications.

Returning to stage (1), the filler to be added can be an organic dye, for instance Rhodamine b. This new composite could then be a useful material for lasers.<sup>17</sup> A porous wet gel can be placed in a leaching solution and one or more of its constituents extracted. The partially extracted wet gel would now have a concentration gradient. Subsequent heat-treatment would lead to the formation of a gradient-index glass (GRIN).<sup>18</sup>

From stage (6), further heating of systems which can be normally meltable to form glasses, would result in glass-like solids (Type B). It has been observed that much lower temperatures than the normal melting temperatures are required to prepare these "glasses". For instance, silica glass of excellent optical quality and in large pieces ( $420 \times 290 \times 10 \text{ mm}$ ) have been prepared by heating to only  $1300^\circ\text{C}$  whereas a conventional melting process would necessitate temperatures in excess of  $2000^\circ\text{C}$ .<sup>19</sup> The much lower heat-treatment temperature and the use of high purity alkoxides would minimize contamination during processing and ensure a high purity optical material. Non-glass forming systems (Type A) yield porous polycrystalline oxides on heating to  $T < 0.5 T_M$ . With the exception of thin films, the removal of porosity can be a problem. For thin films, good optical and electronic properties plus high density are obtained at relatively low heating temperatures. For instance, excellent films of the ferroelectric  $\text{LiNbO}_3$  were prepared from the gel by heating to only  $400^\circ\text{C}$ .<sup>20</sup>

The above sections illustrate that the sol-gel process can be exploited in many ways for optical applications. Because of the many factors which can influence the process, from chemical precursors to final products, the basic scientific knowledge is still inadequate when new optical materials are to be prepared by the sol-gel method. Nevertheless, the enormous potentials of this relatively new processing technique must now be fairly obvious. In the next section, some successful examples will be presented.

### 3. EXAMPLES OF OPTICAL MATERIALS

In the past decade many application of the sol-gel process to the fabrication of optical components have been reported. Some of these have already been successfully developed into commercial products. Others are in the "pilot plant" stage and some are in the "promising" stage of development. Many examples are presented in this Proceedings. The objectives of the present description are to illustrate the wide potentials of the sol-gel process and to provide the reader with sufficient guide-lines for new exploitations.

### 3-1 Dense Glasses

3-1-1 Dense Silica Glass.  $\text{SiO}_2$  glass, because of its low expansion coefficient, transparency in the UV, visible and near - IR and the absence of other cations, is important for many optical applications. Recently, research by L. L. Hench and Co-workers have produced silica glass via the sol-gel method by heat-treatment to only  $1150^\circ\text{C}$ .<sup>21</sup> The properties of the sol-gel derived silica glass are superior to those of all other types of silica glass. For instance, the UV transmission is better, the hydroxyl content is much lower ( $< 1\text{ppm}$ ), the refractive index and density are higher and the thermal expansion is lower.<sup>22</sup> A precision molding technique has also been developed to produce net-shape silica optics with tolerances in the range of  $10 - 50\ \mu\text{m}$ . Grinding of optical elements is thus eliminated and polishing rendered minimal. These ultrahomogeneous silica glass elements have been tested as intra-cavity etalons for argon lasers and shown to have much higher conversion efficiencies.<sup>22</sup>

3-1-2 Gradient Index Glass. A glass rod with a continuous variation of refractive index in the radial direction is used as lenses for copying machines and as connectors for optical fibers. Recently such GRIN glass rods have been prepared by the sol-gel method.<sup>23,24</sup> A  $\text{PbO-K}_2\text{O-B}_2\text{O}_3\text{-SiO}_2$  glass rod of diameter 7 mm was produced with a radial index gradient of  $4 \times 10^{-2}$  in 3 mm. A  $\text{SiO}_2\text{-TiO}_2$  glass rod of diameter 2 mm was found to have a radial index gradient of  $2 \times 10^{-2}$  in 1 mm. The refractive index profile is nearly parabolic. Compositional variation is practically unlimited. The index profile can therefore be altered easily by changes in chemical composition of the wet gel and by the leaching conditions.

### 3-2 Films and Coatings

3-2-1 Ferroelectrics. It has already been mentioned that thin films of  $\text{LiNbO}_3$  have been prepared by the gel method by heating to only  $400^\circ\text{C}$ .<sup>20</sup> Recently, Mackenzie and Co-workers have reported the preparation of a variety of transparent ferroelectric thin films on different substrates.<sup>25</sup> The optical transparencies of two such films are shown in Figure 2. The ferroelectric P-E hysteresis loop of a ( $\text{Sr}_{0.60}\text{Ba}_{0.40}$ )  $\text{Nb}_2\text{O}_6$  film on GaAs is

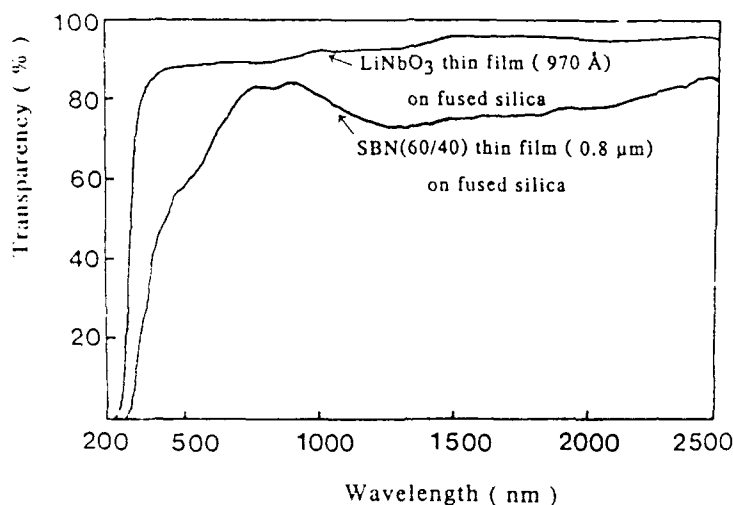


Fig. 2 Optical transparency of ferroelectric films on silica substrate



Fig. 3 Ferroelectric P-E hysteresis loop of SBN film on p-GaAs. Scale of x-axis is 44 kV/cm/div. and of Y-axis is 6.6 mC/cm<sup>2</sup>/div.

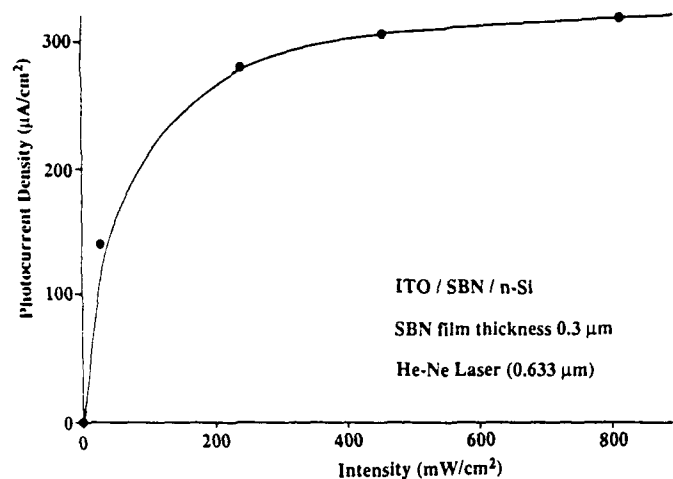


Fig. 4 Photocurrent vs. intensity for a SBN thin film on n-Si.

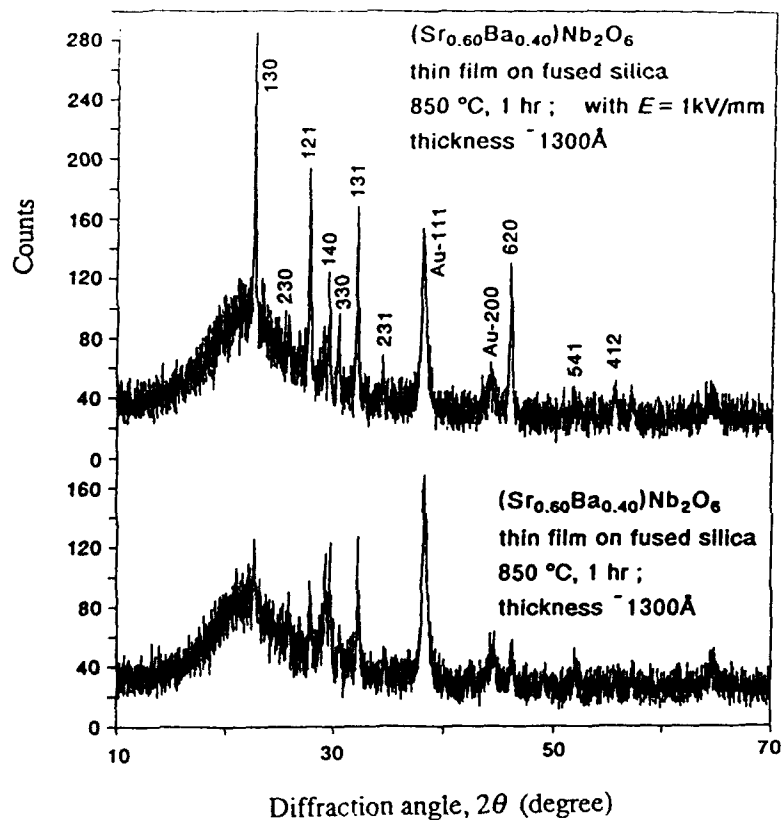


Fig. 5 X-ray diffraction of SBN thin films on fused silica substrate, with and without electric field during heat treatment.



shown in Figure 3. Photovoltaic effects have been clearly observed as exemplified by the photocurrent curve of Figure 4 for SBN on n-Si. Another interesting observation was the influence of an applied electric field during the heating of the gel film. In Figure 5, it is seen that preferred orientation of the SBN film has occurred as a result of the applied field. Further advances in the control of the optical quality of thin  $\text{LiNbO}_3$  films have been made recently at UCLA when two-wave mixing was demonstrated. S. Hirano of Nagoya University has prepared  $\text{LiNbO}_3$  films on sapphire which are "almost" single crystalline.

**3-2-2 Electronically Conductive Films.** Many transparent electronically conductive films have been prepared by the sol-gel process. Some of these are commercially available as coated glass windows as large as 1 m x 1m. The thicknesses available vary from 20 to 300 nm. Common examples are the indium-doped tin oxides and cadmium stannate. A review has been published by Dislich.<sup>26</sup>

**3-2-3 Antireflective Coatings.** The sol-gel process has been successfully applied to the preparation of different types of antireflective coatings.<sup>26,27</sup> The controlled leaching of a gel-derived coating can produce a concentration gradient and change the pore morphology. Through leaching, the reflectivity of a glass surface can be reduced to 1.4%.<sup>28</sup> Double-layer antireflective coatings based on  $\text{SiO}_2$  and  $\text{TiO}_2$  which maintain low reflectivities over a broad range of wavelengths have also been developed via the sol-gel method.<sup>29</sup>

**3-2-4 Ormosils Coatings.** Polymeric materials as optical components suffer from their relatively low hardness. Even the hardest organic polymers which as "CR 39" are much softer than inorganic glasses. Ormosils coatings have been applied to organic polymers and cured at 120°C. The coatings are much more scratch resistant than CR39.<sup>30</sup>

**3-2-5 Silicon Oxynitride Films.** Silicon oxynitride films are of importance in silicon device technologies because of their controllable refractive indices through the N:O ratio, their dielectric properties and their oxidation resistance. They have been prepared via the sol-gel route by first depositing a porous  $\text{SiO}_2$  film and then subjecting the film to a  $\text{NH}_3$  gas treatment at temperatures between 600° and 1100°C.<sup>31</sup> The refractive index could be varied from 1.42 to 1.72 depending on time and temperature and the dielectric constant varied from 3.8 to 5.5. This example is quoted to emphasize the flexibility of the sol-gel process in that it is not limited to oxides only.

### **3-3 Composites**

#### **3-3-1 Organic Dyes in Inorganic Matrices**

Two methods are available for the incorporation of organic dyes into an oxide matrix. In the first method, the dye is dispersed in the sol-gel solution prior to gelation.<sup>17</sup> After gelation, the dye molecules are trapped in an oxide cage. In the second method, the dye molecules are impregnated into the interconnecting fine pores of the dried gel via a monomer solution. The monomer, such as methylmethacrylate is subsequently polymerized.<sup>32</sup> Both methods yield transparent composites. Many organic dyes such as Rhodamine 6G, Rhodamine b, 2-Methyl-4-Nitroaniline have been incorporated into silica matrices.<sup>19,32-34</sup> A new solid state tuner in the 530-630 nm range has been successfully demonstrated recently by the use of the impregnation method with perylene dyes dissolved in methylmethacrylate.<sup>35</sup> Various dyes have also been dispersed in an alumina film by the sol-gel method.<sup>36</sup> Ormosils have also been used as the matrix for laser-active dyes.<sup>37</sup> The behavior of the solid composites was found to be superior to that of the same dyes in a liquid solution. In addition to laser-active dyes, photochromic dyes such as the spiropyranes have also been incorporated into oxide gels and ormosils.<sup>38</sup> Both normal (colorless to colored) and reversed (colored to colorless) photochromisms were obtained.

These early results suggest that sol-gel derived composites are promising materials for information processing.

**3-3-2 Nonlinear Polymers in Gels.** Many newly developed organic polymers have very large optical nonlinearity in comparison with oxide glasses. However, these polymers are difficult to fabricate into optical components of high transparency. If the polymer is incorporated into an oxide gel matrix, materials of high optical quality are obtained. This has permitted Prasad and Karasz to fabricate composites of poly-p-phenylenevinylene (PPV), a leading NLO polymer with a  $c^{(3)}$  of  $9 \times 10^{-9}$  esu in a gel-derived glass. This new material shows considerable promise for optical switching.<sup>39</sup>

**3-3-3 Semiconductor Crystallites in Glass.** The preparation of colored silicate glasses containing ultrafine crystallites of CdS and CdSe was first reported over a hundred years ago. Recently, these glasses have received a great deal of attention because of their nonlinear optical property.<sup>40,41</sup> Single crystals of CdS, for instance, are known to have very high values of nonlinear index at  $\sim 2^\circ\text{K}$ . The bound excitation level in CdS responsible for its high nonlinear coefficient is saturated at  $\sim 2^\circ\text{K}$  but is annihilated at higher temperatures. As the size of a crystal decreases until it approaches that of the exciton dimension, quantum confinement can occur. This should permit the high nonlinearity to be present at room temperature. Indeed, commercial CdS/CdSe glass filters have been shown to have  $c^{(3)}$  values of  $10^{-8}$  -  $10^{-9}$  esu at room temperature. Because of the method used in making these optical glasses, the size distribution of the crystallites is too broad and the average crystallite size somewhat too large. The sol-gel method, in its different variations, offers a promising route to the preparation of this type of CdS-oxide glass composites. Indeed, recent reports suggest that this approach is entirely feasible.<sup>42</sup> More recent work are presented in this proceedings.

#### 4. FUTURE TRENDS

In the above sections, it has been clearly shown that the sol-gel process has enabled the preparation of new and/or improved optical materials. It also permits the fabrication of optical components into shapes not easily achieved by other techniques of processing. As the uniqueness and versatility of the sol-gel process are more widely recognized, there is no doubt that it will be applied to more optical components and devices. Since the gel is formed from a liquid solution and its structure and microstructure are dependent on the overall chemical composition of the liquid, it is not difficult to appreciate that a fundamental understanding of the relationship between the liquid and its resultant gel must be obtained. Without this understanding, future progress in the development of sol-gel optics will be governed by a "hit or miss" approach. The physical chemistry of sol-gel liquid solutions is in its infancy at present. It will be vitally important for optical engineers to collaborate with material scientists and chemists to further exploit this unique process for optical materials and systems. Despite this lack of basic knowledge concerning the structures and properties of sol-gel liquid solutions, significant future advances in a few areas can be identified. These are summarized below.

**4-1 Sol-gels for Nonlinear Optics.** New composites will be developed based on: (a) NLO organic polymers and oxide or ormosil combinations; (b) Organic dyes incorporated into oxide or ormosil matrices by entrapment or by impregnation and (c) semiconductor microcrystals in sol-gel derived matrices. Optical elements of superior transparencies and high NLO coefficients will be fabricated into different shapes.

**4-2 Ferroelectric Thin Films.** Ferroelectric thin films, pure and doped, of superior optical quality will be fabricated on various substrates including semiconductors. As progress develops, the fabrication temperatures will decrease to below  $400^\circ\text{C}$  and the preparation of single crystal films on epitaxially compatible substrates will be possible. Such films will be utilized for holographic memory, infrared detection, optical bistable devices and non-volatile memory devices.

**4-3 New and Improved Oxide Glasses.** The superior optical properties of  $\text{SiO}_2$  glasses prepared by the sol-gel process will lead to applications in UV holography and precision optical imaging devices. Near net-shaped fabrication of lenses based on high purity silica glasses will be followed by other glass

compositions. The GRIN lenses will be fabricated by the leaching and/or ion-exchange process applied to gels. Other new glasses based on compositions which are not normally or easily meltable will be fabricated by the sol-gel method. Examples of these glasses could be  $\text{TiO}_2\text{-SiO}_2$  and  $\text{V}_2\text{O}_5\text{-SiO}_2$ .

4-4 Multifunctional Materials. The sol-gel process permits the preparation of practically unlimited oxide compositions as porous oxide gels. The pore size and distribution are controllable. Organic molecules can be dispersed in the oxide matrix. Ions such as Ag, Pb and Cu, can also be present in the matrix and be reduced to their atomic state. The oxide matrix can be crystallized or vitrified. The pores within the gel can be coated or fully impregnated. The possibilities of preparing new materials, especially multifunctional materials are unlimited. In addition, the gel method readily permits the fabrication of monoliths, films, coatings and fibers. It is timely that innovative exploitations be made at present. It is thus likely that some new and unique optical materials will be developed in the near future.

## 5. ACKNOWLEDGEMENTS

One of us (J. D. Mackenzie) is grateful to the Air Force Office of Scientific Research, Directorate of Chemical and Atmospheric Sciences for the continuing support of sol-gel research at UCLA.

## 6. REFERENCES

1. T. Graham, J. Chem. Soc. 17, 318, 1864.
2. B. Jirgensons and M. E. Straumanis, Colloid Chemistry, McMillan Co., New York, 1962.
3. R. K. Iler, The Chemistry of Silica, John Wiley and Sons, New York, 1979.
4. J. G. Vail, Soluble Silicates, ACS Monograph Series, Reinhold, New York, 1978.
5. C. J. Brinker and G. W. Scherer, Sol-Gel Science, Academic Press, Boston, 1990.
6. J. D. Mackenzie, SPIE Proceedings 878, 128, 1988.
7. J. D. Mackenzie, Chap. 12 in Science of Ceramic Chemical Processing, Ed. L. L. Hench and D. R. Ulrich, John Wiley and Sons, New York, 1986.
8. J. D. Mackenzie, Chap. 43 in Ultrastructure Processing of Advanced Ceramics, Ed. J. D. Mackenzie and D. R. Ulrich, John Wiley and Sons, New York, 1988.
9. W. H. Zacharrai, J. Am. Chem Soc. 54, 3841, 1932.
10. H. Schmidt, G. Philipp, J. Non-Cryst. Solids, 63, 83, 1984.
11. H. H. Huang, B. Orler, G. Wilkes, Polym. Bull. 14, 557, 1985.
12. H. Schmidt, et al, Chap. 48 in Ultrastructure Processing of Advanced Ceramics, Ed. J. D. Mackenzie, D. R. Ulrich, John Wiley and Sons, New York, 1988.
13. E. T. Knobbe, et al, Fourth Conf. Ultrastructure Processing of Ceramics, Tuscon, Arizona, February, 1989, in press.
14. Y. J. Ching, J. D. Mackenzie, Proc. 5th Conf. Better Ceramics Through Chemistry, San Francisco, California, May, 1990, in press.

15. S. Sakka, Chap. 7 in Sol-Gel Technology for Thin Films, Fibers, Preforms, Electronics and Speciality Shapes, Ed. L. C. Klein, Noyes Publications, N. J. 1988.
16. S. S. Kistler, J. Phys. Chem. 36, 52, 1932.
17. D. Avnir, D. Levey, R. Reisfeld, J. Phys. Chem. 88, 5954, 1984.
18. M. Yamanc, J. B. Caldwell, D. T. Moore, J. Non-Cryst. Solids 85, 244, 1986.
19. M. Toki, et al, J. Non-Cryst. Solids, 100, 479, 1988.
20. S. Hirano, K. Kato, J. Non-Cryst. Solids, 100, 538, 1988.
21. L. L. Hench and J. K. West, Chem. Rev. 90, 32, 1990.
22. D. R. Ulrich, Chem. Eng. News 68, 26, 1990.
23. M. Yamane, et al, J. Non-Cryst. Solids, 100, 506, 1988.
24. S. Konishi, K. Shingyouchi, A. Makishima, J. Non-Cryst. Solids, 100, 511, 1988.
25. Y. Xu, C. J. Chen, R. Xu, J. D. Mackenzie, J. Appl. Phys, 67, 2985, 1990.
26. H. Dislich, Chap. 4 in Sol-Gel Technology for Thin Films, Fibers, Preforms, Electronics and Specialty Shapes, Ed. L. C. Klein, Noyes Publications, N.J., 1988.
27. R. B. Pettit et al, Chap. 5 in Sol-Gel Technology for Thing Films, Fibers, Preforms, Electronics and Speciality Shapes, Ed. L. C. Klein, Noyes Publication, N.J., 1988.
28. B. E. Yoldas and D. P. Partlow, Appl. Optics, 23, 1418, 1984.
29. B. C. Yoldas, T. W. O'Keeffe, Appl. Optics 18, 3133, 1979.
30. H. Schmidt, et al, Chap. 48 in Ultrastructure Processing and Advanced Ceramics, Ed. J. D. Mackenzie, D. R. Ulrich, John Wiley and Sons, New York, 1988.
31. C. G. Pantano, R. K. Brow, L. A. Carman, Chap. 6 in Sol-Gel Technology for Thin Films, Fibers Performs, Electronics and Specialty Shapes, ed. L. C. Klein, Noyes Publications, N.J., 1988.
32. E. J. A. Pope, M. Asami, J. D. Mackenzie, J. Mater. Res. 4, 1018, 1989.
33. A Makishima, T. Tani, J. Am. Ceram. Soc. 69, C 72, 1986.
34. T. Tani, et al, J. Appl. Phys. 58, 3559, 1985.
35. R. Reisfeld, et al, Chem. Phys. Letters, 160, 43, 1989.
36. Y. Kobayashi, et al, J. Jon-Cryst. Solids, 105, 198, 1988.
37. E. T. Knoke, et al, Proc. 4th Int. Conf. Ultrastructure Proc. of Ceramics, Glasses and Composites, Tuscon, Arizona, 1989, in press.
38. D. Levy, S. Einhorn, D. Avnir, J. Non-Cryst. Solids, 113, 137, 1989.

39. P. N. Prasad, F. E. Karasz, Y. Yang, C. J. Wang, U. S. Patent Appl. No. 312132, 1989.
40. R. K. Jain, R. C. Lind, J. Opt. Soc. Am. 73, 647, 1983.
41. S. S. Yao, et al, Appl. Phys. Lett. 46, 801, 1985.
42. M. Nogami, K. Nagasaka, E. Kato, J. Am. Ceram. Soc. 73, 1990.

SOL-GEL OPTICS

Volume 1328

**SESSION 1**

**Bulk Solids and Applications**

*Chair*

**J. Zarzycki**

University of Montpellier II (France)



## Chemical Processing of Glasses

Richard M. Laine

Department of Materials Science and Engineering,  
University of Washington and the Washington  
Technology Center, University of Washington, Seattle, WA 98195

ABSTRACT

The development of chemical processing methods for the fabrication of glass and ceramic shapes for photonic applications is frequently Edisonian in nature. In part, this is because the numerous variables that must be optimized to obtain a given material with a specific shape and particular properties cannot be readily defined based on fundamental principles. In part, the problems arise because the basic chemistry of common chemical processing systems has not been fully delineated. The purpose of this paper is to provide an overview of the basic chemical problems associated with chemical processing. The emphasis will be on sol-gel processing, a major subset of chemical processing. Two alternate approaches to chemical processing of glasses are also briefly discussed. One approach concerns the use of bimetallic alkoxide oligomers and polymers as potential precursors to multimetallic glasses. The second approach describes the utility of metal carboxylate precursors to multimetallic glasses.

1. INTRODUCTION

The need for precise control of chemical composition, phase purity, index of refraction, porosity and doping (impurity) levels during processing of complex glass and ceramic shapes, especially for photonics applications, is a major driving force for the development of chemical processing techniques.<sup>1-3</sup> The need for new, low temperature methods for processing complex glass and ceramic shapes, especially for advanced structural materials, provides additional impetus for the development of chemical processing techniques.<sup>4-6</sup>

The literature in these areas has grown tremendously in the last several years<sup>1-10</sup> and it is well beyond the scope of a single paper to provide even a sketchy overview of chemical processing as it exists today. The schematic shown in Figure 1 affords a view of the diversity both in approaches, processing variables and product forms that are encompassed by "chemical processing". From Figure 1, we can define three broad areas that must be considered in any new venture into chemical processing. One area concerns choice of monomer structure and reaction conditions such that the monomer is readily transformed into the desired polymer, gel, or colloid precursor. The second area concerns processing the resultant precursor into the appropriate shape (powder, fiber, film, monolith). Once the final precursor shape is obtained, it is necessary to transform the precursor material into the final glass or ceramic product (powder, film, fiber or monolith).

92-11401



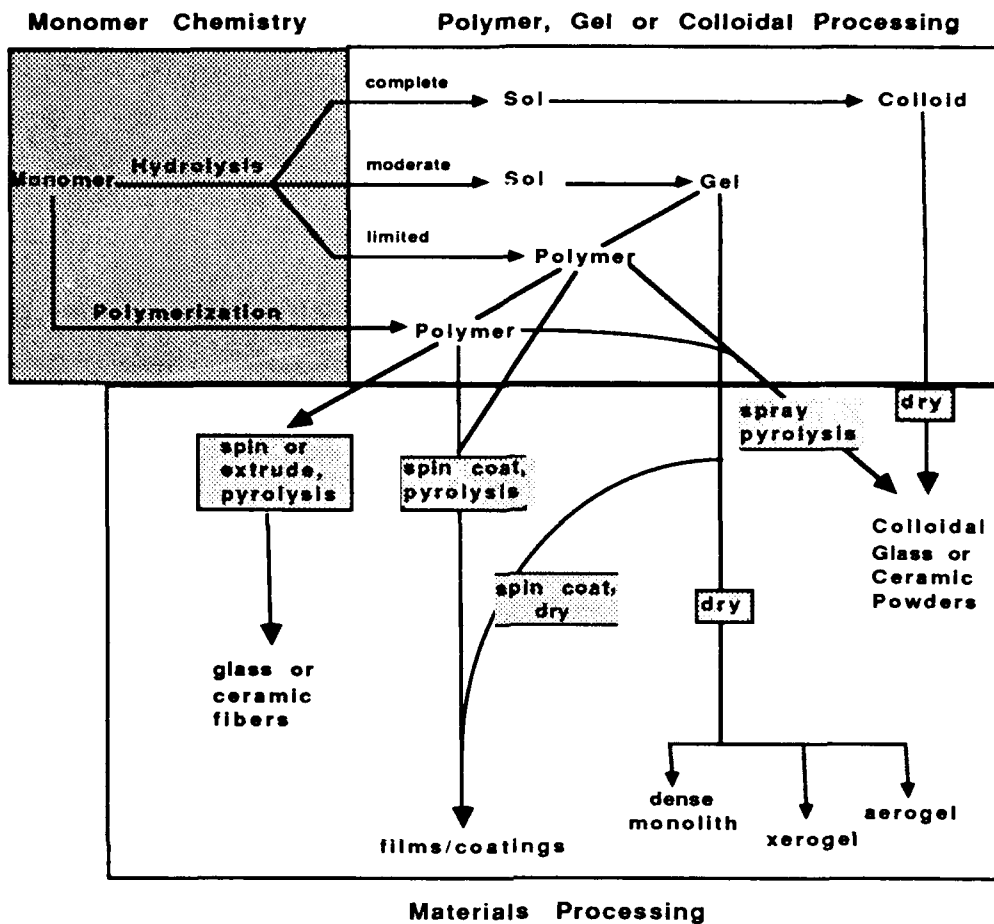


Figure 1. Chemical Processing of Glass and Ceramic Shapes

In this paper, we are concerned with the chemistry that permits the transition from monomer to tractable polymer or gel precursors to oxide glasses. By tractable, we mean that one can process glass or ceramic films, fibers or monoliths from these intermediates without proceeding first to powders. The use of powders implies standard glass or ceramic processing techniques which take advantage of chemically pure and/or uniform powders. We present below an overview of the important chemical reactions that occur during the initial phases of sol-gel processing of glasses and ceramics. This overview is followed by brief discussions of alternatives to sol-gel processing including oxidation of organometallic alkoxide and carboxylate polymers. The emphasis will be on chemical processing of glass, glass/ceramic or ceramic shapes and materials for photonic applications.

## 2. DISCUSSION

We begin by defining what is meant by chemical processing. The basic concept consists of using common, low temperature, inorganic and organo-metallic chemical reactions to form precursors to target materials wherein the elements of the target material are atomically mixed without recourse to standard high temperature processing techniques that rely on



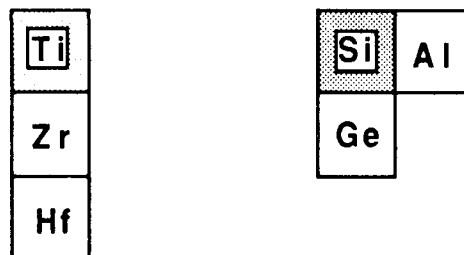
high temperature melt or solid state diffusion reactions. This approach also permits introduction of precise amounts of dopants, again with atomic mixing.

A further advantage to chemical processing is that careful choice of chemical reactions and monomers provides polymer or gel precursors that exhibit appropriate rheological properties. These properties provide access to forms (thin films, coatings and fibers) that are often difficult to fabricate using high temperature processing techniques. Once the desired precursor shape is obtained, conditions can be chosen that permit it to be converted to the target glass or ceramic product while retaining atomic mixing. More detailed discussions of the advantages of chemical processing are presented elsewhere.<sup>1-10</sup>

## 2.1 Sol-gel processing

The phrase "sol-gel processing" is frequently used to define any glass or ceramic processing methodology that employs chemical precursors. As used here, "sol-gel processing" refers to any "chemical processing" approach that relies on hydrolysis of metal-ligand (e.g. M-OR) bonds to form M-O-M bonds. Thus, sol-gel processing becomes a subset of all chemical processing methods that transform M-L (L = ligand) bonds into M-O-M links. We will explore non-hydrolytic methods of forming M-O-M links following a discussion of the chemistry of sol-gel reactions.

Sol-gel processing has been used successfully to incorporate a majority of the elements in the periodic chart into glass or ceramic materials. The sol-gel chemistry of the elements shown below has been studied extensively.



Consequently, our discussions will focus on these elements, especially the chemistry of silicon and titanium. Si chemistry is very similar to that of Ge and Sn. Likewise, the chemistries of Ti, Zr and Hf are very similar. Thus, it can be inferred that what is said for Si or Ti will normally be true for their second and third row equivalents and vice versa.

### 2.1.1 Monomer Structures

We can begin by illustrating (see Figure 2) the structural features of common Si and Ti alkoxide precursors. Figure 2 illustrates the difference between isopropyl and ethyl groups in the two metals. All  $\text{Si}(\text{OR})_4$  compounds are tetrahedral and monomeric in acid or neutral solvents. Ti systems with bulky alkoxy groups, e.g.  $\text{Ti}(\text{OiPr})_4$ , are monomeric and tetrahedral.<sup>11,12</sup> In contrast, Ti systems with smaller alkoxy groups, e.g.  $\text{Ti}(\text{OiEt})_4$ , form trimeric complexes pentacoordinate complexes in non-nucleophilic solvents (e.g. benzene, alkanes) and octahedral species in nucleophilic solvents (e.g. alcohols, THF) with the solvent occupying one coordination site. Alkoxyaluminanes, e.g.  $\text{Al}(\text{OR})_3$ , also exhibit monomer-oligomer behavior dependent on ligand bulk.

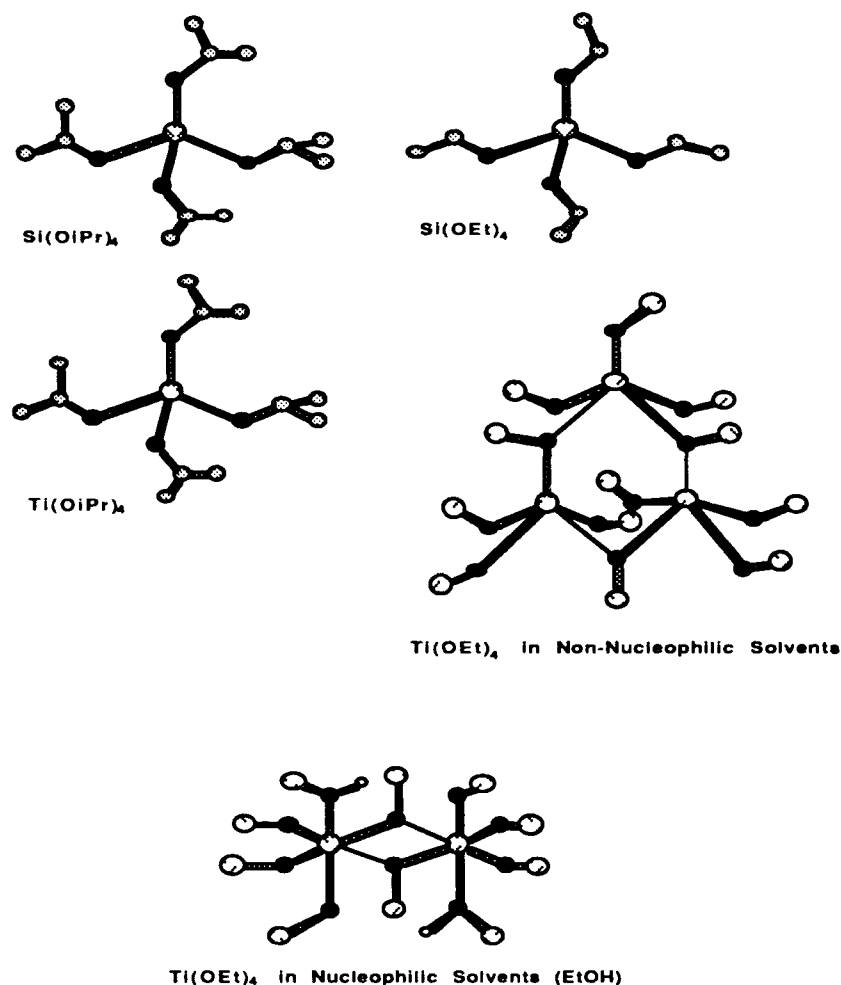
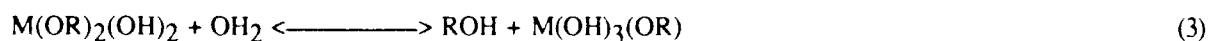
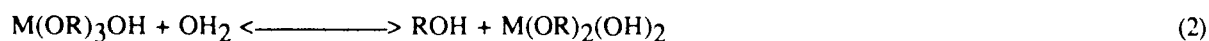
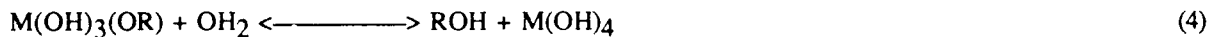


Figure 2. Structural Features in Si and Ti Alkoxide Precursors.

### 2.1.2. Hydrolysis Reactions of Metal Alkoxides.

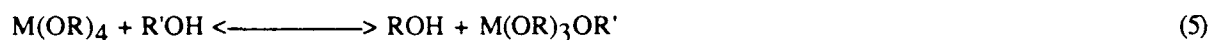
Because we are concerned with making thin films, fibers and monoliths rather than powders; it is important to define the sol-gel parameters necessary to bring about the appropriate intermediates. To obtain useful rheological properties and simultaneously avoid formation of colloidal particles, it is best to choose hydrolysis conditions that lead to linear rather than highly branched and crosslinked intermediates.<sup>13</sup> This is normally accomplished by avoiding complete hydrolysis of the alkoxide precursor. To this end, it is important to understand what types of reactions metal alkoxides can undergo during hydrolysis. The following hydrolysis reactions are common to most metal alkoxides.





For silicon, it is likely to find all four reaction products under most conditions. For other metals, condensation is so rapid or the reverse reaction is so favored that the likelihood of obtaining species such as  $M(OH)_4$  is low. All of the reactions are reversible for all of the metals including Si and under the right conditions, the reverse reaction competes very successfully with hydrolysis. Indeed, this is one reason many fully processed gels contain significant quantities of carbon. Retained carbon in turn diminishes the optical quality, phase purity etc. of the final glass or ceramic products.

Many researchers are unaware of the rapidity of the reverse reaction and run sol-gel reactions using  $M(OR)_4/R'OH/OH_2$  systems.<sup>11,13</sup> The hydrolysis kinetics can be severely affected by alcohol exchange processes:

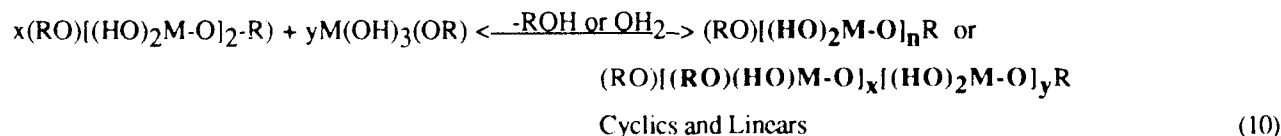
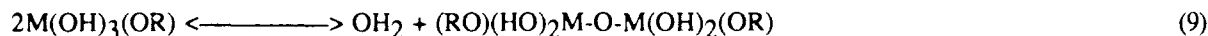
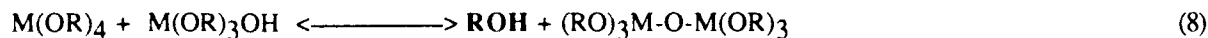


In instances where Ti, Al or related alkoxides are used, alcohol exchange can transform the alkoxide precursor from a monomer to a dimer, trimer or oligomer. The hydrolysis products of oligomeric precursors are very likely to be quite different from those derived from monomers. At worst, one may enhance formation of highly crosslinked, intractable intermediates (see below). At best, the kinetics of hydrolysis (gel time and/or temperature) will be unlike that expected if one is following related literature examples. This is one (of many) reason why two groups studying the same system may report quite different results. Other reasons are discussed below.

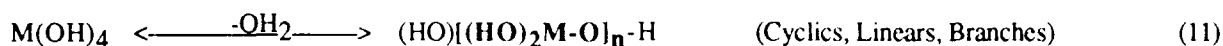
### 2.1.3. Condensation reactions.

Once M-OH groups are formed, further reaction occurs by condensation. The following reactions have been documented for  $Si(OR)_x(OH)_y$  species; however, there is evidence that similar reactions occur in titanium systems.

Low and medium water concentrations:



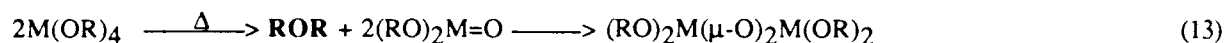
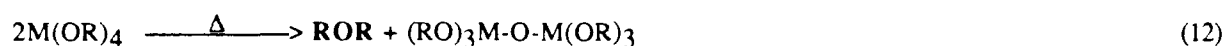
High water concentrations:



The alkoxy groups in the higher  $(RO)[(HO)_2Si-O]_nR$  polymers are much less susceptible to hydrolysis than M-OR groups in monomers and simple oligomers. This provides another explanation for retention of carbon in final, dry gels.

At very high water concentrations, the primary product of hydrolysis is  $Si(OH)_4$  which then condenses to give silica gels and particles. However, the need for a dual solvent system often requires using some alcohol; therefore, one can never truly escape forming some  $(RO)[(RO)(HO)MO]_x[(HO)_2MO]_yR$  polymers during condensation.

The above hydrolysis and condensation reactions can occur at or below room temperature. At higher temperatures, other types of condensation reaction occur that can lead to direct formation of polymers without hydrolysis:<sup>8</sup>



The products of reactions (12) and (13) often form during the distillation of the metal alkoxides. Thus, efforts to purify starting metal alkoxides by distillation may actually lead to less pure rather than higher purity starting materials. Reactions (12) and (13) may be quite useful, if one is intent on producing polymeric rather than gel or colloidal materials.

#### 2.1.4. Mechanisms of Hydrolysis.

In neutral solutions,  $Si(OR)_4$  reacts slowly to form simple hydrolysis products. By comparison, other metal alkoxides react much faster in neutral solution; however, all systems experience significant increases in rates of hydrolysis and condensation in the presence of catalytic amounts of acids or bases. Common acid catalysts include HCl,  $HNO_3$ ,  $H_2SO_4$ ,  $H_3PO_4$ , HF, acetic acid etc. Basic catalysts include metal hydroxides (e.g. KOH, NaOH), ammonium hydroxide ( $NH_4OH$ ), aminium hydroxides (e.g.  $Me_4NOH$ ) etc.

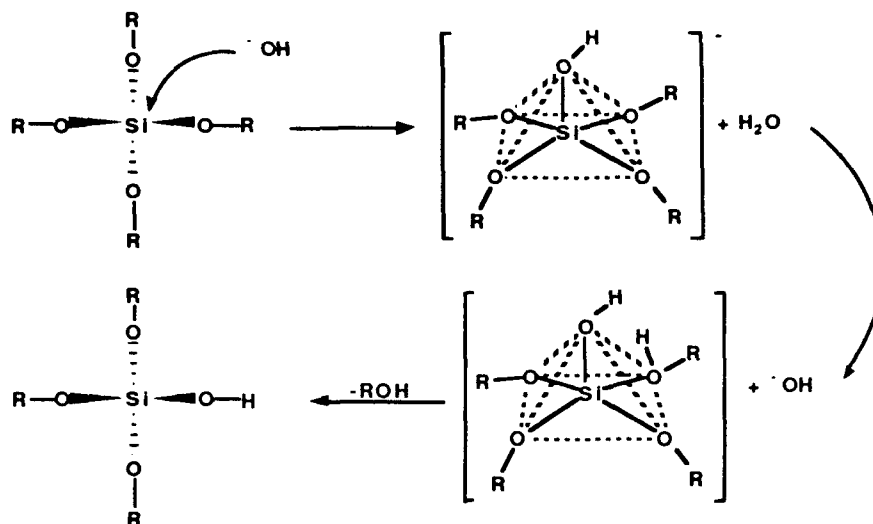
Under otherwise identical conditions, the products deriving from acid catalyzed sol-gel reactions can be quite different from those obtained with basic catalysts. In part, these differences are due to the specific mechanisms of hydrolysis and condensation and, in part to experimental variables. Unfortunately, the only detailed studies on hydrolysis and condensation mechanisms found in the literature concern  $Si(OR)_4$ . Even here, there are still many questions that remain to be answered. Thus, much of sol-gel processing remains an art based on Edisonian tactics.

##### 2.1.4.1. Si

Recent experimental and theoretical results indicate that both acid and base catalyzed hydrolysis of alkoxysilanes proceed via pentacoordinate intermediates. In base catalysis, it has been proposed that  $OH^-$  reacts directly with the silicon center to form a pentacoordinated anion intermediate as shown in Scheme 1.

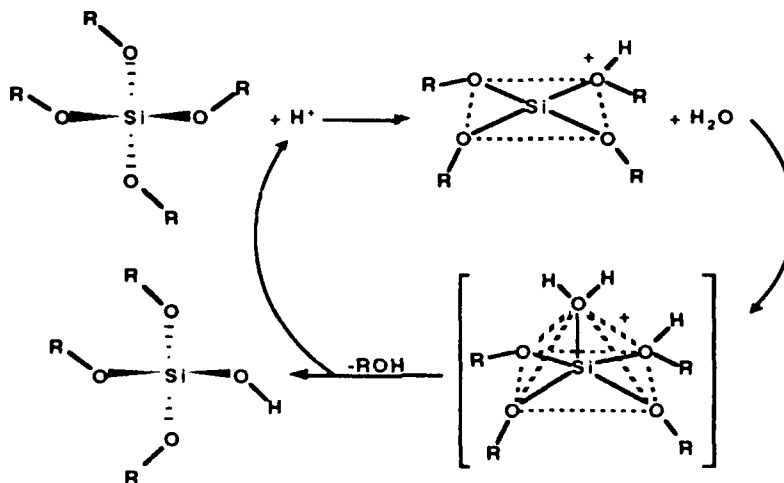
Numerous literature examples of pentacoordinated (and hexacoordinated) Si compounds (see below) provide excellent support for the intermediacy of hypervalent silicon in hydrolysis (and condensation).<sup>14-16</sup> Indeed, pentacoordinated Si is ubiquitous in all areas of silicon chemistry and allows us to pose the question: Why aren't there literature examples of

glasses wherein Si is pentacoordinated?



Scheme 1

The mechanism proposed for acid catalyzed hydrolysis begins with protonation at an alkoxy oxygen.<sup>2c</sup> Protonation makes the silicon sufficiently electropositive to permit attack by free water to form a pentacoordinated intermediate as shown in Scheme 2. Literature support for the existence of pentacoordinated silicon compounds in acid hydrolysis is based



Scheme 2

on volume of activation changes at high pressure.<sup>17</sup> Additional support comes from the fact that acid catalyzed hydrolysis of  $\text{Me}_{4-x}\text{Si(OR)}_x$  is faster for lower values of  $x$ .<sup>18</sup> This is logical given that electron donation by the Me groups will stabilize formation of a positive charge at the alkoxy oxygen. Of interest here is the fact that the compounds  $\text{Me}_{4-x}\text{Si(OR)}_x$  ( $x \neq 4$ ) are not susceptible to base hydrolysis. Thus result permits the conclusion that the mechanism for acid catalyzed hydrolysis differs considerably from that in base catalyzed hydrolysis.

Numerous structure/reactivity hydrolysis rate studies for silicon have been conducted and will not be discussed here; however, as expected, the bulkier the alkyl group the slower the rate of hydrolysis.<sup>17</sup> Also, as expected, increases in temperature typically lead to increases in reaction rates.

One final comment on hydrolysis mechanisms in silicon concerns the use of fluoride compounds to promote hydrolysis. Fluoride either as  $F^-$  or as HF, because of its high Si bond dissociation energy (Si-F BDE  $\approx$  140 kcal/mole, Si-O BDE  $\approx$  128 kcal/mole) will promote hydrolysis by forming pentacoordinate Si-F intermediates even in acid solutions. Thus sol-gel studies with fluoride give anomalous results when compared with other types of catalyzed hydrolyses. Moreover, there is a considerable likelihood that fluoride will remain incorporated in the final glass or ceramic.

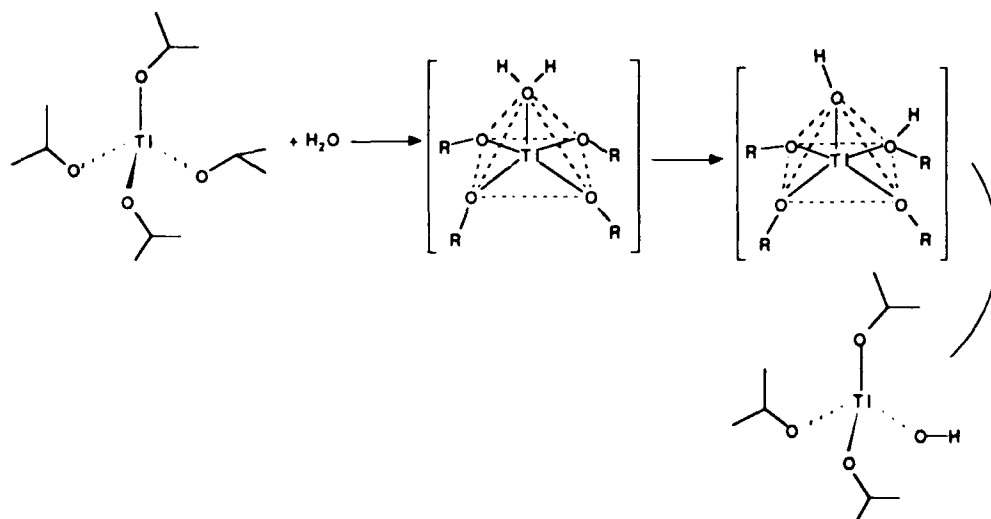
#### 2.1.4. 2. Ti and Zr.

Essentially no other work has been done to ascertain, in detail, the mechanisms of hydrolysis of other metal alkoxides. As noted above the species  $M(OR)_4$  for  $M \neq Si$  hydrolyze much faster than  $Si(OR)_4$ . The reason is that these species are excellent Lewis acids and catalyze their own hydrolysis.

Several groups have studied the hydrolysis kinetics of  $Ti(OR)_4$  and  $Zr(OR)_4$  alkoxides under neutral conditions. Thus, Smit et al<sup>19</sup> have studied the kinetics of hydrolysis of  $Zr(OnPr)_4$  using reaction conditions and analytical techniques essentially identical to those used by Barringer to study the hydrolysis of  $Ti(OEt)_4$ .<sup>20</sup> Smit et al find that if less than four equivalents of water are used, hydrolysis stops at  $(nPrO)Zr(OH)_3$ . Furthermore, essentially no precipitation occurs when less than three equivalents of water are added. They conclude that hydrolysis proceeds in a stepwise manner with only limited condensation. These results closely resemble Barringer's work on  $Ti(OEt)_4$ .<sup>20</sup>

The Smit work was done in ethanol solvent. Alcohol exchange must occur; however, how this exchange affects the hydrolysis kinetics is not clear because all of the straight chain alkoxy titanium complexes including  $Ti(OnBu)_4$  form dimeric and trimeric species.<sup>11,12</sup> Recent work by Sanchez et al<sup>11</sup> on the hydrolysis of  $Ti(OR)_4$ , where  $R = iPr$  or  $nBuO$ , when coupled with the Smit and Barringer works, suggests a plausible hydrolysis mechanism.

Because Ti (IV) alkoxides are well-known Lewis acids, they form pentacoordinate (and hexacoordinate) complexes in the presence of  $H_2O$  akin to those shown in Schemes 1 and 2 for silicon. Hydrolysis occurs from these intermediates:

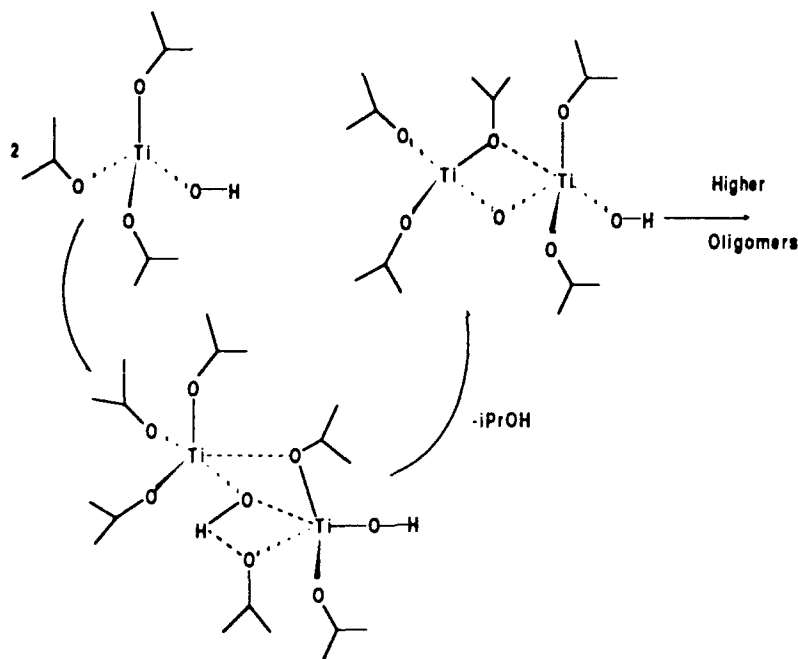


Scheme 3

Once M-OH bonds are formed, condensation must follow and the question is does it result in the formation of linear, branched oligomers, etc and can the degree of each form be controlled to avoid the formation of colloids or intractable gels.

### 2.1.5. Condensation mechanisms

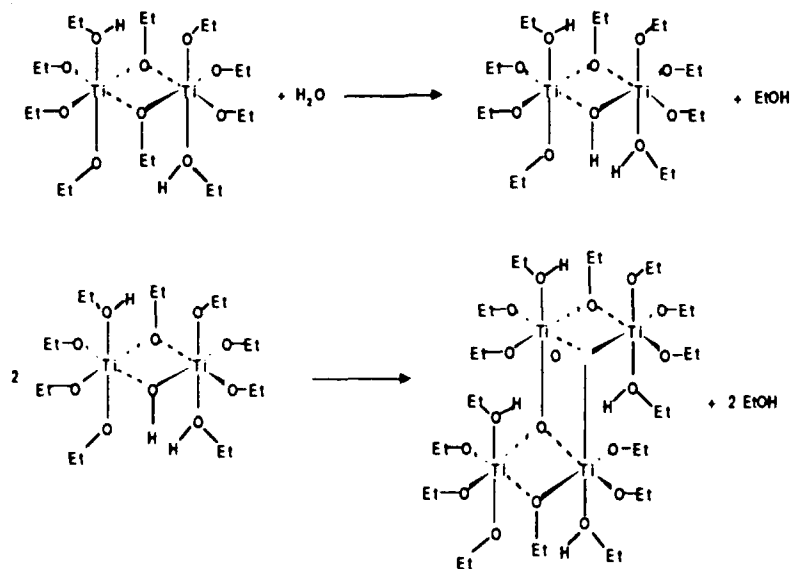
If we assume that tetrahedral  $\text{Ti}(\text{OiPr})_4$  reacts in much the same manner as  $\text{Si}(\text{OR})_4$ ; albeit, much faster, then we can describe general condensation processes as shown below. In Scheme 4, linear polymers are more likely to form. The



Scheme 4

silicon analog, with a basic catalyst, will involve attack of an  $\text{Si-O}^-$  species on another Si center.

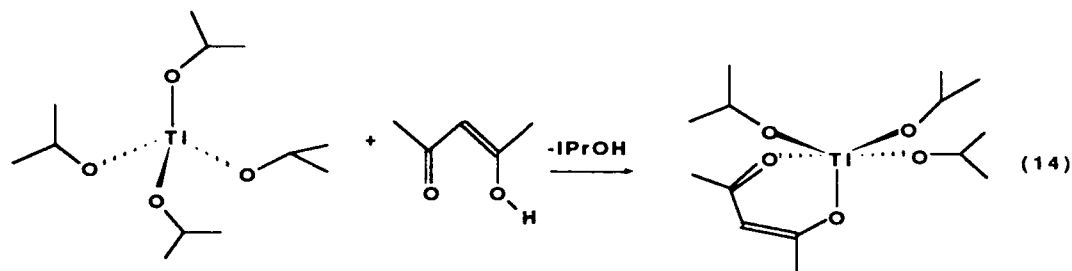
If we start with a less hindered Ti species then we immediately get cluster formation of the type likely to lead to highly branched, colloidal particles:



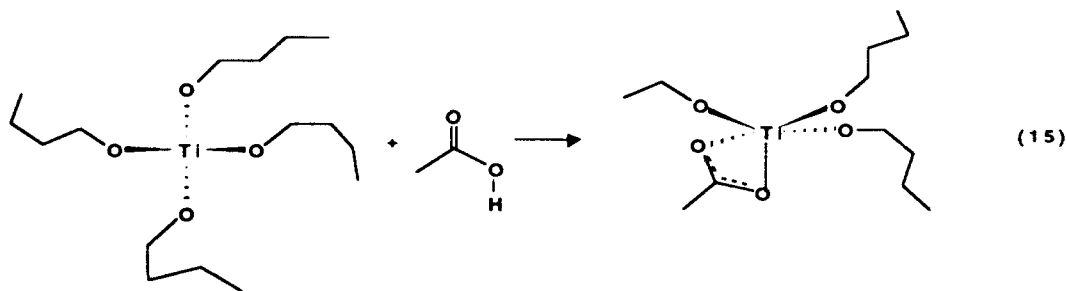
Scheme 5

Sanchez et al<sup>21</sup> have found that in analogous Zr reactions they can actually isolate and obtain a crystal structure of a

species nearly identical to the product in Scheme 4. Sanchez et al<sup>11</sup> have also found a method of reducing the opportunity for reactions such as depicted in Scheme 4 from occurring. They find that if they react  $\text{Ti}(\text{OiPr})_4$  with 2,4-pentanedione (reaction 14) or  $\text{Ti}(\text{OnBu})_4$  with  $\text{CH}_3\text{CO}_2\text{H}$  (reaction 15) that they can obtain unbridged species wherein a fifth ligand



site on Ti is occupied by an unreactive group. These bidentate ligands not only inhibit the formation of bridging species such as shown in Schemes 4 and 5, they also occupy a site that would initially be available for binding water. As a result, the rates of hydrolysis and condensation are slowed down such that they can obtain clear monolithic gels



from either precursor system. These examples suggest ways of modifying the reactivity of the precursor to control the type of intermediates formed and therefore processability. Hench and West have recently discussed this effect in detail.

Detailed discussion of the properties and processing of the resulting oligomeric and polymeric precursors is beyond the scope of this paper but such discussions are available.<sup>1-10</sup>

## 2.2. Organometallic Precursors

We have noted that there is a significant disparity between the rates of hydrolysis of  $\text{Si}(\text{OR})_4$  and the other metal alkoxides.<sup>12</sup> In fact, the rates of hydrolysis of other metal alkoxides have not been carefully measured; however, qualitative results indicate that there can be orders of magnitude variations in rates. These rate differences can be dealt with as Sanchez et al have done, by introducing ligands that modify reactivity. However, consider the preparation of multimetallic glasses and ceramics.

The preparation of processable intermediates to multimetallic glasses via sol-gel processing requires exceptional control of the sometimes exceedingly disparate rates of hydrolysis and condensation of the component metal alkoxides. The possibility of obtaining effective atomic mixing rather than segregation in the precursor is low. Thus, it is extremely difficult to envision developing useful sol-gel approaches to multimetallic glasses; although, it has been done successfully on a commercial scale.

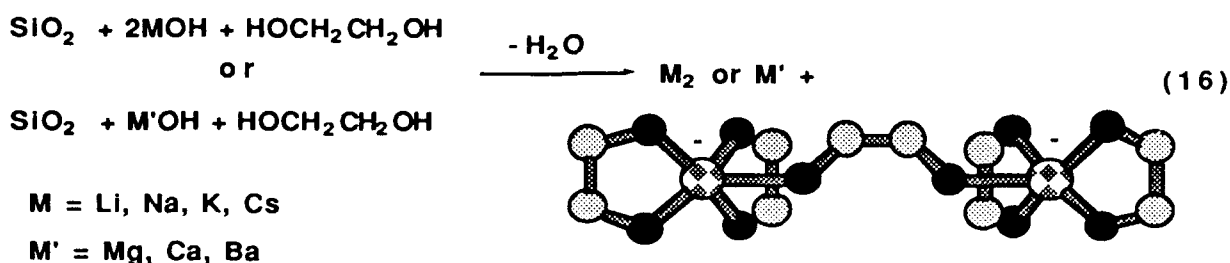
Organometallic precursors offer potential advantages over sol-gel processing of glasses and ceramics for processing



multimetallic glasses. Organometallic precursors rely on preformed bonding arrangements in a polymer species for both atomic mixing and the rheological properties necessary for low temperature manipulation (e.g. fiber spinning). Furthermore, close control of drying does not play a role in organometallic processing of glasses. However, alternate problems do exist, such as effective removal of carbon containing ligands so that carbon impurities are minimized. We will briefly illustrate the possibilities of using polymeric organometallic alkoxide precursors for multicomponent glasses.

### 2.2.1. Bimetallic Alkoxides

We have recently shown that we can synthesize directly from silica, polymeric salts of the following type:<sup>22</sup>



Although, these are discrete molecular species, when mixed with a molar equivalent of another diol, they can be made polymeric simply by heating. These bimetallic polymers provide entrée into a number of standard multimetallic glasses glass compositions, simply by melting in air. For example, the barium salt,  $\text{BaSi}_2(\text{OCH}_2\text{CH}_2\text{O})_5$  decomposes at  $\approx 250^\circ\text{C}$  to essentially pure  $\text{BaO}$ .<sup>22b</sup> Although, this is a simple example it is meant to demonstrate the possibilities of this approach for processing multicomponent glasses. Reference 8 provides an in-depth discussion of bimetallic alkoxides.

### 2.2.2 Metal Carboxylates

As an alternative to metal alkoxides, metal carboxylates also provide access to multimetallic glasses and ceramics. In our own work,<sup>23</sup> we find that 123 superconductor fibers can be made simply by mixing isobutyrate  $[\text{Me}_2\text{CHCO}_2^-]$  complexes of the component metals (Y, Ba, Cu) in the appropriate stoichiometries in THF solvent. In solutions, it appears that the barium and copper complexes form mixed-metal oligomers of the type  $\text{Ba}_2\text{Cu}_2(\text{O}_2\text{CCHMe}_2)_8$  that provide sufficient rheology to spin fibers. These oligomers, when heated in the appropriate atmosphere to  $910^\circ\text{C}$  give intact, flexible, superconducting wires. Other researchers in the area have made numerous other metal oxide thin films<sup>24,25</sup> using this approach including  $\text{SnO}_x$  films.<sup>24a</sup>

These last two approaches to chemical processing of glass are just now becoming potentially useful methods and much more effort will be required to realize their full potential.

## 3. ACKNOWLEDGEMENTS

We would like to thank the Air Force Office of Scientific Research for support of this work through AFOSR contract Nos. F49620-88-C-0143 and F49620-88-C-0059. We would especially like to thank Drs. Clement Sanchez and Florence Babonneau of the Laboratoire de Matière Condensée at the Université de Pierre et Marie Curie (Paris VI) for very helpful discussions, reprints and preprints. We would also to thank Dr. Roger Assink of Sandia Laboratories for timely reprints.

#### 4. REFERENCES

1. a. Ultrastructure Processing of Ceramics, Glasses and Composites, L. L. Hench and D. R. Ulrich eds., Wiley, 1984. b. Science of Ceramic Chemical Processing, L. L. Hench and D. R. Ulrich eds., Wiley, 1986. c. Ultrastructure Processing of Advanced Ceramics, D. J. Mackenzie and D. R. Ulrich Eds, Wiley Interscience, 1988.
2. a. C. J. Brinker and G. W. Scherer, Sol-Gel Science, Academic Press, New York, 1990. b. Sol-Gel Technology for Thin Films, Fibers, Preforms, Electronics and Specialty Shapes, L. C. Klein, Noyes Publ., Park Ridge, N. J., 1988. c. L. L. Hench, J. K. West, Chem. Rev. **90**, 33, 1990.
3. a. Better Ceramics Through Chemistry, C. J. Brinker, D. E. Clark and D. R. Ulrich Eds. Elsevier, 1984. b. Better Ceramics Through Chemistry II, Mat. Res. Symp. Proc. Vol. **73**, C. J. Brinker, D. E. Clark and D. R. Ulrich Eds., Mat. Res. Soc., Pittsburgh, 1986. c. Better Ceramics Through Chemistry III, Mat. Res. Symp. Proc. Vol. **121**, C. J. Brinker, D. E. Clark, and D. R. Ulrich Eds. Mat. Res. Soc., Pittsburgh, 1988. d. Better Ceramics Through Chemistry IV, Mat. Res. Symp. Proc. Vol. **xx**, C. J. Brinker, D. E. Clark, and D. R. Ulrich Eds. Mat. Res. Soc., Pittsburgh in press, 1990.
4. Inorganic and Organometallic Polymers, Am. Chem. Soc. Symp. Ser. Vol. **360**, K. Wynne, M. Zeldin and H. Allcock Ed., 1988.
5. Transformation of Organometallics into Common and Exotic Materials: Design and Activation, NATO ASI Ser. E: Appl. Sci.-No. 141, R. M. Laine Ed.; Kluwer Publ., Amsterdam , 1988.
6. a. R. A. Assink and B. D. Kay, J. Non-cryst. Solids, Vol 99, pp 359-370, 1988. b. B. D. Kay and R. A. Assink, J. Non-cryst. Solids, Vol 104, pp 112-122, 1988. c. R. A. Assink and B. D. Kay, J. Non-cryst. Solids, Vol 99, pp 359-370, 1988.
7. Proceedings of the 4th International Conference on Ultrastructure Processing of Ceramics, Glasses and Composites, D. Uhlmann and D. R. Ulrich eds., in press, 1990.
8. D. C. Bradley, R. C. Mehrotra, and D. P. Gaur, Metal Alkoxides, Academic Press, London, 1978.
9. J. Livage, M. Henry and C. Sanchez, Prog. Sol. State Chem. Vol 4, p 1, 1989.
10. H. Dislich in Transformation of Organometallics into Common and Exotic Materials: Design and Activation, NATO ASI Ser. E: Appl. Sci.-No. 141, R. M. Laine Ed.; Kluwer Publ., Amsterdam page 236, 1988. b. H. Dislich, J. Non-Cryst. Solids vol 57, p 371, 1983.
11. C. Sanchez, F. Babonneau, S. Doeuff and A. Leautic, Ultrastructure Proc. of Advanced Ceramics, J. D. Mackenzie and D. R. Ulrich eds, Wiley, New York, 1988, p 77.
12. a. F. Babonneau, S. DOeuff, A. Leautic, and M Verdaguer, Inorg. Chem., vol 27, p 316, 1988 b. E. P. Giannelis and K. Berglund, Ultrastructure Proc. of Advanced Ceramics, J. D. Mackenzie and D. R. Ulrich eds., Wiley, New York, 1988, p 691. c. K. Berglund, C. L. Przybocki and E. P. Giannelis, Ultrastructure Proc. of Advanced Ceramics, J. D. Mackenzie and D. R. Ulrich eds.,

Wiley, New York, 1988, p 807.

13. J. C. Pouxviel, J. P. Boilot, J. C. Beloeil, J. Y. Lallemand, J. Non-cryst. Solids, vol 89, p 345, 1987.
14. a. A. Boudin, G. Cerveau, C. Chuit, R. J. P. Corriu and C. Reye, Angew. Chem. Int. Ed. vol 25, pp. 474-476, 1986. b. R. J. P. Corriu, R. Perz, and C. Reye, Tetrahed., vol 39, p. 999, 1983.
15. A. Boudin, G. Cerveau, C. Chuit, R. J. P. Corriu and C. Reye, Bull. Chem. Soc. Jpn. vol 61, p 101, 1988.
16. A. Boudin, G. Cerveau, C. Chuit, R. J. P. Corriu and C. Reye, Organometallics, vol 7, pp 1165-1171, 1988.
17. a. T. W. Zerda and G. Hwang, J. Non-Cryst. Solids, in press. b. High Pressure Chemistry, H. Kelm ed, Reidel, Dordrecht (1978).
18. a. H. Schmidt, H. Scholze and A. Kaiser, J. Non-Cryst. Solids, vol 63, p 1, 1984. b. H. Schmidt, B. Seiferling, G. Philipp and K. Deichmann, Ultrastructure Proc. of Advanced Ceramics, J. D. Mackenzie and D. R. Ulrich eds., Wiley, New York, 1988, p 651.
19. P. M. Smit, A. Van Zyl and A. I. Kingon, Mat. Chem. and Phys. vol 17, p 507, 1987.
20. E. A. Barringer, PhD Thesis, Dept. of Materials Science and Eng., MIT, 1983.
21. C. Sanchez, P. Toledano and F. Ribot preprint.
22. a. R. M. Laine, K. A. Youngdahl, P. Nardi, pat pend. b. T. Robinson, R. M. Laine and P. Nardi unpublished results.
23. a. M. L. Hoppe, K. A. Youngdahl, P. A. Kennish and Richard M. Laine. Fourth Internat. Conf. on Ultrastructure Proc. of Glasses, Ceramics, Composites and Polymers, Symp. Proc. in Press. b. R. M. Laine, K. A. Youngdahl, R. A. Kennish, M. L. Hoppe, Z.-F. Zhang and D. J. Ray, in Better Ceramics Through Chemistry IV, Mat. Res. Symp. Proc. Vol. x, C. J. Brinker, D. E. Clark, and D. R. Ulrich Eds. px, 1990.
24. a. J. V. Mantese, A. L. Micheli, A. H. Hamdi, and R. W. Vest, MRS Bulletin, vol 14, p 48, 1989. b. R. W. Vest and J. Xu, IEEE Trans. UFFC (1988) 35, 711. c. J. J. Xu, A. S. Shaik, and R. W. Vest, Thin Solid Films, vol 161, p 273, 1988. d. J. J. Xu, A. S. Shaik, and R. W. Vest, IEEE Trans. UFFC, vol 36, p 307 1989.
25. M. Klee, G. M. Stollman, S. Stotz and J. W. C. de Vries, Sol. St. Comm., vol 67, p. 613, 1988.



Theory and application of spectroscopically active glasses  
prepared by the sol-gel method

Renata Reisfeld\*

Department of Inorganic and Analytical Chemistry  
The Hebrew University of Jerusalem  
Jerusalem 91904 Israel

# ABSTRACT

The sol-gel technique allows preparation of pure inorganic glasses or composite glasses of inorganic and organic nature at low temperature. Incorporation of organic molecules with desired spectral characteristics is the subject of our research. Specific cases include preparation of stable tunable lasers in the visible based on photostable dyes; glasses doped with dyes characterized by double-proton transfer with good separation between absorption and emission; new materials having nonlinear properties; and glasses with dyes sensitive to ambient acidity and basicity. Four types of these glasses are discussed.

## 1. INTRODUCTION

The sol-gel process provides a new approach to the preparation of glasses at low temperature. This technique enables for the first time the introduction into glass of organic molecules having characteristic spectral features. Because of the increased photostability of a dye in an inorganic system due to the fact that the breaking energy of the bonds between the atoms and molecules constituting the glasses is higher than in solution or in polymers a variety of new materials can be designed and prepared. Some systems which were prepared in recent years are discussed in references 1 and 2.

In the present paper recent progress in the new materials prepared in our group is described. These include: materials for photostable solid state tunable lasers in the visible; glasses having well-separated absorption and emission spectra which may be considered for luminescent solar concentrators; glasses which have properties which change reversibly with illumination having nonlinear optical properties; sensors for environmental impurities.

## 2. SOLID-STATE TUNABLE LASERS IN THE VISIBLE

Stable tunable solid-state lasers existing today are based on transition metals<sup>3</sup>, such as Cr(III) and Ti(III) ions which emit in the infrared part of the spectrum. Because of the importance of solid-state tunable lasers in the visible a considerable effort has been extended towards the search for tunable lasers made of solid inorganic materials operating in the visible part of the spectrum<sup>4-9</sup>. The sol-gel enables single or multiple component glasses to be prepared at temperatures low enough in order not to destroy the organic molecules<sup>10</sup>. The process involves hydrolysis and polycondensation of alkoxides, see Fig.1. During the glass preparation an organic molecule<sup>10-12</sup> is added to the solution and homogeneously incorporated in the final glass<sup>10-12</sup>. The resulting photostability of the dye is enhanced in the inorganic host matrix and surpasses that of organic media such as

\*Enrique Berman Professor of Solar Energy

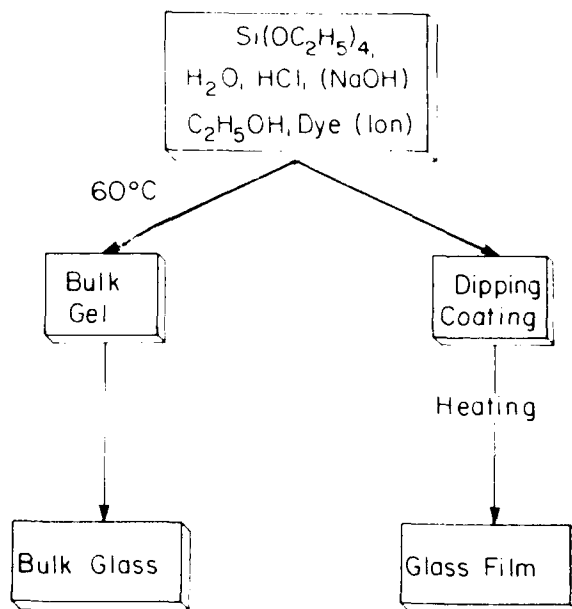
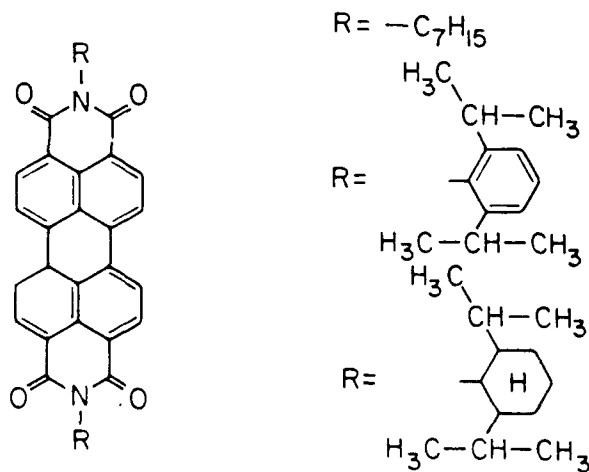


Figure 1. Scheme of preparation of sol-gel bulks and films

polymethylmethacrylate. However, despite this increased photostability lasers prepared by the sol-gel method from conventional laser dyes can survive only a few pulses of exciting laser sources before degradation<sup>4-9</sup>.

Recently perylimide dyes were developed by Seybold and Wagenblast<sup>13</sup> with the following structure:



They are characterized by their extreme photostability and negligible singlet-triplet transfer which is responsible for nonradiative relaxations. The absence of a long-lived triplet state providing enough time for photochemistry to take place allows the existence of stable dyes with high quantum efficiency of fluorescence. Optical characteristics of several perylene dyes are presented in Table I.

Table I. Optical characteristics of perylene dyes.

Dye	$\lambda_{\text{abs}}$ max nm	$\lambda_{\text{em}}$ max nm	extinc. coeff.	quantum effic. %
yellow	474	508	48 000	91
orange	525	540	85 000	100
red	578	613	44 000	96
blue	610	685	63 000	92

The perylene dyes have limited solubility in conventional solvents from which the sol-gel glasses are prepared because of the planar structure of the molecules which facilitates the formation of crystals with high lattice energies. Fortunately perylene dyes can be introduced into composite glasses which are composed of mostly inorganic matrix with an addition of organic polymer<sup>11</sup>. We were able to introduce a variety of perylene dyes into the composite glasses either in bulk glasses<sup>12,14</sup> or into thin films<sup>15</sup>. An example of the bulk glasses doped by the perylene dye BASF-241 is presented in Fig.2 which gives the excitation and emission spectra of the dye in a composite glass. The laser action of this dye was tested by frequency doubled Nd:YAG. The measured threshold was less than 6 $\mu$ J and the slope efficiency was around 8%. This efficiency can be increased by improving the optics of the laser cavity. The laser could also be excited by a copper laser source. There was no change in the laser operation after several thousand excitation pulses. Laser action was also observed in the films prepared by the sol-gel method with dopants BASF-241 and R-300, the absorption and emission spectra of which is given in Fig.3<sup>16</sup>. A different dye based on naphthylimide derivative was recently prepared by Dr. Seybold of BASF Farbenlaboratorium, Ludwigshafen. The absorption and emission spectra of this dye in a sol-gel glass film is presented in Fig.4. The quantum efficiency of this dye is 94%.

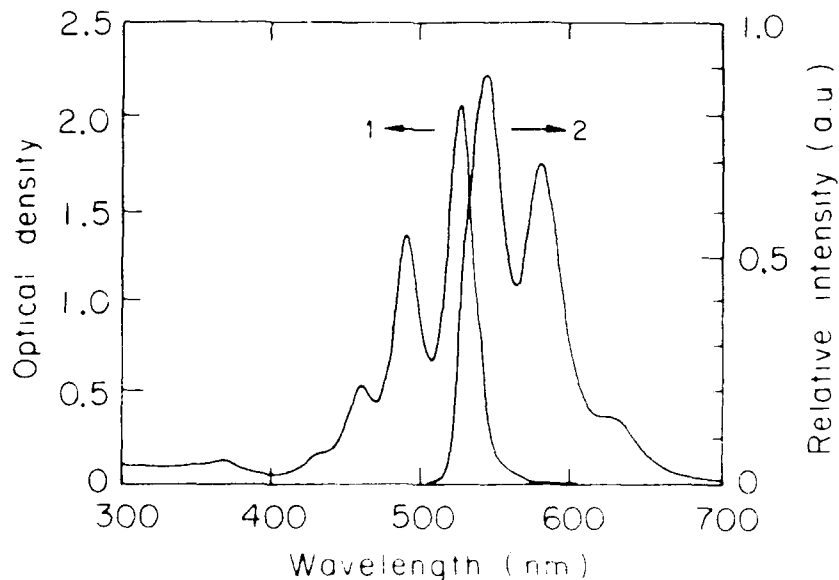


Figure 2. Absorption and emission spectra of perylene dye BASF-241 in a composite material

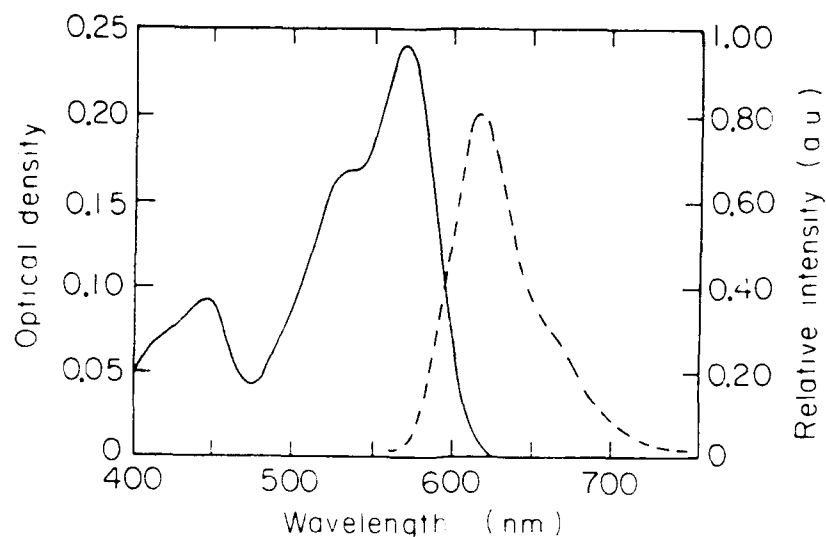


Figure 3. Absorption and emission spectra of R-300 in composite glass-PMMA film

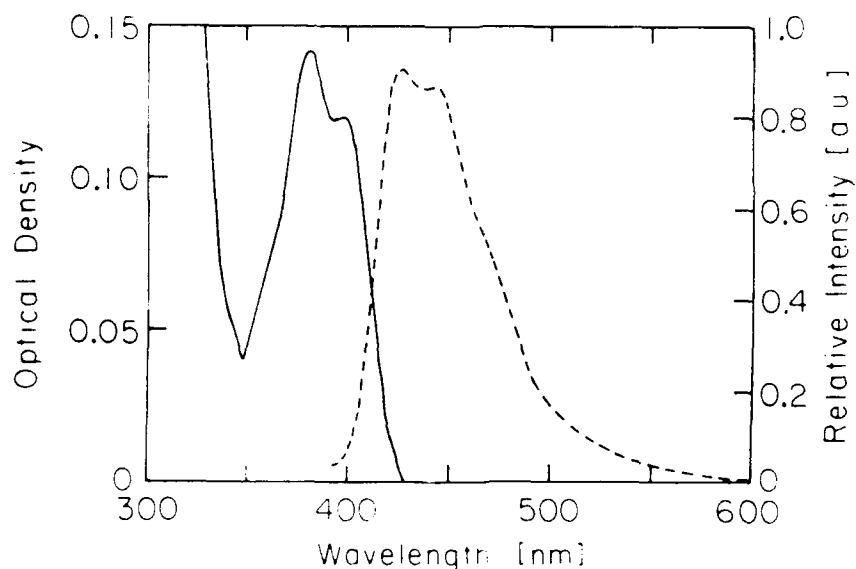


Figure 4. Absorption and emission spectra of the dye KF-42 in sol-gel film

Film lasers may have some advantage over bulk lasers in the future because of the good thermal dissipation and waveguide properties of the films. If the refractive index of the film is higher than that of the glass support the laser radiation is trapped and guided by a total internal reflection in the thin film.

As mentioned above the class of the perylimide dyes are only very slightly soluble in polar organic solvents but dissolve well in apolar solvents such as chloroform. Introduction of a bulky tetrabutyl group into the perylimide ring<sup>17</sup> makes the dye soluble also in a number of polar solvents while retaining a high quantum efficiency of fluorescence. We have recently prepared glasses based on acid hydrolysis of TEOS doped by this dye<sup>18</sup>, the absorption and emission spectra of which

is presented in Fig.5. Laser action was detected on excitation with the green line of a copper laser.

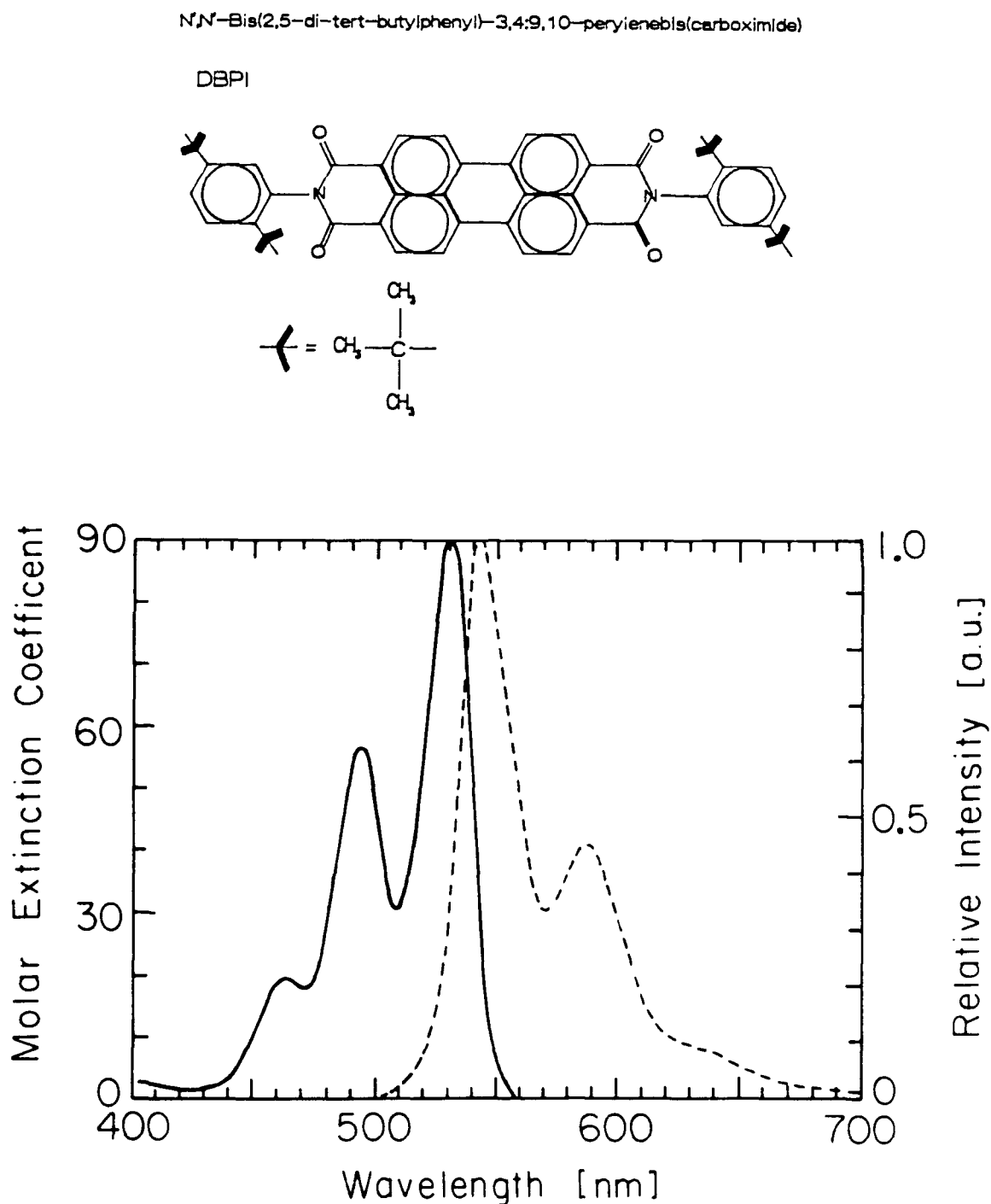
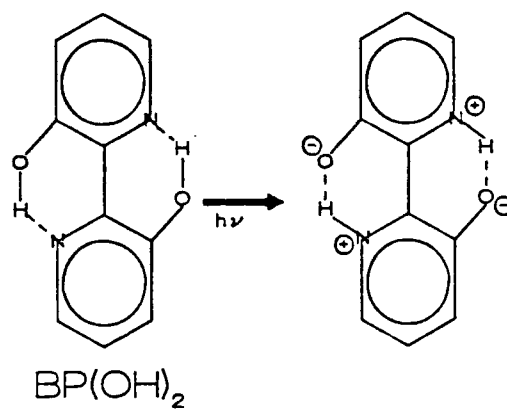


Figure 5. Absorption and emission spectra of DBPI  
(N',N'-Bis(2,5-di-tert-butylphenyl)-3,4:9,10-perylene-bis(carboximide))  
in a bulk glass prepared by hydrolysis and polycondensation of TEOS  
catalyzed by HCl



### 3.OPTICAL PROPERTIES OF [2,2'-BIPYRIDYL]-3,3'-DIOL IN SOL-GEL GLASSES

The absorption and emission spectra of [2,2'-bipyridyl]-3,3'-diol ( $\text{BP(OH)}_2$ ) in solution were studied by the Grabowski group<sup>19-21</sup>. This molecule undergoes an excited state proton transfer reaction as seen from the formula



resulting in a very strong Stokes shift. It has also been recommended as an interesting laser material. We introduced<sup>22</sup> this molecule (prepared by L. Kaczmarek in Warsaw) into glass prepared by hydrolysis of tetraethoxysilane (TEOS) and into glass bulks prepared (a) from Glymo<sup>23</sup> (glycidyloxypropyltrimethoxysilane) with a small addition of tetramethoxysilane (TMOS) and (b) by hydrolysis of PST (3-(trimethoxy-silyl)propylmethacrylate) with a small addition of TMOS. The latter glasses (a) and (b) in their final form are a composite material mainly composed of an inorganic  $\text{SiO}_2$  lattice with a residual organic backbone. The molecule was also

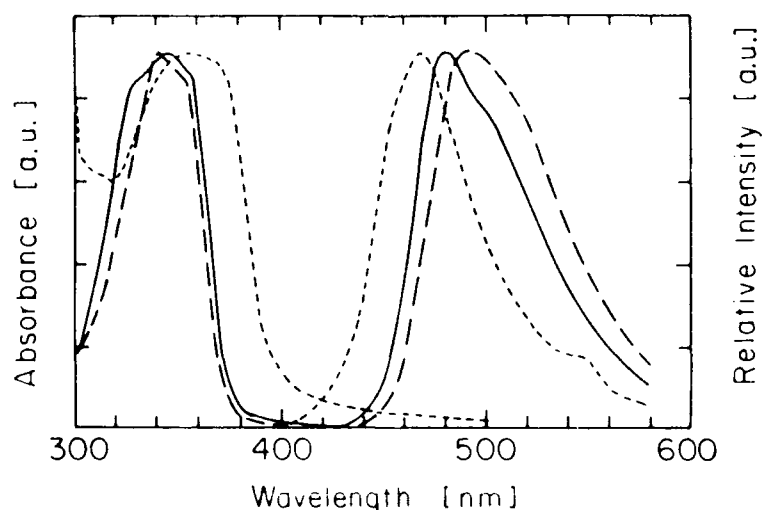


Figure 6. Absorbance and emission spectra of  $\text{BP(OH)}_2$   
 ..... in sol-gel glass film  
 ——— in ethanol  
 - - - in PMMA

Table II. Quantum yields, lifetimes and peak positions of BP(OH)<sub>2</sub> in various media.

Material	concentration [M/L]	absorption $\lambda_{nm}$	emission $\lambda_{nm}$	lifetimes nsec		quantum yield
				calculated	measured	
chloroform	$5 \times 10^{-6}$	341	485	7.95	3.3	$0.40 \pm 0.05$
ethanol	$6.5 \times 10^{-6}$	342	480	4.9	2.2	$0.45 \pm 0.05$
water	$7 \times 10^{-7}$	365	445	5.6	1.0	$0.15 \pm 0.05$
PMMA*	$2 \times 10^{-5}$	342	490	5.2	2.4	$0.45 \pm 0.05$
thin glass film	$2 \times 10^{-4}$	350	470	5.0	0.7	$0.15 \pm 0.05$
PST glass**	$1.2 \times 10^{-4}$	345	485	8.0	4.2	$0.50 \pm 0.05$
Glymo glass***	$1.5 \times 10^{-4}$	345	480	7.9	4.0	$0.50 \pm 0.05$

\* polymethylmethacrylate

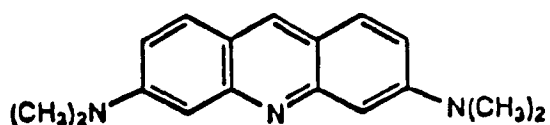
\*\* 3-(trimethoxysilyl)propylmethacrylate

\*\*\* glycidylxypropyltrimethoxysilane

introduced into PMMA (polymethylmethacrylate). An example of absorption and emission spectra of the molecule in a thin glass film, in ethanol solution and in PMMA is presented in Fig.6. The spectra of the molecule in bulk glasses resemble those of PMMA. The absorption and emission maxima together with the radiative lifetimes and measured lifetimes and quantum efficiencies of luminescence obtained from the ratio of the measured and calculated lifetimes are presented in Table II. The high quantum efficiencies of the molecule in PST and Glymo glass and a large Stokes shift which circumvents the self-absorption of the emitted radiation make these new materials promising for lasers in the 480-530 nm range provided that their photostability will be sufficiently high.

#### 4. NONLINEAR MATERIALS BASED ON SOL-GEL TECHNOLOGY

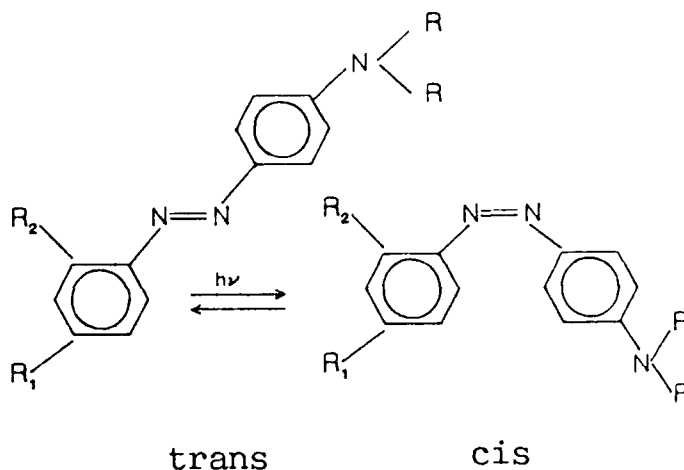
Organic materials in polymers for nonlinear optics have been of great interest in recent years<sup>24,25</sup>. The second order nonlinearity connected with the second order susceptibility  $\chi^2$  can be utilized in the generation of second order harmonics, e.g. creating the green light from the Nd laser. Degenerate four-wave mixing, on the other hand, is based on the third order nonlinearity connected to  $\chi^3$  of the electric susceptibility tensor. Some of the non-inorganic molecules such as fluorescein and its derivatives when introduced into sol-gel glasses show very low saturation values arising from efficient singlet to triplet transfer and were discussed in references 1 and 2. During the last year we have studied extensively the nonlinear behaviour of acridine orange and methyl orange and methyl red in composite glasses.



Acridine Orange

[3,6 - bis(dimethyl amino Acridine)]

cis and trans forms of methyl orange and methyl red



For methyl orange  $R = \text{CH}_3$      $R_1 = \text{NaO}_3\text{S}$      $R_2 = \text{H}$   
 For methyl red     $R = \text{CH}_3$      $R_1 = \text{H}$      $R_2 = \text{COOH}$

The reason for preparation of these materials is their high photostability, absence of pores preventing diffusion of oxygen responsible for the triplet quenching of the molecules. The composite glasses were prepared as follows: TEOS in ethanol with traces of HF as catalyst were used as starting materials for preparation of the gel which was heated to 600°C at a rate of 100°C/hour. The bulk glasses so obtained were then cooled and impregnated by immersing them in a preheated to 35°C mixture of MMA (methylmethacrylate) doped by appropriate concentration of the organic molecule and addition of 2% benzoyl peroxide to assist the polymerization of the MMA in the pores of the glass. After standing for five days in sealed containers the composite glasses were rinsed from the remaining polymer and polished to optical quality. The glasses were stable chemically and mechanically. The saturable absorption in the acridine dyes results from the efficient depopulation of the ground singlet state to the metastable triplet state<sup>26</sup> while in methyl orange the nonlinear properties arise from transformation of the coloured trans-form to the less coloured cis-form (see diagram).

The nonlinear optical properties of the materials were measured by means of nanosecond pump- and probe beam spectroscopy and by the technique of cw laser-induced gratings (LIG)<sup>27</sup>. The laser-induced dynamical gratings in the doped glasses were formed by crossing two coherent chopped beams of equal intensity of a cw argon laser emitting at 514.5 nm in the sample. From the dependence of the intensity of the diffracted beams on the intensity of the incident beams we could estimate the efficiency of the diffracted gratings which is 6.6% for acridine orange and 1.0% for methyl orange. The latter efficiency can be substantially increased by decreasing the angle between the two incident beams. The functional dependence of the diffracted intensity allows also to determine independently the mechanism responsible for the nonlinearity. In acridine the nonlinearity arises from the saturable absorption of the molecules which in methyl red and methyl orange is due to the changes in refractive index possibly due to thermal effects. The existence of the dynamical refraction gratings is connected to optical phase conjugation, a

process that can lead to the correction of a wavefront distortion under conditions in which a beam of light passes twice in opposite directions through an aberrating optical medium. There is a hope that the optical material described above will be used with low intensity light sources for application in phase conjugation and image processing.

## 5. SENSORS FOR ENVIRONMENTAL IMPURITIES

Dyes which can change their colour depending on the environment or with conditions of the preparation when introduced into sol-gel glasses can serve as sensors for detection of environmental and biomedical traces. An example of such a dye is oxazine-170 which can exist in neutral, mono-cation, di-cation and tri-cation forms depending on the environment<sup>28,29</sup>.

Oxazine-170 was introduced into glasses prepared by the sol-gel method using tetramethoxysilane. The absorption and emission of the dye were studied as a function of preparation conditions of the glasses. Extinction coefficients and quantum efficiencies of the cationic form of the dyes revealed much higher values than the molecular form<sup>30</sup>. Several geometries were prepared: bulk glass, glass tubes coated on the inside and glass tubes coated on the outside. It was shown that the colour of the oxazine incorporated into the glasses changes reversibly when exposed to atmospheric ammonia or acid<sup>31</sup>. Waveguides based on this material may serve as optical sensors for ammonia or acid. Comparable results were also obtained when oxazine-170 was incorporated into films of PMMA, however this latter material was less photostable. The response time of colour change depends on the thickness of the films and the velocity of diffusion of ammonia or protons.

## 6. ACKNOWLEDGMENTS

This work was partially supported by the Israel Ministry of Science and Technology and the European Community and the Krupp Foundation.

I am grateful to Professor Christian Jørgensen of Geneva for our continuous and pleasant cooperation on the spectroscopy of sol-gel glasses, to Professor John Mackenzie of UCLA for his generous help in enlightening me in the theory of the sol-gel glass process, to Professor Claus Klingshirn of Kaiserslautern for his contribution to my knowledge in nonlinear optics and to Dr. Gunther Seybold of BASF for providing me continuously with his excellent photostable dyes for production of the lasers. I am indebted to my colleagues and students Dr. Marek Eyal, Dr. Valery Chernyak, David Brusilovsky, Carsten Burgdorff and Raz Gvishi for providing me with many of the experimental data discussed here and to Mrs. Esther Greenberg for her invaluable assistance in preparation of the manuscript.

## 7. REFERENCES

1. R. Reisfeld, "Optical behaviour of molecules in glasses prepared by the sol-gel method". Proc. Winter School on Glasses and Ceramics from Gels, SOL-GEL Science and Technology, Brazil, August 1989, eds. M.A. Aegerter, M. Jafellicci Jr., D.F. Souza and E.D. Zanotto, (World Scientific, Singapore, New Jersey, London, Hong Kong) 323-345 (1989).
2. R. Reisfeld, Spectroscopy and applications of molecules in glasses. J. Non-Cryst. Solids, (1990).
3. R. Reisfeld and C.K. Jørgensen, "Excited states of chromium(III) in

translucent glass-ceramics as prospective laser materials". *Structure and Bonding*, 69, 63-96 (1988).

4. R. Reisfeld, "Criteria and prospects of new lasers based on fluorescent dyes in glasses". *J. Physique, Colloque*, 48, C7 (12) 423-426 (1987).

5. G.B. Altshuler, V.A. Bakhanov, E.G. Dulneva, A.V. Erofeev, O.V. Mazurin, G.F.P. Roskova and T.S. Tsekhomskaya, "Laser based on dye-activated silica gel". *Opt. Spectrosc.*, (8) 62, 707-710 (1988).

6. Y. Kobayashi, Y. Kurokawa, Y. Imai and S. Muto, "A transparent alumina film doped with laser dye and its emission properties". *J. Non-Cryst. Solids*, 105, 198-200 (1988).

7. F. Salin, G. Le Saux, P. Georges, A. Brun, C. Bagnall and J. Zarzycki, "Efficient tunable solid-state laser near 630nm using sulforhodamine 640-doped silica gel". *Optics Letters*, 14, 785-787 (1989).

8. B. Dunn, E. Knobbe, J. McKiernan, J.C. Pouxviel and J.I. Zink, "The optical behavior of organic and organometallic molecules in sol-gel matrices". *Mat. Res. Soc. Symp.* 121, 331 (1989).

9. E.T. Knobbe, B. Dunn, P. Fuqua, F. Nishida and J.I. Zink, "Laser Behaviour and Nonlinear Optical Properties in Organic Dye Doped Sol-Gel Materials", in *Ultrastructure Processing of Ceramics*, ed. D.R. Uhlmann, et al., (Wiley, New York) in press.

10. D. Avnir, D. Levy and R. Reisfeld, "The nature of silica glass cage as reflected by spectral changes and enhanced photostability of trapped rhodamine 6G". *J. Phys. Chem.*, 88, 5956-5959 (1984).

11. E.J.A. Pope and J.D. Mackenzie, "Incorporation of organic dyes in polymer/oxide composites". *MRS Bulletin*, 12, 29-31 (1987).

12. R. Reisfeld, D. Brusilovsky, M. Eyal, E. Miron, Z. Burshtein and J. Ivri, "A new solid-state tunable laser in the visible". *Chem. Phys. Lett.* 160, (1) 43-44 (1989).

13. G. Seybold and G. Wagenblast, "New perylene and violanthrone dyestuffs for fluorescent collectors", *Dyes and Pigments*, 11, 303-317 (1989).

14. R. Reisfeld, D. Brusilovsky, M. Eyal, E. Miron, Z. Burshtein and J. Ivri, "Perylene dye in a composite sol-gel glass: a new solid state tunable laser in the visible range". *Proc. Binational French-Israeli Workshop on Solid State Lasers*, SPIE Proceedings 1182, 230-239 (1989).

15. R. Reisfeld and V. Chernyak, "New solid-state laser configuration based on thin dye-doped glass films". in preparation.

16. R. Reisfeld and G. Seybold, "Stable solid-state tunable lasers in the visible". Lecture to be presented at the International Conference on Luminescence, Lisbon, Portugal, 16-20 July, 1990.

17. H. Langhals, S. Denning and H. Huber, "Rotational barriers in perylene fluorescent dyes". *Spectrochimica Acta*, 44A, (11) 1189-1193 (1988).

18. C. Burgdorff, R. Reisfeld and H.-G. Lohmannsroben, "Spectroscopy and laser characteristics of N',N'-bis(2,5-di-tert-butylphenyl)-3,4:9,10-perylenebis (carboximide) DBPI in sol-gel glasses". in preparation.

19. H. Bulska, A. Grabowska and Z.R. Grabowski, "Single and double proton transfer in excited hydroxy derivatives of bipyridyl". *J. Luminescence*, 35, 189-197 (1986).

20. J. Sepiol, H. Bulska and A. Grabowska, "The dihydroxy derivative of 2,2'-bipyridyl as a new proton-transfer lasing dye". *Chem. Phys. Lett.*, 140, (6) 607-610 (1987).

21. J. Sepiol, A. Grabowska, H. Bulska, A. Mordzinski, F. Perez Salgado and R.P.H. Rettschnick, "The role of the triplet state in depopulation of the electronically excited proton-transferring system [2,2'-bipyridyl]-3,3'-diol". *Chem. Phys. Lett.*, 163, (3,4) 443-448 (1989).

22. M. Eyal, R. Reisfeld and A. Grabowska, "Absorption, emission and lifetime measurements of [2,2'-bipyridyl]-3,3'-diol in sol-gel glasses and PMMA". To be submitted to Chem. Phys. Lett.
23. H. Schmidt, B. Seiferling, G. Philipp and K. Deichmann, "Development of organic-inorganic hard coatings by the sol-gel process", in Ultrastructure Processing of Advanced Ceramics, eds. J.D. Mackenzie and D.R. Ulrich, (Wiley, New York) 651-660 (1988).
24. D.R. Ulrich, "Overview: Non-linear optical organics and devices", in Organic Materials for Non-Linear Optics, Proc. Conf. Applied Solid State Chemistry Group of the Dalton Division of the Royal Society of Chemistry, June 29-30, 1988, eds. R.A. Hann and D. Bloor, (Royal Soc. Chem.) 241-263 (1988).
25. J. Zyss and G. Tsoucaris, "Chemistry, symmetry and optics", in Structure and Optics of Molecular Crystals, ed. M. Pierrot, in Studies in Physical and Theoretical Chemistry, (Elsevier) (1990).
26. S. Graham, R. Renner, C. Klingshirn, W. Schrepp, R. Reisfeld, D. Brusilovsky and M. Eyal, "Pump- and probe beam measurements in organic materials". Paper presented at Int. Conf. Materials for Non-linear and Electro-optics, Cambridge, 1989. Inst. Phys. Conf. Ser. No 103; Section 2.2 157-162 (1989).
27. S. Graham, M. Eyal, M. Thoma, D. Brusilovsky, R. Reisfeld and C. Klingshirn, "Nonlinear optics and laser induced gratings in glasses doped with acridine orange and methyl orange". Lecture to be presented at the International Conference on Luminescence, Lisbon, Portugal, 16-20 July, 1990.
28. R. Gvishi and R. Reisfeld, "An investigation of the equilibrium between various forms of oxazine-170 by means of absorption and fluorescence spectroscopy". Chem. Phys. Lett., 156, (2,3) 181-186 (1989).
29. R. Gvishi, R. Reisfeld and M. Eisen, "Structures, spectra and ground and excited states equilibria of polycations of oxazine-170". Chem. Phys. Lett. 161, (4,5) 455-460 (1989).
30. R. Gvishi and R. Reisfeld, "Spectroscopy of laser dye oxazine-170 in sol-gel glasses". To be published in J. Non-Cryst. Solids.
31. V. Chernyak, R. Reisfeld, R. Gvishi and D. Venezky, "Oxazine-170 in sol-gel glass and PMMA films as a reversible optical waveguide sensor for ammonia and acids". Sensors and Materials, 2, (2) (1990).

**OPTICAL PROPERTIES OF TRANSITION METAL OXIDE GELS**

Clément Sanchez

Laboratoire de Chimie de la Matière Condensée URA 302

Université Pierre et Marie Curie

4 place Jussieu 75252 Paris France

**ABSTRACT**

Transition metal oxide (T.M.O) gels exhibit extrinsic or specific optical properties. This duality is related to the fact that they can be used as transparent amorphous matrices from which high refractive index is expected, or for their mixed valence behaviour. Titanium or Zirconium oxide based gels have been used as transparent matrices in which large concentration of inorganic (Eu (III)) or organic luminophores (Rhodamine 6G , Rhodamine 640, Coumarine 4) have been incorporated. Several specific optical properties related to Titanium oxide based gels such as electrochromism , photoelectrochemistry and photochemistry are also described.

**1.INTRODUCTION**

The sol-gel process opens a land of opportunity for the synthesis of optical materials<sup>1</sup>. Sol-gel chemistry is mainly based on inorganic polymerization reactions. Starting from molecular precursors, a macromolecular oxide network is obtained via hydroxylation-condensation reactions <sup>2,3</sup> which can be controlled by the chemical design of molecular precursors. Transparent transition metal oxide sols and gels can then be synthesized<sup>4</sup>. Rheological properties of sols can be adjust allowing easy deposition of transparent coatings onto glass, ceramic or polymeric substrates <sup>5</sup>. Sol-gel chemistry is performed in solution at lower temperatures than conventionnal chemical methods. Homogeneous doping by mixing components at a molecular level, synthesis of metastable or amorphous phases allowing larger concentrations of chromophores and synthesis of mixed organic-inorganic materials can then be performed.

Silica <sup>6,7,8,9,10</sup> or alumina-silica<sup>11,12</sup> gels have been studied extensively. Less work was devoted to transition metal oxide (T.M.O) based gels (TiO<sub>2</sub>, ZrO<sub>2</sub>...). When compared to silica based compounds T.M.O gels offer similar advantages ; moreover they exhibit a large variety of optical properties arising from the specific electronic structure of transition metal ions. Oxide coatings based on TiO<sub>2</sub> exhibit higher refractive index and have already been used in the glass industry<sup>5</sup>. Electronic d-d transitions can be excited in the visible range giving rise to colored transition metal oxide gels.

**92 4 28 021****92-11403**

When transition metal ions exhibit several valence states, mixed valence compounds are obtained. Then a strong absorption in the visible range due to optically activated electron hopping between metal ions in different valence states is usually observed.

Transition metal oxide gels can be used as electrochromic materials via reversible optical switching performed through electrochemical redox reactions<sup>13,14,15</sup>. Thermally activated electron hopping leads to semiconducting properties<sup>16</sup>. When T.M.O coatings are dipped into a solution, a semiconductor-electrolyte junction occurs allowing a charge separation process: photoelectrochemical devices are based on this phenomenon<sup>17</sup>.

The chemical synthesis of gels is performed in organic solutions around room temperature. Organic molecules or dyes can therefore be easily incorporated into an oxide gel matrix. These mixed organic-inorganic compounds provide new opportunities as optical coatings for applications such as lasers, non linear optics or luminescent materials.

This paper presents some examples of extrinsic or intrinsic optical properties of transition metal oxide based gels.

## 2. RESULTS AND DISCUSSION

### 2.1 Homogeneous doping and stabilisation of metastable phases

Photo-assisted electrolysis of water at the surface of titanium dioxide was first reported by Fujishima and Honda<sup>18</sup>. Most papers published in the literature concern TiO<sub>2</sub> rutile which is the thermodynamically stable phase of titanium dioxide. However the flat band potential of TiO<sub>2</sub> rutile being close to 0 Volts (vs H<sup>+</sup>/H<sub>2</sub>) by positive values so that photoreduction of water cannot be performed at the surface of TiO<sub>2</sub> rutile electrodes without the application of an external voltage. Moreover the band gap of TiO<sub>2</sub> is rather large (3.2 eV for anatase and 3.05 for rutile) and does not fit the solar energy spectrum<sup>19</sup>. Thus the yield for solar conversion of these oxides is quite low (1%). An extension of the spectral response of TiO<sub>2</sub> towards the visible part of the spectrum can be performed by doping with Cr<sup>3+</sup>, while Al<sup>3+</sup> doping can favor kinetics of the minority carriers. Cr<sup>3+</sup>-Al<sup>3+</sup>-doped TiO<sub>2</sub> anatase electrodes can be synthesized via the sol-gel process<sup>17</sup>. When a solution of Ti(OBu<sup>n</sup>)<sub>4</sub>, Al(OBu<sup>s</sup>)<sub>3</sub> and Cr(acac)<sub>3</sub> (98% Ti, 1% Al, 1% Cr) was spin coated onto a titanium foil, an amorphous film was obtained<sup>17</sup>. The amorphous TiO<sub>2</sub> film is heat treated at 500°C under air or an hydrogen-argon gas mixture leading respectively to a stoichiometric or non stoichiometric film of TiO<sub>2</sub> anatase as evidenced by x-ray diffraction<sup>17</sup>. Cyclic voltammetry experiments were carried out under chopped light for different TiO<sub>2</sub> films. These voltammograms recorded in the potential range -



1V to +0.5V (vs. SCE) exhibit the characteristics of n-type semiconductors photodiodes. The photocurrent increases as a positive bias is applied (Figure 1a).

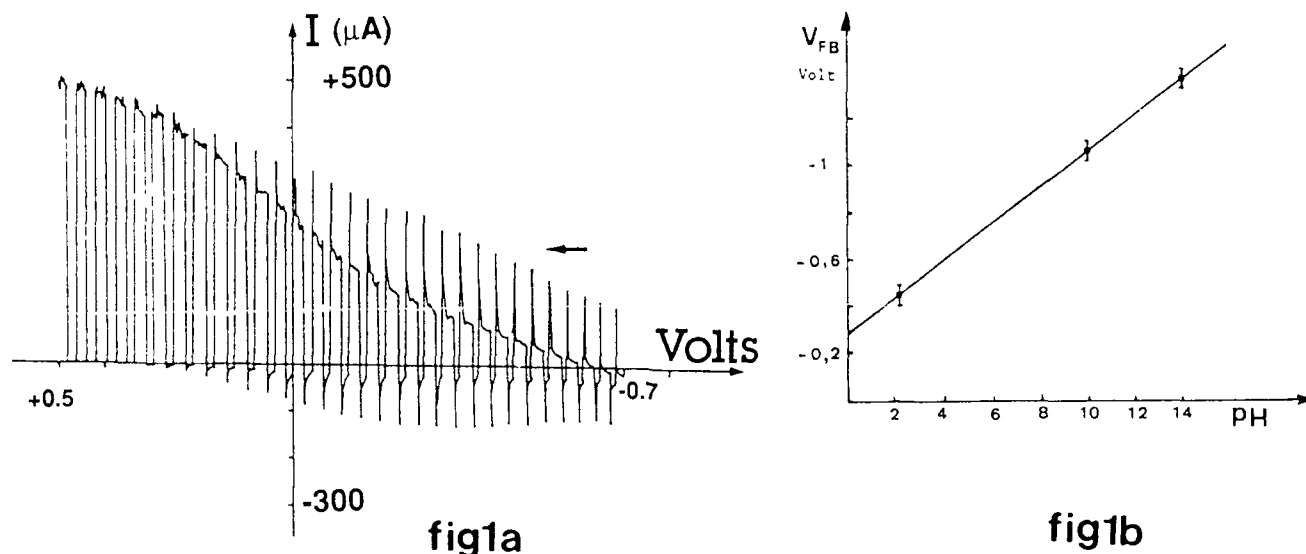


Fig 1a. Cyclic voltammogram of  $\text{Cr}^{3+}$ - $\text{Al}^{3+}$  doped  $\text{TiO}_2$  anatase film recorded under shopped light. Fig 1b. Evolution of the flat band potential  $V_{FB}$  versus pH for  $\text{Cr}^{3+}$ - $\text{Al}^{3+}$  doped  $\text{TiO}_2$  anatase film.

The value of the photocurrent depends on cristallinity and stoichiometry of the oxide film. It decreases from 5 mA/cm<sup>2</sup> for non stoichiometric  $\text{TiO}_2$  anatase down to 300  $\mu\text{A}/\text{cm}^2$  for stoichiometric  $\text{TiO}_2$  and finally to 50  $\mu\text{A}/\text{cm}^2$  for the amorphous  $\text{TiO}_2$  xerogel. The onset of photocurrent for non stoichiometric  $\text{TiO}_2$  anatase films was measured at different pH values ranging from 2 to 14. The flat band potential was determined at different pH values from the onset of the photocurrent following the method proposed by Butler<sup>20</sup>. The flat band potential varies linearly with pH. The slope of 65 mV pH<sup>-1</sup> suggests a nernstian behavior (Fig. 1b). Moreover the value of the flat band potential for  $\text{TiO}_2$  anatase films prepared via sol gel technique is negative with respect to the  $\text{H}^+/\text{H}_2$  potential.

This is not the case for  $\text{TiO}_2$  rutile electrodes prepared by conventional techniques. ac photocurrent measurements were also carried out in order to determine the quantum efficiency versus wavelength recorded at 0V (vs.SCE) for both (1% Cr-1% Al) doped and undoped  $\text{TiO}_2$  anatase films. The quantum efficiency of these films determined from ac photocurrent measurements was of about 50% (at 380 nm). A small extension of the photoresponse towards the visible range was observed for (1% Cr-1% Al) doped  $\text{TiO}_2$  anatase<sup>17</sup>. This example emphasises that metastable phases with better

photoelectrochemical properties can be synthesized via the sol-gel route. Homogeneous doping is also obtained by mixing three components at a molecular level.

## 2.2 Large concentration of luminescent probes can be reached in amorphous gel matrices

TiO<sub>2</sub> based gels have been synthesized following a procedure previously described through hydrolysis and polycondensation of Ti(OBu<sup>n</sup>)<sub>4</sub> in an n-butanol-acetic acid- water mixture<sup>21</sup>. The ratios acetic acid /Ti and water/ Ti are respectively 1.5 and 2.77. The luminescent probe Eu<sup>3+</sup> was introduced at different concentrations between 1% and 24% (atom %) as EuCl<sub>3</sub> dissolved in the hydrolysis solution ( 10% w/w water diluted in butanol )<sup>22</sup>.

Optical absorption spectra of Eu<sup>3+</sup> doped titanium oxide based gels are characterized by the presence of three main absorption bands located at 530nm, 465nm and 393.5nm. They correspond respectively to  $^7F_0 \rightarrow ^5D_1$ ,  $^7F_0 \rightarrow ^5D_2$  and  $^7F_0 \rightarrow ^5D_3$  transitions, the latter transition being the most intense. Its extinction coefficient decreases weakly for the largest Eu(III) concentration suggesting a limit of solubility for the luminophore in titanium oxide based gels smaller than 24%. A typical emission spectrum for Eu<sup>3+</sup> doped titanium oxide based gels is shown in figure 2.

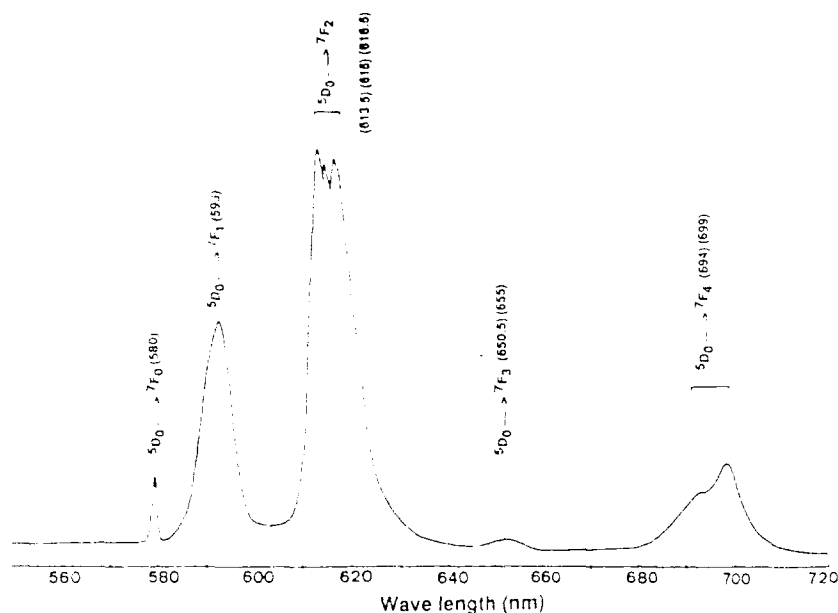


Figure 2 Emission spectra of Eu (III) in a titanium oxide based gel

All transitions are related to the emission of Eu(III) ion<sup>23,24</sup>. Attributions and energy positions of these transitions are reported in figure 2. The  $^5D_0 \rightarrow ^7F_2$  transition is sensitive to the chemical bond

between Eu(III) and its surrounding ligands<sup>23,24,25</sup>. The relative intensity RI between the two main emission transitions ( $^5D_0 \rightarrow ^7F_2$  /  $^5D_0 \rightarrow ^7F_1$ ) (RI = 3.3) is quite different from those reported for aqueous solutions (RI = 0.43)<sup>24</sup> but close to those of Eu<sup>3+</sup>-doped silica gel heat treated at 200°C (RI = 3.48)<sup>23</sup>. Following the arguments developed by R. Reisfeld et al.<sup>23</sup> for silica gels such emission spectra can be related to the fact that Eu(III) cations could be bonded to titanium oxide polymers via (Ti-O)-Eu bonds. Such a reaction occurs even if these gels are not dried and thus still contain a large amount of solvent molecules. This must be related to the higher reactivity of transition metal alkoxides. Interaction between the luminescent probe and the polymeric TiO<sub>2</sub> network is already observed at room temperature while it only occurs around 200°C in the case of silicon oxide gels. The intensity of emission increases with the concentration in Eu(III) except for the highest concentration (24%). This suggests that about 20% of Eu(III) can be introduced in this Eu<sup>3+</sup>-doped titanium oxide based gel without quenching the fluorescence<sup>22</sup>. It emphasizes the interest of amorphous matrices.

### 2.3 Organic molecules inside sol-gel matrices

The chemical synthesis of gels is performed in organic solutions around room temperature. Organic molecules or dyes can therefore be easily incorporated into an oxide gel matrix. Extensive work is being performed by B. Dunn et al.<sup>6,7,11</sup> and by R. Reisfeld et al.<sup>8,9,10,26</sup>. Luminescent dyes (Rhodamine 6G, Rhodamine 640, Coumarine 4) whose molecular structures are shown in figure 3 have been incorporated in titanium, zirconium and aluminium oxide based gels<sup>22,27</sup>.

Rhodamine are laser dyes which belong to the xanthene family. Their optical properties (absorption-luminescence) result from  $\pi-\pi^*$  transitions arising from delocalized  $\pi$  electrons<sup>28</sup>. They lead to strong absorption bands located at 531 nm for R6G and at 569 nm for R640 in water-alcohol solution<sup>26</sup>. A single absorption band is observed when such dyes are diluted ( $C < 10^{-5}$  M). When the dye concentration increases in a polar solvent rhodamine molecules tend to form dimers<sup>26,29</sup> giving rise to two extra absorption bands located for R6G-R6G at 499 nm and 526 nm. The first one is quite strong and is the dominant component of the absorption spectrum of a R6G water solution at concentrations greater than  $10^{-4}$  M (fig 4). Since such dimers do not fluoresce this dimerization of dyes in the ground state decreases luminescence efficiency<sup>30</sup>. The absorption spectrum of R6G dissolved at a concentration of  $10^{-2}$  M inside a TiO<sub>2</sub> based xerogel is also shown in figure 4. The amount of dimeric species is negligible even for such a high concentration. This behavior has been observed for other matrices based on zirconium and aluminium oxide gels<sup>22</sup>.

This effect has already been reported in silica sol-gel glass and assigned to the the formation of silica cages separating luminescent ions<sup>10</sup>.

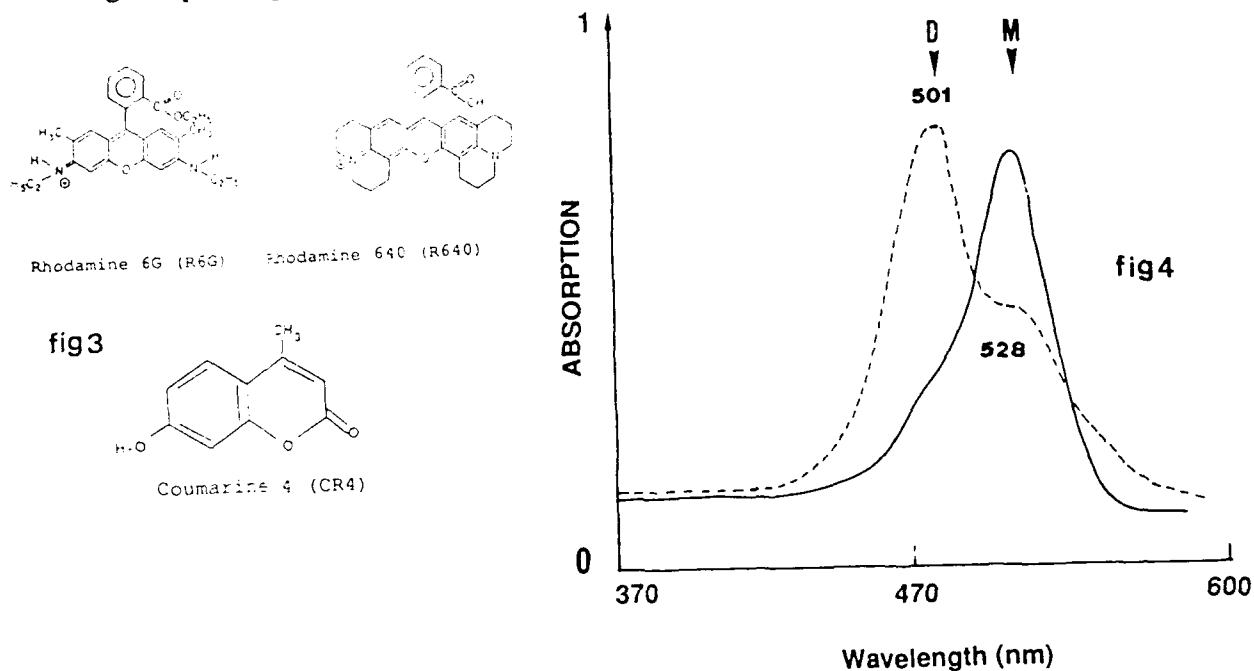


Figure 3. Molecular structures of some laser dyes

Figure 4. Absorption spectra of R6G in water (dotted line) and in a titanium oxide based xerogel (full line)  $C=10^{-2}M$

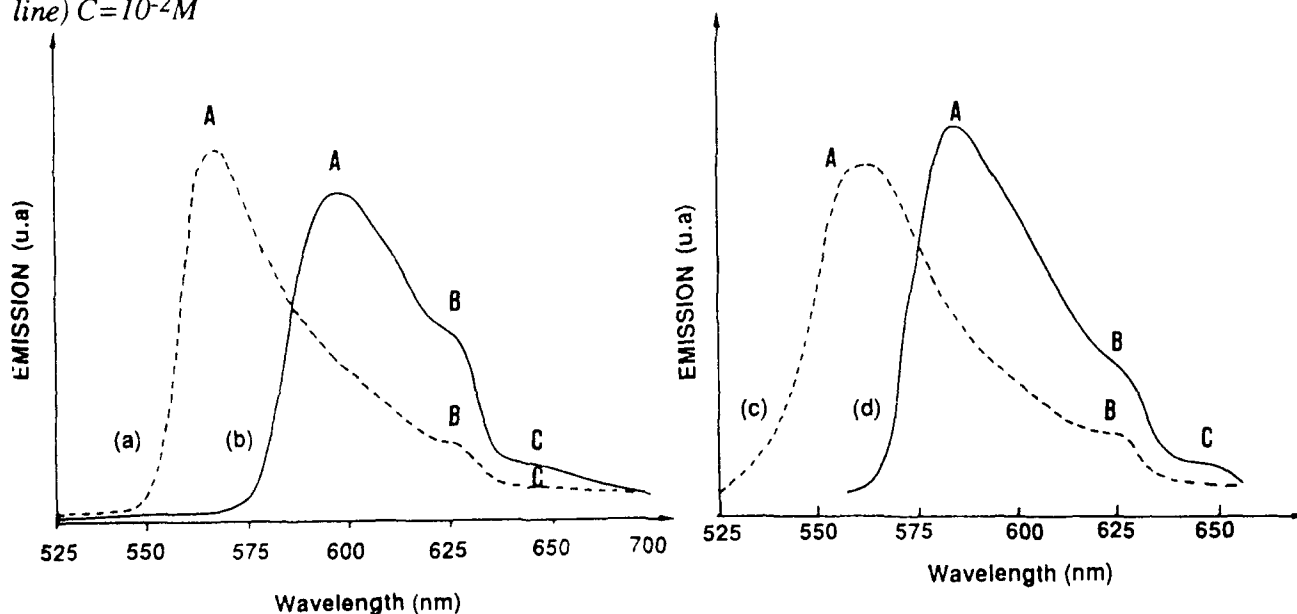


Figure 5. Emission spectra of R6G in titanium oxide based gels ( 5a gel ,  $C=10^{-4}M$ ; (dotted line); 5b gel (tg),  $C=10^{-2}M$  (full line); 5c gel (10 tg)(dotted line) ,  $C=10^{-4}M$ , 5d Xerogel ,  $C=10^{-2}M$  ( full line))

Typical emission spectra of rhodamine in titanium oxide based gel are shown in figure 5. They are characterized by the presence of three main bands A,B, and C located at 598nm, 623nm and 645nm respectively, for a dye concentration of  $10^{-2}\text{M}$ . The strong band A shifts toward the red part of the spectrum ( from 556 nm for  $C=10^{-5}\text{M}$  to 598nm for  $C=10^{-2}\text{M}$ ) when the dye concentration increases. This red shift may be attributed to a specific adsorption of excited state dye molecules on the polymeric oxide network. Such a phenomenon leads to a stabilization of the excited state arising from a restricted freedom of the rotational movements of the dye. As the dye concentration increases the pores of the gel become more and more crowded and a different configuration may thus be adopted by the dyes. Bands B and C are quite broad. Their fluorescence maxima shift slightly ( 2-5 nm) towards the red part of the visible spectrum and only for the higher concentrations. At the same time their relative intensities compared to band A strongly increase. Such bands are probably due to the fluorescence of excimers arising from associations between dyes in the excited and dyes in the ground state  $(R6-G^*-R6G)_n$ <sup>28</sup>. Upon drying xerogels also exhibit fluorescence properties. However even if the concentration of dye by unit volume is increased in the dried state (because of solvent evaporation) the fluorescence spectra look like those of diluted sample (fig. 5d). Band A is blue shifted and band B decreases in intensity while band C related to excimers completely vanishes (fig. 5d). This observation supports again the assumption that in the dried state molecular dilution of dyes should occur, probably because of a preferential adsorption of the dyes at the surface of the amorphous oxide<sup>29</sup>.

All these phenomena are also observed for R640 but in a much more exalted way<sup>27</sup>. For concentrations of about  $10^{-3}\text{M}$  band A vanishes totally while only strong bands B and C are only observed (fig.6). One of the main problem of R640 is related to the fact that at low pH <2 the protonated form is converted into the colorless lactonic form<sup>6</sup>. Many transparent silica sol gel matrices are synthesized at low pH (acid catalysis)<sup>2</sup>. Our first goal was to stabilize such a dye by using transparent transition metal oxide gels synthesized in the presence of organic acids (ACOH)<sup>17</sup> or chelating ligands (acetylacetone)<sup>32</sup> so that the synthesis can be performed into weakly acidic medium typically pH>3. The result was actually not as expected. R640 dissolved into titanium oxide based gels at a concentration of  $10^{-5}\text{M}$  leads to a colorless lactonic form within five days. Such a fast degradation has probably a photochemical origin since no lactonisation is observed when the gel is kept in the dark. As evidenced from UV- visible and ESR measurement,  $\text{Ti}^{3+}$  and super oxide ions ( $\text{O}_2^-$ ) may be involved in such a process<sup>27</sup>. Therefore the synthesis of other transparent matrices which do not exhibit redox properties was performed. Zirconium and aluminum oxide based gels

were synthesized in the same medium as titanium oxide gels. In these gels, R640 does not present any photodegradation even after one year<sup>27</sup>.

Coumarin 4 has also been incorporated into transition metal oxide gels. The most attractive feature of coumarin is the excited state acid-base equilibrium which develops<sup>28</sup>. Four different fluorescent excited forms can exist namely anionic A\*, cationic C\*, neutral N\* and zwitterionic Z\*. The resulting Stoke's shift is large and can be advantageously used for laser pumping. In alcoholic-water mixtures only three forms A\* (440nm), N\* (380-390nm) and Z\* (480nm) with similar relative intensities are observed in the emission spectra. The emission spectra of coumarin 4 in titanium oxide based gels ( $c=10^{-2}M$ ) is shown in figure 7. The anionic form has disappeared and only N\* (380-390nm) and Z\* (480nm) species are observed.

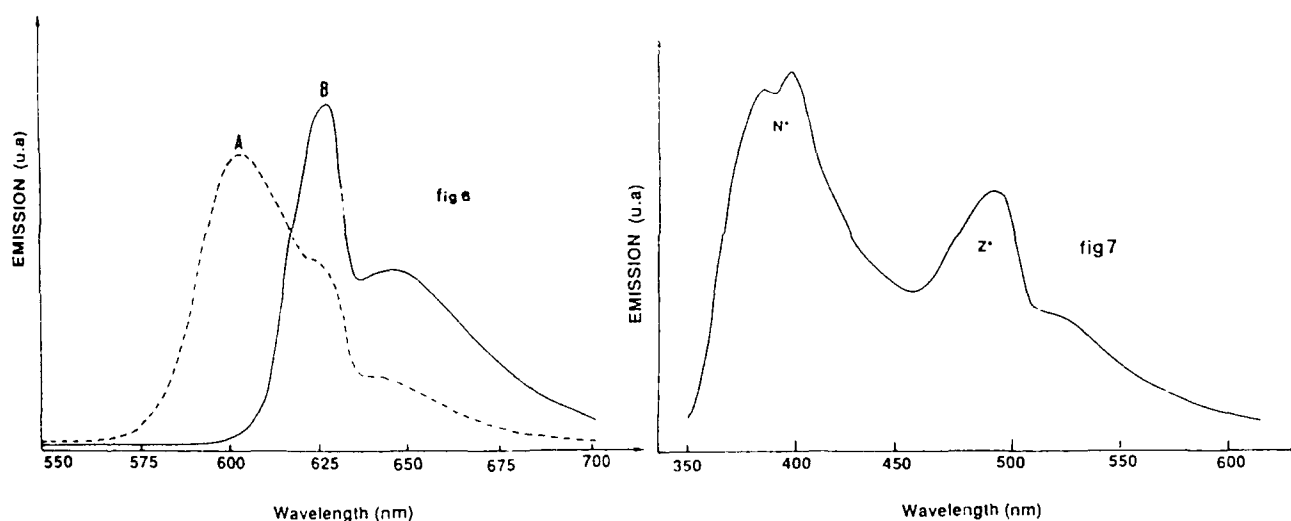


Figure 6 Emission spectra of R640 in titanium oxide based gels:  $C=10^{-5}M$  (dotted line);  $C=10^{-3}M$  (full line)

Figure 7 Fluorescence spectrum of Coumarin 4 in titanium oxide based gels

Titanium oxide or zirconium oxide based xerogels present also luminescent properties. The emission spectra of CR4 in titanium oxide based xerogels shows only the presence of a large band located at 400-410 nm. A similar emission spectrum with a much higher intensity is observed for zirconium oxide based xerogels ( $\lambda = 408$  nm). This transition cannot be assigned to a blue shifted cationic form C\* of coumarin 4 because this latter is stable only at very low pH. This transition corresponds probably to the red shifted luminescence band of the neutral form. This phenomenon probably arises from a preferential adsorption of the excited N\* state in the polymeric T.M.O.

network<sup>31</sup>. The disappearance of charged ionic species  $A^*$ ,  $Z^*$  in xerogel arises probably from a bad screening of the charges resulting from the lack of solvent. Titanium and zirconium alkoxides and their hydrolyzed derivatives are very reactive species<sup>3,33</sup>. Coumarine 4 has an hydroxyl group which should form via alcohol interchange  $CR_4-O-M$  species ( $M = Ti, Zr$ ). The dye can thus be chemically bonded to the polymeric backbone.

## 2.4 Organic molecules bonded to sol-gel polymers.

Organic groups can also be directly bonded to an inorganic network. Chemistry plays a key role for the synthesis of these hybrid materials. Ormocers are extensively studied<sup>34</sup>. Their chemistry is close to that of silicones. They are obtained via the hydrolysis of organo substituted silicic acid esters of the general formula  $Si(OR)_{4-x}R'_x$  where  $R'$  is a non hydrolyzable group bonded to silicon through a Si-C bond. However such chemical tailoring cannot be directly extended to transition metals. The more ionic M-C bond would be destroyed upon hydrolysis. Organic fonctionnalisation of a transition metal oxide backbone can be however performed using complexing agents<sup>32,4</sup>. These organic groups act as network modifiers. They can of course contribute to a specific optical property such as luminescence or non linear optic but their presence can also lead to strong changes in chemical and optical properties as shown in the two following examples. The first one concerns coloration changes in electrochromic display devices based on amorphous titanium oxide layers<sup>17</sup>, while the second one is related to the synthesis of stable colloids with improved photochemical properties<sup>36</sup>.

$TiO_2$  xerogel layers have been synthesized from acetic acid modified alkoxide precursors<sup>17</sup>. The electrochromic layer was made by spin coating. In such a procedure a drop of  $Ti(OBu^n)_3OAc$  - BuOH solution is deposited onto a spinning ITO electrode. Hydrolysis occurs spontaneously onto the substrate leading to transparent thin layers about 0.3  $\mu m$  thick. An amorphous  $TiO_2$  based xerogel is obtained.  $^{13}C$  CP MAS NMR, IR, XANES -EXAFS show that all acetate groups have not been hydrolyzed. Chemical analysis of the xerogel confirms that about 0.30 acetate groups per titanium are still chemically bonded<sup>13</sup>. Electrochromic properties of these layers were studied using the following electrochemical cell : modified  $TiO_2$  xerogel /  $LiClO_4$ -1M Propylen carbonate/ Pt. The layer reversibly turns from transparent to blue within about 1s by applying a voltage of  $\pm 2$ Volts. The energy consumption for coloration and bleaching is about 10mC/cm<sup>2</sup> for an optical density of 0.5. When an electrochromic layer made from spin coating of a butanolic solution of  $Ti(OBu^n)_4$  is tested in the same conditions, optical switching is also obtained but the coloration is grey instead of blue<sup>13</sup>.

Such a difference in coloration can be assigned to the presence of acetate groups chemically anchored to the titanium oxide polymeric network. The ligand field around titanium is therefore modified and the optical spectrum of these two layers are slightly different. As a consequence different colours can be obtained. The chemical modification of alkoxides precursors provides an interesting way for the synthesis of organically modified electrodes.

Transparent  $\text{TiO}_2$  sols are usually produced via the hydrolysis of  $\text{TiCl}_4$  in water or  $\text{Ti}(\text{OPri})_4$  in acid aqueous solutions<sup>35</sup>. Particles about 100Å in diameter are obtained which exhibit good photochemical characteristics<sup>35</sup>. However these sols only absorb U.V. light and are not stable above pH 3. Transparent  $\text{TiO}_2$  based colloids have been synthesized by F.Babonneau et al<sup>36</sup> via the hydrolysis of the modified precursor  $\text{Ti}(\text{OPri})_3\text{acac}$ . These colloids have an hydrodynamic diameter of about 30Å and are made of an oxide core close to  $\text{TiO}_2$  anatase surrounded by a shell of protecting ligands (acac) probably bonded to titanium surface sites<sup>36</sup>. Organic chelating agents have a double role. They increase the chemical stability of  $\text{TiO}_2$  modified colloids that remain stable up to pH 10. Moreover, charge transfer from acetylacetonato ligands to the titanium atom gives rise to a strong absorption of visible light that improves the photochemical efficiency of  $\text{TiO}_2$  sols. They turn blue or pink under visible light irradiation. Their color is due to the reduction of some  $\text{Ti}^{4+}$  to  $\text{Ti}^{3+}$  ions. It depends on the ligand field surrounding  $\text{Ti}^{3+}$  as evidenced from ESR experiments<sup>37</sup>. These modified colloids are stronger reducing agents than other  $\text{TiO}_2$  colloids.

### 3.CONCLUSION

Main advantages of sol-gel chemistry related to some optical properties of TMO gels have been illustrated by several striking examples:

- Mixing of components at a molecular level and synthesis of metastable phases can be performed.
- Amorphous matrices inside which a large amount of luminescent probes can be incorporated without fluorescence quenching.
- Room temperature synthesis allows a good compatibility between organic molecules and oxide based networks.

This latter point together with the fact that coatings and fibers can be easily obtained via the sol-gel process should lead to the most promising future of sol gel optics.

### 4.ACKNOWLEDGEMENTS

Patrick Aschehoug is gratefully acknowledged for his help in luminescence measurements.



## 5. REFERENCES

1. B.J.J. Zelinski. and D.R. Uhlmann, " Gel Technology in Ceramics", J. Phys. Chem. Solids 45, PP.1069-1090, 1984.
2. C.J. Brinker and G. Scherrer , " Sol-Gel Science, the Physics and Chemistry of Sol-Gel rocessing", Academic Press, San Diego, 1989.
3. J. Livage, M. Henry and C. Sanchez, "Sol-Gel Chemistry of Transition Metal Oxides", Progress in Solid State Chemistry 18, PP. 259-341, 1988.
4. C. Sanchez and J. Livage , " Sol-Gel Chemistry from Metal Alkoxide Precursors", New J. of Chem., in print (1990)
5. H. Dislich, "Thin Films From The Sol-Gel Process", in Sol-Gel Technology For Thin Films, Fibers, Preforms, Electronics and Specialty Shapes, Ed L.C.Klein, Noyes Pub, PP. 50-79, 1988.
6. .C Pouxviel, S. Parvaneh, E.T.Knobbe and B.Dunn, "Interactions Between Organic Dyes and Sol-Gel Matrices", Solid State Ionics, 32-33, pp. 646-654, 1989.
7. B Dunn, E.Knobbe, J.M. Mc. Kiernan, J.C. Pouxviel and J.I. Zink, " The Optical Behavior of Organic and Organometallic Molecules in Sol-Gel Matrices" Mat. Res .Soc. Symp. Proc., 121, pp. 331-342, 1988.
8. R. Reisfeld, " Criteria and Prospects of New Lasers Based on Fluorescent Dyes in Glasses" Journal de physique, C7, sup 12, 48, pp. 423-426, 1987.
9. D.Avnir, V.R.Kaufman and R. Reisfeld, " Organic Fluorescent Dyes Trapped in Silica and Silica-Titania Films By the Sol-Gel Method. Photophysical, Film and Cage Properties", J. Non-Cryst. Solids, 74, pp.395-406, 1985.
10. D.Avnir, D. Levy and R. Reisfeld, "The Nature of the Silica Cage as reflected by Spectral Changes and Enhanced Photostability of Trapped Rhodamine 6G", J. Phys. Chem., 88, pp.5956-5959, 1984.
11. J.C Pouxviel, B.Dunn and J.I.Zink, " Florescence Study of Aluminosilicates Sols and Gels doped with Hydroxy Trisulfonated Pyrene" J. Phys. Chem., 93, pp. 2134-2139, 1989.
12. Y. Kobayashi, Y. Kurokawa, Y. Imai, and S.Muto, " A Transparent Alumina Film Doped with Laser Dye and its Emission Properties", J. Non-Cryst. Solids, 105, pp.198-200, 1988.
13. M. Nabavi, S.Doeuff, C.Sanchez and J.Livage, "Sol-Gel Synthesis of Electrochromic Films", Materials Science and Engineering, B3, PP. 203-207, 1989.
14. A chemseddine, M. Henry and J. Livage, "Sol-Gel Derived Electrochromic Layers", Revue de Chimie Minerale, 21, pp. 487-495, 1984.
15. P. Judeinstein and J. Livage, "Role of the Water Content on the Electrochromic properties of  $WO_3 \cdot n H_2O$  thin films, Mat. Sci. Engineer., B3, pp.129-132, 1989.
16. C.Sanchez, F. Babonneau, R. Morineau and J. Livage "Semiconducting Properties of Vanadium Pentoxide Gels", Phil. Mag. B, 47, pp.279-290, 1983.
17. S.Doeuff and C. Sanchez, " Photoelectrochemical Properties of  $TiO_2$  Anatase Films Synthetized via the Sol-Gel Process", C. R. Acad. Sci., Paris, 309, PP. 1137-1142, 1989.
18. A Fujishima and K. Honda, " Electrochemical Evidence for the Mechanism of the Primary Stage of Photosynthesis ", Bull. Chem. Soc. Chem. Jap., 44, pp.1148-1150, 1971.
19. J. G. Mavroides, " Electrode Materials for the Photoelectrolysis of water ", Mat. Res. Bull., 13, pp.1379-1388, 1978.
20. M.A. Butler, "Photoelectrolysis and Physical Properties of the Semiconducting Elctrode  $WO_3$  ", J. Appl. Phys., 48, pp.1914-1920, 1977.
21. S. Doeuff, M. Henry, C. Sanchez and J. Livage, " Hydrolysis of Titanium Alkoxides : Modification of the Molecular Precursors by Acetic Acid", J. Non-Cryst. Solids, 89, pp.206-216, 1987.
22. M. Lecomte, B. Viana and C. Sanchez, " Inorganic and organic luminescent probes in transition Metal Oxide Gels", C. R. Acad. Sci., Paris, in print, 1990.

23. D. Levy, R. Reisfeld and D. Avnir, " Fluorescence of Europium (III) in Silica Gel- Glass as A Probe for Cation Binding and for Changes in Cage Symmetry During Gel Dehydration", *Chemical Physics Letters*, 109, 6, pp. 593-597, 1984.
24. R. Reisfeld, R.A. Velapoldi, L. Boehm and M.I. Shalom, " Transition Probabilities of Europium in Phosphate Glasses " *J. Phys. Chem.*, 75, pp. 3980-3983, 1971.
25. C.K. Jorgensen and R. Reisfeld, " Judd-Ofelt Parameters and Chemical Bonding ", *J. Less-Common Met.*, 93, pp. 107-112, 1983.
26. R. Reisfeld, R. Zusman, Y. Cohen and M. Eyal, " The spectroscopic Behavior of Rhodamine 6G in Polar and Non Polar Solvents and in Thin Glass and in PMMA films", *Chemical Physics Letters*, 147, 2-3, PP. 142-147, 1988.
27. J. Fitreman and C. Sanchez, " Fluorescence of Rhodamine 640 in Sol Gel Matrices", *C. R. Acad. Sci., Paris*, in print, 1990.
28. K.H. Drexhage, "Structure and Properties of Laser Dyes", in *Topics in applied physics*, vol 1, *Dye Lasers*, ed F.P. Schaefer (Springer Verlag Berlin), pp. 144-193, 1977.
29. F.L. Arbeloa, I.L. Gonzalez, P.R. Ojeda, and I.L. Arbeloa, " aggregate Formation of Rhodamine 6G in Aqueous solution" *J. Chem. Soc. Faraday Trans. II*, 78, pp. 989-994, 1982.
30. A. Penkofer and Y. Lu, "Fluorescence Quenching of Rhodamine 6G in Methanol at High Concentration", *Chemical Physics*, 103, PP. 399-405, 1986.
31. E. Lendvay, "Photoluminescence of adsorbed dyes", *J. Phys. Chem.*, 69, pp. 738-743, 1965.
32. C. Sanchez, J. Livage, M. Henry and F. Babonneau, " The Chemical Modification of Metal Alkoxides" *J. Non-Cryst. Solids*, 100, 650, 1988.
33. M. Nabavi, S. Doeuff, C. Sanchez and J. Livage, " The Chemical Modification by The Solvent: a Way to Control Sol- Gel Chemistry", *J. Non-Cryst. Solids*, in print, 1989.
34. H. Schmidt, H. Scholze, and A. Kaiser "Principles of Hydrolysis and Condensation Reaction of Alkoxysilanes", *J. Non-Cryst. Solids*, 63, pp. 1-11, 1984.
35. D. Duonghong, E. Borgarello and M. Grätzel, "Dynamics of Light Induced Water Cleavage in Colloidal Systems", *J. Am. Chem. Soc.*, 103, pp. 4685-4690, 1981.
36. A. Leautic, F. Babonneau and J. Livage, " Structural Investigation of the Hydrolysis-Condensation Process of Titanium Alkoxides  $Ti(OR)_4$  ( $OR=OPr^i$ ,  $OEt$ ) Modified by Acetylacetone", *Chemistry of Materials*, 1, pp. 248-252, 1989.
37. F. Babonneau, A. Leautic and J. Livage, "Structural Investigation of the Hydrolysis Condensation Process of a Modified Titanium Alkoxide", *Mat. Res. Soc. Symp. Proc.*, 121, pp. 317-, 1988.



**Silica glass monoliths from alkoxide gels;  
an old game with new results.**

Y. Sano, S. H. Wang, Ray Chaudhuri and A. Sarkar

Orion Laboratories, Inc.  
550 Via Alondra  
Camarillo, California 93012

**ABSTRACT**

Cylindrical monolithic silica dry gel bodies, up to 250 grams in weight, are routinely produced from alkoxide sols free of colloidal particles, using tetraethyl-orthosilicate precursor. These dry gel bodies, after sintering in controlled chlorinated atmosphere, yielded clear, bubble free, dense glass rods 3.0-4.0 cm in diameter and 15-20 cm in length. Uv-vis-ir spectra, of properly dehydrated and sintered glass samples tested from 180 nm to 3200 nm, showed no detectable absorption peak at 2700 nm and a UV band edge at around 185 nm; implying that resultant glasses are reasonably free of impurities and hydroxyl ions.

Effect of sol composition on gel ultrastructure was carefully investigated. It was found that by careful choice of sol composition, type and amount of catalyst and aging conditions, it is possible to tailor the gel ultrastructure for ease of drying. For example, we have been able to produce gels with unimodal pore distributions, and average pore sizes in the range from 8 to 300 Å and surface area in the range from 150 - 1100 m<sup>2</sup>/gram. As a result of this ability to tailor gel ultrastructure, including pore size, bulk density and skeletal density of the gel bodies, we have been able to optimize gel ultrastructure to maximize its strength, so that it can withstand capillary forces generated during the drying processes.

The result of this preliminary investigation has led us to believe that high quality fused silica glass of much larger sizes can be produced by the alkoxide route; and experiments to scale up the process is under way. Up to date results of this investigation will be presented at the conference.

**92 4 28 022**

**92-11404**



## 1. INTRODUCTION

Commercially available silica glasses today are fabricated by electrical melting of high quality sand or by vapor deposition. The highest purity silica glasses used for transmissive optical components are produced by vapor deposition processes, primarily because in the melting process it is difficult to remove contamination existing in the raw materials and also because it is difficult to prevent recontamination of the melt from its container at the high melting temperatures. In the vapor deposition processes, the silica glass in its final form can be quite expensive because of low processing rates and high investment cost in processing and pollution control equipment. In addition, because of the difficulty in producing vapor deposited glass in useful shapes, significant amount of cutting and polishing is required. Finishing costs therefore, can also be very high. Our objective is to evaluate the potential of producing glasses with optical quality good enough for transmissive optics applications, using a process other than vapor deposition.

The sol-gel process using only organometallic precursors has the potential of producing high purity and extremely homogeneous silica glasses in near net shape form, using relatively low processing temperatures. In this approach, a desired solution of a silica containing alkoxide is mixed with water and alcohol. It is catalyzed with an acid or base; and the solution called sol is poured into molds. Following hydrolysis and condensation reactions in the mold, the sol is converted into a porous gel body. This porous gel is then aged to strengthen the gel, dried and sintered into a clear glass. The process does not require expensive processing equipment and pollution control is not a significant issue.

Thus, in spite of relatively expensive raw materials it is believed that the process can produce inexpensive silica products<sup>1</sup>. A considerable amount of research has gone on in this field for the last 20 years. However, the success in commercially producing large pieces of monolithic silica has been an illusive target. The primary reason for this is the cracking of gel during drying, resulting from stresses in the porous body generated by capillary pressure at the liquid-vapor interface within the pores<sup>2</sup>.

Limited success has been shown in alkoxide gels by using drying control chemical additives called DCCA<sup>3</sup> and hypercritical drying<sup>4</sup>. Other approaches where colloidal silica particles have been added to the alkoxide organometallic precursor sol also has had limited success<sup>5, 6</sup>. However, in this approach, clustering of colloidal particles resulting in formation of crystoballite defects, degassing or bubble formation at high temperatures have been problems<sup>7</sup>.

All colloidal silica sol-gel processing has also had some success<sup>8</sup>. But, in this approach one has to produce colloidal particles by vapor deposition first and then proceed with sol-gel processing. Cost effectiveness of this approach is therefore questionable. The largest pieces of sol-gel glass produced by sol-gel process has been by a colloidal approach as well<sup>9</sup>. However, optical properties of glasses produced by this approach is not good enough for transmissive optics. Based on the above prior art, we believe that the best option is to attempt to solve the problems associated with producing monoliths using alkoxides gels.

Our program in this field started about 2 years ago with the our naivety in not being able to understand why one can so easily form glass monoliths by vapor phase oxidation process. When halides of glass forming materials are passed through a flame to react, spherical soot particles are formed. These particles coalesce at around 650 °C to form a porous body that can easily be sintered into clear glass Monoliths. The question is, why can one not make such monoliths easily by sol-gel process even when the gel structure is chemically bonded from liquid phase reactions. This paper outlines an analysis of the basic issues involved in fabricating monoliths of alkoxide gels and how we went about resolving these. Finally we will present the results of our work at Orion Laboratories, Inc.

## **2. ANALYSIS OF CVD SOOT PREFORM**

First of all, porous soot preform fabricated by axial vapor deposition (NTT) was investigated. In this fabrication process the deposition temperature at the axis of the preform is at maximum and is controlled to around 650 °C, with the temperature at the edge of the preform dropping approximately 100 °C below that of the axis. The bulk density of the soot at axis is higher than that of the edges. However, the average bulk density of such preforms are in the range of 0.2 -0.3 gms/cc. The bulk density of the tested preform was 0.28 gms/cc and the diameter of the porous preform was 28 mm..

The pore size distribution analysis of the preform was done for two portions of the preform, one sample close to the axis and one from the edge of the preform. The average pore radius of the central part was 48 Å, and that of the edge was 68 Å, both with very wide pore size distributions. The BET output of the sample from the edge is shown in Figure 1. It is curious to note that the average pore size is well within the range of pore sizes that can be obtained from alkoxide gels reported in literature. Thus, the capillary force in the pores due to small pore size can not be the sole reason for the cracking of alkoxide gels.

In order to verify this, we took a second preform with similar pore size distribution as mentioned before and dipped it in water for a period of time

sufficient to soak a part of the preform with water, and then let it dry in atmospheric conditions. Curiously, there was no cracking of the preform similar to that seen in normal drying of porous gel of equivalent pore size when it is dried in atmospheric conditions. Thus, it can be concluded that capillary force exerted by water in pore size in the range of 50-70 Å is not large enough to cause cracking of a porous silica matrix produced by vapor deposition.

The question that we had to address was therefore narrowed to what is the difference between the porous body produced by sol-gel compared to that of vapor deposition?

### 3. ANALYSIS OF DIFFERENCES

The key parameters of the porous matrix that controls cracking can be identified as follows:

#### 3.1 Capillary force exerted on the porous body

The capillary force exerted on the porous matrix depends on the pore radius and the properties of the pore fluid. The governing equation is shown below:

$$\Delta P = 2 \gamma \cos \theta / r \quad (1)$$

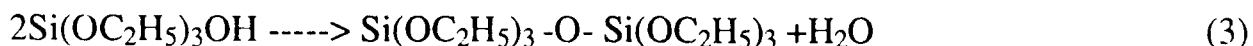
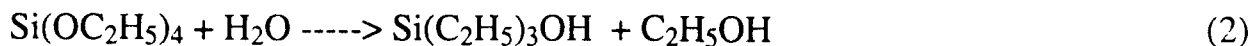
For alkoxide gels, the pore fluid is primarily a mixture of alcohol and water. In the discussion above about vapor deposited preforms, with equivalent pore size and water as a pore fluid, we have shown that the capillary force by itself can not be a problem for a silica matrix. Thus, we have to look beyond this.

#### 3.2 Wall thickness control of porous matrix

Resistance to cracking of a porous body depends on the cross section of the matrix wall and its strength. Strength can be increased by increasing matrix wall thickness either by reducing surface area per unit volume of the gel or by increasing bulk density of the gel. Thus, a comparison of these parameters between vapor deposited preforms and alkoxide gel monoliths becomes critical. Density of vapor deposited preform of 0.28 gm/cc, is surely well within the capabilities of sol-gel process. The surface area is similarly within the capability of sol-gel process, as the vapor deposited gel showed surface area between 150 to 170 m<sup>2</sup>/gm. Thus, too small a wall thickness cannot explain cracking of alkoxide gels either.

### 3.3 Strength of skeletal material

In vapor deposited preform, the porous matrix is fused silica with skeletal density of 2.2 gm/cc. On the other hand, it is difficult to attain a skeletal density of 2.2 gm/cc using the sol-gel process. The reason for this is obvious, if one studies the following gellation reactions of hydrolysis and condensation.



Since, sols are cast and gellation occurs in a closed environment, reaction equilibrium must inhibit completion of reaction at some point, and no more condensation can occur, leaving considerable amount of alkoxide radicals left in the porous matrix. Thus, the Si-O-Si bonds existing in vapor deposited preforms, giving it its strength, is not fully formed in the sol-gel process. The aging step in sol-gel process, used to enhance the strength of the porous body, presumably decreases the amount of alkoxide radicals in the gel. However, we postulated, based on information from literature, that this can not be completely done in a closed system. Thus, one of our efforts was to find ways to eliminate all alkoxide radicals from the porous gel prior to drying, without degrading any of its advantageous features.

In summary, we felt that eliminating alkoxide radicals from the gel prior to drying must be the key to producing monoliths successfully.

### 4. EXPERIMENTAL TAILORING OF GEL PARAMETERS

Basically, we have worked with TMOS, TEOS and Ethyl silicate as our precursor materials, with different concentrations of water and alcohol to form sol. We used diverse combinations of catalysts, and have varied sol composition, aging and drying conditions with basic approaches as reported in literature, but with explicit goal of improving the resistance to cracking of the gel body due to anticipated capillary forces during drying.

Figure 2 shows the ranges of pore sizes we can obtain by sol composition and aging condition tailoring. Figure 3 shows the range of surface area of dry gel that can be produced. Figure 4 shows the range of bulk densities of dry gel we can obtain and Figure 5 shows that through appropriate aging conditions it is possible to produce alkoxide gels with skeletal density of nearly 2.2 gm/cc<sup>10, 11</sup>.

Thus, it is clear that one can come close to replicating the structure of a vapor deposited preform structure with alkoxide gels. We then proceeded to sinter these dry gels, again with well established sintering conditions to produce cylindrical samples of glass.

## **5. RESULTS**

### **5.1 Size of monoliths**

Control of each step of the sol-gel process, including sol composition, aging conditions, drying conditions, sintering conditions and material handling plan are critical in producing high optical quality monolithic silica. We have produced silica glass rods of up to 250 grams. Samples of these will be shown during presentation.

### **5.2 Optical properties**

Figure 6 shows the uv-vis-ir spectrum of glasses produced in our laboratories. It can be seen that we have little difficulty controlling the hydroxyl content of the glass, by a conventional chlorine drying process. We do however still have some impurity absorption problem, as the uv band edge is still at around 200 nm. We have not started working on improving impurity content yet and feel that with using cleaner chemicals and processing conditions the band edge can be moved to around 185 nm.

### **5.3 Glass quality**

Other than visual inspection, the best test of the glass quality is to reheat the glass to about 2000 °C and draw some fiber from it. This permits evaluation of degassing & crystallization problems. We observed no such problems. We have tested the tensile strength of such fiber and compared them to that of our fiber drawn from vapor deposited glass and have not seen any significant difference.

## **6. CONCLUSION**

We feel high quality silica products can be produced by alkoxide gels in a more cost effective manner than vapor deposition and the silica glass produced meets the needs of components for transmissive optics.

Our next step is to scale up the process further, produce glasses of diverse useful shapes and evaluate more carefully the cost potential of this approach.



## **7. ACKNOWLEDGEMENTS**

We would like to thank Prof. J. D. Mackenzie & Dr. E. J. A. Pope of UCLA, for their help in getting us started in this field.

## **8. REFERENCES**

1. J. D. Mackenzie, "Applications of the sol-gel methods for glass and ceramics processing", Chapter 3, Ultrastructure processing of ceramics, glasses and composites, John Wiley & Sons, New York (1984).
2. George W. Scherer, "Measurement of Permeability", J. Non-Cryst. Solids 113 (1989) 107-118.
3. Larry L. Hench, "Use of drying control chemical additives (DCCA) in controlling sol-gel process", Chapter 4, Science of Ceramic Chemical Processing, 52-64, John Wiley & Sons, New York (1986).
4. J. Zarzycki, "Monolithic xerogel- and aerogels for gel-glass processes". Chapter 3, Ultrastructure processing of ceramics, glasses and composites, John Wiley & Sons, New York (1984).
5. M. Toki, S. Miyashita, T. Takeuchi, S. Kanbe and A. Kochi, "A large-size silica glass produced by a new sol-gel process", Journal of Non-crystalline solids 100 (1988) pp. 479-482
6. E.M. Rabinovich, J.B. MacChesney, and D.W. Johnson, Jr., "Gel-derived glasses for optical fibers prepared from alkoxides and fumed silica", Science of Ceramic Chemical Processing, pp.208-216, John Wiley & Sons, New York (1986).
7. M. Nakahara - personal communications
8. G. W. Scherrer and J. C. Luong, "Glasses from colloids", Journal of Non-crystalline Solids, 63 (1984) pp.163-172.
9. R. D. Shoup, "Complex fused silica shapes by a silicate gelation process", Chapter 25, Science of Ceramic Chemical Processing, pp.347-354, John Wiley & Sons, New York (1986).
10. Y. Sano and E. J. A. Pope, Unpublished work.
11. Y. Sano, S. H. Wang, and Ray Chaudhuri, Unpublished work.

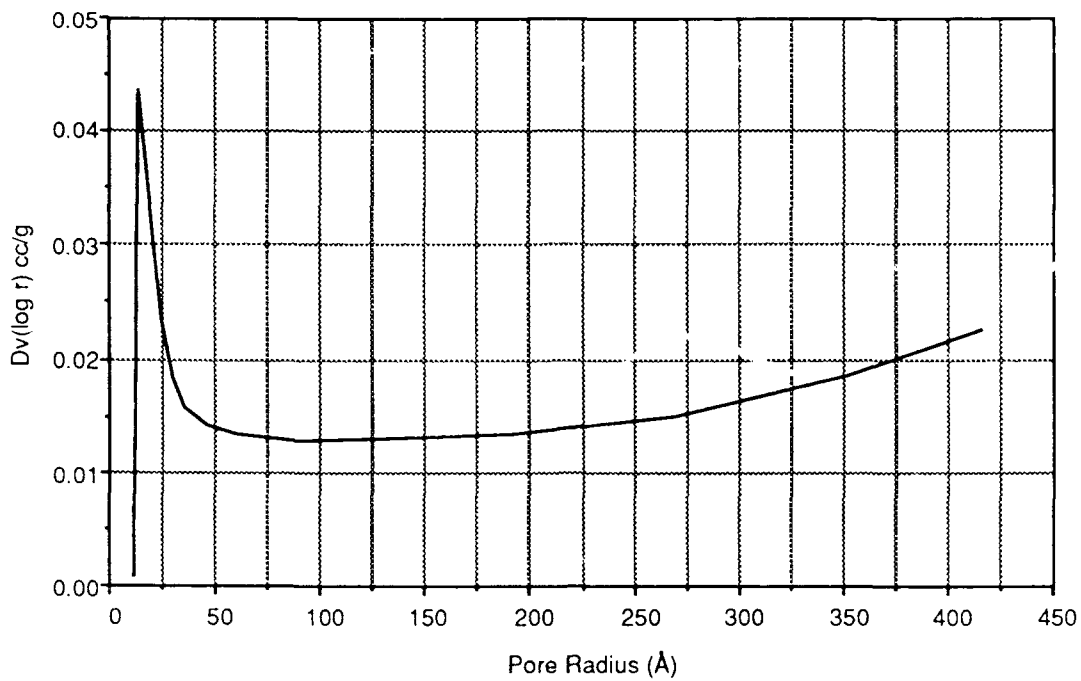


Figure 1 Pore Size Distribution Analysis of the CVD Preform

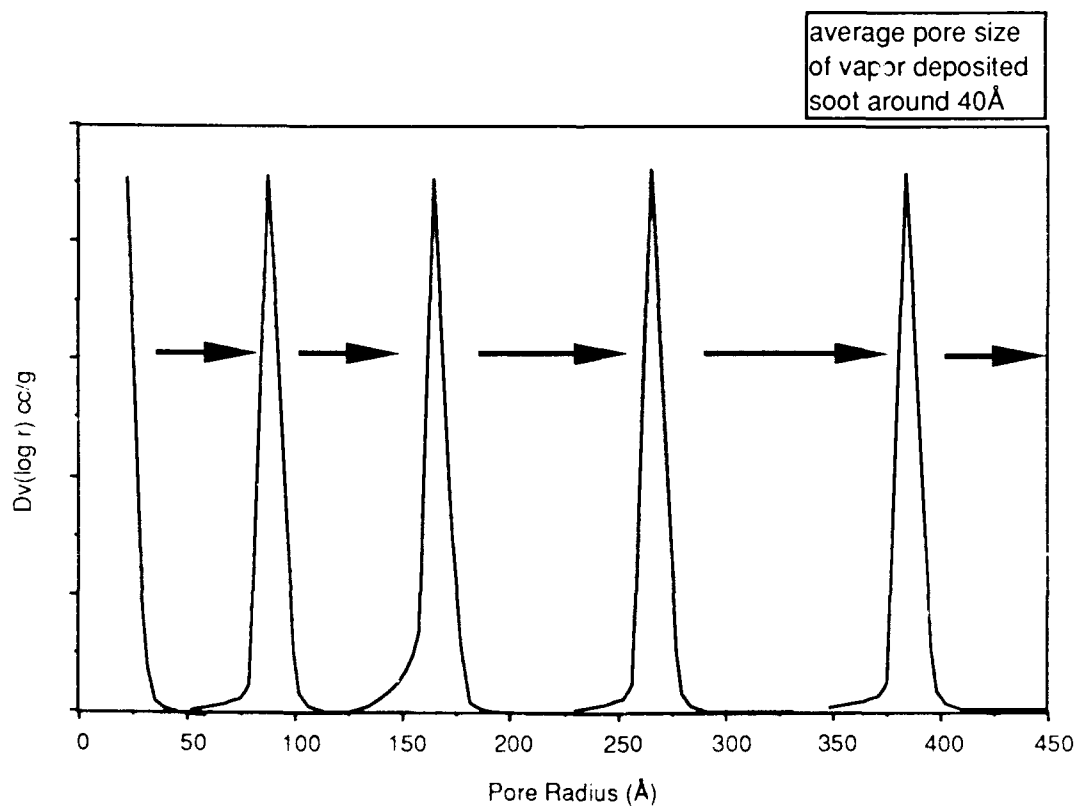


Figure 2. Pore Size Tailoring via Sol Composition and Aging.

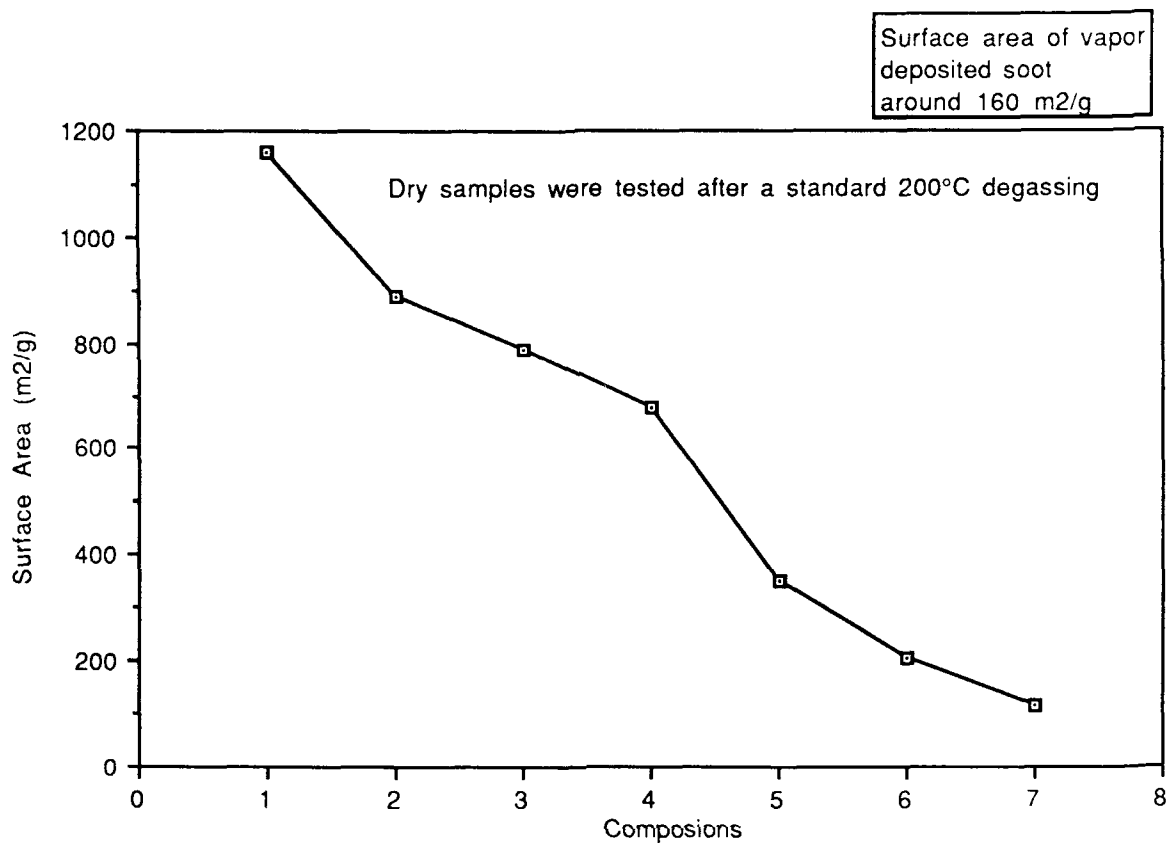


Figure 3. Surface Area of Various Dry Gels

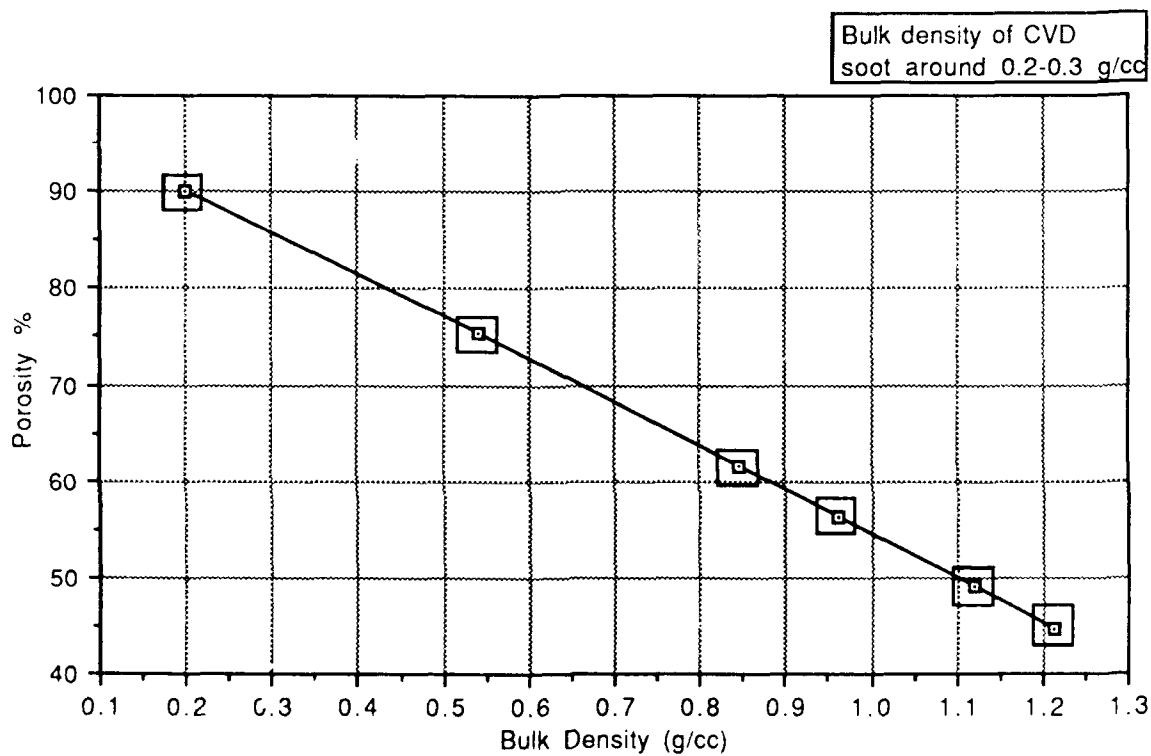


Figure 4. Bulk Density Tailoring

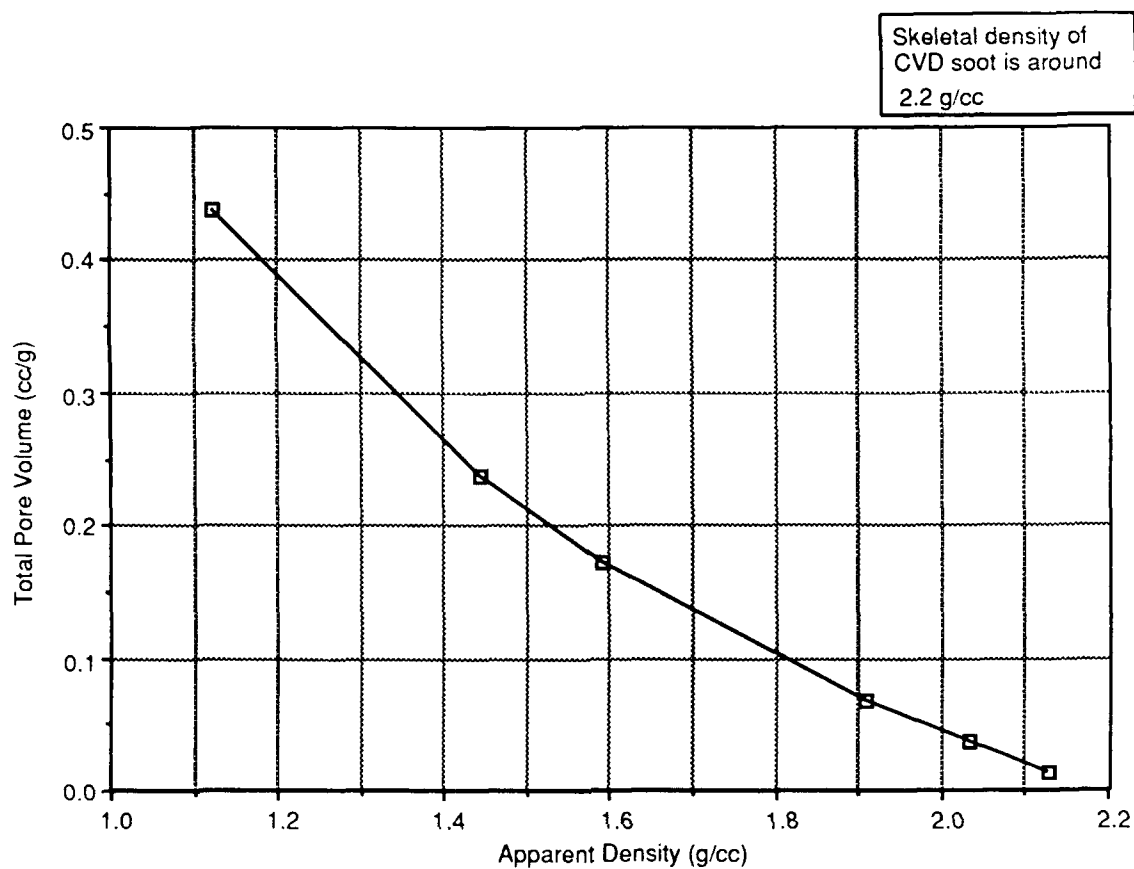


Figure 5. Skeletal Densities of Dry Gels

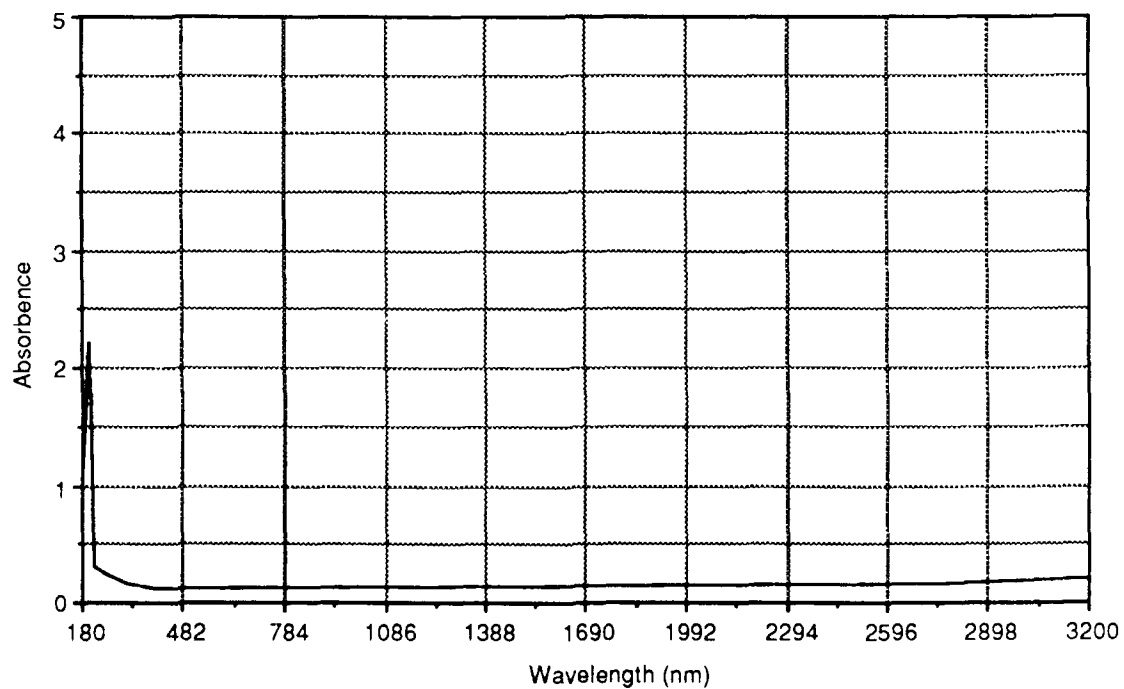
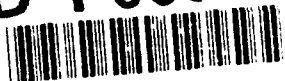


Figure 6. UV-VIS-NIR Light Absorption Curve of a Fully Sintered Gel Glass.



Pregrooving on Glass Disks by the Sol-Gel Method (Part 1)-  
Formation and Evaluation of Pregrooved Glass Disks

Atsunori Matsuda, Yoshihiro Matsuno, Shigeyuki Kataoka,  
Shinya Katayama, Toshio Tsuno, Noboru Tohge\* and Tsutomu Minami\*

Tsukuba Research Laboratory, Nippon Sheet Glass Co., Ltd.  
5-4 Tokodai, Tsukuba, Ibaraki 300-26, Japan

\* Department of Applied Chemistry University of Osaka Prefecture  
Mozu-Umemachi, Sakai, Osaka 591, Japan

### ABSTRACT

Pregrooved glass disks were prepared by the application of the sol-gel coating technique; the soda-lime-silica glass disks were coated with polyethylene glycol(PEG)-containing  $\text{SiO}_2\text{-TiO}_2$  gel films, in which fine patterns were formed by pressing a stamper. The refractive index of the pregrooved layer was matched with that of the glass disks by adjusting the  $\text{TiO}_2$  content. When the weight ratio of PEG with the average molecular weight of 600 to  $\text{SiO}_2\text{-TiO}_2$  oxides was unity, the pitch of the pregrooves formed was unchanged in comparison with that of the stamper used after the heat-treatment at  $350^\circ\text{C}$ , while the land height and the land width of the pregrooves were respectively reduced to 60% and 85% of those of the stamper after the heat-treatment. The noise level of the glass disks with the pregrooved  $\text{SiO}_2\text{-TiO}_2$  layer was lower by 1-2 dB than that of the disks with pure  $\text{SiO}_2$  layer in the frequency range from 0.5 to 2.0 MHz. The lower noise level of the former can be ascribed to the agreement in the refractive index between the pregrooved layer and the glass disks.

### 1. INTRODUCTION

Glass is one of the most promising substrate materials for optical memory disks in terms of optical properties, stability in an ambient atmosphere and so on.<sup>1</sup> In optical memory disks, fine patterns in the submicron scale, so-called pregrooves and preformats, are required for the tracking and the accurate random access. Pregrooves are conventionally formed by a laser beam recording or by a contact printing on photoresist coated on a glass substrate, developing of the photoresist and subsequent etching of the glass substrate.<sup>2-5</sup> These techniques, however, involve complicated processes and need expensive equipments. To overcome these difficulties, the present authors have proposed a novel technique to form pregrooves on glass substrates, based on the sol-gel coating process.<sup>6,7</sup> The technique consists of the following simple steps: (1) formation of an organic polymer-containing gel film on a glass substrate, (2) patterning on the gel film by pressing a stamper against the film, and (3) heat-treatment.

In the present work, pregrooves are formed on soda-lime-silica glass disks of 130 mm in diameter using polyethylene glycol(PEG)-containing  $\text{SiO}_2\text{-TiO}_2$  gel films and the qualities such as dimension accuracies, optical properties, and noise levels of the pregrooved glass disks are evaluated.

92 4 28 023

92-11405



## 2. EXPERIMENTAL

### 2.1. Preparation of coating solutions

The preparation procedure of the coating solution is shown in Fig.1. The  $\text{SiO}_2\text{-TiO}_2$  system was chosen for the present study, since the gel derived  $\text{SiO}_2\text{-TiO}_2$  glass films provided soda-lime-silica glass substrates with an excellent weathering resistance, and since their refractive index was easily controlled by adjusting the  $\text{TiO}_2$  content.<sup>8,9</sup> The procedures are essentially the same as those described previously.<sup>8,9</sup> Silicon tetraethoxide ( $\text{Si}(\text{OEt})_4$ ) in ethanol ( $\text{EtOH}$ ) was first partially hydrolyzed with water, containing 3 wt%  $\text{HCl}$ , at room temperature for 30 min; the molar ratios of  $\text{EtOH}$  and water to  $\text{Si}(\text{OEt})_4$  were 5 and 6, respectively. An appropriate amount of titanium tetra-n-butoxide ( $\text{Ti}(\text{O-nBu})_4$ ) diluted with  $\text{EtOH}$ , the molar ratio of  $\text{Ti}(\text{O-nBu})_4$  to  $\text{EtOH}$  being 20, was then poured into the solution and the stirring was continued for additional 30 min. The solution obtained was further diluted with  $\text{EtOH}$  to control the film thickness. PEG, of which average molecular weight was 600, was then added to the solution and stirred for 10 min. The clear and homogeneous solution obtained in this way served as the coating solution.

### 2.2. Pregrooving on glass disks

The pregrooving process is schematically shown in Fig.2. A chemically strengthened soda-lime-silica glass disk, which was 130 mm in diameter and 1.2 mm in thickness, was coated with the PEG-containing  $\text{SiO}_2\text{-TiO}_2$  solution in a spinning method in an ambient atmosphere (process (a)). A commercially available polycarbonate (PC) substrate with pregrooves of 1.6  $\mu\text{m}$

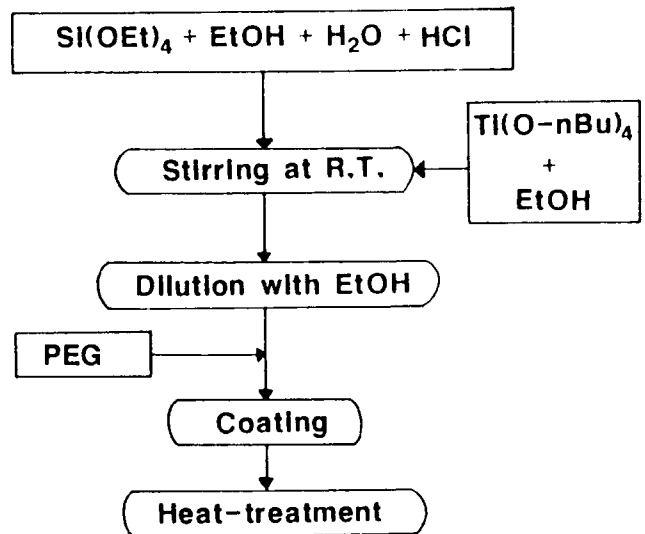


Fig.1. Preparation procedure of polyethylene glycol (PEG)-containing  $\text{SiO}_2\text{-TiO}_2$  solutions.

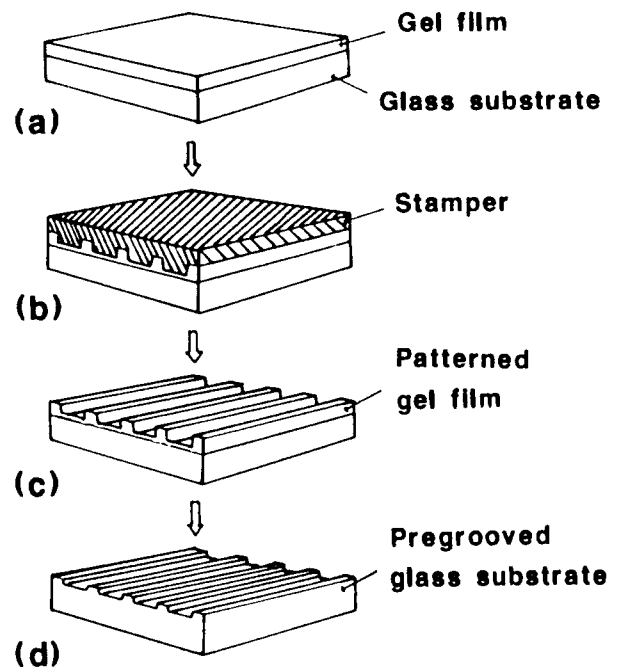


Fig.2. Pregrooving process by the sol-gel method; (a) formation of a gel film on a glass substrate, (b) patterning on the gel film, (c) heat-treatment, and (d) the pregrooved glass substrate.

pitch and 122 nm depth was pressed against the resultant gel film (process (b)). After the film became hard, the stamper was removed and the patterned gel film was heat-treated at 350 °C for 15 min in air using a clean oven to decompose PEG in the gel film and to be densified (process (c)). Through the above processes, the pregrooved glass disk with the negative pattern of the stamper was obtained (process (d)).

### 2.3. Evaluation of pregrooved glass disks

The refractive indices of the coating films were calculated from the reflectivity  $R_m$  of the substrates with the films using equation (1),

$$R_m = (n_c^2 - n_1 n_2)^2 / (n_c^2 + n_1 n_2)^2 \quad (1)$$

where  $n_c$  is the refractive index of the coating film,  $n_1$  is the refractive index of air ( $n_1=1$ ), and  $n_2$  is the refractive index of the substrate. The reflection spectra of the substrate with the film show wavy patterns due to the interference effect. When  $n_c > n_2$ ,  $R_m$  is a peak of the reflection spectra of a half infinite substrate with the film, while when  $n_c < n_2$ ,  $R_m$  is a valley of the reflection spectra.<sup>10</sup> Glass substrates, of which the one side is roughened and painted black, were used as the half infinite substrate. The reflectivity was measured using a spectrophotometer (U-3400, Hitachi, Japan). Dimensions such as land height and land width of pregrooves formed were measured using a scanning electron microscope (JEM-200CX, JEOL, Japan). The weathering tests for glass disks with and without coatings were carried out using a pressure cooker test chamber (TPC-441, Tabai-Espec, Japan). The noise levels were measured using a conventional optical disk tester.

## 3. RESULTS AND DISCUSSION

### 3.1. Organic additives for fine patterning

The organic additives examined in the previous study were listed in Table 1 with their chemical formulae and fine patterning characteristics.<sup>5</sup> Polyvinyl alcohol and cellulose acetate were not suitable because of their insufficient solubilities in the ethanol solutions. Hydroxypropyl cellulose produced gel films which were too hard to emboss fine patterns. In cellulose nitrate, fine patterns were formed on the glass substrates after the heat-treatment, but the optical transmission of the films obtained was low. This poor optical property of the films was due to pits and cracks, which were probably caused by the violent combustion of the additive during the heat-treatment. Formamide, which was studied intensively as a drying control chemical additive (DCCA), had much influence on the gelation of the sols but was not suitable for leaving fine patterns. On the other hand, polyether glycols such as polyethylene glycol (PEG) and polytetramethylene glycol were found to be the most suitable for fine patterning; they had sufficient solubilities in ethanol solutions and no influence on the transparency of the resultant glass films. The effects of the addition of PEG on the viscosity of the solution and on the hardness of the gel films are described in part (2) of this two-part paper.

Table 1. Organic additives examined and the patterning characteristics

Organic additives	Formula	Patterning	Remarks
Polyvinyl alcohol (PVA)	$-\{CH_2CH(OH)\}_n-$	×	Low solubility in alcohol
Cellulose acetate	$-\{C_6H_8O_3(OCOCH_3)_2\}_n-$	×	
Cellulose nitrate	$-\{C_6H_8O_3(NO_3)_2\}_n-$	△	
Hydroxypropyl cellulose (HPC)	$-\{C_6H_7O_5(C_3H_6OH)_3\}_n-$	×	Hard gel film
Polyethylene glycol (PEG)	$HO-(C_2H_4O)_n-H$	○	Good optical property
Polytetramethylene glycol (Terathane®)	$HO-(C_4H_8O)_n-H$	○	
Formamide	$HCONH_2$	×	Hard gel film

× : Failure      △ : Fair      ○ : Excellent

The amount of polyether glycols added to the coating solutions is one of the most important factors, which determine the characteristics of the patterns formed. As the content of polyether glycols in the gel films was increased, the time permitted to form patterns in the gel films was prolonged. However a large amount of polyether glycols caused large shrinkage of the films during the heat-treatment and made the obtained patterns dull. A decrease in the content of polyether glycols in the gel films made the gel films hard and shortened the time permitted for patterning. Under the conditions examined in the present study, the optimum weight ratio of PEG, of which average molecular weight is 600 (PEG600), to  $SiO_2$ - $TiO_2$  oxides is in the range from 0.75 to 1.0.

### 3.2. Refractive index of the films

Figure 3 shows the variations of refractive index of  $91SiO_2 \cdot 9TiO_2$  (in mol%) films with heat-treatment; open and closed circles are respectively for the films obtained without PEG and with the addition of PEG.<sup>9</sup> The weight ratio of PEG600 added to  $91SiO_2 \cdot 9TiO_2$  was unity. The refractive index of the film obtained without PEG almost agrees with that of the glass substrate (=1.51) after the heat-treatment at 400 °C; however, the index of the film with addition of

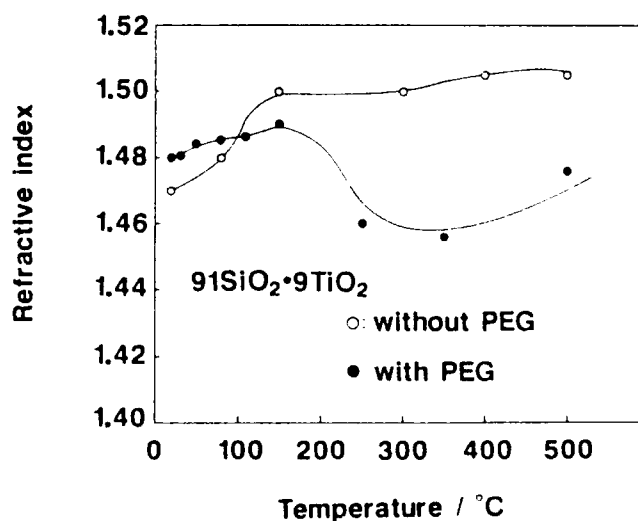


Fig.3. Variations of refractive index of  $91SiO_2 \cdot 9TiO_2$  films with heat-treatment; open and closed circles are respectively for the films obtained without PEG and with the addition of PEG. The weight ratio of PEG600 added to oxides is unity.



PEG is only about 1.47 even after the heat-treatment at 500°C. It has thus been found that the incorporation of PEG into SiO<sub>2</sub>-TiO<sub>2</sub> gel films led to much lower refractive index after the heat-treatment at temperatures over 300°C, which resulted from the increase in porosity of the films due to the decomposition and/or burning of PEG. The porosity and the refractive index of porous films can be related by the following equation;

$$(n_c^2 - 1)/(n^2 - 1) = 1 - P/100 \quad (2)$$

where  $n_c$  and  $n$  are refractive indices of porous coating films and nonporous bulk samples, respectively, and  $P$  is the percent porosity.<sup>10,11</sup> The porosity of the 91SiO<sub>2</sub>·9TiO<sub>2</sub> film obtained with addition of PEG can be calculated from equation (2) to be 17.8 % after the heat-treatment at 400°C for 15 min, assuming the pores of the film are filled only with air. In the calculation, the value (=1.54) of refractive index for the nonporous 91SiO<sub>2</sub>·9TiO<sub>2</sub> bulk glass was used by assuming the additivity in refractive index between SiO<sub>2</sub>(=1.46) and TiO<sub>2</sub>(=2.30). Accordingly, in order to prepare a SiO<sub>2</sub>-TiO<sub>2</sub> film with a refractive index of 1.51, which is for soda-lime-silica glass substrates, by adding PEG600 in the weight ratio of PEG600/oxides=1.0, we should choose the composition of about 83.5SiO<sub>2</sub>·16.5TiO<sub>2</sub> (in mol %) by assuming the porosity of 17.8%.

Figure 4 shows the variations of refractive index of the 83.5SiO<sub>2</sub>·16.5TiO<sub>2</sub> (in mol %) films with heat-treatment<sup>12</sup>; open and closed circles have the same meanings as in Fig. 3. For the films of this composition, a similar feature observed in Fig. 3, i.e. a large decrease in the refractive index resulting from the increase in porosity of the films due to the combustion of PEG, is seen. The refractive index of the as-coated films with addition of PEG is 1.50, and increases slightly from room temperature to 200°C and then decreases sharply down to 1.47 in a range of 200 to 300°C. The index of the films is about 1.51, which almost agrees with that of glass substrates, after the heat-treatment at 400°C, as estimated from their porosity and an additivity in refractive index between SiO<sub>2</sub> and TiO<sub>2</sub>. Thus the refractive index of the pregrooved layer, which is important to design optical memory disks, can be controlled by adjusting the TiO<sub>2</sub> content and heat-treatment conditions.

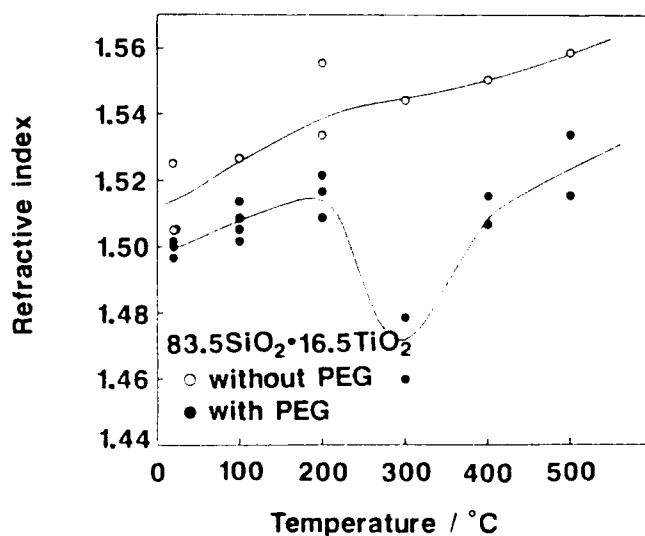


Fig.4. Variations of refractive index of 83.5SiO<sub>2</sub>·16.5TiO<sub>2</sub> films with heat-treatment; open and closed circles have the same meaning as in Fig.3.

### 3.3. Dimensions of pregrooves formed

Figure 5 shows the SEM cross-section of pregrooves fabricated on a glass disk of 130 mm in diameter by the present fine patterning technique. The chemical composition of the pregrooved layer, which was heat-treated at 350 °C, is  $83.5\text{SiO}_2 \cdot 16.5\text{TiO}_2$ , and the weight ratio of PEG600 added to the  $\text{SiO}_2$ - $\text{TiO}_2$  oxides was unity. The pitch of the fabricated pregrooves is 1.6  $\mu\text{m}$ , which precisely coincides with that of the stamper used; whereas the land height and land width of the pregrooves are 70 nm and 500 nm, respectively, which corresponded to 60 % and 85 % of those of the stamper. These results indicate that the shrinkage of the patterned gel films mainly occurs in the vertical direction, and the small shrinkage also occurs in the land width.

### 3.4. Weathering resistance

Weathering resistance of glass disks is very important for practical use of the optical memory disks. The weathering of glass substrates proceeds with the reaction of alkalis in the substrates with carbon dioxide and water in the atmosphere to form salts such as  $\text{Na}_2\text{CO}_3$ .<sup>13</sup> Figures 6 (a) and (b) show the photographs of the glass disks of 130 mm in diameter and 1.2 mm in thickness after weathering tests for chemically strengthened soda-lime-silica glass disks without coating (a) and coated with  $83.5\text{SiO}_2 \cdot 16.5\text{TiO}_2$  films (b); in the weathering test (b), the non-pregrooved films, about 220 nm thick, heat-treated at 350 °C for 15 min were used. The weathering tests were performed for 50 h at 135 °C and 90% R.H. using a pressure cooker test chamber.

The glass disk without coating is

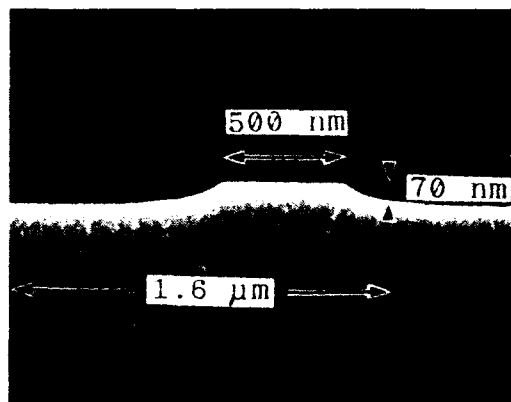


Fig.5. SEM cross-section of  $\text{TiO}_2$ - $\text{SiO}_2$  pregrooves fabricated on a glass disk of 130 mm in diameter by the present fine patterning technique.

(a)

(b)

Fig.6. Photographs of the chemically strengthened soda-lime-silica glass disks of 130 mm in diameter and 1.2 mm in thickness after weathering tests. (a) is for the disk without coating and (b) with  $83.5\text{SiO}_2 \cdot 16.5\text{TiO}_2$  coatings. The weathering tests were performed for 50 h at 135 °C and 90% R.H.

weathered to become opaque and its surface becomes very rough due to the generation of alkali reaction products (Fig. 6(a)). On the other hand, the disk with the coatings is transparent and homogeneous even after the weathering test (Fig. 6(b)). Finely patterned  $\text{SiO}_2\text{-TiO}_2$  layers formed by the sol-gel technique are thus expected to serve as not only pregrooves for optical memory disks but also as effective protective layers, i.e. alkali passivation layer for glass substrates, as well as the layer to control refractive index as described in section 3.2.

### 3.5. Noise levels of pregrooved glass disks

Figure 7 shows the frequency dependence of noise levels in the glass disks fabricated under optimum conditions. Open and closed circles show the disks with pregrooved  $83.5\text{SiO}_2\cdot 16.5\text{TiO}_2$  layer and with pregrooved pure  $\text{SiO}_2$  layer, respectively. The weight ratios of PEG600 added to  $83.5\text{SiO}_2\cdot 16.5\text{TiO}_2$  and  $\text{SiO}_2$  were 0.750 and 0.625, respectively. Each glass disk was heat-treated at  $350^\circ\text{C}$  for 15 min in air using a clean oven and coated with a metal film on the pregrooved layer as a reflective layer for measuring noise levels. The noise level of the glass disks with the pregrooved  $\text{SiO}_2\text{-TiO}_2$  layer is lower by 1-2 dB than that of the disks with pure  $\text{SiO}_2$  in the frequency range from 0.5 to 2.0 MHz. The lower noise level of the former can be ascribed mainly to the agreement in the refractive index between the pregrooved layer and the glass substrate.

Figure 8 shows the radial variation of noise levels for the fabricated glass disks at the 1.0 MHz. Open and closed circles have the same meanings as described in Fig.

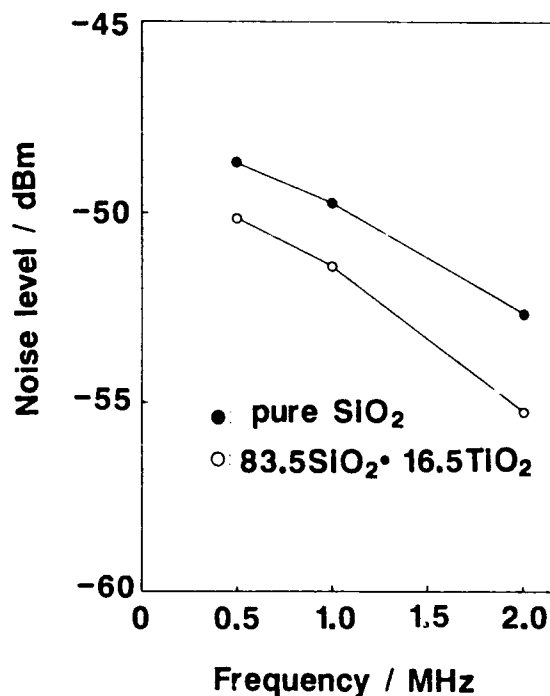


Fig.7. Frequency dependence of noise levels for the fabricated glass disks. Open and closed circles show the disks with pregrooved  $83.5\text{SiO}_2\cdot 16.5\text{TiO}_2$  layer and with pregrooved pure  $\text{SiO}_2$  layer, respectively.

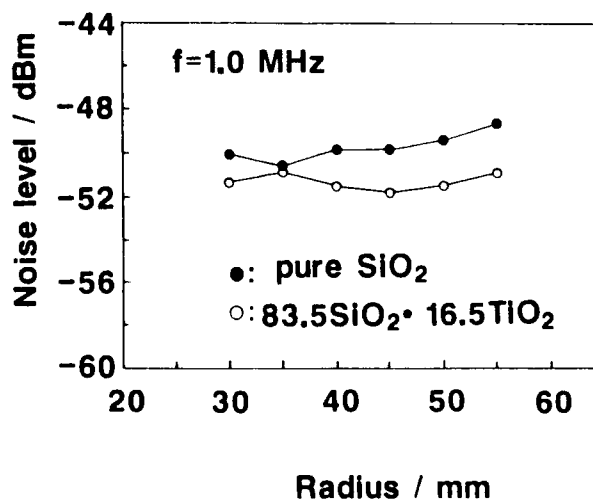


Fig.8. Radial variation of noise levels for the fabricated glass disks at the frequency of 1.0 MHz. Open and closed circles have the same meanings as described in Fig.7.

7. The noise levels of both disks show almost constant values at a given radius, which means that the uniform pregrooves are formed in the whole surface area in both disks of 130 mm in diameter. The noise levels are again 1-2 dB lower in the disks with the  $\text{SiO}_2\text{-TiO}_2$  layer than with the pure  $\text{SiO}_2$  layer.

#### 4. CONCLUSIONS

Pregrooves have been formed on soda-lime-silica glass substrates using polyethylene glycol(PEG)-containing  $\text{SiO}_2\text{-TiO}_2$  gel films and the qualities of the pregrooved glass disks were evaluated. The refractive index of the  $\text{SiO}_2\text{-TiO}_2$  pregrooved layer was matched with that of the glass substrates by adopting the chemical composition of  $83.5\text{SiO}_2\cdot 16.5\text{TiO}_2$  (in mol %) as the layer, in consideration of the porosity which resulted from the decomposition and/or burning of PEG added to the films. When the weight ratio of PEG with the average molecular weight of 600 to  $\text{SiO}_2\text{-TiO}_2$  oxides was unity, the pitch of the pregrooves formed was unchanged compared to that of the stamper used after the heat-treatment at  $350^\circ\text{C}$ , while the land height and the land width of the pregrooves were respectively reduced to 60% and 85% of those of the stamper after the heat-treatment. The  $\text{SiO}_2\text{-TiO}_2$  films provided the glass substrates with a good weathering resistance. The noise level of the glass disks with pregrooved  $\text{SiO}_2\text{-TiO}_2$  layer was lower than that of the disks obtained using pure  $\text{SiO}_2$  layer in the frequency range from 0.5 to 2.0 MHz. The lower noise level of the former can be ascribed to the agreement in refractive index between the pregrooved layer and the glass substrate. It was found that precise pregrooves were uniformly formed on the whole surface area of glass disks of 130 mm in diameter by the newly developed sol-gel fine patterning technique.

#### 5. ACKNOWLEDGEMENT

The authors thank Dr. H. Gokan, Dr. M. Yanagisawa and their colleagues in Functional Devices Research Laboratories of NEC Corporation for helpful discussions.

#### 6. REFERENCES

1. J. Henning, "Polymer Substrates for Optical Discs," Proc. Int. Symp. on Optical Memory, Jpn. J. Appl. Phys., vol.26, Supplement 26-4, pp.9-14, 1985.
2. K. Ohta, J. Hirokane, T. Inui, A. Takahashi, T. Deguchi and T. Okamoto, "Magneto-Optical Disk Substrate Prepared by Reactive Ion Etching," J. Vacuum Soc. of Jpn., vol.28, No.2, pp.77-81, 1985.
3. M. Miyagi, A. Iwasa and H. Yamasaki, "Pregrooved Disk Formed by Dry Etching Technique," Proc. Int. Symp. on Optical Memory, Jpn. J. Appl. Phys., vol.26, Supplement 26-4, pp.83-86, 1987.
4. K. Ohta, Y. Nagahara, J. Hirokane, K. Van and T. Inui, "Magneto-Optical Disk Prepared by Contact Printing (1)," Extended Abstracts (The 35th Spring Meeting); The Japan Society of Applied Physics and Related Societies, No.3, p.869, 29a-ZQ-2, 1988.
5. J. Hirokane, Y. Nagahara, K. Van, A. Takahashi, T. Inui and K. Ohta, "Magneto-Optical Disk Prepared by Contact Printing (2)," Extend-

ed Abstracts (The 35th Spring Meeting); The Japan Society of Applied Physics and Related Societies, No.3, p.869, 29a-ZQ-3, 1988.

6. N. Tohge, A. Matsuda, T. Minami, Y. Matsuno, S. Katayama and Y. Ikeda, "Fine-Patterning on Glass Substrates by the Sol-Gel Method," J. Non-Cryst. Solids, vol.100, pp.501-505, 1988.

7. N. Tohge, A. Matsuda, T. Minami, Y. Matsuno, S. Katayama and Y. Ikeda, "Formation of Organic Polymer-Containing Gel Films and Their Application to the Fine-Patterning Process," J. Ceram. Soc. Jpn., vol.96, No.12, 1127-1130, 1988.

8. A. Matsuda, Y. Matsuno, S. Katayama and T. Tsuno, "Weathering Resistance of Glass Plates Coated with Sol-Gel Derived  $9\text{TiO}_2 \cdot 91\text{SiO}_2$  Films," J. Mater. Sci. Lett., vol.8, pp.902-904, 1989.

9. A. Matsuda, Y. Matsuno, S. Katayama, T. Tsuno, N. Tohge and T. Minami, "Physical and Chemical Properties of  $\text{TiO}_2\text{-SiO}_2$  Films Derived from Polyether Glycol-Containing Gels," J. Am. Ceram. Soc. in press.

10. B. E. Yoldas, "Investigation of Porous Oxides as an Antireflective Coating for Glass Surfaces," Appl. Opt., vol.19, No.9, pp.1425-1429, 1980.

11. K. Kinoshita and K. Nishibori, "Porosity of  $\text{MgF}_2$  Films - Evaluation based on Changes in Refractive Index due to Adsorption of Vapors," J. Vac. Sci. Technol., vol.3, pp.730-733, 1969.

12. Y. Matsuno, A. Matsuda, S. Kataoka, S. Katayama and T. Tsuno, "Pre-Grooving on Glass Substrates for Optical Memory Disks by The Sol-Gel Method," Proc. 1st Jpn Int. SAMPE Symp., pp.295-300, 1989.

13. P. B. Adams, "Glass Corrosion," J. Non-Cryst. Solids, vol.67, pp.193-205, 1984.



Pregrooving on Glass Disks by the Sol-Gel Method (Part 2)-Effects of the Addition of Organic Polymers on the Formation of Glass Films in the  $\text{SiO}_2\text{-TiO}_2$  System

Atsunori Matsuda, Yoshihiro Matsuno, Shigeyuki Kataoka, Shinya Katayama, Toshio Tsuno, Noboru Tohge\* and Tsutomu Minami\*

Tsukuba Research Laboratory, Nippon Sheet Glass Co., Ltd.  
5-4 Tokodai, Tsukuba, Ibaraki 300-26, Japan

\* Department of Applied Chemistry University of Osaka Prefecture  
Mozu-Umemachi, Sakai, Osaka 591, Japan

### ABSTRACT

The effects of the addition of polyethylene glycol(PEG) on the formation of gel-derived glass films in the  $\text{SiO}_2\text{-TiO}_2$  system were studied, aimed at their application to the optical memory disks. The viscosity of the as-prepared sols increased almost linearly with increasing PEG content. The increase in viscosity of the sols during the storage was retarded with decreasing molecular weight of PEG added and with increasing amount of PEG added. The viscosity increase of the sols during the storage, however, showed a similar temperature dependence, i.e. almost the same apparent activation energy was obtained, in the sols containing different amounts of PEG. These findings indicate that PEG added to the  $\text{SiO}_2\text{-TiO}_2$  sols scarcely reacts with the hydrolyzed inorganic species. The hardness of the resultant PEG-containing gel films greatly decreased with increasing PEG content. The gel films containing PEG of the smaller average molecular weight showed the higher hardness and the steeper increase in hardness with increasing the heat-treatment temperature than those containing PEG of the larger average molecular weight. For a high performance in the fine patterning process and densification of the resultant patterned films, PEG of the smaller amount and the smaller molecular weight is favorable, provided the PEG-containing gel films are initially soft enough to emboss fine patterns by pressing a stamper. Incorporated PEG in the  $\text{SiO}_2\text{-TiO}_2$  gel films decomposed completely at temperatures over  $300^\circ\text{C}$  and had a very slight influence on chemical bondings in the resultant films.

### 1. INTRODUCTION

We have developed a fine patterning technique, based on the sol-gel method starting from metal alkoxides.<sup>1-3</sup> In part (1) of this two-part paper, the formation of pregrooves by the technique and the properties of the pregrooved glass disks were described. As described in part (1), when gel-derived  $\text{SiO}_2\text{-TiO}_2$  glass films were used for the formation of pregrooves, the resultant pregrooved glass disks showed excellent weathering resistance and a low noise level.

The key point of the fabrication of pregrooves by this technique is the patterning by pressing a stamper against the gel films, the hardness of which is controlled by incorporation of organic polymers

such as polyethylene glycol (PEG).<sup>1,2</sup> In this part (2), attention will be paid mainly to the effects of the addition of PEG on viscosity of the sols, hardness of the gel films and formation of the gel-derived glass films in the  $\text{SiO}_2$ - $\text{TiO}_2$  system.

## 2. EXPERIMENTAL

The starting solution was prepared from silicon tetraethoxide,  $\text{Si}(\text{OEt})_4$ , and titanium tetra-n-butoxide,  $\text{Ti}(\text{O-nBu})_4$ , in the same way as described in part (1). The chemical composition of  $83.5\text{SiO}_2$   $16.5\text{TiO}_2$  (in mol%) was chosen, since the refractive index of the resultant films of this composition with the addition of PEG agreed with that of glass substrates after a heat-treatment over  $350^\circ\text{C}$  and the pregrooved glass disks showed good characteristics as reported in part (1). The concentration of the equivalent oxides in the solution was 5.08 wt%, which produced the films of about 200 nm in thickness after a final heat-treatment at  $350^\circ\text{C}$  when the solution was spin-coated at 1500 rpm. Various amounts of PEG were added to the above solution and served as a coating solution. The average molecular weights of PEG examined were 200, 600, 1000 and 2000, which were hereafter designated as PEG200, PEG600, PEG1000 and PEG2000, respectively.

The viscosity of the coating solutions and its change during the storage at a given temperature were measured using a rotation viscometer (ELD, Tokyo Keiki, Japan). All the solutions were stored in screw-capped vials. The films were coated on soda-lime-silica glass plates for the measurement of the hardness and on silicon wafers for the IR spectra analysis by a dipping-withdrawing method in an ambient atmosphere. The coating films obtained were heat-treated at a given temperature for 15 min in air using an oven. The hardness of prepared films and its increase with the heat-treatment were measured using a dynamic ultramicrohardness tester (DUH50, Shimadzu, Japan). The hardness,  $H$ , of a film is given by

$$H = kW/D^2 \quad (1)$$

where  $W$  is the load applied to a stylus of the dynamic ultramicrohardness tester,  $D$  is the penetration depth of the stylus under the load  $W$  and  $k$  is  $3.858 \mu\text{m}^2 \cdot \text{mN}^{-1}$  which is a constant decided by the shape of the stylus. The variations of FT-IR spectra of the films during the heat-treatment were measured using an IR spectrophotometer (FTZ-20E/D-V, Digilab, England) in a transmission mode.

## 3. RESULTS AND DISCUSSION

### 3.1. Effects of PEG on the viscosity of sols

Figure 1 shows the viscosity of the as-prepared PEG-containing  $\text{SiO}_2$ - $\text{TiO}_2$  sols at  $25^\circ\text{C}$  against the PEG/oxides weight ratio. The viscosity of the sol increases linearly with increasing PEG content; these results, also observed in the  $\text{B}_2\text{O}_3$ - $\text{SiO}_2$  system<sup>1</sup>, indicate that additivity in viscosity holds for the sols prepared by the present procedure. When PEG of the larger molecular weight is added to the sol,

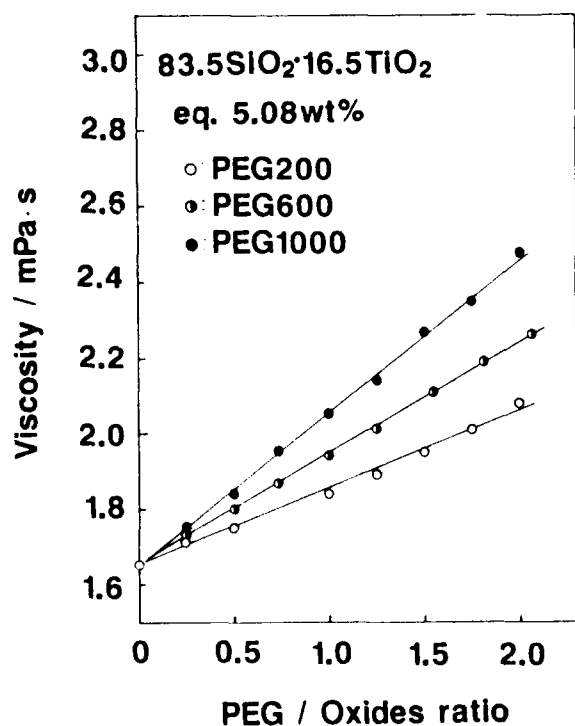


Fig.1. Viscosity of the as-prepared PEG-containing  $\text{SiO}_2\text{-TiO}_2$  sols at  $25^\circ\text{C}$  against the PEG/oxides weight ratio. Open, half-closed and closed circles show PEG of average molecular weight of 200, 600 and 1000, respectively.

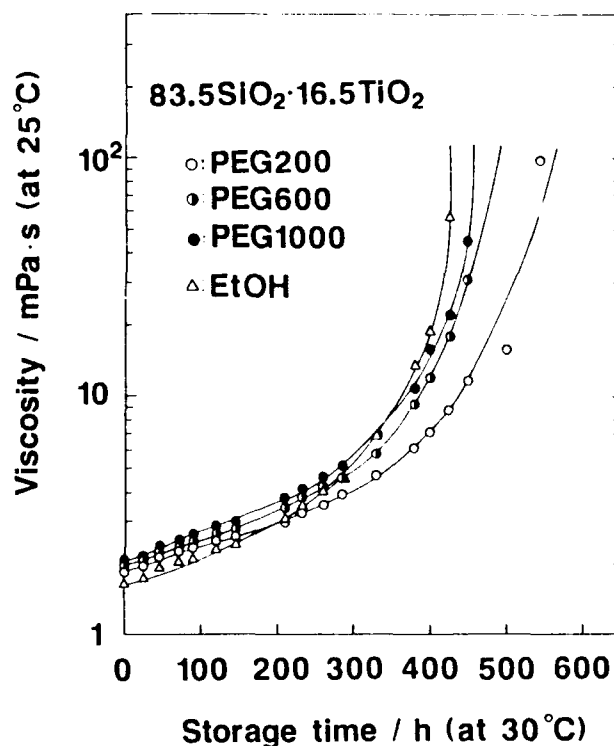


Fig.2. Variations in viscosity of the PEG-containing sols stored at  $30^\circ\text{C}$  as a function of storage time. The viscosity of the solutions was measured at  $25^\circ\text{C}$ . Open, half-closed and closed circles have the same meanings as in Fig.1 and triangles show ethanol. For each sols, the additive/oxides weight ratio is unity.

the sol shows the steeper slope, since the intrinsic viscosity of PEG of larger molecular weight, of course, is higher than that of PEG of smaller molecular weight.

Figure 2 shows the changes in viscosity of the PEG-containing sols stored at  $30^\circ\text{C}$  as a function of storage time. The viscosity of the sols was measured at  $25^\circ\text{C}$ . For each molecular weight of PEG, the weight ratio of PEG added to oxides in the solution was unity. An equal amount of ethanol in place of PEG was also added to the solution and the change in its viscosity was examined for comparison. PEG slows down the viscosity increase during the storage and delays the gelation time in comparison with even ethanol; this finding can be ascribed to the hindrance effects of PEG on the polymerization of hydrolyzed species. PEG of the smaller molecular weight is more effective to hinder the polymerization reaction and to decelerate an increase in viscosity during the storage than PEG of the larger molecular weight.



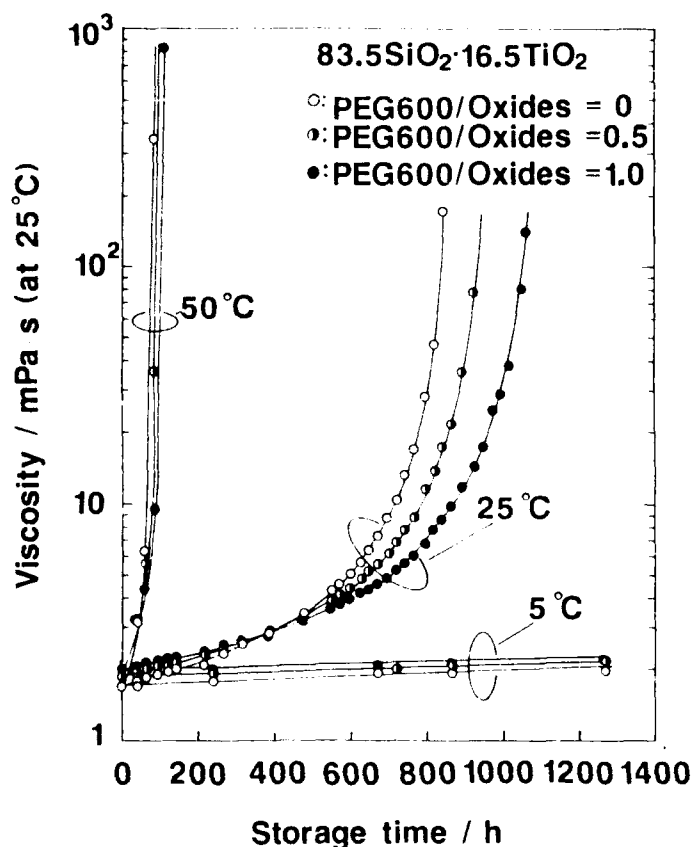


Fig.3. Variations in viscosity of the sols containing different amounts of PEG600 as a function of storage time at temperatures 5, 25 and 50 °C. Open, half-closed and closed circles represent PEG600/oxides weight ratio= 0, 0.5 and 1.0, respectively.

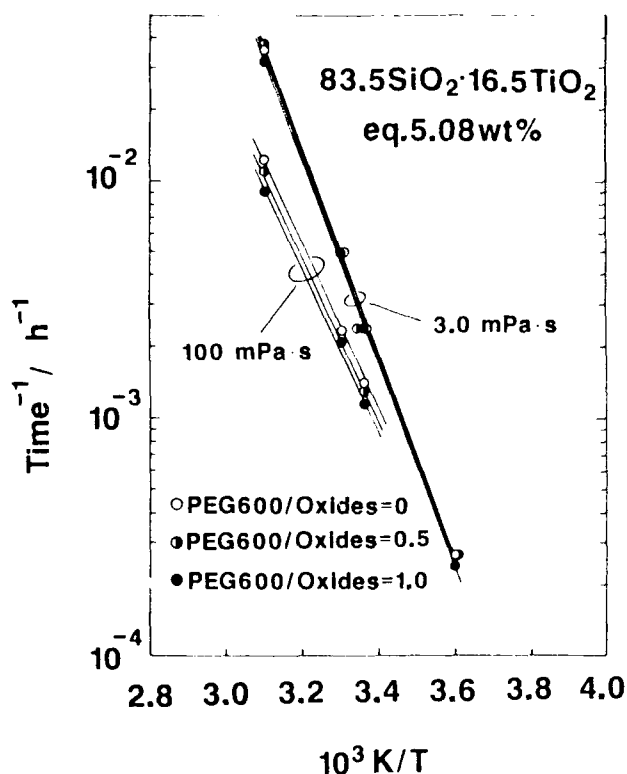


Fig.4. Temperature dependencies of the inverse of the time at which the viscosity of the sols becomes a given value, 3.0 and 100 mPas. Open, half-closed and closed circles have the same meanings as in Fig. 3.

Figure 3 shows the variations in viscosity of the sols containing various amounts of PEG600 as a function of storage time at various temperatures. Open, half-closed and closed circles represent PEG600/oxides weight ratio= 0, 0.5 and 1.0, respectively. At each storage temperature, the increase in viscosity of the sols during the storage slows down and the gelation time of the sols is delayed with increasing PEG content. The storage temperature shows the great effect on the viscosity increase of the sols; as the storage temperature is increased, the viscosity of the sols is drastically increased with time.

The temperature dependence of the viscosity increase is further discussed on the basis of the time at which the viscosity of the sols becomes a given value. In Fig. 4 the inverse of the time at which the viscosity equals 3.0 and 100 mPas is plotted against the reciprocal of absolute temperature. Open, half-closed and closed circles have the same meanings as in Fig. 3. The slope is nearly the same, i.e. almost

the same apparent activation energy for polymerization is obtained in the sols containing different amounts of PEG. This finding indicates that the increase in viscosity of the sols during the storage depends not on the reaction between PEG and hydrolyzed inorganic species but on the polymerization of hydrolyzed inorganic species. From the results observed in Fig.1 and Fig.4, we can conclude that PEG added to the  $\text{SiO}_2\text{-TiO}_2$  solution scarcely reacts with the hydrolyzed inorganic species.

### 3.2. Effects of PEG on hardness of gel films

The feasibility of the patterning greatly depends on the hardness of gel films. Accordingly, the quantitative investigation of the effects of PEG on hardness of the resultant gel films is very important on application of this patterning technique to the pregrooving of glass substrates. Figure 5 shows hardness of the gel films containing various amounts of PEG of different molecular weights. Open, half-

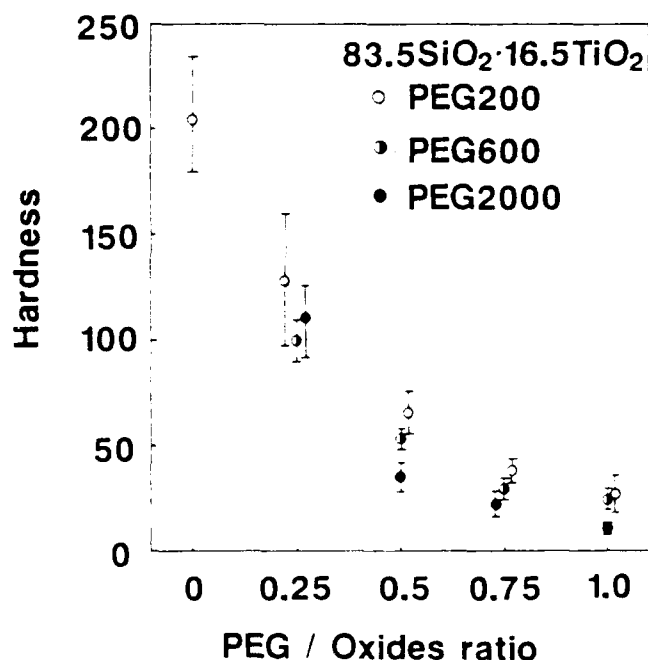


Fig.5 Hardness of the gel films containing various amounts of PEG of different molecular weight. Open, half-closed and closed circles represent the gel films containing PEG200, PEG600 and PEG2000, respectively. All the gel films were formed from as-prepared coating solutions and heat-treated at 50 °C for 15 min.

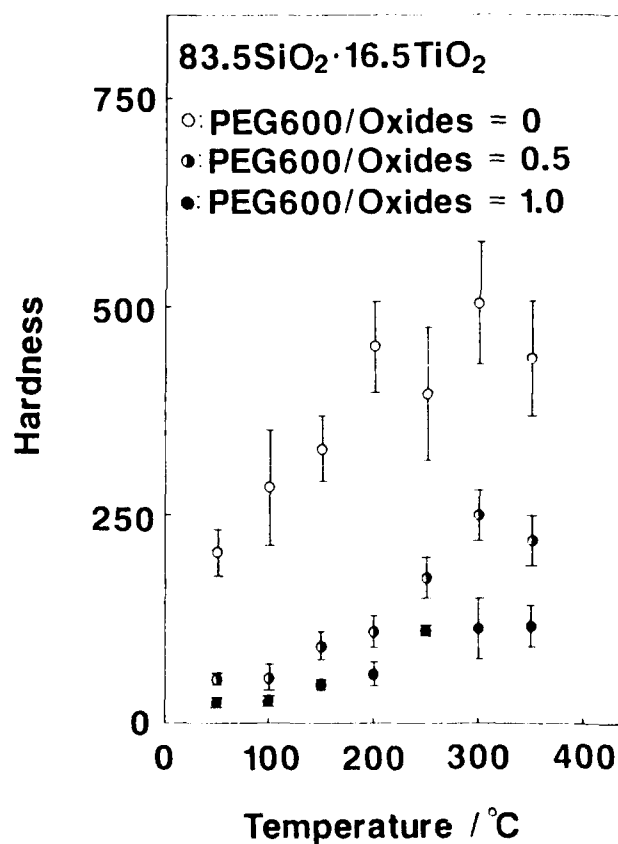


Fig.6. Comparison of hardness of the films containing different amounts of PEG600 as a function of heat-treatment temperature. Open, half-closed and closed circles represent PEG600/oxides weight ratio= 0, 0.5 and 1.0, respectively.

closed and closed circles represent the gel films containing PEG200, PEG600 and PEG2000, respectively. All the gel films were formed from as-prepared coating solutions and heat-treated at 50°C for 15 min because as-coated gel films were too soft to measure their hardness. The values for these films were obtained under the load of 0.245 mN; the load-penetration curve gave almost constant values of hardness in the load-range of 0 to 4.9 mN examined. It is seen that the addition of PEG drastically decreases hardness of the resultant gel films and PEG of larger molecular weight is somewhat effective for the reduction of hardness of the films than PEG of smaller molecular weight.

In the fine patterning technique, the gel film is pressed with a stamper and preheated at an appropriate temperature until the gel film is solidified. When the increase in hardness of the gel films during the preheat-treatment is small, the embossed patterns are dulled out after removing the stamper. The hardening property of the gel films is thus also an important factor, which determines the performance of this patterning process. The hardening process of the gel films is affected by the amount and average molecular weight of the PEG added.

Figure 6 shows the comparison of hardness of the films containing various amounts of PEG600 as a function of temperature heat-treated for 15 min. Open, half-closed and closed circles represent the weight ratios of PEG600 to oxides of 0, 0.5 and 1.0, respectively. As the temperature increases, hardness of all the films increases and tends to level off over 300°C. At a given temperature hardness of the films containing the larger amount of PEG is lower than that of the films containing the smaller amount of PEG. At temperatures below 200°C, PEG added remains in the gel films; thus, PEG should prevent the development of structure in the gel films by dispersing polymerizing species. After a heat-treatment over 300°C, PEG added decomposes completely; the decomposition of PEG generates pores in the gel films and decreases hardness of the films.

Figure 7 shows the variations of hardness of the films obtained with the addition of PEG

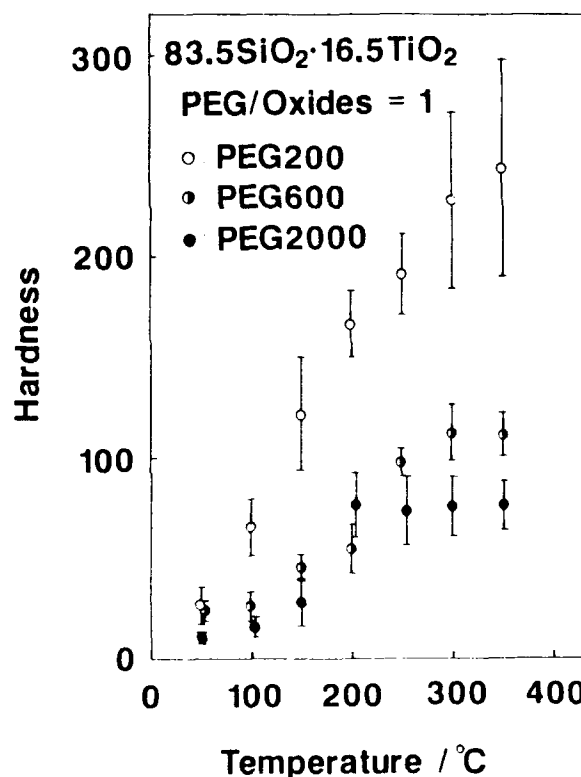


Fig.7. Variations of hardness of the films obtained with the addition of PEG of different molecular weight as a function of heat-treatment temperature. Open, half-closed and closed circles have the same meanings as in Fig.5. For all the films, PEG/oxides weight ratio is unity.

of different molecular weight as a function of heat-treatment temperature. The films were heat-treated for 15 min at each temperature. Open, half-closed and closed circles represent the gel films containing PEG200, PEG600 and PEG2000, respectively. For all the films, the weight ratios of PEG added to oxides were unity. When PEG of the smaller molecular weight is added, the gel films obtained show the higher hardness and the steeper increase in hardness with increasing the heat-treatment temperature.

The addition of large amount of PEG caused large shrinkage of the films during the heat-treatment and made the patterns obtained dull and porous in the fine patterning process. Moreover gel films containing PEG of the smaller molecular weight show the steeper increase in hardness with an increase of the heat-treatment temperature and produce the more densified gel-derived glass films. From the above points of view, PEG of the smaller amount and the smaller average molecular weight is favorable for a high performance in the patterning process and for densification of the resultant patterned films provided the PEG-containing gel films are initially soft enough to emboss fine patterns by pressing a stamper.

### 3.3. Effects of PEG on structure of the films

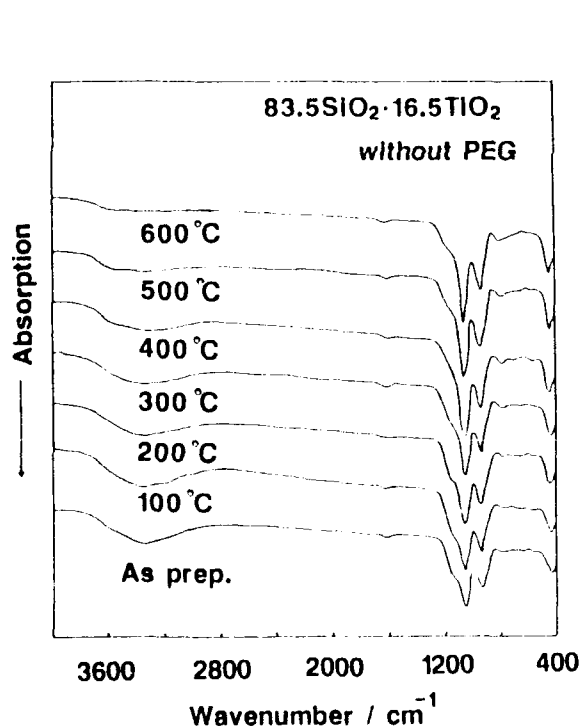


Fig.8. IR absorption spectra of the 83.5SiO<sub>2</sub>·16.5TiO<sub>2</sub> films obtained without PEG as a function of heat-treatment temperature. All the films were heat-treated at each temperature for 15 min.

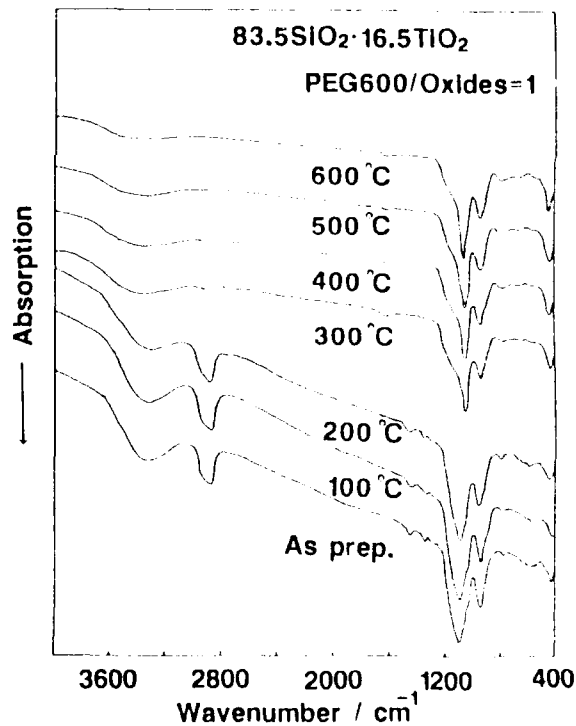


Fig.9. IR absorption spectra of the 83.5SiO<sub>2</sub>·16.5TiO<sub>2</sub> films obtained with the addition of PEG600, the weight ratio of PEG to the oxides being unity, as a function of heat-treatment temperature. All the films were heat-treated at each temperature for 15 min.

In this patterning technique, the patterned gel films are heat-treated to decompose PEG in the films and to be densified. The decomposition temperature of PEG in the gel films is important to determine the minimum heat-treatment temperature in the fine patterning process. Moreover the structure of the gel films and its change with heat-treatment are essential to the understanding of the behavior of PEG in the gel films. Figures 8 and 9 show the IR absorption spectra of the  $83.5\text{SiO}_2 \cdot 16.5\text{TiO}_2$  films obtained without PEG and with the addition of PEG600 as a function of heat-treatment temperature; the weight ratio of PEG to the oxides was unity. In Fig. 8, the strongest absorption peak is seen at around  $1100\text{cm}^{-1}$ , which is due to Si-O-Si bonds.<sup>4,5</sup> The peaks related to Si-O-Si bonds are also observed at 800 and  $440\text{cm}^{-1}$ .<sup>4,5</sup> The broad absorption peak due to O-H bondings can be seen at around 3800 to  $3000\text{cm}^{-1}$ .<sup>5</sup> The absorption peak at  $950\text{cm}^{-1}$  was found to be the overlapping of the band due to Si-OH bonds<sup>6</sup> and the band due to Si-O-Ti bonds.<sup>7</sup> In Fig. 9, additional new peaks such as the strong peak at  $2900\text{cm}^{-1}$ , the weak peaks at 1450 and  $1340\text{cm}^{-1}$ , and the shoulder at around  $1200\text{cm}^{-1}$ , which are respectively assigned to C-H,  $-\text{CH}_2-$  and C-O-C bonds in PEG,  $(\text{HO}(\text{CH}_2\text{CH}_2\text{O})_n\text{H})$ , are observed.<sup>8</sup> These peaks and the shoulder associated with PEG decrease with increasing heat-treatment temperature and disappear over  $300^\circ\text{C}$ . The spectra of the films obtained with addition of PEG almost agree with those of the films obtained without PEG after the heat-treatment over  $300^\circ\text{C}$ , indicating that the addition of PEG to the  $\text{SiO}_2\text{-TiO}_2$  sols has a very slight influence on chemical bondings in the resultant films after the decomposition of PEG.

#### 4. CONCLUSIONS

In this part (2), attention was paid mainly to the effects of the addition of PEG on viscosity of the sols, hardness of the gel films and formation of the gel-derived glass films in the  $\text{SiO}_2\text{-TiO}_2$  system. The viscosity of the as-prepared sols increased almost linearly with increasing PEG content. The increase in viscosity of the sols during the storage was retarded with the decrease in molecular weight of PEG added and with the increase in amount of PEG added. The addition of PEG to the sols, however, affected very slightly the temperature dependence of the viscosity increase of the sols during the storage. These findings indicate that PEG added to the  $\text{SiO}_2\text{-TiO}_2$  sols scarcely reacts with the hydrolyzed inorganic species. The hardness of the resultant PEG-containing gel films greatly decreased with increasing PEG content. The gel films containing PEG of the smaller average molecular weight showed the higher hardness and the steeper increase in hardness with increasing the heat-treatment temperature than those containing PEG of the larger average molecular weight. For a high performance in the fine patterning process and densification of the resultant patterned films, PEG of the smaller amount and the smaller molecular weight is favorable, provided the PEG-containing gel films are initially soft enough to emboss fine patterns by pressing a stamp. Incorporated PEG in the  $\text{SiO}_2\text{-TiO}_2$  gel films decomposed completely at temperatures over  $300^\circ\text{C}$  and had a very slight influence on chemical bondings in the resultant films.

## 5. ACKNOWLEDGEMENT

The authors thank Dr. H. Gokan and Dr. M. Yanagisawa and their colleagues in Functional Devices Research Laboratories of NEC Corporation for helpful discussions.

## 6. REFERENCES

1. N. Tohge, A. Matsuda, T. Minami, Y. Matsuno, S. Katayama and Y. Ikeda, "Fine-Patterning on Glass Substrates by the Sol-Gel Method," J. Non-Cryst. Solids, vol.100, pp.501-505, 1988.
2. Y. Matsuno, A. Matsuda, S. Kataoka, S. Katayama and T. Tsuno, "Pre-Grooving on Glass Substrates for Optical Memory Disks by The Sol-Gel Method," Proc. 1st Japan International SAMPE Symposium, Nov.28-Dec.1, pp.295-300, 1989.
3. A. Matsuda, Y. Matsuno, S. Katayama and T. Tsuno, "Weathering Resistance of Glass Plates Coated with Sol-Gel Derived  $9\text{TiO}_2 \cdot 91\text{SiO}_2$ ," J. Mater. Sci. Lett., vol.8, pp.902-904, 1989.
4. R. Hanna, "Infrared Absorption Spectrum of Silicon Dioxide," J. Am. Ceram. Soc., vol.48, No.11, pp.595-599, 1965.
5. M. Nogami and Y. Moriya, "Non-Crystalline Material Similar to Fused Silica from  $\text{Si}(\text{OC}_2\text{H}_5)_4$ ," J. Ceram. Soc. Jpn., vol.87, pp.37-42, 1979.
6. K. Kamiya, S. Sakka and M. Mizutani, "Preparation of Silica Glass Fibers and Transparent Silica Glass from Silicon Tetraethoxide," J. Ceram. Soc., Jpn., vol.86, No.11, pp.552-559, 1978.
7. S. P. Mukherjee, "Sol-Gel Process in Glass Science and Technology," J. Non-Cryst. Solids, vol.42, pp.477-488, 1980.
8. A. D. Cross and R. A. Jones, "An Introduction to Practical Infra-Red Spectroscopy, Edited by Butter Worth & Co., Ltd., London, 1969.



New developments in sol-gel imaging

Nicholas J. Phillips

Reader in Physics  
Loughborough University of Technology  
Loughborough, Leicestershire, LE11 3TU, UK

### ABSTRACT

This paper addresses the properties of sol-gel silica in relation to its potential to provide new devices for optical imaging. Although the sol-gel method opens the door to unprecedented levels of purity of silica materials, it is also beset with problems of the achievement of extreme optical homogeneity. The work reported discusses experiences with sol-gel silica intra cavity elements in ion lasers and new concepts of imaging and laser structures based on fabrication via porous gel-silica. A new physical model for etalons is proposed which shows advantages of porous gel-silica over conventional fully dense materials.

### 1. INTRODUCTION

The pioneering efforts of Hench and co-workers has led to the development of interesting new optical materials based on ultra-pure silica. Such materials were assumed initially to be reasonably homogeneous and largely devoid of the thermal expansion associated with normal high temperature prepared silica products. Further study has shown that optical homogeneity can be a problem and that the thermal properties are in need of new levels of study.

Work on the intra cavity uses of sol-gel derived silica began in the author's laboratory some three years ago and has continued via support from the S.D.I.O. programme.

A notional view of sol-gel silica, that it can offer a simple solution to the problems of colour centre formation and loss in u.v. ion lasers, was implanted in the author by the observation of unusual levels of conversion efficiency (single line to single mode) when a sol-gel etalon was placed in the cavity of an ion laser.

Observations were made by N.J. Phillips and L. Hench that an uncoated gel-silica Fabry Perot etalon, planar in form, placed in the cavity of an ion laser was capable of creating a single mode of laser output at a level of about 85% or more of the original single spectral line output.

This observation was documented and photographed at the time (c 1987) and led to a concerted programme of study to find the origins of the improvement over the more conventional 50% associated with normal high temperature prepared silica etalons.

It must be remembered that ion laser output radiation carries a heavy cost penalty and that improvements of the type discussed are of great practical and commercial significance.

In the intervening period, studies of carefully prepared gel-silica monoliths have been undertaken inside and outside an ion laser cavity by the author and graduate student (S. Modica) at the Loughborough University facility.

Our work has been directed at trying to find whether there are real bonuses from sol-gel silica in ion lasers or whether our initial observation was lucky and difficult to repeat.

Because of the developmental work involved in the preparation of early samples of gel-silica it has taken a great deal of patience to reach a state of play with the materials, that can lead to a true understanding of their properties. Our findings are

92-11407



that homogeneity is a big problem for intra cavity optics because of the optical feedback situation involved in the laser. Thus deficiencies of optical windows, prisms and etalons are many times more important than for extra-cavity optics.

We have sought to compare the performance of conventional high temperature prepared silica and gel-silica samples. Theoretical study and experiment has led to the conclusion that the real reason for the anomalous performance of the early gel-silica samples was for reasons related to their primitive quality which are explained in this paper.

Following the author's interest in holography and lithography using imaging polymers, it has been a natural trend to investigate uses for sol-gel derived silica in novel forms of imaging or image forming devices and some of these topics are discussed in this paper.

## 2. DEVELOPMENTS IN INTRA CAVITY OPTICAL ELEMENTS FOR ION LASERS USING SOL-GEL DERIVED SILICA

The anomalous performance of etalons described in the introduction has been the driving force for a detailed study of intra cavity elements in ion lasers. The mode selecting etalon conventionally used to create a single mode (and hence long coherence) output is shown in Figure 1.

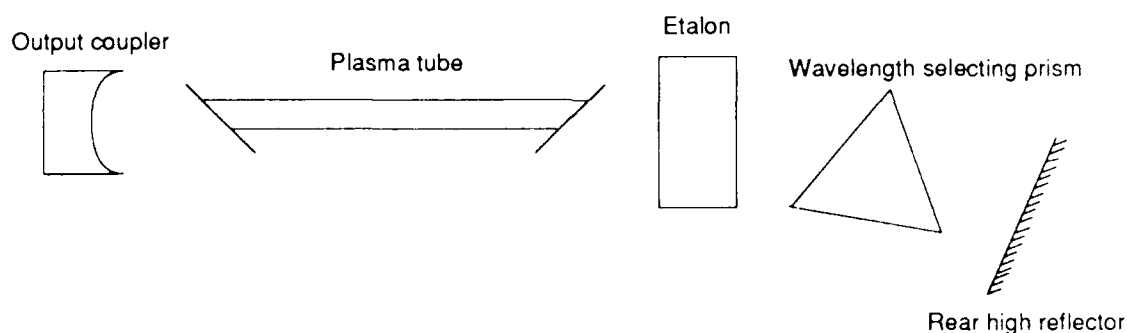


Fig. 1. Conventional ion-laser cavity with mode selecting etalon.

The normal wisdom for the performance of such etalons is that they should be of low finesse for intra cavity applications (since a multiple feedback situation is involved) and should have a free spectral range such that the periodicity of their transmittance roughly equals the width of the gain profile of the laser.

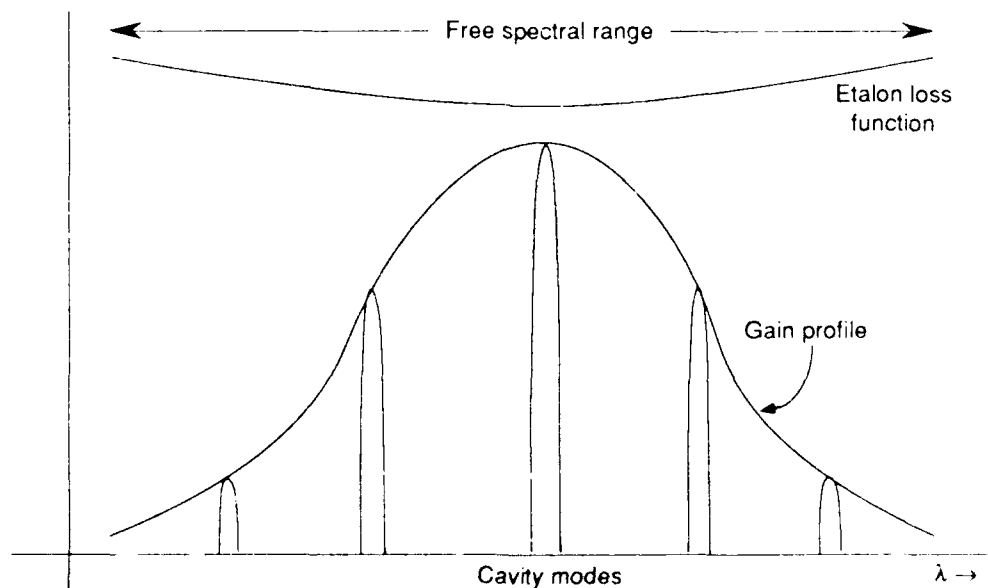


Fig. 2. Free spectral range is matched to gain profile.



If the transmittance is maximised for a given mode then the neighbouring modes can be extinguished by a slight comparative loss.

We note that this control is normally effected by the resonant conditions in the etalon and that there is apparently no reason why sol-gel etalons should perform differently to high temperature prepared silica etalons.

A detailed theoretical study has revealed that longitudinal refractive index gradients (over distances large by comparison with the wavelength of light) in the etalon only influence the single pass phase shift.

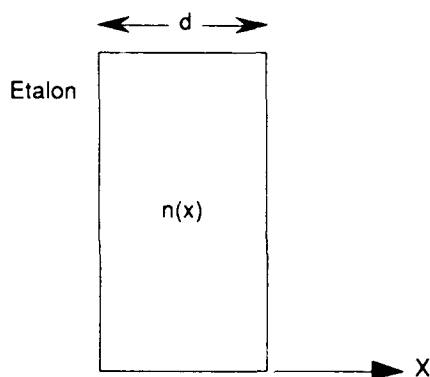


Fig. 3. Axial refractive index gradients over distances  $\gg \lambda_a$  merely alter the single pass phase shift

$$\frac{2\pi}{\lambda_a} n_0 d \rightarrow \frac{2\pi}{\lambda_a} \int_0^d n(x) dx$$

$\lambda_a$  = wavelength in air

$n_0$  = spatially uniform index

This shows that in substance, the theory of the etalon is not significantly changed in relation to its mode selection when weak axial index gradients are present.

Transverse index gradients (orthogonal to the optical axis of the laser) can introduced lensing effects but in a somewhat complex and unpredictable way. A study of their role has not revealed a significant improvement in the mode selecting activity.

The normal attitude of an etalon intra cavity in an ion laser is tipped off orthogonality as shown in the diagram below

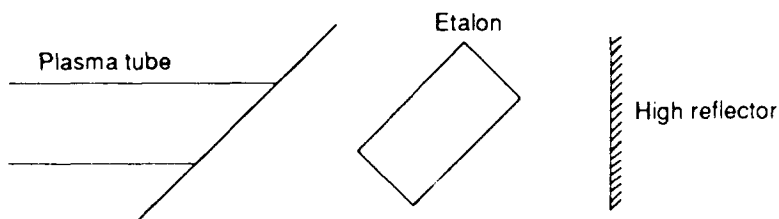


Fig. 4. Etalons used intra cavity in an ion laser are tipped off orthogonality to avoid unwanted lasing off the etalon's surface.

The typical intra cavity etalon has to have a 20% intensity reflectance at each face to provide a deep enough loss curve (high enough finesse) to extinguish the unwanted modes. If such a reflector is lined up orthogonal to the laser's optical axis then commonly lasing takes place between the front surface of the etalon and the output coupler. Tipping the etalon avoids the problem but of course introduces a loss mechanism into the optical cavity. It is largely this constraint that limits the conversion efficiency of the etalon. Relatively expensive curving of the etalon's surface can help to affect this stable cavity problem but adds considerably to the cost and difficulty of manufacture.

As a general comment, we have observed that later samples of gel silica with perfected densification have shown very low levels of Rayleigh scatter due to voids. Early specimens of the material — in particular those provided by Professor Hensch in 1987 — showed notable scatter especially in the intense intra cavity light of the laser.

We propose that the reason for the anomalous performance of early sol-gel etalon samples was due in fact to the presence of micropores. The effect of pore scatter being to introduce an intra cavity loss mechanism which is different in manifestation to that involved in the conventional etalon.

We propose a new model for the etalon as outlined in Figure 5.

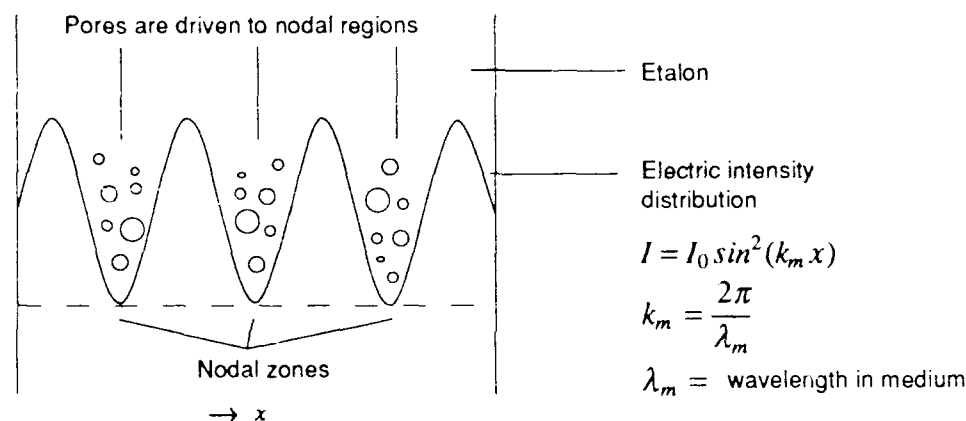


Fig. 5. Proposed etalon mechanism for porous gel silica. Pores are driven towards the nodes of the pattern, leading to index modulation of the etalon. This index modulation is not synergistic with other modes. Finesse is thus self enhancing.

If we consider the electric intensity distribution in the etalon, it is of the Lippmann type i.e. a standing wave pattern of spatial period equal to  $\lambda_m/2$  where  $\lambda_m$  is the wavelength in the medium.

Scattering centres (micropores) are thus subject to large forces which can cause them to migrate and create a spatially periodic index pattern in the solid material. We note that this pattern is of a spatial structure representative of a single mode of the laser. Other modes will not be synergistic with this index pattern and will thus be subject to enhanced loss.

By the above discussion, we can see that the establishment of a single mode condition in the laser is self enhancing.

Such movement of particles in intense laser beams has been observed in the intra cavity interspace between the plasma tube and other components and usually manifests itself in the collection of macromolecules near the beam centre. The intensity is of course subject to both radial and axial gradients. The intra cavity light is a standing wave pattern in a resonator. Thus the largest forces are of axial direction since the intensity changes axially over a distance of the order of  $\lambda_m/4$ . An examination of the problem shows that if  $n_p$  is the refractive index of the pore and  $n_s$  is the index of the bulk silica then

- (a) for  $n_p < n_s$  the pores will move to regions of lower intensity and
- (b) for  $n_p > n_s$  the pores will move to regions of higher intensity.

This proposed mechanism explains very fully the observed phenomena associated with the early anomalous performance of uncoated sol-gel etalons. We note also that

- (a) The uncoated etalon does not risk lasing off its front surface — it exhibits only the  $((n - 1)/(n + 1))^2$  intensity reflectance associated with the refractive index  $n$ .
- (b) Cavity losses can be enhanced by Rayleigh scatter but can, in the case of sol-gel derived silica, be controlled through pore fraction and size. Passive behaviour of pores is simply to enhance Rayleigh scatter and thus induce cavity losses. Such behaviour would **decrease** not **enhance** the finesse.

These facts probably explain the performance of the early gel-silica samples and will clearly form the basis of a new attack on the problem.

We note that the tipped etalon exhibits a **minimal** loss at the Fresnel level or at the level dictated by its enhanced reflectance. Pore scatter can be controlled from virtually nothing up to very high levels.

We conclude this section with the belief that porous silica etalons offer a new line of attack on cavity mode selection. **That pore scatter is potentially a problem is obvious. However, the achievement of a scattering level with such tight control might be difficult by any other known means!**

### 3. NOVEL IMAGING METHODS USING POROUS SILICA

The subject of holography owes much of its success to the influence of recording in ultra-fine grain silver halide media. More recently however skills with real time polymers such as those made by DuPont have opened up new vistas of recording potential.

Most common holographic media are coated in relatively thin layers on to a variety of substrate materials. Thus the halide layers are typically 5  $\mu\text{m}$  to 15  $\mu\text{m}$  thick.

Dichromated gelatin layers have been coated up to several hundred  $\mu\text{m}$  thick but are tricky to handle and very problematic with respect to humidity unless carefully sealed.

Very thick layers of DuPont photopolymer up to 100  $\mu\text{m}$  have been coated and in fact date back to the early 1970s when the material was first released.

Holograms which are very thick exhibit fascinating optical properties. Thus a **thin** transmission hologram made with monochrome light is subject to dispersive replay in white light.

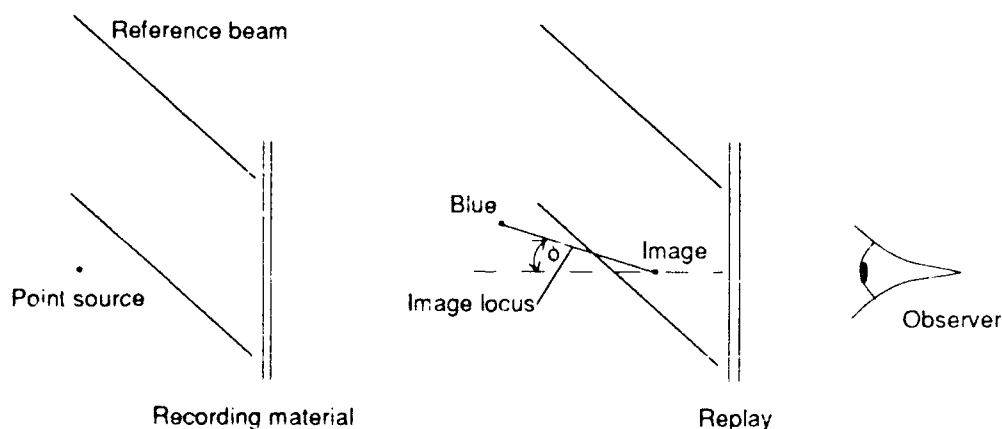


Fig. 6. Showing the replay of a monochromatically recorded 'thin' hologram using white light. The image of the point source smears into a line sloped at the 'achromatic angle'  $\delta$  ( $\tan \delta = \sin \theta$ ).

Thin holograms cannot therefore replay simply in white light.

Thick holograms become angle and wavelength selective.

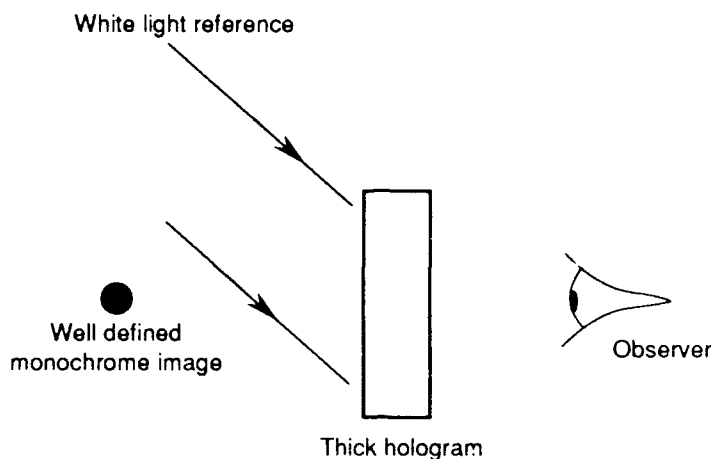


Fig. 7. Thick holograms are selective of angle and wavelength. With sufficient thickness, the hologram will only replay at the recorded reference angle and at the same wavelength as that used in the recording.

This "thick" replay property makes possible the selection of narrow band replay light from a broad spectrum source so as to create a non-blurred image.

Perhaps, more importantly, we can feed the reference light through the edge of a thick hologram:

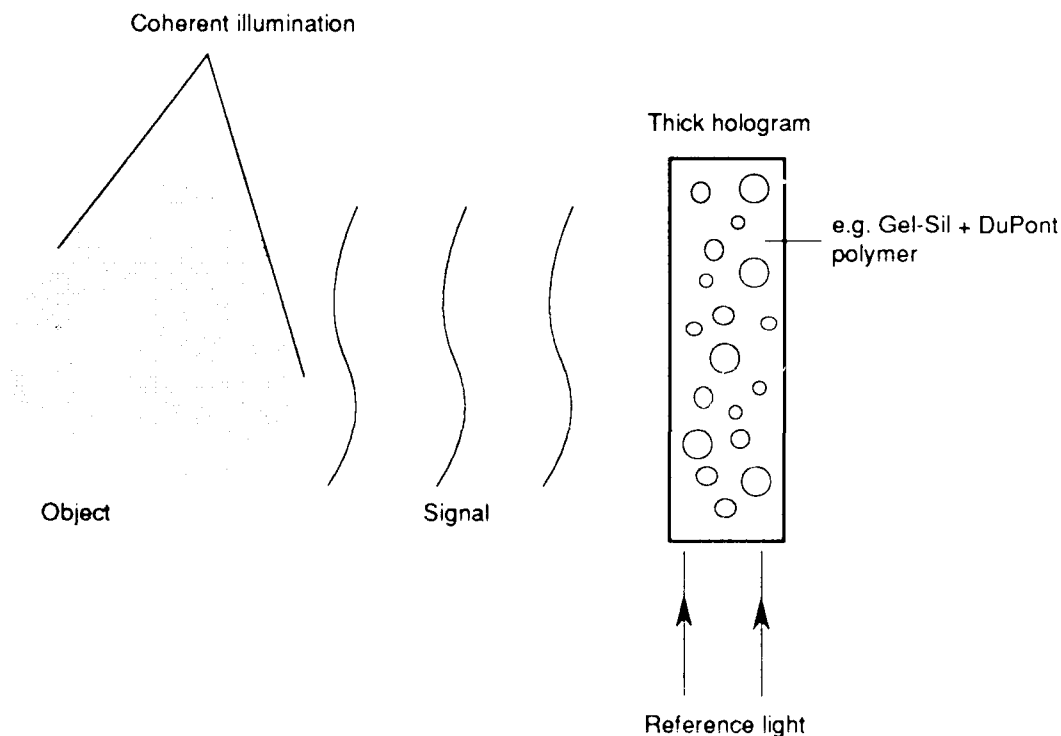


Fig. 8. Edge-lit holograms offer discrete lighting for signs, facia instructions in cars etc.

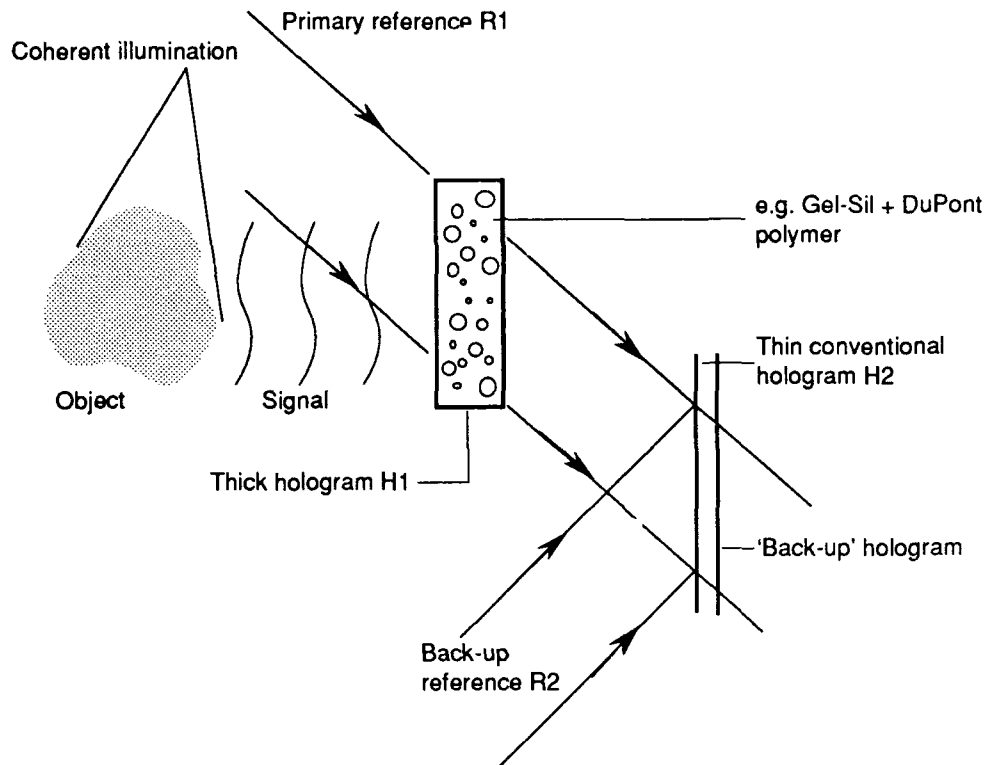


Fig. 9. Very thick holograms probably need a 'back-up' hologram for phase conjugation purposes. This can compensate for distortions of reference R1 in passing through the thick medium. The conjugate R1 can be created using conjugate ray tracing from H2.

Edge-lit holograms can be formed by merely coating the recording material on to a plain substrate but the true volume conversion of the reference to the signal wave is only possible in the configuration of Figure 8. In Figure 9, we see a possible 'back-up' device for very thick holograms to ensure conjugate ray tracing on replay.

Note that an ideal medium for recording holograms can be made from DuPont's polymer embedded in the pores of gel-silica.

Such pore filling techniques invoke scatter reduction if the refractive index of the polymer matches that of the silica. For the DuPont medium and silica, the refractive indices match closely (1.5 — 1.48 respectively) and considerable pore scatter reduction is possible.

Looking at the necessary characteristics of the polymeric medium, we see that the usual variable index polymer formulation involving

#### Binder + Monomer + Initiator + Sensitizer

probably needs to be maintained. In the pores of the silica host, if the monomer moves then it must displace the binder or net movement of molecules will result and possible rupture of the host may take place.

Very thick holograms are almost certain to have problems of distortion of the reference wave on passage through the layer. We propose to overcome this difficulty by the introduction of a thin 'perfect' hologram which is used to recreate the conjugate of the distorted thick reference wave after transmission through the layer, the so called 'back-up hologram'.

#### 4. NOVEL DEVICES FOR OPTICAL COMMUNICATIONS USING POROUS SILICA-POLYMER TECHNOLOGY

The final area of discussion for this paper relates to possibilities offered by sol-gel polymer technology in the area of distributed feedback lasers.

The distributed feedback laser can be understood from the sketch below

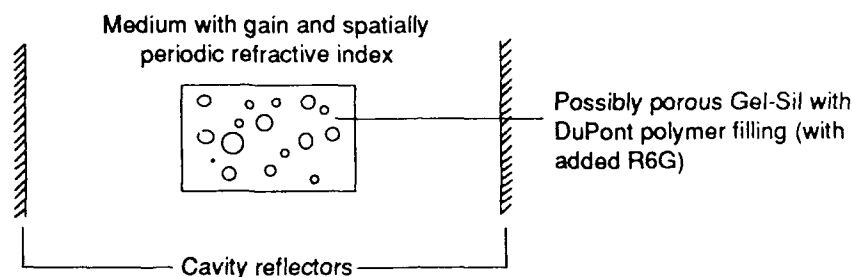


Fig. 10. Simplified view of distributed feedback laser.

The gain medium must have a suitable mechanism for optical gain and also a spatially periodic index. The spatial period must match the wavelength of the light used in the lasing action. Distributed feedback lasers are tunable and offer essential flexibility in communications.

Our research involves investigation of the introduction of fluorescent sensitizers such as Rhodamine 6G into the DuPont polymer followed by recording of the grating structure. Ultimately, we see the advantages of dimensional stability offered by porous gel-silica as of major significance in this area.

#### 5. SUMMARY

In this paper we have addressed topics both old and new which are under investigation at our laboratories.

Gel-silica offers advantages in the formation of novel optical elements and devices but it does seem to be a difficult task to remove the inhomogeneity from its structure during the densification process.

Our programme was triggered off by a chance discovery of unusual properties of primitive gel-silica etalons. A more sophisticated view of the problems associated with the incorporation of gel-silica elements into areas such as laser cavities leads to a cautionary tale based upon complex behaviour associated with the inhomogeneity.

One of the inherent strengths of gel-silica technology is the understanding of how to build pores into the medium. We have proposed in this paper that it is highly probable that the early success of gel-silica etalons was not due to any unusual optical effect based upon bulk homogeneous behaviour but in all probability on the presence of high levels of pore scatter. In referring to our original discovery, we make the point that the presence of an ostensibly unwanted effect can lead to a new approach to optical elements with **controlled** optical loss. The pores of gel-silica may be seen as a major plus point and almost uniquely predictable and controllable compared with other optical micro structures.

This paper concludes with a discussion of two major areas of potential importance for gel-silica technology. Both of these areas rely on the development of predictable gel-silica polymer complexes. These developments have a high chance of success.

## 6. ACKNOWLEDGEMENTS

Special thanks go to Dr. Don Ulrich for his tireless attention and personal support. Thanks are also due to Larry Hench whose ability to solve problems with materials seemingly is without limit. The author also thanks the S.D.I. Innovative Science and Technology Office for its financial support.

Finally, the author wishes to make it clear that the incorporation of polymers into porous silica has been pioneered in the Soviet Union at the State Optics Institute in Leningrad. However, those polymers that have been available for their work have been relatively primitive compared with the sophistication of the DuPont product after some twenty years of development.



New laser media based on microporous glasses.

G.B.Altshuler, V.A.Bakhanov\*, E.G.Dulneva,  
O.V.Mazurin\*, G.P.Roskova\*

Institute of Fine Mechanics and Optics, Department  
of Quantum Electronic, ul. Sablinskaya, 14,  
197101 Leningrad, USSR

\*Institute of Silicate Chemistry of the USSR  
Academy of Sciences, ul. Odoevskogo, 24, korp. 2,  
199155 Leningrad, USSR

#### ABSTRACT

The results of the investigation of new class of the laser media based on dye solutions impregnated microporous glasses are presented. Based on such media high-effective active elements of tunable dye lasers and passive modulators for solid-state lasers are created.

This article is devoted to laser media of the new type - the heterogenous solid-liquid media on the basis of the impregnated by the solutions of the dyes of the microporous glasses. The microporous glasses represent themselves the products of the leaching of heat - treated sodium borosilicate glasses of a certain composition range. As a result of heat treatment is realized the phase separated glass. It consists of two interconnected phases: the silica - rich phase and the chemical unstable sodium - borate - rich phase. If we place this glass in the acid then the ions of sodium and borum will be transfered to the solution. As a result we obtain the porous glass and this pores produce the continious cluster. Therefore it could be easily impregnated by liquids and gases. On the walls of this pores usually the grains of secondary silicon present and the porous glasses themselves on ninty eight percent consists of pure silicon. We now have the technology that permits us to obtain the samples with the volume porosity from ten to fifty percent and the size of this pores could be varied from twenty angstroms up to one thousand angstroms<sup>1-9</sup>.

The microporous glasses ( MPG ) are very good base for the construction disign of the heterogeneous optical materials. At the present time we realized the various composition indicated below:

- MPG + organic dye;
- MPG + anorganic dye;
- MPG + impregnating liquid;
- MPG + impregnating liquid + organic dye;
- MPG + impregnating liquid + anorganic dye;
- MPG + liquid crystall;
- MPG + liquid crystall + organic dye;
- MPG + liquid crystall + anorganic dye;
- MPG + polymer + organic dye;
- MPG + polymer + anrganic dye;

Fig.1 shows the optical characteristics of microporous glasses and solid - liquid media. The optical properties - the refractive index, birefringency and others are varied from the boundary to the center of the sample.

92-11408



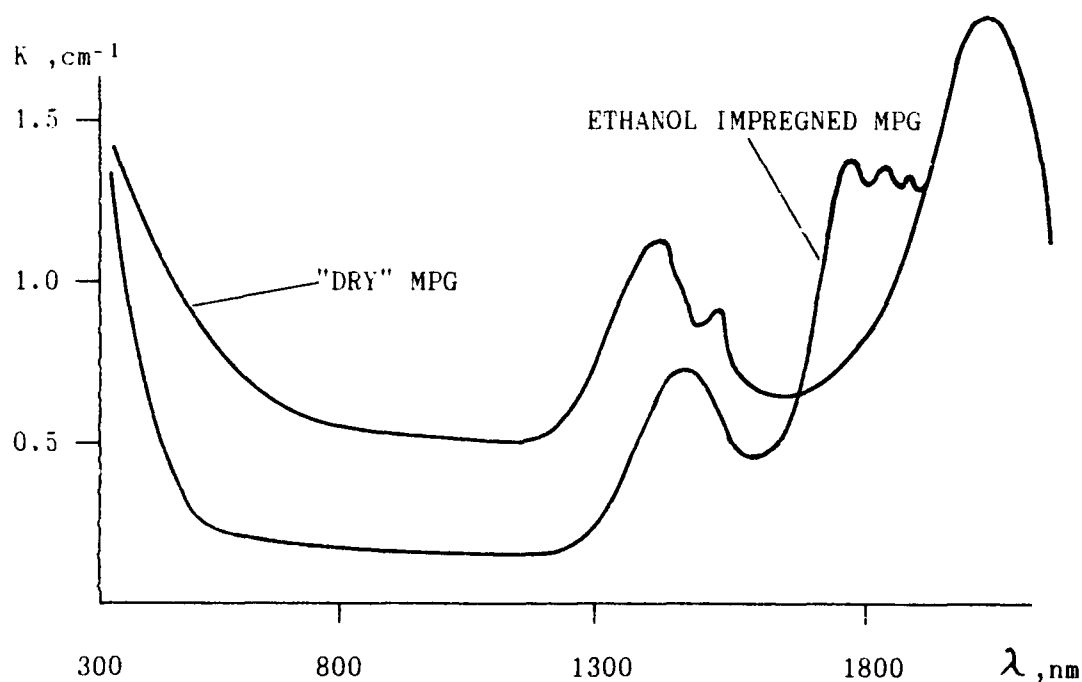


From the spectrum of light losses it is seen that porous glasses and solid - liquid media are transparent in a wide spectral range and at the small sizes of the pores they possess small losses and especially at the filling of these pores by the liquid.

The refraction index of the porous glasses is smallest among the condensed media that is caused by the very small Fresnel losses.

To the present time we have studied in detail the solid-liquid media as the active media for lasers with organic activators.

In the porous glasses we create for the molecules of the dyes absolutely new situation that is connected with interaction of the molecules with the surface of the pore.



Spectral depending of light losses coefficient.

	M P G	MPG + liquid
Refractive index	1.30 - 1.34	1.35 - 1.8
Birefringency	$\pm ( 10^{-4} - 10^{-3} )$	$< 10^{-3}$
Optical damage in SiO <sub>2</sub> units	0.2 - 1.0	0.2 - 0.8

Fig. 1. Optical properties of microporous glass.

Depending of the type of the solvent and dye they could be realized the active centers of two type: first - at the absorption of the solvated molecule of the dye and second - at the weak interaction of the molecule with the walls of the pores. Its important to outline properties of the molecules in the porous glasses from the view point of generation are not detuarated. ( Fig. 2 ).

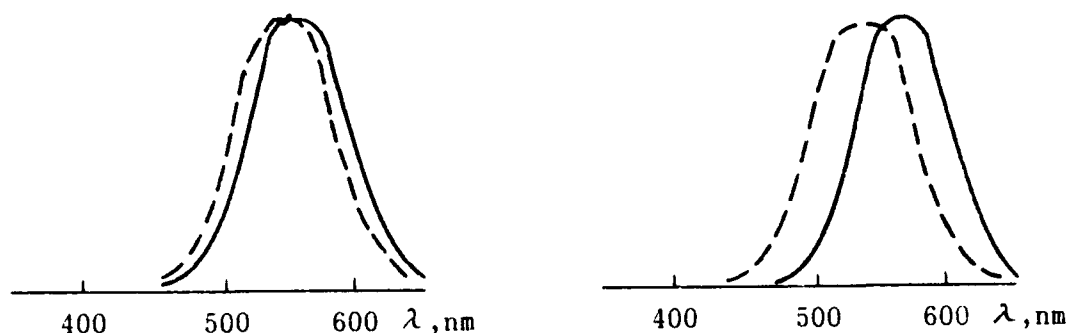


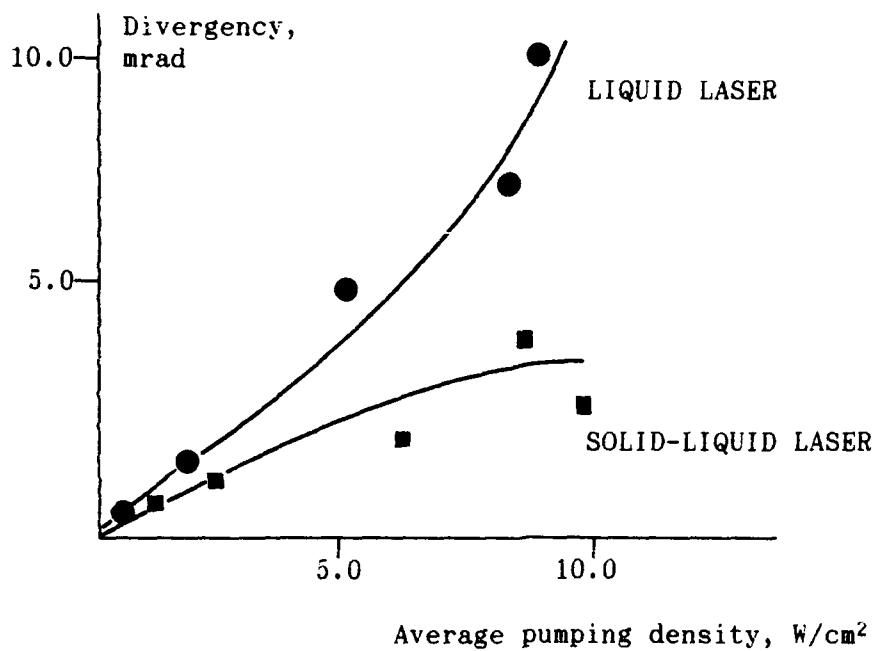
Fig. 2. Dye absorption spectrum in liquid solution (—) and solid - liquid solution (---);  
a) Rh 6G + ethanol, b) Rh 6G + H<sub>2</sub>O

One of the main advantages of the laser on the solid - liquid media compared liquid laser will be the stable spatial energy characteristics of generated radiation that is connected with the dissalaration of the light induced convection. ( Fig. 3 ).

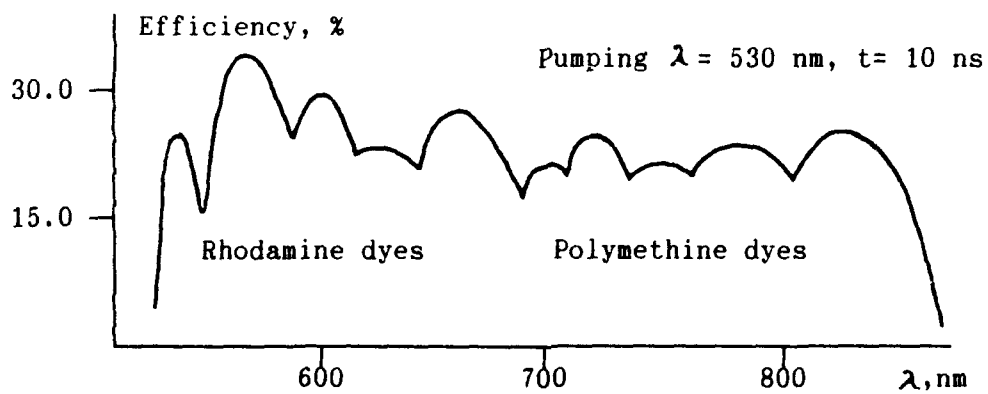
The solid - liquid elements do not require the pumping of the solvent of the dye at the power densities of the pumping power up to ten watt per square centimeters and permit to produce the tuning of the radiation in a very wide optical range.

In solid - liquid elements one can use also the same dyes that in a typical liquid lasers. In this case the energy and spectral characteristics of the both type of lasers quite similar. The problem for the photobleaching of the dye in a solid - liquid matrices could be solved due to the presence of the difuse mixing of the molecules in the volume of solid - liquid media. This is a main advantage of the solid - liquid matrix compared to the polymeric matrix. And this fact is illustrated by Fig. 4 from which one can see that moderate densities of the mean power of high repetition rate pumping the diffusion processes compensate the loss of generating molecules. Recently we discovered the mean for the increase of the resources based upon the application of the directed migration of the dye ions in electric field. Fig. 5 shows the dependence of the stationary in a time efficiency of the laser with coherent pumping depending on the velocity of electrodiffusion of the dyes ions. At the moderate intensities of electric field below one kilovolt per centimeter one can realize the velocities of electrodiffusion up to one millimeter per second, that allows us to use succesfully the active elements at the pumping power at about per fifteen watt per square centimeter. The disign of active element is shown on the Fig. 6. Here you see the solid - liquid element displaced between electrodes and two buffer volumes. This active element in combination with a controled power supply and the set of the buffer volumes allows to automate the processes of optimization of the concentration and allows also to displace in a very operative fashion one dye by another. It is important that the photoproducts are not mixed with a fresh dye.

The unique optical properties of the porous glasses permit us to produce lasers



a)



b)

Fig. 3. Spatial (a) and spectral (b) characteristics of solid - liquid laser media.

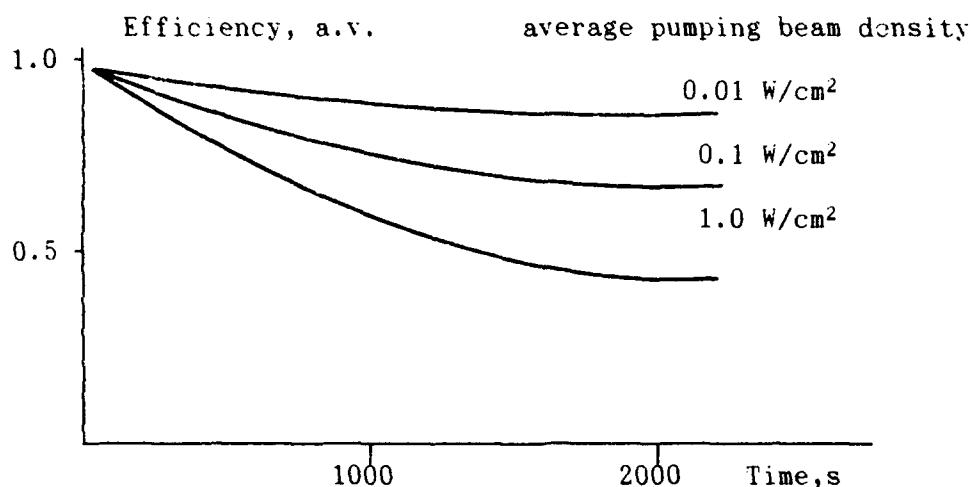


Fig. 4. Solid - liquid media lasers resource Rh 6G with ethanol.

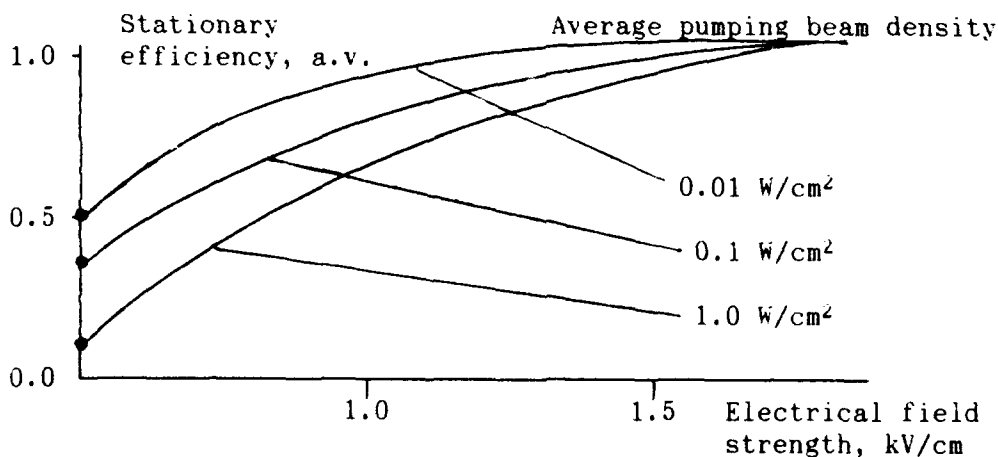


Fig. 5. Solid - liquid media lasers resource Rh 6G with ethanol with electrodiffusion accessories.

with unusual characteristics. For example. Applying special technology inside of the porous glass we can obtain the kind of the waveguide structures. The plates of this glass with deposited on the walls of this porous the dye molecules represent themselves the matrix of the large amount, more then ten on fifth per millimeter square the homogeneously oriented microwave lasers. This matrix placed in optical cavity at the coherent pulsed pumping possesses all the properties of lasers excluding the spatial characteristics. ( Fig. 7 ). The radiation represent itself the beam with angular aperture 30 degree with homogeneous bell - shape distribution of intensity and complete absence the spatial coherence that especially interesting for the high-speed photography and lithography. Second important advantage of the solid - liquid media in lasers is a possibility to use them as a passive modulators. We propose two types of modulators. First type is based upon the effect of

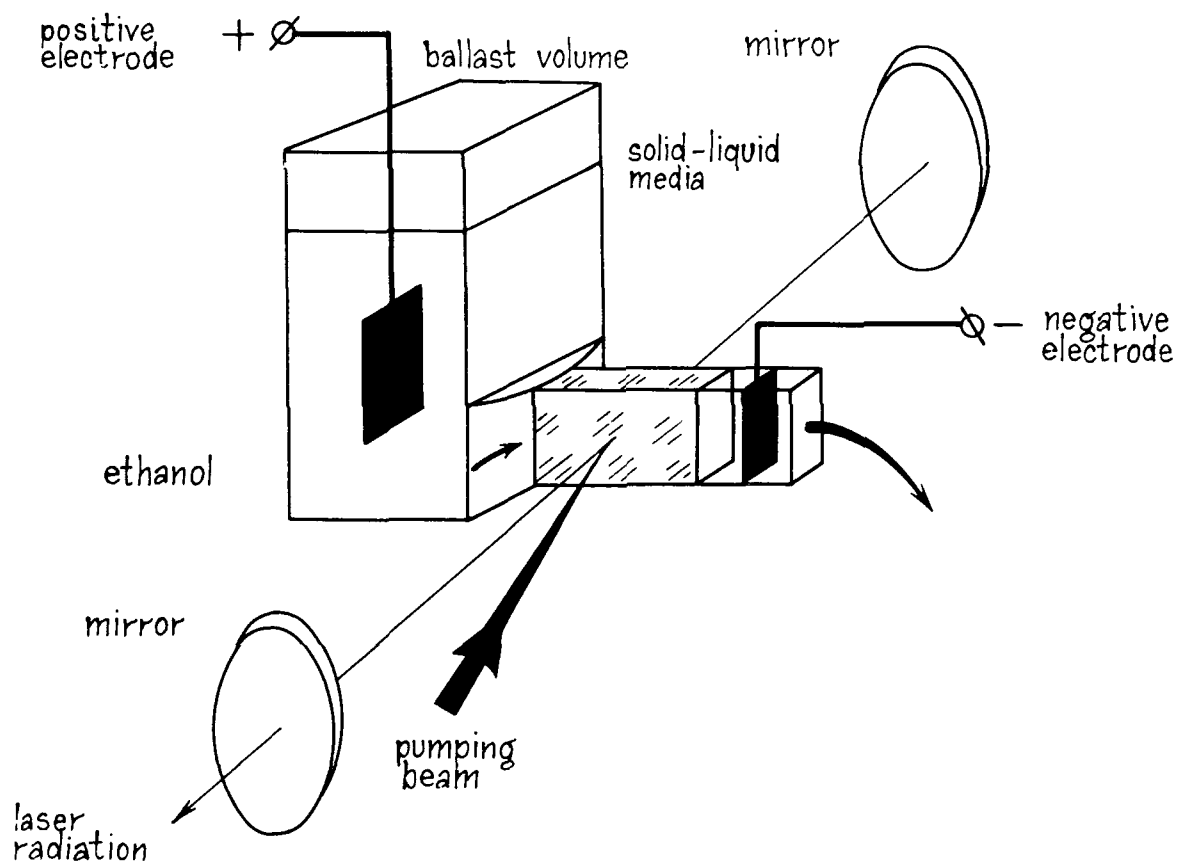


Fig. 6. Solid - liquid media active element with electrodiffusion accessories configuration.

inlightning or darkening by nonactivated solid- liquid media. When the pores are filled by liquids of high nonlinear refractive index, we observe an effect of nonlinear dispersion in the field of powerfull laser pulses. In relation to absolute values of refractive indexes of microporous glass - liquid ratio, as well as to the sign and value of nonlinear addition, the regime of transparency or that of eclipse will realize. This modulators possess many advantages but the main drawback is a very high intensity of the switching on. ( Fig. 8 ).

The second type of the shutter is the shutters on the basis of solid - liquid media activated by saturating absorbers. Our experiments show, that shutters on the basis on solid - liquid media have the advantages comparable to the liquid analogues. They manifest themselves in a two main tendencies. First, the reduction of the length of the pulses and regularization of the enveloping of the pulse - trains in the mode - locked regime. The second - improvement of the spatial distribution of generated radiation. This properties are shown on the example of neodymium - glass laser with the liquid shutters with the same dye. ( Fig. 9 ).

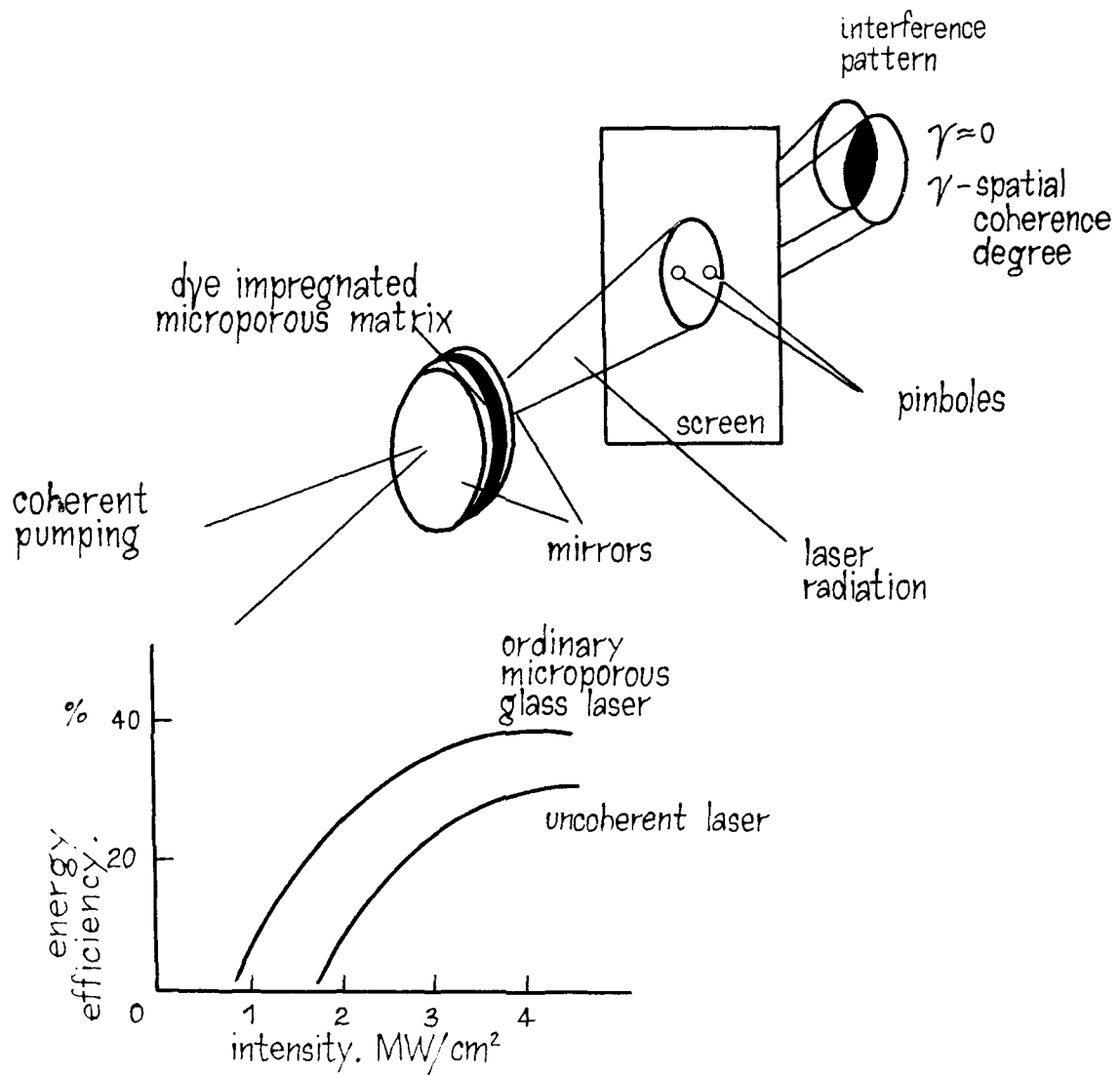


Fig. 7. Spatial incoherent laser.

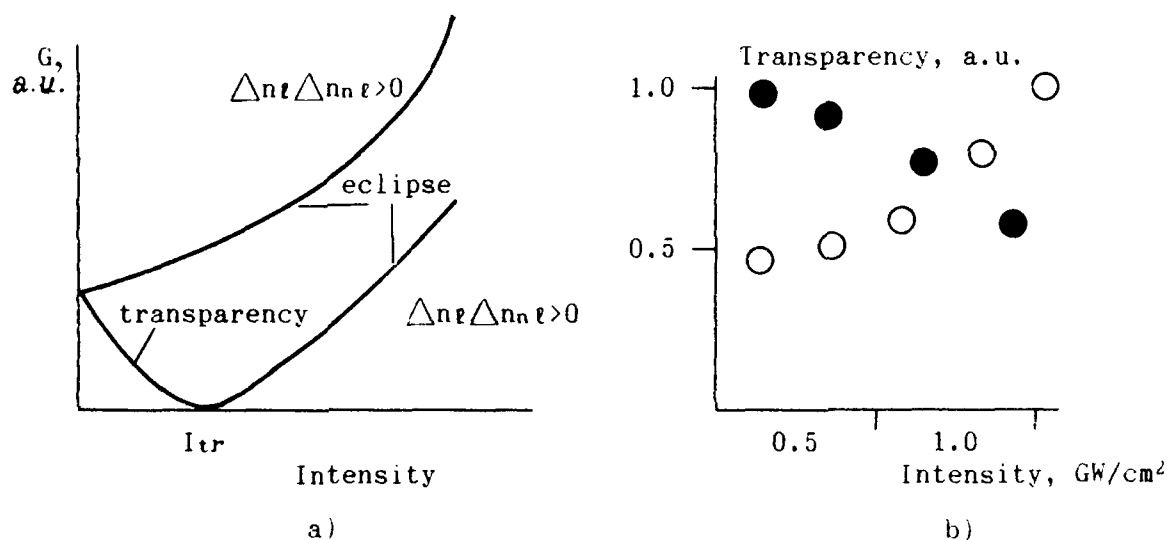


Fig. 8. Dependence of the scattering cross section a) and transparency b) of the solid - liquid nonlinear media.

$\Delta n_l$  - the difference between linear refractive indexes of liquid and glass;

$\Delta n_{nl}$  - the difference between nonlinear refractive indexes of liquid and glass;

$G$  - scattering cross section;

$$G \sim (\Delta n_l + \Delta n_{nl})^2;$$

Transparency when  $G = 0$ : 1.  $\Delta n_l = -\Delta n_{nl}$  ;  
 2.  $\Delta n_{nl} = n_2 \cdot I_{tr}$  ,  $I_{tr} = -\Delta n_l / n_2$  ;

$n_2$  - coefficient of the nonlinear refractive index.

Main advantages:

- spectral unselectivity;
- no absorption;
- unlimited lifetime;

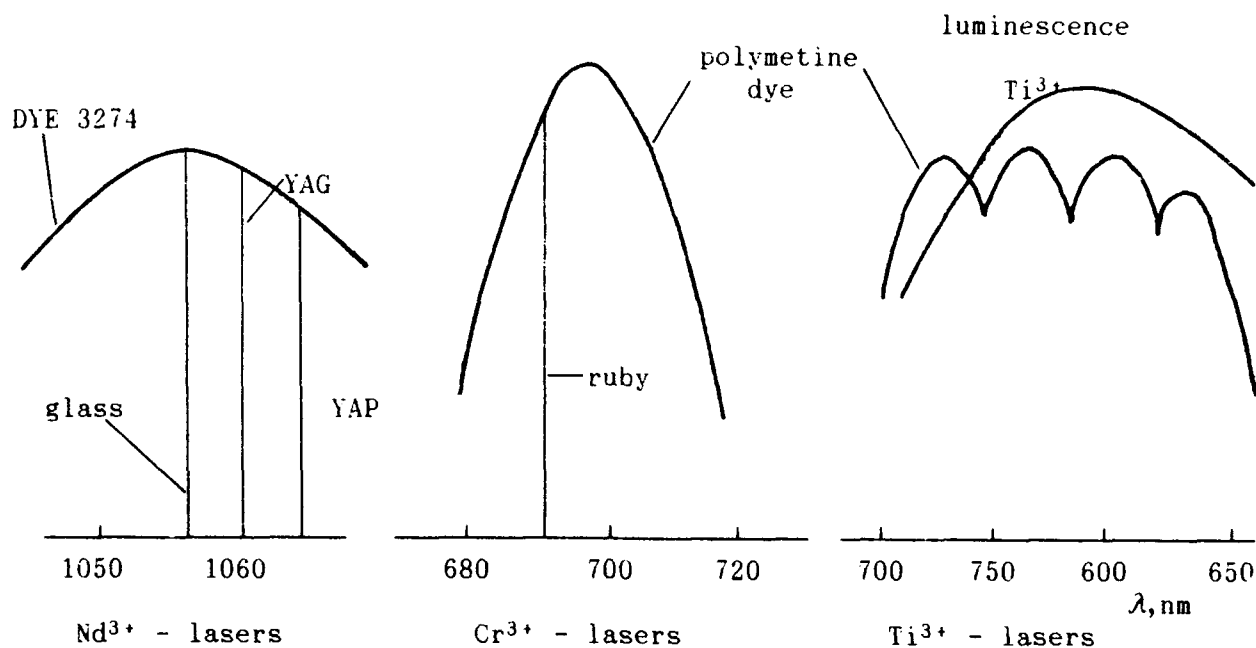


Fig. 9. Laser modulators based on dye doped microporous glasses.

In conclusion, the solid - liquid media are give absolutely new possibilities, new horizons for obtaining of lasers materials.

#### REFERENCES

1. G.B.Altshuler, E.G.Dulneva, I.K.Meshkovsky, K.I.Krylov. "Solid state active media based on dyes". *J. Appl. Spectrosc. ( USA )* v.36, N4, p.415-421.
2. G.B.Altshuler, E.G.Dulneva, K.I.Krylov, I.K.Meshkovsky, V.S.Urbanovich. "Output characteristics of a laser utilizing Rhodamin 6G in microporous glass." *Sov. J. Quantum Electron. ( USA )* v.13, N6, p.784-788.
3. G.B.Altshuler, V.A.Bakhanov, E.G.Dulneva, L.G.Kelbakh, E.I.Krylov. "Optical breakdown in microporous quartz glasses." *Sov.Phys.-Tech. Phys. ( USA )* v.29, N1, p.105-106.
4. G.B.Altshuler, V.A.Bakhanov, E.G.Dulneva, I.K.Meshkovsky. "Optical characteristics of active elements made of microporous quartz glass." *Opt. & Spectrosc. ( USA )* v.55, N2, p.216-219.
5. G.B.Altshuler, E.G.Dulneva, A.V.Erofeev, I.K.Meshkovsky, A.V.Okishev. "Phototropic switches made of microporous glass activated with dye molecules." *Sov. J. Quantum Electron. ( USA )* v.15, N5, p.722-724.
6. G.B.Altshuler, E.G.Dulneva, V.B.Karasev, A.V.Okishev, L.S.Telegin. "Subpicosecond pulses from a neodymium-glass laser with a solid-liquid phototropic shutter." *Sov. Tech. Phys. Lett. ( USA )* v.11, N2, p.96-97.
7. G.B.Altshuler, E.G.Dulneva, A.V.Erofeev. "Field-induced transport of laser dyes in porous glass matrix." *Sov.Phys.-Tech. Phys. ( USA )* v.30, N8, p.941-942.
8. G.B.Altshuler, V.A.Bakhanov, E.G.Dulneva, A.V.Erofeev, O.V.Mazurin, G.P.Roskova. "Laser based on dye-activated silica- gel." *Opt. & Spectrosc. ( USA )* v.62, N6, p.709-710.
9. G.B.Altshuler, V.A.Bakhanov, E.G.Dulneva, O.V.Mazurin. "Spatial dispersion of anisotropy of high-silica microporous glasses." *Opt. & Spectrosc. ( USA )* v.63, N1,



SOL-GEL OPTICS

Volume 1328

**SESSION 2**

**NLO and GRIN Materials**

*Chair*

**Donald R. Uhlmann**  
University of Arizona



# THIRD ORDER OPTICAL PROPERTIES OF QUASI-TWO DIMENSIONAL CONJUGATED DISCS: SILICON NAPHTHALOCYANINE

N.Q.Wang, Y.M.Cai, J.R.Heflin, J.W.Wu\*, D.C.Rodenberger and A.F.Garito

*Department of Physics  
University of Pennsylvania, Philadelphia, PA 19104*

## ABSTRACT

Since the basic phthalocyanine structure intrinsically possesses high thermal and oxidative stabilities, phthalocyanines incorporated into sol-gel glasses provide an attractive approach for realizing highly stable nonlinear optical media. Experimental results recently obtained for the nonresonant and resonant third order optical properties of metallophthalocyanines are reviewed in this paper.

## 1.INTRODUCTION

The macroscopic second order,  $\chi_{ijk}^{(2)}(-\omega_3; \omega_1, \omega_2)$ , and third order,  $\chi_{ijkl}^{(3)}(-\omega_4; \omega_1, \omega_2, \omega_3)$ , nonlinear optical susceptibilities of conjugated  $\pi$ -electron organic and polymer structures are known to be unusually large, and their microscopic origin and virtual excitation processes can be successfully described by many-electron theory of highly correlated quasi-one(1D) and two(2D) dimensional systems.<sup>1-3</sup> For 2D metallophthalocyanines,<sup>4-10</sup> studies of the resonant third order optical properties of disc-like silicon naphthalocyanine(SINC) (Figure 1), randomly dispersed in glassy polymer films, demonstrated that SINC behaves as an optical Bloch system, exhibiting absorption saturation of the large oscillator strength( $\alpha_0$  of order  $10^5 \text{ cm}^{-1}$ ) Q band in the near infrared range and an associated, large, intensity dependent refractive index  $n_2$  of order  $1 \times 10^{-4} \text{ cm}^2/\text{kW}$ .<sup>5-7</sup> These properties allowed the first observation of absorptive optical bistability occurring through the nonlinear electronic excitations of a random solid medium.

The development of random glassy materials containing molecular units with large nonlinear optical susceptibilities is a major approach toward realizing nonlinear optical media that possess both important primary nonlinear optical properties and secondary material properties such as thermal, mechanical, chemical, and oxidative stabilities. The basic concept of molecular doped sol-gel glasses for nonlinear optics has been widely

\* Present address: Lockheed Palo Alto Research Lab, Palo Alto, Ca. 94304



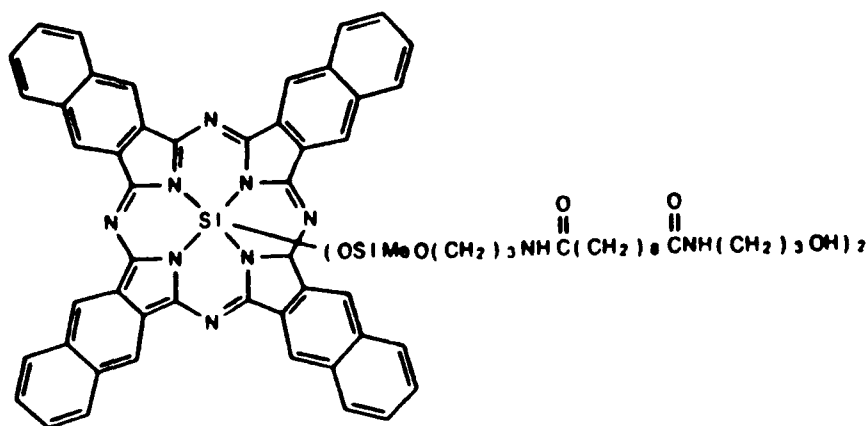


Figure 1 Schematic diagram for the molecular structure of SINC.

presented. Because of its large  $\pi$ -electron conjugation, the phthalocyanine structure intrinsically possesses one of the highest thermal and oxidative stabilities known for organic structures. Phthalocyanines incorporated into sol-gel glasses by doping, or directly by covalent binding, provide an attractive approach to realizing highly stable nonlinear optical media that can satisfy both primary and secondary property requirements. In this paper, we review experimental results recently obtained for the nonresonant and resonant third order optical properties of a metallophthalocyanine.

## 2.LINEAR OPTICAL PROPERTIES OF SINC

The absorption spectrum of SINC dissolved in dimethylformamide (DMF) is shown in Figure 2. After a wide transparent region(850nm-2000nm), SINC exhibits a characteristic, vibronically coupled, large oscillator strength Q band centered at 778 nm, followed by another transparent region(500 nm-600 nm), and a B(Soret) band located near 335 nm. The Q and B bands are due to widely separated  $S_0(1^1A_g) \rightarrow S_1(1^1E_u)$  and  $S_0(1^1A_g) \rightarrow S_2(2^1E_u)$   $\pi$ -electron transitions, respectively, as is well-established for metallophthalocyanines and related metalloporphyrins of  $D_{4h}$  symmetry.<sup>11-13</sup> In fluorescence measurements, a red emission from the  $S_1$  state is observed in nearly mirror symmetry of the Q-band. Strickler-Berg analysis<sup>14</sup> of the Q-band spectrum yields a radiative lifetime for the  $S_1$  state of 8.8 ns which is consistent with pump-probe measurements of transient absorption at 532nm and transient bleaching at 770nm. The transparent regions allow third harmonic measurements with little or no absorption at the fundamental and harmonic frequencies.

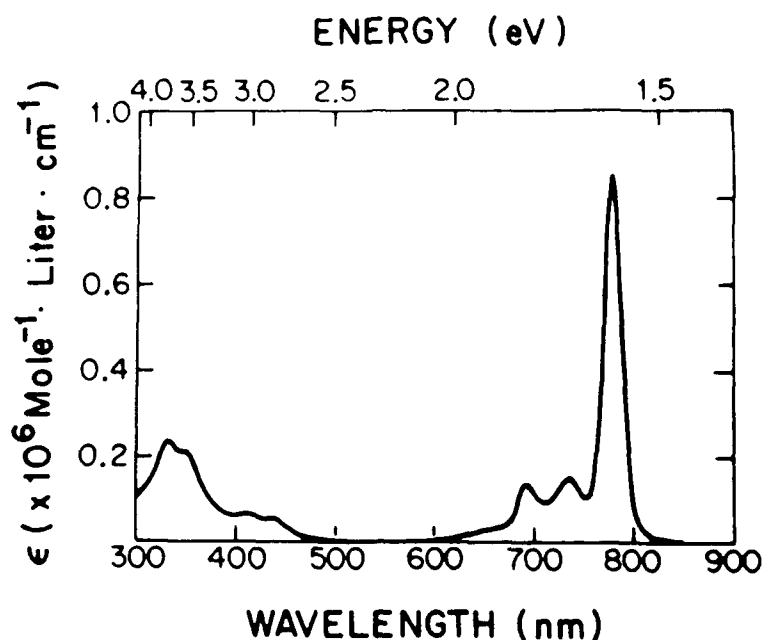


Figure 2 Linear absorption spectrum of SINC in DMF . The Q band absorption peak occurs at 778 nm(1.59eV) and the B band peak is 335 nm(3.70eV) . The solution is transparent between 850-2000nm and between 500-600 nm.

### 3. NONRESONANT THIRD ORDER OPTICAL PROPERTIES OF SINC

Third harmonic generation measurements of SINC dissolved in DMF were performed using the Maker fringe technique at the fundamental wavelengths 1907nm and 1543nm.  $\chi_L^{(3)}(-3\omega; \omega, \omega, \omega)$  of the solution is obtained through the relation<sup>15</sup>

$$\frac{(A_m^L)_{\text{corr}}}{A_m^R} = \frac{\left[ T_G \frac{l_c^G \chi_G^{(3)}}{n_{3\omega}^G + n_\omega^G} - T_L \frac{l_c^L \chi_L^{(3)}}{n_{3\omega}^L + n_\omega^L} (t_\omega^{(2)})^3 \right]^2}{\left[ T_G \frac{l_c^G \chi_G^{(3)}}{n_{3\omega}^G + n_\omega^G} - T_R \frac{l_c^R \chi_R^{(3)}}{n_{3\omega}^R + n_\omega^R} (t_\omega^{(2)})^3 \right]^2} \quad (1)$$

where

$$(A_m^L)_{\text{corr}} = \frac{2(A_m^L)_{\text{obs}}}{e^{-3a_\omega l} + e^{-a_{3\omega} l}} \quad (2)$$

is the mean value of the fringes of the liquid solution corrected for any absorption at  $\omega$  and  $3\omega$ , and R refers to the reference liquid.

Determination of  $\chi_L^{(3)}$  of the liquid solution from Eq.(1) requires the knowledge of  $\chi^{(3)}$  of the glass window and the solvent. The following values<sup>16</sup> have been used in our calculations: at 1907nm,  $\chi_G^{(3)}=0.584 \times 10^{-14}$  esu,  $\chi_{DMF}^{(3)}=0.631 \times 10^{-14}$  esu;

at 1543nm,  $\chi_G^{(3)}=0.591 \times 10^{-14}$  esu,  $\chi_{DMF}^{(3)}=0.650 \times 10^{-14}$  esu.

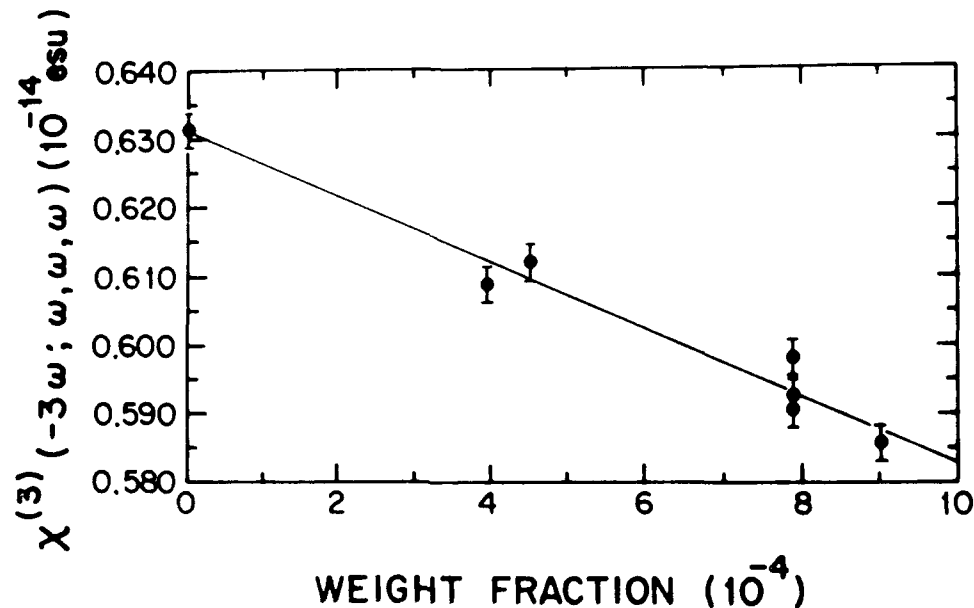


Figure 3 Concentration dependence of  $\chi_L^{(3)}(-3\omega; \omega, \omega, \omega)$  for solutions of SINC in DMF at 1907 nm fundamental wavelength.

Figure 3 shows the concentration dependence of the solution  $\chi_L^{(3)}$  at the fundamental wavelength of 1907 nm. The values of  $\chi_L^{(3)}$  decrease linearly with increased concentration of SINC. Since the  $\gamma_2$  value of DMF is known to be positive, the  $\gamma_1$  value of SINC is thus observed to be negative in sign. In the infinite dilution limit where  $w \rightarrow 0$ , the microscopic third-order susceptibility  $\gamma_1$  of the solute is obtained from the following expression<sup>15</sup>

$$v_0 \frac{\partial \chi_L^{(3)}}{\partial w} \Big|_0 + \chi_2^{(3)} \frac{\partial v}{\partial w} \Big|_0 + v_0 \chi_2^{(3)} \left( 1 - \frac{4}{n^2 + 2} \frac{\partial n^2}{\partial w} \Big|_0 \right) = \frac{1}{M_1} \left( \frac{n^2 + 2}{3} \right)^4 N_A \gamma_1 \quad (3)$$

where  $M_1$  is the solute molecular weight,  $\chi_2^{(3)}$  the macroscopic third harmonic susceptibility of the solvent,  $N_A$  Avagadro's number and the subscript 0 denotes the infinite dilution limit. At 1907 nm,  $\gamma_1$ , which is the isotropically averaged value  $\langle \gamma \rangle$  for SINC, is found to be  $-410 \pm 30 \times 10^{-36}$  esu. THG measurements at 1543 show that  $\chi_L^{(3)}$  is

independent of the SINC concentration, and, therefore,  $\langle\gamma\rangle$  is less than the experimental uncertainty of  $\pm 30 \times 10^{-36}$  esu.

$\langle\gamma\rangle$  of SINC can be understood in terms of the key examples of type I and type II third order virtual excitation processes schematically illustrated in Figure 4. The state  $S_n$  is a postulated large cross-section singlet state accessible through  $S_1$  and  $S_2$ . The  $S_0 \rightarrow S_1 \rightarrow S_0 \rightarrow S_1 \rightarrow S_0$  virtual excitation process shown in (a) is a type I term deriving from the large oscillator strength  $S_0 \rightarrow S_1$  Q band excitation. A dominant type II term is shown in (b) where the  $S_0 \rightarrow S_1 \rightarrow S_n \rightarrow S_1 \rightarrow S_0$  virtual excitation process involves both the  $S_0 \rightarrow S_1$  and  $S_1 \rightarrow S_n$  virtual transitions. Correspondingly, less important type I and type II virtual processes are illustrated in (c) and (d), respectively, where each involves the  $S_0 \rightarrow S_2$  transition. Since the  $S_0 \rightarrow S_1$  transition is much stronger than the  $S_0 \rightarrow S_2$  transition, the virtual excitation processes shown in (a) and (b) dominate those shown in (c) and (d). Further, as a general rule, 2D conjugated structures have smaller nonresonant  $\langle\gamma\rangle$  values than their 1D analogs.<sup>6</sup>

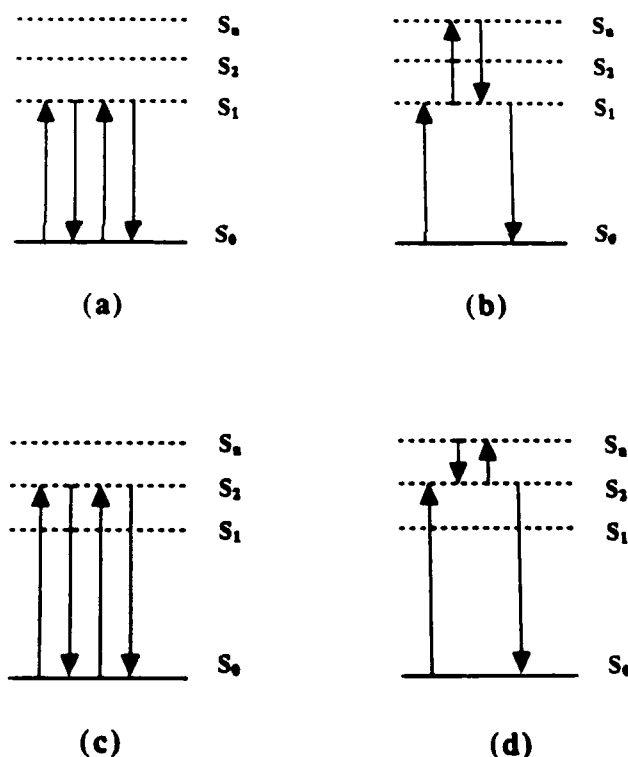


Figure 4 Key examples of third order virtual excitation processes contributing to  $\gamma_{ijk}(-3\omega; \omega, \omega, \omega)$  of SINC. The (a) type I and (b) type II virtual excitation processes that involve the  $S_0 \rightarrow S_1$  virtual transition dominate the (c) type I and (d) type II processes that involve the  $S_0 \rightarrow S_2$  transition.

For the fundamental laser frequencies used in the present experiment of SINC, the third harmonic frequencies are larger than the Q band excitation energy at 1.59 eV. The  $3\omega$  resonance of the Q band occurs for a fundamental frequency that is one-third of the Q band

excitation energy or 0.53 eV(2334 nm), and the  $3\omega$  resonance of the 3.70 eV B band occurs for a fundamental frequency of 1.23 eV(1005 nm). Since 1907 nm is above the  $3\omega$  resonance at 2334 nm, the experimentally measured value of  $\langle\gamma\rangle$  is negative for that fundamental wavelength. The close proximity of 1907 nm to 2334 nm also implies that  $\langle\gamma\rangle$  is near resonantly enhanced and, therefore, large in magnitude. The fundamental wavelength of 1543 nm, however, is well between the  $3\omega$  resonances of the Q and B bands, and the experimental value is very small since it lies in the crossover region between these resonances.

#### 4. RESONANT THIRD ORDER OPTICAL PROPERTIES

A saturable absorber exhibits the important resonant properties of nonlinear absorption and nonlinear refraction with increased incident light intensity. Absorption saturation has been long known for metallophthalocyanine liquid solutions<sup>13</sup> and only recently has it been reported for polymer films in the case of SINC.<sup>6</sup> Picosecond single beam and pump-probe measurements of SINC liquid solutions have been carried out. Figure 5 shows the saturation behavior typically observed in the single beam measurements of the intensity dependence of the absorption coefficient  $\alpha L$  for 30 ps pulses at 770nm within the Q-band. SINC was dissolved in transparent cyclohexanone. The data were analyzed as described previously.<sup>6</sup> The solid line in Figure 5 is the least squares fit to a Bloch-type saturable absorber of the form

$$\alpha(I)L = \frac{\alpha_0 L}{1 + I/I_s} + \alpha_B L \quad (4)$$

where  $I_s$  is the threshold power for the saturation,  $\alpha_0 L$  gives the low intensity linear absorption, and  $\alpha_B L$  is the unsaturable background absorption. The behavior is qualitatively the same as that observed earlier for SINC films. For 30 ps pulses, the threshold intensities for saturation in the liquid samples were in the range of 30-100 MW/cm<sup>2</sup>. The range in  $I_s$  values reflect sample to sample variations. In the presence of impurities and aggregation, both  $I_s$  and  $\alpha_B L$  increase significantly.

From the saturable absorption measurements as a function of pulse duration, one can estimate the nonlinear refractive index  $n_2$  as described earlier for SINC films.<sup>6</sup> From the optical susceptibility  $\chi(\omega)$  for a Bloch type system, one obtains

$$n_2 = \frac{1}{3} \left[ \frac{4\pi}{n_0} \right]^2 \chi^{(3)} = - \left( \frac{\alpha_0 \lambda}{4\pi I_s} \right) \left( \frac{\Delta}{(1+\Delta^2)^2} \right) \quad (5)$$

where  $\alpha_0$  is the linear absorption coefficient,  $\Delta$  is the detuning  $(\omega - \omega_0)/\Gamma$ , and  $I_s$  is the saturation power. The similar saturation behavior seen for the liquid and films is important

because the value of  $n_2$  for a SINC film is of order  $10^{-4} \text{ cm}^2/\text{kW}$  which is the largest  $n_2$  value obtained for a conjugated structure.<sup>6</sup>

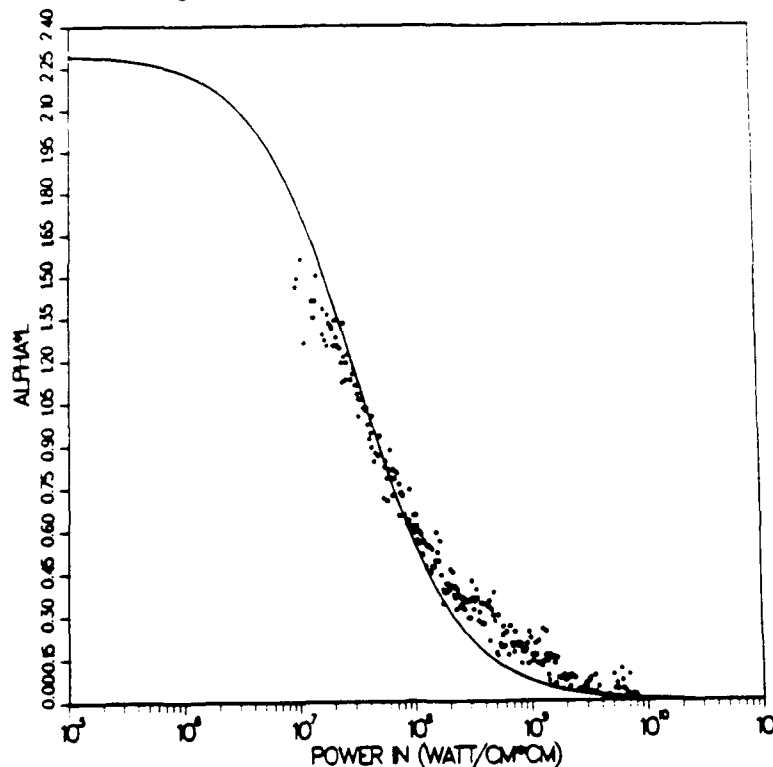


Figure 5 Saturable absorption measured at pulse width  $\tau_p = 30 \text{ ps}$  and wavelength  $\lambda = 770 \text{ nm}$ . The solid line is the least squares fit to Eq. (4).

## 5. CONCLUSION

The nonresonant and resonant optical properties of SINC liquid solutions were studied by THG and saturable absorption measurements. At a fundamental wavelength of 1907 nm, the isotropically averaged third harmonic susceptibility  $\langle \gamma \rangle$  was measured to be  $-410 \pm 30 \times 10^{-36} \text{ esu}$ , while at 1543 nm,  $\langle \gamma \rangle$  was less than the experimental sensitivity of  $\pm 30 \times 10^{-36} \text{ esu}$ . Liquid SINC solutions can be described as easily saturable, optical Bloch systems that exhibit absorption saturation behavior similar to SINC films which have unusually large values for the linear absorptivity coefficient  $\alpha_0$  of order  $10^5 \text{ cm}^{-1}$  and intensity dependent refractive index  $n_2$  of order  $10^{-4} \text{ cm}^2/\text{kW}$ . The  $n_2$  value is the largest obtained so far for a conjugated structure and is the basis for the electronic absorptive optical bistable behavior.

## 6. ACKNOWLEDGEMENTS

This research was generously supported by AFOSR and DARPA (grant F49621-85-C-0105), Penn Research Fund, and partially by NSF/MRL (grant DMR-85-19059). We



gratefully acknowledge discussions with Dr. K. Y. Wong and the generous SINC sample supply from Drs. P. Kalyanaraman and J. Sounik of Hoechst-Celanese.

## 7. REFERENCES

- [1] J.R.Heflin, K.Y.Wong, O.Zamani-Khamiri and A.F.Garito, Phys. Rev. B **38**, 1573(1988); and in Nonlinear Optical Properties of Polymers, A.J.Heeger, D.Ulrich, and J.Orenstein, eds.(Mater. Res. Soc. Proc. **109**, Pittsburgh, PA, 1988) pp.91-102.
- [2] Z.G.Soos and S.Ramasesha, Chem. Phys. Lett. **153**, 171(1988); J. Chem. Phys. **90**,1067(1989).
- [3] B.M.Pierce, J. Chem. Phys. **91**, 791(1989).
- [4] Z.Z.Ho, C.Y.Ju, and W.M.Heatherington, J. Appl. Phys. **62**, 716(1987).
- [5] J.W.Wu, R.A.Norwood, J. R. Heflin, K. Y. Wong, O. Zamani-Khamiri, and A. F. Garito, Topical Meeting on Nonlinear Optical Properties of Materials, 1988 Technical Digest Series, Vol. 9(Optical Society of America, Washington, D.C., 1988) pp.28-31.
- [6] J. W. Wu, J. R. Heflin, R. A. Norwood, K. Y. Wong, O. Zamani-Khamiri, A. F. Garito, P. Kalyanaraman, and J. Sounik, J. Opt. Soc. Am. B **6**, 707 (1989).
- [7] A. F. Garito and J.W.Wu, Proc. SPIE **1147**, 2(1990).
- [8] P.N.Prasad, M.K.Casstevens, J.Pflegler, and P.Logadon, Proc. SPIE **878**, 106(1988).
- [9] J.S.Shirk, J.R.Lindle, F.J.Bartoli, C.A.Hoffman,Z.H.Kafafi, and A.W.Snow, Appl. Phys. Lett. **55**, 1287(1989).
- [10] A. Kaltbeitzel, D. Neher, C. Bubek, T. Sauer, G. Wegner, and W. Caseri, in *Electronic Properties of Conjugated Polymers*, eds. H. Kuzmany, M. Mehring, and S. Roth (Springer Ser., New York, 1989).
- [11] B. L Wheeler, G. Nagasubramanian, A. J. Bard, L. A. Schectman, D. R. Dininny, and M. E. Kenney, J. Am. Chem. Soc. **106**, 7404 (1984).
- [12] See, for example, M. Gouterman, in *The Porphyrins*, ed. D. Dolphin (Academic, New York, 1978) Vol. 3, Chap. 1.
- [13] W. F. Kosonocky and S. E. Harrison, J. Appl. Phys. **37**, 4789 (1966).
- [14] S.J.Strickler and R.A.Berg, J. Chem. Phys. **37**, 814(1962).
- [15] N.Q.Wang,Y.M.Cai,J.R.Heflin, and A.F.Garito, Mol.Cryst.Liq.Cryst.(In press).
- [16] J.R.Heflin,Y.M.Cai, and A.F.Garito, International Conference on Quantum Electronics Technical Digest Series 1990, Vol.8,(Optical Society of America, Washington, D.C. 1990) p.38; J.R.Heflin, Y.M.Cai, and A.F.Garito(to be published).



Obtention of  $\text{CdSe}_x \text{S}_{1-x}$  precipitates in sol-gel matrices

Carol M. Bagnall\* and Jerzy Zarzycki

Laboratory of Science of Vitreous Materials  
University of Montpellier 2  
34095 Montpellier Cedex 2, France

### ABSTRACT

Various methods of obtaining fine colloidal precipitates of cadmium sulfo-selenides in  $\text{SiO}_2$  gel matrices are described. These materials, which are of interest in optoelectronic applications, can be prepared by diffusion of various reactants in wet gels.

The influence of different preparative parameters on the diffusion characteristics, the possibility of obtaining distribution gradients and, in particular, the interest of sonocatalysis (ultrasonic irradiation) are briefly presented.

### 1. INTRODUCTION

Semiconductor-doped glasses have attracted much attention recently because of their large third-order optical susceptibility. Important applications of these systems in Q switches, degenerate four-wave mixing, optical phase conjugation and optical bistability have been reported. In addition, the very small semiconductor microcrystallites formed by aggregation in these glasses also present interesting quantum-confinement effects<sup>1-3</sup>. Typical systems are constituted by glasses containing  $\text{CdSe}_x \text{S}_{1-x}$  crystallites which are usually formed by dissolving  $\text{Cd}^{2+}$ ,  $\text{Se}^{=}$  and  $\text{S}^{=}$  ions in an oxide glass matrix. A subsequent thermal treatment of the system leads to the formation of colloidal agglomerates and finally of microcrystallites.

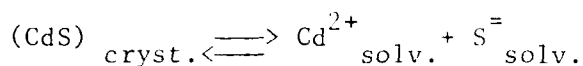
The commercially available glasses (Schott) Code OG590 contain  $\text{CdSe}_x \text{S}_{1-x}$  crystallites with  $x \approx 0.2$ ; their size is about 150 Å diameter and the size distribution is characterized by a standard deviation of about 50 Å. This prevents the observation of quantum effects in these glasses but more uniform size distribution and smaller crystal diameters can be obtained by careful treatment of the parent matrix. Crystallites of 30 to 80 Å with 24 Å to 44 Å standard deviation have been produced by Corning<sup>4</sup>.

Small colloidal CdS particles were also obtained as very diluted systems in water and acetonitrile with typical dimensions in the range 10-100 Å. Correlations between their size and electronic absorption, resonance Raman and luminescence spectra were also reported<sup>5-7</sup>. Thin films of CdS deposited by magnetron sputtering on fused silica substrates were also studied<sup>8</sup>. These films consist of small intersecting islands of material of about 100 Å.

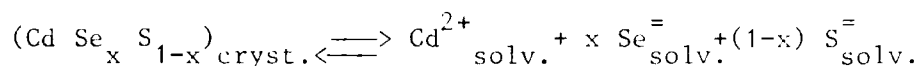
In the present work attempts to prepare analogous materials by sol-gel methods are described. Sol-gel techniques may be used to synthesise oxide (generally  $\text{SiO}_2$ -based) matrices. The introduction of CdS or  $\text{CdSe}_x \text{S}_{1-x}$  particles may be accomplished by chemical reactions of the type:

\* Present address: Thorn Lighting Limited, Melton Road, Leicester LE 4 7PD England.





and



The reactions take place in the interstitial liquid of the gel and various configurations may be used in order to introduce the different components which should influence particle size and their distribution.

Some of the components may be introduced into the sol prior to gelation and the missing components diffused from external sources or all the components may be successively introduced by diffusion methods. The reaction which takes place within the pores of the gel filled with interstitial liquid depends on the solubility product of the forming precipitate and the kinetics will be influenced by the concentration gradients, i.e. by the size and geometry of the pores which control the diffusive fluxes.

Classically, a gel matrix is prepared by hydrolysis and polycondensation of various alkoxides, e.g. for  $SiO_2$ : tetramethoxysilane  $Si(OCH_3)_4$ , TMOS or tetraethoxysilane  $Si(OC_2H_5)_4$ , TEOS. As, however, these reactants and water are immiscible, the addition of a common solvent, usually an alcohol, is indispensable to ensure initial homogeneity. This can be avoided by using ultrasonic irradiation during sol formation.

Sonocatalysis leads to gels which have a higher density, smaller pore-size (typically of  $\sim 30$  Å diameter) and more uniform pore-size distribution<sup>9</sup>.

The satisfactory drying of the gels requires the addition of drying control chemical additives (DCCA's) which are introduced into the sol before gelling. The use of these compounds results in narrower size distribution of pore sizes<sup>10</sup>.

The combination of sonocatalysis with DCCA's should therefore create optimal conditions for small and regular pore-size formation which in turn should influence the size of the precipitated crystallites within the gel matrix.

The use of the chalcogenide particles containing gels for optical applications necessitates that the surfaces of the gel pieces be satisfactorily polished and that the dried gels do not condense vapour from the ambient atmosphere. The best solution is superficial or total impregnation with a material of identical optical index which seals the pores without impairing the optical transmission. Impregnation with polymers (e.g. PMMA) has been proposed<sup>11</sup>. In this work we used  $SiO_2$  as sealant as has already been reported in a previous communication<sup>12</sup>.

## 2. PREPARATION OF THE HOST GELS

Pure silica gels were used as matrices for  $CdS$  and  $CdSe_x S_{1-x}$  precipitates. Two main classes were tested:

a) "Classic" gels formed from alkoxides in the usual way, containing various DCCA's: formamide, acetamide, glycerol. The preparation of the classic formamide-containing gel follows essentially the recipe indicated by Hensch<sup>10</sup>: 15 cm<sup>3</sup> of TMOS, 12.5 cm<sup>3</sup> of formamide and 12.5 cm<sup>3</sup> of methylalcohol are stirred for 5 minutes with a magnetic blender. Then 2 cm<sup>3</sup>  $HNO_3$  and 18.2 cm<sup>3</sup>  $H_2O$  are added and stirring continued for a further 10 minutes. The liquid is poured into a plastic container which is then hermetically sealed and gelation is obtained at 50°C. The gels are then aged for 12h.

In the case of other DCCA's, 10 cm<sup>3</sup> of acetamide or 10 cm<sup>3</sup> of glycerol were substituted for 12.5 cm<sup>3</sup> of formamide.

b) "Sonogels" using ultrasonic irradiation. The compositions used were identical to the preceding ones, except that the 12.5 cm<sup>3</sup> of alcohol was omitted. The mixture was insonated for 3 minutes with an energy density of 0.6 w cm<sup>-3</sup> and then poured into plastic containers hermetically sealed. As before, gelation was obtained at 50°C and the gels aged for 12 hours. The reactants used for Cd chalcogenide precipitates were: Cd(NO<sub>3</sub>)<sub>2</sub> and K<sub>2</sub>SeO<sub>4</sub>. Thioacetamide CH<sub>3</sub>CSNH<sub>2</sub> (TAA) served as the source of S<sup>=</sup> ions.

The following methods of introducing the various reactants were used :

#### 2-1 Successive diffusions method

In this method, already indicated by ROY<sup>13</sup>, the pure SiO<sub>2</sub> aged gel was removed from the syneresis liquid and washed with distilled water. The first reactant, usually Cd(NO<sub>3</sub>)<sub>2</sub> in water solution, was then diffused for 1-4 days. After rinsing in distilled water, the second reactant, generally thioacetamide, was diffused, immersing the specimen in a solution of TAA in water. To measure the diffusion coefficient, the space between the specimen and the vessel containing the TAA solution was partially filled with polyethyleneglycol (PEG) leaving only the upper specimen face in contact with TAA. This arrangement enables the axial progress of the reaction front to be easily monitored.

#### 2-2 Simple diffusion method

In this method Cd(NO<sub>3</sub>)<sub>2</sub> (and eventually K<sub>2</sub>SeO<sub>4</sub>) were dissolved in the initial mixture before gelling. The resulting gels containing Cd<sup>2+</sup> (and eventually Se<sup>=</sup>) ions were then placed in contact with the TAA solution. It should be noted that before diffusion of TAA the initially Se-doped gels were colourless. This seems to indicate that the reaction between Cd<sup>2+</sup> and Se<sup>=</sup> did not occur before the introduction of S<sup>=</sup> ions. The precipitate layer is yellow-orange with a shift towards red as the proportion of Se increases.

In a limited number of cases diffusion from a gas phase without direct contact with TAA solution was tested. The presence of the reactive atmosphere containing TAA was sufficient to bring about a faint yellow colouration, the Cd-containing gels being placed singly in the vicinity of an open container filled with TAA solution at 50°C for periods of up to 3 weeks. Sometimes coloured bands appeared in glycerol-containing gels.

#### 2-3 Solid couple diffusion method

In this method two separate gels, one containing Cd(NO<sub>3</sub>)<sub>2</sub> (and evt. K<sub>2</sub>SeO<sub>4</sub>) and the second TAA, are put in contact with each other forming a diffusion couple. Contact is maintained for 1 hour, then the gels are separated and maintained at 50°C. This permits the extent of the reaction to be limited and produces lighter, more transparent specimens. It is possible to obtain in this way concentration gradients in precipitated particles which give rise to optical density gradients.

It is to be noted that Cd-containing gel becomes more intensely coloured than its TAA-doped counterpart - this seems to indicate that the transport velocity of S<sup>=</sup> ions is higher than that of Cd<sup>2+</sup> ions.

In the case of gels containing glycerol as DCCA, coloured bands were observed in some of the diffusion experiments.

### 3. DIFFUSION MEASUREMENTS

When a compound diffuses through a gel containing a substance which will form a sparingly soluble precipitate with this compound, the precipitate will usually appear as a dense mass with a fairly sharp plane diffusion front. The process obeys Fick's diffusion law.

If  $c_1$  and  $c_2$  are respectively the concentrations of the external diffusing compound and of the substance contained in the gel and  $D_1$  and  $D_2$  their corresponding diffusion coefficients, assumed to be constant :

$$\frac{\partial c_1}{\partial t} = D_1 \frac{\partial^2 c_1}{\partial x^2}$$

and

$$\frac{\partial c_2}{\partial t} = D_2 \frac{\partial^2 c_2}{\partial x^2}$$

At the diffusion boundary they satisfy the relation :

$$D_1 \frac{\partial c_1}{\partial t} + D_2 \frac{\partial c_2}{\partial t} = 0$$

The diffusion front defined by the distance  $x_f$  from the interface will advance as a function of time  $t$  according to the formula :

$$x_f = k_1 \sqrt{2D_1 t} \quad (1)$$

where  $k_1$  is the solution of the so-called "Adair's equation" <sup>14-15</sup>

$$\frac{\text{sq exp } (-\frac{1}{2} k^2)}{G(k)} = \frac{\text{exp } (-\frac{1}{2} k^2 s^2)}{\frac{1}{2} - G(ks)} \quad (2)$$

In this equation  $G(\xi)$  is defined as

$$G(\xi) = \frac{1}{\sqrt{2\pi}} \int_0^\xi \exp(-\frac{1}{2} n^2) dn \quad (3)$$

or, in terms of error functions :

$$\text{erf}(\xi) = \frac{2}{\sqrt{\pi}} \int_0^\xi \exp(-n^2) dn$$

$$G(\xi) = \frac{1}{2} \text{erf}\left(\frac{\xi}{\sqrt{2}}\right)$$

Furthermore,  $q = c_{10}/c_{20}$  is the ratio of the initial concentrations  $c_{10}$  and  $c_{20}$  of the two reacting species and the parameter

$$s = (D_{10}/D_{20})^{1/2}$$

can be calculated from the diffusion constants  $D_{10}$  and  $D_{20}$  at infinite dilution of the two reactants using Nernst equation.

According to the relation (1) the plot of  $x_f$  vs  $\sqrt{t}$  should be linear. In the diffusion experiments presented here the advance of the diffusion front  $x_f$  is followed measuring the thickness of the coloured precipitate layer and a "penetration coefficient" :

$$p = x_f^2/2t \quad (4)$$

evaluated.

The solution of the Adair's equation (2) then yields the factor  $k_1$  and the diffusion coefficient  $D_1$  of the external reactant is given by the relation :

$$D_1 = p/k_1^2 \quad (5)$$

In our case we have assumed  $s=1$  which can be shown to be equivalent to Adair's "negative ion convention". This amounts to assuming that the in situ reactant effectively removes the incoming reactant and diffuses in the opposite direction to the incoming reactant at the same speed. This is a reasonable assumption when  $q > 10$  i.e. when, for  $s=1$ ,  $k_1 > 1.5$ . For smaller  $q$  values, however, the influence of  $s$  is greater and when, at constant  $q$ ,  $s$  increases,  $k_1$  decreases which means that by assuming  $s=1$  the  $D_1$  is then underestimated.

#### 4. RESULTS

##### 4-1 Preparation of CdS precipitates

###### 4-1-1 Successive diffusions method

Figures 1a and 1b show the results obtained respectively for glycerol-containing "classic" gels and "sonogels". In these experiments the concentration of the inner component  $\text{Cd}(\text{NO}_3)_2$  was kept constant at  $c_2 = 3.49 \times 10^{-3} \text{ mol/l}$  and the concentration  $c_1$  of the external infusing component (TAA) was varied between  $19 \times 10^{-3} \text{ mol/l}$  and  $30 \times 10^{-3} \text{ mol/l}$

The results show that in all cases there is a very fast uptake of TAA resulting in the formation of a superficial layer of CdS (of about 2.5 mm in 20 minutes) followed by a much slower increase in thickness.

Table I shows the corresponding diffusion parameters  $p$ ,  $k_1$  and  $D_1$  calculated for both the "fast" and "slow" diffusion stages. In the fast diffusion the coefficient  $D_1$  is seen to be practically constant and close to  $1.5 \times 10^{-5} \text{ cm}^2 \text{ s}^{-1}$ . In the second stage the diffusion coefficients of classic gels are higher than those of sonogels and depend on the TAA concentration while those for sonogels are practically independent of TAA concentration.

###### 4-1-2 Single diffusion method

When the inner reactant  $\text{Cd}(\text{NO}_3)_2$  is not diffused separately but incorporated before gelation, the diffusion pattern is modified.

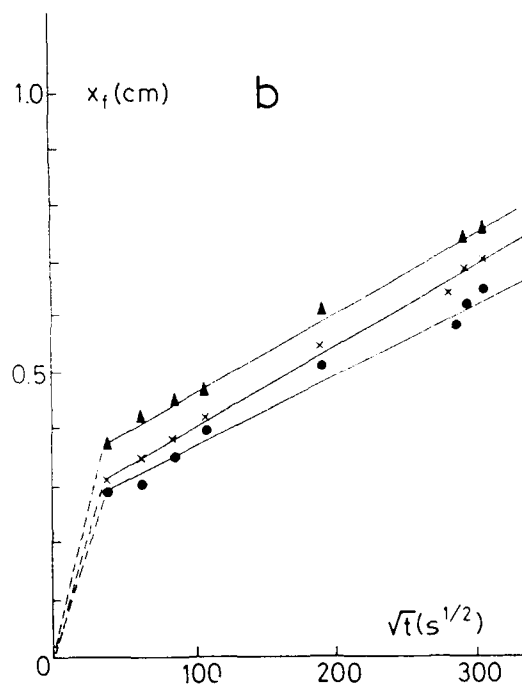
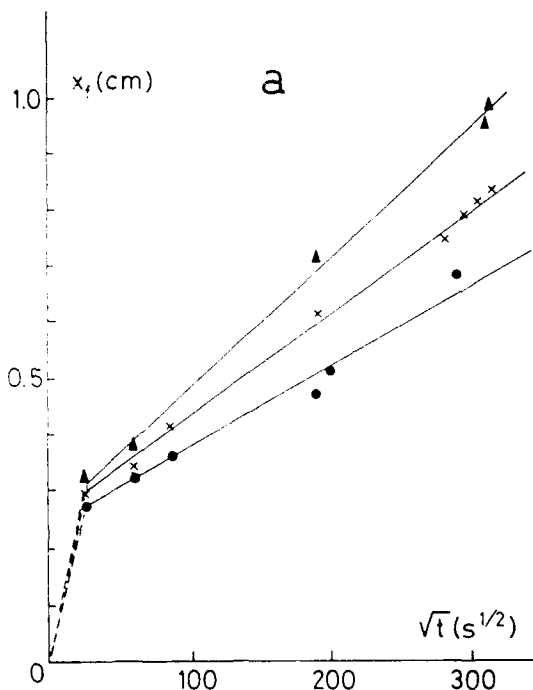


Fig.1 - Diffusion of TAA into glycerol-silica gels containing  $3.29 \times 10^{-3} \text{ mol/l Cd(NO}_3)_2$  previously introduced by diffusion, for various TAA concentrations:

● :  $19 \times 10^{-3} \text{ mol/l}$  ; × :  $26 \times 10^{-3} \text{ mol/l}$  ; ▲ :  $30 \times 10^{-3} \text{ mol/l}$

a) classic gels

b) sonogels

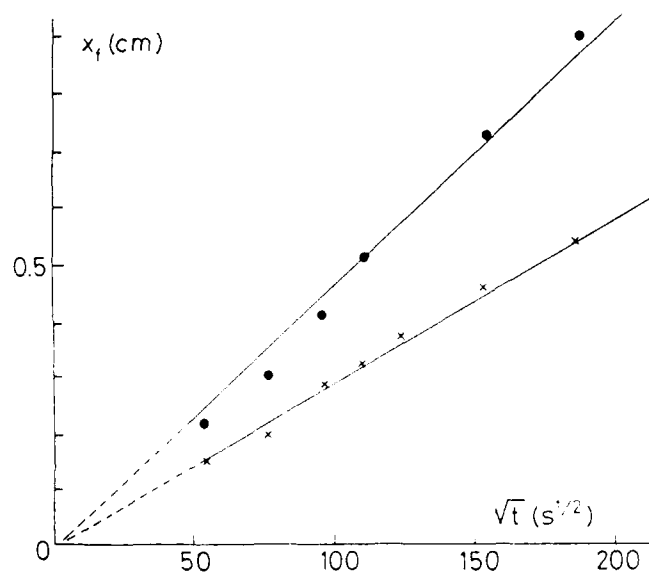
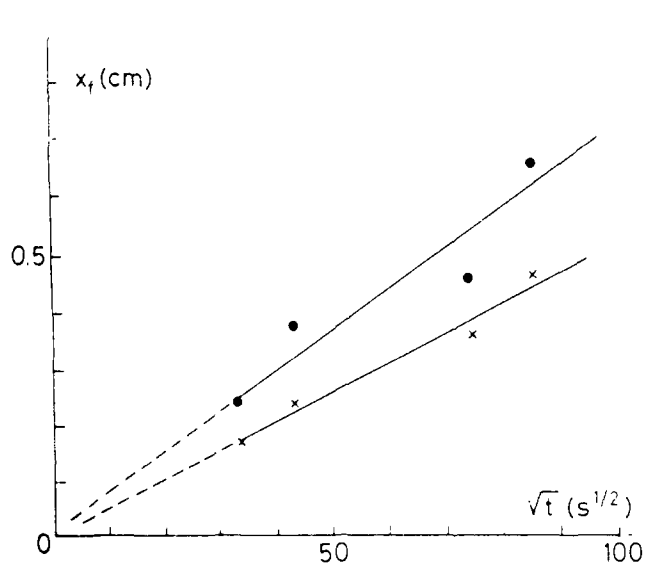


Fig.2 - Diffusion of TAA into formamide-silica gels with  $3.29 \times 10^{-3} \text{ Cd(NO}_3)_2 \text{ mol/l}$  for two TAA concentrations :

× :  $1.73 \times 10^{-3} \text{ mol/l}$  ; ● :  $13.9 \times 10^{-3} \text{ mol/l}$

Fig.3 - Diffusion of TAA of concentration  $13.9 \times 10^{-3} \text{ mol/l}$  into formamide-silica gels containing  $1.29 \times 10^{-3} \text{ mol/l Cd(NO}_3)_2$  and  $2.5 \times 10^{-4} \text{ mol/l K}_2\text{SeO}_4$

● : classic gels ; × : sonogels

Table I

Diffusion of TAA of concentration  $c_1$  in silica gels containing  
 $c_2 = 3,29 \times 10^{-3}$  mol/l of  $\text{Cd}(\text{NO}_3)_2$

Gel Type and DCCA	$c_1 \times 10^3$ mol/l	$k_1$	FAST DIFFUSION $t < 20$ min.		SLOW DIFFUSION $t > 20$ min.	
			$p \times 10^5$ $\text{cm}^2 \text{s}^{-1}$	$D_1 \times 10^5$ $\text{cm}^2 \text{s}^{-1}$	$p \times 10^6$ $\text{cm}^2 \text{s}^{-1}$	$D_1 \times 10^6$ $\text{cm}^2 \text{s}^{-1}$
CLASSIC GLYCEROL	19	1.45	3.2	1.52	0.88	0.42
	24	1.52	3.75	1.55	1.62	0.70
	26	1.56	3.5	1.44	1.65	0.67
	30	1.65	4.2	1.54	2.72	1.0
SONO GLYCEROL	19	1.45	3.5	1.67	0.76	0.36
	22	1.51	3.5	1.52	0.76	0.33
	26	1.56	3.75	1.48	0.76	0.31
	30	1.65	5.7	2.09	1.02	0.37

Figure 2 shows typical results for a formamide-containing sonogel. The diffusion is more regular in the beginning and shows a very progressive slowing down for higher diffusion times.

Table II assembles the initial diffusion parameters obtained for classic gels and sonogels with different DCCA's. It can be seen that when TAA concentration increases the penetration coefficients  $p$  increase but the diffusion constants  $D_1$  actually decrease. The type of gel influences  $D_1$  :

$$D_1(\text{sono-formamide})/D_1(\text{classic-formamide}) \sim 0.7 - 0.8$$

$$D_1(\text{sono-formamide})/D_1(\text{sono-glycerol}) \sim 0.8$$

Table II

Diffusion of TAA of concentration  $c_1$  in silica gels containing  
 $c_2 = 1,28 \times 10^{-3}$  mol/l  $\text{Cd}(\text{NO}_3)_2$

Gel Type and DCCA	$c_1 \times 10^3$ (mol/l)	$k_1$	$p \times 10^5$ $\text{cm}^2 \text{s}^{-1}$	$D_1 \times 10^5$ ( $\text{cm}^2 \text{s}^{-1}$ )
CLASSIC	1.73	0.79	1.25	1.96
FORMAMIDE	13.9	1.72	2.45	0.83
SONO	1.73	0.79	0.60	1.25
FORMAMIDE	13.9	1.72	1.73	0.58
SONO	1.73	0.79	1.0	1.60
GLYCEROL	13.9	1.72	2.1	0.71



#### 4-2 Preparation of $\text{CdSe}_x\text{S}_{1-x}$ precipitates

Figure 3 shows typical diffusion plots obtained for a formamide-sonogel compared to a classic formamide gel. The gels contained  $1.28 \times 10^{-3} \text{ mol/l}$   $\text{Cd}(\text{NO}_3)_2$  and  $2.5 \times 10^{-4} \text{ mol/l}$   $\text{K}_2\text{SeO}_4$ . The TAA concentration was  $13.9 \times 10^{-3} \text{ mol/l}$ . The diffusion parameters are contained in Table III which shows results obtained for a series of sono- and classic gels with formamide or DCCA as a function of TAA concentration.

Table III

Diffusion of TAA of concentration  $c_1$  in silica gels containing  $c_2 = 1,28 \times 10^{-3} \text{ mol/l}$   $\text{Cd}(\text{NO}_3)_2$  and  $2,5 \times 10^{-4} \text{ mol/l}$   $\text{K}_2\text{SeO}_4$

		Classic Gels			Sono Gels	
DCCA	$c_1 \times 10^3$ (mol/l)	$k_1$	$p \times 10^5$ ( $\text{cm}^2 \text{ s}^{-1}$ )	$D_1 \times 10^5$ ( $\text{cm}^2 \text{ s}^{-1}$ )	$p \times 10^5$ ( $\text{cm}^2 \text{ s}^{-1}$ )	$D_1 \times 10^5$ ( $\text{cm}^2 \text{ s}^{-1}$ )
FORMAMIDE	1.74	0.79	0.16	0.26	0.09	0.15
	3.47	1.09	0.33	0.28	0.21	0.18
	6.94	1.42	0.52	0.26	0.29	0.14
	8.00	1.48	0.55	0.25	0.31	0.14
	10.90	1.59	0.61	0.24	0.31	0.12
	12.50	1.68	0.68	0.24	0.38	0.13
	13.89	1.73	0.70	0.23	0.44	0.15

Figure 4 shows the evolution of the diffusivity  $D_1$  as a function of the TAA concentration. It can be seen that  $D_1$  is practically independent of (TAA). This justifies the original assumption in the Fick's equations that  $D_1$  is independent of concentration. The average value of the diffusion constants are :

$$\begin{aligned}
 D_1 \text{ (classic)} &= 0.25 \pm 0.03 \text{ cm}^2 \text{ s}^{-1} \\
 D_1 \text{ (sono)} &= 0.145 \pm 0.03 \text{ cm}^2 \text{ s}^{-1} \\
 \text{and} \\
 D_1 \text{ (sono)} / D_1 \text{ (classic)} &\sim 0.6
 \end{aligned}$$

#### 5. GENERAL DISCUSSION OF THE RESULTS

Specimens obtained by the double diffusion method give rise to rather opaque precipitate layers. The opacity can be reduced by diminishing the  $\text{Cd}(\text{NO}_3)_2$  concentration. The TAA concentration and temperature are less effective in controlling the degree of transparency.

The initial stage of rapid diffusion is linked with abundant precipitation of chalcogenide particles and their agglomeration into voluminous precipitates which can attain  $0.5 \mu\text{m}$  and more as shown by electron microscopy (Fig.5a). In this method the original solvent elimination, followed by rinsing in distilled water, enlarges the pores, eliminating the residual groups and parts of the gel skeleton. This is favourable to the increase of particle size of the precipitate by diffusion, agglomeration and coarsening.

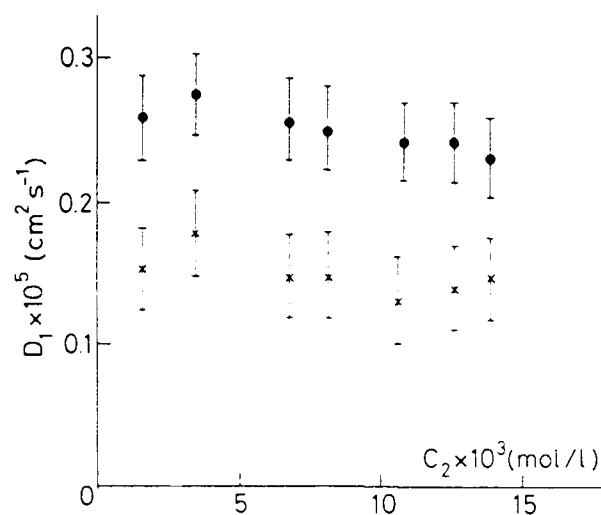


Fig.4 - Diffusion constant  $D_1$  of TAA in formamide-silica gels containing  $1.28 \times 10^{-3} \text{ mol/l Cd(NO}_3)_2$  and  $2.5 \times 10^{-4} \text{ mol/l K}_2\text{SeO}_4$  as a function of TAA concentration  $C_2$ .

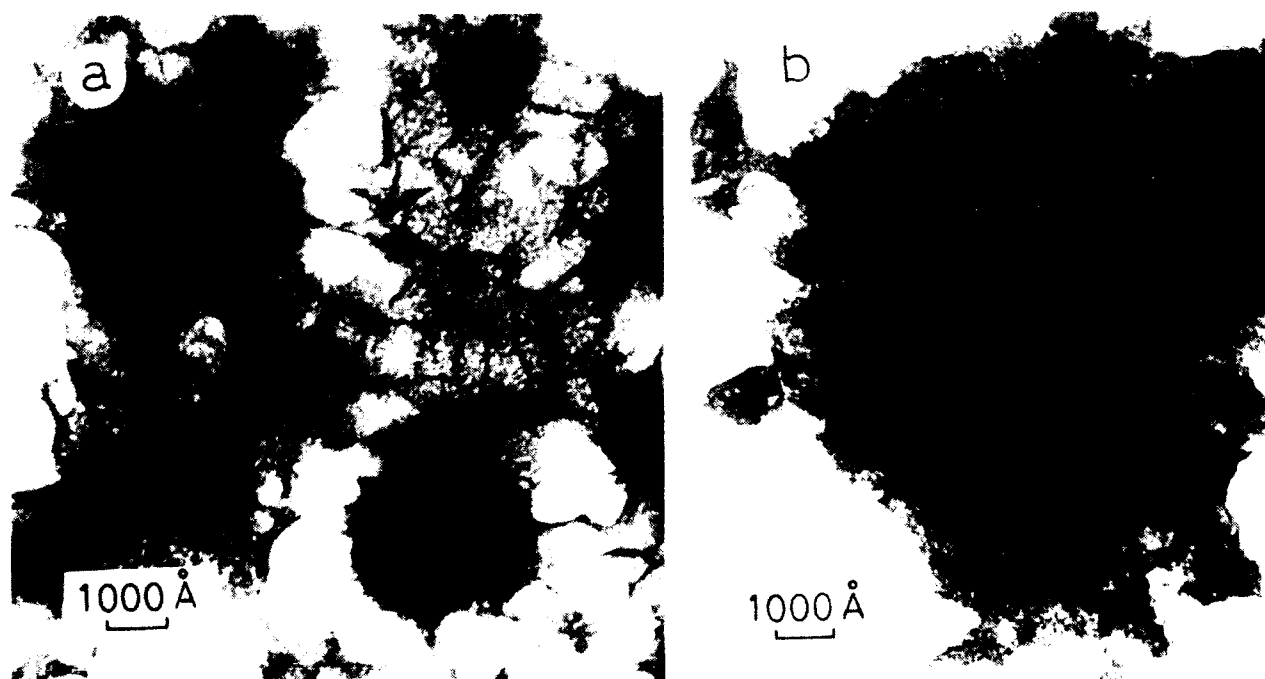


Fig.5 - Transmission electron micrographs of classic formamide-silica gels containing  $\text{CdSe}_x\text{S}_{1-x}$  particles obtained by:

a) double diffusion method.

b) single diffusion method.

In contrast, simple diffusion methods where the gel skeleton is intact and contains a highly dispersed  $\text{Cd}(\text{NO}_3)_2$  in the micropores, lead to very small size precipitates which are trapped in the individual pores and do not coalesce easily.

The transparency of the samples can be complete and correspondingly, electron microscopy shows only uniform darker veils obscuring the pores without resolved particles - the size of which is probably below 100 Å (Fig.5b).

The simple diffusion method is thus to be adopted in optical applications.

Behaviour during drying and final impregnation depends on the method used to prepare the host gel. In general it has been observed that sonogels show a lesser tendency to break into fragments on drying than do the "classic" gels. With regard to the various DCCA's tested, the gels containing formamide, and especially acetamide, show the best resistance against fragmentation, while glycerol-containing gels are the worst and also give rise to non-uniform precipitation. The volume shrinkage of gels on drying varies with the DCCA used in the order :  
(glycerol) < (formamide) < (acetamide).

## 6. ACKNOWLEDGEMENTS

One of us (C.M.Bagnall) wishes to thank the C.N.R.S. for financial support during her stay in Montpellier.

## 7. REFERENCES

1. N. Peyghambarian and S.W. Koch, "Femtosecond and coherent effects in bulk  $\text{CdSe}$  and  $\text{CdSe}_x\text{S}_{1-x}$ -doped glasses", *Revue Phys. Appl.* **22**, 1711-1715, 1987.
2. J.T. Remillard and D.G. Steel, "Narrow nonlinear-optical resonances in  $\text{CdSe}$ -doped glass", *Optics Letters*, **13** (1) 30-32, 1988.
3. H. Jerominek, M. Pigeon, S. Patela, Z. Jakubczyk, C. Delisle and R. Trémbay, " $\text{CdS}$  microcrystallites-doped thin-film glass waveguides", *J. Appl. Phys.* **63** (3) 957-959, 1988.
4. N.F. Borelli, D.W. Hall, H.J. Holland and D.W. Smith, "Quantum confinement effects of semiconducting microcrystallites in glass", *J. Appl. Phys.* **61**, 5399-5409, 1987.
5. R. Rosetti, J.L. Ellison, J.M. Gibson and L.E. Brus, "Size effects in the excited electronic states of small colloidal  $\text{CdS}$  crystallites", *J. Chem. Phys.* **80** (9), 4464-4469, 1984.
6. R. Rosetti, R. Hull, J.M. Gibson and L.E. Brus, "Excited electronic states and optical spectra of  $\text{ZnS}$  and  $\text{CdS}$  crystallites in the 15 to 50 Å range ; evolution from molecular to bulk semiconducting properties", *J. Chem. Phys.* **82** (1) 552-559, 1985.
7. R. Rosetti, S. Nakahara and L.E. Brus "Quantum size effects in the redox potentials, resonance Raman spectra and electronic spectra of  $\text{CdS}$  crystallites in aqueous solution", *J. Chem. Phys.* **79** (2) 1086-1088, 1983.
8. J.H. Simons, E.M. Clausen Jr. and B.G. Potter Jr., "Nonlinear-optical composite materials using  $\text{CdS}$ " in *Ultrastructure Processing of Advanced Ceramics*, pp.661-669, J.D.Mackenzie and D.R.Ulrich, Eds., Wiley, N.Y., 1988.
9. J. Zarzycki, "Sonogels-Development and Perspectives" in *4th Intern. Conf. on Ultrastructure Processing of Ceramics, Glasses and Composites*, Tucson (AZ), 12-19 Feb. 1989.

10. L. Hench, "Use of Drying Control Chemical Additives (DCCA's) in controlling sol-gel processes" in *Science of Ceramic Chemical Processing*, pp. 52-64, L.L.Hench and D.R.Ulrich, Eds., Wiley, N.Y. 1986.

11. E.J.A. Pope and J.D. Mackenzie, "Porous and dense composites from sol-gel", *Proc.Mat.Res.Soc.* 73, 809-814, 1986.

12. C.M. Bagnall and J. Zarzycki, "The use of solution impregnation to dope silica gels with Cd, Se and S", *J. Non-Cryst.Sol.* (in press).

13. R. Roy, S. Kumarneni and D. Roy, *Mater. Res. Symp. Proc.*, 27, 342, 1984.

14. G.S. Adair, "The penetration of electrolytes into gels II : The application of Fourier's linear diffusion law". *Biochemical J.* 14, 762-779, 1920.

15. S. Shinohara, "A theory of one-dimensional Liesegang phenomena", *J. Phys. Soc. Japan*, 29 (4) 1073-1087, 1970.



Preparation of semiconducting sulfides microcrystalline-doped silica glasses by the sol-gel process

Masayuki Nogami, Michie Watabe, and Katsumi Nagasaka

Aichi Institute of Technology  
1247 Yakusa, Toyota 470-03, Japan

### ABSTRACT

The sol-gel process has been applied successfully to the preparation of small-particle-size ZnS, CdS or PbS-doped silica glasses with a significant quantum size effect. Gels prepared through the hydrolysis of complex solutions of  $\text{Si}(\text{OC}_2\text{H}_5)_4$  and acetate of Zn, Cd or Pb were heated at 500 to 900°C, then reacted with  $\text{H}_2\text{S}$  gas to form fine microcrystals doped glasses. From X-ray diffraction analyses and transmission electron micrographs, these crystals were cubic ZnS, hexagonal CdS and cubic PbS crystal, respectively, and their sizes were 2 to 8 nm in diameter. In the optical absorption spectra, the absorption edge exhibited a blue shift compared with those of the bulk sulfides crystals. Size dependence of energy shift was discussed in relation to size quantization of electron-hole in microcrystals. The nonlinearity was estimated to be  $1.5 \times 10^{-10}$  esu for 2% CdS doped glass.

### 1. INTRODUCTION

Recently, there has been a significant increase of interest in nonlinear optical materials. Glasses doped with small size semiconductors, in which the electron and hole wave functions are quantum confined by a deep potential well, have large, resonant third-order nonlinearity. Jain and Lind first studied high, nonlinear optical properties of  $\text{CdS}_x\text{Se}_{(1-x)}$  doped glasses<sup>1</sup>. Since then, although many results have been published, the glasses measured are commercial filter glasses and the dopants are limited to a few crystals such as  $\text{CdS}_x\text{Se}_{(1-x)}$  or  $\text{CuCl}$ <sup>2-7</sup>. It is desired that many different type of semiconductor crystals can be incorporated into glasses, which enables us to extend the studies beyond the limitation of  $\text{CdS}_x\text{Se}_{(1-x)}$  or  $\text{CuCl}$ .

The authors have been conducting a study of the preparation of glasses containing small size semiconductor particles by the sol-gel process and first reported the CdS microcrystals doped silica glasses<sup>8,9</sup>. Sol-gel process is superior to the conventional glass melting method because it provides glasses of unusual compositions with high purity and good homogeneity at temperatures significantly lower than those required by the melting method.

In this study, we report the preparation of ZnS, CdS or PbS microcrystals doped silica glasses by the sol-gel process. Crystal structure and size were determined and the blue shift in the optical absorption of the obtained glasses were investigated in relation to the quantum size effect of their crystals. The nonlinearity of CdS doped glass was also estimated by the degenerate four-wave mixing method.

### 2. EXPERIMENTAL PROCEDURE

#### 2.1. Preparation of glasses and their reaction with $\text{H}_2\text{S}$ gas

Sulfides doped glasses were prepared by synthesis of silica glasses containing 4.2% ZnO, 4.4% CdO and 4.5% PbO, respectively, and subsequent reaction with  $\text{H}_2\text{S}$  gas. The process is represented schematically in fig.1.  $\text{Si}(\text{OC}_2\text{H}_5)_4$  was at first partially hydrolyzed by dropping it into a mixed solution of  $\text{H}_2\text{O}$ ,  $\text{C}_2\text{H}_5\text{OH}$  and  $\text{HCl}$  of which the molar ratio was 1, 1 and 0.0027 mol, respectively, per 1 mol of  $\text{Si}(\text{OC}_2\text{H}_5)_4$ . After this solution was stirred for 1 h, the each metal acetate dissolved in  $\text{CH}_3\text{OH}$  was added, followed by stirring for 1 h at room temperature. The resultant homogeneous solution was hydrolyzed by adding the mixed solution of  $\text{H}_2\text{O}$ ,  $\text{C}_2\text{H}_5\text{OH}$  and  $\text{NH}_4\text{OH}$  as a catalyst. In this second hydrolysis reaction, the molar ratio was maintained at 4, 1 and 0.0027 mol, respectively, per 1 mol of



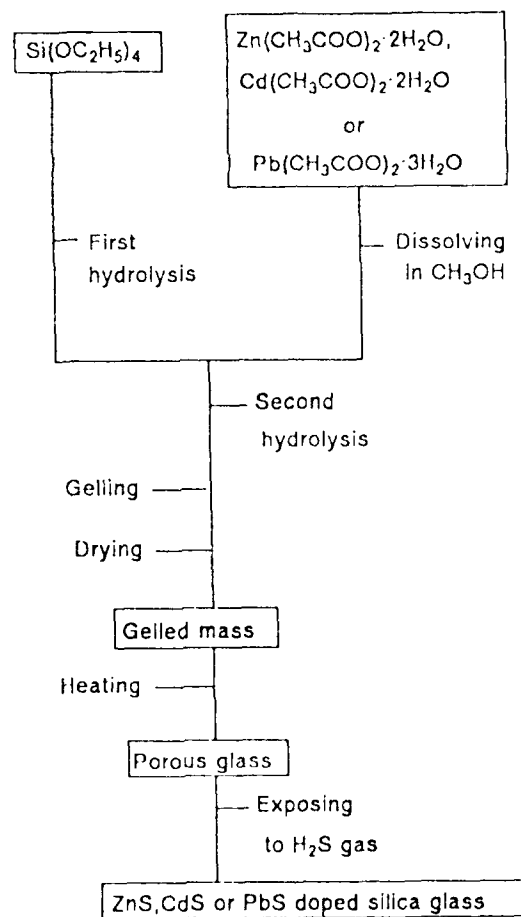


Fig. 1. Schematic representation of the sol-gel process

$\text{Si}(\text{OC}_2\text{H}_5)_4$ . After stirring for 1 h, the solution was poured into a polystyrene container and was left for 2–3 d with cover to form a stiff gel, followed by drying without cover for 3–4 d at room temperature.

This gel was heated at  $50^\circ\text{C}/\text{h}$  to  $500\text{--}900^\circ\text{C}$  and kept for 2 h. Reaction of glass with  $\text{H}_2\text{S}$  gas was performed by flowing the dried  $\text{H}_2\text{S}$  gas at 25 to  $400^\circ\text{C}$  in a glass tube which was previously placed under vacuum by a rotary pump.

## 2.2. Measurement of $\text{N}_2$ gas adsorption

Surface measurement of glasses was performed by  $\text{N}_2$  gas adsorption using a Micromeritics Instrument (Flowsorb II, 2300). The specific surface area and the pore size distribution were calculated by BET equation and the Cranston-Inkley model, respectively.

## 2.3. Characterization of microcrystals doped glasses

The X-ray diffraction measurements were carried out using a Rigaku diffractometer (Rad-C System) with a copper  $\text{K}\alpha$  wavelength and a graphite monochromator. The diffracted X-ray was collected by scanning between  $2\theta = 20$  and  $60^\circ$  in  $0.04^\circ$  steps and counting for 100 s.

Glass microstructures were also studied with a JEM-2000FX transmission electron microscope.

Optical absorption spectra of the glasses 0.1 to 0.5 mm thick were measured in the range 200 to 3000 nm with a Shimadzu UV-3100S spectrometer.

### 3. RESULTS AND DISCUSSION

#### 3.1. Sulfide microcrystals precipitation

The gels prepared by the sol-gel process were porous, with a mean pore radius ranging from 1 to 1.5 nm, and they contained physically and chemically adsorbed water and organic compounds on their particle surfaces. When heated, these gels shrank according to dehydration-condensation reaction and sintering, which resulted in collapse of the pores. The porous structure remained unchanged in glasses heated below 900°C, at which temperature the gels transformed into impervious, nonporous glasses. Specific surface area of glasses heated for 2 h at 500°C is listed in table 1, 420 to 550 m<sup>2</sup>/g, in which large difference is not observed between the compositions.

Exposing the porous glasses to H<sub>2</sub>S gas changed their colors to yellow and brown to black for CdO and PbO containing glasses, respectively, whereas the glass containing ZnO remained transparent. These phenomena indicate the formation of sulfide crystals in the glass matrices.

Figure 2 shows the XRD patterns of glasses heated at 500°C(a) and then reacted with H<sub>2</sub>S gas at various times and temperatures(b, c and d). The glass heated at 500°C only shows the typical amorphous halo pattern, whereas the XRD patterns of glasses reacted with H<sub>2</sub>S gas have several broad peaks on a background due to the amorphous phase. Comparing the peak profiles with JCPDS files<sup>10</sup>, the data files are fitted quite well to the cubic ZnS, hexagonal CdS and cubic PbS crystal for patterns (b), (c) and (d), respectively, and all the peaks can be indexed to diffraction lines of each crystal as seen in figs. 2(b), (c) and (d).

The size of crystal was determined from broadening of the diffraction lines, using the Scherrer's formula  $D = 0.9 \lambda / (\beta \cos \theta)$ , where  $\lambda$  is X-ray wavelength and  $\beta$  is the line broadening. The value of line broadening, defined as the full-width at half-maximum(FWHM) intensity of the broad diffraction line, was obtained by taking the instrument broadening into account<sup>11</sup>. The mean diameters of the microcrystals were calculated as 4.0, 5.8 and 5.7 nm for figs. 2(b), (c) and (d), respectively.

Transmission electron microscopy was used to confirm the results obtained by XRD analyses. Figure 3 shows the TEM micrographs of fracture surfaces. The particles observed are practically spherical, of which average sizes coincide with the results of XRD analyses. Hereafter, the size of crystals was determined from the XRD experiments. It was found that the crystal size increased with increasing the exposure time and temperature to H<sub>2</sub>S gas.

Table 1  
Specific surface area of glasses heated for 2 h at 500°C

	Surface area (m <sup>2</sup> /g)
ZnO	424
CdO	554
PbO	538

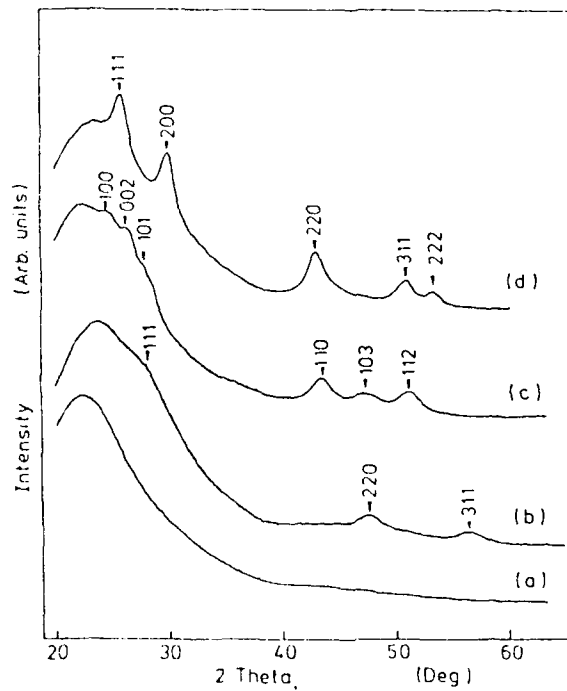


Fig. 2. XRD patterns of glass heated (a) for 2 h at 500°C, and glasses containing ZnO (b), CdO (c) or PbO (d) reacted with H<sub>2</sub>S gas (b) for 5 h at 250°C, (c) for 20 h at 25°C or (d) for 1 h at 250°C after heating at 500°C.

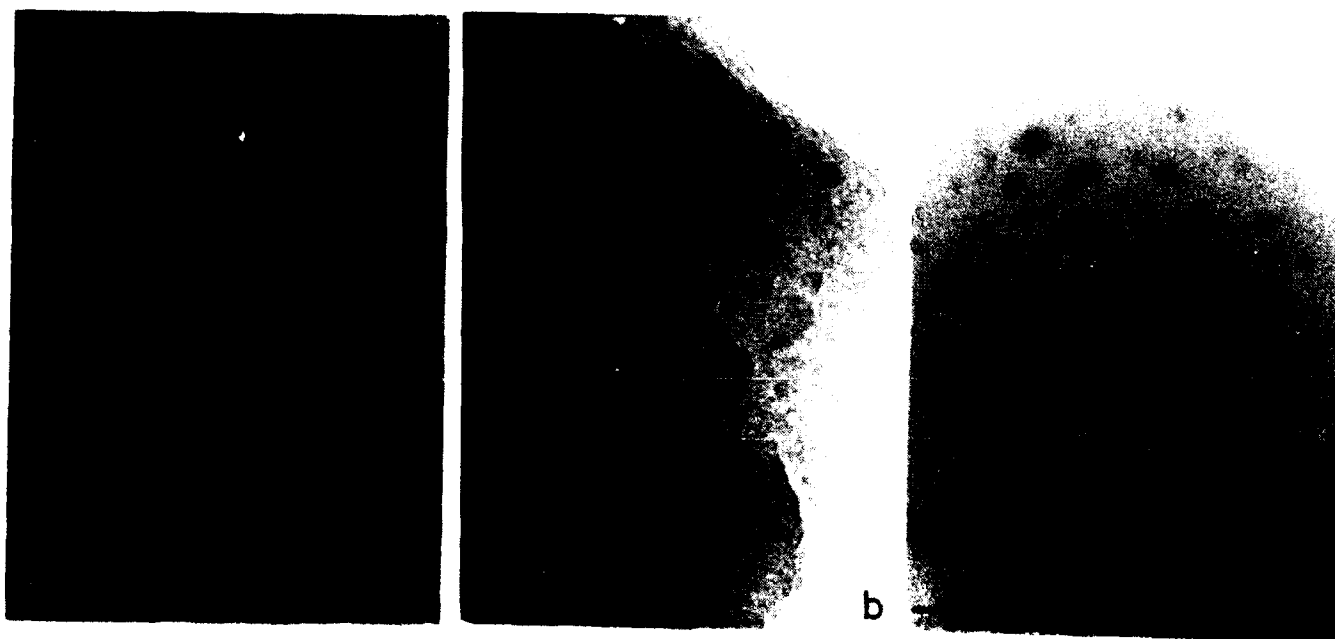


Fig. 3. Transmission electron micrographs of glasses containing ZnO(a), CdO(b) or PbO(c) reacted with H<sub>2</sub>S gas (a) for 4 h at 100°C, (b) for 20 h at 25°C or (c) for 23 h at 250°C after heating at 500°C.



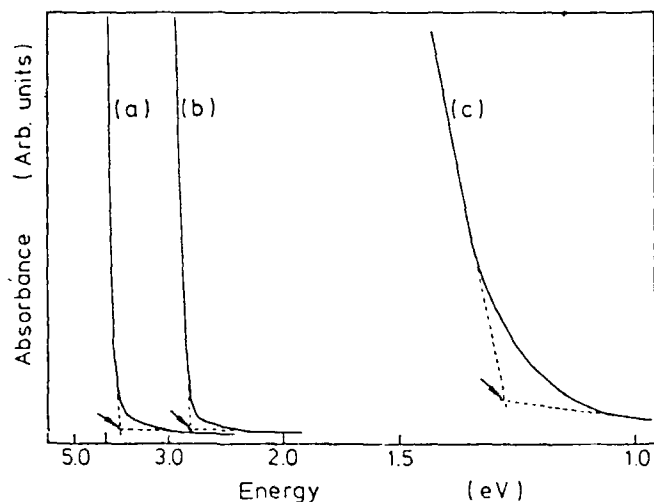


Fig. 4. Absorption spectra of glasses containing ZnO (a), CdO (b) or PbO (c) reacted with  $H_2S$  gas (a) for 5 h at  $250^\circ C$ , (b) for 2 h at  $25^\circ C$  or (c) for 1 h at  $250^\circ C$  after heating at  $500^\circ C$ .

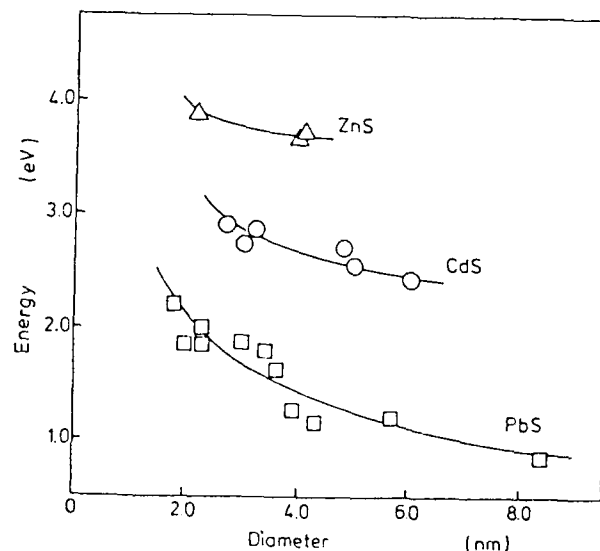


Fig. 5. Relations between the energy gap and the crystal size.

### 3.2. Optical absorption spectra

Figure 4 shows the absorption spectra of glasses containing ZnO, CdO and PbO, respectively, heated for 2 h at  $500^\circ C$ , followed by reaction with  $H_2S$  gas at various times and temperatures. The absorption edge of PbS containing glass shows a long tail, suggesting the broad distribution of particles size. The absorption is assigned to a transition from the highest hole subband to the lowest electron subband level, and the gap energies, obtained by interpolating the absorbance at zero, are 3.73, 2.74 and 1.20 eV for figs. 4(a), (b) and (c), respectively. Comparing with the band gaps of ZnS, CdS or PbS bulk crystals, the values of fig. 4 correspond to 0.09, 0.21 and 0.79 eV of blue shifts. The blue shift proves the quantum size effect of the microcrystals doped in the matrices. The blue shift energy was found to decrease as the exposure time and temperature to  $H_2S$  gas increase.

### 3.3. Quantum size effect of sulfides microcrystalline doped glasses

The blue shifts of absorption edge can be considered due to the quantum size effect of the carrier confinement. The charge carriers in the semiconductor particles are in potential wells defined by the conduction and valence bands of the particles and the dielectric glass matrix. This carrier confinement leads to the creation of discrete levels in the conduction and valence band in small particles. Therefore, the energy gap should increase with decreasing the crystal size.

To examine the quantum size effect of our sulfides doped glasses, the absorption edge and crystallite size of glasses reacted with  $H_2S$  gas at various conditions were determined from the absorption spectra and XRD analyses, respectively. Figure 5 shows the relations between the energy gap and crystallite size. As the crystallite size decreases, the band gap energy increases. Crystal size dependence of these quantum size effects was examined by the models of Brus<sup>12</sup> and Wang et al<sup>13</sup>.

Finally, the nonlinear optical properties were studied using forward degenerate four-wave mixing (DFWM) method. From the DFWM experiment, the nonlinearity of 2% CdS doped glass was estimated to be  $1.5 \times 10^{-10}$  esu at 390 nm which was the wavelength correspond to the band gap energy.

#### 4. ACKNOWLEDGMENTS

The authors wish to thank A. Nakamura, Nagoya University, for the nonlinearity measurements and helpful discussions and K. Kotani, Industrial Research Institute, Aichi Prefectural Government, for TEM measurement. This work was supported in part by The Nippon Sheet Glass Foundation for Materials Science and The Ookura Foundation.

#### 5. REFERENCES

1. R.K. Jain and R.C. Lind, "Degenerate Four-Wave Mixing in Semiconductor-Doped Glasses," *J. Opt. Soc. Am.*, **73**, 647-53(1983).
2. A. I. Ekimov and A. A. Onushchenko, "Quantum Size Effect in the Optical Spectra of Semiconductor Microcrystals," *Sov. Phys. Semicond.*, **16**, 775-77(1982).
3. A. I. Ekimov, A. L. Efros, and A.A. Onushchenko, "Quantum Size Effect in Semiconductor Microcrystals," *Solid State Commun.*, **56**, 921-24(1983).
4. N. F. Borrelli, D. W. Hall, H. J. Holland, and D. W. Smith, "Quantum Confinement Effects of Semiconducting Microcrystallites in Glass," *J. Appl. Phys.*, **61**, 5399-409(1987).
5. Y. Fuyu and J. M. Parker, "Quantum Size Effects in Heat Treated Cd(S,Se) Doped Glasses," *Mater. Lett.*, **6**, 233-37(1988).
6. B. G. Potter, Jr., and J. H. Simmons, "Quantum Size Effects in Optical Properties of CdS-Glass Composites," *Phys. Rev. B*, **37**, 10838-45(1988).
7. A. Nakamura, H. Yamada, and T. Tokizaki, "Size-Dependent Radiative Decay of Excitons in CuCl Semiconducting Quantum Spheres Embedded in Glasses," *Phys. Rev. B*, **40**, 8585-88(1989).
8. M. Nogami, K. Nagasaka, and E. Kato, "Preparation of Small-Particle-Size, Semiconductor CdS-Doped Silica Glasses by the Sol-Gel Process," *J. Am. Ceram. Soc.*, **73**, (1990).
9. M. Nogami, K. Nagasaka, and M. Takata, "CdS Microcrystal-Doped Silica Glass Prepared by the Sol-Gel Process," in press in *J. Non-cry. Solids*, (1990).
10. JCPDS files, No. 50566 (ZnS), No. 60314 (CdS), No. 50592 (PbS).
11. A. P. Klug and L. E. Alexander, *X-ray Diffraction Procedures*, Chapter 9. Wiley, N.Y., (1974).
12. L. E. Brus, "Electron-Electron and Electron-Hole Interactions in Small Semiconductor Crystallites: The Size Dependence of the Lowest Excited Electronic State," *J. Chem. Phys.*, **80**, 4403-09(1984).
13. Y. Wang, A. Suna, W. Mahler, and R. Kasowski, "PbS in Polymers. From Molecules to Bulk Solids," *J. Chem. Phys.*, **87**, 7315-22(1987).



Preparation of CdS-doped glasses by the sol-gel method

Noboru Tohge, Masahiro Asuka and Tsutomu Minami

Department of Applied Chemistry, University of Osaka Prefecture  
Mozu-Umemachi, Sakai-Shi, Osaka-Fu 591, Japan

### ABSTRACT

CdS-doped  $\text{SiO}_2$  glasses have been prepared through the sol-gel process. A methanol solution of cadmium nitrate and thiourea in a molar ratio of 1:2 was added to the  $\text{SiO}_2$  sol prepared from silicon tetraethoxide. The mixed solution was left for gelation at 50 °C and thereby complexes of cadmium nitrate with thiourea were confined in the gel. The gel obtained was then heat-treated at 350 °C in air for the decomposition of the complexes to CdS, the elimination of residual organics, and the densification. The above process produced the transparent  $\text{SiO}_2$  glasses doped with CdS microcrystallites up to Cd/Si = 0.05. The optical absorption edge of the CdS-doped glasses moved to longer wavelengths from that of non-doped  $\text{SiO}_2$  glasses with increasing Cd/Si ratio. The size of CdS microcrystallites in the glasses was further controllable with the additional heat-treatment at around 400 °C in a 10%  $\text{H}_2\text{S}$ /90% Ar stream. For these CdS microcrystallite-doped glasses, the peak of photoluminescence was shifted to shorter wavelengths relative to the absorption edge of CdS crystal, in agreement with the blue shift of the optical absorption edge; these shifts were indicative of the quantum size effects.

### 1. INTRODUCTION

Semiconductor microcrystallites doped in glasses exhibit optical properties different from bulk crystals due to the quantum size effects.<sup>1-3</sup> One of the practical interests in these materials is the very fast and strong optical nonlinear response, which has a potential application to optical switching and signal processing.<sup>4,5</sup> For the manifestation of the strong nonlinearity in these materials, it is essential to control the size and its distribution of the doped microcrystallites. Commercially available cut-off filters are typical glasses doped with semiconductor microcrystallites such as  $\text{CdS}_x\text{Se}_{1-x}$  and produced by the conventional melt-quenching method. Various doping techniques have also been studied extensively to improve the above characteristics and to extend the variety of doped semiconductors: modified melt-quenching,<sup>6</sup> sputtering<sup>7,8</sup> and so on.

The sol-gel process is an alternative method to dope semiconductor microcrystallites to glasses. Nogami et al. have recently prepared CdS microcrystallite-doped  $\text{SiO}_2$  glasses through the sol-gel process; CdO-containing  $\text{SiO}_2$  glasses were first prepared by the usual sol-gel method and then CdO in the glasses was sulfurized to CdS on exposure to a  $\text{H}_2\text{S}$  stream.<sup>9,10</sup> On the other hand, the present authors have proposed a different sol-gel process for the doping of semiconductor microcrystallites to glasses. In the process, metal salts and thiourea are added to sols which are pre-

pared from metal alkoxides, confined in gels on gelation, and then thermally decomposed to metal sulfides in the gels; CdS microcrystallite-doped  $\text{SiO}_2$  glasses have been prepared by this process.<sup>11</sup> The above process is based on the fact that metal salts form complexes with thiourea and the aqueous solutions containing these complexes are used for the preparation of the sulfide films by the spray-pyrolysis in air.<sup>12-14</sup>

The present paper concerns with the formation of complexes of cadmium salts with thiourea in alcohol solutions, the formation process of CdS microcrystallite-doped  $\text{SiO}_2$  glasses, and the optical properties of the resultant doped glasses.

## 2. EXPERIMENTAL

Silicon tetraethoxide,  $\text{Si}(\text{OEt})_4$ , was diluted with ethanol, EtOH, and hydrolyzed with  $\text{H}_2\text{O}$ , which contained 0.3 % HCl, the molar ratios of EtOH and  $\text{H}_2\text{O}$  to  $\text{Si}(\text{OEt})_4$  being 10 and 5, respectively. Proper molar ratios of cadmium salt and thiourea,  $\text{SC}(\text{NH}_2)_2$ , were dissolved in methanol, MeOH;  $\text{MeOH}/\text{Si}(\text{OEt})_4$  was 10. A variety of cadmium salts such as nitrate, chloride, acetate, and sulfate were examined as a starting material in terms of solubility in alcohol. Among them,  $\text{Cd}(\text{NO}_3)_2 \cdot 4\text{H}_2\text{O}$  was found to be the most soluble in MeOH and hence used through the present work. An appropriate amount of the methanol solution thus prepared was mixed with the above  $\text{SiO}_2$  sol and left for gelation at 50 °C; the sol gelled typically in about 20 h. After being dried, the obtained gel was heat-treated in air for the decomposition of the complexes of  $\text{Cd}(\text{NO}_3)_2$  with  $\text{SC}(\text{NH}_2)_2$  to CdS, the elimination of residual organics, and the densification. Some gels were subjected to further heat-treatment in various atmospheres to control the size of precipitated CdS; the details of the heat-treatment will be described below.

The gels were thermally analyzed with a differential thermal analysis/thermogravimetry (MAC, TG/DTA 2000) to determine heat-treatment conditions. The optical absorption spectra of the doped glasses were measured at room temperature using a UV-visible spectrophotometer (Hitachi, U-3200). The photoluminescence spectra was measured at 77 K using a fluorescence spectrophotometer (Shimadzu, RF-501). The x-ray diffraction patterns were obtained using a rotating cathod x-ray diffractometer (Rigaku, RAD-rA). The size of the doped crystallites was evaluated using a transmission electron microscope (JEOL, JEM-2000). The IR spectra were measured using an IR spectrophotometer (Hitachi, 260-50) by the KBr method.

## 3. RESULTS AND DISCUSSION

### 3.1 Formation of complexes of cadmium salts with thiourea

As mentioned above, cadmium salts,  $\text{CdX}_2$  ( $\text{X} = \text{Cl}^-$ ,  $\text{NO}_3^-$ , or  $\text{CH}_3\text{COO}^-$ ), form complexes,  $\text{Cd}[\text{SC}(\text{NH}_2)_2]_n\text{X}_2$ , with  $\text{SC}(\text{NH}_2)_2$  in aqueous solution;  $n$  depends on the preparation conditions.<sup>10-12</sup> The formation of the complexes of  $\text{Cd}(\text{NO}_3)_2$  with  $\text{SC}(\text{NH}_2)_2$  in methanol solutions was studied from the x-ray diffraction and IR spectra on the crystal-

line residue, which remained after evaporating the solvent from the solution of both components in various molar ratios. The x-ray diffraction patterns showed that the residues were of different single phases for  $\text{Cd}(\text{NO}_3)_2 : \text{SC}(\text{NH}_2)_2 = 1:1$  and  $1:2$ , whereas they were of multiphases for  $\text{Cd}(\text{NO}_3)_2 : \text{SC}(\text{NH}_2)_2 = 1:3$  and  $1:4$ .

Figure 1 shows the IR spectra of  $\text{SC}(\text{NH}_2)_2$  (a) and the crystalline residue after the evaporation of methanol for  $\text{Cd}(\text{NO}_3)_2 : \text{SC}(\text{NH}_2)_2 = 1:2$  (b). Taking notice of the absorption peaks associated with  $\text{S}=\text{C}$  bonding in thiourea ( $740$  and  $635\text{ cm}^{-1}$ ),<sup>13</sup> these peaks are shifted toward lower wavenumbers ( $710$  and  $620\text{ cm}^{-1}$ ) in the residue. These peak shifts indicate the coordination of a sulfur atom in thiourea to a  $\text{Cd}^{2+}$  ion and thereby the formation of the complexes of  $\text{Cd}(\text{NO}_3)_2$  with  $\text{SC}(\text{NH}_2)_2$ ; the presence of  $\text{NO}_3^-$  ions is shown by the absorption peak at  $825\text{ cm}^{-1}$ . The formation of the complexes was also confirmed for  $\text{Cd}(\text{NO}_3)_2 : \text{SC}(\text{NH}_2)_2 = 1:1$ .

The thermal analysis in air on the thiourea complex of  $\text{Cd}(\text{NO}_3)_2$  is shown in Fig.2;  $\text{Cd}(\text{NO}_3)_2 : \text{SC}(\text{NH}_2)_2 = 1:2$ . Remarkable weight loss in a temperature range from  $160$  to  $250^\circ\text{C}$ , accompanied with two exothermic peaks, is ascribable to the decomposition of the complex and the simultaneous combustion of the volatile products. The x-ray measurement showed that the decomposition product at  $300^\circ\text{C}$  was hexagonal  $\text{CdS}$ , though the weight loss at this temperature ( $53\%$ ) is rather smaller than that expected from the conversion of  $\text{Cd}[\text{SC}(\text{NH}_2)_2](\text{NO}_3)_2$  to  $\text{CdS}$  ( $63\%$ ). The gradual weight loss observed over  $300^\circ\text{C}$  probably arises from the decomposition of the remaining complexes and/or the oxidation of resultant  $\text{CdS}$ ; the x-ray

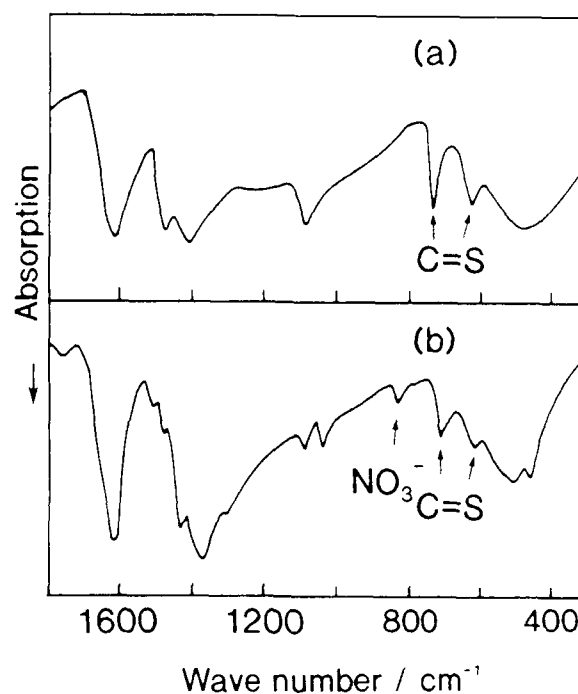


Fig.1. IR spectra of  $\text{SC}(\text{NH}_2)_2$  (a) and the crystalline residue obtained from a methanol solution of  $\text{Cd}(\text{NO}_3)_2$  and  $\text{SC}(\text{NH}_2)_2$  in the molar ratio of  $1:2$  (b).

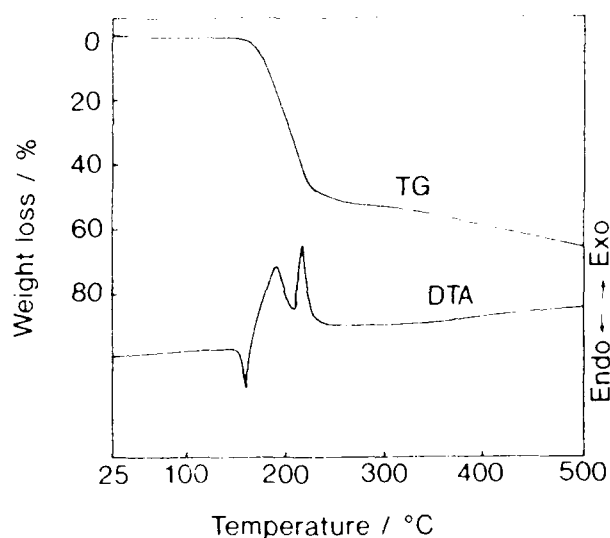


Fig.2. DTA/TG curves in air for the complex of  $\text{Cd}(\text{NO}_3)_2$  with  $\text{SC}(\text{NH}_2)_2$ , in the molar ratio of  $1:2$ .

diffraction measurement on the samples heat-treated up to 500°C showed the presence of CdO in CdS. The above results show that the complexes are formed between  $\text{Cd}(\text{NO}_3)_2$  and  $\text{SC}(\text{NH}_2)_2$  in alcohol solutions and are thermally decomposed to CdS at around 250°C in air. In the further study, the molar ratio of  $\text{Cd}(\text{NO}_3)_2$  to  $\text{SC}(\text{NH}_2)_2$  is kept to be 1:2, taking consideration of the evaporation of sulfur during the heat-treatment.

### 3.2 Heat-treatment of the gels

Figure 3 shows an example of the DTA/TG curves in air for the dried gels, Cd/Si being 0.01. There is a gradual decrease in weight up to 200°C, due to the evaporation of the remaining solvent and water. A small but abrupt decrease in TG at around 330°C, accompanied with an exothermic peak, results from the combustion of the residual organics in the gel. This finding means that the heat-treatment in this temperature range is very important to eliminate the residual organics, though the complexes of  $\text{Cd}(\text{NO}_3)_2$  with  $\text{SC}(\text{NH}_2)_2$  is expected to decompose to CdS below 250°C in the gels as well. The gels were hence heat-treated at 350°C for 10 h in air for the elimination of the residual organics and the densification.

The above heat-treatment gave the transparent yellow glasses up to Cd/Si = 0.05, whereas there was a tendency for the glasses to become opaque over Cd/Si = 0.05; when the heat-treatment was insufficient, the glasses became dark brown. The optical absorption spectra of the glasses obtained are shown in Fig.4 for different Cd/Si ratios (0.001, 0.01, 0.03, and 0.05), along with the spectrum of the non-doped  $\text{SiO}_2$  glass prepared under the same conditions. The fundamental absorption edge of the doped glasses is shifted to longer wavelengths with respect to that of the non-doped  $\text{SiO}_2$  glass, as the Cd/Si ratio is increased; the absorption edge of the glass of Cd/Si = 0.05 almost corresponds to that of bulk CdS crystal. This finding implies that CdS microcrystallites precipitate in the glasses, and their size and/or

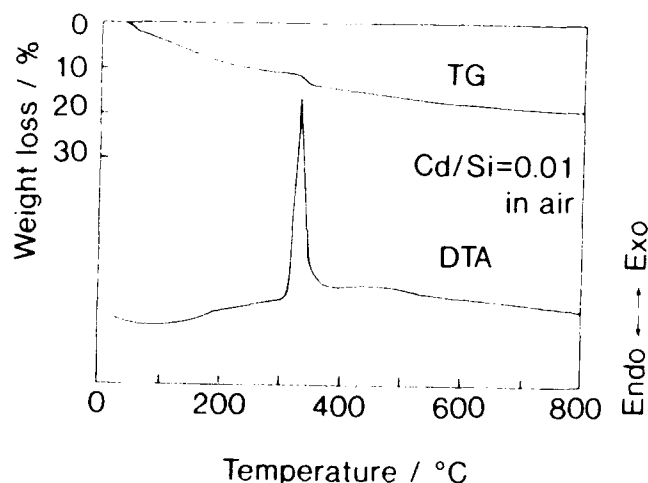


Fig.3. DTA/TG curves of dried gel of Cd/Si = 0.01 in air; the heating rate was 10°C/min.

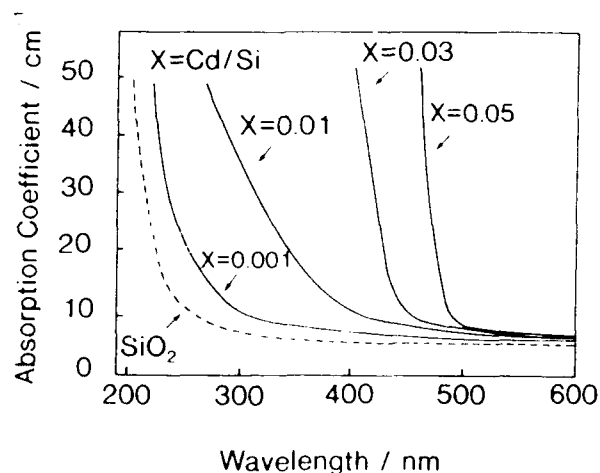


Fig.4. Optical absorption spectra of the CdS-doped glasses, along with the spectrum of the non-doped  $\text{SiO}_2$  glass; X = Cd/Si.

number increase with increasing Cd/Si ratio.

The crystalline phase of the CdS microcrystallites precipitated in the glasses was studied from the x-ray diffraction measurement. For the glasses of Cd/Si below 0.05, however, the scattering intensity was too weak to identify the crystalline phase of the precipitated CdS. Figure 5 shows the x-ray diffraction patterns of the doped SiO<sub>2</sub> glass of Cd/Si = 0.07 (a), of the non-doped SiO<sub>2</sub> glass (b), and the subtraction of (b) from (a), (c); these data were obtained in a step scanning mode at an interval of 0.05 deg with counting time of 100 sec at each point. The main peaks observed in the pattern (c) can be indexed as hexagonal CdS.

### 3.3 Properties of CdS-doped SiO<sub>2</sub> glasses

The doped glasses were further heat-treated at 400°C for various periods in various atmospheres (air, N<sub>2</sub>, Ar, vacuum, or 10% H<sub>2</sub>S/90% Ar stream) to control the size of the precipitated CdS microcrystallites. In the former four atmospheres, however, it was difficult to prevent sulfur from evaporating out of the glasses; the evaporation of sulfur was suggested from the bleaching of the yellow color of the glasses on heat-treatment. The glasses were hence heat-treated in a 10% H<sub>2</sub>S/90% Ar stream.

Figure 6 shows an example of the change in optical absorption spectra with additional heat-treatment at 400 °C for the glass of Cd/Si=0.03, along with the spectrum of the non-doped SiO<sub>2</sub> glass. The spectrum of the glass treated for 0 h corresponds to that of the glass of

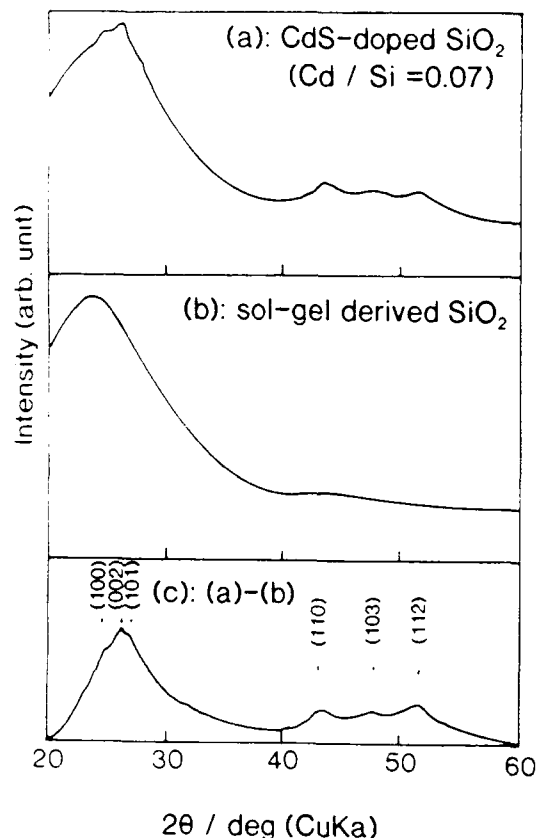


Fig.5. X-ray diffraction patterns for the CdS-doped SiO<sub>2</sub> glass of Cd/Si = 0.07 (a), the non-doped SiO<sub>2</sub> glass (b), and the subtraction of (b) from (a), (c).

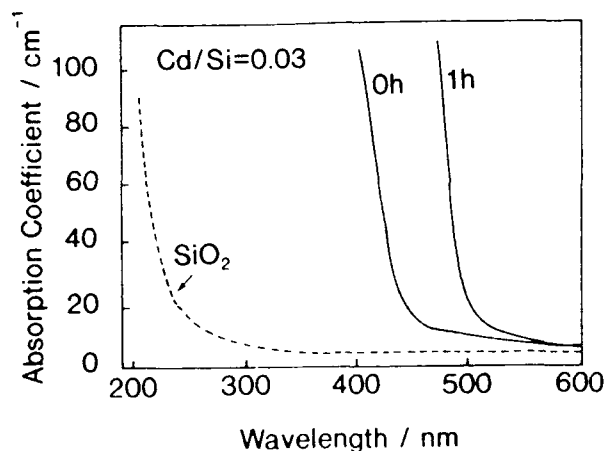


Fig.6. Change in optical absorption spectra with additional heat-treatment at 400 °C in a 10% H<sub>2</sub>S/90% Ar stream for the glass of Cd/Si = 0.03.

Cd/Si = 0.03 in Fig.4. The fundamental absorption edge is shifted to longer wavelengths with increasing treatment time. On the other hand, the glasses prepared from gels containing  $\text{Cd}(\text{NO}_3)_2$  but no  $\text{SC}(\text{NH}_2)_2$  was heat-treated under the same conditions and the shift of the absorption edge was compared with that of the glasses in Fig.6, to check the influence of the sulfurization of residual CdO in the glasses. As a result the shift of the absorption edge was found to be smaller in the former glasses than that in the latter. The shift of the absorption edge observed in Fig.6 is hence considered to result from the growth of the CdS microcrystallites rather than the sulfurization.

Figure 7 shows the photoluminescence spectra for the doped  $\text{SiO}_2$  glasses of Cd/Si = 0.03, the absorption spectra of which were shown in Fig.6. The spectra were measured with the excitation of 280 nm at 77 K. The spectra are maximized at 432 and 474 nm for the samples without (0 h) and with additional heat-treatment (1 h), respectively. The shift of peak energies of the luminescence almost agrees with that of band gap of the glasses in Fig.6, taking consideration of the temperature dependence of the band gap in CdS crystal ( $1.7 \times 10^{-4}$  eV/K). The result of the photoluminescence measurement therefore indicates that the blue shift of the absorption edge observed in Fig.5 is due to the quantum size effects.

Figure 8 shows the TEM photograph of the CdS microcrystallite-doped  $\text{SiO}_2$  glass of Cd/Si = 0.03, additionally heat-treated at 400°C for 1 h. In the speckled texture characteristic of glass, contrasted spots of the precipitated CdS microcrystallites

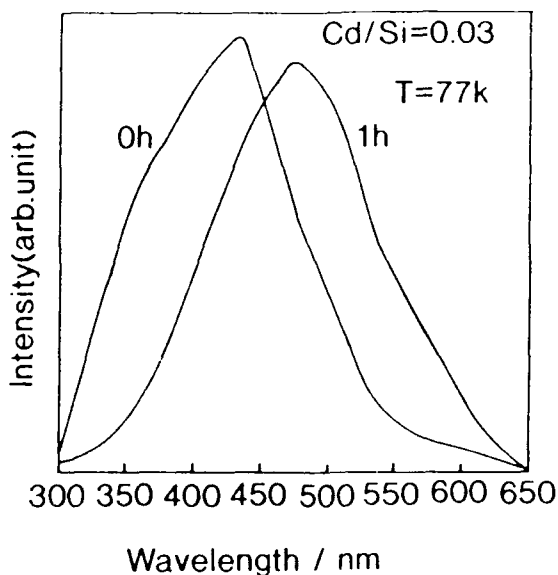


Fig.7. Photoluminescence spectra at 77 K of the CdS microcrystallite-doped  $\text{SiO}_2$  glasses of Cd/Si = 0.03, with and without additional heat-treatment at 400°C for 1 h in a 10%  $\text{H}_2\text{S}/90\%$  Ar stream.

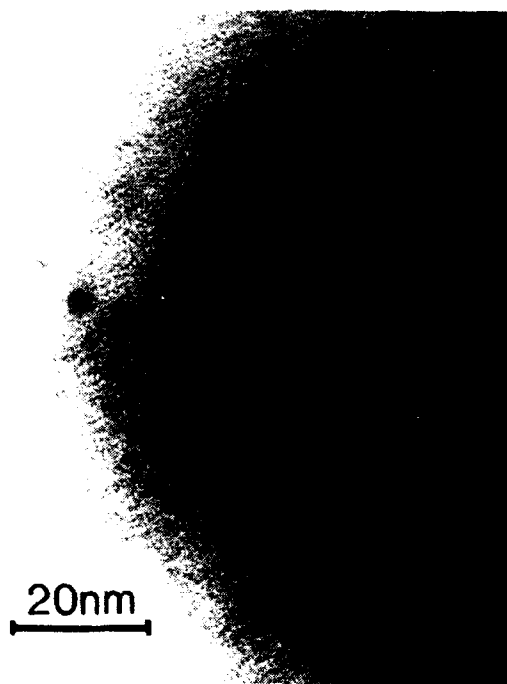


Fig.8. TEM photograph of the CdS-doped  $\text{SiO}_2$  glass of Cd/Si = 0.03, additionally heat-treated at 400°C for 1 h in a 10%  $\text{H}_2\text{S}/90\%$  Ar stream.



are distributed. The size of the spots is about 6 nm in average. For the doped glasses of Cd/Si = 0.03 without the additional heat-treatment, the size of the CdS microcrystallites was about 3 nm. These TEM observations directly support that the shift of absorption edge observed in Fig.6 is due to the change in size of precipitated CdS microcrystallites.

#### 4. Conclusion

A sol-gel process to dope CdS microcrystallites into SiO<sub>2</sub> glasses have been proposed. A salient feature of the present process is the confinement of the complexes of cadmium salts with thiourea into SiO<sub>2</sub> gels. It has been shown that the confined complexes are decomposed to CdS microcrystallites in the gels on heat-treatment in air. The size of the microcrystallites is controllable by the additional heat-treatment at around 400 °C. The optical absorption edge and the photoluminescence peak of the CdS-doped glasses are shifted to shorter wavelengths relative to that of CdS crystal, indicating that the quantum size effects occur. The present process is also applicable to the doping of selenide semiconductors when selenourea is used in place of thiourea and now under study.

#### ACKNOWLEDGEMENT

The authors are indebted to Prof. Dr. S. Anpo of the Department of Applied Chemistry for his kind permission of the use of a fluorescence spectrophotometer and to Dr. H. Tsuda of the Department of Metallurgy for his technical assistance for TEM observation.

#### REFERENCES

1. J. Warnock and D. D. Awschalom, "Quantum Size Effects in Simple Colored Glass", Phys. Rev. B, vol.32, pp.5529-31, 1985.
2. A. I. Ekimov, A. L. Efros and A. A. Onushchenko, "Quantum Size Effect in Semiconductor Microcrystals", Solid State Commun., vol.56, pp.921-24, 1985.
3. N. F. Borrelli, D. W. Hall, H. J. Holland and D. W. Smith, "Quantum Confinement Effects of Semiconducting Microcrystallites in Glass", J. Appl. Phys., vol.61, pp.5399-409, 1987.
4. R. K. Jain and R. C. Lind, "Degenerate Four-Wave Mixing in Semiconductor-Doped Glasses", J. Opt. Soc. Am., vol.73, pp.647-53, 1983.
5. N. Finlayson, W. C. Banyai, C. T. Seaton, G. I. Stegeman, M. O'Neill, T. J. Cullen and C. N. Ironside, "Optical Nonlinearities in CdS<sub>x</sub>Se<sub>1-x</sub>-Doped Glass Waveguides", J. Opt. Soc. Am. B, vol.6, pp.675-84, 1989.
6. S. Omi, S. Yoshida, Y. Asahara, A. Ikushima and J. Yumoto, "Properties of Semiconductor-Doped Glasses with CdS<sub>x</sub>Se<sub>1-x</sub> Microcrystallites Made by an Alternative Technique", Proc. 1st Japan Internat. SAMPE Symposium, pp.307-11, 1989.
7. H. Nasu, K. Tsunetomo, Y. Tokumitsu and Y. Osaka, "Semiconducting CdTe Microcrystalline-Doped SiO<sub>2</sub> Glass Thin Films Prepared by Rf-Sputtering", Jpn. J. Appl.

Phys., vol.28, pp.L862-64, 1989.

8. I. Tanahashi, A. Tsujimura, T. Mitsuyu and A. Nishino, "Optical Properties of CdS Microcrystallites-Doped Thin-Film Glass", Extended Abst. Topical Meeting of Glasses for Optoelectronics, pp.60-63, 1989.

9. M. Nogami, K. Nagasaka and E. Kato, "CdS Microcrystalline-Doped Silica Glasses Prepared by the Sol Gel Process", J. Non-Cryst. Solids, 1990 (in press).

10. M. Nogami, K. Nagasaka and E. Kato, "Preparation of Small-Particle-Size Semiconductor CdS-Doped Silica Glasses by the Sol-Gel Process", J. Am. Ceram. Soc., 1990 (in press).

11. N. Tohge, M. Asuka and T. Minami, "Doping of CdS Semiconductor Crystallites to SiO<sub>2</sub> Glasses by the Sol-Gel Process", Chemistry Express, vol.5, 1990. (in press)

12. D. Richards, A. M. El-Korashy, R. J. Stin and P. C. Karukar, "Highly Photoconducting O<sub>2</sub>-Doped CdS Films Deposited by Spray Pyrolysis", J. Va. Sci. Technol. A, vol.2, pp.332-35, 1984.

13. M. Krunk, E. Melikov and E. Sork, "Formation of CdS Films by Spray Pyrolysis", Thin Solid Films, vol.145, pp.105-09, 1986.

14. M. K. Karanjai and D. Dasgupta, "Preparation and Study of Sulphide Thin Films Deposited by the Dip Technique", Thin Solid Films, vol.155, pp.309-15, 1987.



## Graded Index Materials by the Sol-gel Process

Masayuki Yamane, Atsuo Yasumori, Mitsunobu Iwasaki and Kazutaka Hayashi

Tokyo Institute of Technology, Department of Inorganic Materials,  
2-12-1, Ookayama, Meguro-ku, Tokyo 152, Japan

## ABSTRACT

A gradient-index glass rod of about 13 mm in diameter and 20 mm in length with the refractive index difference of about 0.05 between center and perimeter has been prepared by the sol-gel process from a precursor solution consisted of tetramethoxysilane, tetraethoxysilane, boron ethoxide and aqueous solution of lead acetate. A bubble free wet gel of about 35 mm in diameter and 50 mm in length was obtained by adding acetic acid to the precursor solution as a buffering agent. The liquid in the micropores of the wet gel was totally replaced with acetone. Then the compositional gradient of lead was formed in radial direction of the gel by soaking in an ethanolic solution of potassium acetate. A transparent r-GRIN rod of about 13 mm in diameter was obtained by sintering the gel at 550°C.

## 1. INTRODUCTION

Gradient index (GRIN) glass rods, particularly those having a continuous variation in refractive index in radial direction (r-GRIN rods), have been applied in a wide variety of optical and optoelectronic devices such as compact photocopiers, communication relay systems, medical imaging systems, and so on<sup>1-3</sup>. Most of the r-GRIN rods used in these fields are currently manufactured by ion-exchange method, in which  $Tl^+$  or  $Cs^+$  ions contained in a glass rod as index-modifying ions are exchanged with  $K^+$  ions by immersing the glass rods in a  $K^+$ -containing fused salt bath<sup>4-8</sup>. This method is good for the precise control of the profile of refractive index with large  $\Delta n$ , i.e., with a large difference of refractive index between center and perimeter of the rod.

However, there are some devices in which the employment of r-GRIN rods by ion-exchange technique is not suitable or very difficult. For example, in a device which is used at a high temperature, the migration of alkali ions, therefore the distortion of refractive index-profile during its use, is inevitable in a GRIN lens based on the ion-exchange. Thus the development of r-GRIN lens of alkali free system is practically important to meet this requirement. The other examples are those which use lenses of large size such as cameras, binoculars, etc. *et al.*<sup>9</sup>. Because the maximum diameter of the r-GRIN rod produced by ion-exchange technique has been only a few mm or even less due to the small diffusion coefficient of  $Tl^+$  or  $Cs^+$  in glass. The r-GRIN lens of large size provides many advantages over homogeneous glass in the design of optical systems for cameras, binoculars etc. These advantages include greater simplicity by the reduction of total number of optical elements and improved performance<sup>10-11</sup>.

The sol-gel process, which begins with the formation of precursor sols by introducing the index-modifying cations in the form of either alkoxide or aqueous metal salt solution, is advantageous over others in the production of r-GRIN rods used in the fields where the material by ion-exchange technique is not appropriate<sup>12-15</sup>.

92-11413



92 4 28 031

The r-GRIN rod of alkali free system is manufactured by the partial leaching of Ti ions and subsequent drying and sintering of the gel of  $\text{TiO}_2\text{-SiO}_2$  or  $\text{TiO}_2\text{-SiO}_2\text{-Al}_2\text{O}_3$  system prepared from metal alkoxide precursors<sup>13,16,17</sup>. The method which was developed on the binary system by Shingyouchi et. al<sup>13</sup> and later extended to the ternary systems by Caldwell et. al<sup>17</sup> is relatively simple and good for the precise control of refractive index profile, although the  $\Delta n$  of the material is not very large.

The r-GRIN rod having large diameter can be prepared by the sol-gel method using aqueous metal salt solution<sup>14,15</sup>. The method in which the formation of compositional gradient of index modifying ions is made quickly by the interdiffusion of ions in the liquid phase filling the micropores of a gel, is advantageous to get a materials of large diameter in a short time. The advantages of this process also include the followings; (1) a large amount of index modifying cations such as lead can be incorporated into the gel, thus making large index changes possible, (2) almost any two ions can be interdiffused regardless of valence, thus making the wide variety of optical constants possible. Therefore, the production of the material having the diameter larger than 10 mm with  $\Delta n$  of 0.05 or more, which is hardly attainable by other processes such as ion-exchange, molecular stuffing and so on<sup>18,19</sup>, can be expected to the sol-gel process, although the technique has not yet been established.

This paper reports the study on the elimination of the underlying problems in the production of such r-GRIN rods<sup>20</sup> having large diameter and large  $\Delta n$  by the sol-gel process using aqueous metal salt solution. The main techniques introduced in the study were; (1) the introduction of acetic acid in the precursor sol as a buffering agent to control gelling time for the elimination of bubble inclusion during casting of a sol, (2) total replacement of acetone for water in a gel, before the formation of concentrational gradient of lead, in order to minimize the distortion of the formed concentrational profile due to the migration of lead ions and to eliminate the deformation of the gel upon drying, (3) the employment of ethanolic solution of potassium acetate as a source for potassium ion which was necessary to modify the change in glass property caused by the partial extraction of lead, and (4) the total replacement of acetone for ethanol after the formation of concentrational profile of lead.

## 2.EXPERIMENT

### 2.1.Gel preparation

The experiment was carried out on the precursor sol corresponding to a glass of the composition  $26\text{PbO-}7\text{B}_2\text{O}_3\text{-}67\text{SiO}_2$  (mol%) using tetramethoxysilane (TMOS), tetraethoxysilane (TEOS), triethoxyboron ( $\text{B}(\text{OEt})_3$ ), and aqueous lead acetate solution (aq-PbAc) as starting materials.

A mixture of 30 ml of TMOS, 30 ml of TEOS and 12.4 ml of  $\text{B}(\text{OEt})_3$  was hydrolyzed with 25 ml of aqueous HCl solution of pH=2. The mixture was then added to 107.6 ml of 1.25 mol/l aq-PbAc at the existence of 20 ml of acetic acid and stirred for 2.5 min. The eventual solution, a sol, was casted in a polypropylene vial of about 35 mm inside diameter up to the depth of about 50 mm and held at 30°C with a cover of aluminum foil. This procedure of gel preparation is illustrated in Fig. 1.

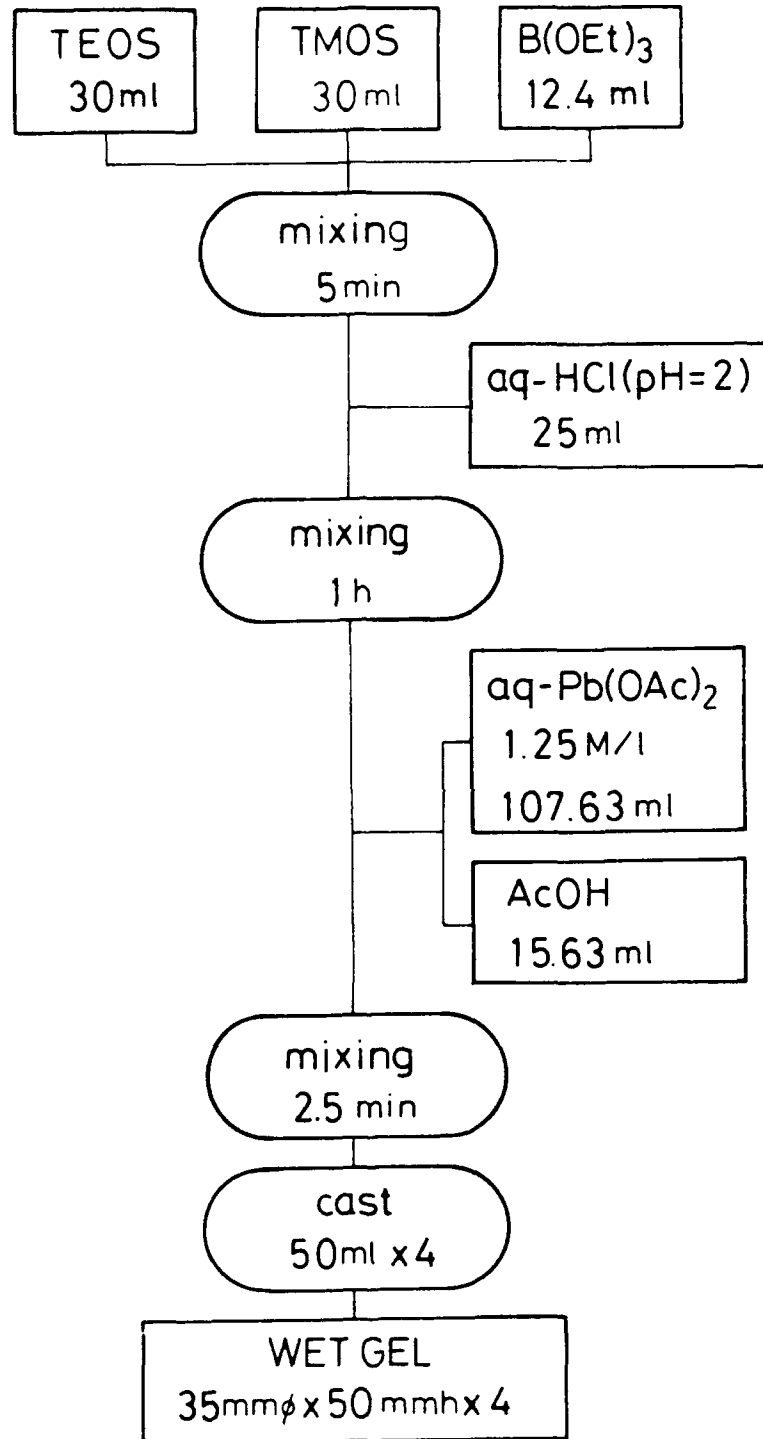


Fig.1. Flow chart for gel preparation.

## 2.2.Pretreatment of a wet gel

A wet gel formed in a polypropylene vial was subjected to pretreatments before the formation of concentrational gradient, in order to enhance gel strength and to replace acetone for water in the micropores. The flow chart of this process is shown in Fig. 2.

The enhancement of gel strength, which was necessary to keep the gel monolithic throughout the process and to avoid the deformation during drying, was made by aging at 30°C for 5 days. The gel was then transferred in a 50 ml bath of isopropanol-water system (iso-PrOH/H<sub>2</sub>O=80/20 in Vol) saturated with lead acetate to be soaked at 60°C for 2 days for the purpose of further aging and the extraction of acetic acid without reducing lead content. Next, the gel was soaked successively in 50 ml baths of isopropanol-aceton system of the compositions iso-PrOH/Aceton=80/20, 50/50, 0/100 (in Vol) at 30°C for 2 days, respectively, in order to totally replace acetone for the liquid in the micropores.

## 2.3.Formation of concentrational gradient of lead

After the total replacement of acetone for the liquid in the micropores, a wet gel containing fine crystals of lead acetate on micropore wall was soaked in 0.61 mol/l ethanolic solution of potassium acetate at room temperature for 2-48 h. During this treatment, the concentrational gradient of lead ions was formed in the radial direction by the gradual dissolution of the precipitated fine lead acetate crystals and subsequent diffusion of lead ions through micropores. The gel was then transferred to a bath of isopropanol-acetone system for the complete removal of the intermingled ethanol during the treatment and the reprecipitation of the dissolved lead acetate crystals. The flow chart of this step is shown in Fig.3.

## 2.4.Drying and sintering

The gel thus treated was placed on a teflon sheet in a glass container and covered with an aluminum foil. The drying of the gel was made by slowly evaporating acetone through a pin-hole formed on the aluminum foil. At the end of drying, the gel was about 20 mm in diameter and 30 mm in length and free from crack.

The dried gel was placed in a fused quartz reaction tube which was, in turn, placed horizontally in an electric furnace, and subjected to the heat treatment for densification. The heat treatment consisted of a 5°C/h ramp in temperature from room temperature up to 550°C with 24 h isothermal treatments at 200°C, 360°C, 460°C, 510°C, and a 48 h isothermal treatment at 550°C. Oxygen gas was fed into the reaction tube at a rate of about 60 ml/min up to a temperature slightly above 460°C, at which point helium was substituted for oxygen for the remainder of the heating cycle. At the end of the 550°C treatment, the temperature was reduced to room temperature at a rate of 60°C/h.

## 2.5.Measurement of refractive index profile of glass

The profile of refractive index of gel-derived glass was determined on a disc sample of about 1mm thickness which was cut out of the central part of the cylindrical glass, by both interferometry using He-Ne laser beam of wavelength 632.8 nm, and the measurement of the reflectivity of d-line (583 nm) at various points of the surface of the disc sample.

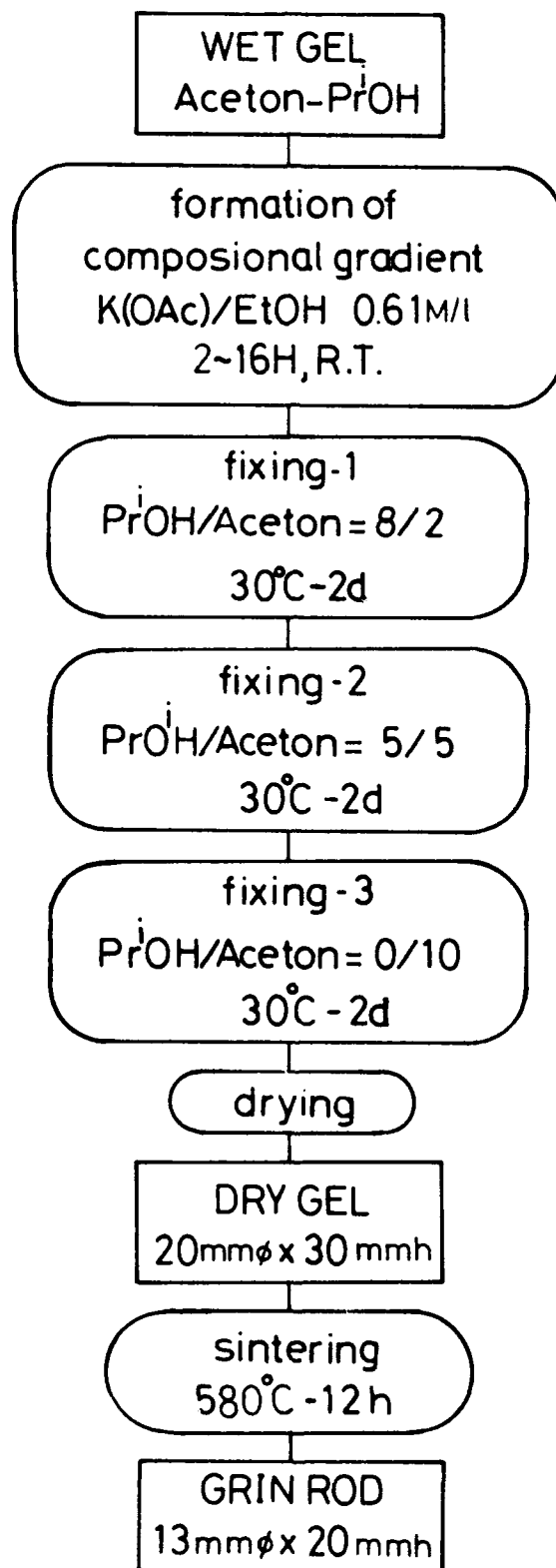


Fig.2. Flow chart of treatment for the complete replacement of acetone for water.

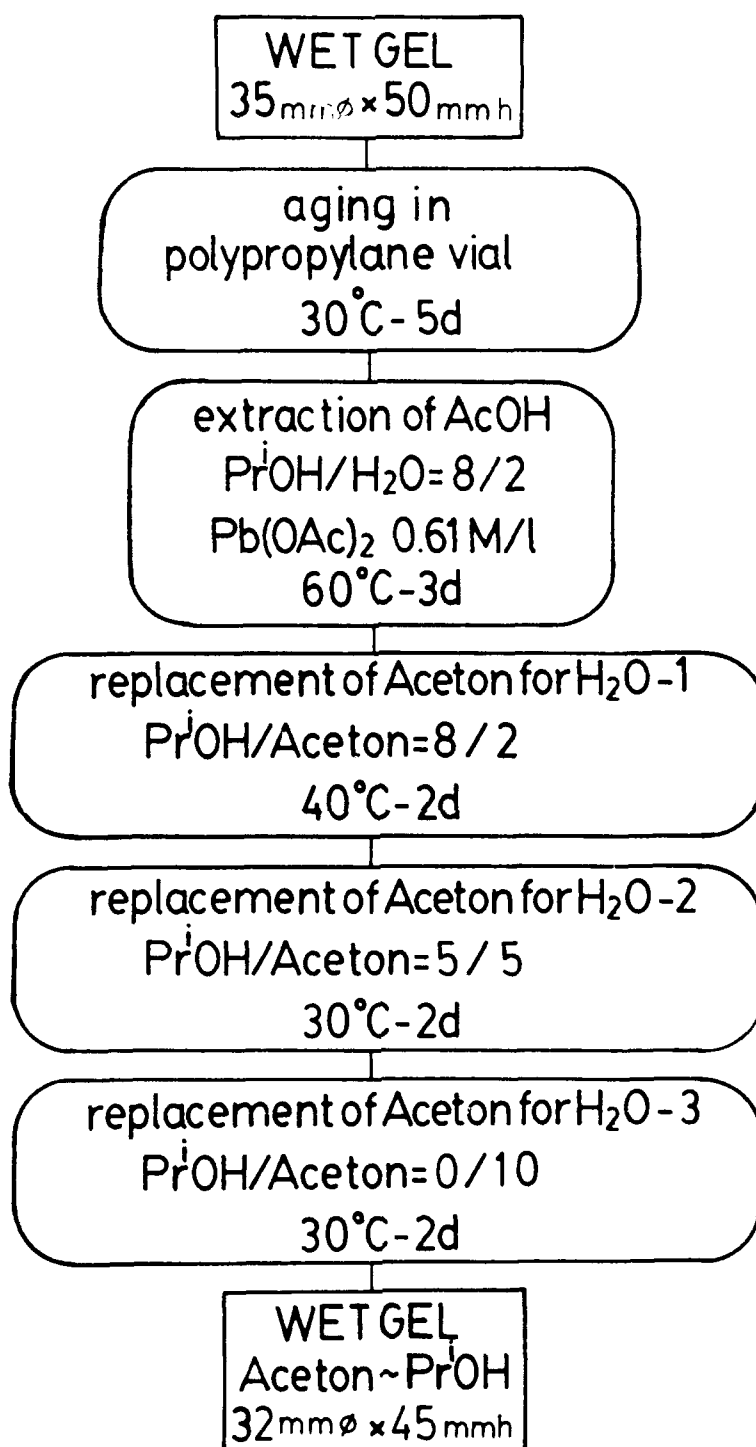


Fig.3. Flow chart for the formation of compositional gradient of lead, and dry and sintering of a gel.



### 3.RESULTS AND DISCUSSION

#### 3.1.Profiles of refractive index

Glasses obtained by immersing gels in ethanolic solution of potassium acetate for various length of time and subsequent replacement of acetone for ethanol, and drying and sintering according to the prescribed heating cycle were about 13 mm in diameter and 20 mm in length. They were clear, transparent and free from bubbles.

The interferogram of the sample obtained by sintering the gel after the soaking for 4 h to form the compositional gradinet is shown in Fig.4. The smooth fringe pattern in the figure shows that the glass has continuous variation in refractive index from center toward perimeter and free from bubbles or other defects which cause the local distortion of the refractive index profile.

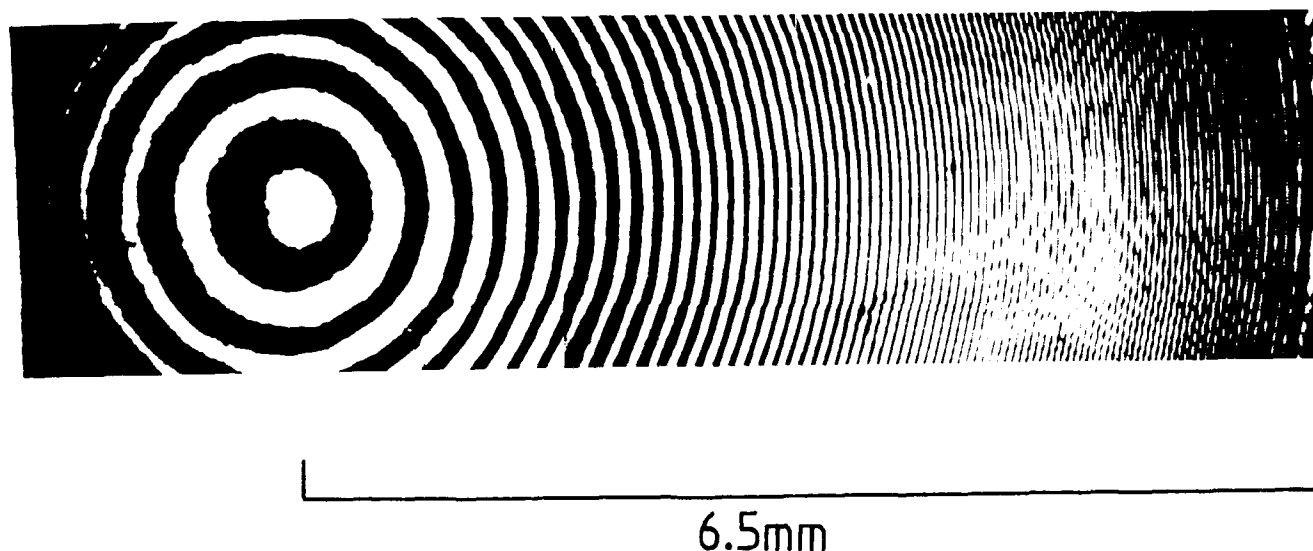


Fig.4. Interferogram of a GRIN rod obtained by the soaking for 4 h.

The contour lines of refractive indices determined by reflectivity measurements on the same sample are shown in Fig. 5 at the contour interval of 0.005. The lines which consisted of data points plotted at the interval of 0.25 mm are close to circles except for those in the mid center and near perimeter. The local distortions observed on some contour lines are attributed to dusts. The maximum value of the refractive index was about 1.65 at the center, and the minimum was about 1.60 at the perimeter. The maximum value of 1.65 is lower by 0.03 than the estimated value of 1.68 for the lead borosilicate glass aimed in the preparation of precursor sol i.e.,  $26\text{PbO}-7\text{B}_2\text{O}_3-67\text{SiO}_2$  (mol%). This difference is due to the loss of lead ions during both aging and the replacements of acetone for the liquid in the micropores of the gel before and after the formation of compositional gradient of lead<sup>21</sup>.

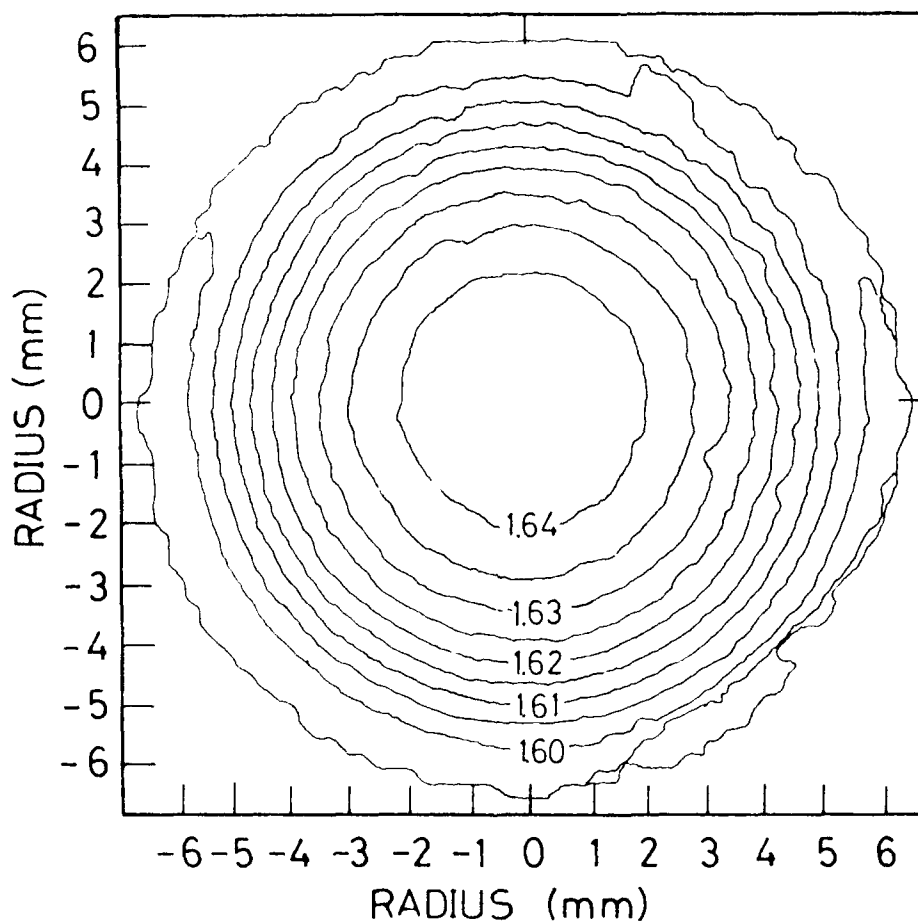


Fig.5. Refractive index contour lines of r-GRIN rod obtained by sintering the gel after soaking for 4 h.

The refractive index profile in the radial direction determined from the contour lines is shown in Fig. 6 for the glass rods obtained after various soaking times in the ethanolic solution of potassium acetate. The curves whose maxima decreased with the increasing soaking time are nearly parabolic in the region up to 3 mm from the center, but deviated thereafter as they approached to the perimeter. This deviation from parabolic curve, which is obviously undesirable and must be removed, is due to the incomplete elimination of the migration of lead ions. That is, lead ions which migrated from center during the stepwise replacement of acetone for ethanol in the process shown in Fig. 3, piled-up as lead acetate crystals in the vicinity of perimeter.

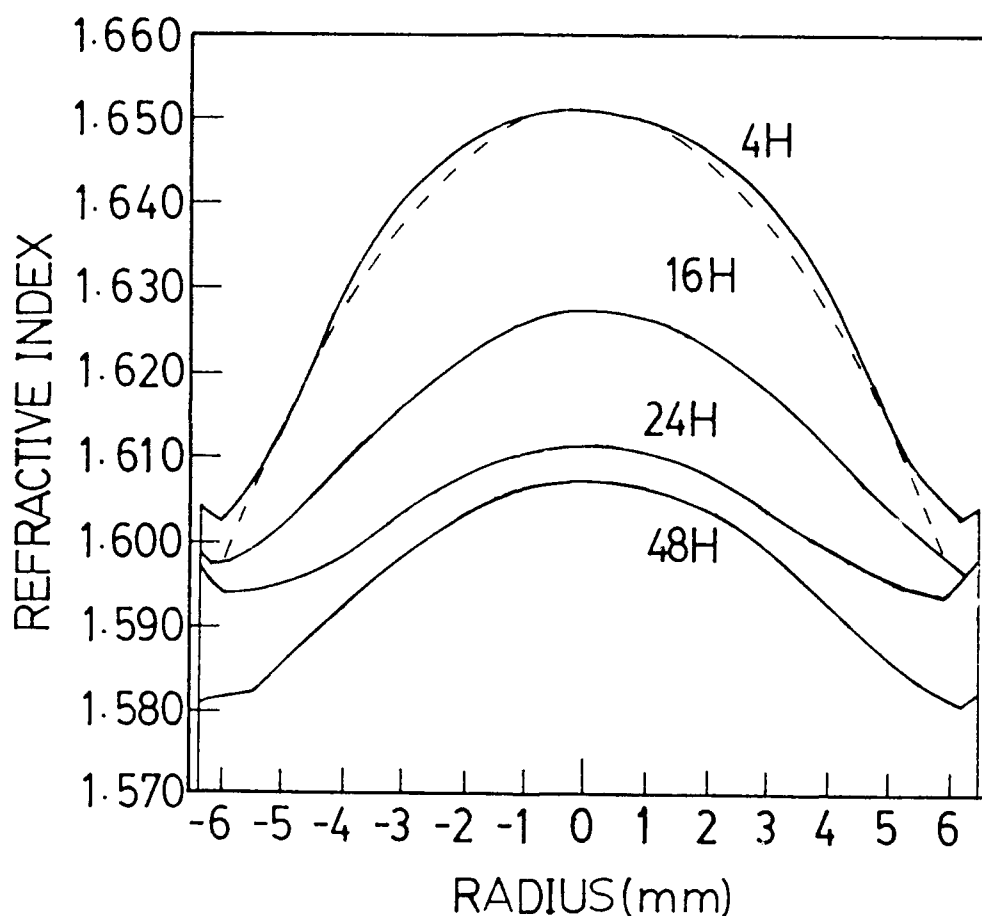


Fig.6. Change in refractive index profile of gel-derived r-GRIN rods with soaking time.

Since it is very difficult to completely eliminate the migration of lead ions during replacement of acetone for ethanol in the gel of large diameter, it is better to add one more step of treatment to remove the piled lead acetate than to elaborate the condition for further improvement of the reduction of lead migration. One of the effective ways to be added for the removal of the piled lead acetate crystals will be to dissolve them out by immersing the gel once again in ethanolic solution of potassium acetate for short period of time, say 15 min, after the total replacement of acetone for ethanol according to the flow chart shown in Fig. 3. This treatment may result in another interminglement of small amount of ethanol into acetone in the vicinity of gel surface. But the extraction of small amount of ethanol with acetone to a level at which the migration of lead ions does not take place will be made without difficulty before it penetrates deeply into the micropores. If this removal of the piled lead acetate can be made without changing the concentrational gradient of lead in the central part of the gel, the value of refractive index at the perimeter of the rod will decrease from 1.60 to about 1.55. Then the value of  $\Delta n$  in the eventual glass will increase up to about 0.1 as it is known from the curves shown in Fig. 6 with a broken line.

### 3.2. Comparison with r-GRIN rod by other processes.

The diameter and  $\Delta n$  of r-GRIN rod obtained in this study is compared with those of other methods in Fig. 7. The values of  $\Delta n$  for the materials by respective methods shown in the figure represent the practical maxima, whereas the value for the present study, which is already higher than most of the others, can be increased further as it was mentioned in the above. Thus, the advantage of the sol-gel process in the preparation of r-GRIN rods with large diameter and large  $\Delta n$  is obvious.

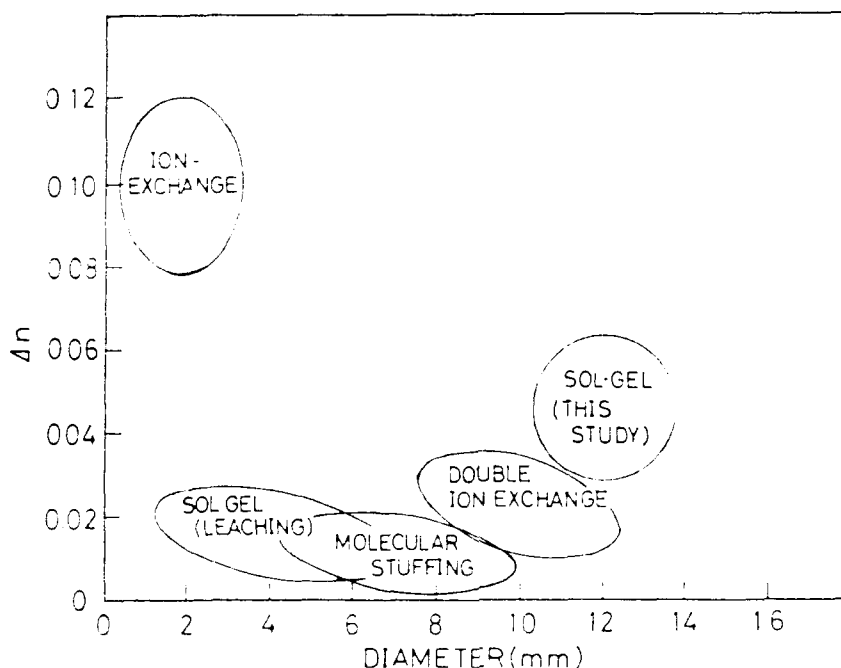


Fig.7. Comparison of the diameter and  $\Delta n$  of r-GRIN rods by various methods.

The next step of the study for the establishment of the process is, therefore, the investigation of the optimum conditions on the removal of the piled lead acetate crystals without changing the compositional gradient in the central part of the gel so that the parabolic profile of refractive index is obtained throughout the radial direction. Once this process is established on the  $\text{PbO-B}_2\text{O}_3\text{-SiO}_2$  system, it will not be so difficult to apply the technique to a new system of interest such as those containing Ba, La, Nb, etc. as index-modifying cations.

#### 4. REFERENCES

1. L. Pugliese and D. T. Moore, "Gradient Index Optics," *Photonics Spectre*, vol.5, pp.71-77, March 1987
2. W. J. Tomlison, "Application of GRIN-Rod Lenses in Optical Fiber Communication Systems," *Appl. Opt.*, vol.19, pp.1127-1130, 1980
3. M. Kawazu and Y. Ogura, "Application of Gradient-Index Fiber Arrays to Copy Machines," *Appl. Opt.* vol.19, pp.1105-1112, 1980
4. A. D. Pearson, W. G. French and E. G. Rawson, "Preparation of a Light Focusing Glass Rod by Ion-Exchange Techniques," *Appl. Phys. Lett.* vol.15, pp.76-77, 1969
5. I. Kitano, K. Koizumi, H. Matsumura, T. Uchida and M. Furukawa, "Light-Focusing Fiber Guide Prepared by Ion-Exchange Techniques," *Jap. J. Appl. Phys.*, vol.39, pp.63-70, 1970
6. H. Kita, I. Kitano, T. Uchida and M. Furukawa, "Light-Focusing Glass Fibers and Rods," *J. Am. Ceram. Soc.*, vol.54, pp.321, 1971
7. T. Yamagishi, K. Fujii and I. Kitano, "Fabrication of a New Gradient-Index Rod Lens with High Performance," *J. Non-Cryst. Solids*, vol.47, pp.283, 1982
8. T. Miyazawa, K. Okada, T. Kubo, K. Nishizawa, I. Kitano and K. Iga, "Abberation Improvement of Selfoc Lenses," *Appl. Opt.* vol.19, pp.1113-16, 1980
9. L. G. Atkinson, S. N. Houde-Walter, D. T. Moore, D. P. Ryan and J. M. Stagaman, "Design of a Gradient-Index Photographic Objective," *Appl. Opt.* vol.21, pp.993, 1982
10. J. B. Caldwell and D. T. Moore, "Design of Gradient-Index Lens Systems for Disc Format Cameras," *Appl. Opt.*, vol.25, pp.3351-3355, 1986
11. D. S. Kindred and D. T. Moore, "Design, Fabrication, and Testing of a Gradient-Index Binocular Objective," *Appl. Opt.*, vol.27, pp.492-95, 1988
12. K. Shingyouchi, S. Konishi, K. Susa and I. Matsuyama, "Radial Gradient Refractive Index Glass Rods Prepared by a Sol-gel Method," *Electron. Lett.*, vol.22, pp.99-100, 1986
13. K. shingyouchi, S. Konishi, K. Susa and I. Matsuyama, "r-GRIN  $\text{TiO}_2\text{-SiO}_2$  Glass Rods Prepared by a Sol-Gel Method," *Electron. Lett.*, vol.22, pp.1108-10, 1986
14. M. Yamane, J. B. Caldwell and D. T. Moore, "Preparation of Gradient-Index Glass Rods by the Sol-Gel Process," *J. Non-Cryst. Solids*, vol.85, pp.244-46, 1986
15. M. Yamane, H. Kawazoe, A. Yasumori and T. Takahashi, "Gradient-Index Glass Rods of  $\text{PbO-K}_2\text{O-B}_2\text{O}_3\text{-SiO}_2$  System Prepared by the Sol-Gel Process," *J. Non-Cryst. Solids*, vol.100, pp.506-510, 1989
16. S. Konishi, K. Shingyouchi and A. Makishima, "r-GRIN Glass Rods by a Sol-Gel Method," *J. Non-Cryst. Solids*, vol.100, pp.511-13, 1988
17. J. B. Caldwell, T. M. Che, R. W. Cruse, R. M. Mininni, R. E. Nikles, V. N. Warden and M. A. Banash, "Study on the Reproducible Production of GRIN (Gradient-Index) Glass Rods by a Sol-Gel Process," Better Ceramics Through Chemistry IV, to be published
18. J. H. Simmons, R. K. Mohr, D. C. Tran, P. B. Macedo and J. A. Litovitz, "Optical Properties of Waveguide Made by a Porous Glass Process," *Appl. Opt.*, vol.18, pp.2732-33, 1979

19. S. Ohmi, H. Sasaki, Y. Asahara, Y. Yoneda and T. Izumitani, "Gradient-Index Rod Lens Made by a Double Ion-Exchange Process," *Appl. Opt.*, vol.27, pp.496-99, 1986
20. M. Yamane, "Gradient-Index Materials by Sol-Gel Process," Proc. 4th Intern. Conf. Ultrastructure Processing of Ceramics, Glasses, Composites, Feb. 22-25, Tucson AZ, 1989, to be published
21. H. Maeda, M. Iwasaki, A. Yasumori and M. Yamane, "Reduction of Lead Migration During Drying of a Gel," *J. Non-Cryst. Solids*, to be published



## Sol-gel derived gradient index optical materials

Tessie M. Che, J. Brian Caldwell and Robert M. Mininni

Enimont America Inc. Research & Development Center  
2000 Cornwall Road, Monmouth Junction, NJ 08852

### ABSTRACT

Gradient index optics will play an increasingly important role in applications such as fax machines, photocopiers, fiber optic couplers and cameras. In this paper, we present an overview of various sol-gel methods for making gradient index materials.

### 1. INTRODUCTION

Gradient index (GRIN) optics has become a prominent part of modern optics. GRIN materials are characterized by a refractive index distribution which varies spatially in a controlled manner. For example, cylindrical glass rods with plane-parallel faces can be made with a refractive index higher along the central axis than at the outer edges. Such a rod will act as a positive, converging lens. The use of gradient index glass in optical systems provides many advantages over homogeneous glass. These advantages include greater simplicity by reduction of the total number of optical elements in a system and improved performance. In general, GRIN designs require fewer elements than their homogeneous counterparts. Thus, definite benefits exist with respect to size, weight, and economics when using GRIN materials in fiber and integrated (miniaturized systems) optical applications. Furthermore, some systems can be designed using GRIN lenses which would be virtually impossible to configure using homogeneous lenses.

Interest in the use of gradient index optics for imaging systems has existed since 1887, when Exner discovered that insect eyes are composed of tiny radial gradient index rods<sup>1</sup>. An early radial gradient index lens was made by Robert W. Wood in 1905<sup>2</sup>. A "Wood" lens can be made from a mixture of glycerin and gelatin, which is allowed to gel in a cylindrical mold pressed between two parallel plates. The cylindrical gel is then soaked in water, which diffuses into the gelatin, replacing some of the glycerol and lowering the index. The resulting GRIN gelatin lens can form an image just as a conventional lens does. Radial gradient index glass was first made by Otto Schott<sup>3</sup>, who used differential cooling techniques in which molten glass was placed in a metal cylinder and cooled very rapidly. Unfortunately, the resultant glass was birefringent.

Since 1969, most of the research in GRIN optics has been carried out by a small but dedicated group of optical scientists. Steady progress has been made in gradient index optical theory, design, testing, and application<sup>4-7</sup>. However, material fabrication currently represents the major limiting factor in the full development of GRIN optics. Existing fabrication methods<sup>8</sup> include neutron irradiation, chemical vapor deposition, polymerization, and ion stuffing, but to date, the most successful has been ion exchange.

Using ion exchange methods, Nippon Sheet Glass (NSG) Corporation started commercial production<sup>9</sup> of radial GRIN lenses in the late 1960's. Produced under the trade name SELFOC Micro-Lens, these lenses range in size from 1.0 to 3.0 mm in diameter, with the index gradient produced by the exchange of  $Ti^{+}$  or  $Cs^{+}$  ions for  $K^{+}$  or  $Na^{+}$  ions in a silicate glass. Today, SELFOC lenses are used widely in photocopier<sup>10</sup> and facsimile lens arrays<sup>11</sup>, medical endoscopes<sup>12</sup>, video or compact disk systems<sup>13-16</sup>, and a wide variety of devices for splitting, and coupling light in optical fiber telecommunication applications<sup>17-20</sup>. Limitations of currently available SELFOC materials produced by ion exchange

92 4 26 032

92-11414



techniques include small size, poor environmental and thermal stability, and a limited variety of optical characteristics such as index profile dispersion and base index of refraction.

Numerous lens design studies<sup>21-24</sup> have revealed that useful applications exist for GRIN lenses in cameras, telescopes, and microscopes, as well as waveguides. Unfortunately, the economical fabrication of large diameter GRIN elements remains a major roadblock in the development of these applications.

In recent years, significant progress has been made in using sol-gel methods to prepare large diameter (>5 mm) optical quality GRIN lenses of various compositions. In this paper, we compare the existing sol-gel methods for making radial GRIN materials, and present some physical and optical properties of the resulting GRIN glasses.

## **2. MATERIAL CONSIDERATIONS**

GRIN optics is a technology which has been awaiting the development of new materials. Whether or not sol-gel methods will be applied for the commercial fabrication of GRIN elements is still to be determined. Success will undoubtedly depend on the creativity and efforts of researchers in diverse disciplines. A close interaction between material and optical scientists would certainly favor the attainment of that "happy medium" between optical materials specified by lens designers and those attainable by sol-gel methods. In any case, a researcher planning to fabricate gel-derived GRIN materials would do well to build a personal knowledge base which encompasses the optics and properties of existing homogeneous and gradient index glasses, existing GRIN fabrication methods, and of course, sol-gel technology.

Consideration of a GRIN lens application can help to identify a target glass composition; and candidate compositions can be selected by consulting various references on homogeneous glass<sup>25,26</sup> and by calculation using models which correlate the optical and physical properties of glasses<sup>27-33</sup>. For example, GRIN lenses with relatively large diameters (>10 mm), a large variation of refractive index ( $\Delta n = \Delta n > 0.05$ ) and low dispersion ( $V_{10} > 50$ ) would find wide ranging applications in camera lenses<sup>21,22</sup>, microscope objectives<sup>23</sup>, and eyepieces<sup>24</sup>. In order to meet these specifications, a gradient index material would have to exhibit a large  $\Delta n$  and a small variation of dispersion (measured as  $n_F - n_C$ ) as a function of radial position. Such lenses could be achieved if the central portion of the GRIN rod consisted of a high-index low-dispersion glass, such as a barium or lanthanum silicate, and the outer portions of the rod consisted of a low-index glass such as an alkali silicate with a dispersion similar in value to that in the center of the rod. For certain applications, low GRIN dispersion is not required, and a lead or titanium silicate composition in the central portion of the GRIN rod would be suitable. Regardless of the  $\Delta n$  and GRIN dispersion requirements, it is necessary to maintain a relatively constant value of thermal expansion within the rod in order to avoid cracking or excessive stress birefringence.

The imaging characteristics of a radial GRIN lens are basically dependent upon the following optical properties<sup>6,8,21</sup>:

- 1) Size of  $\Delta n$  (index-of-refraction change) - The greater the radial composition gradient, the greater  $\Delta n$ .
- 2) Profile shape and symmetry - Gaussian, Lorentzian, parabolic and linear profiles have been obtained with ion exchange methods. SELFOC lenses exhibit symmetrical parabolic index profiles<sup>18</sup>.



3) Depth of the gradient - determines the size of the GRIN element.

4) Chromatic variation of the index profile.

Discussion of GRIN characterization techniques has been published previously<sup>6,8</sup>. Mach Zehnder interferometric methods have proven to be relatively straightforward and accurate; and commercial interferometers are now available<sup>34</sup>. Figure 1 shows a typical interferogram and radial index profile plot for a gel-derived GRIN glass lens.

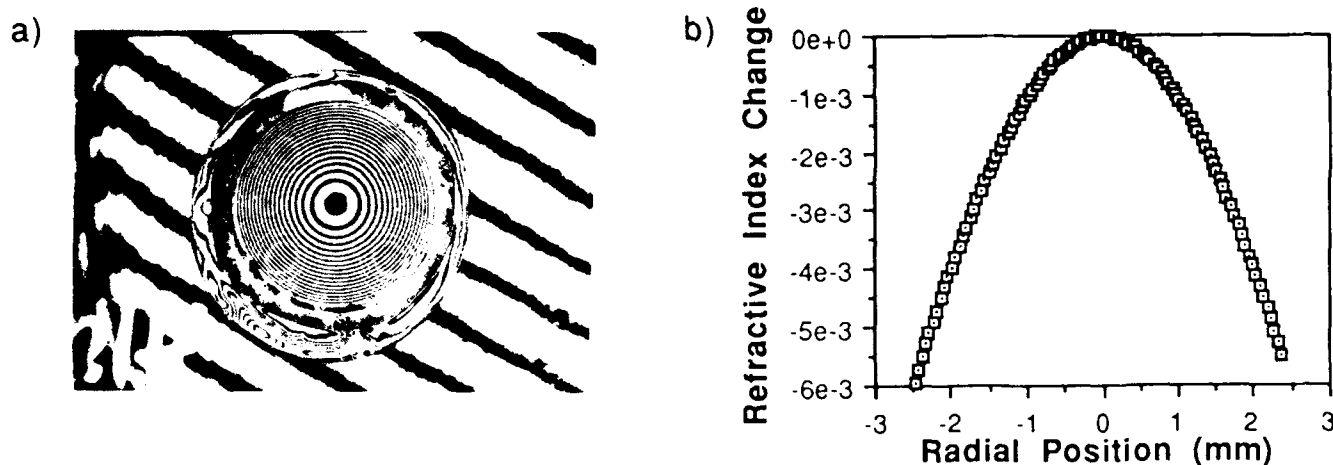


Figure 1a) Mach Zehnder interferogram of a  $\text{TiO}_2\text{-SiO}_2$  GRIN lens, and b) plot of refractive index versus radial position data taken from interferogram.

Whether or not sol-gel techniques can actually be used to make a specified multicomponent GRIN glass will, of course, be determined by experimentation. However, insight can be gained from the extensive literature available on sol-gel technology<sup>35-44</sup> and by comparing the intrinsic properties of gel-derived glasses with those of high temperature glass melts<sup>45</sup>. Presumably, once a sol-gel method is developed for making a small GRIN lens of a specific composition, the potential for making a larger piece exists. In particular, sol-gel processing techniques which have recently been developed for the preparation of large silica xerogels<sup>46-50</sup> and aerogels<sup>51-55</sup> hold promise for the preparation of large multicomponent GRIN glasses.

### 3. EARLIER GRIN GLASS FABRICATION METHODS

Various techniques have been used in the past for the fabrication of GRIN lenses and are discussed elsewhere<sup>6,8</sup>. However, for the purpose of comparison, the methods of ion exchange in solid glass, stuffing/unstuffing of porous glass, and phase separation/leaching are presented here. These and the sol-gel methods discussed in Section 4.0 are similar in that all these techniques involve immersion of a substrate in a liquid phase to induce diffusion of index modifiers resulting in a gradient index profile in the substrate.

### 3.1. Ion exchange.

Ion exchange is the only method which has been commercially developed for the production of GRIN lenses. This process involves exchanging ions from a molten salt bath with those in a dense glass.

In the fabrication of SELFOC Microlenses, a borosilicate glass rod containing  $Tl^+$  and  $Na^+$  ions, is immersed in a high-temperature molten  $KNO_3$  salt bath. Under these conditions, ion diffusion within the glass occurs with partial substitution of the  $Tl^+$  and  $Na^+$  in the glass rod by  $K^+$  from the salt bath. As ion exchange proceeds, a nearly parabolic refractive-index distribution corresponding to  $Tl^+$  ion concentration is formed in the cylindrical glass rod. After a specified time, the rod is removed from the bath, cut into lengths, and both ends are polished flat. Available SELFOC rod lenses<sup>18,19,56</sup> range in diameter size from 1-3 mm with a maximum  $\Delta n$  of 0.124.

Numerous factors affect the final refractive index distribution in GRIN glass made by the ion exchange process. These include: base glass composition, ions to be exchanged, diameter of the rod, temperature of the bath and the ion exchange time. For example, in order to avoid deformation of the glass rod during the diffusion process, it is necessary to keep the temperature of the molten salt bath below the glass softening point. This restriction limits the choice of index modifying ions to those which can both increase the optical index of the glass and are capable of diffusion at such temperatures. For SELFOC glasses, ions such as  $Tl$ ,  $Cs$ ,  $Rb$ ,  $K$ ,  $Na$  or  $Li$ , which fulfill both these requirements, are used. Unfortunately, complications arise from the toxicity of ions like  $Tl$ , and from the fact that glasses containing  $Tl$  ions are characterized by high dispersion of refractive index.

Another limitation of the ion exchange method is that processing times are very long. In borosilicate glass, exchange times of 10-99 hours are needed for each millimeter of depth, which can result in profile control and stressing problems due to prolonged periods of heating and cooling<sup>57</sup>. For these and other reasons, ion exchange methods have not been commercially applied to the production of radial GRIN rods greater than 3 mm in diameter.

### 3.2. Stuffing and unstuffing of porous glass.

The use of porous glasses for the fabrication of gradient index glass was first carried out by Macedo<sup>58</sup> in 1976. In this technique<sup>58-61</sup> a porous glass preform made by leaching a phase separated glass in acid is stuffed with index modifying ions such as  $Cs^+$  or  $Tl^+$  by precipitation of a salt solution. A concentration gradient of the modifier ions is then created by redissolving the salt and allowing it to diffuse out of the preform. The diffusion process is halted by precipitation after the desired composition profile is achieved, and the preform is dried and sintered.

In the stuffing/unstuffing method, dopant diffusion times can be of the order of 20 minutes per millimeter<sup>57</sup>, which is several orders of magnitude faster than that for an ion exchange process in dense glass. Unfortunately, such short diffusion times make it difficult to produce small diameter (less than 5 mm) GRIN rods in a consistent manner. Furthermore, though this technique can be used to prepare lenses of 10 mm aperture, these lenses can often exhibit index gradients which are not uniform. This is due primarily to non-uniform pore size distributions created in the porous glass during the phase separation and leaching process. When the pore size distribution of the porous glass is not uniform, the resulting index profile is also not uniform due to localized variations in the concentration of index modifying ions. In addition, the porosity of porous glasses made by phase-separation methods is generally less than 50%, which limits the amount of dopant which can be stuffed into the glass, which in turn limits the  $\Delta n$  to a maximum of 0.03, even when  $Tl^+$  is used as the dopant.

### **3.3. Phase separation and leaching.**

This technique<sup>62</sup> is similar to the stuffing/unstuffing method in that the initial steps involve phase separating a suitable glass by heat treatment and then leaching away the soluble phase in an acid solution. In this reference case, however, the starting glass contains a significant amount of germanium dioxide which is not completely removed during leaching. A concentration profile of  $\text{GeO}_2$  is thus created by the processes of dissolution and diffusion. Other components such as  $\text{Na}_2\text{O}$  and  $\text{B}_2\text{O}_3$  are almost completely removed during leaching. After leaching, the now porous glass is washed, dried and sintered. GRIN glass rods with index changes of up to 0.015 over a radius slightly larger than 2 mm have been made by this technique.

The phase separation and leaching technique has several advantages over the stuffing/unstuffing technique. First, it is simpler since the stuffing and unstuffing steps are avoided. Second, larger concentrations of the index modifier can be introduced during the melting of the raw glass. Third, the final glass is more refractory since single valence ions are nearly absent.

The primary disadvantage of the last two methods which involve phase separation and leaching processes is that the selection of phase separable glasses is very limited.

## **4. SOL-GEL METHODS USED FOR GRIN GLASS FABRICATION**

Given the limitations inherent in the GRIN fabrication methods discussed above, it is not surprising that an interest in sol-gel methods has developed. Some of the advantages of sol-gel techniques include:

- (1) Greater diffusion coefficients - which can result in time savings as much as two orders of magnitude in comparison to ion exchange processes.
- (2) Low energy consumption during most of the process.
- (3) The ability to introduce a broader variety of index modifying dopants into the sol-gel preform.
- (4) Multi-component compositions can be formed into glasses of different sizes and shapes.

An early proposal to use sol-gel methods for the fabrication of gradient index materials was made by Mukherjee<sup>63</sup> in 1981. In the same year, patents on sol-gel<sup>64,65</sup> derived GRIN glasses were filed by researchers at Sumitomo Electric, Osaka, Japan.

To date, the existing sol-gel methods used to obtain radial gradient rods with parabolic index profiles all involve wet gel leaching and can be divided into two general categories - the leaching of wet gels containing (1) metal salt dopants or (2) metal alkoxide dopants. The basic steps involved in making GRIN glass by the leaching of wet gels are shown in Figure 2. Research carried out using these sol-gel techniques is summarized in Table I, and described in the following sections.

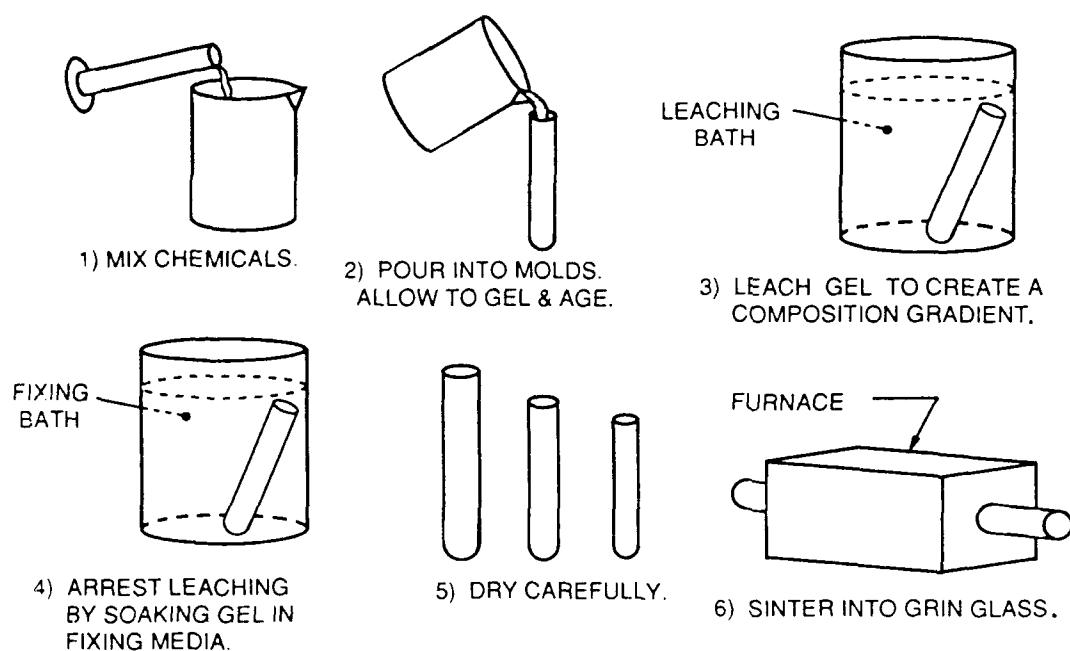


**Figure 2. General procedure for making GRIN glass by leaching of wet gels.**

**TABLE I. Sol-gel derived GRIN glass rod lens systems.**

LEACHING METHOD	PROPERTIES	REF.
<b>4.1. GELS with METAL SALT DOPANTS</b>		
4.1.1. Ti, Cs, Rb out H, NH <sub>4</sub> , K in SiO <sub>2</sub> gel matrix	10-13 mm diam. rods w/ good focusing abilities	64-68
4.1.2. Pb out, K in B <sub>2</sub> O <sub>3</sub> -SiO <sub>2</sub> gel matrix	6-13 mm diam. rods $\Delta n = 0.02 - 0.05$	69-73
<b>4.2. GEL with METAL ALKOXIDE DOPANTS</b>		
4.2.1. Ge, Ti, Ta out H in SiO <sub>2</sub> gel matrix	2-3.4 mm diam. rods <sup>a</sup> $\Delta n = 0.015 - 0.025$	74-81
4.2.2. Zr, Ti, Ge out H in Gel matrices: SiO <sub>2</sub> , B <sub>2</sub> O <sub>3</sub> -SiO <sub>2</sub> , Al <sub>2</sub> O <sub>3</sub> -SiO <sub>2</sub>	3-8 mm diam. rods $\Delta n = 0.013 - 0.028$	6a, 83

(a) For GeO<sub>2</sub>-SiO<sub>2</sub> and TiO<sub>2</sub>-SiO<sub>2</sub> systems only.

#### 4.1. Leaching of gels with metal salt dopants.

In this approach, a gel is first prepared by reacting one or more silicon alkoxides with an aqueous solution of metal salt dopants. The doped gel is placed either in water or in an aqueous metal salt solution to partially leach out the first dopant and partially leach in a second dopant, creating concentration gradients of the dopants within a silica gel matrix. Once the desired gradients are obtained and fixed into place (e.g., by precipitation of the dopants), the gel is then dried and sintered into GRIN glass.

##### **4.1.1. Leaching of gels with metal salt dopants**

-  $\text{Ti}^+$ ,  $\text{Rb}^+$  or  $\text{Cs}^+$  out and  $\text{H}^+$ ,  $\text{NH}_4^+$ ,  $\text{K}^+$  in.

To overcome the problems associated with the use of phase separated/leached porous glass, researchers investigated the use of silica gel<sup>64-68</sup> as the so-called "porous glass body." U.S. Patent 4,528,010 describes a method<sup>68</sup> involving the stuffing and unstuffing of a gelled body to make a GRIN glass using thallium, rubidium or cesium ions as the index modifying dopants. In one example, a solution of cesium and ammonium silicates was acidified and allowed to gel. The resulting gel rod was leached in a 1M aqueous ammonium nitrate solution containing 30wt%  $\text{KNO}_3$  and fixed in propanol. This resulted in a gel which exhibited a  $\text{Cs}^+$  radial gradient which decreased outwardly, while the  $\text{NH}_4^+/\text{K}^+$  ion gradient decreased radially inward. The gel was then dried and sintered to form a transparent GRIN glass rod with a diameter of 10mm. A 1/4 x (pitch) rod lens was prepared from this sample, and found to have "very good focusing ability".

##### **4.1.2. Leaching of gels with metal salt dopants**

-  $\text{PbO-K}_2\text{O-B}_2\text{O}_3\text{-SiO}_2$  system.

This approach was first investigated<sup>69,70</sup> in 1986. Since then a steady increase in the physical dimensions and the magnitude of  $\Delta n$  for a  $\text{PbO-K}_2\text{O-B}_2\text{O}_3\text{-SiO}_2$  GRIN system has been achieved<sup>69-73</sup>, as shown in Table 2.

**Table 2. Improvement of the  $\text{PbO-K}_2\text{O-B}_2\text{O}_3\text{-SiO}_2$  GRIN glass system.**

YEAR	ROD DIMENSIONS (mm diameter x mm length)		DELTA-N/PROFILE SHAPE		REF.
	XEROGEL	GRIN GLASS			
1986	10 x 20	6 mm diam.	$\Delta n = 0.02$	"w-shaped"	69
1987	12 x15	7 x 9	$\Delta n = 0.04$	nearly parabolic	71,72
1990	24 mm diam.	13 x 20	$\Delta n = 0.05$		73

The general procedure used<sup>70</sup> involves mixing a silicon alkoxide with water, a boric acid solution and an aqueous metal salt solution, such as  $\text{Pb}(\text{NO}_3)_2$ . The resulting gel was then immersed in a  $\text{KNO}_3$  solution. Through diffusion,  $\text{Pb}^{+2}$  ions were partially leached out of the gel matrix and replaced by  $\text{K}^+$  ions. The gel was then dried and sintered into glass. An early sol-gel GRIN sample<sup>69</sup> prepared by this

method contained cracks and bubbles, and exhibited an asymmetric "W-shaped" index profile. The probable cause of the strange index profile as well as the main difficulty with the metal salt technique is that the lead and potassium index modifiers are ions which are not easily incorporated into the structural gel network under these reaction conditions. These cations remain in the liquid phase filling the micropores of the wet gel and are free to migrate during the drying step, which leads to asymmetry in the final index profile.

Significant improvements on the original process<sup>72,73</sup> have been made. Technical problems recently addressed include: i) the elimination of bubbles trapped during casting of the sol, ii) migration of index-modifying cations during drying, and iii) deformation/fracture of the gel during drying. To avoid trapping bubbles in the gel, acetic acid was added as a buffering agent to the precursor solution to slow gelation. Use of this solution provided a bubble free wet gel with the dimensions of 35 mm diam. x 50 mm length.

Another key improvement made was to precipitate the lead salts within the gel prior to and after leaching by soaking the gel in acetone. By replacing the liquid in the micropores of the wet gel with acetone, lead ion migration in the pre-leached gel was substantially reduced. To generate the radial lead/potassium compositional gradients, the gel was soaked in an ethanolic solution of potassium acetate. After the leaching step and formation of the desired composition gradient, ethanol was completely replaced by acetone. The steps involving the precipitation of lead and potassium by acetone help to effectively fix the dopant concentration profile, which is maintained during the drying and sintering process. Acetone also helps to eliminate the deformation of the gel during drying.

The method of leaching gels with metal salt dopants offers the potential of preparing unique gradient glass combinations of alkali, alkaline earth and rare earth ions in silica. Certain glass compositions of this type would provide very desirable optical and physical properties. For example, a  $\text{PbO-K}_2\text{O-SiO}_2$  GRIN glass system<sup>6a</sup> could result in a lens material exhibiting a large  $\Delta n$  and minimal stress-induced birefringence due to differential thermal expansion gradients in the glass.

#### **4.2. Leaching of gels with metal alkoxide dopants.**

The difference between this technique and that discussed in the Section 4.1. is that the index modifying dopants are introduced into the sol-gel solution as metal alkoxides. The principle advantage of using metal alkoxide reactants is that the index modifying species are easily incorporated into the gel structure and do not migrate during drying as is the case for metal salt dopants. This offers greater control over the index profile.

##### **4.2.1. Leaching of two-component (binary) gels with metal alkoxide dopants.**

Binary gel systems<sup>74-81</sup> which have been developed for the preparation of GRIN glasses have generally consisted of silica and an index modifying oxide such as germania, titania or tantalum oxide. A summary of the activity in this area is given in Table 3.

**Table 3. Development of binary metal alkoxide GRIN systems by Hitachi researchers.**

YEAR	COMPOSITION	RESULT	REF.
1985	TaO <sub>x</sub> -SiO <sub>2</sub> HF-leached	2.6 mm diam x 10 mm long rod Reported: $n = 1.54$ center/1.46 surface	75
1985	TiO <sub>2</sub> -SiC <sub>2</sub> acid leached	2.7 mm diam x 10 mm long rod Reported: $n = 1.56$ center/1.46 surface	74
1986	GeO <sub>2</sub> -SiO <sub>2</sub> water leached	3 mm diam rod Parabolic index profile with axial symmetry, N.A. = 0.27 $\Delta n = 0.025$	76
1986	TiO <sub>2</sub> -SiO <sub>2</sub> HCl leached	2 mm diam x 10 mm long rod Nearly parabolic index profile with axial symmetry, N.A. = 0.2 $\Delta n = 0.015$	77
1987-88	GeO <sub>2</sub> -SiO <sub>2</sub> TiO <sub>2</sub> -SiO <sub>2</sub>	Diffusion, microstructural studies. Correlation with index profiles.	79-81

A typical preparation of a GeO<sub>2</sub>-SiO<sub>2</sub> GRIN glass is described here. Tetramethoxysilane was reacted with a solution of tetraethoxygermanium, ethanol, water and hydrochloric acid to provide a gel. The gel was placed in water to partially leach out the germanium dopant, and then washed in methanol to fix the germanium dopant concentration gradient. Finally, the gel was dried and sintered into a gradient index glass. The product glass rods were 2 mm in diameter with  $\Delta n = 0.013$ .

Choosing the appropriate leaching reagent is important to ensure the selective removal of index modifying dopants from the wet gel. From leaching studies<sup>79</sup>, Hitachi researchers concluded that for the GeO<sub>2</sub>-SiO<sub>2</sub> and TiO<sub>2</sub>-SiO<sub>2</sub> systems, germanium and titanium dopants were selectively leached out of the gels due to their greater solubility in the respective leaching reagents than silica. From diffusion studies<sup>78</sup>, Shingyouchi et al showed that the diffusion behavior of the titanium species out of the wet gel is similar to that of electrolyte ions in water. Thus, formation of these radial GRIN rods is controlled predominantly by diffusion of the index modifying dopants. The diffusion coefficients of the leached dopants, which were estimated from refractive index profiles, using a mathematical treatment based on diffusion in a cylinder, were found to be  $3.0 \times 10^{-6}$  and  $1.1 \times 10^{-6}$  cm<sup>2</sup>/s for Ge and Ti ionic species, respectively<sup>80</sup>.

In addition, the concentration gradient of the dopant in the leached wet gels was found to be maintained in the densified glasses, as evidenced by the fact that there was no observed change in the dopant concentration profiles during drying and sintering.

The main disadvantage of the binary metal alkoxide gel process is that these binary systems generally yield gels which shrink considerably during drying. This large shrinkage results in a dense gel which is difficult to sinter without fracturing or bloating. The bloating problem is presently being addressed

in homogeneous  $\text{GeO}_2\text{-SiO}_2$  glasses<sup>82</sup>. One drawback of the  $\text{TiO}_2\text{-SiO}_2$  system is that these binary gels tend to crystallize at elevated temperatures if the  $\text{TiO}_2$  content exceeds ~5 mole%.

#### 4.2.2. Leaching of multicomponent (3 or more component) gels with metal alkoxide dopants.

Difficulties inherent in binary metal alkoxide sol-gel systems such as cracking during drying or sintering, and devitrification can be avoided by using 3 or more starting components<sup>6a,83</sup>. Gradient index glass rods produced by this method can range in diameter size from 3 mm to 8 mm, and have refractive index gradients of up to 0.03. In addition, the gradient index profile typically can be made to be symmetrical and nearly parabolic in shape. Table 4 lists the compositions of multicomponent gels made with metal alkoxide dopants which have been successfully processed into transparent GRIN glass<sup>6a</sup>.

TABLE 4. Multicomponent Gel-derived GRIN Glasses	
System	$\Delta n$ (rod diameter size = 3 - 8mm)
$\text{TiO}_2\text{-Al}_2\text{O}_3\text{-SiO}_2$ (a)	0.013
$\text{TiO}_2\text{-Al}_2\text{O}_3\text{-B}_2\text{O}_3\text{-SiO}_2$ (a)	0.015
$\text{TiO}_2\text{-Al}_2\text{O}_3\text{-GeO}_2\text{-SiO}_2$ (a)	0.015
$\text{ZrO}_2\text{-GeO}_2\text{-SiO}_2$ (b)	0.028
$\text{ZrO}_2\text{-Al}_2\text{O}_3\text{-B}_2\text{O}_3\text{-SiO}_2$ (b)	0.021
(a) $\text{H}_2\text{SO}_4$ leached, methanol fix; (b) $\text{HCl}$ leached, methanol fix.	

Large diameter (>5 mm) radial gradient-index glass rods can be readily made with  $\text{TiO}_2$  or  $\text{ZrO}_2$  as the primary refractive index modifier, if one or more additional oxide components are used. The reproducible preparation of  $\text{TiO}_2\text{-SiO}_2$  GRIN glasses based on the  $\text{TiO}_2\text{-Al}_2\text{O}_3\text{-SiO}_2$  gel system has recently been demonstrated<sup>84</sup>.  $\text{ZrO}_2$  systems were studied since the use of Zr oxide as an index modifier results in a lower index profile dispersion than when Ti oxide is used. The amount of  $\text{SiO}_2$  in the gel should be at least 60 - 98 mole%. Less than 60%  $\text{SiO}_2$  will result in a gel which is too weak to withstand the processing steps, and greater than 98% will not yield useful refractive index changes.

Gel preparation was based on the partial hydrolysis method developed by Yoldas<sup>85</sup> to prepare binary silicate gels from metal alkoxides. A silicon alkoxide was mixed with organic solvents, e.g., methanol and dimethylformamide, and partially hydrolyzed by adding a small amount of acidic water to the reaction mixture. After partial hydrolysis, the different metal alkoxides which include index modifiers such as titanium and zirconium, and gel modifiers such as boron, aluminum and germanium were added. Additional water was then added to facilitate gelation. Prior to gelation, the solution was poured into a plastic cylindrical mold.

For most of the systems listed in Table 4, gelation typically occurred within a few hours at room temperature. The gel rods were aged in tightly sealed containers for 1 day at room temperature, and then for another day at 60 °C. After aging, the gels were cooled and placed in leaching baths in order to partially leach out and create a concentration profile of the index modifying dopant. The choice of leaching medium is determined by the solubility properties of the component being removed. Leaching solutions for the different systems are listed in Table 4. Neither sulfuric nor hydrochloric acids will disrupt the  $\text{SiO}_2$  structure of the gel to any significant extent as long as the  $\text{SiO}_2$  content of the gel is greater than 65mole%, and the gel has been properly aged. Gels which have not been aged long enough can completely dissolve in the leaching bath. Leaching times typically range from 5 to 50 hours for a



15mm diameter cylindrical gel. A longer leaching time will remove more dopant from the gel, generally resulting in a smaller index change in the final glass.

After leaching, the gel was placed in an organic solvent, typically methanol, in order to "fix" the concentration profile in place. The fixing media precipitates the index modifying components and removes the acid solution. If this fixing step is neglected, undesired migration of the non-silicate components can occur during the drying process.

The gel was then dried to produce a porous oxide body with a greater amount of index modifying dopants at its center than at its edge. Leached gels can usually be dried in one or two days without cracking. Wet gels can be easily dried by hypercritical alcoholic solvent evacuation but the resulting dry gel is often more prone to devitrification during sintering than one dried by xerogel techniques. The dry gel then was sintered into glass by controlled heating to temperatures as high as 1550 °C.

Addition of aluminum di(sec-butoxide) acetoacetic ester chelate to the pre-gel solution of TiO<sub>2</sub> based systems increases the pore diameter of the final leached xerogel, and allows the gel to be dried and sintered without cracking. After leaching, very little alumina remains in the finished GRIN glass because it is completely extracted during the leaching and fixing steps. The addition of the aluminum chelate to the ZrO<sub>2</sub>-SiO<sub>2</sub> gel system also results in greatly enlarged pores, unfortunately, the ZrO<sub>2</sub>-Al<sub>2</sub>O<sub>3</sub>-SiO<sub>2</sub> gels tend to crystallize. The addition of GeO<sub>2</sub> and B<sub>2</sub>O<sub>3</sub> dopants to the titania and zirconia based systems helps to prevent crystallization and bloating during the sintering process. The addition of germania also increases the overall change in refractive index obtained in the GRIN lens.

## **5. CONCLUSIONS**

Although sol-gel methods for making gradient index glass are relatively new, some very encouraging results have been reported. Radial GRIN rods with diameters of 5 mm or more and of a variety of compositions can now be routinely fabricated in the laboratory. One of the key advantages of the sol-gel technique is its compositional flexibility, since sol-gel precursors for almost all index modifying metals are available. By comparison, the conventional ion exchange technique is limited for all practical purposes to the use of single valence ions for creating an index gradient.

A variety of gel processing techniques are currently in use, but at the present time it is not clear whether or not one of them has a definite advantage over the others. The current state of the art only hints at the full potential of the sol-gel method, and it is likely that further work in this field will be very rewarding.

## **6. ACKNOWLEDGEMENTS**

The authors gratefully acknowledge the support of Enimont, Italy. We would also like to express our appreciation to Mark Banash, Michele Chang, Richard Cruse, Randall Nikles, Grace Sagona and Victor Warden for helpful discussions and assistance in the preparation of this manuscript.

## 7. REFERENCES

1. S. Exner, *Die Physiologie der Facetterierten Augen von Krebsen und Insekten*, 8 volumes, Franz Deuticke, Leipzig und Wein, 1891.
2. R.W. Wood, *Physical Optics*, pp. 71-77, MacMillan Co., New York, 1905.
3. H. Hovestadt, *Jena Glass and Its Scientific and Industrial Applications*, p. 67, London, 1902.
4. D.T. Moore, "Gradient-Index Optics: Aspects of Design, Testing, Tolerancing, and Fabrication," Ph.D. thesis, University of Rochester, New York, 1974.
5. E.W. Marchand, *Gradient Index Optics*, Academic Press, New York, 1978.
6. J. B. Caldwell, a) "Sol-Gel Methods for Making Radial Gradient-Index Glass," Ph. D. thesis, University of Rochester, 1989; b) "Optical design with Wood lenses," in Proceedings of the OSA International Lens Design Topical Meeting, Monterey, CA (June 11-14, 1990).
7. The proceedings of eight Topical Meetings on Gradient-Index Optical Imaging Systems have been published in the following Applied Optics:
  - a) Volume 19, No. 7 (1 April 1980).
  - b) Volume 21, No. 6 (15 March 1982).
  - c) Volume 22, No. 3 (1 February 1983).
  - d) Volume 23, No. 11 (1 June 1984).
  - e) Volume 24, No. 24 (15 December 1985).
  - f) Volume 25, No. 19 (1 October 1986).
  - g) Volume 27, No. 3 (1 February 1988).
  - h) to be published (Summer 1990).
8. D.T. Moore, "Gradient-Index Optics: A Review," *Applied Optics* 19(7), 1035-1038 (1980).
9. I. Kitano, K. Koizumi, H. Matsumura, T. Uchida, and M. Furukawa, *J. Jpn. Soc. Appl. Phys. Suppl.* 39, 63 (1970).
10. M. Kawazu and Y. Ogura, "Application of Gradient-Index Fiber Arrays to Copying Machines," *Applied Optics* 19(7), 1105-1112 (1980).
11. J.D. Rees, "Non-Gaussian Imaging Properties of GRIN Fiber Lens Arrays," *Applied Optics* 21(6), 1009-1012 (1982).
12. D.C. Leiner and R. Prescott, "Correction of Chromatic Aberrations in GRIN Endoscopes," *Applied Optics* 22 (3), 383-386 (1983).
13. K. Takada, "Graded Refractive Index Lens System," U.S. Patent 4,701,032 (Oct 20, 1983).
14. H. Nishi, H. Ichikawa, M. Toyama and I. Kitano, "Gradient-Index Objective Lens for the Compact Disk System," *Applied Optics* 25(19), 3340-3344 (1986).
15. D.T. Moore, "Spherical Gradient-Index Lens Designs for Video-Disk Pickup Lens or the Like," U.S. Patent 4,457,590 (July 3, 1984).
16. J. Benschop and J. Braat, "Gradient-Index Objectives for CD Applications," *Applied Optics* 26(7), 1195-1200 (1987).
- 17a) W.J. Tomlinson, "Aberrations of GRIN-Rod Lenses in Multimode Optical Fiber Devices," *Applied Optics* 19(7), 1117-1126 (1980).
- b) W.J. Tomlinson, "Applications of GRIN-Rod Lenses in Optical Fiber Communication Systems," *Applied Optics* 19(7), 1127-1138 (1980).
18. SELFOC literature published by Nippon Sheet Glass America, Inc., 28 Worlds Fair Drive, Somerset, NJ 08873.
19. Literature on SELFOC lenses - *Introduction to Graded-Index Rod Lenses - GRIN-Rod Lens Starter Kit F-GRK1 Instruction Manual* (May 1986), published by Newport Corp., P.O. Box 8020, 18235 Mt. Baldy Circle, Fountain Valley, CA 92728.
20. P.J. Murphy and T.P. Coursolle, "Fiber Optic Displacement Sensor Employing a Graded Index Lens," *Applied Optics* 29(4), 544-547 (1990).
21. L.G. Atkinson, S.N. Houde-Walter, D.T. Moore, D.P. Ryan and J.M. Stagaman, "Design of a Gradient-Index Photographic Objective," *Applied Optics* 21(6), 993-998 (1982).
22. J.B. Caldwell and D.T. Moore, "Design of Gradient-Index Lens Systems for Disc Format

- Cameras," *Applied Optics* **25**(19), 3351-3355 (1986).
23. D.P. Ryan, "Chromatic Properties of Index of Refraction Gradients in Glass," Ph.D. thesis, pp. 7-38, University of Rochester, New York, 1983.
  24. J.P. Bowen, J.B. Caldwell, L.R. Gardner, N. Haun, M.T. Houk, D.S. Kindred, D.T. Moore, M. Shiba and D.Y.H. Wang, "Radial Gradient-Index Eyepiece Design," *Applied Optics* **27**(3), 3170-3176 (1988).
  25. O.V. Mazurin, M.V. Streltsina and T.P. Shvaiko-Shvaikovskaya, *Handbook of Glass Data*, published by Elsevier, New York -  
*Part A: Silica Glass and Binary Silicate Glasses* (1983).  
*Part B: Single-component and Binary Non-silicate Oxide Glasses* (1985).  
*Part C: Ternary Silicate Glasses* (1987).
  26. T.S. Izumitani, *Optical Glass*, American Institute of Physics Translation Series, New York, 1986.
  27. M.L. Huggins and K.H. Sun, "Calculation of Density and Optical Constants of a Glass from its Composition in Weight Percentage," *J. Opt. Soc. Am.* **26**, 4 (1936).
  28. M.L. Huggins, a) "The Density of Silicate Glasses as a Function of Composition," *J. Opt. Soc. Am.* **30**, 420 (1940); b) "The Refractive Index of Silicate Glasses as a Function of Composition," *J. Opt. Soc. Am.* **30**, 495 (1940); c) "The Dispersion of Silicate Glasses as a Function of Composition," *J. Opt. Soc. Am.* **30**, 514 (1940).
  29. M.L. Huggins, K.H. Sun, and D.O. Davis, "The Dispersion of Silicate Glasses as a Function of Composition. II," *J. Opt. Soc. Am.* **32**, 635 (1942).
  30. S.D. Fantone, "Design, Engineering, and Manufacturing Aspects of Gradient Index Optical Components," Ph.D. thesis, U. of Rochester, New York, 1979.
  31. S.D. Fantone, "Refractive Index and Spectral Models for Gradient-Index Materials," *Applied Optics* **22**(3), 432-440 (1983).
  32. P.O. McLaughlin and D.T. Moore, "Models for the Thermal Expansion Coefficient and Temperature Coefficient of the Refractive Index in Gradient-Index Glass," *Applied Optics* **24**(24), 4342-4348 (1985).
  33. D.P. Ryan-Howard and D.T. Moore, "Model for the Chromatic Properties of Gradient-Index Glass," *Applied Optics* **24**(24), 4356-4366 (1985).
  34. Gradient Lens Corporation, 207 Tremont Street, Rochester, New York 14608.
  35. R.K. Iler, *The Chemistry of Silica*, Wiley, New York, 1979.
  36. S. Sakka, "Gel Method for Making Glass," in *Treatise on Materials Science and Technology*, Volume 72, pp.129-167, Academic Press, 1982.
  37. H. Dislich, "Glassy and Crystalline Systems from Gels: Chemical Basis and Technical Application," *J. Non-Cryst. Solids* **57**, 371-388 (1983).
  38. J.D. Mackenzie, "Applications of Sol-Gel Methods for Glass and Ceramic Processing," in *Ultrastructure Processing of Ceramics, Glasses and Composites*, L.L. Hench and D.R. Ulrich, editors, pp. 15-26, Wiley, NY, 1984.
  39. J. Zarzycki, "Processing of Gel Glasses," in *Glass: Science and Technology*, Volume 2, D.R. Uhlmann and N.J. Kreidl, editors, pp. 209-249, Academic Press, New York, 1984.
  40. J.D. Mackenzie, "Applications of the Sol-Gel Process," *J. Non-Cryst. Solids* **100**, 162-168 (1988).
  41. D.R. Ulrich, "Prospects of Sol-Gel Processes," *J. Non-Cryst. Solids* **100**, 174-193 (1988).
  42. L. Klein, editor, *Sol-Gel Technology for Thin Films, Fibers, Preforms, Electronics and Specialty Shapes*, Noyes Publications, New Jersey, 1988.
  43. L.L. Hench and J.K. West, "The Sol-Gel Process," *Chem. Rev.* **90**, 33-72 (1990).
  44. C.J. Brinker and G.W. Scherer, *Sol-Gel Science - The Physics and Chemistry of Sol-Gel Processing*, Academic Press, 1990.
  45. J.D. Mackenzie, "Amorphous Oxides from Gels," in *Ultrastructure Processing of Advanced Ceramics*, J.D. Mackenzie and D.R. Ulrich, editors, pp. 589 - 601, Wiley, New York, 1988.
  46. S. Sakka, "Chemical Preparation of Glass," in *Proceedings of the 1st International Conference on Advances in the Fusion of Glass* (American Ceramic Society), 2.1-2.27,

- Alfred, New York, June 14-17, 1988 .
47. T. Adachi and S. Sakka, a) "The Role of N,N-Dimethylformamide, a DCCA, in the Formation of Silica Gel Monoliths by the Sol-Gel Method," *J. Non-Cryst. Solids* **99**, 118-128 (1988);  
b) "Sintering of Silica Gel Derived from the Alkoxysilane Solution Containing N,N-Dimethylformamide," *J. Non-Cryst. Solids* **100**, 250-253 (1988).
  48. S.H. Wang, C. Campbell and L.L. Hench, "Optical Properties of Silica-Gel Glasses," in *Ultrastructure Processing of Advanced Ceramics*, J.D. Mackenzie and D.R. Ulrich, editors, pp. 145-157, Wiley, New York, 1988.
  49. L.L. Hench, M.J.R. Wilson, C. Balaban and J.L. Nogues, "Sol-Gel Processing of Large Silica Optics," in *Proceedings of 4th International Conference on Ultrastructure Processing of Ceramics, Glasses and Composites*, Tucson, AZ, 1989.
  50. H. Okazaki, T. Kitagawa, S. Shibata and T. Kimura, "Mechanical Strength Improvement of Sol-Gel Derived Dry Gels for Optical Fiber Preforms," *J. Non-Cryst. Solids* **116**, 87-92 (1990).
  51. J.W. Zarzycki, M. Prassas and J.E.H. Phalippou, "Preparation of Monolithic Silica Aerogels, the Aerogels Thus Obtained and Their Use for the Preparation of Silica Glass Articles and of Heat Insulating Materials," U.S. Pat. 4,432,956 (1984).
  52. M. Prassas, J. Phalippou and J. Zarzycki, a) "Synthesis of Monolithic Silica Gels by Supercritical Solvent Evacuation," *J. Materials Science* **19**, 1656-1665 (1984);  
b) "Sintering of Monolithic Silica Aerogels," in *Science of Ceramic Chemical Processing*, L.L. Hench and D.R. Ulrich, editors, pp. 156-167, Wiley, New York, 1986.
  53. P.H. Tewari, A.J. Hunt and K.D. Lofftus, a) "Ambient-Temperature Supercritical Drying of Transparent Silica Aerogels," *Mater. Lett.* **3** (9,10), 363-367 (1985); b) "Structure and Chemistry of Sol-Gel Derived Transparent Silica Aerogels," in *Science of Ceramic Chemical Processing*, L.L. Hench and D.R. Ulrich, editors, pp. 123-130, Wiley, New York, 1986.
  54. J.G. van Lierop, A. Huizing, W.C.P.M. Meerman and C.A.M. Mulder, "Preparation of Dried Monolithic SiO<sub>2</sub> Gel Bodies by an Autoclave Process," *J. Non-Cryst. Solids* **82**, 265-270 (1986).
  55. J. Fricke, "Aerogels," *Scientific American*, pp. 92-97, May 1988.
  56. T. Miyazawa, K. Okada, T. Kubo, K. Nishizawa, I. Kitano and K. Iga, "Aberration Improvement of Selfoc Lenses," *Applied Optics* **19**(7), 1113-1116 (1980).
  57. L. Pugliese and D.T. Moore, "Gradient Index Optics," *Photonics Spectra*, pp. 71-76, March 1987.
  58. P.B. Macedo and T.A. Litovitz, U.S. Pat. 3,938,974 (1976).
  59. J.H. Simmons, R.K. Mohr, D.C. Tran, P.B. Macedo and T.A. Litovitz, "Optical Properties of Waveguides made by a Porous Glass Process," *Applied Optics* **18**(16), 2732-2733 (1979).
  60. P.B. Macedo, J.H. Simmons and S. Murai, "Method of Producing a Glass Article Having a Graded Index Profile of a Parabolic Nature," U.S. Pat. 4,302,231 (Nov 24, 1981).
  61. S. Ohmi, S. Shingaki, H. Sakai and Y. Asahara, "Process for Producing Glass Product having Gradient of Refractive Index," U.S. Pat. 4,640,699 (Feb 3, 1987).
  62. A. de Panafieu, Y. Nemaud, C. Baylac, M. Turpin, M. Faure and F. Gauthier, "The Production of Low Loss Optical Fibers by the Technique of Phase Separation and Leaching," *Physics and Chemistry of Glasses* **21**, 22-24 (1980).
  63. S.P. Mukherjee, "Gradient Index Lens Fabrication Processes: A Review," in the *Proceedings of a Topical Meeting on Gradient-Index Optical Imaging Systems*, May 4-5, 1981, Honolulu, Hawaii, Optical Society of America, pp. TuA1-1 to TuA1-5 (1981).
  64. S. Kurosaki, "Producing Graded Index Optical Glass Articles from Doped Silica Gel Bodies," UK Pat. Appl. GB 2084990A (Sept 15, 1981).
  65. S. Kurosaki and M. Watanabe, "Producing Graded Index Optical Glass Articles from Silica Gel Bodies," UK Pat. Appl. GB 2086877 (Sept. 15, 1981).
  66. S. Kurosaki and M. Watanabe, "Process for the Production of an Optical Glass Article," U.S. Pat. 4,389,233 (Jun 21, 1983).
  67. S. Kurosaki, "Process for the Production of an Optical Glass Article," U.S. Patent

- 4,436,542 (Mar 13, 1984).
68. T. Edahiro, N. Inagaki and S. Kurosaki, "Process for Producing Optical Glass Product," U.S. Pat. 4,528,010 (July 9, 1985).
  69. M. Yamane, J.B. Caldwell and D.T. Moore, "Preparation of Gradient-Index Glass Rods by the Sol-gel Process," *J. Non-Cryst. Solids* **85**, 244-246 (1986).
  70. M. Yamane, "Method and Composition for the Manufacture of Gradient Index Glass" U.S. Patent 4,686,195 (Aug. 11, 1987).
  71. M. Yamane, H. Kawazoe, A. Yasumori and T. Takahashi, "Gradient-Index Glass Rods of PbO-K<sub>2</sub>O-B<sub>2</sub>O<sub>3</sub>-SiO<sub>2</sub> system prepared by the Sol-Gel Process," *J. Non-Cryst. Solids* **100**, 506-510 (1988).
  72. M. Yamane, H. Kawazoe, A. Yasumori and T. Takahashi, "Preparation of Pb-Containing Glass by the Sol-gel Process - Reduction of Pb-migration during drying," *J. Non-Cryst. Solids* **99**, 160-167 (1988).
  73. M. Yamane, A. Yasumori, M. Iwasaki and K. Hayashi, "GRIN Rods of Large Diameter and Large Delta-N", to be published in "Better Ceramics Through Chemistry IV," MRS Symposia Proceedings, April 1990.
  74. K. Shingyouchi and K. Susa, "Refractive index gradient in glass," Jap. Pat. 61,183,136 (Aug 15, 1986).
  75. K. Shingyouchi and K. Susa, "Refractive index gradient in glass," Jap. Pat. 61,183,137 (Aug 15, 1986).
  76. K. Shingyouchi, S. Konishi, K. Susa and I. Matsuyama, "Radial Gradient Refractive-Index Glass Rods prepared by a Sol-Gel Method," *Electronic Letters* **22**(2) 99-100 (1986).
  77. K. Shingyouchi, S. Konishi, K. Susa and I. Matsuyama, "r-GRIN TiO<sub>2</sub>-SiO<sub>2</sub> Glass Rods prepared by a Sol-Gel Method," *Electronic Letters* **22**(21) 1108-1110 (1986).
  78. K. Shingyouchi, A. Makishima, M. Tutumi, S. Takenouchi and S. Konishi, "Determination of Diffusion Coefficient of Titanium Ion in TiO<sub>2</sub>-SiO<sub>2</sub> Wet Gel Prepared from Metal Alkoxides During Leaching," *J. Non-Cryst. Solids* **100**, 383-387 (1988).
  79. S. Konishi, K. Shingyouchi and A. Makishima, "r-GRIN rods prepared by a Sol-gel Method," *J. Non-Cryst. Solids* **100**, 511-513 (1988).
  80. K. Shingyouchi, A. Makishima and S. Konishi, "Determination of Diffusion Coefficients of Dopants in Wet Gels During Leaching," *J. Am. Ceram. Soc.* **71**(2) pp. C-82 to C-84 (1988).
  81. A. Makishima, K. Shingyouchi, Y. Kitami and M. Tsutsumi, "Microstructural Studies of Leached TiO<sub>2</sub>-SiO<sub>2</sub> Gel," *J. Non-Cryst. Solid* **102**, 275-279 (1988).
  82. K. Susa, I. Matsuyama, S. Satoh and T. Suganuma, "Sol-gel Derived Ge-doped Silica Glass for Optical Fiber Application I. Preparation of gel and glass and their characterization," *J. Non-Cryst. Solids* **119**, 21-28 (1990).
  83. J.B. Caldwell and D.T. Moore, "Sol-Gel Method for Making Gradient-Index Glass," U.S. Patent 4,797,376 (Jan 10, 1989).
  84. J.B. Caldwell, T.M. Che, R.W. Cruse, R.M. Mininni, R.E. Nikles, V.N. Warden and M.A. Banash, "Studies on the Reproducible Production of GRIN (Gradient Index) Glass Rods by a Sol-Gel Process," to be published in "Better Ceramics Through Chemistry IV," MRS Symposia Proceedings, April 1990.
  85. B.E. Yoldas, "Formation of Titania-Silica Glasses by Low Temperature Chemical Polymerization," *J. Non-Cryst. Solids* **38** and **39**, 81-86 (1980).



## Sol-gel derived r-GRIN doped-silica lenses

Shirou Konishi

Cable Research Laboratory, Hitachi Cable, Ltd.  
5-1-1 Hitaka-cho, Hitachi, Ibaraki 319-14, Japan

ABSTRACT

A new technique for producing radial gradient refractive index (r-GRIN) titanium-doped silica lenses has been developed employing a sol-gel leaching method. The obtained lenses possess a parabolic index distribution and give good images with high resolution. They also show high coupling efficiency with optical fibers and enable a low-loss large distance space transmission of light between optical fibers. Furthermore the sol-gel r-GRIN lenses show a high degree of environmental stability as expected for the doped-silica lenses.

1. INTRODUCTION

R-GRIN lenses have been widely used with the development of optical communication<sup>1</sup> and sensing systems. Many different techniques such as ion-exchange, chemical vapour deposition (CVD) and molecular stuffing have been explored to fabricate them<sup>2</sup>. Most of the r-GRIN lenses available today, however, are produced by an ion-exchange method using multicomponent glasses. Although the multicomponent r-GRIN lenses show fairly good optical quality, they do not possess good environmental stability due to their material compositions. Therefore it is desirable to develop a new method which can produce r-GRIN lenses with both good optical quality and environmental stability. In this paper we present a fabrication method and environmental characteristics of r-GRIN lenses produced by a newly developed sol-gel leaching method. The fabrication process consists of preparation of wet gels from a mixture of silicon and titanium alkoxides, formation of a titanium concentration gradient in the wet gels by diffusion controlled selective leaching of the titanium component, and drying of the leached wet gels followed by sintering of the dry gels. Cracking of the gels and light scattering of the densified glasses which are often observed in the sol-gel derived glasses have been overcome by careful control of the entire process. The fabricated r-GRIN lenses possess a well-defined parabolic index distribution, and also give good images with high resolution even after they are elongated by heat treatment. Since they function as a good collimating and focusing lens, they allow a low-loss large distance space transmission of light between optical fibers. Moreover, they exhibit a high degree of stability in an adverse environment such as high temperature, high humidity and strong radiation as expected for high-silica glasses.

2. FABRICATION

The sol-gel process to fabricate the doped-silica r-GRIN lenses<sup>3</sup> is outlined in Fig. 1. The process starts with preparation of individual n-propanol solutions of silicon tetramethoxide [ $\text{Si}(\text{OMe})_4$ ] and titanium tetra-n-butoxide [ $\text{Ti}(\text{O-n-Bu})_4$ ]. The two solutions are mixed together and a small amount of ammonia water is added to the solution followed by the introduction of formamide. The resultant sol solution is poured into glass tubes. Rod shaped wet gels are obtained as a result of gelation. After aging for a few days, the gels are immersed in hydrochloric acid to leach out the titanium component. The leached gels are then heated up to 140°C in the open air to obtain the dry gels. Finally, the dry gels are sintered into the densified glasses. The wet gels and the densified glasses are approximately 6 and 2 mm in diameter and 30 and 10 mm in length, respectively. Some details of the process are described below.

92 4 28 033

92-11415



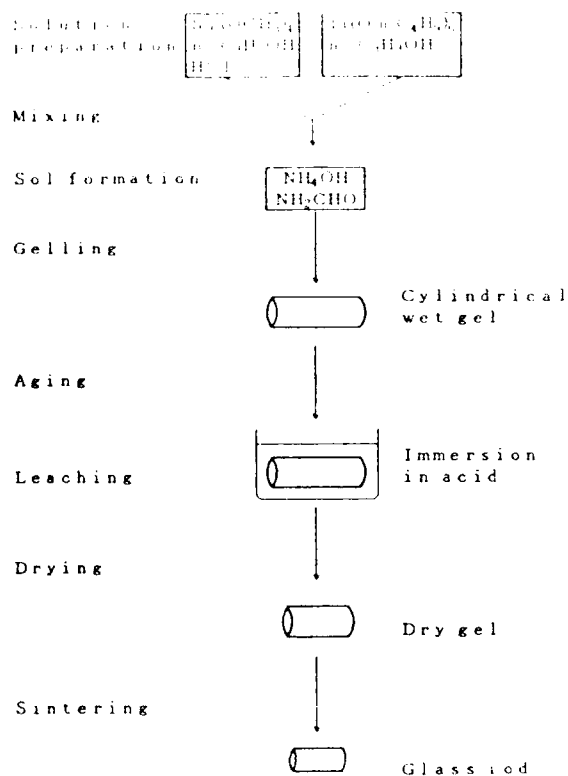


Fig. 1. Outline of the sol-gel process to produce r-GRIN lenses.

## 2.1 Solution preparation

Since  $\text{Si(OMe)}_4$  and  $\text{Ti(O-n-Bu)}_4$  are very different in their sol-gel reactivity, it is important to prepare sol and gel solutions with good homogeneity. We adopted a stepwise process to attain this, i.e., partial hydrolysis of  $\text{Si(OMe)}_4$  in n-propanol by addition of a small amount of hydrochloric acid followed by addition of  $\text{Ti(O-n-Bu)}_4$  diluted with n-propanol and then introduction of an ammonia water for adjustment of pH of the resultant sol solution. This procedure yields a clear solution without the formation of titanium dioxide precipitation. Formamide was also added to the solution as a Drying Control Chemical Additive (DCCA) to avoid cracking during drying of the wet gels.

## 2.2 Leaching

For formation of a titanium concentration gradient inside the wet gels, we have to make a proper choice of leaching reagent for titanium and further to confirm that the selective leaching of titanium out of the wet gel is predominantly controlled by diffusion. We found that acid, particularly, hydrochloric acid, is suitable for selective leaching of titanium out of a  $\text{Si(OMe)}_4$ - $\text{Ti(O-n-Bu)}_4$  wet gel. Fig. 2 shows the time dependence of the leached amount of silicon and titanium from a wet gel in 10% hydrochloric acid. The solid curve for titanium is calculated using the diffusion equation for a cylinder and assuming a diffusion coefficient of  $1.1 \times 10^{-6} \text{ cm}^2/\text{s}$  for the titanium component. The curve fits the experimental data well and verifies that the selective leaching of titanium is diffusion controlled.<sup>4</sup>

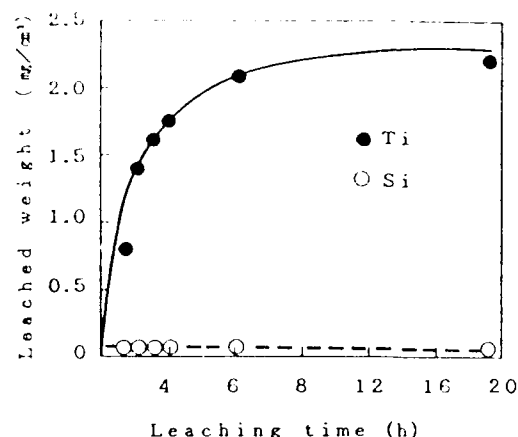


Fig. 2. Diffusion controlled leaching of the titanium component out of a wet gel.

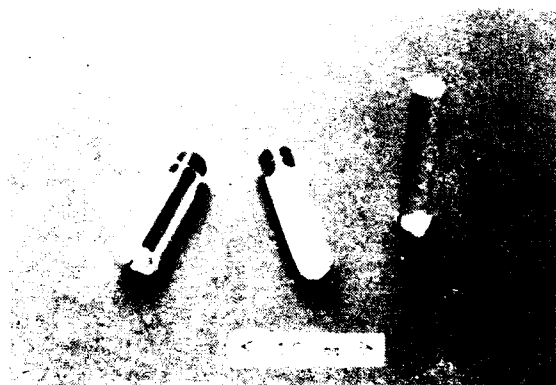


Fig. 3. Photograph of the sol-gel derived r-GRIN lenses.

### 2.3 Drying and sintering

Careful control of the drying and sintering of the gels is also needed to obtain clear glasses which are crack-free and show no light scattering due to micropores. The leached wet gels are washed thoroughly with water to remove the hydrochloric acid inside them. The washing is followed by drying in which the gels are gradually heated from room temperature to 140°C in the open air. Fast drying is apt to cause cracking of the gels. Then the dry gels are heated in an electric furnace up to 600°C in an oxygen atmosphere to remove organic residues by oxidation. Finally, the gels are heated to 1250°C in a helium atmosphere to obtain bubble-free clear glasses. Fig. 3 shows a photograph of the sol-gel derived r-GRIN lenses.

## 3. OPTICAL PROPERTIES

### 3.1 Refractive index profile

As described in the preceding section a concentration gradient of titanium is formed inside the wet gels by diffusion controlled leaching. It is not certain, however, if this concentration gradient of titanium is retained through the later process after leaching. Fig. 4 shows an example index profile of the fabricated rods examined with a transmission interference microscope. The observed index profiles fit the parabolic equation well

$$n(r) = N_0(1 - g^2 r^2) \quad (1)$$

Where the value of  $N_0$  is around 1.5 and that of  $g$  varies from 0.09 to 0.13 mm<sup>-1</sup> depending on the fabrication conditions. The observation of the parabolic index distributions is a confirmation that the concentration gradient of titanium inside the gels is retained through their fabrication, including drying and sintering after leaching.

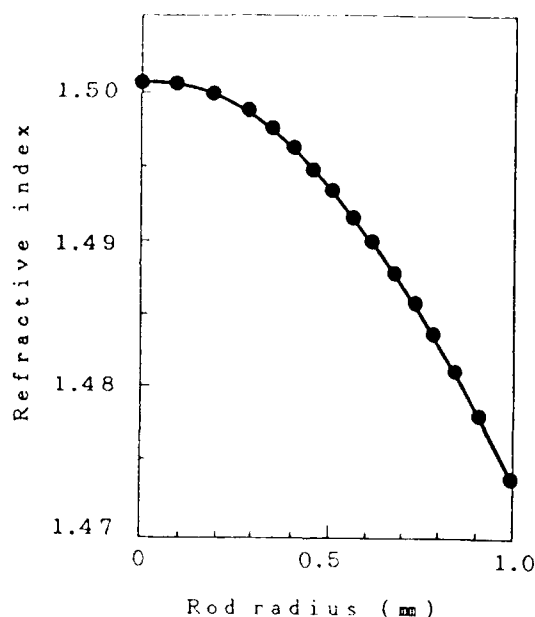


Fig. 4. Radial index profile of a sol-gel r-GRIN lens.

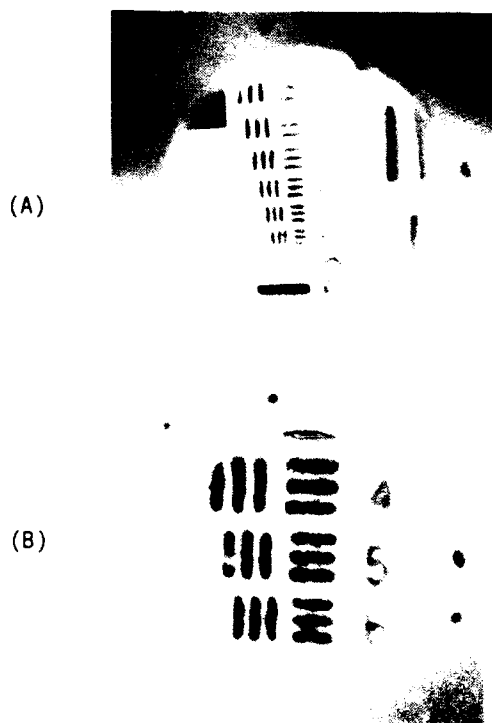


Fig. 5. Images formed by sol-gel r-GRIN lenses.

(A) 2 mm in diameter.

(B) 1 mm in diameter.



### 3.2 Image formation

We need to examine image formation by the sol-gel r-GRIN rods. Since the radial index profile is a well defined parabola with good axial symmetry, images with little distortion are expected. Furthermore, the smooth index gradient arising from molecular level composition changes is likely to yield high resolution of the obtained images. One more important point to be noted is that the fabricated r-GRIN rods can be elongated by heating just as is the case of producing silica optical fibers, in which large-sized preforms are elongated to thin optical fibers. The elongation of r-GRIN glasses by heating without changes of index profile is possible only for doped-silica. Figure 5 shows optical micrographs of the resolution target images formed by the sol-gel r-GRIN rods. A mother rod of 2 mm in diameter gives the image (A), whereas a rod elongated to 1 mm in diameter from the mother rod shows the image (B). These images confirm the above described expectations. The resolution of the lenses is evaluated to be higher than 100 lp/mm.

### 3.3 Beam collimation

Optical characteristics of the r-GRIN rods as a lens vary with their length. Therefore their length is adjusted to meet each specific purpose. One of the commonly used lengths is a quarter pitch, which is useful for collimation. We prepared nearly quarter pitch rods and examined their collimating power. Two photographs are shown in Fig. 6 giving a visible demonstration of the beam collimation ability; the output beam from a standard graded index (GI) optical fiber (50  $\mu$ m in core diameter) is introduced into a translucent plastic. (A) is the case without a r-GRIN rod and (B) with a quarter pitch sol-gel rod attached near the fiber end. The two cases are clearly distinguished and show how the quarter pitch r-GRIN lenses work as a collimator. Fig. 7 shows numerical data for diameters of the output beam from optical fibers, a GI fiber and a single mode (SM) fiber when a nearly quarter pitch sol-gel r-GRIN lens is placed close to the fiber end for each. The experimental setup is also given in the figure. The beam diameter increases with expansion of spacing, giving approximately 4 mm for a GI fiber and 1 mm for an SM fiber at the spacing of 400 mm, because the collimation effect is not perfect. However, if we compare these values with those of r-GRIN lensless cases, in which a GI fiber gives about 200 mm and an SM fiber about 80 mm beam diameters at the distance of 400 mm from the fiber end, we can appreciate the degree of the collimation effect by the sol-gel r-GRIN lenses.



Fig. 6. Spreading of the output beam from a GI fiber.  
(A) without a sol-gel r-GRIN lens.  
(B) with a sol-gel r-GRIN lens.

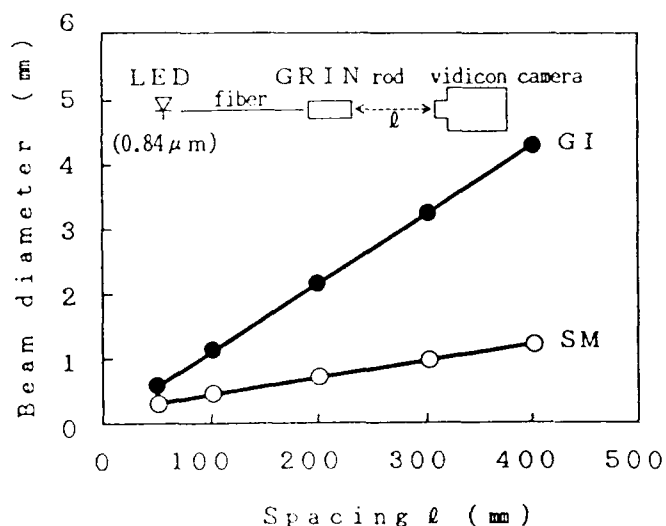


Fig. 7. Diameters of the output beams from optical fibers after passing through a nearly quarter pitch sol-gel r-GRIN lens.

### 3.4 Coupling with optical fibers

The r-GRIN lens is being used in a number of fiber optic devices<sup>5</sup>. The aim of the r-GRIN lens is to collimate the diverging light from an input fiber and direct the light onto a receiving r-GRIN lens which focuses the light onto a receiving fiber. That is the r-GRIN lens functions as a collimator and a focuser. The gap between the two r-GRIN rods depends on device requirements. In many applications, a large gap between the two lenses are needed with minimal loss increase. Fig. 8 shows lens spacing dependence of insertion loss when a pair of quarter pitch sol-gel r-GRIN rods are coupled with optical fibers. The experimental conditions for the measurements are also given in the figure. A 2 km long input fiber and a 3 m long receiving fiber are used. The results are shown for three different types of input and receiving fiber pairs. The loss is defined as  $10 \log (P_o/P)$ , where  $P_o$  is the light power inputted to a r-GRIN lens from the input fiber and  $P$  is the power received by a short fiber. Among the three fiber pairs, the GI  $\leftarrow$  SM pair gives the smallest loss value of about 1 dB and it is almost independent of the lens spacing. The other two pairs give a nearly equal loss value of approximately 2 dB up to the spacing of 200 mm, but thereafter the loss increase of the GI  $\leftarrow$  GI pair is larger than that of the SM  $\leftarrow$  SM pair. These results are reasonable, because the SM fiber is smaller both in core diameter and in numerical aperture (NA) than the GI fiber.

The point we want to stress here is that such a low-loss large distance space transmission of light between optical fibers using the r-GRIN lenses as the present case has not been reported before. That is, the loss increase with lens spacing is much larger for r-GRIN rods produced by other methods. Therefore we believe that the sol-gel r-GRIN lens would be a great help to those devices which need a low-loss large distance space transmission of light.

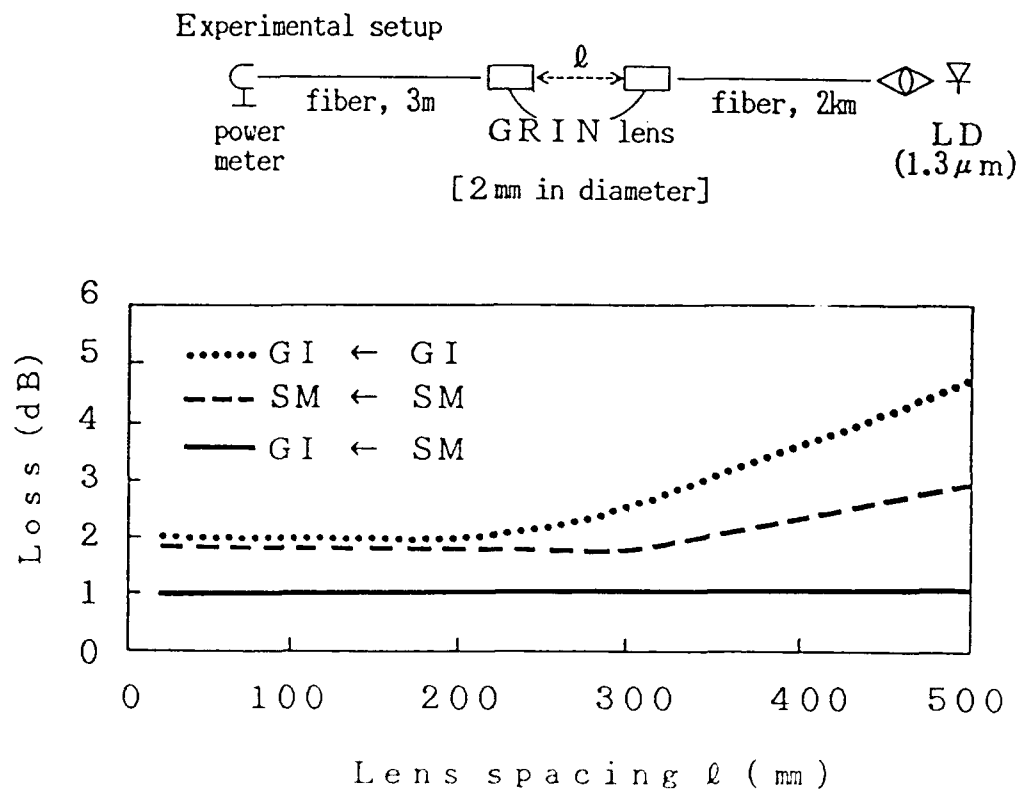


Fig. 8. Coupling efficiency of optical fibers using a pair of r-GRIN lenses.

#### 4. ENVIRONMENTAL STABILITY

Since the sol-gel r-GRIN lenses have a doped-silica composition, they are expected to show much higher performance in an adverse environment than the multicomponent glass lenses. The stability has to be evaluated experimentally. We evaluated the environmental stability of the sol-gel r-GRIN lenses based on changes in their appearance and in coupling efficiency before and after exposure of the lenses under each environment. The GI - GI fiber pair was used in the experimental setup of Fig. 8. The results are shown in Table 1 together with those for commercially available multicomponent r-GRIN lenses for comparison. For the heat resistance experiment the lenses were heated up to 1000°C in air and maintained at the temperature for 2 hours. The sol-gel lenses show no melting, no deforming, nor discoloring and the optical loss increase was zero, whereas the multicomponent lenses melt around 670°C. For the humidity resistance experiment the lenses were placed in a chamber with a water vapour pressure of 2 atm at 121°C for 10 hours. The sol-gel lenses show no changes in appearance and in optical transparency, while the multicomponent lenses become white due to devitrification. For the acid resistance experiment the lenses were immersed in 1 N hydrochloric acid at room temperature for 5 hours. The sol-gel rods show no changes at all, but the multicomponent rods undergo whitening and cracking. We also performed a radiation response experiment using  $^{60}\text{Co}$   $\gamma$ -rays. Radiation resistance is important for optical devices used in such environment as nuclear power stations and space stations. Fig. 9 shows the  $\gamma$ -ray dose dependence of the coupling loss increase. The sol-gel lenses show a gradual increase in loss with dose increase, while the multicomponent lenses undergo a steep increase due to deep coloration, which causes practically no transmission of light at the dose of  $10^6$  rad. Thus, strong resistance to harsh environment is confirmed for the sol-gel r-GRIN lenses.

Table 1. Environmental Stability of r-GRIN glass lenses.

environment	loss increase (dB), $0.84\ \mu\text{m}$	
	sol - gel	multicomponent
1000°C, 2h in air	0	$\infty$ (melting)
121°C, 2 atm water vapour, 2h	0	$\infty$ (devitrification)
25°C, 1N-HCl, 5h	0	$\infty$ (devitrification)
$10^6$ rad, $\gamma$ -rays in air	1.0	$\infty$ (coloration)

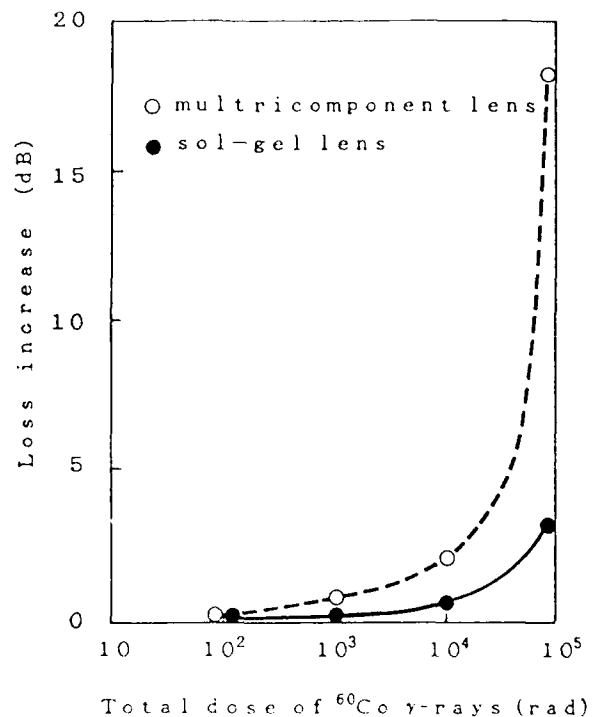


Fig. 9. Radiation response of r-GRIN glass lenses.

## 5. CONCLUSIONS

We have developed titanium-doped silica r-GRIN rod lens using the sol-gel leaching method. The fabricated lenses showed well-defined parabolic index profiles and gave good images with high resolution even after being elongated from a mother rod by heating. They functioned as a good collimator and also showed high coupling efficiency with optical fibers, which allowed a low-loss large distance space transmission of light between optical fibers. Examination of environmental stability of the lenses revealed their high degree of resistance to heat, humidity, acid, and  $\gamma$ -radiation as expected for the doped-silica composition. The sol-gel r-GRIN lenses having both good optical quality and high stability in an adverse environment will be versatile materials with many applications.

## 6. ACKNOWLEDGMENTS

The author is grateful to the following people in Hitachi Cable Laboratory, Mr. H. Endo for his technical assistance throughout the work and Mr. T. Fukabori and Mr. H. Morinaga who kindly helped in the coupling loss measurements.

## 7. REFERENCES

1. W. J. Tomlinson, "Application of GRIN-Rod Lenses in Optical Fiber Communication Systems," App. Opt. 19, pp. 1117-1126, 1980.
2. D. T. Moore, "Gradient-Index Optics : a Review," App. Opt. 19, pp. 1035-1038, 1980.
3. K. Shingyouchi, S. Konishi, K. Susa, and I. Matsuyama, "r-GRIN  $\text{TiO}_2$ - $\text{SiO}_2$  Glass Rods Prepared by a Sol-Gel Method," Electron. Lett. 22, pp.1108-1110, 1986.
4. K. Shingyouchi, A. Makishima, M. Tutumi, S. Takenouchi, and S. Konishi, "Determination of Diffusion Coefficient of Titanium Ion in  $\text{TiO}_2$ - $\text{SiO}_2$  Wet Gel Prepared from Metal Alkoxide during Leaching," J. Non-Cryst. Solids. 100, pp.383-387, 1988.
5. J. C. Palais, "Fiber Coupling Using Graded-Index Rod Lenses," App. Opt. 19, pp.2011-2018, 1980.

SOL-GEL OPTICS

Volume 1328

**SESSION 3**

**Composites and Lasers I**

*Chair*

**Larry L. Hench**  
University of Florida



# Sol-Gel Processed Inorganic and Organically Modified Composites for Nonlinear Optics and Photonics

Paras N. Prasad\*

\*Photonics Research Laboratory, Department of Chemistry,  
State University of New York at Buffalo, Buffalo, N.Y. 14214

## ABSTRACT

The newly emerging field of Nonlinear Optics and Photonics offers tremendous opportunities for optical engineers and materials scientists. The approach used for sol-gel optics i.e. the use of sol-gel processing can play a very important role for the development of novel materials and device structures for nonlinear optics and photonics. In this paper, chemical processing using the sol-gel method is reported for preparation of new composite materials of both a silica glass and a  $V_2O_5$  gel with a  $\pi$  conjugated polymer poly-p-phenylene vinylene up to 50% by weight. The composite films show highly improved optical quality with large third-order nonlinear optical coefficient, the latter derived from the conjugated polymer. Optical waveguiding through the film has been achieved. Nonlinear optical studies using femtosecond degenerate four wave mixing, optical Kerr gate switching and power dependent waveguide coupling have been successfully performed. Also, to investigate the use of such films for optical recording, a two dimensional grating structure has successfully been produced.

## 1. INTRODUCTION

Photonics has been labelled as the technology for the 21st century. It is a multidisciplinary field which has captured the imaginations of scientists and engineers worldwide. Sol-gel processing can provide new ceramic composite materials with multifunctionalities needed for photonics applications. In this article I hope to highlight this point.

Photonics describes the technology in which a photon is used to transmit, process and store information with an obvious gain in speed, bandwidth and density of information processing. The technology, therefore, deals with high density optical data storage, optical processing of information and image analysis. In addition, there is a need for devices to provide sensor protection against laser threat.

Some of the needed operational functions are frequency conversion, light modulation and optical switching. For these functions one needs nonlinear optics which describes processes occurring under the influence of a laser pulse. The resulting polarization in the medium can be written in the form of a power series expansion in the electric field strength as

$$P = \chi^{(1)} \cdot E + \chi^{(2)} : EE + \chi^{(3)} :: EEE + \dots \quad (1)$$

The term  $\chi^{(1)}$ , the linear susceptibility, describes the linear optical effect such as absorption, refraction, etc. under ordinary light intensities and is related to the refractive index of the medium as

$$1 + 4\pi\chi^{(1)} = n^2 \quad (2)$$

The terms  $\chi^{(2)}$  and  $\chi^{(3)}$  called second and third order nonlinear susceptibilities, respectively, describe the second and third order nonlinear optical

92 4 28 034

92-11416



processes. For all optical processing of information, the important nonlinear process is third order, the manifestations of which are third-harmonic generation and intensity dependence of refractive index. It is the latter which provides the method of light control by light. Conjugated polymers with extensive  $\pi$ -electron delocalization have emerged as an important class of third-order nonlinear optical materials because the  $\pi$ -electrons make a large contribution to optical nonlinearity. In addition to having a large nonlinear coefficient  $\chi^{(3)}$  needed so that a nonlinear component can be switched with low energy pulses, the materials must also have mechanical strength, environmental stability, high optical damage threshold and low optical losses. Organic polymeric materials are in general optically lossy. Inorganic glasses, particularly silica, are excellent photonic media; high quality fibers and films with extremely low optical losses can be prepared. However, the nonlinear optical coefficients of these glasses are extremely low. There is a need, therefore, to optimize both the nonlinear coefficient  $\chi^{(3)}$  and the optical losses. An obvious approach will be to make a composite of a conjugated polymer and an inorganic glass. The preparation of such composites run into two difficulties (i) High temperature processing of glass cannot be used as most polymers decompose by 300-350° C. (ii) Because of the incompatibility of the organic polymeric and inorganic glass structures, generally a phase separation occurs at higher compositions.

We have recently developed such composites using the sol-gel chemical processing method.<sup>4</sup> In our opinion, this approach opens up an important avenue to produce novel composite structures for applications in both photonics and electronics. In this paper, the merits of the sol-gel processing technique for photonics are briefly discussed. Then, the characterization of these composites, their nonlinear optical studies and optical wave guide experiments are presented.

## 2. MERITS OF THE SOL-GEL PROCESSED COMPOSITES

Sol-gel processing of composite structures offers the following advantages for photonics:

a) tremendous flexibility to introduce multifunctionality desired for device applications. This flexibility enables: 1. Preparation of numerous composite structures incorporating various inorganic and organic species because of the sol-gel low temperature chemical processing. 2. Use of infiltration to incorporate molecular species into the pores and layers. 3. Conducting chemistry in the pores and layers before densification. 4. Making novel unusual molecular composites of the sol-gel glass and a third-order nonlinear optical polymer.

b) opportunity to make various guided-wave structures such as planar waveguides, channel waveguides and fibers.

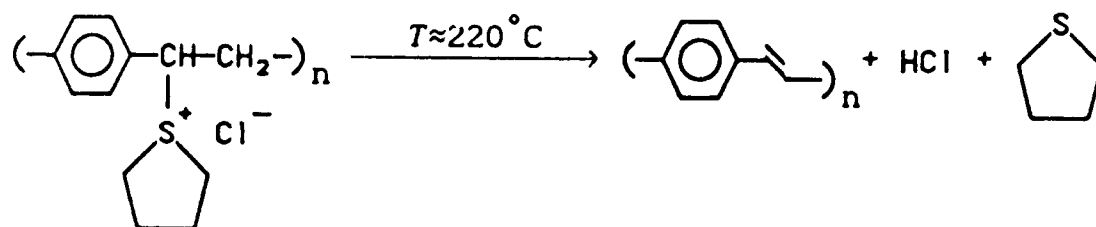
c) Electric field poling during gelation, for dipole alignment needed for second order effect, as poling is more effective due to increased molecular mobility of the structure.

d) opportunities to prepare composites with unusual electronic and optical properties by using heterostructures consisting of mixed valence inorganic semiconductors and p-type organic semiconductors.

## 3. THE NEW COMPOSITE GLASS-POLYMER MATERIALS

Using the sol-gel processing technique we have prepared several inorganic oxide, conjugated polymer composites in which the two components are homogeneously mixed in large compositions (up to 50% by weight) without phase separation. The conjugated nonlinear optical polymer is poly-p-phenylene vinylene (abbreviated as PPV, shown below). In our approach we start with a water soluble sulfonium salt polymer

precursor of PPV which when cast in the film form and heated above 230° C undergoes the following elimination reaction to produce the conjugated polymeric structure of PPV.<sup>5</sup>



Precursor polymer

PPV

To prepare the new composites, the PPV polymer precursor is homogeneously mixed with the sol-gel precursor in a common solvent in very high compositions. The film is cast and during the heat treatment the polymer precursor converts into the final conjugated polymer. The result is an optically transparent film of wave guiding quality (i.e., very low optical losses). The formation of this compatible blend is due to a synergistic effect occurring during the chemical transformation of each component. We do not know at this stage if they are molecularly mixed. However, the excellent optical quality clearly indicates that if domains exist, they are much smaller than the wavelength of light.

We have prepared composites of the PPV polymer with the sol-gel processed silica glass and  $V_2O_5$  gel. In both cases optical quality films were obtained. The U.V. visible absorption spectra of both silica:PPV and  $V_2O_5$  gel:PPV composites indicate quantitative conversion of the PPV precursor to the conjugated PPV structure. At this stage, only the silica:PPV composite has been characterized in more detail. Both DSC and TGA thermal analysis have been performed on this composite material. The results indicate that the conversion of the PPV precursor to the final conjugated PPV structure is indeed facilitated in the composite structure. The conversion temperature shifts from 230° C, found for the pure PPV precursor, to 140° C in the composite structure.

A number of linear and nonlinear optical studies have been performed on the composite films. A film of about one micron thickness was used to conduct optical waveguide studies. At 1.06 $\mu$ , propagation distances of upto 2 cm through the film were readily achieved. An estimation of the waveguide loss is about ~4dB/cm. We believe that by optimizing the processing variables, this loss can be greatly reduced. The waveguide prism coupling experiment also yielded information on the refractive indices of the TE and TM modes at 1.06 $\mu$ . These two modes of propagation differ in the polarization of the wave. In the TE mode, the electric field vector of the propagating waveguide mode lies in the plane of the film, while for the TM mode it is outside the plane of the film.<sup>6</sup> The refractive indices are 1.72 and 1.60 for the TE and TM modes at 1.06 $\mu$  indicating a birefringence even in the as-cast film. The higher refractive index for the TE mode may be the result of a preferential alignment of the polymer chains in the plane of the film. In the optical waveguiding arrangement with the prism coupler we have also obtained the Raman spectra of the



film; the bands due to the PPV polymer correlate nicely with those obtained for the pure PPV material.

Nonlinear optical studies have been carried out in both the bulk configuration and the waveguide geometry. A convenient method to measure the third-order nonlinear optical coefficient  $\chi^{(3)}$  and its time-response is degenerate four wave mixing (DFWM) which has been described in detail elsewhere. The method can best be understood by using a grating picture. Two coherent beams of same frequency interact in a medium such as the silica: PPV film. They set up an intensity modulation pattern due to interference. Since for a third order material, the refractive index is dependent on the intensity, a refractive index modulation (grating) results. A third beam, the probe beam, of same frequency is diffracted from this grating to produce the signal, the intensity of which is proportional to the square of  $\chi^{(3)}$ . The decay of the signal intensity as a function of the time delay of the probe beam with respect to the interfering beams gives direct information on the response time of the third-order optical nonlinearity. We have conducted this study using 400 femtosecond pulses from a Nd:Yag laser pulse compressed amplified system at 602 nm. The  $\chi^{(3)}$  value obtained is  $\sim 3 \times 10^{-10}$  esu for a ~50:50 composite; this value is fairly high. The response time is limited by the pulse width of the laser. We have also conducted the DFWM studies using 50 femtosecond pulses from an amplified colliding-pulse mode-locked laser system. The nonlinearity in the composite shows response on this time scale, again limited by the pulse width. Using 50 femtosecond pulses, we have also performed an Optical Kerr gate experiment in which a strong pump beam creates an optically induced birefringence in the nonlinear medium. This birefringence is detected by passing a linearly polarized probe beam through the medium and detecting the switching on of the transverse component through a polarizing analyzer. We have observed optical switching in 50 femtoseconds. Figure 1 shows the results of the Kerr gate study. We therefore observe ultrafast nonlinear response in femtoseconds for this composite material.

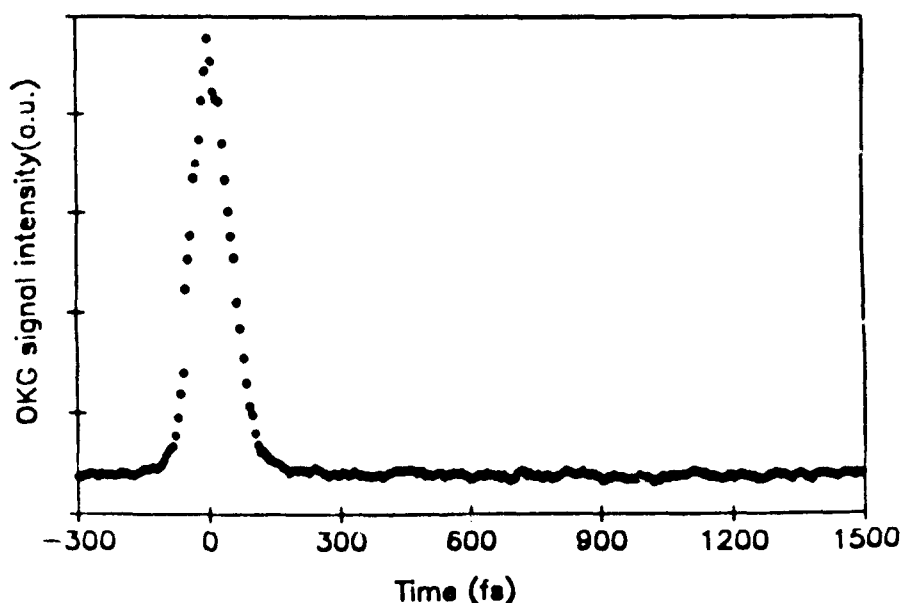


Figure 1: Optical Kerr-gate signal for the sol-gel silica: PPV composite as a function of time delay between the pump and probe beam

In the waveguide arrangement, we have investigated the third-order optical nonlinearity by investigating the power dependent coupling angle at  $1.06\mu$  using a grating coupler arrangement.<sup>9,10</sup> The film of the silica:PPV composite is deposited on a quartz substrate on which input and output grating couplers have been fabricated using the ion milling technique. The input wave couples through the grating at a specific angle which is determined by the refractive index of the film. As the intensity of the beam is increased, the refractive index of the film changes leading to a change of the coupling angle.<sup>10</sup> We have successfully observed this intensity dependent coupling angle behavior. This phenomenon is also of interest from device application point of view as it can be used for optical switching and optical power limiter operations.

From device application perspective, we have also investigated the films of the silica:PPV composite for the fabrication of two-dimensional gratings. Crossing of two femtosecond pulses at 602 nm was used for this fabrication. For a two dimensional grating, the film is rotated by  $90^\circ$  and the crossing angle is changed. The result is optical recording of a two dimensional grating of two different periods. Our preliminary investigation indicates that the grating is not formed by laser ablation but is a result of intensity dependent two-photon absorption which induces chemical changes in the polymer precursor and/or produces laser densification of the composite. Figure 2 shows the diffraction pattern of a He-Ne laser beam from the grating. It clearly exhibits the two different grating spacing in

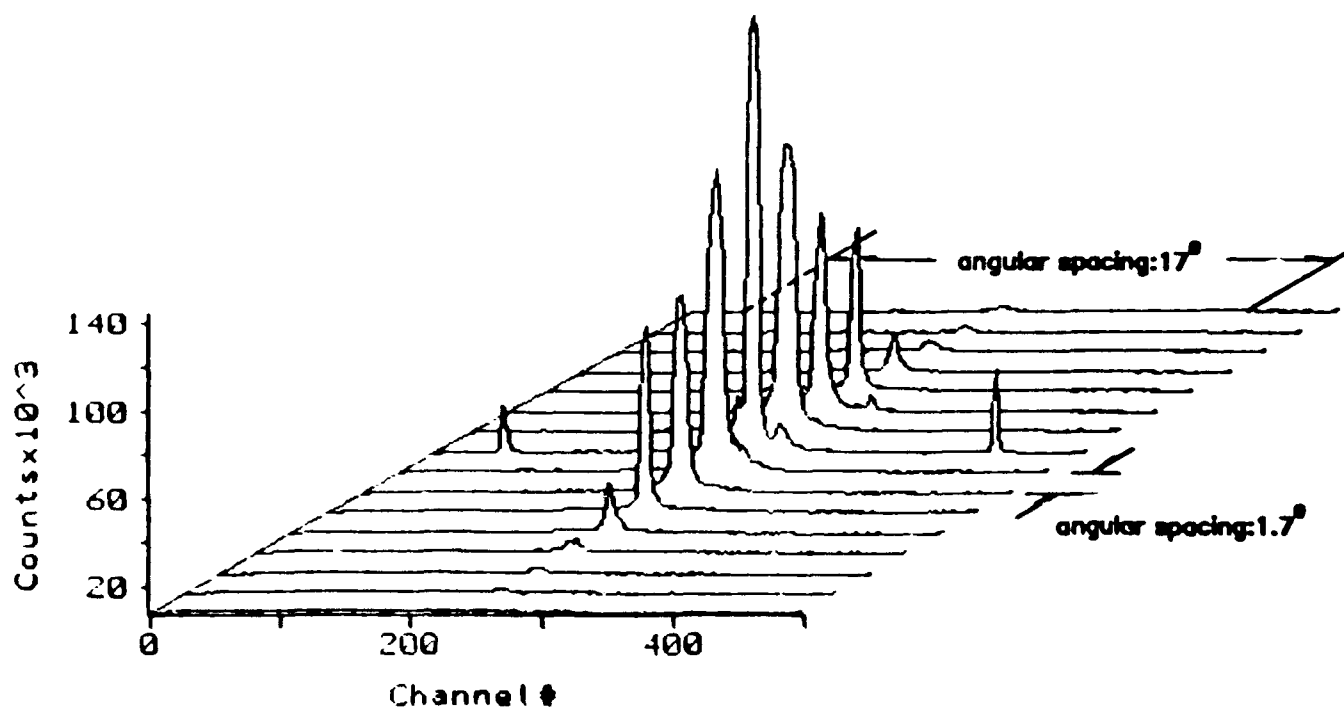


Figure 2: Diffraction pattern from a two-dimensional grating fabricated in the silica:PPV film

the two transverse directions. Such composite films, therefore, can also be useful for optical recording.

#### 4. ACKNOWLEDGEMENT

This research was supported by the Office of Innovative Science and Technology - Defense Initiative Organization and the Air Force Office of Scientific Research, the directorate of Chemical and Atmospheric Sciences through contract numbers F4962087C0097 and F4962090C0021.

#### 5. REFERENCES

1. Y. R. Shen, The Principles of Nonlinear Optics, Wiley & Sons (New York, 1984).
2. "Nonlinear Optical and Electroactive Polymers", Eds. P. N. Prasad and D. R. Ulrich, Plenum Press (New York, 1988).
3. P. N. Prasad and D. J. Williams, "Introduction to Nonlinear Optical Effects in Molecules and Polymers", Wiley & Sons (New York, in Press).
4. C. J. Wung, Y. Pang, P. N. Prasad and F. E. Karasz, *Polymer* (in Press).
5. D. R. Gagnon, J. D. Capistran, F. E. Karasz, R. W. Lenz and S. Antoun, *Polymer* 28, 567 (1987).
6. G. I. Stegeman, *Thin Solid Films* 152, 231 (1987).
7. M. Samoc and P. N. Prasad, *J. Chem. Phys.* 91, 6643 (1989).
8. C. J. Wung and P. N. Prasad, unpublished result.
9. Y. Pang and P. N. Prasad, unpublished result.
10. R. Burzynski, D. N. Rao and P. N. Prasad, unpublished result.
11. G. S. He, G. Xu, C. J. Wung, and P. N. Prasad, unpublished result.



## Solid-state tunable lasers based on dye-doped sol-gel materials

B. Dunn\*, J.D. Mackenzie\*, J.I. Zink<sup>†</sup> and O.M. Stafsudd\*

University of California, Los Angeles, \*Department of Materials Science and Engr.

†Department of Chemistry and Biochemistry •Electrical Engineering Department  
Los Angeles, California 90024

## ABSTRACT

The sol-gel process is a solution synthesis technique which provides a low temperature chemical route for the preparation of rigid transparent matrix materials. The luminescent organic dye molecules, rhodamine 6G and coumarin 540A have been incorporated, via the sol-gel method, into aluminosilicate and organically modified silicate host matrices. Synthesis, laser oscillation and photostability for these systems are reported. The improved photostability of these materials with respect to comparable polymeric host materials is discussed.

## 1. INTRODUCTION

The sol-gel technique offers a low temperature method for synthesizing amorphous materials which are essentially inorganic. The process is based on hydrolysis and condensation reactions of organometallic compounds in alcoholic solutions. The most widely investigated system involves silica-based glasses which are prepared by polymerization of a silicon alkoxide,  $\text{Si}(\text{OR})_4$ .<sup>1,2</sup>

The ability to synthesize inorganic polymers using sol-gel processing with little or no heating makes it possible to dope these gels with a variety of organic and organometallic molecules.<sup>3-11</sup> Luminescent molecules have been widely investigated and it is evident that numerous dyes maintain their luminescent properties in sol-gel matrices.<sup>3-5,8-10</sup> The emission properties of the molecules have been used to optically probe sol-gel chemistry<sup>3-6,9</sup> and structure.<sup>4,8</sup> Another active area for organic doped sol-gel glasses is to use dopants to induce selected optical properties and to synthesize new optical materials. Among the properties reported to date are photochromism,<sup>1,2</sup> nonlinear optical effects ( $\chi^{(3)}$ ),<sup>13</sup> and tunable laser action.<sup>14-18</sup> The latter was achieved by incorporating organic laser dyes in a sol-gel matrix and thus represents a potentially important direction for solid-state laser materials.

Organic laser dyes have been widely reported as having desirable properties for optical gain and laser applications. Finding suitable host materials for these organics is problematic and, in the case of laser dyes, devices have been primarily restricted to liquid state applications. There are a number of devices, however, where solid state gain media would be quite advantageous. Attempts have been made to fabricate solid state organic dye materials using polymeric hosts such as poly (methyl methacrylate), poly(carbonate), poly(styrene) and poly(vinyl alcohol).<sup>19-21</sup> These hosts, however, have been shown to be inherently lacking in mechanical and thermal properties, photostability, and refractive index uniformity. Inorganic glasses, on the other hand, do possess extremely good optical, thermal, and chemical stability. Unfortunately, typical melt glasses require processing temperatures which would cause the rapid decomposition of most organic species.

92 4 28 035

92-11417



Prior studies have shown that laser oscillation can be obtained in organic dye-doped oxide matrices synthesized by the sol-gel technique. To date rhodamine, coumarin and perylene dyes have been lased in various matrices including silica, alumina, aluminosilicate, organic modified silicates (ORMOSIL) and sol-gel composites.<sup>14-18</sup> Although much of the work is at the demonstration stage, some extremely promising results have been reported: optical gain of  $40\text{ cm}^{-1}$ ,<sup>16</sup> slope efficiency in the range of 20% and laser thresholds as low as  $1\text{ }\mu\text{J}$ .<sup>17</sup> In view of the number of dyes and dopants available, the prospect of achieving a wide range of sol-gel based tunable solid state lasers is of substantial interest to the optical materials community.

The present paper reviews our recent work with rhodamine and coumarin dyes in aluminosilicate and ORMOSIL hosts. The emphasis of the studies is the photodegradation characteristics of these systems. Although earlier work indicated that sol-gel matrices exhibited good photodecomposition properties because of matrix isolation,<sup>3</sup> photodegradation under laser action represents a more rigorous measurement as well as a more relevant one. The synthesis and laser oscillation characteristics of these materials are also presented.

## 2. SYNTHESIS

The organically modified silicate gels were synthesized in a fashion similar to the methods described previously.<sup>22,23</sup> The initial precursor solution was composed of a 1:1:1:3.5 molar ratio of TMOS / methyl methacrylate (MM) / 3-(trimethoxysilyl) propyl methacrylate (TMSPM) / 0.04 N HCl, in a homogeneous solution. After one day at room temperature, the dye was dissolved into the sol and the solution was placed into acrylic cuvettes. The doped ORMOSIL was kept uncovered at room temperature for about 3 days, until approximately one half of the initial volume had evaporated. Starting dye concentrations in the ORMOSIL solutions were  $2.0 \times 10^{-3}$  and  $5 \times 10^{-4}$  mol/l for coumarin 540A (C:540A) and rhodamine 6G (R6G), respectively. After this composition was found to produce rhodamine-doped materials with poor gain,<sup>24</sup> the composition was modified with epoxy-silane. In this case the starting sol consisted of a 3:1.5:3:1.5:3:16 molar ratio of TMOS / MM / ethylene glycol (EG) / TMSPM / 3-glycidoxypropyl trimethoxysilane (GPTMS) / 0.04 N HCl. The epoxy functionalities incorporated into ORMOSIL gels are believed to form internal diols under appropriate hydrolytic conditions.<sup>22</sup> Diols such as ethylene glycol are known to have good solvation properties for the R6G dye.<sup>25</sup> The glycol was added to the composite polymer to help stabilize the monomeric form of R6G in the rigid host matrix.

After 2 to 3 weeks of hydrolysis and aging, the gels had lost approximately 50% of their initial volume. The volume change arises primarily from the loss of methanol, which is a product of the organometallic hydrolysis reaction. These samples were then removed from their cuvettes and heated to  $55^\circ\text{C}$  for an additional three weeks in order to remove any remaining volatile components and/or unreacted monomer. The resulting monoliths had faces which were nearly plane parallel, having good surface and volume optical quality. Absorption measurements indicated that scatter in the dye-doped ORMOSILs was approximately  $2\% \text{ cm}^{-1}$ .

The aluminosilicate samples were prepared by slowly adding a solution of 10 ml of isopropanol and 5 ml distilled water to a solution containing 10 ml of the aluminosilicate precursor diisobutoxyaluminumoxytriethoxysilane and 10 ml of isopropanol.<sup>9</sup> The coumarin

and rhodamine dyes were dissolved in the isopropanol beforehand. The sol was decanted into polystyrene cuvettes and sealed with wax film. Gelation of the sol was complete after  $\approx 3$  days. The gels were allowed to age in the sealed cuvettes for one week after gelation. A small hole was subsequently pierced in the film to allow slow evaporation of alcohol and water. When the gels were fully dried xerogels ( $\sim 4$  weeks after drying began) the monoliths were removed from the cuvettes and then used in the experiments *as cast*, with no polishing or surface treatment.

### 3. EXPERIMENTAL

The range of optical measurements employed in characterizing the dye-doped gels and ORMOSILs was described previously.<sup>8,9,16</sup> The most commonly used techniques are fluorescence, optical gain, laser oscillation and photostability. In the laser oscillation results reported here, the doped xerogels or ORMOSILs were transversely pumped by a FL 2001 Lambda Physik dye laser at either 540 nm (for R6G) or 460 nm (for C-540A). The pump beam was focussed to a line with a cylindrical lens ( $f = 5$  cm) which was mounted on a translation stage to allow focussing without disturbing the alignment of the pump beam on the sample. The oscillation cavity consisted of a 90% reflective parabolic mirror ( $f = 25$  cm) and a 35% reflective planar output coupler. The output of the laser cavity was directed with two aluminum mirrors through an iris onto a MgO scatterplate. Collecting optics brought the scattered laser beam into a 1/4 m single grating monochromator. The free running laser output spectrum was recorded periodically in order to quantitatively determine reduction in output intensity of the doped gel laser materials as a function of the number of pump pulses. The repetition rate was varied from 1 Hz to 25 Hz.

### 4. RESULTS

#### 4.1. Aluminosilicate gels

The spectra for the rhodamine 6G and coumarin 540A free running lasers are shown in figures 1 and 2 as a function of the number of pump pulses. In both cases, free standing monoliths were used as processed, with no polishing. The output for the R6G is centered at about 570 nm, and the bandwidth is approximately 5 nm. The laser spectrum is much narrower than the corresponding fluorescence spectra for this system.<sup>16</sup> The bandwidth is typical of a free running laser which runs many modes simultaneously due to lack of a wavelength selective grating or prism in the cavity. The different output wavelengths of the modes can be seen in the spectra as the variations in peak shape; the exact mechanism which determines the relative intensities of the different modes is not yet known. The bandwidth for the R6G laser stays roughly constant with increasing numbers of pump pulses.

The spectrum of the free running laser for coumarin 540A doped aluminosilicate xerogel as a function of the number of pump pulses is shown in Figure 2. The output is centered at about 557 nm with a bandwidth of 10 nm. The laser spectrum is also much narrower than the fluorescence spectra.<sup>16</sup> The wavelength maximum blue-shifted with increasing numbers of pump pulses. The maximum of the spectrum after 900 pulses can be seen as a shoulder on the spectrum of the free running laser after 600 pulses. The bandwidth, however, stays roughly constant with increasing numbers of pump pulses.

**TABLE 1.**  
**Spectral output of aluminosilicate and ORMOSIL laser resonators**

Dye	Matrix	Pump $\lambda$ (nm)	Laser Emission Peak (nm)	Osc. Bandwidth (FWHM in nm)
Coumarin 540A	ORMOSIL	460	525	21
Coumarin 540A	Aluminosilicate	460	557	10
Rhodamine 6G	ORMOSIL	539	568	8
Rhodamine 6G	Aluminosilicate	540	570	5

The intensity of the laser output for both rhodamine and coumarin samples decreases with the total number of pulses which have pumped the sample. The rate of this decrease varies with concentration, pump power, and pump rate. A set of degradation plots is shown in Figure 3 for the R6G samples. A continuously decreasing decay rate which could not be fit to an exponential or a double exponential curve was observed in all experiments. Samples pumped at 1 Hz retained 50% of this initial output intensity after about 1500 pulses. This is considerably better than the behavior of the coumarin lasers where the 50% level for the initial output intensity was reached after only about 300 pulses.

The decay rate for R6G was modestly accelerated by increasing the pump rate. 1200 pulses were required to reduce output to 50% at 10 Hz whereas 800 were required at 25 Hz. The best R6G sample studied exhibited laser action even after 40,000 pulses. In these studies the photodegradation was not counteracted by changing the focal point of the pump beam to a fresh area of the gel, either by translation of the gel or beam or by refocussing. It is important to note that full output could be regained by pumping a new region.

#### 4.2 Ormosils

Broad band laser oscillation was easily obtained in all of the dye-doped ORMOSILs tested. The details are summarized in Table 1. The laser emission peak for the C-540A samples occurred at 525 nm with an oscillation bandwidth of 21 nm (FWHM) while the laser emission peak for R6G was observed at 568 nm with a bandwidth of 8 nm. The coumarin-doped samples represented the only materials where the fluorescent emission spectrum had a bandwidth (495 to 575 nm, FWHM) which closely corresponded to the overall width and specific oscillation wavelengths of the free-running laser (498 to 574 nm). The oscillation bandwidths for rhodamine doped ORMOSILs were found to be substantially narrower than the coumarins. In this case the fluorescence band for R6G doped ORMOSIL had a FWHM bandwidth of 55nm (541 to 596 nm) that was considerably larger than the detectable oscillation range for these materials (41 nm, from 557 to 598 nm).

Figure 4 shows the decrease in laser output intensity of the rhodamine and coumarin doped ORMOSILs as a function of the number of laser pump pulses. It can be seen that both materials could be pulsed for more than 3000 shots, corresponding to a reduction of emission by about a factor of 4. Although there was a decrease in emission intensity, the spectral laser emission characteristics of the doped ORMOSILs were unchanged by the large number of laser pulses, as was observed with the aluminosilicate materials (see Figs. 1 and 2). It is interesting to note that the coumarin doped gel appears to have a double exponential decay plot.

## 5. DISCUSSION

The results clearly demonstrate the ability of aluminosilicate gels to support laser action. Although optical gain was not measured, the gain values are apparently in the range observed for alcoholic solutions as laser action was achieved using as-formed samples without any polishing. Xerogels contain no residual liquid, however, solvents are known to be left adsorbed on the pore walls.<sup>26</sup> Narrowing of the laser oscillation band as compared to the luminescence spectrum was observed with both R6G and C-540A dyes. The effect may be the result of dye/matrix interactions and attachment of the molecules to pore walls. In addition, the free running laser spectrum of C-540A is red shifted with respect to the luminescence spectrum. This behavior is similar to that of coumarins in silica matrices where the red shift is associated with greater solvent polarity of siloxane groups and silanols as compared to the initial sol.<sup>24</sup>

The laser behavior exhibited by ORMOSILs underscores the chemical variability available with this synthesis method. The methacrylate modified silica gel used with C-540A is clearly an excellent host. Large values for optical gain have been measured and laser oscillation was obtained over a wide spectral range.<sup>16</sup> In contrast this matrix leads to dimer formation with R6G and correspondingly poor optical properties.<sup>24</sup> The ORMOSIL approach, however, enables the silica gel matrix to be suitably modified so that an environment favorable to R6G is created. Specifically, epoxy functionalities were utilized to form interal diols. Diol solvation within the matrix tends to support the monomeric molecular form of R6G. The success of this approach is evident by the fact that laser oscillation was readily obtained. Although the R6G doped ORMOSILs did not perform with the laser bandwidth exhibited in the C-540A material, the prospects for optimizing the ORMOSIL composition to obtain a more suitable matrix are excellent.

One of the most important issues to be considered for laser materials prepared by the sol-gel technique is the photostability of these materials. Laser characteristics of dye-doped PMMA and many other doped polymers have been examined extensively and represent an appropriate basis for comparison. Although laser oscillation was obtained in many cases, poor photostability limited the ultimate usefulness of polymeric laser hosts. Itoh et. al. reported optical gain of several coumarin dyes in PMMA.<sup>20</sup> Using a nitrogen laser pump source (337 nm) the best of the dyes reported could be used to several hundred oscillatory pulses, while other coumarin dyes could not be made to oscillate for as many as 100 pulses. More recently, Gromov et. al. reported on the photodegradation of modified poly(methyl methacrylate), MPMMA, doped with rhodamine 6G and other selected dyes.<sup>19</sup> They showed that R6G exhibited photobleaching (loss of 20% output) after 180 pump pulses ( $1\text{J}/\text{cm}^2$ ) at 532 nm. Their data indicated that R6G doped MPMMA laser materials would have dropped by 90% after some 300 pulses, due to rapid steady-state photodegradation once the pulse count exceeded the critical pulse number,  $N_{\text{cr}}$ .



The photostability of sol-gel laser materials is just beginning to be explored. The R6G doped aluminosilicate xerogel laser material compares favorably to that of R6G in other matrices. A reduction of output pulse energy to 50% of its initial value occurs after about 1500 pulses at 1Hz, and a reduction to 10% would require more than 4000 pulses. These values are comparable to those of R6G in ORMOSILS which were reduced by a factor of 4 after 3000 pulses. Extrapolation of the decay curve (Fig. 4) indicates that the R6G doped ORMOSIL gel would have undergone a 90% reduction in emission intensity after approximately 5300 laser pulses. This represents a useful lifetime improvement by a factor of more than 15 with respect to results with MPMMA. In other sol-gel results, an R6G-doped alumina thin film required about 600 pump pulses to reduce the laser emission to 50% of its initial value.<sup>14</sup>

Coumarin 540A is substantially more stable in the ORMOSIL host than in the aluminosilicate xerogel. The double exponential decay plot (Figure 4) seems beneficial as the laser emission was reduced by a factor of 6 after absorption of more than 6000 pulses of 500 MW/cm<sup>3</sup>. This represents an apparent improvement for doped ORMOSIL gels of some 10 to 100 times as compared to coumarin doped PMMA described by Itoh et. al.<sup>20</sup> In contrast, the photostability of C-540A in the aluminosilicate matrix is considerably poorer than that of R6G. In this case, the 50% laser intensity level was reached within 300 pulses, although laser action was still detected after 1500 pulses.

The high photostability of the dye-doped ORMOSIL laser materials and the R6G/aluminosilicate system is probably due to the isolation of the active species. The main decomposition pathway in solution is through reaction of the solvent with the triplet state.<sup>27</sup> By isolating the molecules within the inert matrix, their active life is extended.<sup>3</sup> These isolated molecules would be, presumably, less likely to have their emission quenched because the concentration of deactivating species in their local environment is small. It is interesting to note that the R6G in either the ORMOSIL or the aluminosilicate xerogel exhibits similar photostability characteristics, while C-540A is substantially different in the two matrices. Isolation effects are likely to be highly specific to dye/matrix interactions. Finally, recent work in our laboratories indicates that the photostability of rhodamine B when pumped at 337 nm is greater than that of the reference alcoholic solution.<sup>28</sup>

The ability for R6G to sustain laser action for extended periods of time deserves additional consideration. It is probable that high concentrations ( $1 \times 10^{-3}$  M) are required to obtain laser action because only a small portion of the laser dye is completely surrounded by the oxide matrix. The condensation and polymerization mechanisms involved in the sol-gel process would allow most of the dye to remain in solution as the small alumina particles formed, leaving large amounts of the R6G adsorbed on the walls of the pores and channels in the crosslinking and drying gel. These non-encapsulated dye species may not have the enhanced photostability of the microencapsulated molecules, and emission from them could fade quickly while the encapsulated dyes would continue to be active. This explanation accounts for the rapid decay within the first several hundred pulses followed by the much slower decreases observed in the photostability curves shown in figure 3. The encapsulated molecules give the R6G aluminosilicate xerogel its lasting luminescent component which enables the laser to remain active after 40,000 pulses

## 6. ACKNOWLEDGEMENTS

The authors gratefully acknowledge the assistance of E. Knobbe, P. Fuqua, F. Nishida, J. McKiernan, S. Yamanaka, S. Parvanch, J.C. Pouxviel, E. Bescher and H. Dai in these studies. The research has been supported by the NSF (DMR 87-06010 for B.D. and J.I.Z.) and AFOSR (J.D.M.).

## 7. REFERENCES

1. J. D. Mackenzie and D. R. Ulrich, eds. Proc. Third Intern. Conf. on Ultrastructure Processing Wiley, New York, 1988.
2. C. J. Brinker, D. E. Clark and D. R. Ulrich, eds. Better Ceramics Through Chemistry II, MRS Symp. Vol 73, (1986) and Better Ceramics Through Chemistry III, MRS Symp. Vol 121 (1988) (Materials Research Society, Pittsburgh)
3. D. Avnir, D. Levy, R. Reisfeld, J. Phys. Chem. **88**, 5956 (1984) .
4. D. Avnir, R. Kaufman and R. Reisfeld, J.Non-Cryst.Solids, **74**, 395 (1985) .
5. V. Kaufman and D. Avnir Langmuir, **2**, 717 (1986).
6. R. Reisfeld, R. Zusman, and M.Eyal, Chem.Phys.Lett., **147**, 142, (1988) .
7. V. R. Kaufman, D. Avnir, D. Pines-Rojanski, D. J. Huppert, J. Non-Cryst. Solids **99**, 379, (1988) .
8. J. McKiernan, J.-C. Pouxviel, B. Dunn, J. I. Zink, J. Phys. Chem. **93**, 2129 (1989).
9. J.-C. Pouxviel, B. Dunn, J. I. Zink, J. Phys. Chem. **93**, 2134 (1989).
10. A. Makishima and T. Tani, J. Am. Ceram. Soc., **69**, 4 (1986)
11. E. J. Pope and J. D. Mackenzie, MRS Bull., **12**, 29 (1987)
12. D. Levy, S. Einhorn, D. Avnir, J. Non-Cryst. Solids, **113**, 137 (1989)
13. F. Nishida, B. Dunn, E. T. Knobbe, P. D. Fuqua, R. B. Kaner and B. R. Mattes, Better Ceramics Through Chemistry IV, MRS Symp. San Francisco, April 1990 (In Press)
14. Y. Kobayashi, Y. Kurokawa and Y. Imai, J. Non-Cryst. Solids, **105**, 198 (1988)
15. B. Dunn, E. Knobbe, J. McKiernan, J. C. Pouxviel and J. I. Zink, Proc. MRS Symp. **121**, 331 1988
16. E. T. Knobbe, B. Dunn, P. D. Fuqua and F. Nishida, Appl. Optics, (In Press)
17. F. Salin, G. LeSaux, P. Georges, A. Brun, C. Bagnall and J. Zarzycki, Opt. Letts., **14**, 785 (1989)
18. R. Reisfeld, D. Brusilovsky, M. Eyal, E. Miron, Z. Burstein, and J. Ivri, Chem. Phys. Letts., **160**, 43 (1989)
19. D. A. Gromov, et. al., J. Opt. Soc. Am. B, **2**, 1028 (1985)
20. U. Itoh, M. Takakusa, T. Moriya, and S. Saito, Jap. J. Appl. Phys., **16**, 1059 (1977)
21. R. M. O'Connel and T. T. Saito, Opt. Eng., **22**, 393 (1983).
22. C. A. Capozzi and L. D. Pye, Proc. SPIE, **970** (1988)
23. H. Schmidt and B. Seiferling, Proc.MRS Symp., **73**, 739 (1986)
24. E. Knobbe, B. Dunn, P. D. Fuqua, F. Nishida and J. I. Zink, Fourth Intern. Conf. on Ultrastructure Processing, ed. by D. R. Uhlmann et. al., (Wiley, New York) In Press.
25. J. M. Yarborough, Appl. Phys. Lett., **24**, 629 (1974).
26. J.-C. Pouxviel, J. P. Boilot, A. Lecomte, A. J. Dager, J. Phys. (Paris), **48**, 921 (1987).
27. M. Yamashita, H. Kashiwagi, IEEE J. Quantum Electron., **QE 12**, 90 (1976)
28. E. Bescher, H. Dai, J. D. Mackenzie and O. Stafsudd, unpublished results.

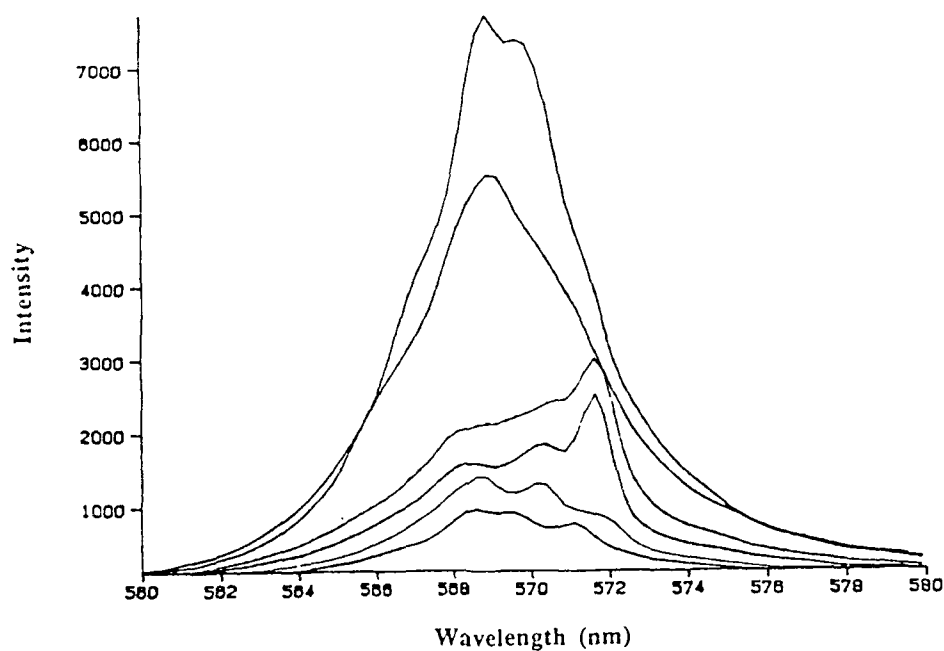


Figure 1. Spectrum of the free running laser of R6G ( $1 \times 10^{-3}$  M) in an aluminosilicate matrix as a function of the number of pump laser (540 nm) pulses. From top to bottom the spectra were obtained after 60, 900, 1950, 2700, 3600, and 4500 pulses.

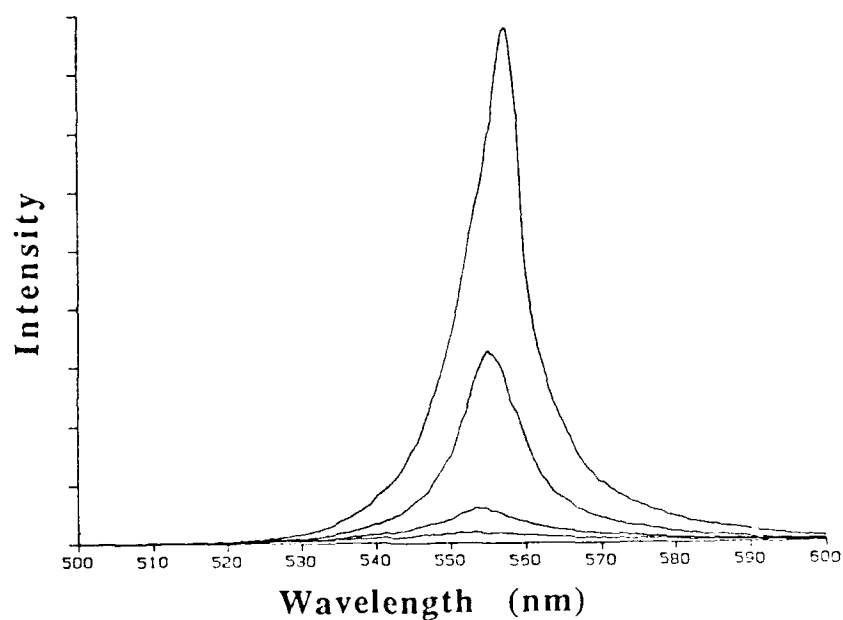


Figure 2. Spectrum of the laser output of coumarin 540A in an aluminosilicate xerogel pumped at 460 nm. In order of decreasing intensity, they were taken after 600, 900, 1200, and 1500 pump pulses.

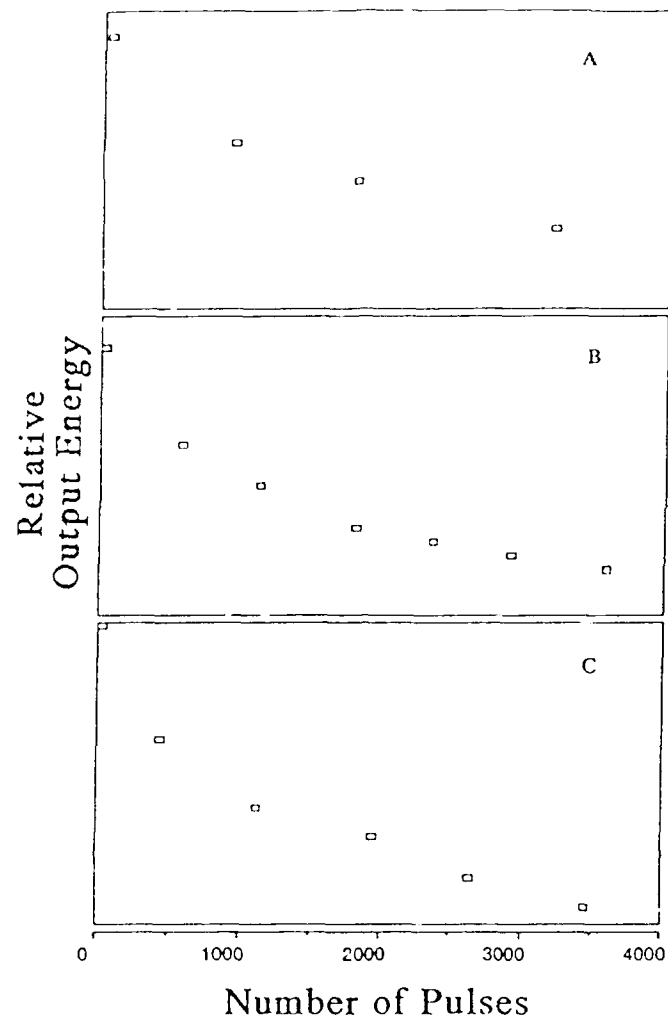


Figure 3. Dependence of the laser output intensity on the number of pump pulses at A) 1 Hz B) 10 Hz C) 25 Hz. The pump wavelength is 511 nm and the initial concentration of R6G is  $5 \times 10^{-4}$  M.

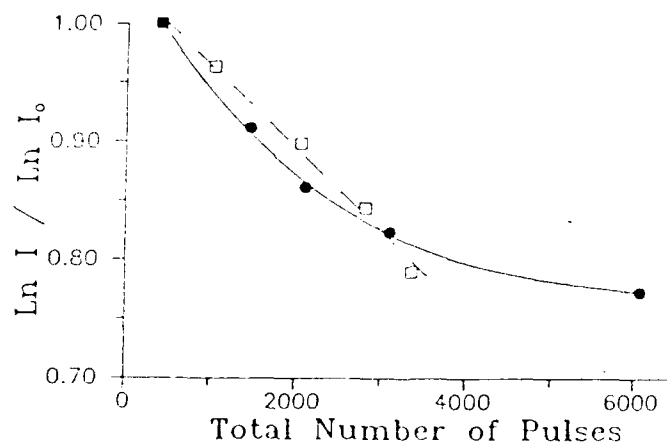


Figure 4. Photodegradation characteristics of C153:A (dots) and R6G:G (squares) ORMOSIL gels.



Sol-gel glass solid state lasers doped with organic molecules

C. Whitehurst, D.J. Shaw, and T.A. King

Physics Department, Schuster Laboratory

University of Manchester, Manchester. M13 9PL.

United Kingdom

### Abstract

When doped with organic dye laser molecules, porous sol-gel prepared silica constitutes a solid state dye laser medium. In this study such media have been shown to exhibit laser action using: (a) a krypton fluoride, 249nm, laser pump producing nano-second laser pulses and, (b) a coumarin 504 (507nm) pump producing microsecond laser pulses. The lasing thresholds were measured as  $140\text{kW/mm}^3$  and  $1.8\text{kW/mm}^3$  respectively, with lifetimes of 10-20 and 50-100 shots respectively.

### 2.Introduction

Organic molecule solutions provide a reasonably efficient and broadly tunable range of intense laser sources, (figure 1), with some limitation of convenience and flexibility in use because of their liquid medium. Many of the dyes in the visible region possess high quantum yields of fluorescence, absorption and emission. However, the full potential of the lasing dye media cannot be realised because the liquid host adversely affects many thermodynamic, spectroscopic and kinetic properties of the dye. These include non-radiative quenching of upper lasing levels, spectral shifts and thermal instability. The use of a solid matrix may be expected to enhance the lasing properties of organic dyes, reducing thermal restrictions, impurity quenching, dimerisation and the affects of photodegrading



impurities. The use of a solid dye matrix greatly increases the handling convenience by reducing laser complexity and removing the need for pumps, pipes and reservoirs. The method of doping sol-gels used here involves adsorbing dye molecules onto pore surfaces; this results in the production of a uniformly distributed (visually inspected by a scanned laser beam) dye dispersed within the sol-gel sample. Since this method involves doping after the sol-gel medium has been formed it can be referred to as "post-doping." The advantage of this method is that samples can be partially densified to intermediate but high temperatures thus increasing their physical strength and optical quality whilst retaining relatively large specific surface areas. Provision of solid state media for dyes has been accomplished elsewhere by incorporating dye molecules within the hydrolysis and condensation sequence of  $\text{Si}(\text{OCH}_3)_4$ <sup>1-5</sup>. The resulting gel is then dried for a few days at 60°C. The dye is thus uniformly embedded in the resulting silica matrix. The fluorescence properties of dye molecules in the sol-gel matrix have been described<sup>6</sup> where it was shown that the concentration of rhodamine 6G dimers within a sol-gel matrix was found to be negligible when compared with the concentration in solution. Laser action of such 'predoped' samples using different dyes has been reported on nanosecond timescales<sup>7-9</sup>.

### 3.Experimental

Recent advances in sol-gel processing<sup>1-5</sup> have made it possible to produce an optically transparent, amorphous and monolithic silica with formation temperatures around room temperature. Such sol-gel prepared silica samples<sup>4</sup> have a microporous structure on a nanometer scale and contain hundreds of square meters of surface per gram of silica. Heating to

1150 °C fully densifies the silica while heating to an intermediate temperature partially densifies the material. Monolithic sol-gel samples, supplied by Geltech Inc., in disc form, and densified to various temperatures were doped with rhodamine 6G by immersion in a solution of rhodamine 6G in methanol. After doping for 48 hours, samples were removed and left to dry in a temperature controlled environment at 2°C. This reduces the vapour pressure of the methanol solvent as it evaporates since it has been shown that vapour pressures in excess of 20 Torr can lead to catastrophic cracking of samples. Samples were left in this environment for one week or longer. Table 1 lists the various dopant concentrations and samples used. This method of doping sol-gels which essentially involves adsorbing dye molecules onto pure surfaces, results in the production of a uniformly distributed (to the eye) dye dispersed within the sol-gel sample.

SAMPLE NUMBER	DENSIFICATION TEMPERATURE/°C	DYE DOPANT CONCENTRATION/M
1	700	$10^{-4}$
2	400	$2 \times 10^{-4}$
3	850	$2 \times 10^{-4}$
4	500	$5 \times 10^{-4}$
5	850	$5 \times 10^{-4}$

TABLE 1: SAMPLE PREPARATION

#### 4. Laser studies

Optical pumping of rhodamine 6G molecules was provided for using two different laser pumps. Initially a krypton fluoride excimer laser was used, emitting a 7ns pulse at 249 nm with up to 200mJ of energy per pulse. Later work has used a coumarin 504 flashlamp pumped dye laser emitting light at 507nm in a pulse 3.7 $\mu$ s long and giving up to 1 J per shot. By using a cylindrical lens (as shown in figure 2) a 'strip' of doped sol-gel could be transversely pumped. A laser cavity was formed by placing a high reflecting mirror and a 80% output mirror coupler on either side of the excited region. A helium-neon laser was used to align the cavity. The sample could be rotated within the cavity and was mounted on an x-y stage so as to enable fresh areas of dye to be pumped. Spectral profiles were measured with an EG&G optical multichannel analyser (OMA) and temporally with an appropriate photodiode (or a transient digitiser for excimer laser work). Sample 1 was used with the KrF laser and the remaining samples were used with the coumarin 504 laser.

#### 5. Results

Figure 3 shows the temporal profiles of the lasing and fluorescence pulses of sample 1 under excitation by the KrF laser. The profiles of the KrF laser excitation pulse and laser emission from a cuvette of R6G in methanol are shown for comparison. The profiles clearly show laser action in sample 1 and the spectral line profiles is shown in figure 4. Each track of dye exhibited laser action 3 or 4 times before undergoing photodissociation under excitation from the 249nm UV excitation. The disc was then rotated to expose fresh dye. By increasing the energy of the pump beam until a lasing



pulse was observed the lasing threshold was measured as  $140\text{kW/mm}^3$ .

Samples 2-5 were pumped with the coumarin 504 laser, which emits lower energy photons and so is less likely to photodegrade dye molecules. Figures 5 and 6 are the spectral and temporal profiles of sample 5 clearly showing a broadband laser pulse centred on 577nm and a pulse length of  $1.8\mu\text{s}$ . Sample 5 gave up to 10 shots on each track before having to be rotated to expose fresh dye, whereas other samples only gave 2 or 3 shots. The lasing threshold was measured as  $1.8\text{ kW/mm}^3$ . The degree of dimerisation was assessed by measuring the absorbance curves of samples and comparing with a  $5 \times 10^{-5}\text{ M}$  R6G in methanol solution. The shoulder just below 500 nm in figure. 7a is a result of dimers in the solution and is absent in the absorbance profile of sample 5 as shown in figure 7b.

#### 6. Conclusion

Lasing action of rhodamine 6G doped sol-gel prepared silica, has been demonstrated on both a nanosecond and microsecond timescale. This report is the first on the longer time microsecond laser emission from sol-gel glass doped with an organic molecule. From the range of samples used we can say that higher temperature densified discs (up to  $850^\circ\text{C}$ ) are easier to dope without sample cracking and produce more stable and longer lasting lasing media, higher concentrations ( $5 \times 10^{-4}\text{M}$ ) dopant solution also produce longer lifetime discs. Low temperature ( $400^\circ\text{C}$ ) densified sol-gels are unsatisfactory because of their sensitivity to temperature and humidity fluctuations. Laser excitation with the coumarin 504 laser required a lower energy threshold than the krypton fluoride laser as the former excites electrons directly into the S1 upper lasing band. The krypton fluoride

laser excites electrons into the S2 band, some of which then relax into the S1 band, and hence is an inherently less efficient mechanism. The absorbance spectra show that dye molecules are essentially isolated within the sol-gel matrix and are immobile since attempts to leach out the dye molecules fail. The success of producing microsecond laser pulses indicates the feasibility of a flashlamp excited dye-doped sol-gel glass laser, utilising rod or waveguide slab geometries.

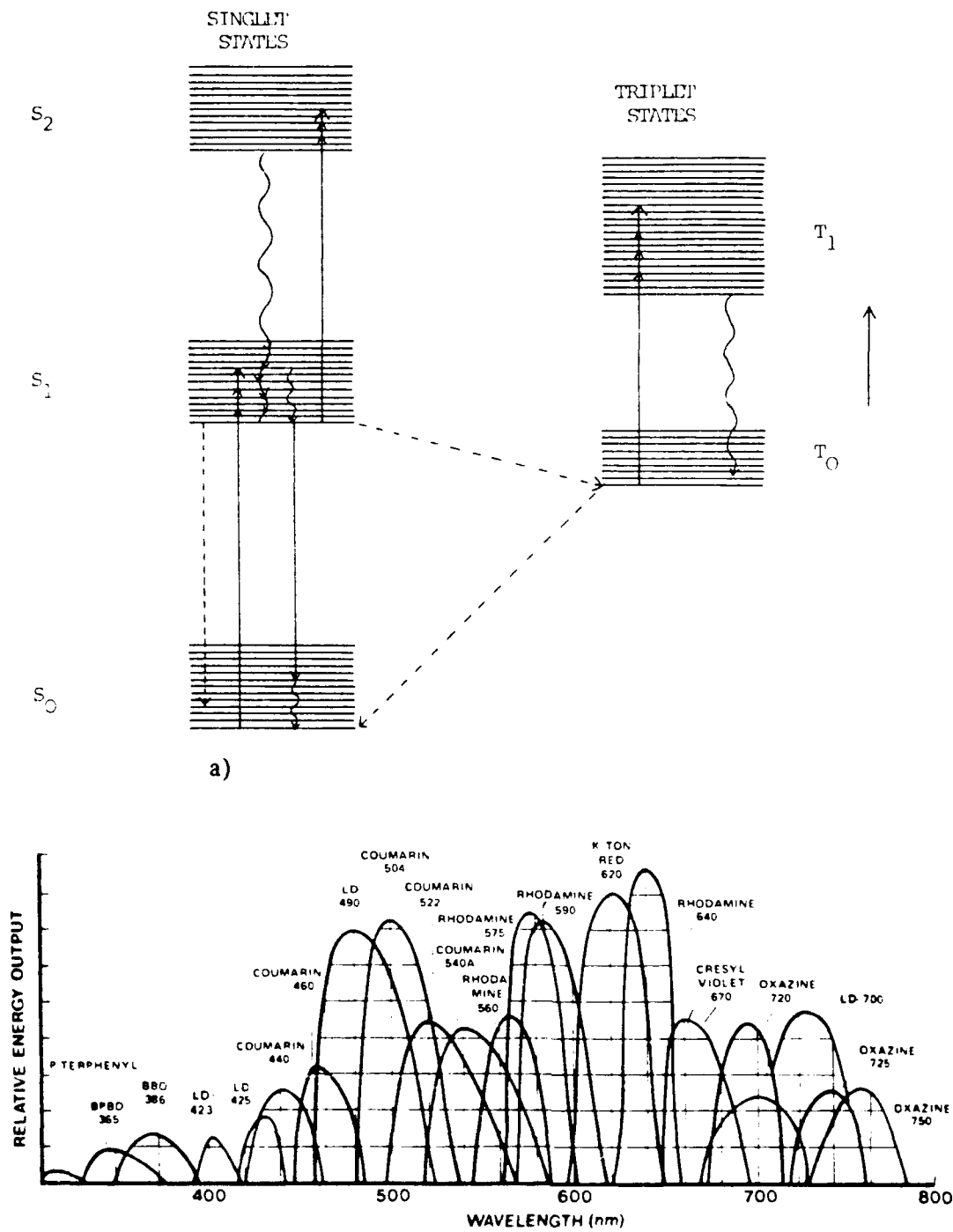
### 7. Acknowledgements

This forms part of a wider research programme in collaboration with the Advanced Materials Research Center, University of Florida and Geltech Inc. we have enjoyed extensive discussions with Professor Larry Hench and Dr. Jon West of the Advanced Materials Research Center, University of Florida.. This research has been sponsored by the Air Force Office of Scientific Research under contract number F49620-88-C-00. The United States government is authorised to reproduce and distribute reprints for governmental purposes notwithstanding any copyright notation hereon.

### 8. References

1. L. L. Hench and D. R. Ulrich (Eds) Ultrastructure processing of ceramics glasses and composites, Wiley (1984).
2. J. Brinker, D. E. Clark and D. R. Ulrich (Eds) Better ceramics through chemistry North Holland 1984.
3. G. Ortel and L.L. Hench, Journal of Non-Crystalline Solids, 79, 177, 1986.
4. L. L. Hench and J. K. West, "The Sol-Gel Process," Chem. Rev. 90 pp 33-72, 1990.

5. L. L. Hench and S. H. Wang, "The Sol-Gel Glass Transformation of Silica" Phase transitions, Gordon and Breach Science Publishers Inc., London 1990.
6. D. Avnir, D. Levy and R. Reisfeld, "The Nature of the Silica Cage as Reflected by Spectral Changes and Enhanced Photostability of Trapped Rhodamine 6G" *J. Phys.Chem* (88) pp5956-5959, 1984
7. F. Salin, G. Le Saux, P. Georges, A. Brun, C. Bagnall and J. Zarzycki, "Efficient tunable solid-state laser near 630nm using sulforhodamine 640-doped silica gel" *Optics Lett.* 14 pp 785-787, 1989.
8. R. Reisfeld, D. Brusilovsky, M. Eyal, E. Miron, Z. Burshtien and J. Ivri "Perylene dye in a composite sol-gel glass - a new solid state tunable laser in the visible region" *SPIE Vol 1182*, French Israeli workshop on solid state lasers, pp230-239, 1988.
9. R. Reisfeld, "Criteria and prospects of new lasers based on fluorescent dyes in glasses" *J de Physique Colloque C7*, Supplement No. 12, Tome 48, pp.C7 423-6, 1987.



b)

Figure 1

a) Dye molecule energy levels

b) Tuning range of commonly available dyes (source: Exciton Inc.)

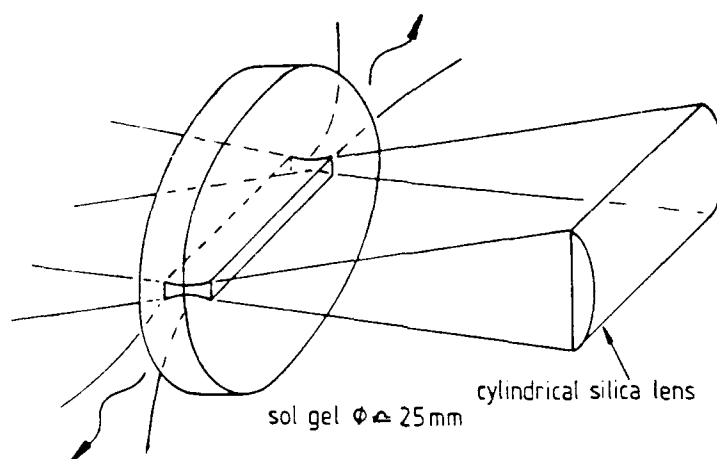


Figure 2: Pumping geometry, either 7ns 249nm KrF laser  
or 3.7 $\mu$ s coumarin 504 laser.

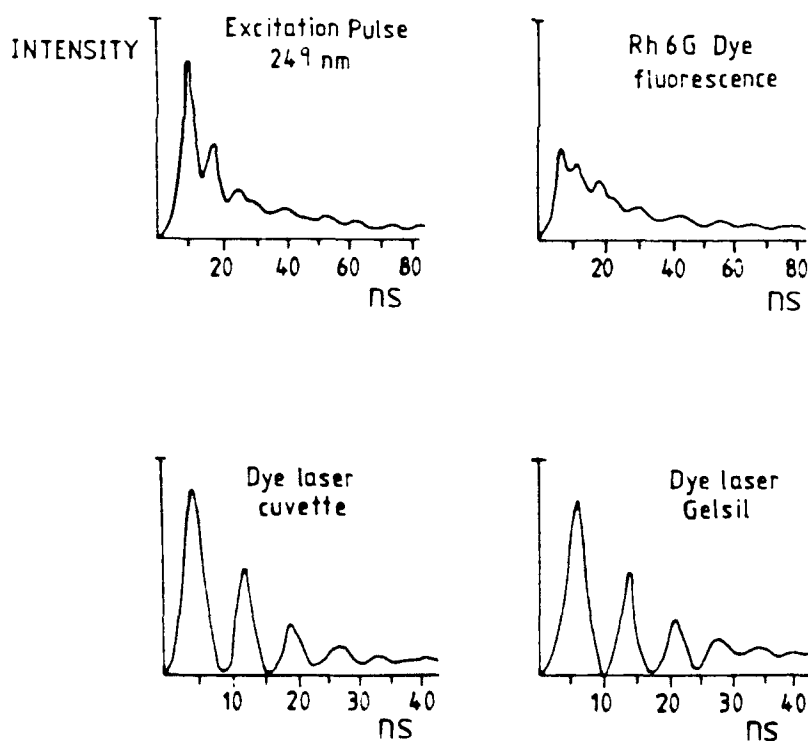


Figure 3: Temporal profiles of sample 1, R6G in methanol and krypton fluoride  
excimer laser excitation.

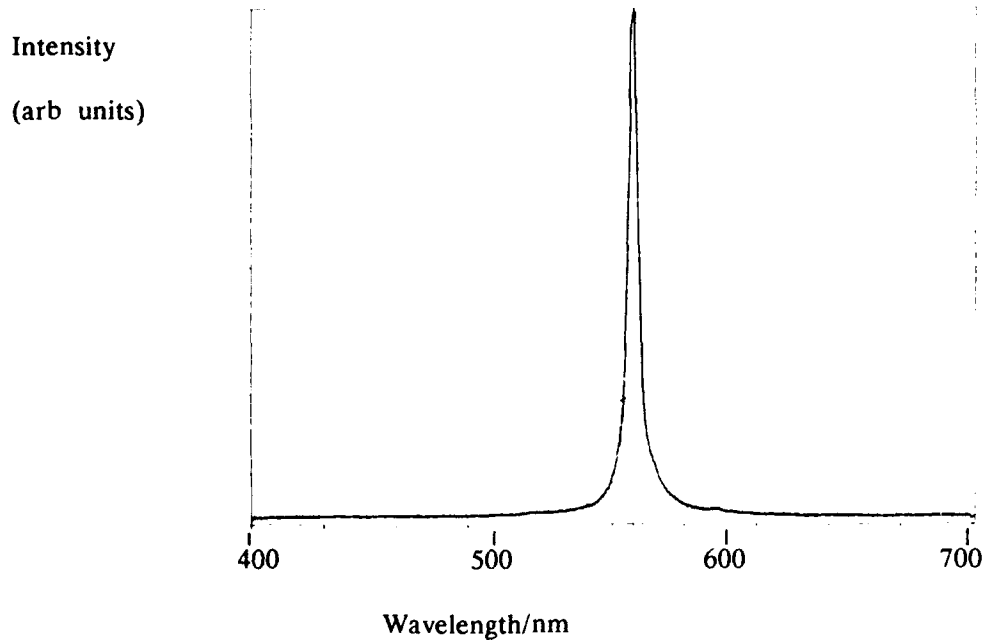


Figure 4: Spectral line profile of lasing pulse for sample 1.

KrF laser excitation; peak emission 560nm, fwhm 4nm.

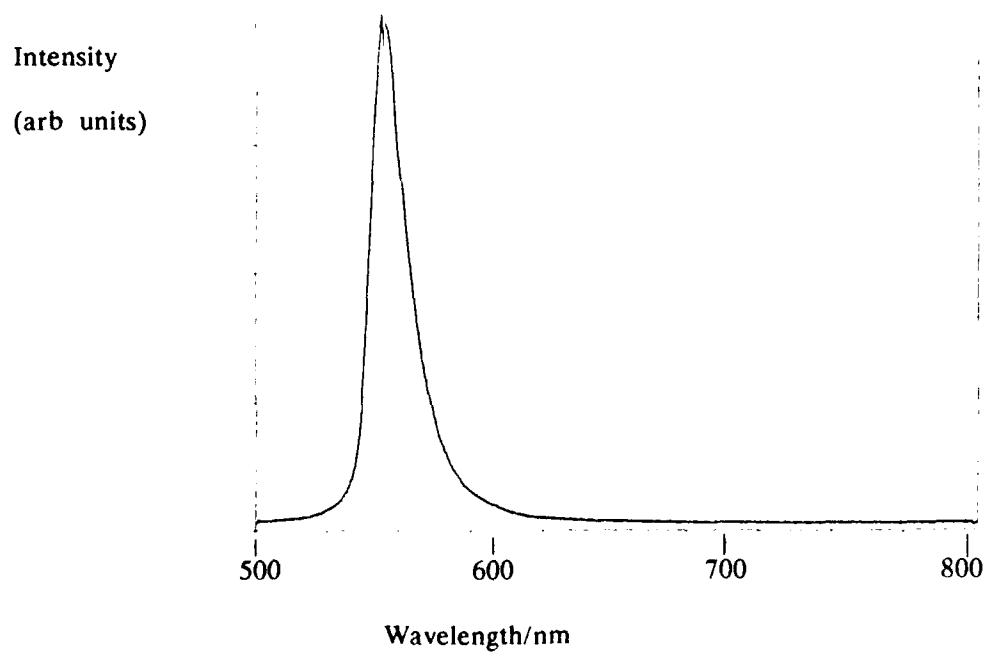


Figure 5: Spectral line profile of lasing pulse for sample 5.

coumarin 504 excitation; peak emission 577nm, fwhm 18nm.

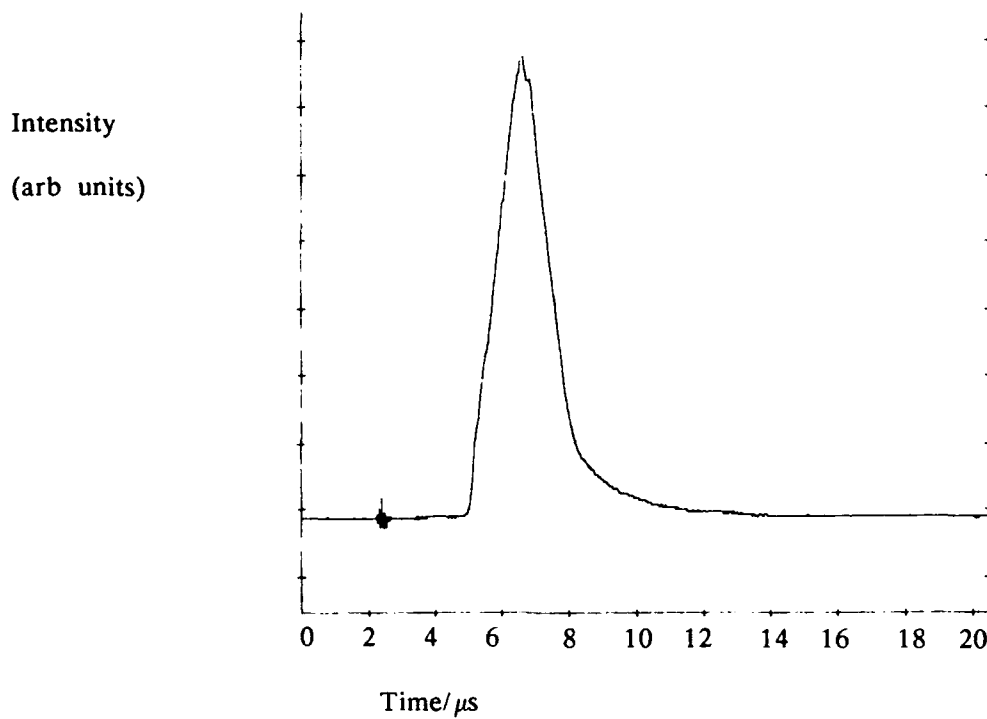


Figure 6: Temporal lasing pulse profile for sample 5  
coumarin 504 excitation, fwhm  $1.8\mu\text{s}$ .

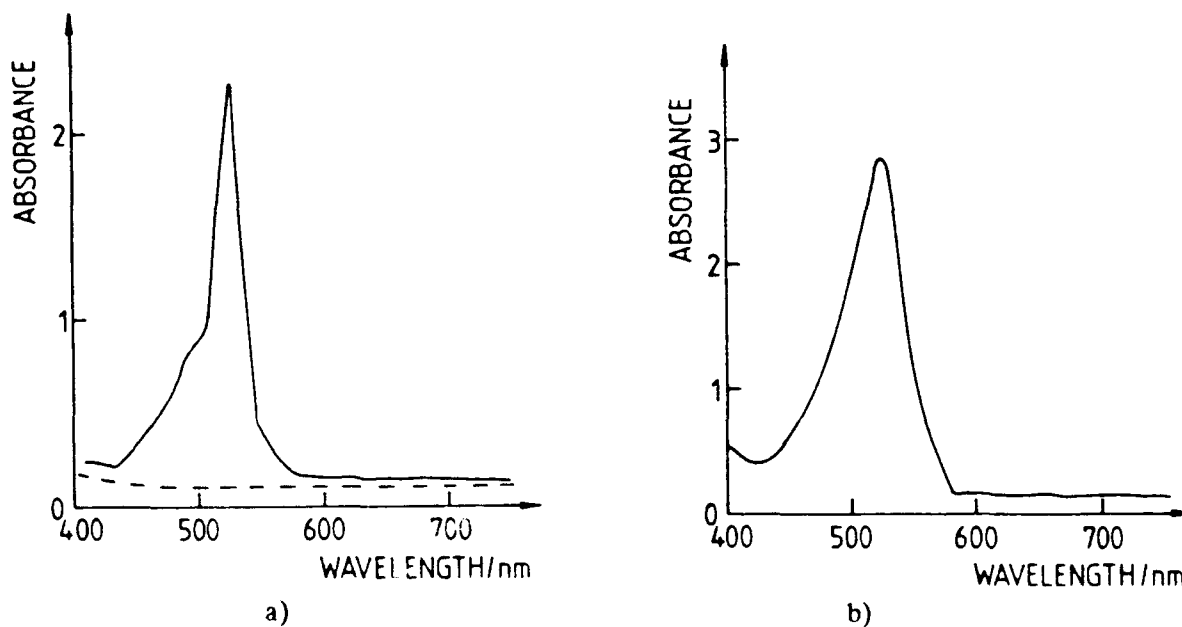


Figure 7: Absorbance curves; a) --- undoped sol-gel.  
—  $5 \times 10^{-5}$  molar rhodamine 6G in methanol  
b) sample 5



TRANSPARENT GEL AND XEROGEL OF THORIUM PHOSPHATE :  
OPTICAL SPECTROSCOPY WITH :  $\text{Nd}^{3+}$ ,  $\text{Er}^{3+}$ ,  $\text{Eu}^{3+}$ ,  $\text{Cr}^{3+}$  AND RHODAMINE 6G.

M. GENET, V. BRANDEL, M.P. LAHALLE, E. SIMONI

Institut de Physique Nucléaire, Groupe de Radiochimie, Université de Paris-Sud  
B.P. N° 1, 91406 Orsay Cedex (France)

### ABSTRACT

Chemical conditions for thorium phosphate gel preparation have been determined. The transparency is of good optical quality and the gel is very stable for a long time. Under drying condition, this gel can give rise to the xerogel which is still transparent. We can also prepare this xerogel by simple evaporation at room temperature of a very concentrated solution of thorium phosphate. From this viscous medium, the xerogel can be obtained in various kinds of shapes : threads, slabs and blocks. Solidification time depends on the final volume desired and spreads from few minutes to several weeks. Absorption spectrum of pure gel and xerogel have been recorded. Gel and xerogel doped with very well known probes like  $\text{Nd}^{3+}$  and  $\text{Er}^{3+}$  were examined to compare their optical properties with aqueous medium of the same chemical composition.  $\text{Eu}^{3+}$  doped gel and xerogel were also studied using their fluorescence properties.

The optical properties of  $\text{Cr}^{3+}$  in doped gel and xerogel allowed us to determine the kinetics of hydration sphere modification during the drying period. Finally, as xerogel synthesis takes place at room temperature, fragile organic dye can be used as dopant, so Rhodamine 6G absorption and emission spectra have been studied in these conditions. When, at that time, the xerogel is doped with Coumarin 460 and  $\text{Tb}^{3+}$ , an energy transfer is observed between dye and  $\text{Tb}^{3+}$  ions, which contributes to enhance the fluorescence of  $\text{Tb}^{3+}$  ions.  $\text{Eu}^{3+}$  behaves similarly.

In conclusion, gel and xerogel of thorium phosphate tested with usual probes such as 3d, 4f ions and dyes seem to be very promising matrices.

### 1. INTRODUCTION

Most of spectroscopic data related to doping ions have been obtained in matrices such as glasses, polycrystals and single crystals. Very few results were done in gels and xerogels, the main reason being opacity of these materials. Among a lot of thorium compounds, we found that phosphate gel and xerogel were transparent<sup>1</sup> and were very convenient matrices for spectroscopic studies in UV, visible and near infra-red regions. We specially investigated the pure material freshly prepared and we examined its evolution during thermal treatments. We studied dryness behaviour of thorium phosphate gel and xerogel by DTA, TGA, NMR and IR spectroscopy. We also used doped gels and xerogels with uranyl ions where luminescence of  $\text{UO}_2^{2+}$  was followed as samples were dried<sup>2</sup>. From these results, the best conditions of gel and xerogel preparations were determined and we were able to begin spectroscopy studies of doped materials.

### 2. SYNTHESIS OF THORIUM PHOSPHATE GEL AND XEROGEL

#### 2.1. Gel of thorium phosphate.

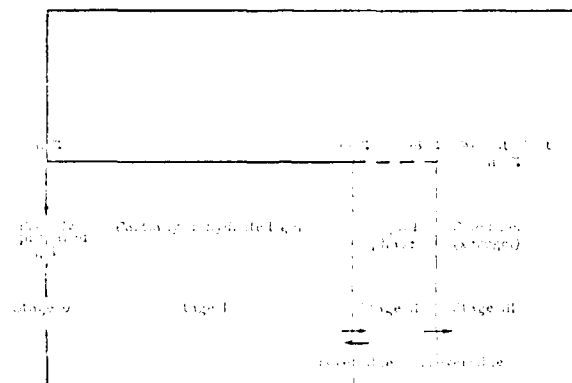
This gel can be obtained from any kind of soluble thorium salts, but we mostly used thorium chloride prepared in the laboratory<sup>3</sup>. When we mixed a 0.1 M  $\text{ThCl}_4$  aqueous solution at pH = 0.5 (adjusted with HCl) with a 0.1 M solution of orthophosphoric acid, transparent gel is formed in few minutes. Gelation time depends on concentration of both reactants, and on final pH of the solutions. It can reach several days for low concentration of thorium and phosphate ions in acid medium. The ratio  $r = \text{thorium/phosphate}$  expressed in molar concentrations were chosen equal to 3/4 or 1/1. The former value corresponds to the stoichiometry of thorium orthophosphate, the later was fixed arbitrarily. If the gel is not kept in a closed vessel, it spontaneously loses weight at room temperature. After few weeks, the weight loss is about 95 % and we observe a correlated decreasing of the volume of the order of 20. The gel phase disappears and is replaced by a liquid phase. This concentrated solution still keeps on evaporation and leads to a solid phase that we call xerogel. Different steps concerning dryness at room temperature are shown on the following scheme :

92 4 28 037

92-11419







The same process can be obtained faster at higher temperature to get thin films, but never over 50° C to preserve the transparency of the xerogel.

## 2.2. Xerogel of thorium phosphate.

The xerogel can be directly prepared from concentrated solution equivalent to the liquid phase previously observed in the gel dryness scheme. This solution is made by mixing  $\text{ThCl}_4$ , 8  $\text{H}_2\text{O}$  and  $\text{H}_3\text{PO}_4$  15 M in saturated conditions. We observe that gaseous  $\text{HCl}$  evolves from this viscous solution, and if we let evaporation go on, we finally obtain a transparent thorium phosphate xerogel in a solid state. From this hyperconcentrated and syrupy medium, various shapes of xerogels can be synthesized : threads, films, blocks. The solidification time is as long as the needed volume is important. For example, a cubic centimeter volume of xerogel is prepared in about one week and a film of few tenths of microns in few minutes.

To get doped gel and xerogel, doping ions are added either in thorium chloride solution or phosphoric acid before mixing. We mainly used chloride salt as dopant.

## 3. OPTICAL WINDOW TRANSPARENCY OF PURE MATERIALS.

### 3.1. Gel of thorium phosphate.

Gel is made of a mixing of diluted thorium chloride and phosphoric acid solutions, thus its absorption spectrum is in good agreement with the gel composition, that is to say : 98 % of water amount. So, the absorption in UV is due to water and chloride ions. The limit of transparency in infrared is comparable to that observed in pure water with a broad absorption peak at 970 nm.

### 3.2. Xerogel of thorium phosphate.

We have shown in Fig. 1 a typical absorption spectrum of a 2 mm sample thickness recorded with a Cary 17. Optical window of xerogel is wider than that of the gel according to the less amount of water. In the UV domain, absorption band of chloride ions around 262 nm is clearly seen, and the absorption front in the near infra-red is shifted up to 1350 nm if we consider that weak bands at 980 nm and 1180 nm are not enough intense to prevent spectroscopic studies in this domain. The presence of band absorption in this infra-red region is due to overtones and band combinations of vibration modes of the remaining water.

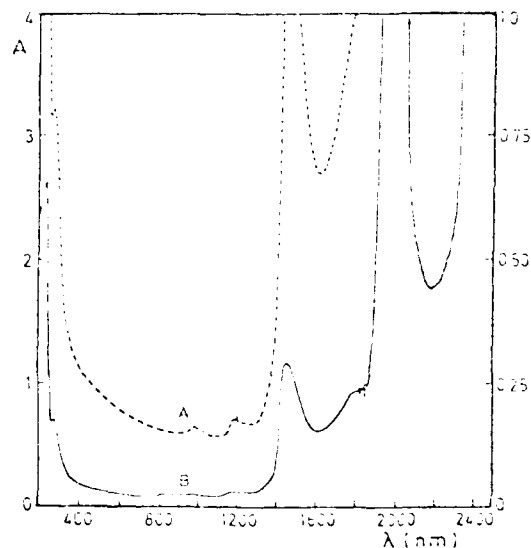


Fig. 1 - Absorption spectra of pure thorium phosphate xerogel (thickness 2 mm) :  
A - Absorbance scale from 0 to 1.  
B - Absorbance scale from 0 to 4.

The high level background, with an average absorbance of 0.2 in the visible part, could be readily improved with a well polished material.

By cooling down, the gel at 77 K transparency is lost and the gel becomes opaque, while the xerogel is still transparent at 4 K which allows to set up spectroscopy studies at low temperature.

#### 4. ABSORPTION SPECTRUM OF $\text{Nd}^{3+}$ AND $\text{Er}^{3+}$ .

$\text{Nd}^{3+}$  and  $\text{Er}^{3+}$  ions have been chosen taking into account that their absorption spectra are very well known and so, these ions can be used as local probes to test the host quality of the material. We specifically check rare earth behaviour through the  $^4\text{I}_{9/2} - ^2\text{G}_{7/2}$  transition of  $\text{Nd}^{3+}$  at 575 nm and for  $\text{Er}^{3+}$  through the pure transition  $^4\text{I}_{15/2} - ^4\text{G}_{11/2}$  located at 379 nm.

##### 4.1. Gels doped with $\text{Nd}^{3+}$ and $\text{Er}^{3+}$ .

We observed no differences between absorption spectra of  $\text{Nd}^{3+}$  and  $\text{Er}^{3+}$  in gel of thorium phosphate compared to those of the same ions in aqueous solutions of identical chemical composition, that means the same pH and the same  $\text{H}_3\text{PO}_4$  concentration. All measurements were performed with  $10^{-2}$  M for the rare earth concentration.

##### 4.2. Xerogels doped with $\text{Nd}^{3+}$ and $\text{Er}^{3+}$ .

Their absorption spectra are shown in Fig. 2 and 3. They look differently from those of corresponding gel and solution. For  $\text{Nd}^{3+}$  ions, the maximum of the absorption band is shifted towards low energy region and a fine structure composed of four peaks at least appears. The spectrum of  $\text{Er}^{3+}$  ions is still made of an unique line whose energy is increasing a little. The splitting of  $\text{Nd}^{3+}$  band and the energy shift for both ions are interpreted as local crystal fields in the xerogel, associated to a lowering of the symmetry around  $\text{Nd}^{3+}$  and  $\text{Er}^{3+}$  ions. Phosphate ions exist at high concentration in the xerogel and could be introduced by complexation through the hydration sphere of the lanthanide ions with a modification of the symmetry site.

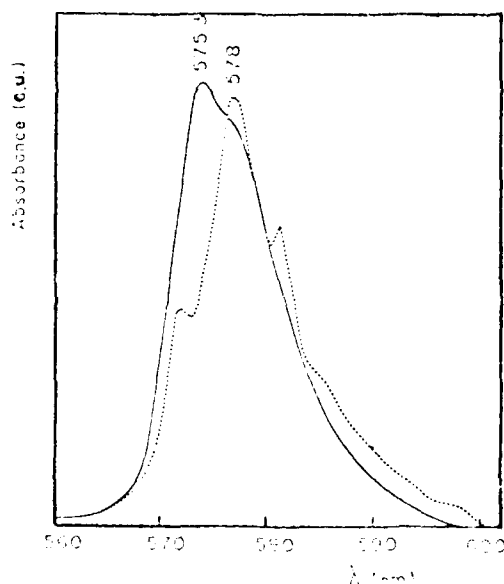


Fig. 2 - Absorption spectra of  $\text{Nd}^{3+}$  :  
— aqueous solution and "nitrate" gel,  
--- "nitrate" xerogel

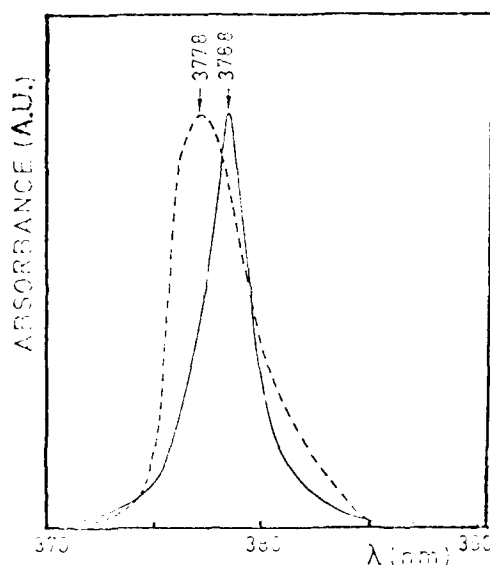


Fig. 3 - Absorption spectra of  $\text{Er}^{3+}$  in :  
— aqueous solution and "nitrate" gel,  
--- "nitrate" xerogel.

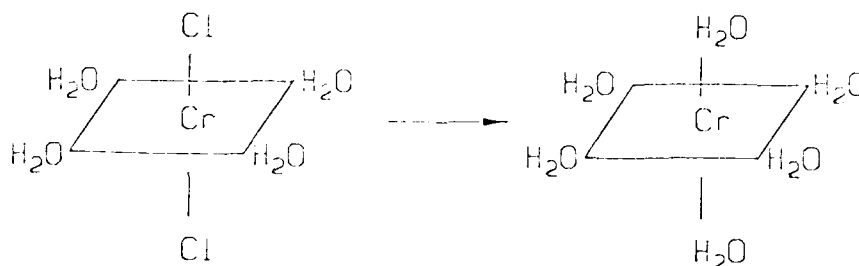
## 5. EMISSION SPECTRA OF $\text{Eu}^{3+}$ .

Gels and xerogel were doped with  $\text{Eu}^{3+}$ , emission and lifetime were measured. As these results will appear soon<sup>4</sup>, we just like to mention that a very weak emission has been obtained in gel with  $10^{-2}$  M europium ion concentration, but xerogel in the same conditions shows a fluorescence comparable with those observed in glasses and crystals.

## 6. DRYING KINETICS STUDY WITH $\text{Cr}^{3+}$ .

We previously noticed a "solid state" effect when compared absorption spectra of  $\text{Nd}^{3+}$  and  $\text{Er}^{3+}$  in gel and in xerogel. It is well known that 3d elements are much more sensitive to crystal fields than lanthanides. So we chose to study the modification of  $\text{Cr}^{3+}$  absorption spectrum (at  $10^{-2}$  M) during transformation of gel into xerogel under drying conditions. This spectrum is made of two very broad bands located around 440 and 630 nm. Furthermore, the behaviour of  $\text{Cr}^{3+}$  in aqueous solution and crystal compounds are quite understood and bring us a qualitative support to interpret what we observed in gel and xerogel.

All along this study, we used a chromium compound corresponding to the formula : Bis-chloro-tetraaquo chrome (III) chloride dihydrate, that is to say :  $[\text{Cr}(\text{H}_2\text{O})_4\text{Cl}_2] \text{Cl} \cdot 2 \text{H}_2\text{O}$ . Aqueous solution of this salt gives immediately, after dissolution, chemical species characteristic of the complex cation :  $[\text{Cr}(\text{H}_2\text{O})_4\text{Cl}_2]^+$ . This cation structure changes as the time goes by and, after 24 hours, we get an hexaaquo chrome (III) ion with an octahedral symmetry. Both ions are shown below :



This modification of hydration sphere of chromium ions is easily seen in Fig. 4. Maximum of the two main peaks varies with time and are shifted to the blue. As the structure of the ion changes, the symmetry and the crystal field change. For chromium, it is higher in hexaaquo ion than in the starting one, due to the fact that water molecules create a greater field than chloride ions.

The same experiments have been realized with thorium phosphate gel and concentrated solutions leading to xerogel by evaporation. Results are plotted in a diagram in Fig. 5. This figure shows the displacement in function of time of chromium absorption peaks for different kinds of studied systems. We estimate that equilibrium in the medium is reached when we are not able to evaluate a change in the wavelength determination. The time reported on the scheme corresponds to the time elapsed to get a constant value of the wavelength.

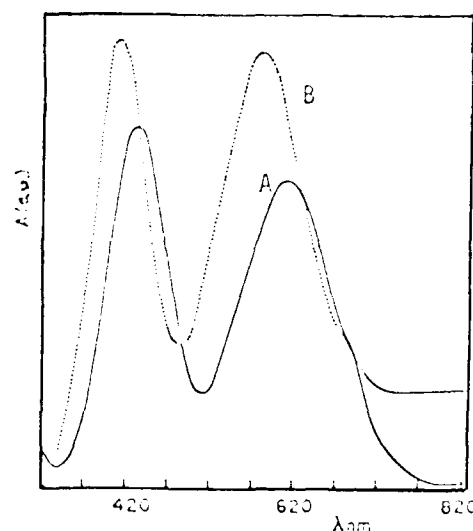


Fig. 4 - Absorption spectra of chromium (III) in aqueous solution :  
A - Just after dissolution of chromium salt,  
B - After 24 hours.

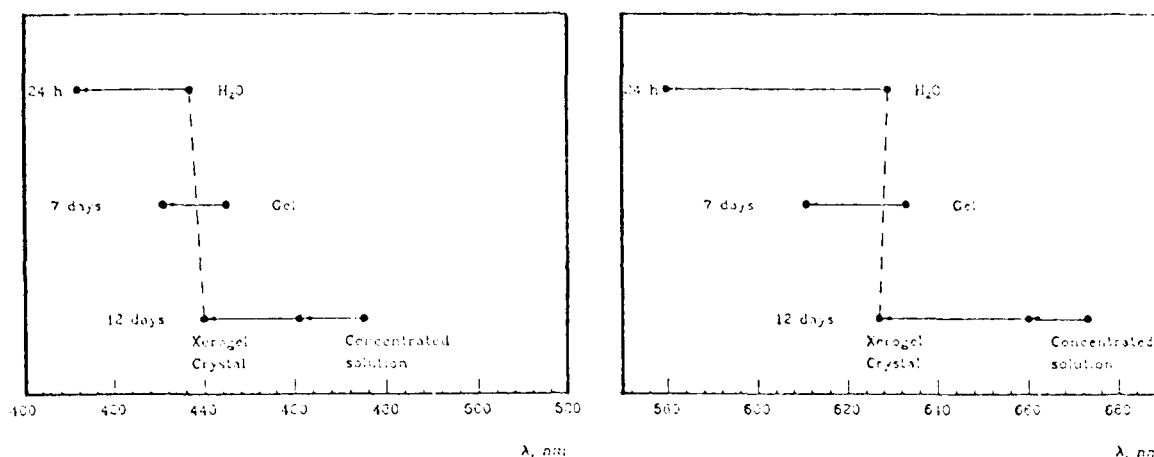


Fig. 5 - Summary scheme of variation with time of absorption maxima for chromium (III) in various conditions.

In gel and concentrated solution freshly prepared, absorption bands of chromium are moved to higher wavelengths. Both medium contain an important concentration of chloride ions which could contribute to decrease the crystal field value in the beginning. The effect is roughly proportional to the chloride ions concentration namely 0.5 M for gel and about 12 M for concentrated solution. Phosphate ion is not a good complexing agent for  $\text{Cr}^{3+}$ , nevertheless it may play a role in peak displacement which is difficult to analyze. After 7 days, chromium ion spectrum is stabilized in gel. It is partially rehydrated. Chloride ion has been exchanged with water molecule. The final state corresponds to a field with an intermediate value between 4 and 6  $\text{H}_2\text{O}$ .

For the concentrated solution, 12 days are necessary to get no change in wavelength values. At the beginning peaks are red shifted, effect is more important than in gel. Stabilization time is longer, certainly due to the low content of water (about 30 % by weight) and to the dynamics of the medium which is decreasing as the viscosity is increasing. Diffusion coefficients of ions are reduced with time and modification of hydration sphere of  $\text{Cr}^{3+}$  ions is less and less affected. At the end,  $\text{Cr}^{3+}$  in solid xerogel shows the same absorption spectrum as the first experiment in aqueous solution. The crystallized chromium salt used in these studies gives also an identical spectrum. So, in these conditions, we can estimate that chromium is present in xerogel as  $[\text{Cr}(\text{H}_2\text{O})_4\text{Cl}_2]^+$  ions.

Similar experiments done only qualitatively with  $\text{Co}^{2+}$  ions as dopant in xerogel, show a colour change in connection with humidity atmosphere. They slowly change from weak pink to dark blue as the amount of water in air is less abundant. This can be explained by a symmetry change of hydrated cobalt ions which is transformed from hexaaquo ion in an octahedral symmetry in a tetrahedral tetra aquo complex. This important effect is entirely reversible.

These modifications show us how much the time is long to get a stable gel and xerogel. Synthesis of these compounds needs few minutes or few days but after this preparation period equilibrium of the material takes place in few days for the gel and almost two weeks for the xerogel.

## 7. XEROGEL DOPED WITH RHODAMINE 6G .

We take profit of the fact that material is synthesized at room temperature to study how organic dye properties are modified in xerogel compared to aqueous solutions. We use this medium as reference instead of organic liquid phase like alcohol, acetone, etc... because of the chemical nature of the xerogel which is of inorganic type. Gels, doped with organic dye, are not yet studied.

We report in Fig. 6 absorption spectrum of Rhodamine 6G ( $10^{-4}$  M) in aqueous solution, concentrated thorium phosphate solution and xerogel. We notice a drastic change between pure water and the two mediums which contain an important concentration of hydroxonium ions. They surely react with Rhodamine 6G and so, the spectrum is shifted in the blue. It has been supposed that at  $10^{-4}$  M dimerisation of the dye is not enough important to explain the observed modification of the spectrum.

The excitation of Rhodamine 6G by a nitrogen laser at 337 nm leads to an emission spectrum characteristic of the dye, without any modification of the general feature usually observed. Nevertheless, a shift of about 27 nm in the red has been recorded between pure water and xerogel (Fig. 7).

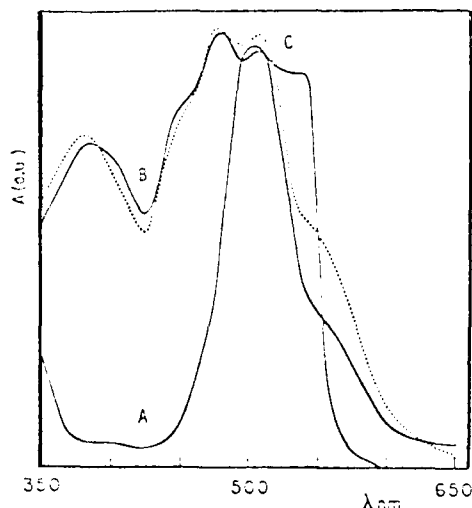


Fig. 6 - Absorption spectra of Rhodamine 6G ( $10^{-4}$ M) :  
A - Aqueous solution ; B - Concentrated thorium phosphate solution ; C - Xerogel.

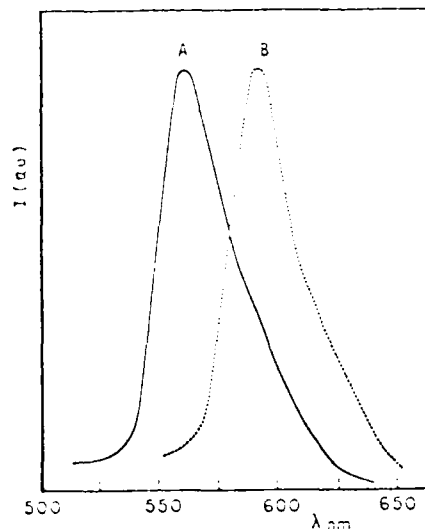


Fig. 7 - Emission spectra of Rhodamine 6G ( $10^{-4}$  M) :  
A - Aqueous solution,  
B - Xerogel.

The emission of Rhodamine 6G at 590 nm is identical in the xerogel and in organic liquid medium. We conclude that the interaction of the dye in its excited state with the xerogel and organic phase is of the same nature.

Photodegradation of the dye by means of an intense mercury lamp is quite comparable to that already observed in the same kind of material <sup>5</sup>.

#### 8. ENERGY TRANSFER IN XEROGEL BETWEEN COUMARIN 460 AND $Tb^{3+}$ .

We recently prepared xerogel doped with Coumarin 460. Excitation at 337 nm gives an emission of this dye over a broad band peaked at 390 nm instead of the "normal" one regularly seen at 460 nm as it is indicated by the reference number of this dye. Like for Rhodamine 6G, we suggest a matrix effect to explain such a change of the emission wavelength. Separately, xerogel has been doped with  $Tb^{3+}$  ions (1 % in mole, referred to thorium amount expressed in mole) and fluorescence has been excited at 337 nm. We observed a very weak emission at 544 nm on one of the more intense lines of  $Tb^{3+}$ , as shown in Fig. 8a.

A mixture of both Coumarin 460 and  $Tb^{3+}$  ions has been made in a same xerogel. Excitation by nitrogen laser gives rise to an intense fluorescence of terbium ions (Fig. 8b). For a constant value of terbium concentration (1 %), different concentrations of Coumarin 460 were tried (Fig. 9). It appeared that the efficiency of Coumarin 460 on  $Tb^{3+}$  measured at  $\lambda = 544$  nm is maximum for the dye amount of 0.1 % in the xerogel. We found that lifetime of  $Tb^{3+}$  ions is constant and equal to 0.30 ms, whatever the compound we excite namely, xerogel :  $Tb^{3+}$  or xerogel : Coumarin 460 +  $Tb^{3+}$ . In these conditions, we can expect that fluorescence takes place through an energy transfer mechanism and not via a direct excitation of a complex species between  $Tb^{3+}$  and Coumarin. Several checks are necessary to conclude.

In the same type of experiment,  $Eu^{3+}$  shows with Coumarin 460 the same behaviour. The dye greatly enhances the fluorescence of  $Eu^{3+}$ .

It seems, through literature, that this kind of pair : dye + lanthanide ion, was rarely investigated in an inorganic transparent solid.

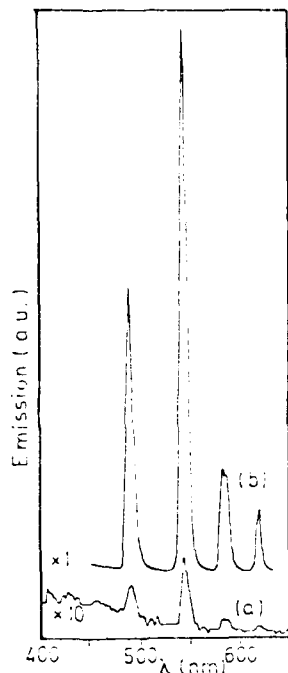


Fig. 8 - Emission spectra of  $Tb^{3+}$  ions (1 %) in :  
A - Xerogel,  
B - Xerogel doped with Coumarin 460.

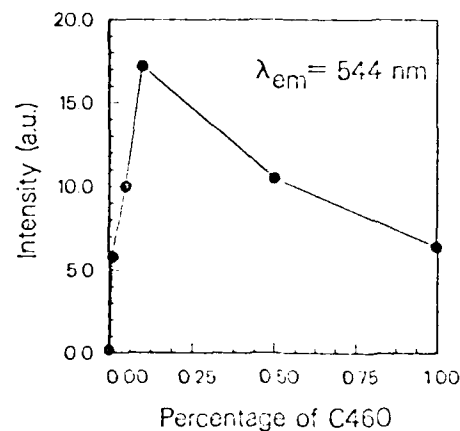


Fig. 9 - Variation of emission intensity of  $Tb^{3+}$  ions (1 %) in xerogel doped with various concentrations of Coumarin 460.

## 9. CONCLUSION.

Gels and xerogels of thorium phosphate have been tested in terms of their capability of being good matrices for optical spectroscopy studies. It appears that gels, from this point of view, do not bring any more advantages when they are compared to the corresponding aqueous solutions. On the other hand, xerogels, due to their broad optical window, allow us to use them up to 1350 nm in the near infra-red. Furthermore, they can be easily and homogeneously doped at room temperature, either with inorganic ions or organic compounds as well. For example, it has been shown with  $Cr^{3+}$  ions that the stabilisation of hydration sphere of these ions varies with the amount of water which is contained in gels and xerogels.

Xerogels, doped with Rhodamine 6G, exhibit the same emission band as in an organic liquid phase, while the absorption spectrum of the dye is slightly disturbed by acidity of the medium. Finally, we found that a xerogel simultaneously doped with Coumarin 460 and  $Tb^{3+}$  leads to a high increase of terbium fluorescence when the dye is excited by a nitrogen laser. To our knowledge, this is a very rare example of an energy transfer between a dye and a lanthanide ion in an inorganic and transparent solid.

## 10. REFERENCES.

1. M. Genet and V. Brandel, C.R. Acad. Sci. Paris, 307, II, 545, 1988.
2. V. Brandel, G. Iroulart, E. Simoni, M. Genet and J.P. Audi re, New. J. Chem. 14, 113, 1990.
3. M. Hussonnois, J.C. Krupa, M. Genet, L. Brillard and R. Carrier, J. Crystal Growth 51, 11, 1981.
4. V. Brandel, G. Iroulart, E. Simoni and M. Genet (submitted to New J. Chem.).
5. D. Avnir, D. Levy and R. Reisfeld, J. Phys. Chem. 88, 5956, 1984.



## NEW TECHNOLOGY OF OPTICAL COMPONENTS BASED ON LOCAL LASER THERMOCONSOLIDATION OF POROUS GLASSES AND COATS.

V.P.Veiko, E.B.Iakovlev, G.K.Kostjuk, V.A.Chuiko, P.A.Fomichov, V.S.Kozhukharov.\*  
Leningrad Institute of Precise Mechanics and Optics. Department of Laser Technology.  
USSR, 197101, Leningrad, Sablinskaja str.14.

\* Institute of Chemical Technology. Sofia; Bulgaria, Bul. "Kl. Okhridski" 8.

### ABSTRACT.

A new laser method is reported for manufacturing of microoptical components including high-aperture microlenses and microobjectives which can be used in fiber-optic communication links, in integrated optic devices, in the laser technique and technology, as well as in scanning optics. The physical model of the local laser thermoconsolidation process is described. The main types of the microoptical elements and their specific parameters are presented.

### 1. INTRODUCTION.

At present optical methods and, devices for information recording, storage, transmission and processing are being developed stormily. They include fiber-optic communication, cable television, laser digital, and analogue recording of information, and in the nearest future also optical-electronic and optical computers. To improve all this devices further dimension time and spectrum densitation of data communication channels, processing and storage of information are necessary. These problems can be successfully solved with the help of microoptical components.

This paper presents the consideration of authors proposed of laser technology of microoptical components and matrices which has the efficiency in several orders greater than traditional technology. Its main idea lies in local laser thermoconsolidation of porous optical media (glasses, ceramics, coats). New technology is based on two important principles:

1. To form microoptical component (MOC) it is possible to use process of spontaneous thermoconsolidation (sintering) of porous glass in viscosity - fluidity phase due to its tendency to the state with minimum surface energy. The process is initiated and guided by controlled local laser heating which provides a high quality of microoptical components.
2. Accuracy and reproduction of MOC are provided thanks to stabilization of the process by introducing of a strong feedback in temperature and the time of action and also in optical parameters of elements (refraction index and radius of the curvature).

### 2. SOURCE MATERIALS.

For MOC fabrication porous silicate glass (PG) has been chosen as a basic material, it is obtained on industrial scale by acid-alkaline treatment of samples made of sodium-borosilicate glass Na 7/23 (the composition range 80-90% SiO<sub>2</sub>, 2.5 - 20% B<sub>2</sub>O<sub>3</sub>, 0.5 - 5% N<sub>2</sub>O<sub>3</sub>), undergone a double thermal treatment (650°C, 24 hours and 530°C, 72 hours). Porous glass has been chosen as a basic of optical components due to the following reasons:

- 1) in the process of sintering its density changes and it leads to appreciable changes of refraction index;
- 2) by PG local sintering it is possible to change its form in the action zone due to shrinkage;

92-11420

92 4 28 038



3) sintered porous silicate glass possesses a good optical quality, approaching in its composition to pure  $\text{SiO}_2$ , and strong chemical structural bonds provide sufficient mechanical strength in spite of great internal stresses and developed surface (up to  $300 \text{ m}^2/\text{gr}$ );

4) changing parameters of thermal and chemical treatment it is possible to vary average sizes of pores, their dispersion and the whole volume, and also optical (refraction index, attenuation coefficient), thermophysical and other properties of transfer material.

### 3. PHYSICAL MECHANISM OF LAZER THERMOCONSOLIDATION.

Action of  $\text{CO}_2$ -laser radiation results in surface heating of glass, which leads to its softening, that is, to sharp decrease of silicate matrix viscosity. A viscous flowing of softened glass layers is caused by own internal stresses and surface tension. This flowing will continue until glass attains thermodynamically equilibrium state with minimum free surface forces (or until it is cooled). This state is reached at minimum porosity of volume and minimum surface area of glass-air separation to which its spherical form corresponds. (Fig.1).

Complete analysis of microoptical component formation process at local sintering is rather complicated. Thus let's evaluate only sintering time of surface layer in porous glass, when changes of glass thermophysical and optical properties, caused by its sintering, don't play any essential role.

It is assumed that sintering of surface layer occurs under conditions close to stationary ones, that is, while sintering the viscosity of glass quartz base doesn't change much. Let's consider work of

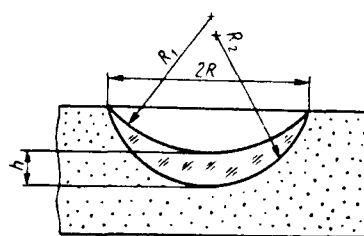


Fig. 1. Geometry of zone of action at laser local sintering of porous media.

surface forces  $W_\alpha = -\alpha d\Delta S/dt$  at pores jointing to be expended on overcoming of viscous flowing power of silicate base  $W_\eta = 2\eta(d\varepsilon/dt)^2 V$ , where  $\alpha$  - glass specific surface energy;  $\Delta S$  - surface changing at sintering process;  $\eta$  - viscosity of silicate base at sintering temperature;  $\varepsilon$  - relative deformation of the object;  $V$  - the volume of deformation area. To describe geometry of pores in subsurface glass layer a model of cylindrical pores is used. Then  $d\Delta S/dt$  will be proportional to changing the pore radius ( $r$ ) on the depth  $\Delta h$ ,  $d\Delta S/dt \sim 2\pi\Delta h dr/dt$ , and relative deformation  $\varepsilon \sim \pi r^2 n$ ,  $V \sim \Delta h$ ,  $n$  - pore concentration. Making  $W_\alpha$  equal to  $W_\eta$ , we get the time required for complete sintering of the pore radius  $r_0$  at the given glass porosity  $m$ :

$$t_c \sim 4mr_0\eta/3\alpha$$

One should take into consideration that while producing optical elements by laser local sintering of porous optical media thermomechanical stresses always appear and they can lead to the sample failure. The most dangerous is the border between sintered and unsintered areas where tensile stresses occur. Their amount depends on the volume of shrinkage area and increases with its rise, though viscous flowing of glass during the sintering process results in their partial relaxation. That's why maximum dimensions of optical components are limited by mechanical strength of porous sample.



#### 4. LASER SET FOR PRODUCING OPTICAL COMPONENTS.

Experimental set on laser local sintering of PG was built on the base of 100 W CO<sub>2</sub>-laser and provided:

- 1) control of important process parameters (light flow density  $q$ , the time of action  $\tau$ , the range of radiation zone  $R_0$ , as well as lateral distribution  $q(R)$ ;
- 2) the possibility of control of cross-section geometry of the action zone by laser beam redistribution;
- 3) visualization of the profile of the upper (on the border with air) and lower (on the border with the source glass) refracting surfaces due to the scanning of the action zone by He-Ne laser beam;
- 4) control of brightness temperature in the action zone.

#### 5. CHARACTERISTICS OF THE OPTICAL COMPONENTS.

Let's consider optical characteristics of microlenses which can be obtained on the basis of local sintering of porous glasses. The lens whose form is given on the Fig.1, at real refraction indexes of sintered and unsintered glasses can be only negative. To produce a positive lens it's necessary to remove a concave surface of shrinkage, that is, to make the lens flat-convex. Focal length  $F$  of such lens is known to be determined by the curvature radius of spherical surface  $R_2$  and the difference between refraction indexes  $\Delta n$  of the media separated by this surface:  $F = R_2 / \Delta n$ . The refraction index of sintered porous glass is 1.46, while of porous glass at the 0.63 mkm wavelength change, depending on its porosity, (according to authors readings) from 1.33 up to 1.22, that is,  $\Delta n$  amounts to 0.1-0.24. Numerical aperture of microlenses, obtained by the method of local laser sintering of porous glasses, may be determined as  $A \sim R_0 / F \sim \Delta n$  and for a number of glasses it will amount to 0.1-0.24. Dependence of MOC geometrical parameters on the action zone is given in Fig.2.

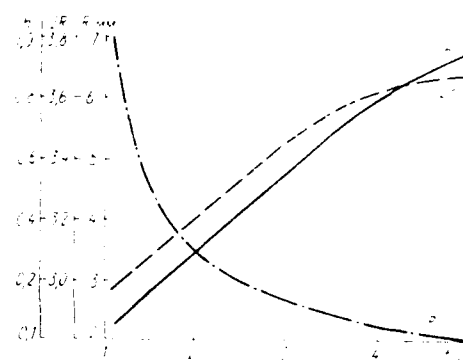


Fig. 2. Dependence of MOC geometrical parameters  $H(0)$ ,  $D_0(\Delta)$ ,  $R(0)$  on the duration of action

The improvement of microlenses characteristics (increase of aperture, decrease of focal spot diameter) requires the increase of  $\Delta n$ , that may be achieved by introducing oxides of metals in sintering zone by the method similar to impregnation.

#### 6. LASER FORMATION OF OPTICAL RASTERS IN SOL-GEL COAT.

Formation of long-focus optical rasters based on sol-gel coats is of interest. Physical nature of focusing element formation in porous coats seems to be nearly the same as in porous glasses. After covering sol from solution and its preliminary drying thus formed gel-like coats are subjected to laser action of CO<sub>2</sub>-laser profiled beam. Thermoconsolidation zone has refraction index of monolithic hard coat, its profile (curvature of the lens surface) being determined by the surface thickness, beam profile and action regime. For TiO<sub>2</sub> ( $n=2.5$ ) coat with the number of layers up to 15 at the each layer thickness 1000 Å it was possible to obtain long-focus ( $f=30$  mm) lens rasters, radiation correctors with the pupil of every element from 0.5 to 3 mm (at raster capacity up to 100 elements).

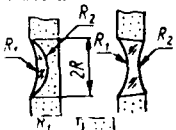


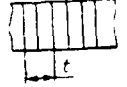

## 7. KINDS OF OPTICAL COMPONENTS.

Using the method of laser local sintering of porous optical media it is possible to obtain a great variety of optical microelements from double-concave diverging components up to rather light-powerful planar gradient positive elements and aspherical lenses. Mirror elements are obtained while depositing the reflecting films on surfaces formed during the sintering process.

While scanning or projecting a laser beam on a sample surface, it is possible to produce successively or simultaneously a passive integral optical scheme containing necessary quantity of homogeneous (raster, diffraction grating, wave guide) or non-homogeneous (distribution correctors elements).

Exposing to radiation successively two sides of a glass sample it is possible to obtain planar "telescopic" and double and even more complicated optical assemblies like objectives, oculars, condensers, etc. Types and parameters of some obtained microoptical components are given in Table 1.

Table 1. TYPES AND PARAMETERS OF MICROOPTICAL COMPONENTS.

Microelement	Form (construction)	Optical parameters, mm			
		2R	R1	R2	F
Negative microlenses (spherical, cylindrical)		0.3 5	0.3-20 4-12	0.2-1.5 2.5-10	2-25
Reflecting MOC		0.2 7	0.4-2 5-20	- -	0.2-10
Positive microlenses (spherical, cylindrical) <sup>1</sup>		0.1 4	- -	0.1-0.5 3-10	2-5 10-30
Components with distributed refraction index <sup>2</sup>		-	-	-	-
Beam-strength microdiaphragms		0.02-3	-	-	-

<sup>1</sup> Numerical aperture up to 0.24

<sup>2</sup> Step 0.15 - 2 mm

One can easily imagine devices which may be constructed on the basis of these components by means of their joining, gluing together, etc. They include functional sets of microoptical components (for fiber-optical communication lines - connectors, disconnectors, couplers, multiplexers, demultiplexers, etc.; imaging elements and their rasters; amplitude and phase distribution correctors; Fresnel elements; soft diaphragm; matching optical filters, etc.

Proposed method gives the opportunity to obtain microoptical components with optical and mechanical strength and has considerable advantages over conventional methods:

- 1) high efficiency;
- 2) possibility of minimization of microoptical elements sizes up to 10 mkm and increasing the density of their package up to  $10^{-6} \text{ cm}^{-2}$ ;
- 3) possibility of obtaining aspherical elements.

#### 8. REFERENCES.

1. V.P.Veiko, G.N.Dulnev, G.K.Kostjuk, I.K.Meshkovsky, V.A.Chuiko, E.B.Jakovlev. Sov. Patent N1108283, Bullet. of patents N30, 1984.
2. O.S.Molchanova. Sodium-borosilicate and porous glasses. Leningrad, Oborongis, 1961.
3. J.E.Gegusin. Physics of sintering. Moscow, Nauka. 1967.

SOL-GEL OPTICS

Volume 1328

**SESSION 4**

**Composites and Lasers II**

*Chair*

**Leonard H. Caveny**

Innovative Science and Technology/SDIO



**Interaction between host matrices and fluorescent species trapped  
in metal alkoxides derived gels.**

C. Guizard, J.C. Achddou, A. Larbot, L. Cot

Laboratoire de Physicochimie des matériaux CNRS UA 1312  
ENSC, 8, rue de l'Ecole normale 34053 Montpellier (France)

G. Le Flem, C. Parent

Laboratoire de Chimie du Solide CNRS LP 8861  
Université de Bordeaux I, 351, cours de la Liberation 33405 Talence (France)

C. Lurin

KODAK PATHE Centre de Recherches et de Technologie  
Zone Industrielle 71102 Chalon sur Saône (France)

**ABSTRACT**

The sol-gel method has been identified as a very promising direction to prepare host matrices for trapping photoactive species. A wide variety of such activator are sensitive to environmental parameters and have been used both for sol-gel processing investigation and photoactive materials preparation. Depending on the organic or inorganic nature of the fluorescence probe, different fluorescence effects have to be expected in metal oxide matrix derived from a sol-gel process. Special attention has been given to the interaction between three fluorescent species ( $\text{Eu}^{3+}$ ,  $\text{Nd}^{3+}$ , pyrene) and three inorganic matrices (silica, titania, zirconia). Fluorescence phenomena have been investigated related to the nature of the probe and its incorporation mode into the host matrix.

**1. INTRODUCTION**

Potential applications for doped amorphous materials exhibiting luminescence and lasing properties have been already discussed in the literature.<sup>1,2,3,4</sup> Two important fields for future needs have been identified : renewable energy sources and communications. Focusing on the sol-gel process, various organic and inorganic dyes were embedded in gel matrices aiming at applications in solid state dye laser and optical sensing technologies. Compared to organic matrices, inorganic ones offer a more rigid structure which prevents undesirable dye aggregation and lowering of photochemically efficiency. The purpose of this work is to give an insight of interactions between host matrices and fluorescence species trapped in metal alk oxides derived gels prepared in reversed micelles microemulsion.

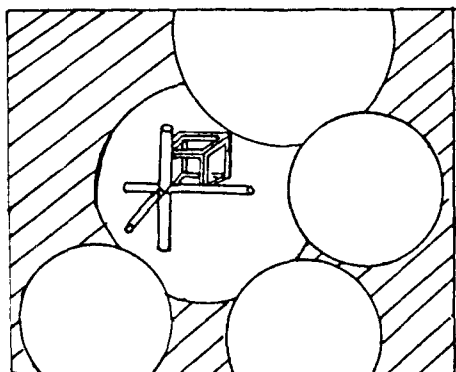
This new versatile method to prepare monolithic metal-organic derived gels using titanium, zirconium or aluminum alkoxides has already been presented<sup>5</sup> and is used for this work. The sol-gel transition is achieved in a reversed micelle microemulsion. The little amount of water solubilized inside the micelles provides a controlled alkoxide hydrolysis. By this way, the hydrolysis kinetics of this family of highly reactive alkoxides can be monitored and monolithic transparent gels of titania, zirconia as well as silica have been obtained

**92 4 28 039**

**92-11421**



Many techniques have been performed to investigate the structure of this kind of gel : gaz phase chromatography,<sup>6</sup> thermoporometry,<sup>7</sup> small angle X-ray and neutron scattering.<sup>8</sup> The resultant structural model exhibits three porosity levels as illustrated in Fig. 1 :



- crossbars of inorganic matters form a local microporous structure.

- the crossbars network inside the particles, that corresponds to the mesostructure, contains the mesoporosity; this level has a fractal structure.<sup>8</sup>

- the juxtaposition of particles of different sizes builds up the macrostructure and determines the macroporosity.

Fig. 1 : Illustration of the structural model of a Titania gel realized with a reversed micelles microemulsion.

Main advantages of this sol-gel process are the ability to govern the kinetics by only three parameters and the possibility to elaborate for each alkoxide a gel with very little size monodisperse particles and thus with very good optical transparency. Moreover, desordered fractal systems are presented presently an intensive activity. In this context it was interesting to study this kind of gel by a probe method to know whether it corroborates or not the previous model.

The gels obtained by hydrolysis / condensation reaction of tetramethyl orthosilicate (TMSO) have been widely studied by virtually all modern analytical techniques.<sup>6,7</sup> Since a few years, photoprobes have been used for investigating the sol-gel process. Photochemistry and photophysics offer today a wide variety of probes which are highly sensitive to environmental parameters such as polarity, viscosity, porosity and local geometry. For example, pyrene is used as a probe for the evolution of pore network,<sup>9,10,11</sup> the hydroxy trisulfonated pyrene molecule has been used to detect pH variations,<sup>12</sup> the spiroopyrans molecules,<sup>13</sup> rhodamine 6G<sup>14,15</sup> and rhodamine B<sup>15,16,17</sup> can probe the silica cage polarity and the ability to isolate molecules.  $\text{Eu}^{3+}$  is a local symmetry probe<sup>18</sup> but many others rare earths, as  $\text{Nd}^{3+}$  and  $\text{Tb}^{3+}$ ,<sup>19</sup> are conceivable to investigate a sol-gel system. In this paper, we will focus our attention on the results concerning  $\text{Eu}^{3+}$ ,  $\text{Nd}^{3+}$  and pyrene.

In desordered systems,  $\text{Eu}^{3+}$  is generally situated in low symmetry sites. Its emission spectrum is composed of the the electric-dipole transitions  $^5\text{D}_0 \rightarrow ^7\text{F}_{0,2,4,6}$  and of the the magnetic-dipole transition  $^5\text{D}_0 \rightarrow ^7\text{F}_1$ . As the electric-dipole transitions are forbidden in a centrosymmetric site, their intensities are dependent on the surrounding medium symmetry. On the contrary, the magnetic-dipole transition is insensitive to the surrounding of the ion and may therefore be used as a reference for comparison with other transition strenghts. Thus a large R ratio of the fluorescence intensities for the  $^5\text{D}_0 \rightarrow ^7\text{F}_2$  and  $^5\text{D}_0 \rightarrow ^7\text{F}_1$  transitions ( $R = ^5\text{D}_0 \rightarrow ^7\text{F}_2 / ^5\text{D}_0 \rightarrow ^7\text{F}_1$ ) implies a low symmetry field for the  $\text{Eu}^{3+}$  site.<sup>20, 21</sup>

Concerning  $\text{Nd}^{3+}$ , its environment can be described by the three Judd-Ofelt intensity parameters, calculated from the absorption spectra. This parameters,  $\Omega_2$ ,  $\Omega_4$  and  $\Omega_6$ , have been largely studied in various materials.<sup>19</sup> More accurately  $\Omega_2$  is strongly enhanced by covalent bonding and  $\Omega_6$  increases when the rigidity of the cage decreases.  $\text{Eu}^{3+}$

and  $\text{Nd}^{3+}$  have the same chemical nature and a similar affinity with the different alkoxides. Thus, the  $\text{Nd}^{3+}$  insertion have been performed to corroborate the results obtained with  $\text{Eu}^{3+}$ .

Pyrene shows many interesting photophysical properties that have contributed to the wide use of this molecule as a probe for heterogeneous systems. It tends to form excimers by an intramolecular complexation process between an excited  $\text{Py}^*$  and a ground state  $\text{Py}$ .

Its characteristic fluorescence spectrum (Fig. 2.1) is composed of a blue emission (between 360 and 430 nm) due to the monomer form and of a green one (between 460 and 530 nm) due to the excimer form. It is one of the few condensed aromatic hydrocarbons which shows significant fine structure due to vibronic bands in its monomer fluorescence spectrum. The solvent dependency of vibronic bands intensities in pyrene monomers fluorescence was first investigated by Nakajima<sup>22</sup> and by Kalyanasundaram.<sup>23</sup>

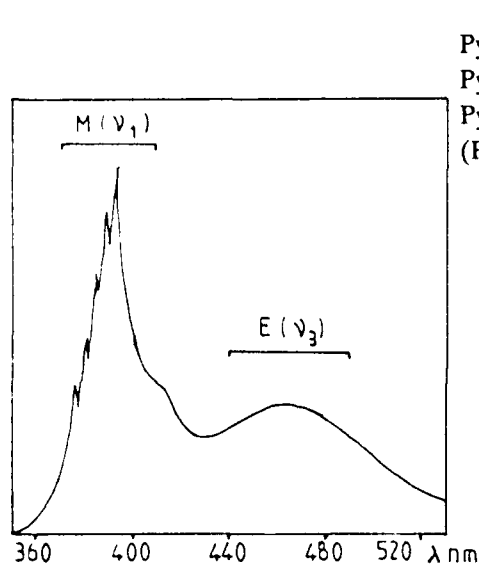


Fig 2.1 : Characteristic fluorescence of a decane solution doped with pyrene.

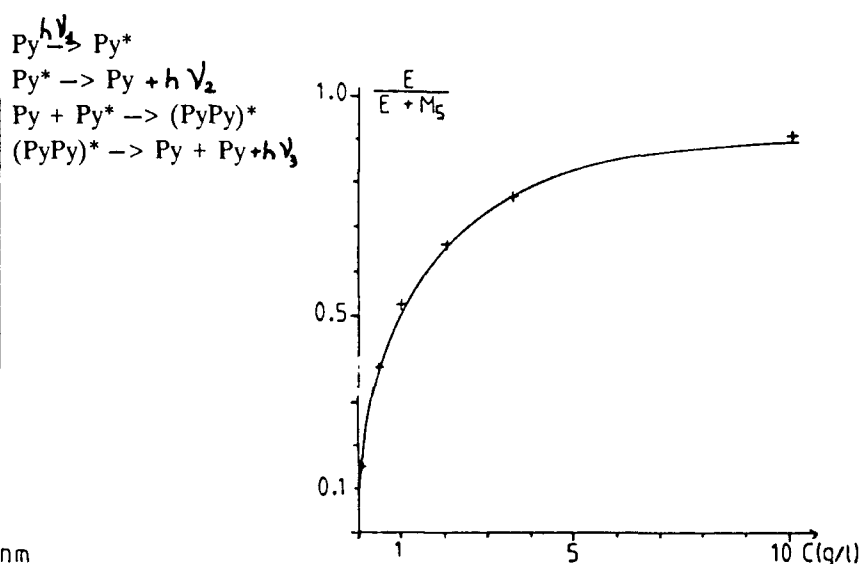


Fig 2.2 : Evolution of the excimer proportion in a decane solution versus concentration.

For the sake of convenience in the following discussions, the five predominant peaks of the monomers emission are listed as  $M_1$  to  $M_5$ . For the excimers emission, we will consider the maximum intensity level,  $E$ . It is well known, now, that the intensity ratio of peaks  $M_3/M_1$  serves as a measure of the solvent polarity.<sup>23</sup> It increases from 0.63 in the case of  $\text{Py}$  solubilized in water to 1.65-1.80 in hydrocarbon solvents. To evaluate the excimer formation, we will use the intensity ratio  $E/E + M_5$  which increases with the concentration (Fig. 2.2).

## 2. EXPERIMENTAL

The solutions are prepared from the following alkoxides : titanium isopropoxide, zirconium n-propoxide and Silicon methoxide. The reversed micelle microemulsions are realized by mixing the suitable quantities of water, decane and a oil soluble surfactant. We used the alkylaryl polyether alcohols triton X35 and X45 (Rhoom and Hass) as surfactant; they have respectively 3 and 4 average oxide units in the ether side chain. The sol-gel process begins after the

addition of the micellar solution on to the alkoxides. Different gelation times can be chosen according to  $n$  and  $h$ , respectively the water/surfactant molar ratio and the water/alkoxide molar ratio. If we want to elaborate a transparent gel with high optical properties, it is necessary to choose the gel formation parameters in order to reach the gel state slowly. All chemicals details concerning the preparation of these gels are given in Ref. 5.

The rare earths ions were incorporated under their chloride hexahydrate forms in proportion varying from 1 to 2% compared to the alkoxide. pyrene was purchased from Kodak and was recrystallized from ethanol before use. The probe can be incorporated using four different ways :

1- probes are dissolved in pure alkoxides which are then reacted with micellar solution.

2- probes are dissolved in the micellar solution before the addition on to the alkoxide solution.

3- probes are added into the sol before gelation.

4- probes are adsorbed on a dry washed gel prepared by soaking the adged gel in solvent like decane or hexane to remove the surfactant.

Gels were studied in tightly sealed tubes excepted for the fourth way.  $\text{Eu}^{3+}$  and pyrene were respectively recorded under a 393 nm and 350 nm excitation wavelength on a home-built apparatus and corrected with respect to the spectral responses of the monochromator and photomultiplier. The fluorescence spectra were carried out at 300 K because they exhibited same resolution at the liquid nitrogen temperature. Absorption spectra recorded on a Cary 17 (Varian) spectrophotometer and on a UV-Visible 3100 Shimadzu spectrophotometer were used for absorption measurement. The Judd-Ofelt parameters calculated from the two recordings systems were similar ( $\pm 5\%$ ). All the values listed below have been calculated from the Cary 17 recordings.

### 3. RESULTS

#### 3.1. Inorganic probes

##### 3.1.1. In the pure alkoxides (Fig. 3)

The ratio  $R$  has been calculated by planimetry. It is about 7.2 for the titanium alkoxide and changes to 4.33 for the zirconium alkoxide. These values can be compared to  $R=1$  measured in the case of an aqueous solution and show that  $\text{Eu}^{3+}$  is in a very dissymmetrical site. That ties up with the fact that the alkoxides can be coordinated in molecular aggregates (from 2 to 6) by the intermediate of hydrogen bindings. This aggregation can prevent a symmetrical arrangement around the probe.

##### 3.1.2. In the micellar solutions (Fig. 4)

$\text{Eu}^{3+}$  chloride hexahydrate is a strongly hydrophilic probe and its solubility in organic solvents is very low. In the presence of reversed micelles, it is preferentially solubilized in the internal hydrophilic regions.

The ratio  $R$  varies from 0.9 to 1.2. This kind of spectrum is typical of the  $\text{Eu}^{3+}$  emission dissolved in water or alcohol. In this case, the probe has a well definite site : inside the reversed micelle and surrounded by the water molecules and by the OH groups of the surfactant. Various conflictig models have been suggested.<sup>24,25,26</sup> Considering the  $\text{Eu}^{3+}$  fluorescence spectra, the micelle structure seems to strongly depend on the surfactant nature (Fig. 4). Both



reversed micellar solutions studied have been prepared using the same components ratio. The only difference is the surfactant hydrophilic head groups nature. Our results can not confirm one of the proposed structure. In fact they only give evidence that the reversed micellar aggregates are centrosymmetrical, especially in the case of the X35 surfactant, characterized by a smaller hydrophilic head.

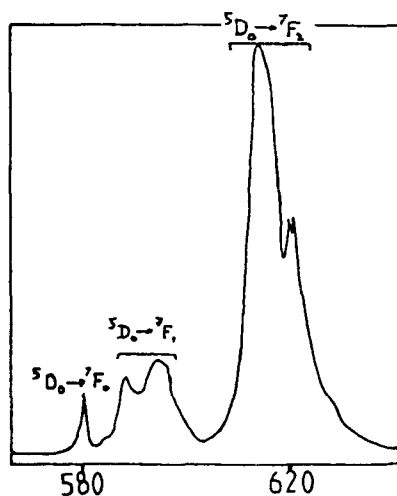


Fig.3 : Fluorescence spectrum of titanium alkoxides doped with  $\text{Eu}^{3+}$

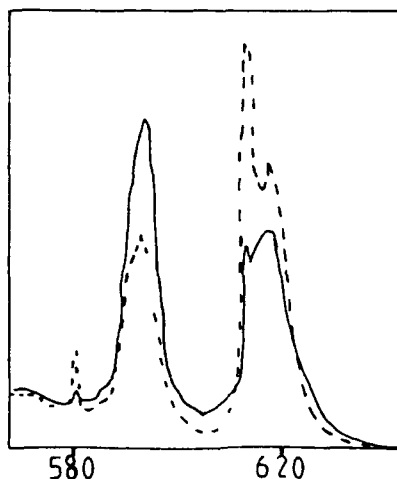


Fig. 4 : Fluorescence spectra of a micellar solution doped with  $\text{Eu}^{3+}$ .  
— : X 35, ---- : X 45.

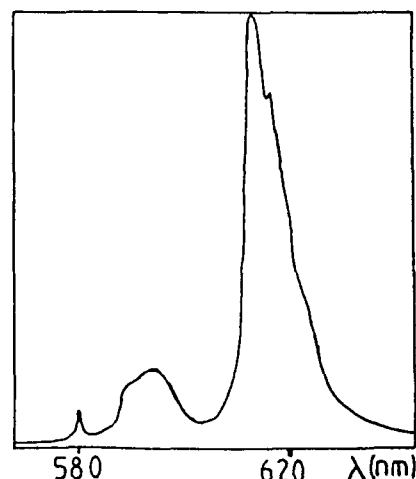


Fig. 5 : Fluorescence spectrum of a titania gel elaborated by the first way.

### 3.1.3. During the sol-gel transition

The  $\text{Eu}^{3+}$  fluorescence has been analysed in relation with the incorporation way of the probe. In this part, we will focus our attention on the results concerning titania gels.

In the first way, the probe is incorporated by the pure alkoxide intermediate. The  $\text{Eu}^{3+}$  fluorescence spectra in the resulting gels (Fig. 5) present only one significant difference with the precursor solution (Fig. 3) : the ratio  $R$  has changed from 7.2 to 4.6.  $\text{Eu}^{3+}$  is no more surrounded by coordinated alkoxides molecules. A chromatographic analysis has proved that most of the alkoxides groups react. Two different mechanisms can explain these results :

- during the sol-gel transition, the coordination degree is reduced, titanium alkoxides react individually and a different  $\text{Eu}^{3+}$  environment appears formed by the inorganic network.
- the aggregates react between each others by the intermediate of the external functions and then the  $\text{Eu}^{3+}$  surrounding environment is not destroyed but disturbed. No conclusion can be drawn from the different aspect of the  $5D_0 \rightarrow 7F_2$  band (Fig. 3 and Fig. 5).

If the probe is incorporated by the micellar solution intermediate (second way),  $\text{Eu}^{3+}$  emission in the gel is similar to the previous one and strongly differs from the  $\text{Eu}^{3+}$  spectrum in the micellar solution (Fig. 4). The water that made up the  $\text{Eu}^{3+}$  coordination shell in the micellar solution has been quickly consumed to perform the hydrolysis. Thus,  $\text{Eu}^{3+}$  undergoes an important modification of its environment. A new  $\text{Eu}^{3+}$  solvation shell appears which is

composed of the oxygen of the Ti-O-Ti and of the OH groups just formed and also with the oxygens of the unreacted OR fonctions.

To make sure that the introduction of the probe have no influence on the gel formation, it was necessary to consider the third and fourth ways of incorporation. For both ways, the fluorescence spectra of the final gel are roughly the same. The slight variation of  $R$  ( $R=4.1$  to  $R=4.7$ ) only indicates that  $\text{Eu}^{3+}$  adsorbed on a washed gel has a lightly more dissymmetrical surrounding. That was foreseeable, because in case three, the particles can go on growing around the probe. So the solvation shell of  $\text{Eu}^{3+}$  is practically the same whatever the incorporation way we choose.

Concerning the fourth way, if the rare earth was really adsorbed on the surface of the gel particles, we should have noted some differences especially in the widths of emission spectra bands; this is an indication of the fact that  $\text{Eu}^{3+}$  gets to the inside gel cages porosity using the "bottle-neck" geometry of the gel. At this place, it can thus have an arrangement of coordinative bonds of identical symmetry than before. We must also consider the fact that after washing a doped gel,  $\text{Eu}^{3+}$  is still trapped in the gel whatever the solvent we use. Moreover, the probe luminescence is insensitive to an exchange of the decane by hexane or by a very different kind of solvent as alcohol or water. We have proved by an infrared spectroscopic study that the solvent and the surfactant were still detectable in a dry washed gel, showing that the remaining chemical substances were contained in the  $\text{TiO}_2$  crossbars and adsorbed on their surfaces. These results prove that the probe is trapped inside the microporosity of the  $\text{TiO}_2$  crossbars (first and second ways) or adsorbed at the junctions of the network structure. On this system, we have performed many kinetics but we did not have seen any spectral differences between a doped sol, a gel and a gel after the syneresis phenomenon. The probe doesn't detect any variation in the symmetry or in the nature of its first neighbours; they were organized definitely at the real beginning of the sol-gel transition; this proves that the gel state is obtained by few condensation reactions between particles formed during the first minutes of the reactions.

The Neodymium insertion can be performed by the same ways. A characteristic absorption spectrum is presented on Fig. 6. Considering that  $\text{Eu}^{3+}$  and  $\text{Nd}^{3+}$  have the same chemical nature and a similar affinity with the titanium alkoxide, they will occupy the same position in the system. The former kinetic informations have been wholly confirmed by this probe. For the different doped gels, we have recorded their absorption spectra using the same conditions; it is thus reliable to compare the Judd-Ofelt intensity parameters that are given on table 1.

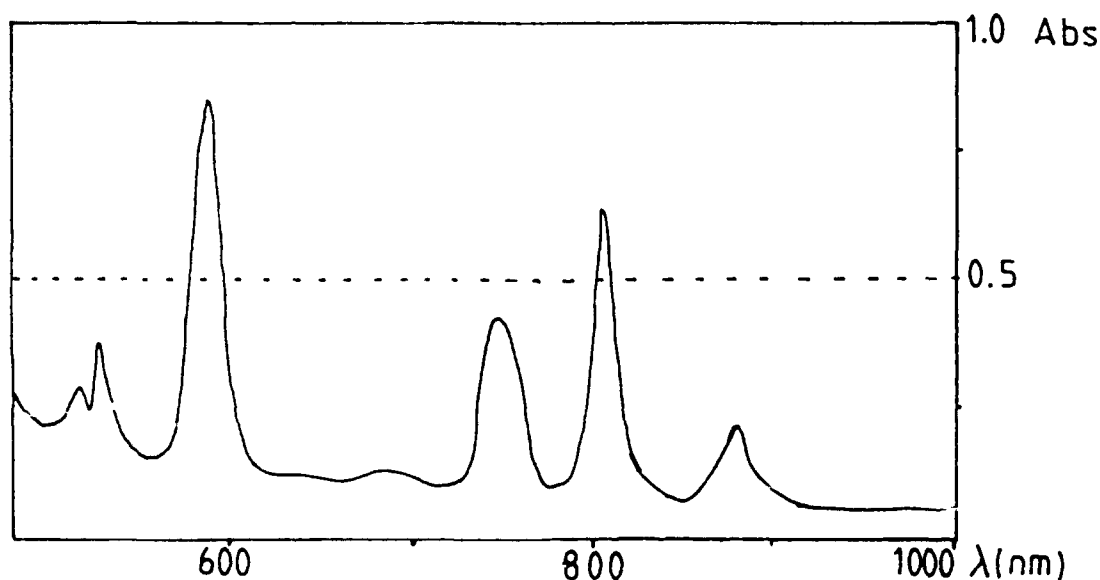


Fig. 6 : absorption spectra of a titanium gel doped with  $\text{Nd}^{3+}$ .

	$\Omega_2 \cdot 10^{20}$	$\Omega_4 \cdot 10^{20}$	$\Omega_6 \cdot 10^{20}$
Pure alkoxide doped with $\text{Nd}^{3+}$	8.38	6.89	6.25
Doped gel (first way)	7.05	6.30	6.16
Micellar solution	0.71	5.62	6.86
Doped gel (second way)	5.15	7.56	6.75
Gel doped after the sol elaboration	5.97	6.12	6.1

Table 1 : Judd-Ofelt parameters for the titanium gels elaborated by the different ways; we have listed the parameters of the precursor solutions and of the corresponding gels.

The  $\Omega_2$  parameter varies from  $0.71 \cdot 10^{20}$  to  $8.38 \cdot 10^{20}$  and as soon as the probe is in the vicinity of alkoxides molecules this parameter becomes much higher than in the micellar solution; the maximum value has been measured for the pure titanium alkoxide doped with  $\text{Nd}^{3+}$ ; that clearly indicates that there is covalent bondings between Neodymium and its ligands which are the OR groups of the titanium alkoxide. Many of these functions are hydrolysed during the sol-gel process and, so, some of the covalents bondings disappeared. That explains the medium values measured in the different gels. Concerning the  $\Omega_6$  parameter, the variations are not large enough to deduce anything from; we can only say that the rigidity of the gel cage is lightly higher than in a solution but we are still far from the rigidity of an oxide ( $\Omega_6 = 4 \cdot 10^{20}$ ).

All those results have been confirmed using the zirconium alkoxide. The case of the silicon alkoxide is slightly different : the  $\text{Eu}^{3+}$  fluorescence spectra are always the same as in the pure alkoxide. So, the  $\text{Eu}^{3+}$  setting doesn't change and is essentially built of alkoxides with low hydrolysis rate; that must be linked with the fact that it is the lowest reactive alkoxide.

### 3.2. pyrene incorporation

Kaufman and al. have published a similar study in a classical sol-gel system;<sup>9,10</sup> they carried out the polymerization of  $\text{Si}(\text{OCH}_3)_4$  in the presence of surface active agents and pyrene as a probe molecules. They observed prolonged oscillations in the  $E/E + M_5$  ratio during the sol-gel transition.

So, we have to determine a concentration field where the both forms, monomers and excimers, coexist. Kinetic studies have been performed on the titanium alkoxide using different concentrations of Py : 0.3 g/l, 1.05 g/l, 1.6g/l and 3.6g/l. The second and the third kinetics are the only ones situated inside the previous field. As these two kinetics have provided absolutely the same information, all the results presented below correspond to a pyrene concentration of 1.05 g/l.

#### 3.2.1 In the micellar solution

Pyrene is a strongly hydrophobic probe and its solubility in water is very low. In the pyrene fluorescence spectrum at this concentration (1.05 g/l) we have measured the significant ratio  $M_3/M_1 : M_3/M_1 = 1.80$ .

In the case of the pyrene solubilized in decane at the same concentration, the ratio  $M_3/M_1$  becomes 2.8. This observation permits us to say that, in presence of such micelles, pyrene is preferentially solubilized in the exterior hydrophobic region of these aggregates and in the vicinity of the surfactant molecules.

### 3.2.2. During the sol-gel process

On the figure 7, we have represented the evolution, versus time, of the excimers proportion (Fig. 7.1) and the  $M_3/M_1$  (Fig. 7.2) ratio during the sol-gel transition. The gel point is situated by an arrow; and the dotted lines correspond to the different values characterizing the pyrene fluorescence in reversed micelles and in decane.

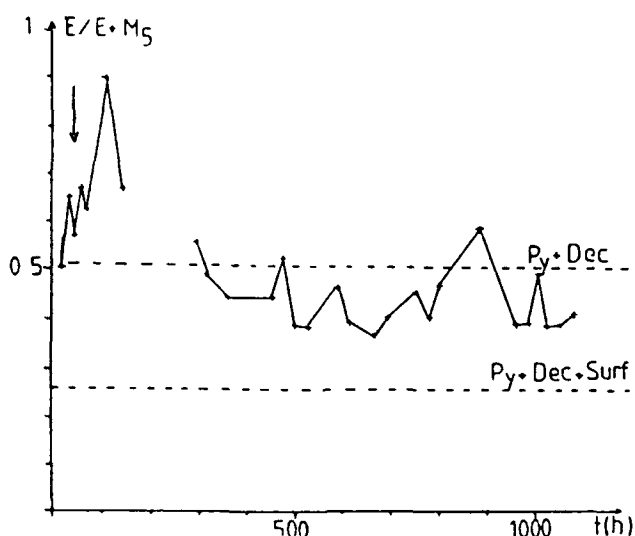


Fig. 7.1 : Representation of the excimers proportion versus time during the sol-gel transition of titanium.

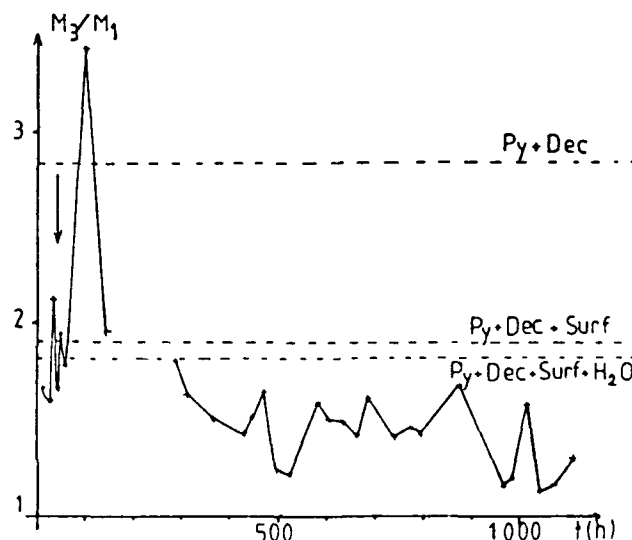


Fig. 7.2 : Representation of the  $M_3/M_1$  ratio versus time during the same sol-gel transition.

At the beginning of the kinetic we observe large variations in the  $E/E + M_5$  as well as in  $M_3/M_1$ , and then the amplitude of the fluctuations gets smaller.

We have recorded many times the fluorescence spectra of a micellar solution doped with pyrene; thus we have evaluated the experimental error at less than 5%; consequently, that can not be at the origin of the oscillatory behavior we observe.

The oscillations, we have observed, can be considered as chaotic, in fact we have never been able to follow continuously a change of the former ratio from a maximum to a minimum. Moreover, a similar sample has been analysed during many days under a constant 350 nm excitation; by this way we know that the excitation energy could have an influence only at the right beginning of this experiment. Under these new conditions, the two ratio, presented on Fig. 8.1 and 8.2, do not exhibit any chaotic evolutions.

The oscillations for the  $M_3/M_1$  ratio are situated below the characteristic level of the micellar solution doped with the same pyrene concentration; this observation proves that the system has a stronger polarity certainly because of the proximity of the  $TiO_2$  crossbars. We must also note the direct correlation between an increasing of the excimers proportion and a decreasing of the media polarity during the first thousand hours of the kinetics. If we divide a solution in two parts before gelation, we observe the same phenomena with a real synchronicity and, considering that the

fluctuations are not continuous, it seems to us uncertain that structural evolutions, i.e. reversible polycondensation reactions as suggested by Kaufman and coll.,<sup>10</sup> are at the origin of this chaotic behavior.

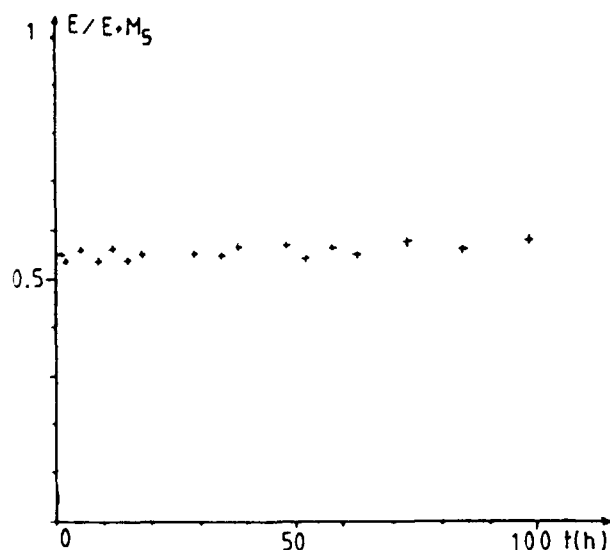


Fig. 8.1 : evolution of the excimer proportion versus time, under a constant excitation.

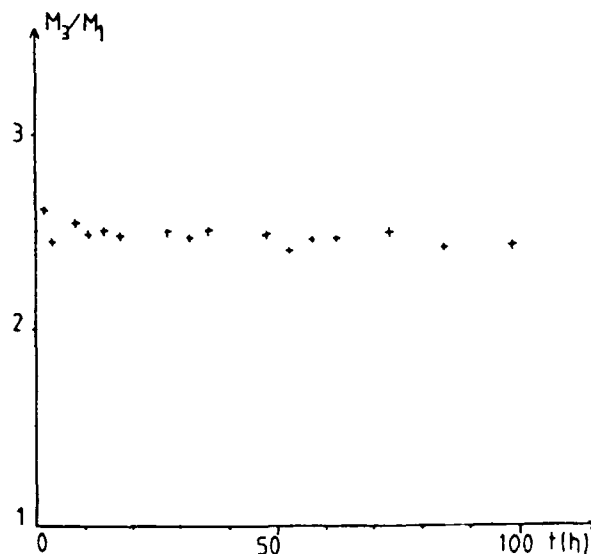


Fig. 8.2 : evolution of the  $M_3/M_1$  ratio versus time, under a constant excitation.

In order to study aging of the gel as an open system, it was separated of its syneresis liquid during kinetic evolutions. For the liquid we have measured constant values :

$$E/E + M_5 = 0.297$$

$$M_3/M_1 = 1.43$$

Concerning  $M_3/M_1$ , this value corresponds roughly to the average value all along the kinetics, showing that an important amount of the probe molecules are surrounded by this kind of liquid.

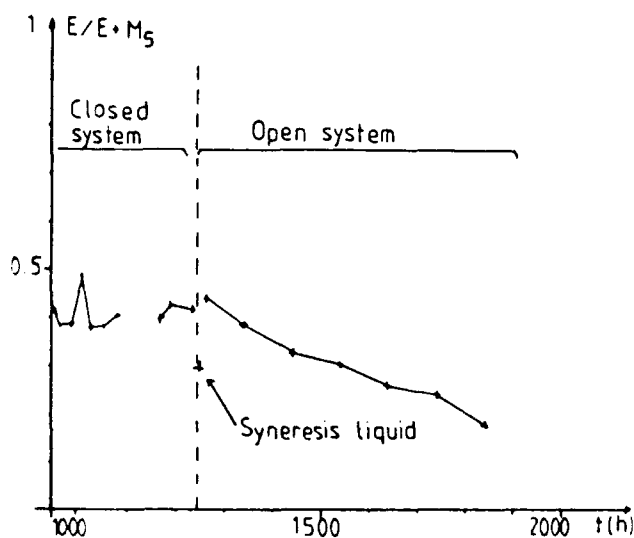


Fig. 9.1 : evolution of the excimer proportion versus time, in the case on an open system.

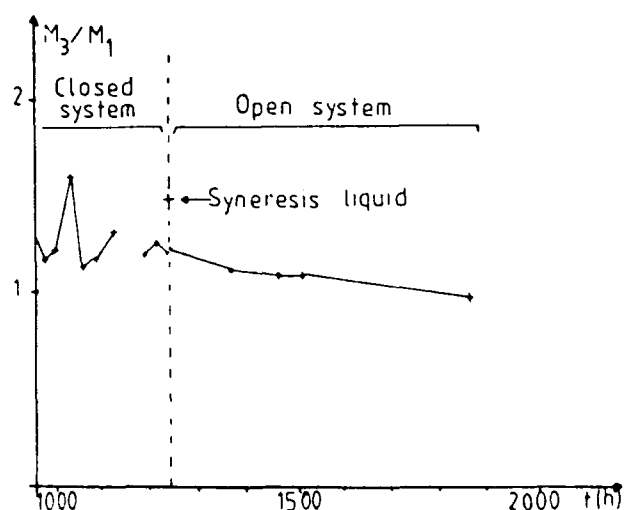


Fig. 9.2 : evolution of the  $M_3/M_1$  ratio versus time, in the case on an open system.

In the case of the open system, the gel contracts significantly and the liquid throwing out is collected and does not stay in contact with the gel. The kinetics performed with these new conditions are presented on Fig. 9.1 and on Fig. 9.2. They do not exhibit any fluctuation; the interaction between pyrene and the micellar solution becomes thus evident. The pyrene molecules, inside the gel, tend to be preferentially under the monomer form. The lowering of the excimer proportion must be linked with the fact that the liquid contained in the gel leaves out the structure; but the fluorescence intensity measured for the monomers wavelengths region remains high, showing that this trapped molecules were at the origin of the monomers emission, all along the kinetics.

So, we can describe two possible simultaneous locations for this kind of probe molecules :

- Inside the microporous volume of the gel, we have a little part of the pyrene molecules; considering that pyrene has a 10 Å diameter, it can be located individually in this kind of pores. No oscillations have been observed at this level. The molecules are trapped in this structure and are prevented from aggregation.

- Inside the macroporous volume of the gel, we have a large amount of pyrene which induces the fluctuations on the excimers proportion in the fluorescence recordings. These fluctuations are not only due to the interaction between pyrene and the liquid inside this volume, but also to the interaction between pyrene and the titanium alkoxide. In fact, we have performed kinetics with the others alkoxides; and no fluctuations have been observed; so, we think that the origin of this phenomenon is a triangular effect between the probe, the titanium alkoxide and the micellar solution certainly by the surfactant intermediate as suggested by Kaufman and al.. The titanium alkoxide is the only one that has the ability to change of oxidation number : from Ti(IV) to Ti(III). A possible explanation could be this electronic charges transfer; we have already proved that this reduction reaction was strongly enhanced by this surfactant family<sup>27</sup> and we also know that pyrene can be easily photoionized in a micellar system by a blue light excitation.<sup>28</sup>

The applicability of these electronic charges transfer theory to the chaotic behavior in this system is still under study.

#### 4. CONCLUSION

We have determined, in this kind of sol-gel matrix, three different host sites, which are the microporosity, the mesoporosity and the macroporosity; depending of the organic or inorganic nature of the fluorescence probe different sites will be occupied; so, that corroborates the previous model we have elaborated by a classical thermoporometry study. This one have brought many others informations :

- The reversed micellar aggregates are centrosymmetrical; they are destroyed as soon as they are in contact with the alkoxides. The alkoxides aggregates are not centrosymmetrical and it is possible that during the sol-gel transition, they are not destroyed but only disturbed.

- The formation kinetic of the TiO<sub>2</sub> crossbars is very quick; they contains a microporosity which is a closed porosity; inside this crossbars, the inorganic probes are definitively trapped. This probe environment is completely organized at the real beginning of the sol-gel transition.

- An organic probe as pyrene can also be efficiently trapped inside the mesoporosity of this gel. This cage effect remains after an ageing process. But, the fluctuation phenomenon, which occurs inside the macroporosity of a titania gel, is not for the moment completely understood; it seems to us that the excitation energy can be at the origin of a photoelectrical process between the titanium alkoxide and the pyrene molecules which induce these fluctuations.

## 5. REFERENCES

1. G. Blasse, "The physics of new luminescence materials," *Mat. Chem. and Physics*, Vol. 16, pp. 201-236, 1987.
2. R. Reisfeld, "Future technological applications of rare earth doped materials," *J. of the Less Common Metals*, vol. 93, pp. 243-251, 1983.
3. G. Boulon, "Luminescence in glassy and glass ceramics materials," *Mat. Chem. and Phys.*, vol. 16, pp. 301-347, 1987.
4. Y. Kobayashi, Y. Imai, K. Kurokawa, "Preparation of a transparent alumina film doped with organic dye by the sol-gel process," *J. of Mat. Science Letters*, Vol. 7, pp. 1148-1150, 1988.
5. C. Guizard, M. Stitou, A. Larbot, "Sol-gel transition in reversed micelles microemulsion," *Mat. Res. Soc. Symp. Proc.*, M.R.S., vol. 121, pp. 115-124, 1988.
6. C. Guizard, A. Larbot, L. Cot, "Principes fondamentaux de la transition sol-gel en milieu micellaire inverse," *Greco Sol-Gel 93*, C.N.R.S., Vol. 1, pp. 11-32, 1989.
7. J.F. Quinson, J. Dumas, M. Chatelut, J. Serughetti, C. Guizard, A. Larbot, L. Cot, "Porous texture of inorganic gels after aging in different solvents," *J. of non Cryst. Solids*, Vol. 113, pp. 14-20, 1989.
8. J. Marignan, C. Guizard, A. Larbot, "Local structure of titania gels," *Europhysics Letters*, Vol. 8(7), pp. 691-696, 1989.
9. V.R. Kaufman, D. Levy, D. Avnir, "A photophysical study of the sol-gel transition in silica," *J. of non Cryst. Solids*, Vol. 82, pp. 103-109, 1986.
10. V.R. Kaufman, D. Avnir, "Prolonged Chaotic oscillations during the gel-xerogel transition in Silicon tetramethoxide polymerization as detected by pyrene excimerization," *Mat. Res. Soc. Symp. Proc.*, M.R.S., Vol. 73, pp. 145-156, 1986.
11. R. K. Bauer, R. Borenstein, "Surface photochemistry : translation motion of organic molecules adsorbed on silica gel and its consequences," *J. of the Am. Chem. Soc.*, Vol. 104, pp. 4635-4644, 1982.
12. J.C. Pouxviel, B. Dunn, J.I. Zink, "Fluorescence study of alumino-silicate sols and gels doped with hydroxy trisulfonated pyrene," *J. of Phys. Chem.*, Vol. 93, pp. 2134-2139, 1989.
13. D. Levy, D. Avnir, "Effect of the changes in the properties of silica cage along the gel-xerogel transition on the photochromic behavior of trapped spiropyrans," *J. of Phys. Chem.*, Vol. 92, pp. 4734-4738, 1988.
14. D. Avnir, D. Levy, "The nature of the silica cage as reflected by spectral changes and enhanced photostability of trapped rhodamine 6G," *J. of Phys. Chem.*, Vol. 88, pp. 5956-5959, 1984.
15. D. Avnir, V.R. Kaufman, "Organic fluorescence dyes trapped in silica and silica titania thin films by the sol-gel method," *J. of non Cryst. Solids*, Vol. 74, pp. 395-406, 1985.
16. D.I. Santos, "Optical properties of dye molecules adsorbed on fractal structures," *J. of non Cryst. Solids*, Vol. 82, pp. 165-170, 1986.
17. R. Reisfeld, M. Eyal, D. Brusilovsky, "Luminescence enhancement of rhodamine 6G in sol-gel films containing silver aggregates," *Chem. Phys. Letters*, Vol. 153:23, pp. 210-214, 1988.
18. D. Levy, R. Reisfeld, D. Avnir, "Fluorescence of  $\text{Eu}^{3+}$  trapped in silica gel-glass as a probe for cation binding and for changes in cage symmetry during gel dehydration," *Chem. Phys. Letters*, Vol. 109:6, pp. 593-597, 1984.
19. C.K. Jorgensen, R. Reisfeld, "Judd-Ofelt parameters and chemical bondings," *J. of the Less Common Metals*, Vol. 93, pp. 107-112, 1983.
20. R. Reisfeld, R.A. Velapoldi, L. Boehm, "Quantum efficiencies and radiationless transitions of  $\text{Eu(III)}$  in phosphate glasses," *The J. of Phys. Chem.*, Vol. 76:9, pp. 1293-1297, 1972.
21. R. Reisfeld, "Spectra and energy transfer of rare earths in inorganic glasses," *Structure bonding*, Vol. 13, pp. 53-98, 1973.
22. A. Nakajima, "Variation in the vibrational structures of fluorescence spectra of naphthalene and pyrene in water and in aqueous surfactant solution," *J. of Mol. Spectrosc.*, Vol. 61, pp. 467-475, 1976.
23. K. Kalyanasundaram, J.K. Thomas, "Environmental effect on vibronic band intensities in pyrene monomer fluorescence and their application in studies of micellar systems," *J. of the Am. Chem. Soc.*, Vol. 99:7, pp. 2039-2044, 1977.
24. J. Rouviere, J.M. Couret, M. Lindhemmer, J.L. Dejardin, "Ionic diffusion coefficients of sodium chloride in water-hexane mixture," *Journal de chimie physique*, Vol. 76:3, pp. 289-296, 1979.

25. M. Kotlarczyk, J.S. Huang, S.H. Chen, "Structure of AOT reversed micelles determined by small angle neutron scattering," *J. of Phys. Chem.*, Vol. 89, pp. 4382-4386, 1985.
26. E. Hirschorn, M.B. Mathews, "Equilibrium and kinetics of water exchange between rayon and detergent micelles in a hydrocarbon medium," *J. of Colloid Science*, Vol. 14, pp. 430-440, 1959.
27. C. Guizard, J.C. Achddou, C. Lurin, "Reversible photochromism in titanium gels realized with the reversed micelles microemulsion technique," To be published.
28. J.K. Thomas, "Radiations induced reactions in organized assemblies," *Chemicals Reviews*, Vol. 80:4, pp. 283-299, 1980.





## Porous Optical Composites

S. T. Reed, C. S. Ashley, C. J. Brinker, R. J. Walko  
Sandia National Laboratories  
Albuquerque, NM 87185

Robert Ellefson, and John Gill  
E.G.& G. Mound Applied Technologies  
Miamisburg, OH 45342

### ABSTRACT

Previous studies have shown that sol-gel matrices are excellent low temperature hosts for various optically-active materials, both organic and inorganic. Optical properties of these composites depend upon such factors as the structure of the matrix and size, shape, and degree of dispersion of the optically-active phase. We discuss factors that control the shrinkage and clarity of silicate aerogel host matrices and report on novel composites in which the optical properties are controlled by solid-vapor and/or solid-liquid reactions within the host matrix.

### 1. INTRODUCTION

The radioluminescent light (RL) program at Sandia National Laboratories and E.G.& G. Mound Applied Technologies is conducting research to improve radioactively-powered light sources and to develop power supplies based on this technology. Current studies have focused on developing a volumetric light source powered by radiation. The volumetric light is intended to improve light output over current technology while enhancing safety. We report on the results of an optically active aerogel/phosphor composite in which light output is controlled by aerogel properties, concentration and dispersion of the phosphor, and source of excitation radiation.

Aerogel/phosphor composites are prepared by suspending a commercial phosphor powder in a sol. After gelation, aging, and supercritical solvent extraction, a beta source is placed in proximity to the phosphor grains through the aerogel pores. The beta particles excite the phosphor and cause it to luminesce. This light source should have a higher light output than conventional surface RL lights because light is emitted not only from the aerogel surface but also from within some portion of the aerogel volume. Thus, it should have some of the intensity-additive properties of a true volumetric light source.

Uses for self-powered radioluminescent lights include emergency lighting for aircraft, submarines, and ships, instrumentation panel and docking lights for space applications, lighting where electrical power is difficult or impossible such as remote runway lighting, and low energy radiation detection (e.g.,  $T_2$  detector).

---

This work is supported by the US DOE under contracts #DE-AC04-76DP00789 and #DE-AC04-88-DP43495

92 4 28 040

92-11422



If the light output from the aerogel/phosphor volumetric light is great enough then it is economically feasible to use it as a scintillator in a two-step betacell to produce electrical power. This concept is schematically represented in Fig. 1. Beta particles bombard a scintillator, producing photons. The photons are then absorbed by the photocell, generating electrical power.

### 1.1. Conventional technology

In a gas tube RL light prepared using current technology, a phosphor powder is deposited on the inside surface of a glass tube using phosphoric acid or an organic binder to adhere the phosphor to the tube surface. The tube is subsequently evacuated and backfilled with approximately one atmosphere of tritium gas (Fig. 2). Beta particles produced by radioactive decay of tritium atoms excite the phosphor particles and some of the energy is released as light.

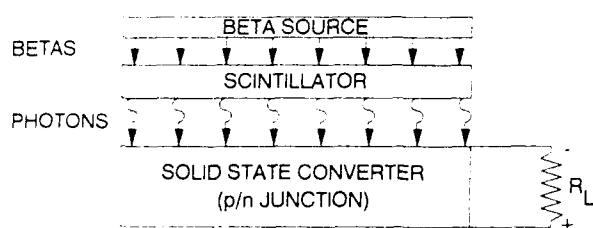


Fig. 1. A schematic of a two-step betacell conversion.

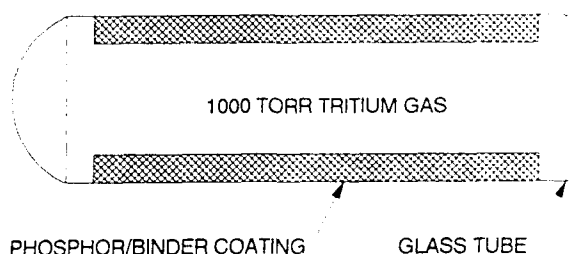


Fig. 2 Schematic of conventional gas tube RL light.

There are three effects that limit the maximum light output of such light sources. First, tritium gas has a very low beta particle energy ( $E_{avg} = 6 \text{ keV}$ ) which causes self-absorption of the beta particle and limits beta particle penetration into the phosphor particles to  $\sim 1\text{-}2$  microns. In other words, the beta particles that excite the phosphor on the inside of the glass tube can only come from a limited gas thickness. Computer simulations predict this thickness to be about 2 cm for 1 atmosphere of pure tritium gas.<sup>1</sup> In practice, a spacing of  $\sim 0.3$  cm is typically used with 1.3 atmospheres of tritium to optimize the light output per Curie of tritium gas used.

Second, although the phosphor materials are very reflective, the phosphor layer quickly becomes opaque to light for deposits only a few particles thick. Therefore, increasing the thickness of the phosphor deposit or increasing the tritium pressure does not significantly increase the light output.

Finally, the organic binder used to glue the phosphor particles to the inside of the glass tube can darken due to radiation damage from tritium beta particle bombardment, thereby reducing the intensity of the light over time.

In addition, gas tube RL lights are extremely fragile. If a tube is fractured, the tritium gas will rapidly leak out and may pose a contamination threat in a confined space.

## 2. AEROGEL/PHOSPHOR COMPOSITE

To overcome the limitations of current RL tube technology we are studying a composite consisting of a cathodo-luminescent phosphor suspended in a silica aerogel. The high porosity of the aerogel allows intimate mixing of the tritium with the phosphor throughout the aerogel matrix. The clarity of the silica aerogel is not affected by radiation-induced darkening.<sup>2</sup> This composite will have characteristics of a volumetric light source and thus be inherently brighter than a conventional RL tube providing: 1) the aerogel matrix is sufficiently transparent to the emitted beta particles so that most of the energy is deposited in the phosphor, and 2) the aerogel/phosphor matrix is optically transparent to the emitted light such that most of the light generated within its volume can escape. Ideally, a highly transparent aerogel matrix prepared under conditions where little shrinkage occurs during processing will produce the most desirable host material for phosphor incorporation.

### 2.1. Aerogel clarity and shrinkage

Clear silica aerogels can be prepared using tetramethylorthosilicate (TMOS) or tetraethylorthosilicate (TEOS) as precursors. TEOS is often the precursor of choice because of the toxicity of TMOS. Recent advances have produced highly transparent aerogels using a base-catalyzed TEOS system, resulting in more robust aerogels with significantly less shrinkage than acid-catalyzed aerogels.<sup>3,4</sup> Scattering (lack of clarity) in base-catalyzed aerogels occurs not only from the small spherical linkages that make up the aerogel skeleton but also as a result of slight differences in aerogel density.<sup>5</sup> The clarity of aerogels is influenced by TEOS concentration, amount of water for hydrolysis, pH, and gelation temperature.<sup>6,7</sup>

Aerogels can be prepared by direct removal of solvent (usually ethanol or methanol) under supercritical conditions or by a safer, low temperature process involving exchange of ethanol with liquid CO<sub>2</sub>. Some workers have found that CO<sub>2</sub> processing of base-catalyzed gels produces slightly clearer aerogels than direct (high temperature) processing.<sup>4</sup> Transmission spectra of base catalyzed TEOS aerogels formed using the CO<sub>2</sub> process show absorption due to adsorption of H<sub>2</sub>O in the gel. The clarity of these aerogels improves upon heating in air at elevated temperatures.<sup>6</sup>

A near-zero-shrinkage (NZS) aerogel composition and process, developed at Sandia National Laboratories, was chosen as the matrix for phosphor particle loading. The NZS aerogel reduces stresses due to shrinkage during aging (syneresis) and during critical point drying. Stresses arising from particle/matrix interactions and matrix collapse around the particle are also minimized. Particle loaded aerogels exhibit improved mechanical strength, an observation that may be analogous to the strength imparted to concrete by aggregate.

### 2.2. Composite clarity

For optical clarity of the composite, diffuse scattering resulting from phosphor agglomeration must be minimized. The size, distribution, shape and light absorption of the phosphor will influence the total internal scattering of the composite.<sup>8</sup> Maximum light output is achieved under conditions where the phosphor particles are small and act as "point sources" of light. Ideally, the emitted light is neither absorbed nor scattered by the matrix or by other particles.

### 3. EXPERIMENTAL METHODS

#### 3.1. Preparation of aerogel/phosphor composites

A partially condensed silica sol containing 1 mole  $\text{H}_2\text{O}$ /mole TEOS was prepared as discussed previously.<sup>9</sup> Commercial phosphor powder (nominal particle size  $\sim 20$  microns) was added to the sol to give the required loading (grams phosphor/milliliter of sol) and the mixture was agitated to break up phosphor agglomerates. Dilute  $\text{NH}_4\text{OH}$  was added to give a final concentration of  $\sim 0.04$  M. After gelation, the phosphor/gel composite was aged at  $50^\circ\text{C}$  to strengthen the polymeric network. The samples were sealed into a commercial critical point drying chamber (Polaron Equipment Ltd.) and flushed with liquid  $\text{CO}_2$  at  $\sim 900$  psi replacing ethanol within the gel pores with  $\text{CO}_2$ . The chamber temperature was raised above the critical temperature for  $\text{CO}_2$  ( $31.5^\circ\text{C}$ ), causing an increase in chamber pressure to  $\sim 1200$  psi, followed by a slow venting procedure to ambient pressure.

#### 3.2. Tritiation of aerogel/phosphor composites

For the RL lights considered here, tritium is the preferred radioisotope. However, other isotopes may be considered for specific applications. In general, any radiation source could be used, as long as it does not generate radiation damage either to the luminescent species or the aerogel matrix during the expected lifetime of the device. Examples of other potential isotopes are  $\text{Ni}^{63}$  and  $\text{C}^{14}$ . Like tritium, both of these are pure negative beta emitters which minimize external radiation levels. Positive beta emitters, in general, are not acceptable for RL lights because of the high level of annihilation gamma rays associated with them. Alpha particle emitters are also not acceptable because of the potential for excessive radiation damage to the luminescent species and the aerogel matrix. X-ray and low energy gamma emitters may be usable depending upon the threshold for radiation damage and/or radiation safety considerations.

The brightness of the RL lights is measured in foot-lamberts (fL) using a luminance meter (Minolta LS110) with a precision of 0.02 fL. Commercially available RL tube lights have a light output of  $\sim 0.3$  fL. For comparison, a 25 watt frosted light bulb and a motion picture screen have luminance values of about 2500 fL and 10 fL, respectively.

The phosphor/aerogel RL light system being investigated can be powered by tritium in various forms: low pressure gas, high pressure gas, tritiated water, tritoxyl bonding to the silica matrix, and organic occluders dispersed within the phosphor/aerogel composite. Each of these tritium forms have unique technical advantages and limitations depending upon the ultimate use of the RL light. For example, the use of tritium which is chemically bound to an organic will provide a safe, proliferation-resistant light, but will have poor resistance to radiation damage. Our experiments have incorporated tritium in the aerogel pores as a low pressure gas or on the aerogel surface as tritoxyls (by  $\text{H}=\text{T}$  exchange and tritolysis of siloxane bonds). Incorporation of tritium-loaded organics into these aerogel/phosphor composites is reported elsewhere.<sup>10</sup>

## 4. RESULTS AND DISCUSSION

### 4.1. Tritium gas experiments

An aerogel containing GTE 1260 phosphor powder (ZnS:Cu:Al) at a final concentration of 0.5 grams of phosphor/ml of sol was prepared as described above. Samples were evacuated and backfilled with  $T_2$  gas at E.G. & G. Mound Applied Technologies, Miamisburg, OH. The brightness of the lights was monitored as a function of increasing  $T_2$  pressure and compared to a similar experiment performed with bulk GTE 1260 powder. The results of this experiment are summarized in Fig. 3.

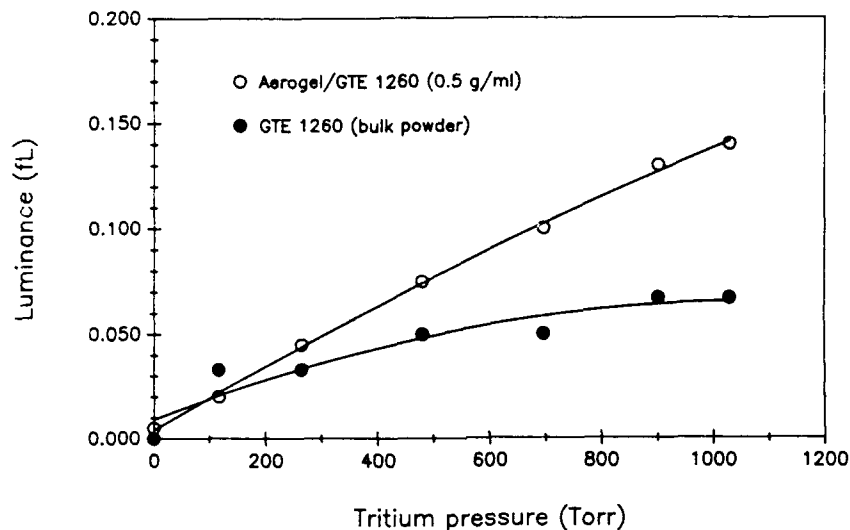


Fig. 3. Luminance (brightness) measurements of aerogel/phosphor and bulk phosphor as function of tritium gas pressure.

There is an nearly linear increase in optical brightness as a function of gas pressure up to 1030 torr. The light output for the aerogel/phosphor composite is greater than that for bulk phosphor powder shown for comparison. However, the composite brightness is lower than that of a commercially available RL tube light ( $\sim 0.3$  fL). One possible explanation is that the beta particles are partially absorbed by the aerogel matrix. The aerogel/phosphor composite properties, e.g., aerogel porosity, phosphor concentration, and phosphor dispersion, were not optimized for maximum light output when loaded with  $T_2$  gas.

To study the relationship of brightness and phosphor concentration, aerogel composites with phosphor concentrations ranging from 0.01 to 0.5 g/ml were loaded with  $T_2$  gas. The results of this experiment are summarized in Fig. 4. This curve suggests that phosphor concentrations greater than 0.5 g/ml will result in even brighter lights. In fact, we have found that higher phosphor concentrations result in phosphor agglomeration in the aerogel and lower light output. Increased phosphor concentration and brighter lights may be achieved through the use of dispersants or surfactants. The reduced agglomeration will minimize scattering of light and the phosphor will behave as a more ideal "point source" of light. However, there will be a phosphor concentration beyond which the composite is no brighter than the bulk phosphor powder. In

this case, as with the bulk powder, most of the light originates in the near-surface region and the overall brightness is substantially lower.

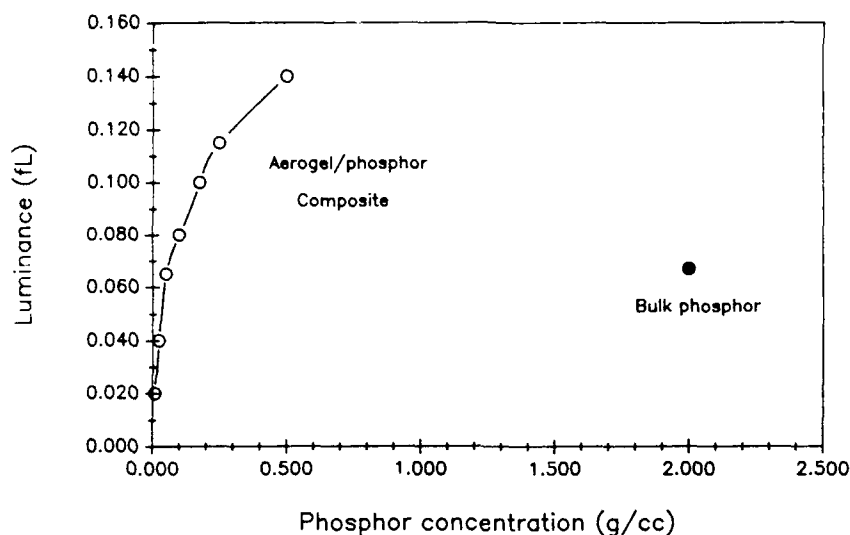


Fig. 4. Luminance measurements of aerogel/phosphor composites over a range of phosphor concentrations at 1030 torr tritium gas. For comparison, the luminance of bulk phosphor powder (density  $\sim 2$  g/cc) is shown.

#### 4.2. $T_2/T_2O$ experiments

Several small pieces of an aerogel phosphor composite (0.5 gm/ml GTE 1260) were exposed first to  $T_2$  gas and subsequently to  $T_2O$  vapor. At 760 torr of tritium gas the brightness of the pieces was 0.08 fL. Immediately upon exposure to  $T_2O$  vapor the brightness of the pieces began to increase. A maximum brightness of 4.6 fL was achieved after about 10 hours vapor exposure. This level of brightness is more than 4 times greater than the brightest RL tube light ( $\sim 1$  fL) and about 10 times brighter than typical commercially available tube lights -- a record brightness for a tritium based light. After about 15 hours exposure the brightness began to diminish and the samples appeared to have shrunk, probably due to pore collapse within the aerogel caused by the large quantity of physisorbed water in the pores. When the  $T_2O$  vapor was removed from the sample a residual brightness of  $\sim 0.2$  fL was measured. This may be due to chemisorption of  $T_2O$  onto the aerogel surface as tritoxyls. As before, these composites were not optimized in any way to maximize the uptake of tritium onto the aerogel surface.

#### 4.3. Long-term brightness and gas analysis

Long-term luminance measurements are being made on several tritium-gas-loaded samples. Interestingly, the light output from these samples continues to increase. Fig. 5 shows a typical sample with an initial brightness of 0.12 fL after loading with tritium gas. After  $\sim 135$  days exposure to the same volume of tritium its brightness increased to 0.32 fL. The tritium gas was pumped off at 135 days and the sample retained a brightness of 0.2 fL. At  $\sim 181$  days, the sample was evacuated and reloaded to 998 torr with  $T_2$  gas. This re-exposure to tritium resulted in an even higher luminance (0.44 fL).

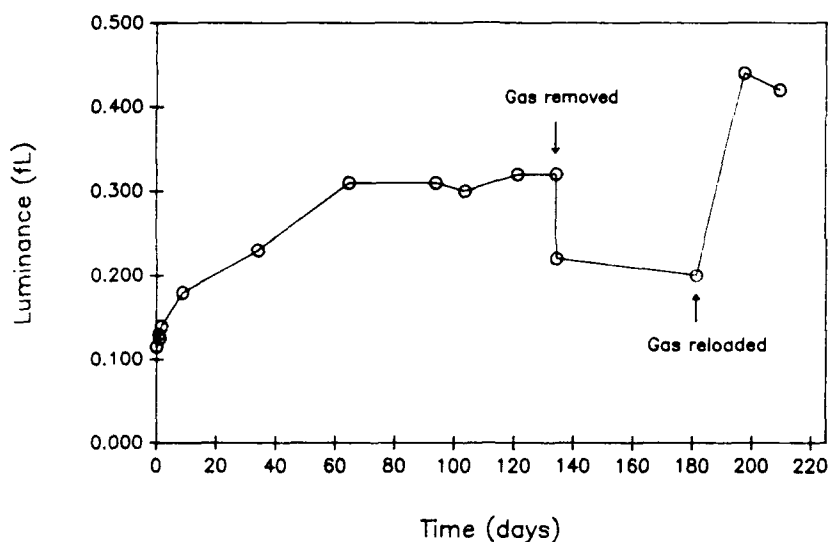


Fig. 5. Long term luminance measurements of an aerogel/phosphor composite (0.25 g/ml) following  $T_2$  gas loading.

Residual gas analysis was performed on three similar tritium-gas-loaded composites. After  $\sim 135$  days, the gases were removed from the composite samples and were found to contain  $>60\%$  hydrogen and only  $\sim 30\%$  tritium. Two samples also exhibited traces of  $CT_4$ . These results suggest that a beta-catalyzed exchange reaction of  $H=T$  is occurring mainly at hydroxyls (OH) located on the aerogel surface and at H-containing organics in the aerogel matrix.<sup>11</sup> All three gas analyses showed  $\sim 4\%$   $He^3$ , a radioactive decay product of tritium.

The residual light measured after  $T_2$  removal, as shown in Fig. 5, can be attributed to tritium that is chemically bound to the aerogel surface. The increased brightness seen when tritium is re-introduced results from an even higher concentration of tritium in close proximity to the phosphor (chemically bound  $T + T_2$  gas). Extremely high brightness levels may be achieved by controlled, sequential loading of tritium onto the aerogel/phosphor composite.

#### 4.4. Discussion of $H=T$ exchange

Loading of tritium onto the composite surface can be accomplished by three methods: 1) complete hydroxylation followed by exposure to tritium gas, 2) complete dehydroxylation followed by exposure to  $T_2O$ , and 3) incorporation of H-containing organics followed by exposure to tritium gas.

A high output light source may be prepared by first fully hydroxylating the aerogel surface then exposing it to  $T_2$  gas, whereupon the exchange reaction occurs, allowing the replacement of surface protium (H) with tritium (T). It has been well established that the aerogel surface has the capacity for 4-5 hydroxyl (OH) groups per square nm of surface.<sup>12</sup> Based on an aerogel density of 150 mg/cc and a surface area of 600-1200  $m^2/gm$ , there is the potential for up to  $9 \times 10^{20}$  OH/cc! Saturation of the surface with OT approximates a tritium loading equivalent to 15-20 atmospheres. The exchange reaction can be accelerated by higher temperatures and/or pressures. In addition, if surface protium is completely replaced and if extraneous water is absent, the aerogel/phosphor source is radiochemically stable.

Maximization of surface tritoxyls can also be achieved by fully dehydroxylating the surface followed by exposure to  $T_2O$ . A preferred process involves heating above  $250^\circ C$  to form defect silicate structures which readily react upon subsequent exposure to  $T_2O$  to form  $Si-OT$ .<sup>13</sup> Higher  $T_2O$  loading (and higher light output) may be obtained by continuing to expose the aerogel to  $T_2O$  vapor after complete tritoxylation of the surface. This may result in classical hydrogen ( $T-OT_2$ ) bonding of additional  $T_2O$  onto surface OT groups. There are obvious practical limitations to this approach due to the extreme toxicity of  $T_2O$ .

H=T exchange also occurs with H-containing organics located on the aerogel surface. These may be residual molecules from incomplete solvent removal during aerogel processing or from incomplete hydrolysis of TEOS. Alternatively, H-containing organics may be incorporated into the aerogel to increase the number of potential exchange sites per cc of aerogel compared to the number of sites available with tritoxylation. With careful selection of the organic to minimize radiation damage this concept would allow an extremely safe and stable light source.

#### 4.5. Optical depth measurements

In an ideal volumetric light source, the brightness would be proportional to the volume. In practical sources, however, scattering and absorption limit the thickness from which light can escape. This thickness is the optical depth.

To confirm the volumetric source nature of the aerogel/phosphor composite, phosphor loaded samples with thicknesses of 0.9, 1.8, and 5.3 mm were filled with 746 torr of  $T_2$  gas. Precautions were taken to assure that the volumes of gas over the samples were identical and independent of sample thickness. Brightness measurements made after only one day were inconclusive. However, additional measurements, taken 41.7 days after tritium exposure, showed dramatic differences in brightness as a function of sample thickness. This is evidence of a volumetric effect since the brightnesses would be identical for a surface source. From this limited data, the optical depth can only be estimated at  $> 1.8$  mm.

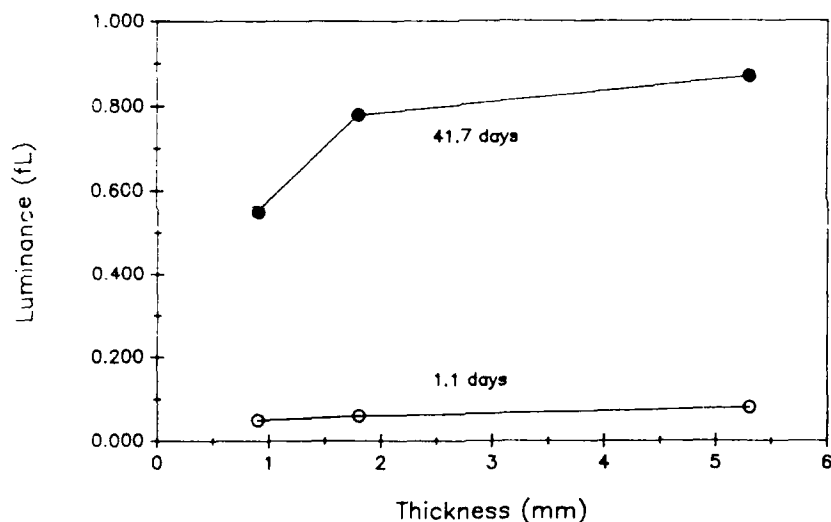


Fig. 6. Brightness measurements of aerogel/phosphor composite samples (0.5 g/ml) with thicknesses of 0.9, 1.8, and 5.3 mm. Initial measurements were taken after 1.1 days exposure to  $T_2$  gas and final measurements were made at 41.7 days.



## 5. SUMMARY

The goal of the RL light program is to overcome the limitations of conventional RL gas tube technology and produce brighter lights while enhancing safety. Current studies have focused on the development of a volumetric light source using an aerogel/phosphor composite activated by tritium. These lights have potential applications where electrically powered lights are impractical. They may also be used to illuminate a photocell for long-term generation of low levels of electricity.

Increases in tritium gas pressure and phosphor concentration result in more light from the composite. A phosphor loading of 0.5 g/ml consistently produces the brightest lights. The addition of surfactants to the sol should reduce phosphor agglomeration at higher loadings and result in even brighter lights.

Composites exposed to low pressure tritium gas were not initially as bright as commercially available RL tube lights. However, the brightness of these composites actually increased with time. Our preliminary results suggest a H=T exchange reaction with any H present in the composite, either as OH or H in residual organic molecules. A record setting aerogel/phosphor composite RL light was made by physisorbing T<sub>2</sub>O onto a composite surface.

Optical depth experiments showed that light output increased as a function of sample thickness. This is evidence of a true volumetric effect since the brightness is independent of thickness for a surface source. The optical depth was estimated at > 1.8 mm.

Further work includes optimization of aerogel clarity and density, phosphor loading in the composite, and composite pretreatment to maximize tritium uptake on the aerogel surface.

## 6. ACKNOWLEDGEMENTS

The authors gratefully acknowledge the support of Lee Leonard of the U.S. Department of Energy, Germantown, MD. The technical support of Ed Lewis of E.G.& G. Mound Applied Technologies during the tritium loading experiments is greatly appreciated.

## 7. REFERENCES

1. R. J. Walko, unpublished.
2. C. J. Brinker, unpublished.
3. R. E. Russo and A. J. Hunt, "Comparison of Ethyl versus Methyl Sol-Gels for Silica Aerogels Using Polar Nephelometry", *J. Non-Cryst. Solids*, vol. 86, pp. 219-230, 1986.
4. P. H. Tewari, A. J. Hunt, K. D. Lofftus, and G. Lieber, "Microstructural Studies of Transparent Silica Gels and Aerogels", Better Ceramics Through Chemistry, eds. C. J. Brinker, D. E. Clark, and D. R. Ulrich, vol. 73, pp. 195-205, Materials Research Society, Pittsburgh, 1986.
5. A. J. Hunt and P. Berdahl, "Structure Data from Light Scattering Studies of Aerogel", Better Ceramics Through Chemistry, eds. C. J. Brinker, D. E. Clark, and D. R. Ulrich, vol. 32, pp. 275-280, North-Holland, New York, 1984.

6. P. H. Tewari, A. J. Hunt, and K. D. Lofftus, "Advances in Production of Transparent Silica Aerogels for Window Glazings", Aerogels, ed. J. Fricke, vol. 6, pp. 31-37, Springer Proceedings in Physics, 1986.
7. C. A. M. Mulder and J. G. van Lierop, "Preparation, Densification and Characterization of Autoclave Dried SiO<sub>2</sub> Gels", Aerogels, ed. J. Fricke, vol. 6, pp. 68-75, Springer Proceedings in Physics, 1986.
8. A. R. Mahoney, Sandia National Laboratories, private communication.
9. C. J. Brinker, K. D. Keefer, D. W. Schaefer, and C. S. Ashley, "Sol-Gel Transition in Simple Silicates", J. Non-Cryst. Solids, vol. 48, pp. 47-64, 1982.
10. C. L. Renschler, T. J. Shepodd, and J. Gill, Sandia National Laboratories and E.G.& G. Mound Applied Technologies, manuscript in preparation.
11. K. E. Wilzbach, "Tritium-Labeling by Exposure of Organic Compounds to Tritium Gas," J. Am. Chem. Soc., vol. 79, pp. 1013, 1957
12. C. J. Brinker and G. W. Scherer, Sol-Gel Science, pp. 620-628, Academic Press, Inc., New York, 1990.
13. C. J. Brinker, D. R. Tallent, E. P. Roth, and C. S. Ashley, "Defects in Gel-Derived Glasses", Defects in Glasses, eds. F. L. Galeener, D. L. Griscom, and M. J. Weber, vol. 61, pp. 387-411, Materials Research Society, Pittsburgh, 1986.

**Gel-silica hybrid optics****L. L. Hench, J. K. West, F. F. Zhu and R. Ochoa****Advanced Materials Research Center, University of Florida  
One Progress Blvd., #14, Alachua, Florida 32615****ABSTRACT**

Sol-gel processing is used to make two new types of silica optics, Type V fully dense silica and Type VI optically transparent ultraporous silica. Type VI silica is an ideal matrix for impregnation with second phases that are optically active, resulting in a hybrid optical material with a unique combination of properties. The processing and characteristics of several hybrid optical devices are discussed including hybrid dye lasers, scintillators and wavelength shifters, transpiration cooled windows, and laser written waveguides. Advantages of the hybrid optical components are discussed along with potential applications.

**1. INTRODUCTION**

In recent years, sol-gel processing has made it possible to produce with high reliability Type V fully dense silica as well as Type VI optically transparent ultraporous silica optical components.<sup>1-3</sup> The ultrastructure of porous silica gels can be controlled to meet specific application requirements.<sup>2</sup> Type VI gel-silica, first reported by Hench et al.<sup>1</sup> in 1988, is a porous monolithic material exhibiting excellent optical quality,<sup>1</sup> good thermal and chemical stability,<sup>4</sup> and reasonably high mechanical strength.<sup>5</sup>

There are several advantages of Type VI gel-silica optics: 1) near net-shape casting eliminates grinding and minimizes final polishing and finishing, which lowers the production cost of the material and makes very small precision optical components possible; 2) the reliability of processing offers high degree of success, which further reduces overall cost of silica optics; 3) the porous structures can be controlled over a broad range of different pore sizes and different values of volume fraction of porosity to meet the requirements for hosting second phases of different molecular sizes; 4) there are interconnecting pore channels throughout the whole structural network and second phases can be incorporated into the matrix through these channels; and 5) the surface chemistry of the pore network can be tailored molecularly for the organic impregnants.

Recently, research work on optical devices has been one of the largest growth fields in high technology industry due to fast signal transmittance, miniaturization, and high efficiency. Hybrid optics offers another growth opportunity for this field. The second phases in the hybrid optics can be optically active, which, along with the molecularly tailored host material, offers a wide range of multifunctional characteristics in optical operations. For example, Type VI gel-silica is an excellent candidate host material for making optical devices such as hybrid dye lasers, scintillators and wavelength shifters, transpiration cooled windows, and laser written waveguides, GRIN optics, and micro-optical arrays.

The conventional methods of making optical silica involve either very high temperatures or complicated and costly processes. For example, melting of the natural quartz at high temperatures results in low purity vitreous silica which usually degrades the intrinsic properties of the optical material.<sup>1,2</sup>

Diffusion (ion-exchange) and chemical vapor deposition (CVD) are successful techniques, especially in glass waveguide fabrication and the optical fiber field, but they have some major disadvantages. Since diffusion processes are relatively slow, in most cases heating is needed to enhance the process. The CVD method is versatile, but rather complex, expensive, and difficult to tailor to small sizes or complex shapes.

**92 4 28 041****92-11423**

Type VI porous gel-silica offers the opportunity to incorporate optically active phases into the porous structure at room temperature within hours and doesn't require complex equipment or precision controls. This type of vitreous silica offers a broader range of volume fraction of porosity (0.02-0.72) and the average pore radii (1.2-10.0 nm) as compared to a leached sodium boro-silicate glass (0.23-0.25, and 3-4 nm, respectively).<sup>6</sup> Combined with excellent chemical and thermal stability, and high mechanical strength and reliability, this new generation of optically active gel-silica hybrid optics provides promising characteristics for new optical devices.

The objectives of this paper are: 1) review sol-gel processing of Type VI gel-silica with variable porous structures and properties; 2) discuss the processing of the composite materials and the characteristics of various hybrid optical devices such as solid state dye lasers, scintillators and wavelength shifters, transpiration cooled windows, and laser written optics. Data for the characterization of these hybrid optical devices are presented along with a discussion of the advantages and potential applications.

## 2. SILICA GEL MATRICES

There are two methods of preparing hybrid optical materials using sol-gel technology: (1) doping second phases at the sol stage; and (2) impregnating second phases into a rigid gel matrix after the gel has been dried and stabilized. Stabilization, as shown in Fig. 1, is considered as a prerequisite step for impregnation of the second phase of either an aqueous or non-aqueous solution. In this paper, we focus on the second method because it offers the flexibility to incorporate different optically active phases with different molecular weights and sizes once the porous matrices are made.

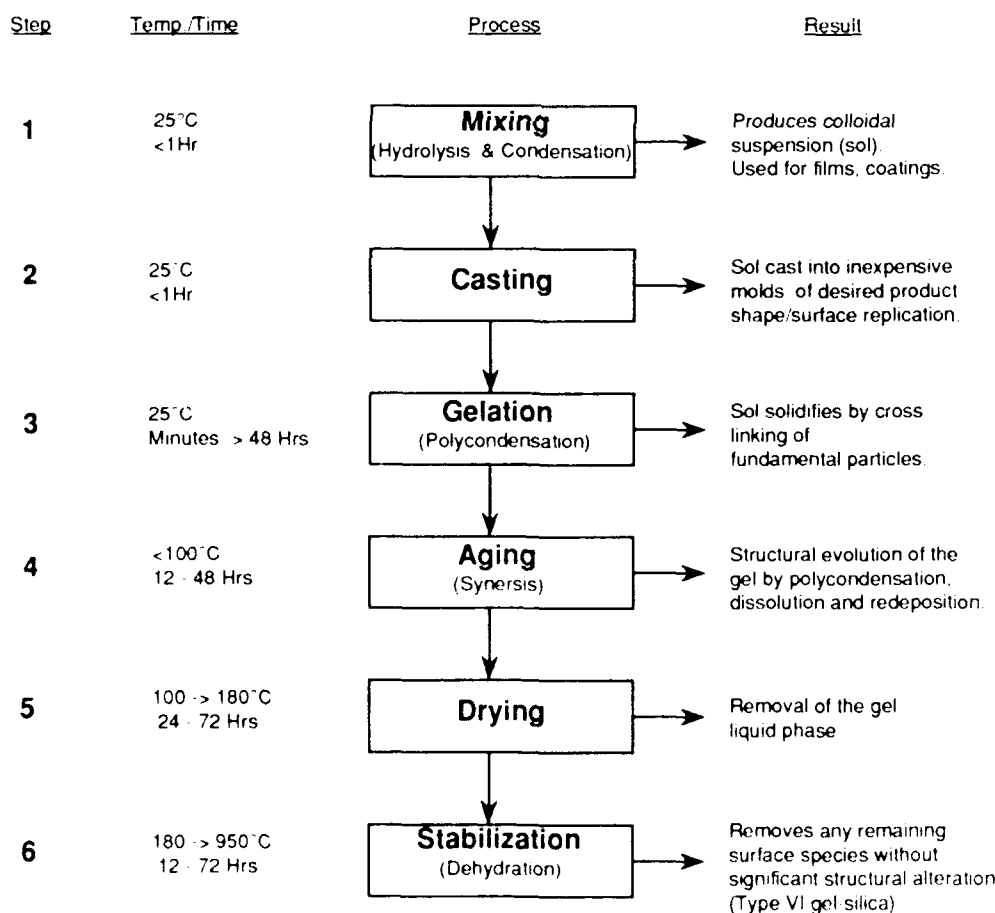


Fig. 1. Sol-gel processing sequence for Type VI ultraporous silica.

A major advantage of the second method is that the gel matrix can be pre-heated to obtain desirable environmental stability and strength prior to impregnation. In most cases, the second phases are organic materials which decompose at relatively low temperatures. Doping of such organic substances at the sol stage, i.e., Method 1, eliminates the possibility of heating the composite materials at high temperatures without losing the useful properties of the organic substances.

Typical steps of the sol-gel processing of Type VI vitreous silica are illustrated in a flow chart in Fig. 1.<sup>2</sup> Careful selection of the catalysts during hydrolysis (mixing) of the alkoxide precursors is essential in controlling the solution chemistry which further controls the average pore size of the rigid gel after drying. It is interesting to note that the subsequent heat treatments of the rigid gel do not change the average pore size much as long as the heating is below a certain temperature ( $<1000^{\circ}\text{C}$ ). By using HF along with  $\text{HNO}_3$  as the catalysts, the average pore radius of the gel changes over a broad range (1.2-10.0 nm).<sup>3,5</sup> Heat treatments, however, do change other pore properties such as the volume fraction of porosity and the surface area of the gel as shown in Fig. 2. Based on these results, the required pore properties can be produced both by controlling the solution chemistry during hydrolysis of the alkoxide and by the subsequent heat treatments.

Thermal stability is an important property when a gel is expected to experience temperature changes in its applications. Wang,<sup>6</sup> Zhu, et al.<sup>7</sup> and Elias<sup>3</sup> studied the thermal stability of porous gel-silica monoliths as a function of processing history. Their work included the processing and characterization of gels with different pore size distributions, and they used dilatometry to identify thermal stability of the gel. A thermal hysteresis loop, which was plotted as the relative length change against the specimen temperature, was obtained after heating and cooling the gel in a dilatometric measurement. The integrated area of the hysteresis loop was used as a parameter to quantify the thermal stability of the specimen. When the area of the loop reaches zero, the gel becomes thermally stable. The area below the curve in Fig. 3 represents a thermally stable region in which the gel does not have any dimensional changes before and after it is heated below a specific temperature and then cooled to room temperature, i.e., in order to use a gel at a certain temperature, this gel has to be heated to a temperature high enough to reach thermal stability.

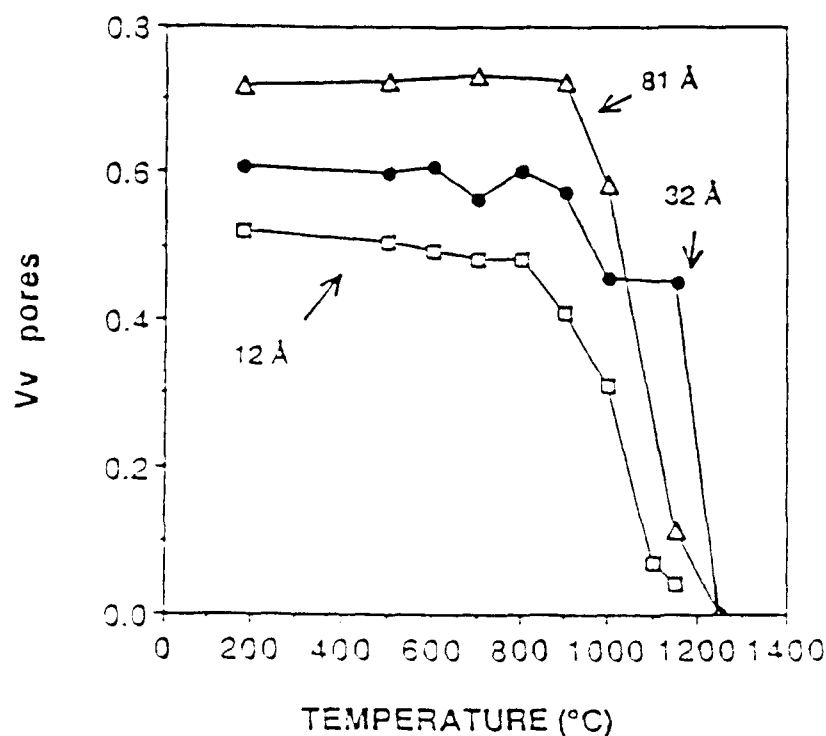


Fig. 2. Variation of volume fraction of porosity ( $V_v$ ) as a function of processing for silica gels with average pore radii of 1.2, 3.2 and 8.1 nm.<sup>5</sup>

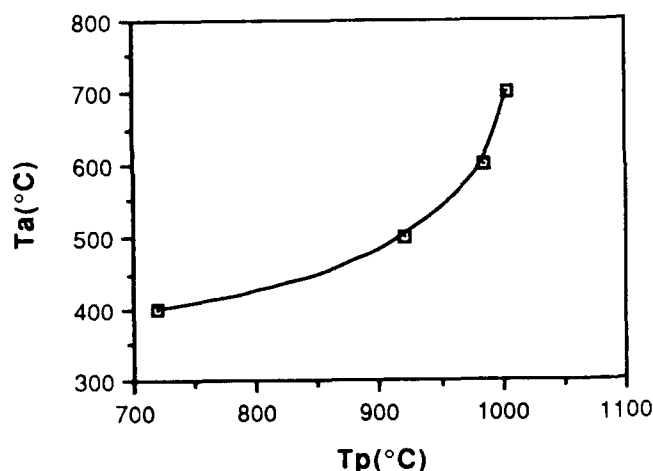


Fig. 3. Application temperature ( $T_a$ ) vs processing temperature ( $T_p$ ) for a gel with 1.2 nm pore radius. The area below the curve corresponds to a thermally stable zone.<sup>6</sup>

Figure 4 is a typical transmittance spectrum for Type VI gel-silica heated to 900-950°C. Because of the very small size of pores (1.2 nm), the material is optically transparent. Chemical stability, mechanical strength and thermal shock resistance are also very important properties for some applications. By heating to 800-900°C for stabilization, the concentration of silanols on the surface of the pore network can be controlled, thereby making the material chemically stable when exposed to an aqueous environment. High mechanical strength and thermal shock resistance ensure that the gel will withstand the stresses which may develop during drying of the gel after impregnation and which may result from the temperature changes in an optical system. These physical characteristics of the gel-silica monoliths are maintained when doped with second phases.

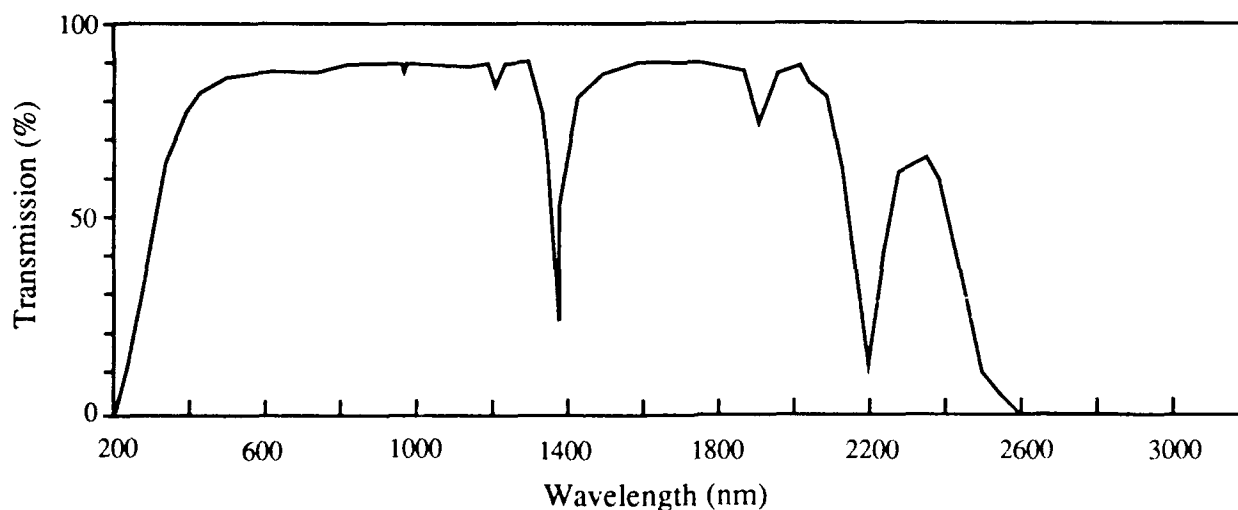


Fig. 4. Typical transmission spectrum of Type VI ultraporous silica heated to 900-950°C.

### 3. HYBRID DYE LASERS

For the last two decades, solid state dye lasers have been studied by a number of scientists worldwide in order to obtain lightweight and storable solid state systems, inexpensive to fabricate and safe to handle.<sup>8-12</sup>

There are several advantages of a solid state dye laser system over a fluid counterpart: (1) a fluid pumping and flow system is eliminated, making it more compact, easy to handle and less expensive to operate; (2) the dye molecules are separated by the pore walls such that dimerization and aggregation can be minimized;

(3) thermal and photo stability are improved since the gel-silica can tolerate heat well above decomposition temperatures of most organic solvents; (4) initial impurities in the dye are isolated and do not interfere by destructive (photo)processes; and (5) the solid cage of the porous matrix reduces internal rotational modes in the dye. Rotational relaxation of the excited state of the dye molecules is one of the main modes of non-radiative energy loss.

In most solid state dye laser systems, inorganic crystals, glasses and polymers are used as host materials or saturable absorbers.<sup>12-14</sup> Recently, porous structures have been used to incorporate dye molecules in the solid state systems.<sup>8,10,15</sup> Type VI gel-silica is superior among these porous structures due to its excellent optical quality, flexibility of controlling the pore size, range of volume fraction of porosity and surface area, high chemical and thermal stability, and high purity and homogeneity. High purity of the gel structure via sol-gel processing gives the dye molecules a better chemical environment. In addition, Type VI gel-silica has high transmittance in a broader spectral region as compared to plastic host media.

In our recent work, rectangular gel-silica specimens of 6 X 6 X 10 mm were stabilized to 800°C for 4 hrs. The ends of the rectangles were polished to 600 grit and are parallel to each other. Other surfaces of the specimens were not polished and were kept in as-cast condition.

The laser dye used in this study, developed by Lee,<sup>16</sup> was 4-{2-(5-phenyl-oxazolyl)} 1-methylpyridinium p-toluenesulfonate (4PyPO-MePTS). This dye is water soluble which is a major advantage in processing, handling, and use of the composite. The dye also has exceptionally high photostability.

Type VI gel-silica monoliths with pore sizes ranging from 1.2 to 11 nm were filled with the dye solution, and tested using methods discussed in another publication.<sup>15</sup> The impregnated gel-silica monoliths exhibited good environmental, chemical and thermal stability.

In brief, the impregnated gel was tested in a single cavity using nitrogen laser pumping at 337.1 nm in a transverse configuration where the rectangular nitrogen laser beam was focused to a line within the specimen. The maximum average power of the system was 50 mW, the maximum energy per pulse, 2.5 mJ, and the pulse duration, 800 ps.

Laser dye solutions were compared with the dye impregnated gel-silica. The samples were pumped by the nitrogen laser beam splitted from the primary laser source in an amplifier stage to increase the population density of the signal. The amplification factors obtained are based upon this single path mode. The particular wavelength was selected through a grating system.

The transmittance spectra from 200 to 900 nm are shown in Fig. 5. The major features of these spectra for 4PyPO-MePTS water solutions and for the dye impregnated gel-silica specimens are an absorption at the region between 300 and 430 nm due to the presence of the dye. Therefore, it is possible to use a nitrogen laser at 337.1 nm as the primary source for pumping. The high transmittance of the gel matrix throughout the whole spectral region indicates that this is an ideal host material for the impregnated optical devices.

Figure 6 shows the fluorescence spectra at 509.5 nm for the dye laser specimens under different test conditions. In these experiments, the dye solution was compared with the dye impregnated gel-silica. As shown in Fig. 6, the dye solution pair have the highest intensity (43) as compared to 32 for the solution/gel-silica pair. However a gain of 23 was observed after amplification with a single pass of the laser beam at 509.5 nm through the dye gel-silica sample. A much higher gain is expected when the ends of the rectangular gel specimen are optically smooth and parallel to each other.

---

\*Aldrich Chemical Company, Inc., Milwaukee, Wisconsin.

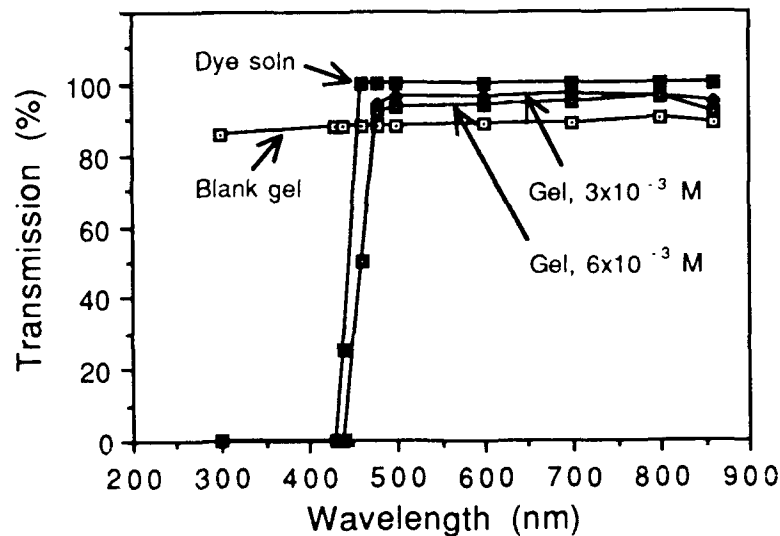


Fig. 5. Transmission spectra of (1) 4PyPO-MePTS solutions in either  $3 \times 10^{-3}$  M or  $6 \times 10^{-3}$  M; and (2) the 4PyPO-MePTS impregnated gels. Two dye concentrations were used in impregnation.

### Fluorescence Spectra at 509.5 nm

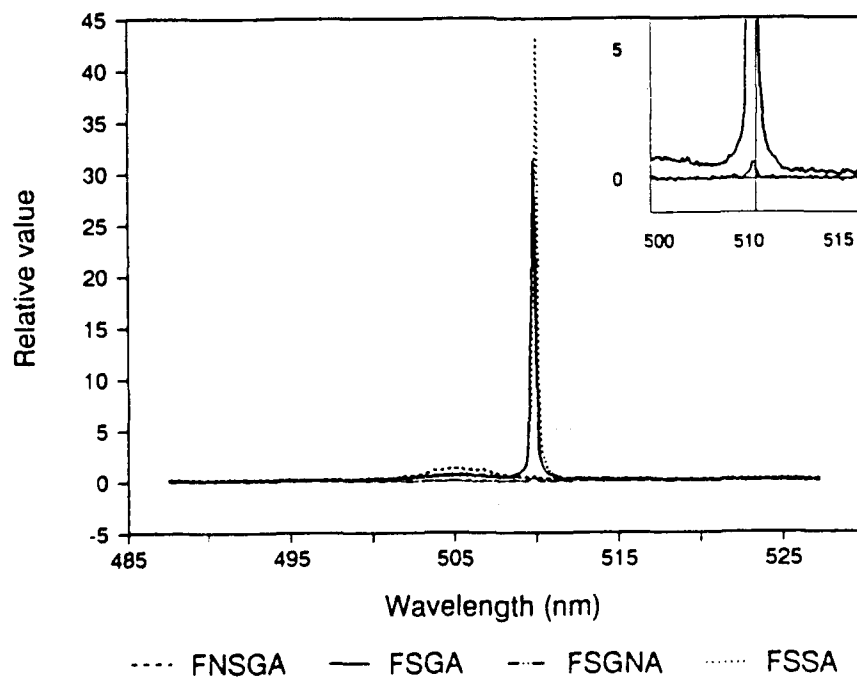


Fig. 6. Fluorescence spectra at 509.5 nm of (1) 4PyPO-MePTS impregnated gel with the amplifier (FNSGA); (2) the dye solution and the impregnated gel with the amplifier (FSGA); (3) same as in (2) but without the amplifier (FSGNA); and (4) two dye solutions with the amplifier (FSSA).



Figure 7 compares the tuning curve for 4PyPO-MePTS or R6G impregnated gel-silica over the blue-green spectral region with the corresponding dye solution. The relative energy of the laser output for 4PyPO-MePTS water solution shows a maximum at 510 nm (curve 1). This result is consistent with Contnoir's data<sup>17</sup> where he also used water as the solvent. The maximum of the power output for the 4PyPO-MePTS impregnated gel-silica appears almost at the same wavelength (curve 2). By using a grating system, however, the signal intensity of this solid state sample shows a maximum at a slightly shorter wavelength (505 nm, curve 3). In contrast, the tuning peak of the R6G impregnated gel-silica shifted to longer wavelength compared to the dye solution (curves 4 and 5). The similarity among these cases is that the tuning ranges of the dye solutions are wider than their solid state counterparts (Fig. 7 and Table 1).

The spectroscopic properties of both liquid and solid state 4PyPO-MePTS and R6G dye lasers developed by Berry and King<sup>18</sup> using the same Type VI gel-silica host matrices are summarized in Table 1. With R6G, two kinds of host materials are compared including Type VI sol-gel derived silica and microporous quartz glass (MQG), which is a leached sodium boro-silicate glass. The gel-silica used in this study has a higher volume fraction of porosity (0.5) and smaller average pore radius (1.2 nm) as compared to MQG with <0.25 volume fraction of pores and 3-4 nm in the average pore radius. The maximum of the fluorescence spectra reported by Avnir, et al.<sup>10</sup> and Berry and King<sup>18</sup> are very close to each other. However, Efendiev, et al.'s fluorescence spectrum shows a maximum located at lower wavelength along with a lower value of the volume fraction of porosity of the glass matrix.<sup>8</sup> With 4PyPO-MePTS, the peak shifted to a lower wavelength for the solid state dye laser compared to that for the solution case.

#### 4. SCINTILLATORS AND WAVELENGTH SHIFTERS

Fast radiation hard scintillators have been developed by Noguès, et al.<sup>19</sup> using Type VI gel-silica as the matrix with a 1.2 nm average pore radius and 0.35 volume fraction of porosity to host organic fluors such as B-PBD, P-TP and P-QP. The silica matrix provides high  $\gamma$ -ray radiation resistance compared to the organic plastic scintillators and the organic fluor provides fast scintillation response. Both properties are advantageous for high-speed counting necessary for high-energy physics applications.

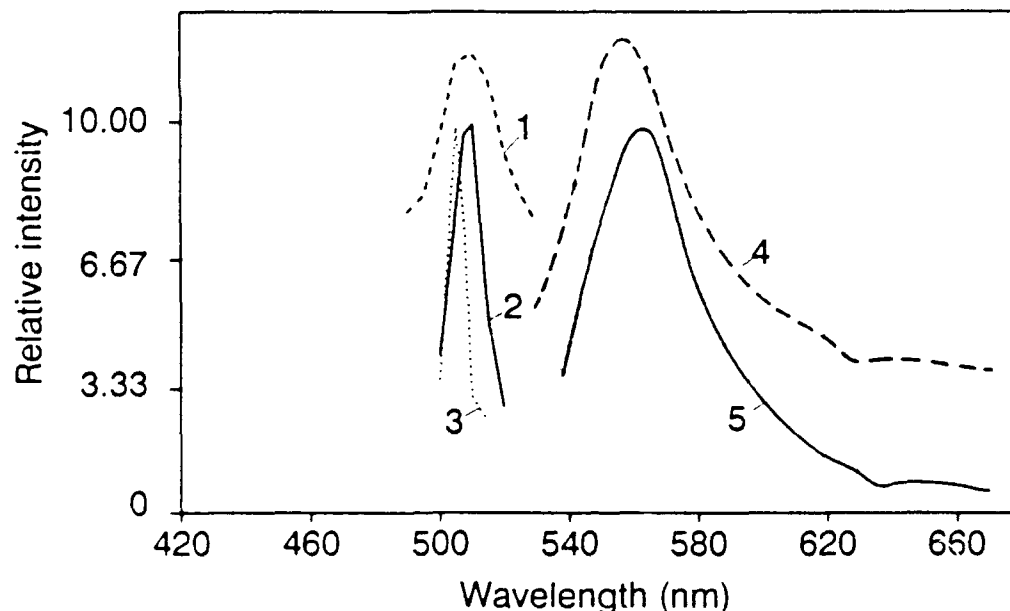


Fig 7. Tuning curves of the 4PyPO-MePTS or R6G impregnated gel-silica and the dye solutions 1-4PyPO-MePTS water solution; 2-4PyPO-MePTS impregnated gel-silica with data from the total energy output; 3-4PyPO-MePTS impregnated gel-silica with data after grating; 4- R6G water solution;<sup>10</sup> and 5-R6G impregnated gel-silica.<sup>10</sup>

Table 1. Summary of spectroscopic properties of selected dyes  
--liquid versus solid host

<u>Dye</u>	<u>Solvent/solid host</u>	<u>Tuning range</u> (nm)	<u>max</u> (nm)	<u>Reference</u>
4PyPO-MePTS	H <sub>2</sub> O	40	508.8	17
	Gel-silica*	15	505.0	This work
R6G	H <sub>2</sub> O	80	553.4	10
	Silica gel	70	558.6	10
	Methanol	--	294.6	18
	Gel-silica	--	559.6	18
	Ethanol	--	560.1	8
	MQG**	--	545.4	8

\* For gel-silica, the average pore radius is 1.2 nm and the volume fraction of porosity is 0.5.

\*\*For MQG, the average pore radius is 3-4 nm and the volume fraction of porosity is 0.23-0.25.

The problem encountered with B-PBD, P-TP and P-QP is that their fluorescence spectra typically peaks at wavelengths below 400 nm at which the gel matrix has certain absorption. To solve this problem, Noguès, et al.<sup>19</sup> used 3-HF as a wavelength shifter to absorb the <400 nm radiation of the primary fluor and to re-emit in wavelengths of  $\approx$  500-600 nm. These wavelengths are advantageous as they are less absorbing in glass than the shorter wavelengths and also result in high quantum efficiency for silicon photodiodes. When analyzed for scintillation efficiency with  $\alpha$ -,  $\beta$ -, and  $\gamma$ -ray sources, the light output was reported to be only 6-7 times lower than the much more highly developed plastic scintillators.

## 5. TRANSPIRATION COOLED WINDOWS

A novel use of sol-gel derived porous Type VI silica monoliths for high performance rocket guidance system windows was demonstrated by Fosmoe and Hench.<sup>20</sup> Their results show that UV transmission is maintained at temperatures above 1000°C and that transpiration flow is possible through optically transparent porous gel monoliths. Samples with average pore radius in the low mesopore range, approximately 5.0 nm, were evaluated in an attempt to increase transpiration velocities to well above 1 cm/sec needed for transpiration cooling.<sup>21</sup>

The shock wave preceding a rocket under high mach conditions involves an intense thermal boundary next to the exterior surface of the rocket.<sup>22</sup> If this exterior surface is an optical transmission window with a temperature dependent bandpass, the increased temperature resulting from the radiant and conductive heat from this boundary layer to the window will dramatically affect its optical throughput. Radiant transfer can be decreased with a reflective surface. Such a reflective surface will not, however, reduce the large amount of heat transferred by conduction. A very effective method for lowering the conduction is transpiration cooling. This is a flow of fluid, in this case, a gas, through a porous exterior surface which effectively reduces the boundary layer temperature gradient with respect to distance from the surface. This lowers the conduction transfer rate. Transpiration velocities as low as 1 cm/sec lead to a significant cooling effect. Higher transpiration velocities bring more significant results.

Maximum He transpiration cooling at velocities up to 3 cm/sec was measured for a 5.0 nm sample at 3.2 MPa. Transpiration velocities of only 0.6 cm/sec result in cooling effects as large as 44°C from 160°C.<sup>20</sup>

It is apparent from Fosmoe and Hench's work<sup>20</sup> that the permeability of the porous gels to He flow is quite high. The Reynold numbers calculated in their study are on the order of  $10^{-7}$  at low pressures to  $10^{-3}$  at high pressures. These values indicate that the flow is laminar in nature. It appears that for the most part there is an incompressible laminar flow through a highly porous consolidated medium which can be treated as a continuum. It is expected that the flow rate will increase in proportion to the pressure gradient across the sample. Additional studies are in progress to determine the effects on the thermal boundary under conditions closer to practical applications.

## 6. LASER WRITTEN WAVEGUIDES

In 1988, Ramaswamy et al.<sup>23</sup> reported for the first time the fabrication of waveguiding regions in porous gel-silica by laser induced heating. Sol-gel optical waveguides with tracks of higher refractive indexes,  $\approx 40$  by  $15 \mu\text{m}$  in dimension, were produced by scanning the substrate gel glass with a focused  $\text{CO}_2$  laser beam pulsed with variable duty cycles to permit controlled variation on the average power. As the gel surface densifies under local heating, the surface refractive index increases producing tracks allowing the light to be guided. An obvious advantage of laser densification is that this process is amenable to automation and does not require photolithography.

A year later, Shaw et al.<sup>24</sup> confirmed the results of controlled densification of silica gels using a continuous wave  $\text{CO}_2$  laser at  $10.6 \mu\text{m}$  and with a  $193 \text{ nm}$  ArF excimer laser radiation. They pointed out that the threshold for permanent densification by  $10.6 \mu\text{m}$  radiation on the partially densified sol-gel derived glass is  $4.6 \text{ J/cm}^2$  and that for optical damage the threshold is  $6.3 \text{ J/cm}^2$ .

Figure 8 shows the variation of the refractive index as a function of the degree of densification of Type VI gel-silica substrates. In gel-silica glasses, the higher the densification temperature and the longer the holding time, the greater the degree of densification. Full densification occurs around  $1150^\circ\text{C}$  where the refractive index reaches 1.465.

By radiating the surface with the  $10.6 \mu\text{m}$  laser beam, an increase in the refractive index occurs in the exposed region of the gel substrate. The magnitude and spatial definition can be controlled by an appropriate choice of average laser power and the beam profile.

The index change,  $\delta n$ , is determined by measuring the refractivity off the center of the waveguiding region. Using the samples densified at  $900^\circ\text{C}$  for 12 hours with 71% densification, typical values of 0.06 for  $\delta n$  were obtained using  $\text{CO}_2$  laser treatment. It is obvious that this technique is capable of fabricating waveguides with complex patterns by controlled scanning of a focused laser beam and is amenable to automation since the index change can be monitored during the process. However, single mode waveguide fabrication will require use of excimer laser radiation to achieve the required dimensions of the densified tracks.

More recently, a transient model for heat conduction in a silica gel was proposed to simulate three dimensional temperature distribution in the gel irradiated by a moving  $\text{CO}_2$  laser.<sup>25</sup> Both the refractivity of the gel surface and the strong attenuation of the laser energy in the gel medium are accounted for by a detailed radiation analysis. The energy absorbed by the gel was found to be confined in a  $10 \mu\text{m}$  thickness. The laser irradiation was treated as a boundary condition. The heat diffusion equation was solved by an alternating-direction-implicit method. Parameters tested in this study encompass the laser power and moving speed, the heat transfer coefficient and the thermal diffusivity of the gel medium.

The significance of this modeling<sup>25</sup> is that it provides an analytical basis for the thermal effect of laser densification on a gel-derived silica glass. The properties of the gel glass are known to be strongly related to its processing temperature and the resulting ultrastructure. The results presented in this work permit a prediction of the change in the glass properties with temperature.

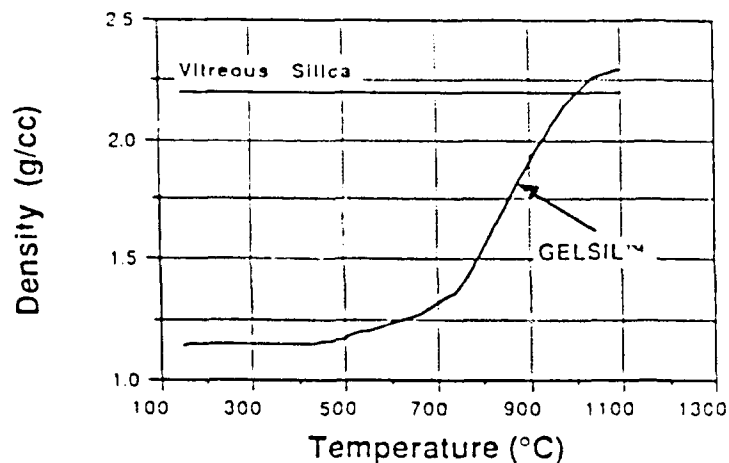
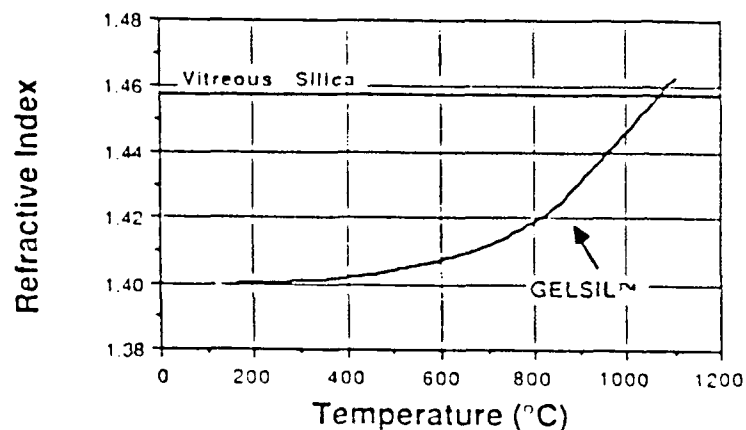


Fig. 8. Variation of density and refractive index as a function of densification temperature for a Type VI silica gel.



## 7. SUMMARY

Sol-gel processing has resulted in two new kinds of silica optics, Type V fully dense silica and Type VI optical transparent ultraporous silica. Type VI gel-silica is ideal for precision transmissive optics with very high transmission throughout the VUV, UV, Vis, and NIR. Type VI gel-silica is an ideal matrix for impregnation with second phases that are optically active. The flexibility of controlling the volume fraction of porosity, average pore radius and the surface area over a broad range, by solution chemistry at the early stage of processing and subsequent heat treatments, makes this an unique material for hybrid optical components. It is possible to cool the optics by transpiration cooling; to impregnate organic polymers into the matrices to produce new optical devices such as scintillators and wavelength shifters, and solid state dye lasers. It is also possible to fabricate waveguides by localized heating using a laser beam. Additional applications are expected in the near future.

## 8. ACKNOWLEDGEMENTS

The authors are grateful for the financial support of the Air Force Office of Scientific Research under contract #F49620-88-C-0073 and the encouragement of D. R. Ulrich throughout this research.

## 9. REFERENCES

1. L. L. Hench, S. H. Wang and J. L. Noguès, SPIE, 877, 76 Multifunctional Materials, 1988.
2. L. L. Hench and J. K. West, Chem. Rev., 90, pp. 33-72, 1990.
3. E. Elias, Masters Thesis, University of Florida, 1989.
4. B. F. Zhu, G. F. Wang and L. L. Hench, the 4th Ultrastructure Conference, Tucson, AZ, 1989.
5. W. Vasconcelos, Ph.D. Thesis, University of Florida, 1989.
6. G. F. Wang, Masters Thesis, University of Florida, 1988.
7. B. F. Zhu, G. F. Wang, J. K. West and L. L. Hench, to be published.
8. T. S. Efendiev, Y. V. Kostennich and A. N. Rubinov, Appl. Phys. B33, 167, 1984.
9. O. G. Peterson and B. B. Snavely, Appl. Phys. Lett., 12, 238, 1968.
10. D. Avnir, D. Levy and R. Reisfeld, J. Phys. Chem., 88, 5956, 1984.
11. G. B. Altshuler, V. Bakhanov, E. G. Dulneva and J. K. Meshkovskii, Opt. Spektrosk., 55, 369, 1983.
12. S. Muto, A. Ando, O Yoda, T. Hanawa and H. Ito, Trans. IECE, Japan E70 317, 1987.
13. H. Wang and L. Gampel, Opt. Commun. 18, 444, 1976.
14. V. Danilov, A. Eremenko, S. Lan'kova, D. Savel'ev and A. Stepanov, Bull. of the Academy of Sciences of USSR (Physics Series), 47, 86, 1983.
15. B. F. Zhu, R. Ochoa, and L. L. Hench, to be published.
16. L. A. Lee and R. A. Robb, IEEE J. Quantum Electronics, QE-16, 7, 777, 1980.
17. L. J. Cotnoir, Appl. Opt., 20, 2332, 1981.
18. A. J. Berry and T. A. King, private communication.
- 19a. J. L. Nogués, S. Majewski, J. K. Walker, M. Bowen, R. Wojcik, and W. V. Moreshead, J. Am. Ceram. Soc., 71 (12), pp. 1159-1163, 1988.
- 19b. J. L. Nogués, C. Balaban, W. V. Moreshead and R. S. Sheu, Advanced Ceramics, eds. WP. E. Longo, S. N. Monteiro and J. D. Filho (Florida-Brazil Institute, Rio de Janeiro, p. 51, 1989.
- 20a. L. L. Hench and A. G. Fosmoe, II, 1989 MRS Fall Meeting in Boston, Mass.
- 20b. A. G. Fosmoe II and L. L. Hench, 1990 MRS Spring Meeting in San Francisco, CA.
21. U. Kurzweg, private communication.
22. J. D. Anderson, Introduction to Flight, 3rd ed., McGraw-Hill, New York, 1989, p. 125.
23. R. V. Ramaswamy, T. Chia, R. Srivastava, A. Miliou and J. K. West, SPIE, 878, 86, Multifunctional Materials, 1988.
24. D. J. Shaw, A. J. Berry and T. A. King, private communication.
25. T. Chia, L. L. Hench, C. Qin and C. K. Hsieh, 1990 MRS Spring Meeting in San Francisco, CA.



## PMMA - Impregnated Silica Gels: Synthesis and Characterization

R. Abramoff\* and L. C. Klein

Rutgers-The State University of New Jersey  
Ceramics Department  
P.O. Box 909  
Piscataway, NJ 08855-0909

ABSTRACT

Shaped microporous silica has been prepared by a sol-gel process. The resulting silicas have 50% open porosity. The open porosity is filled by immersing the shapes in methyl methacrylate (MMA) and polymerizing with ultraviolet radiation. The fully impregnated silica is recovered in net shape.

The outstanding feature of the PMMA-impregnated silica is its transparency. There is little loss from scattering because of the nanometer scale of the microstructure and the similarity in index of refraction for silica and PMMA. The flexure strength of the silica-PMMA composite has been measured in 4-point bending. The strength increases at slower strain rates because the PMMA provides crack blunting. The composites can withstand thermal shocks up to about 150°C without losing strength. The thermal expansion coefficient for the range 0 to 150°C follows a mixing rule for 50% silica - 50% PMMA. While the mechanical behavior of the composite largely follows that of bulk PMMA, the microhardness is 3 to 5 times greater than for bulk PMMA.

1.0 INTRODUCTION

The sol-gel process has produced in recent years a number of interesting optical materials in both bulk<sup>1</sup> and fiber<sup>2</sup> form. The sol-gel process has also been used for optical waveguides on glass substrates.<sup>3</sup> Another class of optical materials which uses the sol-gel process to prepare a microporous host is the class of gels doped with organic dyes. The organic molecules incorporated into gels include fluorescent dyes, laser dyes and non-linear optics. The inorganic hosts include alumina,<sup>4</sup> titania-silica,<sup>5</sup> aluminosilicates,<sup>6</sup> zeolites,<sup>7</sup> though primarily the host has been silica.<sup>8,9</sup> In all of these cases, the host material needs to be transparent. In addition the host material must be environmentally stable.

It has been found that silica gels are environmentally stable when impregnated with PMMA (polymethyl methacrylate)<sup>10,11,12,13</sup> and that the impregnated gels are also suitable hosts for organic molecules.<sup>9,14</sup> In most of these studies,<sup>11,12,13</sup> monolithic silica gels were infiltrated with MMA (monomer) following processing that involved catalysis with HF and firing to 800°C. After this treatment, the xerogels were 33% porous and had a median pore diameter of 10 nm. The porosity was infiltrated with monomer solution which polymerized in-situ. The resulting composites

---

\*Present Address: Code 3891, Naval Weapons Center, China Lake, CA 93555

92-11424



92 4 28 042

consisted of two fully percolating phases, a silica matrix and an organic polymer impregnant. Silica/PMMA composites were used to encapsulate electro-optically active organic compounds such as 2-methyl-4-nitroaniline (MNA). Electro-optical DC Kerr Effect and solid state deuteron NMR measurements were made.<sup>14</sup> In a comparison to conventional optical cells, silica/PMMA composites were found to have better optical quality and retained dimensional stability to about 90°C. The composites were abrasion resistant and could be machined to complex shapes.

While the process described here is an interesting one for optical cells, it may also be a practical process for large scale windows once the process is simplified. When comparing sol-gel optics with conventional silica optics, the sol-gel process can hardly do better than duplicate the properties of conventional silica. However, when comparing silica/PMMA composites with bulk PMMA (Plexiglass<sup>TM</sup>), the composite can have better properties in terms of resistance to rain erosion, solvent crazing and weathering. Improvements in these properties have not been quantified, but qualitatively it is safe to say that the composites do not suffer from loss of transparency under conditions where PMMA does.

The objective of this study is to synthesize a silica/PMMA composite in the simplest way possible. Knowing that MMA readily adsorbs on acidic silica surfaces,<sup>15</sup> even silica gels without high temperature treatment are expected to fill with MMA. Once silica/PMMA composites are fully impregnated and rigid, mechanical, thermal and optical properties can be evaluated and the environmental stability can be assessed.

## 2.0 SYNTHESIS

Silica gels were prepared from a solution of tetraethylorthosilicate (TEOS), distilled deionized water and ethanol. Equal volumes of distilled TEOS and ethanol were used. The molar ratio of water: TEOS was 16.<sup>16</sup> The solution was catalyzed with 0.1 M HNO<sub>3</sub> and was stirred for 30 minutes. Ten ml of the solution were poured into polystyrene tubes and capped. The solutions gelled while in an oven for 7 days at 50°C, followed by 10 days at 70°C. The tubes then were uncapped and samples were dried in lots of 100 at 50°C for 14 days. Xerogels were removed from the tubes and dried 2 more days at 50°C. Finally, the gels were outgassed 24 hours at 250°C to remove physically adsorbed species.

A monomer solution of 1 g benzoyl peroxide (97%) catalyst per 100 ml MMA (methylmethacrylate, inhibited) was prepared (Aldrich Chemicals, Milwaukee, WI). After outgassing, each xerogel was immersed immediately in a borosilicate vial containing 11 ml of monomer solution (Figure 1a). The solution was allowed to infiltrate for 2 hours and then the sealed vials were subjected to 7 days of longwave UV illumination (Figure 1b) with a UV intensity of about 2000 micro W/cm<sup>2</sup>. Once the PMMA was polymerized, the vials were cracked off and the PMMA surrounded silica gels were treated at 200°C in a mechanical convection oven for 30 minutes (Figure 1c). This is a temperature about 100° above the glass transition temperature of bulk PMMA and is also high enough to promote a moderate rate of depolymerization. This treatment turned the thick PMMA shell rubbery so that it could be peeled off by hand to recover net shape PMMA/silica gel composites (Figure 1d).

As Figure 1 is intended to show, the samples are roughly cylindrical. The diameter at the center of the composites is 5.60 mm and the length is about 33 mm.

According to nitrogen sorption analysis of the outgassed silica before infiltration, the surface area of the matrix is  $900 \text{ m}^2/\text{g}$ , and the porosity is almost completely microporous (less than  $2.0 \text{ nm}$  in diameter) and cylindrical in shape. The skeletal density is about  $2.27 \text{ g/cm}^3$ , and the open porosity is 52.5%. Following infiltration and polymerization, the composite is close to theoretical density calculated by a mixing rule. The total weight gain during infiltration followed by polymerization is 50%. The density of the composite is  $1.60 \text{ g/cm}^3$ .

### 3.0 TRANSPARENCY

Optical transmission was measured on a Perkin-Elmer Lambda 9 UV-VIS-NIR spectrophotometer. Rods of outgassed silica xerogel, silica-PMMA composite, and PMMA of  $10 \text{ mm}$  length were cut or ground to length on a diamond saw, briefly hand ground dry on 600 grit abrasive paper, and polished with 1 micron diamond paste. Samples were mounted on a mask with a  $4 \text{ mm}$  aperture and the reference beam was obscured by a similar mask. Scan parameters included a slit width of  $2 \text{ nm}$ , a scan speed of  $480 \text{ nm/min}$ , and a response time of  $0.5 \text{ sec}$ . Automatic background correction was employed. The transmission curves were recorded and compared to see any changes in transparency.

The silica gel, PMMA and the composite were largely transparent over the range  $380\text{--}800 \text{ nm}$ . The transmission curves are shown in Figure 2. Transmission is highest in PMMA alone. Lower transmission is seen in the silica gel which may be the result of scattering from a few large pores. The transmission for the composite is nearly identical to the transmission for silica gel despite the difference in handbook values for index of refraction,  $1.46$  for silica and  $1.49$  for PMMA.

### 4.0 MECHANICAL PROPERTIES: STRENGTH AND MICROHARDNESS

Strength measurements were made by the four point flexure technique. The flexure fixture had a support span of  $2.540 \text{ cm}$  ( $1.000''$ ) and a load span of  $1.270 \text{ cm}$  ( $0.500''$ ). A gear driven Instron materials testing machine with a  $1000 \text{ lb}$  load cell was used. Crosshead speeds were between  $.05 \text{ cm/min}$  ( $0.02''/\text{min}$ ) and  $5.08 \text{ cm/min}$  ( $2.0''/\text{min}$ ). A rapid strain rate was necessary to prevent plastic deformation in bulk PMMA. Composite samples were measured after exposure to ambient conditions. Water adsorption in composites corresponded to an increase in weight of  $1.8\%$  while in PMMA it was only on the order of  $.1\%$ . Sample test sets numbered 20 for silica/PMMA composites and PMMA.

Table 1 lists the strengths of silica-PMMA composites at the various strain rates. The distributions of Table 1 are illustrated in Figure 3. The strength distributions are represented by a two parameter Weibull analysis.<sup>17</sup> At the highest strain rate estimated to be  $3 \times 10^{-2}/\text{sec}$ , composites had a mean strength of about  $30 \text{ MPa}$ . Upon decreasing the strain rate by one decade, to  $3 \times 10^{-3}/\text{sec}$ , the mean strength increased to about  $100 \text{ MPa}$ . Strength then remained about the same as strain rate was twice again decreased by one decade. The dramatic increase in flexure strength upon decrease of strain rate from  $3 \times 10^{-2}/\text{sec}$  to  $3 \times 10^{-3}/\text{sec}$ , likely is due to the "brittle-ductile" transition of the polymer phase.<sup>18</sup> In polymers, both brittle and ductile fracture involve plastic deformation. In thermoplastics such as PMMA, brittle fracture is characterized by localized crazing and localized volume increase. Ductile behavior is characterized by constant volume



shear yielding in the bulk and also by crack tip blunting. The brittle and ductile mechanisms are competitive but not mutually exclusive.

The apparent brittle-ductile transition of the silica-PMMA composite results in higher strength for the composites at low and moderate strain rates. The reason for this may be crack blunting and shear yielding of the PMMA, which reduces the stress at the crack tip, thereby increasing flexure strength. In comparison, pure PMMA had a mean strength of about 120 MPa when PMMA was measured at the highest strain rate. At this strain rate of  $3 \times 10^{-2}$ /sec, bulk plastic deformation was avoided. However, PMMA rods fractured at a strain rate of  $3 \times 10^{-4}$ /sec were observed to be permanently bent. The strengthening mechanism for the PMMA in the composite is no longer evident when strengths were measured at 100°C. Apparently, the decrease in stiffness of the MMA at elevated temperature diminishes its ability to provide crack blunting.

Vickers hardness was measured on a Zwick 3212.00 hardness tester. Test parameters included an impact speed of 0.3 mm/sec, an indent time of 30 sec, and a load of 1.0 kg. All samples were left in rod shape and were rested on a V-block. The values as determined by the Zwick computer were corrected for cylindrical surfaces. The number of samples per test was 10 and each sample was indented once.

Table 2 summarizes the results of hardness tests. Bulk PMMA exhibited the lowest hardness. Porous xerogels were more than twice as hard as PMMA. The silica-PMMA composites were by far the hardest.

Table 1: Strengths of Silica-PMMA Composites vs Strain Rate

Strain Rate (sec <sup>-1</sup> )	Strength (MPa)	Weibull Parameter m	R <sup>2</sup>
3 x 10 <sup>-2</sup>	34 +/-2	3.2	.94
3 x 10 <sup>-3</sup>	96 +/-5	4.6	.95
3 x 10 <sup>-4</sup>	99 +/-5	4.7	.96
3 x 10 <sup>-5</sup>	93 +/-5	4.4	.97

Table 2: Vicker's Hardness

Material	Vicker's Hardness (MPa)
PMMA	152 +/- 1
Silica Xerogel, exposed	355 +/- 3
Silica Xerogel, fresh	413 +/- 2
Silica-PMMA composite, exposed	881 +/-11
Silica-PMMA composite, fresh	988 +/- 8

## 5.0 THERMOMECHANICAL PROPERTIES: THERMAL SHOCK AND THERMAL EXPANSION

The resistance of PMMA-silica composites to thermal shock damage was evaluated qualitatively and quantitatively. Samples were heated in a mechanical convection oven and then quenched in ice-water to give shocks corresponding to between 75 and 200°C. The frequency of damage visible to the naked eye was then recorded and flexure strength was measured at a crosshead speed of 0.0508 cm/min (0.02"/min). Damage was observed with the unaided eye at a temperature difference of 90°C or greater. At a temperature difference of 150°C and above, all samples appeared damaged. The damage was in the form of cracks that extended throughout the bulk of the sample. The number of cracks observed increased with increasing temperature difference, though all samples retained their overall shape. The mean flexure strengths for each set of 5 samples is plotted on Figure 4 vs temperature difference. Strength dropped sharply for a temperature difference of 150°C or greater. In total, 24 of the 50 samples survived the ice water quench test without visible damage.

Thermal analysis was performed on the Perkin-Elmer Series 7 Thermal Analysis System. A heating rate of 10°C was used in all tests and temperature was varied from -25 to 200°C. Coefficient of thermal expansion was calculated by the Perkin-Elmer software. Thermal mechanical analysis in flowing helium was performed on 7 mm long rods of silica-PMMA composite. A probe load of 100 mN was used.

The trace is shown in Figure 5. The mean thermal expansion coefficient is  $3.6 \times 10^{-5}/^{\circ}\text{C}$ , where the expansion coefficient for bulk silica is  $5 \times 10^{-7}$  and that for bulk PMMA is  $7 \times 10^{-5}$ . The composite was cycled without any apparent damage.

## 6.0 SUMMARY

In summary, the synthesis of silica-PMMA composites has been simplified and carried out in large quantities. The benefit of the PMMA impregnant on the silica xerogel is to render it less sensitive to moisture. The improvement of environmental stability by PMMA impregnation is quite evident even before intentional application of stress. While porous xerogels typically exhibit limited shelf life due to the stresses caused by adsorption and desorption of water, composites in the open remain intact even after years of exposure. Only composites that are intentionally scratched exhibit a shelf life short enough to be observed.

The mechanical properties, flexure strengths and hardness have been evaluated. Overall, the mechanical behavior of the composite is more like that of bulk PMMA than bulk silica except that the hardness is much higher than bulk PMMA. The thermomechanical properties have been evaluated. Despite a large thermal expansion mismatch, the composite expanded and contracted without disruption. The maximum exposure temperature for the composite is recommended to be no higher than about 100°C for extended periods of time. Preferably, the composite would only see service at room temperature to -50°C. Finally, the composite material is transparent in the visible range so its use as a window is conceivable.

## 7.0 ACKNOWLEDGEMENT

The financial support of the Office of Naval Research under Contract N00014-87-K-0529 is greatly appreciated.

## 8.0 REFERENCES

1. L. L. Hench, S. H. Wang, J. L. Nogués, "Gel-silica optics," SPIE 878, 76-85 (1988).
2. K. Kamiya, T. Yoko, H. Suzuki, "Hydrolysis-condensation reaction of tetraethyl orthosilicate (TEOS) for glass fiber-drawing," J. Non-Cryst. Solids 93, 407-414 (1987).
3. R. V. Ramaswamy, T. Chia, R. Srivastava, A. Miliou and J. West, "Gel silica waveguides," SPIE 878 86-93 (1988).
4. Y. Kobayashi, Y. Imai, Y. Kurokawa, "Preparation of transparent alumina film doped with organic dye by the sol-gel process," J. Mat. Sci. Lett., 7 1148-1150 (1988).
5. D. Avnir, V. Kaufman, R. Reisfeld, "Organic fluorescent dyes trapped in silica and silica-titania thin films by the sol-gel method. Photophysical, film and cage properties," J. Non-Cryst. Solids 74 395-406 (1985).
6. J. C. Pouxviel, B. Dunn and J. I. Zink, "Fluorescence study of aluminosilicate sols and gels doped with hydroxy trisulfonated pyrene," J. Phys. Chem. 93 2134-2139 (1989).
7. S. D. Cox, T. E. Gier, G. D. Stucky and J. Bierlein, "Inclusion tuning of nonlinear optical materials: Switching the SHG of p-nitroaniline and z-methyl-p-nitroaniline with molecular sieve hosts," J. Am. Chem. Soc. 110 2986-2987 (1988).
8. H. Nasu and J. D. Mackenzie, "Nonlinear optical properties of glasses and glass-or gel-based composites," Optical Engineering 26 102-106 (1987).
9. E. J. A. Pope and J. D. Mackenzie, "Incorporation of organic dyes in polymer/oxide composites," MRS Bull. 12 March/May, 29-31 (1987).
10. B. Abramoff and L. C. Klein, "Mechanical behavior of PMMA-impregnated silica gels," 4th Int. Ultrastructure Conference, Tucson, AZ, February 19-24, 1989.
11. E. J. A. Pope and J. D. Mackenzie, "Oxide non-oxide composites by sol-gel," in Better Ceramics through Chemistry II, C. J. Brinker, D. E. Clark, and D. R. Ulrich, Materials Research Society, Pittsburgh, PA 73 809-814 (1986).
12. E. J. A. Pope and J. D. Mackenzie, "Novel composite materials for space structures and systems," 32nd International SAMPE Symposium, 760-771 (1987).
13. E. J. A. Pope, M. Asami and J. D. Mackenzie, "Transparent silica gel-PMMA composites," J. Mater. Res., 4 1018-1026 (1989).
14. T. M. Che, R. V. Carney, G. Khanarian, R. A. Keosian, and M. Borzo, "Electro-optical DC Kerr effects and solid state deuteron NMR studies of stable gel-derived glass-organic polymer composites," J. Non-Cryst. Solids, 102 280-287 (1988).
15. D. L. Allara, Z. Wang and C. G. Pantano, "Characterization of organic adsorbates on model glass surfaces," J. Non-Cryst. Solids 120 93-101 (1990).
16. L. C. Klein, T. A. Gallo and G. J. Garvey, "Densification of monolithic xero-gels below 1000°C," J. Non-Cryst. Solids 63 23-33 (1984).
17. S. B. Batdorf, "Fundamentals of the statistical theory of fracture," Fracture Mechanics of Ceramics: Vol. 3, Flaws and Testing, eds. R. C. Bradt, D. P. H. Hasselman, and F. F. Lange, Plenum Press, New York, 1978, pp. 1-30.
18. A. J. Kinloch and R. J. Young, Fracture Behavior of Polymers, Applied Science, Essex, 1983, pp. 33-36, 107, 139.

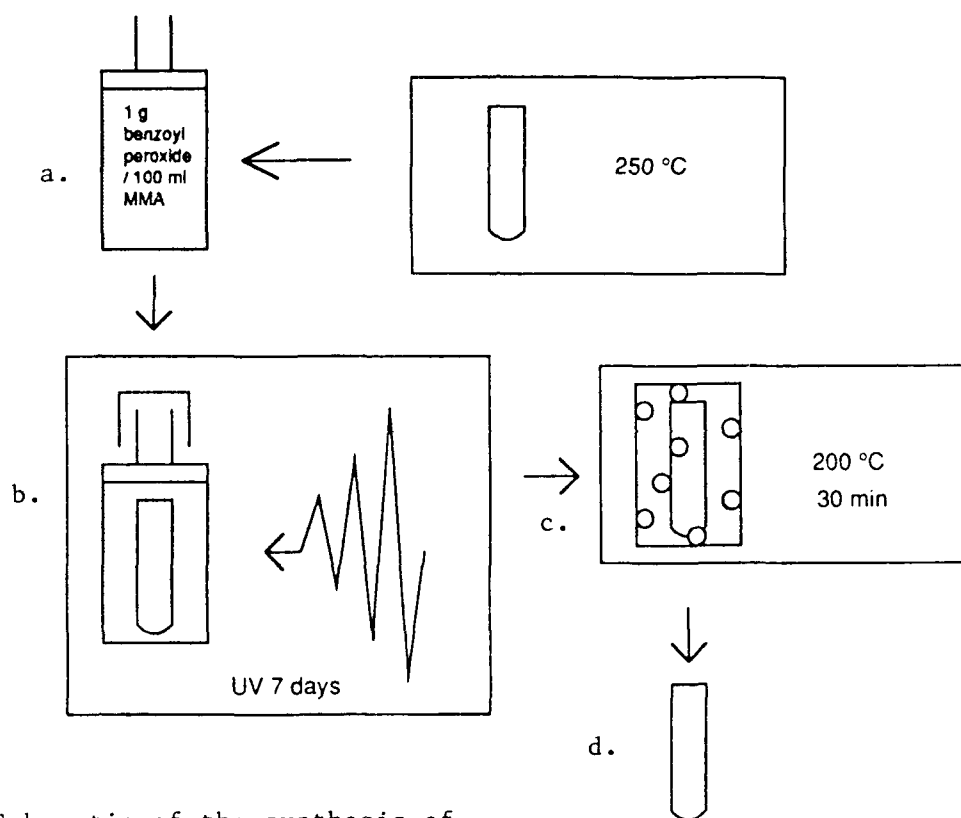


Figure 1: Schematic of the synthesis of silica/PMMA composites

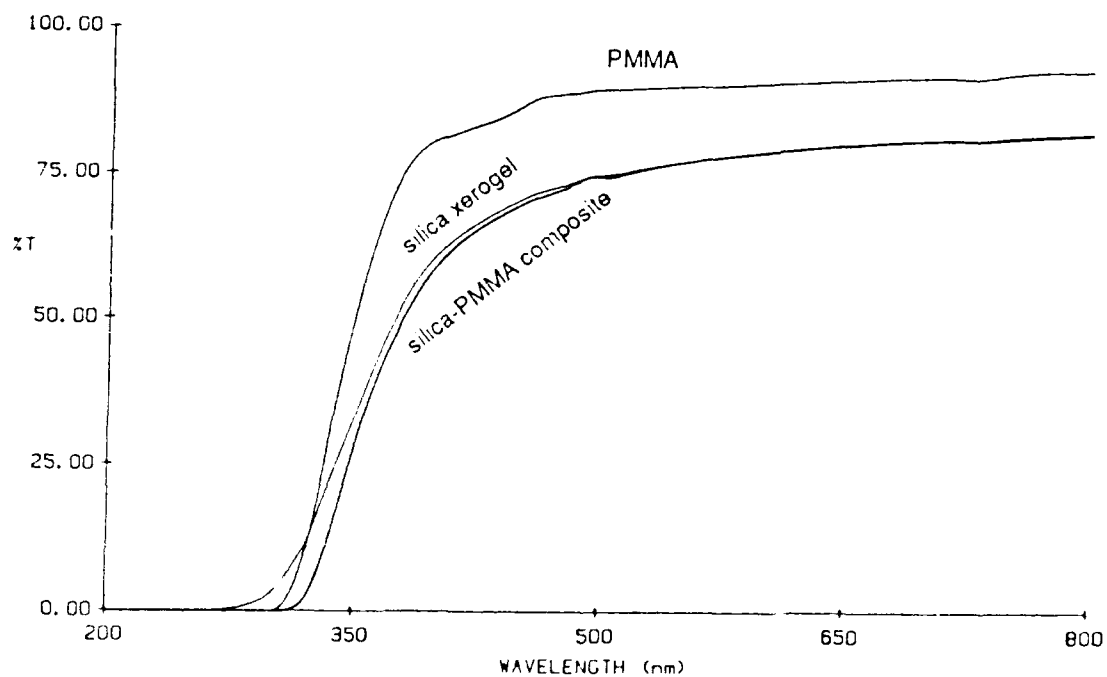


Figure 2: Percent of incident radiation transmitted for 10 mm thick samples

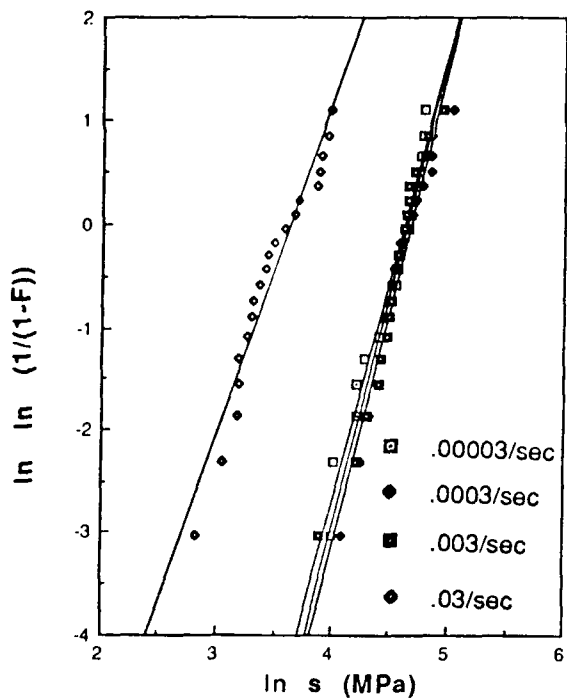


Figure 3: Strength distributions for 4 strain rates in silica/PMMA composites

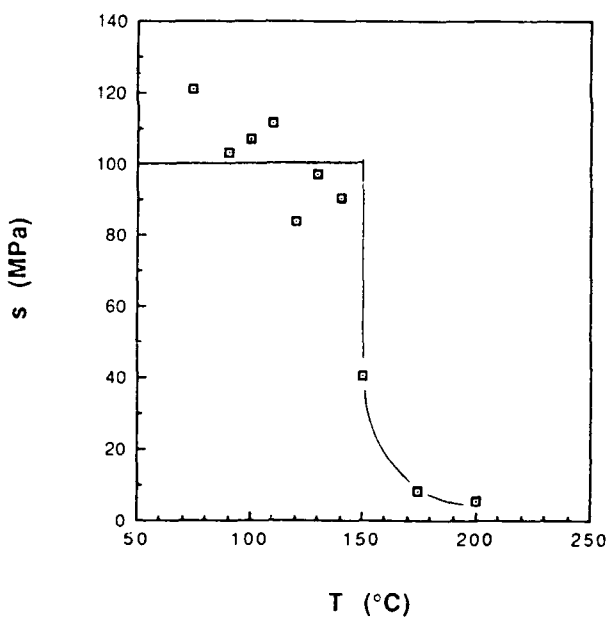


Figure 4: Flexure strength of samples after being subjected to thermal shock

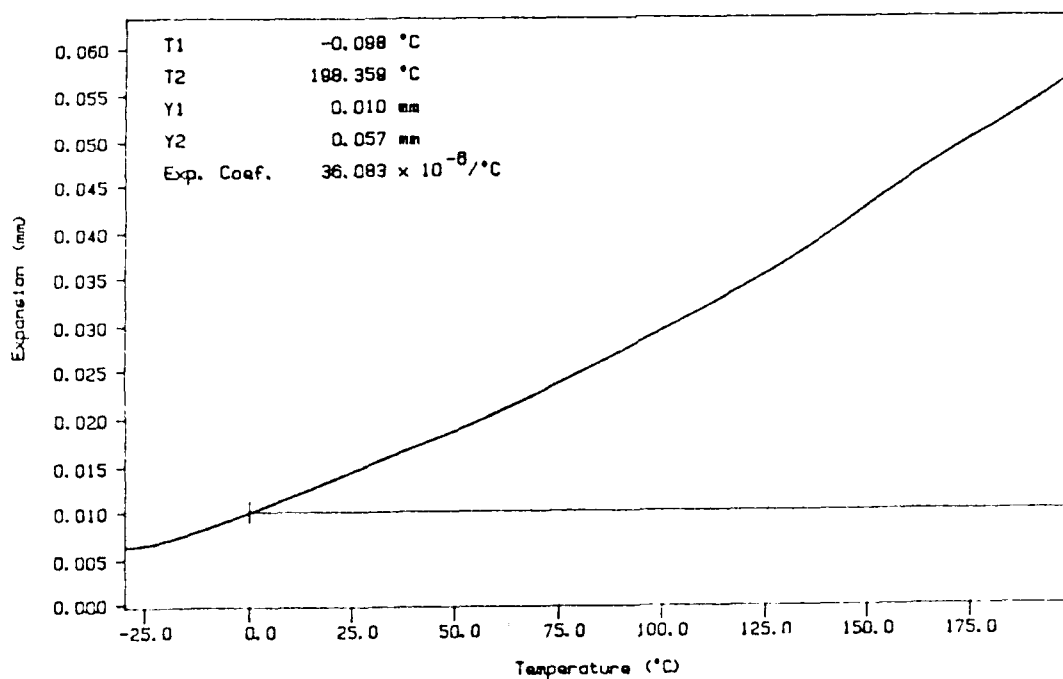


Figure 5: Thermomechanical analysis used to determine thermal expansion coefficient for silica/PMMA composite over the range 0 to 200°C



Inorganic-organic composites (ORMOCERS) for optical application.

Helmut Schmidt and Michael Popall\*

Institut für Neue Materialien der Universität des Saarlandes  
Gebäude 43, Im Stadtwald, D-6600 Saarbrücken, Fed. Rep. Germany

\*Fraunhofer-Institut für Silicatiforschung  
Neunerplatz 2, D-8700 Würzburg, Fed. Rep. Germany

#### ABSTRACT

Organically modified ceramics (ORMOCERS) have been prepared with respect to optical applications. The investigations show that materials can be synthesized with interesting properties for a variety of potential applications. They can be used as hard coatings for the protection of optical polymers, e.g. CR 39 or fluorescent dye containing PMMA. The incorporation of dyes leads to active optical matrices, e.g. fluorescent coatings and the introduction of components with high refractive increments to refractive index numbers  $n_D \leq 1.68$ . For microoptic applications, materials suitable for photolithographic patterning or direct laser writing have been developed.

#### 1. INTRODUCTION

For optical applications two types of materials have gained importance: glasses and polymers. Glasses are characterized by high processing temperatures and a costly shaping and finishing process, polymers can be processed at lower temperatures but show a poorer performance with respect to optical properties like  $n_D$  or  $D'$ , as shown in Fig. 1.<sup>1</sup> In addition to optical data distinctly differing from those of inorganic glasses, the mechanical surface properties of polymers exclude many practical applications. Therefore, protective coatings tailored for polymers have to be developed which are suitable for the mechanical and optical data of polymers and which provide sufficient surface protection. ORMOCERS can be located between glasses and polymers, as described in 2.2. They are hybrid materials the properties of which should be able to be adapted to a variety of requirements. The basic principles of ORMOCER synthesis has been described elsewhere.<sup>2-4</sup> Similar principles have been used by Wilkes<sup>5</sup> to synthesis high refractive index composites. First optical ORMOCER materials have been synthesized for contact lens applications.<sup>6</sup> A multicomponent system with various specific properties such as high oxygen permeation, intrinsic hydrophilicity and high mechanical strength was developed on the basis of the ORMOCER principle.

The question arises how far ORMOCERS can be used as a principle for materials for various optical applications. In this paper, data of ORMOCERS, as they have been developed in the Fraunhofer-Institut

92-11425

92 4 28 043



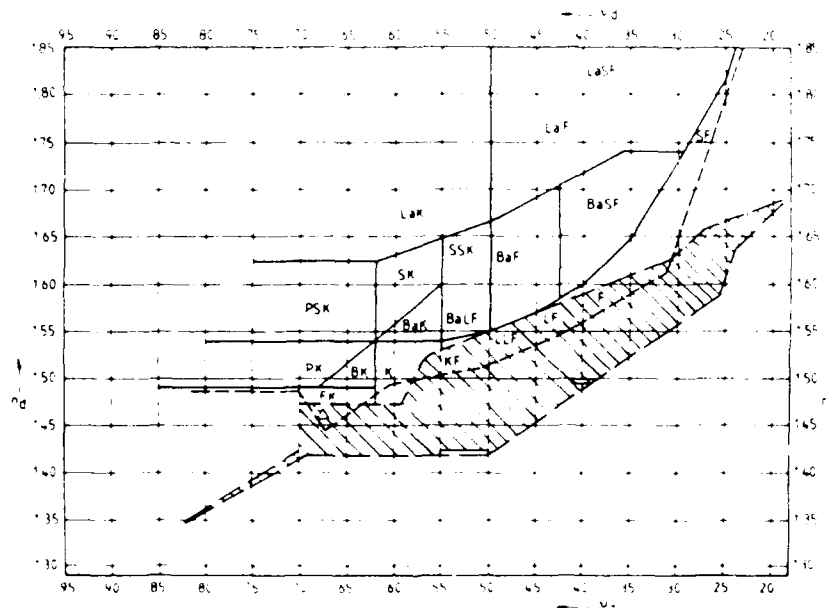


Fig. 1. Properties of optical glasses and polymers in the  $n_D/v_D$  plot. The written symbols refer to optical glasses of Schott Glaswerke company. The full circles refer to ORMOCERS (see also Chapter 2.2.).

für Silicatiforschung, are presented for an overview over the state of the art.

## 2. RESULTS AND DISCUSSIONS

### 2.1. Protection of surfaces

If materials from organic polymers are used for high performance optical components, the surfaces have to be protected from mechanical impact. The coating materials have to be adapted to the thermal expansion and to the modulus of elasticity of the substrate. As shown in <sup>7</sup>, the thermal expansion coefficient  $\alpha$  of ORMOCERS can be varied within a wide range (Fig. 2) and easily be adapted to a polymeric substrate.

Other requirements for polymer coatings are low curing temperatures and high abrasive resistance (compared to the substrate). The question of "surface hardness" is a difficult one and strongly depends on the practical stress conditions. In many cases, "soft" materials (e.g. rubber tires) under special circumstances can show a better performance than "hard" materials. As experiments have shown, the incorporation of inorganic ("brittle") components into a polyethylene oxide polymer<sup>8</sup> can increase the abrasion resistance of the polymer substantially. These materials are composed of  $TiO_2$ ,  $SiO_2$

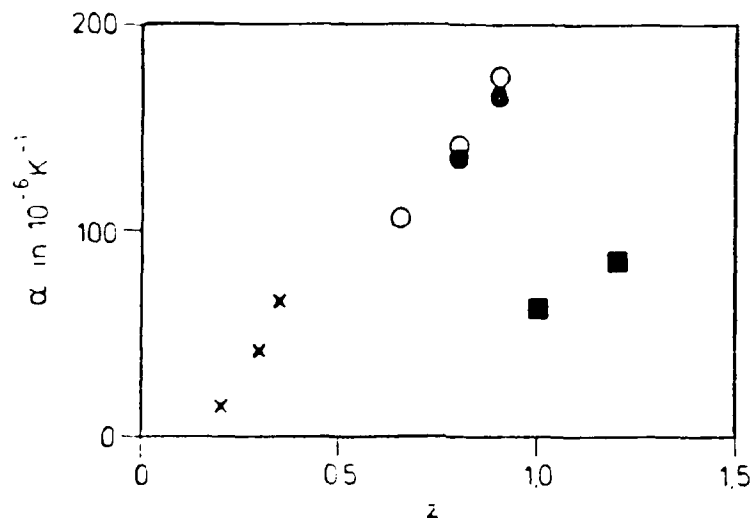
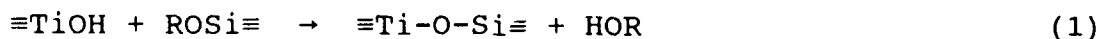


Fig. 2.  $\alpha$  as a function of  $z$ ;  $z$  = fraction of organic to inorganic groups. x  $\text{C}_6\text{H}_5\text{Si}\equiv$ ; O epoxy-Si $\equiv$ ; ● methacryl-Si $\equiv$ ; ■  $(\text{C}_6\text{H}_5)_2\text{Si}=\text{}$ .

and  $\text{SiO}_{3/2}(\text{CH}_2)_2\text{OCH}_2-\overline{\text{CHCH}_2\text{O}} = 20 : 10 : 70$  (molar ratio). The homogeneity of this system is achieved by the homogeneous generation of water in the mixture of the precursors (alkoxides). This leads to a controlled hydrolysis and condensation and highly reactive components like  $\text{Ti}(\text{OEt})_4$  are linked by a condensation step (equation (1))



to slower reacting components. This process control allows to synthesize coating materials with a tailored viscosity and a shelf life of several months. An industrial production for CR 39 and other eye glass lens materials has been established with this material.<sup>8,9</sup> The adhesion to CR 39 can be promoted by  $(\text{RO})_3\text{Si}(\text{CH}_2)_3\text{NH}_2$  as adhesion promoter (Fig. 3).

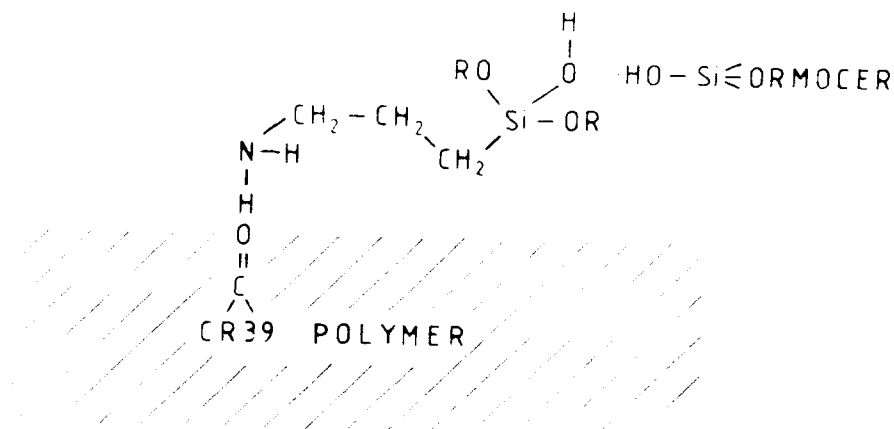


Figure 3. Adhesion model of the ORMOCER to CR 39 surfaces.



The low curing temperature of only 90 - 100 °C can be explained by the sol-gel condensation which takes place by simply evaporating the solvent and the fact that the organic polyethylene chain leads to sufficient matrix relaxation behavior to densify these materials at the indicated low temperatures. One important point is, that due to the active curing (the final "infinite" network is generated by condensation during the curing step), low molecular weights (500 - 1000 D) can be used in the coating laquers. Suitable viscosities can be obtained by high solid contents (up to 80 wt.%, which is rather high compared to polymer based laquers). As a consequence, high coating thicknesses can be obtained by one step processes (5 - 10  $\mu\text{m}$ ). The abrasion resistance of the coatings is very good and haze measurements after a standardized taber abrader treatment (200 rev.) show about 2 % (flat glass  $\approx$  1 %, CR 39 uncoated 20 %). The UV stability of the coating is fully sufficient for eye glass requirements. Due to the  $\text{TiO}_2$ , the material shows an electronic conductivity of about  $10^{-5}$ - $10^{-6} \sigma$ , which is sufficient to be used as a transparent electrode material.

For higher UV stabilities,  $\text{TiO}_2$  has to be replaced by  $\text{Al}_2\text{O}_3$  as network formers. The preparation of the Al-containing materials is described in detail in <sup>10</sup>. The materials are prepared from (I)  $(\text{RO})_3\text{Si}(\text{CH}_2)_2\text{OCH}_2-\text{CHCH}_2\text{O}$ , (II)  $\text{Al}(\text{OR})_3$ , and (III)  $\text{C}_6\text{H}_5\text{Si}(\text{OR})_3$ ,  $\text{CH}_3(\text{CH}_2)_2\text{Si}(\text{OR})_3$  or  $\text{CH}_2=\text{CHSi}(\text{OR})_3$  alternatively.  $\gamma$ -aminopropyltriethoxysilane can be added as adhesion promoter for PMMA, analogous to the  $\text{TiO}_2$  coatings. The scratch resistance of this type of coatings is high and in the same range as the  $\text{TiO}_2$  coatings. Depending on the type of substituting group in (III), various properties can be obtained: propyl leads to low  $\text{H}_2\text{O}$  take-up and these coatings are very stable against moist conditions (weathering for 14 days at 100 % r.h. and 40 °C). The ORMOCER coatings directly employed to the sputtered metal layers<sup>11</sup> provide sufficient chemical and mechanical protection (Fig. 4).

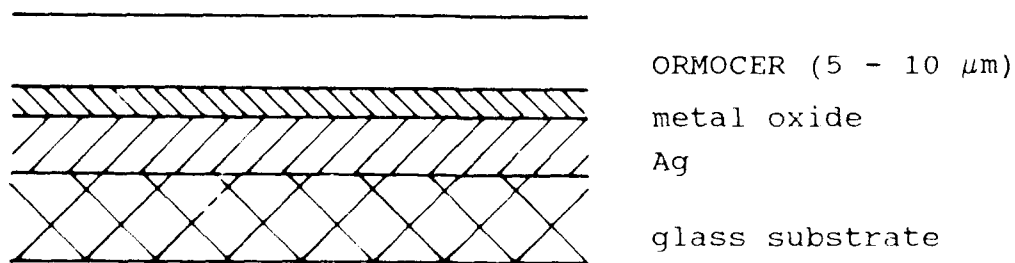


Fig. 4. Metallization protection ORMOCER coating.

The introduction of  $(\text{RO})_3\text{Si}(\text{CH}_2)_2\text{OCOCH}(\text{CH}_3)=\text{CH}_2$  instead of (III) leads to photocurable compositions if photocatalysts (e.g. IRGACURE 184, Ciba Geigy company) are added. All these types of coatings can be prepared with homogeneities suitable for optical coatings.

If necessary, the coatings can be prepared even with thicknesses up to 100  $\mu\text{m}$ . This was developed for coloured coatings with fluorescent dyes included. As shown in <sup>12</sup>, dyes of the perylene type can be incorporated and the system can be used for solar collectors. The incorporation of organic components into such systems is almost unlimited. NLO molecules can be introduced as shown by Dunn<sup>13</sup> and Prasad<sup>14</sup>.

## 2.2. Bulk materials

The first optical bulk materials have been developed for contact lens applications.<sup>6</sup> In this case, rods (10 cm in lengths, 2.5 cm in diameter) have been molded from viscous precursors and photocured by MMA polymerization). The rods were cut into blanks and mechanically machined to contact lenses.

In other experiments,  $\text{C}_6\text{H}_5$  containing silanes were combined with  $\text{TiO}_2$  or  $\text{ZrO}_2$  by condensation of  $(\text{C}_6\text{H}_5)_2\text{Si}(\text{OH})_2$  and  $\text{Ti}(\text{OEt})_4$  or  $\text{Zr}(\text{OPr})_4$  as precursors (50 % toluene as solvent).  $\gamma$ -glycidyloxypropyl silane and methacrylic acid glycidylester (MGE) were added in order to reduce the brittleness of the systems. In Fig. 5 the  $n_D/\nu_D$  diagram of the systems without MGE and in Fig. 6 the effect of MGE on various material data is given. The results are in accordance with Lorentz-Lorenz calculations, if the correct densities are used.

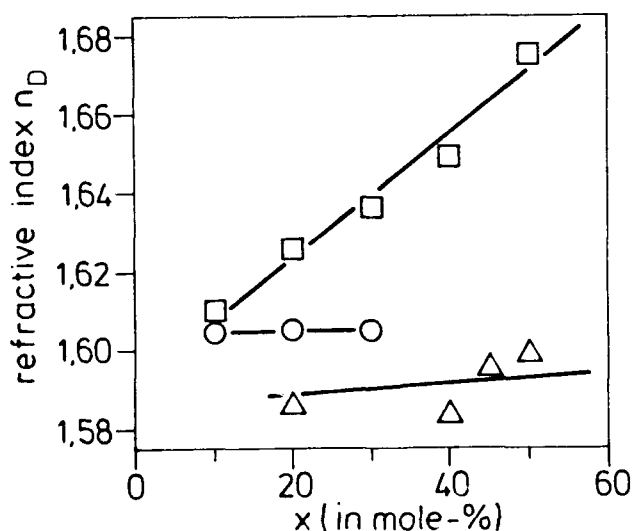


Fig. 5. Effect of  $\text{M}(\text{OR})_4$  on the refractive index of ORMOCERS.

□  $(100-x)\text{C}_6\text{H}_5)_2\text{Si}(\text{OH})_2/x\text{Ti}(\text{OEt})_4$ ; ○  $(100-x)\text{C}_6\text{H}_5)_2\text{Si}(\text{OH})_2/x\text{Zr}(\text{OPr})_4$ ; Δ  $(80-x)(\text{C}_6\text{H}_5)_2\text{Si}(\text{OH})_2/x\text{Zr}(\text{OPr})_4/20\gamma$ -glycidyloxypropyl triethoxysilane (molar ratio of precursors).

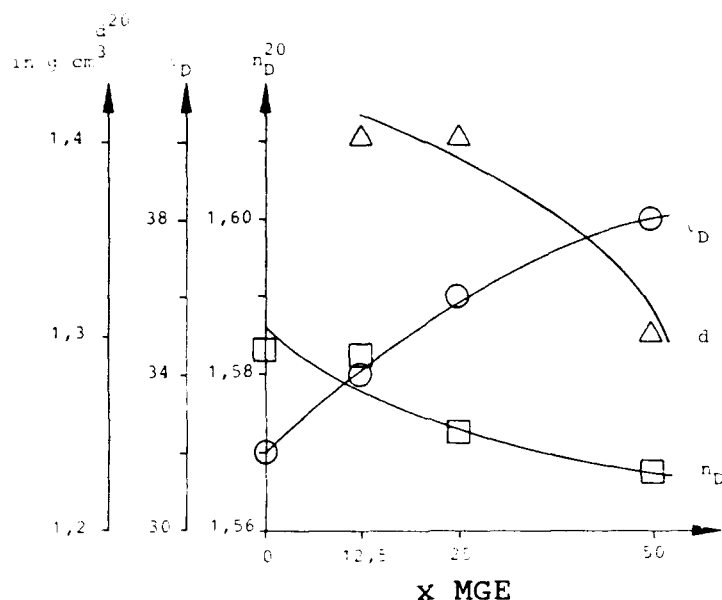


Fig. 6. Density,  $\rho_D$  and  $n_D$  of ORMOCERS as a function of the addition of MGE in the system  $40(\text{C}_6\text{H}_5)_2\text{Si}(\text{OH})_2/40\text{Zr}(\text{OPr})_4/20\gamma\text{-glycidyloxypropyl triethoxysilane}/x\text{MGE}$ ; molar ratio).

The results show that  $n_D$  values between 1.57 and 1.68 can be obtained with ORMOCERS. Lower values can be easily prepared, too. For higher values, further optimization is necessary. As shown in <sup>7</sup> the density of ORMOCERS does not increase with increasing content of inorganic components as it should be expected from the density of the crystalline phase. For example, a 40 wt.% containing glycidyloxypropyl based ( $\equiv$  POE chain containing) ORMOCER, which is expected to have a density of about  $2.5 \text{ g/cm}^3$  only shows a value of about 1.6. This means that the ORMOCER is not a ceramic polymer composite in a conventional sense (a physical mixture of crystalline  $\text{ZrO}_2$  and the polymer), but a composite in which the  $\text{ZrO}_2$  plays the role of a threedimensional network former similar to a threedimensional cross-linking organic group.

The materials can be prepared as coatings and as bulk products. Most of them show a very good abrasion resistance and can be used as protective transparent coatings, too.

The incorporation of inorganic ions into ORMOCERS is possible, too. As described in <sup>15</sup> the incorporation of  $\text{V}^{4+}$  ions into a  $\gamma$ -glycidyloxypropyl silane based ORMOCER leads to coatings with an effective absorption band in the near infrared for solar protection. If  $\text{ZrO}_2$  or  $\text{TiO}_2$  are substituted by  $\text{Al}_2\text{O}_3$ ,  $n_D$  values down to 1.35 can be obtained.

### 2.3. Patternable ORMOCERs

For microoptic or integrated optic applications, the formation of geometrical structures is an important feature. Therefore, ORMOCERs for photolithographic or laser writing processes have been developed. The synthesis of these materials is described elsewhere.<sup>16</sup> The process consists of three steps, the preparation of an ORMOCER precursor for coating techniques with high homogeneity and transparency, the lithographic step after coating and the development step of the patterns and final curing.

As photopolymerizing step the crosslinking methacryloxy groups bond to Si were chosen. For achieving thick coatings with a one step coating, the solid content of the precursor should be as high as possible. This can be obtained by a solvent-free processing using modified silanes only. The slowly reacting silanes also allow the preparation of stable coating laquers with a shelf live of several months. If network formers with high reactivity with respect to condensation, e.g.  $\text{Al(OR)}_3$  is used, patternability can be provided, but the shelf live is reduced drastically.<sup>17</sup>

A suitable system consisting of organo silanes and  $\text{SiO}_2$  was developed from  $\gamma$ -glycidyloxypropyl trimethoxysilane :  $\gamma$ -methacryloxypropyl trimethoxysilane : vinyl trimethoxysilane :  $\text{Si(OEt)}_4$  = 39 : 39 : 18 : 4 (molar ratio) by refluxing the precursors for several hours with about 50 % of the water necessary for complete hydrolysis. By spin-on techniques substrates can be coated up to about  $13\ \mu\text{m}$  thickness in a one step process. The coatings can be polymerized, if about 0.1 wt.% photoinitiator (e.g. IRGACURE 184) is added. If a laser writing technique is used, as shown in <sup>16</sup> and <sup>17</sup>, the width of the patterns depends strongly on the laser intensity. After light exposure, the patterns were developed either with diluted NaOH or acetone.<sup>16</sup> Under these conditions, the ORMOCER is sufficiently polymerized but not to be redissolved. The width increases with laser exposure time which can be attributed to light reflection from the interface and chain propagation into "dark" areas. Fig. 7 shows an example of a patterned ORMOCER.



Fig. 7. Developed ORMOCER patterns received by laser writing 600 W/cm<sup>2</sup>, scanning rate: 2 mm/s (bar refers to 10  $\mu\text{m}$ )

This technique allows to generate dielectrics for SMD techniques for microelectronics as well as wave guides for optics. In combination with active components (e.g. inorganic ions or organic molecules with special functions) the ORMOCERS open interesting perspectives.

#### 4. CONCLUSIONS

As the data have shown, ORMOCERS with interesting optical properties and a potential for optoelectronic applications can be prepared. As a consequence of the high number of compositions and processing parameters, most of the discussed systems are not yet optimized. Three groups of materials already have been developed to a state which clearly shows the application potentials: transparent hard coatings, transparent bulk materials and materials for patterning. The combination with active components will be an interesting task for future work.

#### 5. ACKNOWLEDGEMENT

The authors want to thank Dr. H. Meyer and Dr. J. Schulz for their helpful discussions and experimental work, the Bundesminister für Forschung und Technologie and several industrial companies for their financial support.

#### 6. REFERENCES

1. B. Lintner, N. Arfsten, H. Dislich, H. Schmidt, G. Philipp, and B. Seiferling, "A First Look at the Optical Properties of ORMOSILs", *J. Non-Cryst. Solids* 100, pp. 378-382, 1988.
2. H. Schmidt, "Organically Modified Ceramics, Materials with History or Future?", In: *Proceedings Fourth International Conference on Ultrastructure Processing of Ceramics, Glasses and Composites*, February 1989, *J. Non-Cryst. Solids* (in print).
3. H. Schmidt, "Organically Modified Silicates as Inorganic-Organic Polymers", *ACS Symposium Series No. 360*, pp. 333-344, 1988.
4. H. Wolter and H. Schmidt, "Isolationsschichten auf der Grundlage organisch modifizierter Keramiken und deren Applikation", *DVS-Berichte* 129, 1990.
5. G. L. Wilkes, B. Wang, A. Brennan, D. Rodrigues, and H. Huang, "New Hybrid Inorganic-Organic Materials Made by the Sol-Gel Method", In: *Proceedings of MRS Fall Meeting November 1989, Boston, Mat. Res. Soc. Symp. Proc.* (in print).
6. G. Philipp and H. Schmidt, "New Materials for Contact Lenses Prepared from Si- and Ti-Alkoxides by the Sol-Gel Process", *J. Non-Cryst. Solids* 63, pp. 283-292, 1984.
7. H. Schmidt, "Organic Modification of Glass Structure - New Glasses or New Polymers?", *J. Non-Cryst. Solids* 112, pp. 419-423, 1989.

8. H. Schmidt, B. Seiferling, G. Philipp, and K. Deichmann, "Development of Organic-Inorganic Hard Coatings by the Sol-Gel Process", In: Ultrastructure Processing of Advanced Ceramics, Eds.: J. D. Mackenzie and D. R. Ulrich, John Wiley & Sons, New York, pp. 651-660, 1988.

9. K. Buchner, "ORMOCERe in der industriellen Praxis - Beispiel Augenoptik bei Rupp und Hubrach", Oral Presentation at the Meeting "Glasforum" of German Glass Society, May 5, 1990.

10. G. Philipp, B. Seiferling, H. Schmidt, A. Kaiser, and K. Hofmann, "Verfahren und Zusammensetzung zur Herstellung von kratzfesten Materialien", European Patent Application No. 0358011, August 17, 1989.

11. G. Schottner, "Protective Coatings by Sol-Gel-Techniques", Oral Presentation at 52nd Dr. Wilhelm and Else Heraeus Seminar, May 1989, Bad Honnef/FRG.

12. K. H. Haas, H. Schmidt, and H. Roggendorf, "Incorporation of Fluorescent Dyes into ORMOCER Coatings", In: Extended Abstracts of the Topical Meeting on Glasses for Optoelectronics, December 1, 1989, Ed.: The Ceramic Society of Japan, Tokio/Japan, pp. 68.1-68.4, 1989.

13. E. T. Knobbe, B. Dunn, and J. I. Zink, "The Development of Optical Properties in Organic-Doped Sol-Gel Materials", In: Proceedings Fourth International Conference on Ultrastructure Processing of Ceramics, Glasses and Composites, Tucson, February 1989, John Wiley and sons, publishers (in print).

14. P. N. Prasad, "Nonlinear Optical Processes in Polymers and Sol-Gel Composites", In: Proceedings Fourth International Conference on Ultrastructure Processing of Ceramics, Glasses and Composites, Tucson, February 1989, John Wiley and sons, publishers (in print).

15. F. Hutter, H. Schmidt, and H. Scholze, "Iron(II)- or Vanadium(IV)-Containing Siliceous Gels", J. Non-Cryst. Solids 82, pp. 373-377, 1986.

16. M. Popall, H. Meyer, H. Schmidt, and J. Schulz, "Inorganic-Organic Composites (ORMOCERs) as Structured Layers for Microelectronics", In: Proceedings of MRS Spring Meeting, April 1990, San Francisco, Mat. Res. Soc. Symp. Proc. (in print).

17. M. Popall and H. Meyer, "Entwicklung von photostrukturierbaren ORMOCERen für Multilayer", Oral Presentation at VDI/VDE Seminar "Anwendung der laserinduzierten Metallabscheidung für Multi Chip Module, March 1990, Berlin.



## Synthesis and Properties of Transparent $\text{ZrO}_2$ Containing $\text{SiO}_2$ Polymethacrylate Polymers

R. Nass and H. Schmidt  
Institut fuer Neue Materialien der Universitaet des Saarlandes  
D-6600 Saarbruecken (Fed. Rep. Germany)

E. Arpac  
Inoenuue Universitat  
44069 Malatya (Turkey)

### Abstract

The synthesis of zirconia modified polymerized methacryloxypropylsilane as a new material with a potential for optical application has been investigated. The material is synthesized by copolymerizing 3-methacryloxypropyl trimethoxysilane and zirconium propylate chelated by methacrylic acid. The methacrylic acid serves as a complexing agent and participates in the polymerization process in order to incorporate the zirconia homogeneously into the polymer. Transparent bulk materials have been prepared by this process.

### 1. Introduction

The properties of ORMOCERS prepared by the sol-gel process<sup>1</sup> can be varied in a wide range by composition and processing conditions. Materials with a high refractive index thereby generally require the incorporation of inorganic components like  $\text{ZrO}_2$  or  $\text{TiO}_2$  as inorganic network formers<sup>2</sup>. But due to the high reactivity of zirconium- and titanium alkoxides, the addition of water for hydrolysis must be carried out very carefully. In order to improve the processing properties of these metalalkoxides chemical modification with  $\beta$ -dicarbonyl compounds or carboxylic acids is often used<sup>3</sup>. In general, complexing ligands can be used to control hydrolysis and condensation<sup>3,4</sup>, but this does not necessarily lead to a molecular distribution of the metal oxide within the polymeric matrix, as to be concluded from<sup>4</sup>. For the molecular scale fixation of metal oxides within the matrix the use of polymerisable complex formers seems to be a suitable route as shown in<sup>5</sup>. In this case,  $\beta$ -diketonates with polymerisable ligands were used. For  $\text{Zr}(\text{OPr}^n)_4$ , the complexation with methacrylic acid was investigated. Mechanical properties of  $\text{ZrO}_2$  containing polymers have been reported<sup>6,7</sup>. In this paper, the preparation of bulk materials with respect to optical applications is investigated. Therefore, a three component system prepared from  $\text{Zr}(\text{OPr}^n)_4$ , methacrylic acid, and 3-methacryloxypropyl trimethoxysilane was investigated. Therefore a synthesis route in order to achieve homogeneous monoliths had to be developed. Therefore, hydrolysis and condensation of the silane as well as of the complexed zirconia precursor was investigated, too.

92 4 28 014

92-11426



## 2. Experimental

Hydrolysis of 3-methacryloxypropyl trimethoxysilane was investigated with 0.15 - 0.3 mole  $H_2O$ /mole silane. Thereby a pH of 5.5 was adjusted by bubbling through the reaction mixture  $CO_2$ . Due to the immiscibility with water, the mixture is diphasic and was stirred for 16 hrs in order to obtain a homogeneous solution. The residual water content after this time was determined by Karl Fischer titration. For the preparation of a  $ZrO_2$  containing polymethacryloxypropyl siloxane, one mole of the silane was prehydrolysed with 1.5 mole water as described before. The prehydrolysed clear solution was cooled down with an ice bath to  $0^\circ C$  and 0.2 mole zirconium propoxide and 0.2 mole methacrylic acid were added. After 30 minutes, additional 0.4 mole water was added. For polymerization a photoinitiator (IRGACURE 164, Ciba Geigy company 5 wt.%) was added and methanol and propanol were removed by vacuum treatment. The remaining highly viscous liquid was poured into plastic tubes (4 mm in diameter, 50 mm in length) and exposed to UV irradiation for 3 minutes.

## 3. Results and Discussion

### 3.1 Reactions of 3-methacryloxypropyl Trimethoxysilane (MPT)

The investigation of the hydrolysis reaction of MPT was carried out since previous experiments had shown a strong dependance of the drying behavior of the UV cured rods on the amount of the water addition to the silane.  $CO_2$  was used as a slightly acid catalyst because it can be easily removed from the reaction mixture. Independent of the added amount of  $H_2O$ , the concentration of the residual  $H_2O$  remained constant after 16 hrs. In Fig. 1 the concentration of the residual water in the reaction mixture is shown as a function of the added water.

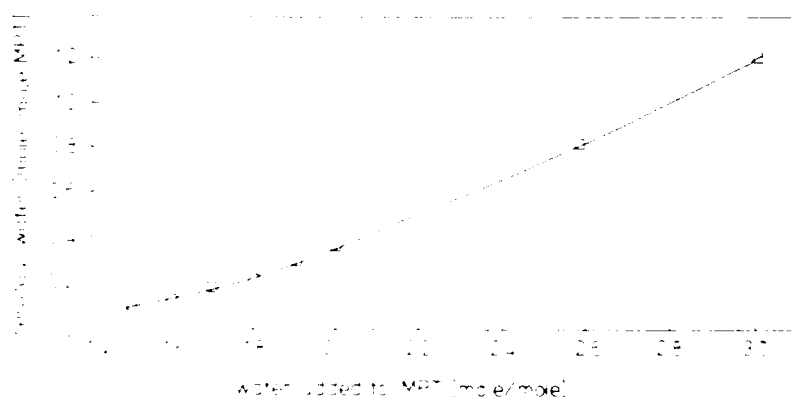


Figure 1: Residual water content as a function of water added to MPT after a reaction time of 16 hrs; pH: 5.5

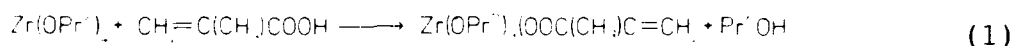
As one can clearly see, only with initial concentrations of  $<1.5$  mole



H<sub>2</sub>O the H<sub>2</sub>O content of the reaction mixture becomes very low ( $\leq 0.1$  mole). The following UV curing experiments showed that only with low H<sub>2</sub>O contents monoliths could be obtained. For the monoliths preparation, 1.5 mole H<sub>2</sub>O were chosen as standard preparation conditions.

### 3.2 Complex Formation

The formation of the Zr(OR)<sub>4</sub> methacrylic acid complex is described elsewhere<sup>7</sup>.



As shown by IR spectroscopy, a bidental chelate complex is formed by substituting one OR group of Zr(OR)<sub>4</sub>. The reaction of this complex with various concentrations of H<sub>2</sub>O was investigated by Karl Fischer titration. The results show that only 1.5 mole H<sub>2</sub>O per mole complex are consumed and a stable sol with very fine particle sizes (3-10 nm, determined by dynamic light scattering) is obtained. From this sol, a crystalline material can be received by evaporating the solvents. The crystallized phase can be redissolved in ethanol and purified by this method: the slightly yellow colour, as a result of the complex formation, disappears. The redissolved complex can be used for monolith preparation as an alternative way.

### 3.3 Preparation of Monoliths

Monoliths were prepared from a solvent-free sol of prehydrolysed 3-methacryloxypropyl trimethoxysilane and the modified zirconium propoxide. Solidification takes place by copolymerization of the methacrylate groups as well as by condensation of hydroxyl and alkoxyl groups. Therefore the formation of an inorganic/organic network as shown in Fig. 2 can be assumed.

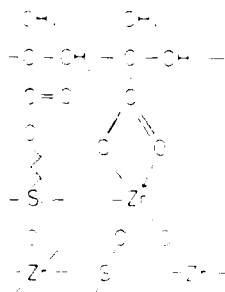


Figure 2: Network model of the transparent monoliths

The polymerisation step was followed by IR spectroscopy. The IR

spectroscopy of a polymerised sample is shown in Fig. 3.

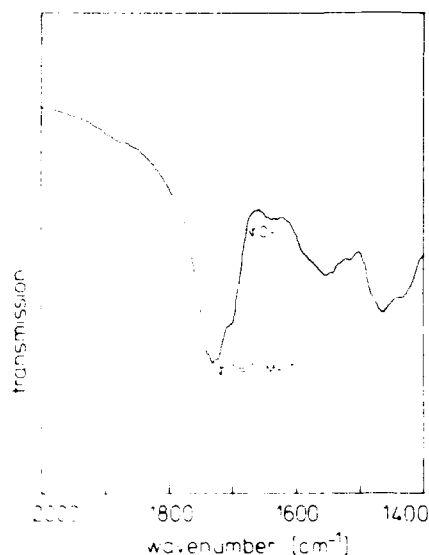


Figure 3: IR-spectrum of the polymerised monolith

As one can see, the C=C double bond at  $1640\text{ cm}^{-1}$  has almost disappeared showing a high polymerization yield. The effect of excess water in the reaction mixture leads, as already indicated, to a disaggregation of the rod. There is no clear explanation for this effect, but one reason might be that condensation is leading to a brittle material before polymerisation takes place; enhanced polymerisation then can cause internal stresses finally leading to cracking.

The results show that due to the chemical modification, the zirconia can be incorporated into the inorganic/organic network on a very small scale. Therefore a homogeneous distribution of the zirconium compound can be assumed which was proved by TEM micrographs (Fig. 4). Upto a magnification of  $10^6$  no phase separation could be detected. The dash spots do not indicate phase separation but are caused by elementary carbon from the sample preparation.



Figure 4: TEM micrograph of a monolith; the bar refers to 80 nm; the square indicates an area with only a few carbon spots.

Monoliths, 4 mm in diameter and 50 mm in length, exhibit an average fracture strength of 79 MPa, which is surprisingly high. The optical transparency of the material was measured by UV/VIS-spectroscopy (Fig. 5).

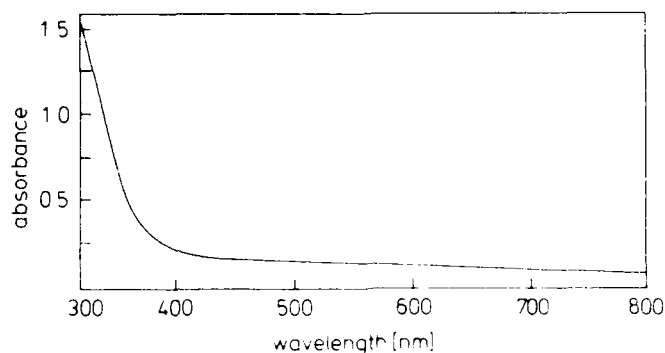


Figure 5: UV/VIS-spectrum of a monolith

Due to the pale yellow colour of the material, the absorption increases below 350 nm. This result can be attributed to impurities, e.g. of transition metal complexes with higher extinction coefficient ( $\text{Fe}^{3+}$ ), because the zirconium alkoxide was stored in iron containers and used without further purification. As already shown, the colour can be removed by purifying the zirconium complex.

A value of 1.51 was determined for the refractive index. This result might be due to the low zirconia content of only 17 mole%. Therefore, further experiments have to be carried out in order to increase the zirconia content as well as the refractive index. The high mechanical strength combined with the good optical transparency of this type of material show an interesting potential for optical applications, especially because further optimization and variations of composition are possible in a wide range.

#### 4. Acknowledgement

This research was performed during the authors stay at the Fraunhofer Institut fuer Silicatiforschung, Wuerzburg, Federal Republic of Germany. The financial support of the Bayrisches Staatsministerium fuer Wirtschaft is gratefully acknowledged.

#### 5. References

1. H. Schmidt, "Organically Modified Ceramics, Materials with History or Future?", In: Proc. Fourth Int. Conf. on Ultra structure Processing of Ceramics, Glasses and Composites, Febr. 1989. J. Non-Cryst. Solids (in print).

2. B. Lintner, N. Arfsten, H. Dislich, H. Schmidt, G. Philipp and B. Seiferling, "A First Look at the Optical Properties of ORMOSILs", *J. Non-Cryst. Solids*, vol. 100, pp. 378-382, 1988.
3. J. Livage, M. Henry and C. Sanchez, "Sol-Gel Chemistry of Transition Metal Oxides", *Prog. Solid State Chem.*, pp. 1-83, 1989.
4. R. Naß and H. Schmidt, "Preparation and Properties of Chelated Aluminiumalkoxides", In: *Proceedings Second International Conference on Ceramic Powder Processing Science*, Berchtesgarden, October 1988 (in print).
5. Y. Sanchez, "Organically Modified Sol-Gel Materials", Oral Presentation at 52nd Dr. Wilhelm und Else Heraeus Seminar, May 1989, Bad Honnef, FRG.
6. H. Schmidt, "Inorganic-Organic Composites by Sol-Gel Techniques", In: *Proc. MRS Fall Meeting*, November 1989, Boston, Mat. Res. Soc. Symp. Proc. (in print).
7. R. Naß, E. Arpac and H. Schmidt, "Monolithic Gel Preparation from Chemically Modified Zirconium Alkoxides", In: *Proceedings Third International Conference on Ceramic Powder Processing Science*, San Diego, February 1990 (in print).



# Preparation and optical properties of amorphous silica doped with functional organic molecules by the sol-gel process

Akio Makishima, Kazuki Morita, Hiroyuki Inoue  
University of Tokyo, Department of Materials Science, 7-3-1 Hongo,  
Bunkyo-ku, Tokyo 113, JAPAN

and  
Toshiro Tani  
Electrotechnical Laboratory, Umezono 1-1-4, Tsukuba-city, Ibaraki  
305, JAPAN

## ABSTRACT

Molecular dispersions of amorphous siliceous materials doped with organic molecules, TPPS, were prepared by a sol-gel process in which  $\text{Si}(\text{OC}_2\text{H}_5)_4$  was hydrolyzed in neutral solution. An amorphous silica which was doped with TPPS on the order of  $1 \times 10^{-5}$  mol/mol  $\text{SiO}_2$  showed photochemical hole burning at 4 K. The TPPS/a- $\text{SiO}_2$  was heat-treated at various temperatures and the change of optical spectrum were observed as a function of temperature. It was found that the sample was comparatively stable upto 200 °C.

## 1. INTRODUCTION

Recently the sol-gel process for preparing oxide glasses has been extensively studied and developments in the technique for preparation of oxide glasses from metal alcoholates through hydrolysis, gelling, and heating at low temperatures have been reviewed.<sup>1-3</sup> The authors reported the preparation of amorphous silicas doped with organic molecules, which have various kinds of properties, such as photochemical hole burning, photo-conductivity, and laser emission, using the sol-gel process.<sup>4-6</sup> In order to obtain oxide glasses it is common to use the high-temperature melting technique; doping of thermally dissociative components in these glasses has never been realized due to the high melting temperatures. By adopting the sol-gel process, however, we successfully obtained organic-molecule-doped amorphous siliceous materials in molecular dispersion, which are air stable. One of the samples thus obtained, which was doped with 1,4-dihydroxy-9,10-anthraquinone (DAQ,quinizarin), showed photochemical hole burning at 4 K. Photochemical hole burning is a kind of photobleaching technique which utilizes a site-selective photoinduced reaction to form a persistent hole in the inhomogeneously broadened absorption band by laser light irradiation.<sup>4</sup> The phenomenon has attracted wide attention because it can be applicable in high-density optical data storage.

It is said that the photochemical hole burning (PHB) takes place by the effects of photon energy on the proton of the OH in the structure of the DAQ as shown in Fig.1. In this case the proton of the OH is placed OUTSIDE of the structure. However the TPPS (Tetraphenylporphinetetrasulfonic acid) has a structure as shown in Fig.2, and it is said that the PHB takes place by the irradiation of photon energy to the proton of NH of the INSIDE of the TPPS structure. The location of the proton of the NH changes as the results of photo tauomerization by the action of the photon energy as shown in Fig.2. Therefore it is interesting to see what will happen to the TPPS doped amorphous silica by the irradiation of the laser light and to observe whether the PHB takes place or not in this amorphous materials prepared by the sol-gel process. The process usually needs some heat treatment to stabilize the structure of the silica gel and dehydrate or collapse the micro or meso-pores in the gel. However in the present case to much higher temperature treatment deteriorates the functional organic molecules in the silica matrix. Therefore it is also important to see how high temperature we can heat-treat the TPPS-doped-siliceous materials. In this study we observed the optical spectrum of the sample which was heat-treated at various temperatures.

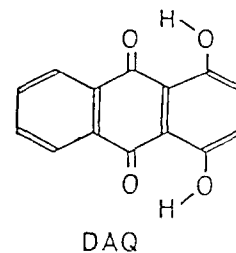


Fig.1. The structure of DAQ.

92-11427



92 4 28 015

## TPPS

$\alpha, \beta, \gamma, \delta$ -Tetraphenylporphinetetrasulfonic acid

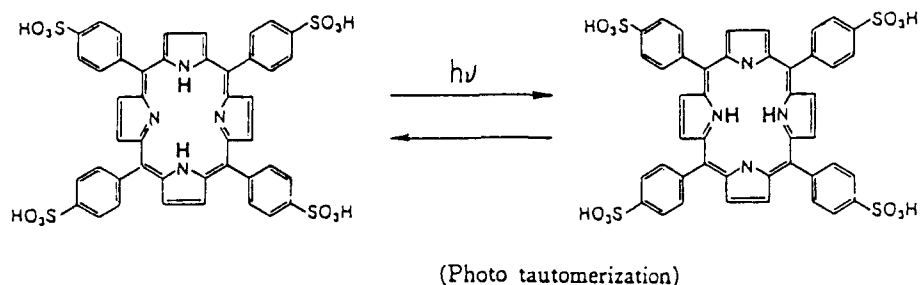


Fig.2. The change of structure of TPPS by the light.

### 2.EXPERIMENTAL PROCEDURE

We used tetraethoxysilane ( $\text{Si}(\text{OC}_2\text{H}_5)_4$ ), ethanol and TPPS as starting materials. The organic material was dissolved in ethanol on the order of  $10^{-5}$  mol/mol. Organic compound/ethanol solution (11.4 mL),  $\text{Si}(\text{OC}_2\text{H}_5)_4$  (10.0 mL), and distilled water (3.7 mL) were mixed together to attain a homogeneous solution in a 100 mL beaker. The hydrolysis for gelling was carried out at 60 °C with 50% relative humidity for about one month and the gel thus obtained was kept at 40 °C with 50% relative humidity. Some of the samples were heat treated from 100 °C to 300 °C for 10 min and their visible range optical absorption spectrum were measured by the conventional methods. Photochemical hole burning was observed for the sample by using a  $\text{N}_2$ -dye laser at 4 K; the details of the experiment was reported before.<sup>7</sup>

### 3.RESULTS AND DISCUSSION

We obtained monolithic solid samples from homogeneous solutions which were neutral. The organic compound seemed to be homogeneously doped in the monolithic solids without macroscopic segregation. The monolithic disks were 28 mm in diameter and 2 mm in thickness. The concentration of the organic dopant in the amorphous silica was ca.  $1 \times 10^{-5}$  mol/mol  $\text{SiO}_2$ . Some of the observed optical spectra of the TPPS/a- $\text{SiO}_2$  heat-treated at various temperatures are shown in Fig.3, and the change of the absorbances at 420 nm in the Fig.3 is plotted in Fig.4. These results indicate that the TPPS in the silica matrix is stable upto ca. 200 °C and about 300 °C the molecules dissociate or may burn-out. We can heat-treat the sample nearly upto 200 °C to stabilize the structure of the gel and dehydrate the water contents in the gel. The colors of organic compound/ethanol solution and the corresponding organic/amorphous silicas thus prepared are nearly same. The color of the TPPS doped amorphous silica is dark grey.

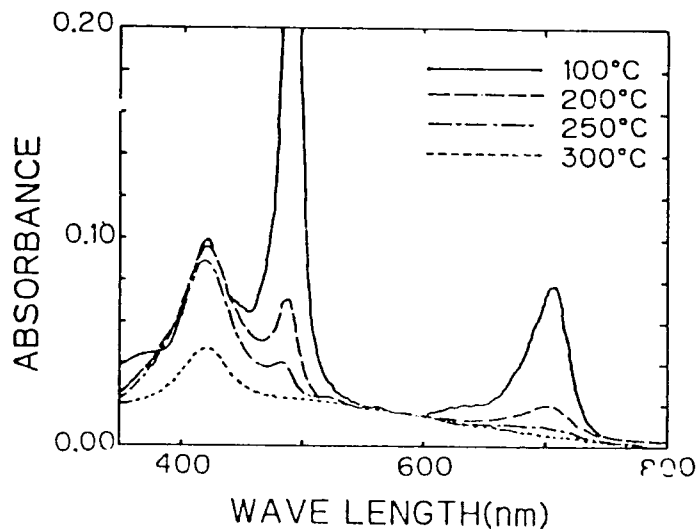


Fig.3. The optical absorptions of TPPS/a- $\text{SiO}_2$  heat treated at various temperatures.

Taking some of the TPPS/amorphous silica as an example, the position of the peaks of the optical absorption spectrum in the visible wavelength region of the organic compound ethanol solution are almost identical with those of the organic-compound-doped sample (Fig.5), indicating that the organic compound is molecularly dispersed in the monolithic sample. The molecular dispersion of the TPPS/amorphous silica was further confirmed by measuring the photochemical hole burning of the sample at 4 K (liquid helium temperature). By use of a  $N_2$  dye laser, the sharp hole at 640 nm was observed for the TPPS/amorphous silica sample (Fig.6), and the details of the observed PHB will be discussed elsewhere.

The TPPS is said to be weak for the strong acid and also basic solution. When the basic hydrolysis of  $Si(OC_2H_5)_4$  was used to prepare the sample, the doping of the TPPS was unsuccessful and monolithic samples were not prepared. Two-layered solids resulted with many cracks, and the organic compounds were not homogeneously distributed in the layers.

The reasons why doping the TPPS into the amorphous silica was unsuccessful for the present process of hydrolysis with  $NH_4OH$  solution are not clearly explained at present, but two factors might be involved: syneresis and microstructure. After mixing the raw materials to attain a homogeneous solution containing TPPS and storing the solution 4 d at 60 °C and 50% relative humidity, we observed that syneresis took place, and gel and liquid coexisted in the beaker. Subsequent drying of the gel and liquid parts for a week at 40 °C with 50% relative humidity resulted in a sample with many cracks and two-layered solids. On the contrary, for the sample obtained by hydrolysis with neutral solution syneresis could not be observed and organic-compound doped monolithic silica was obtained as Nogami and Moriya<sup>8</sup> reported that many spherical particles of 10 nm diameter were observed in samples prepared by hydrolysis with  $NH_4OH$ , but such particles were not observed in samples prepared by hydrolysis with neutral solution. These differences in the microstructures<sup>8</sup> would affect doping of the organic compounds.

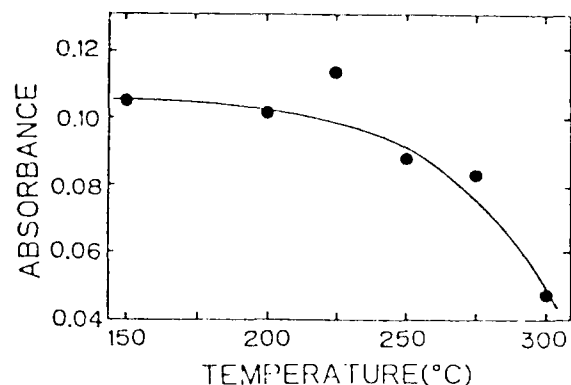


Fig.4. The change of absorbances at 420nm of TPPS/a-SiO<sub>2</sub> heat-treated at various temperatures.

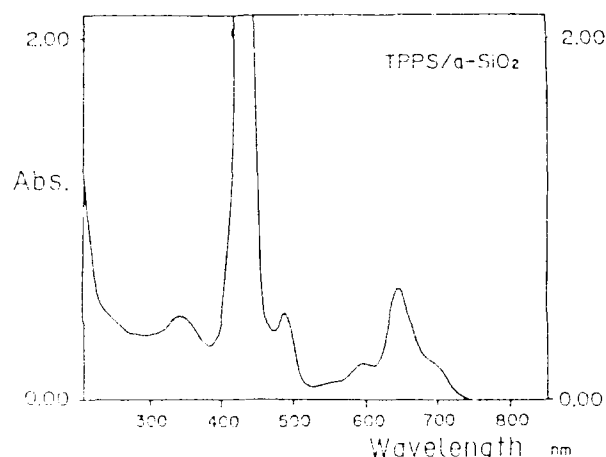


Fig.5. The observed optical spectrum of TPPS/a-SiO<sub>2</sub>.

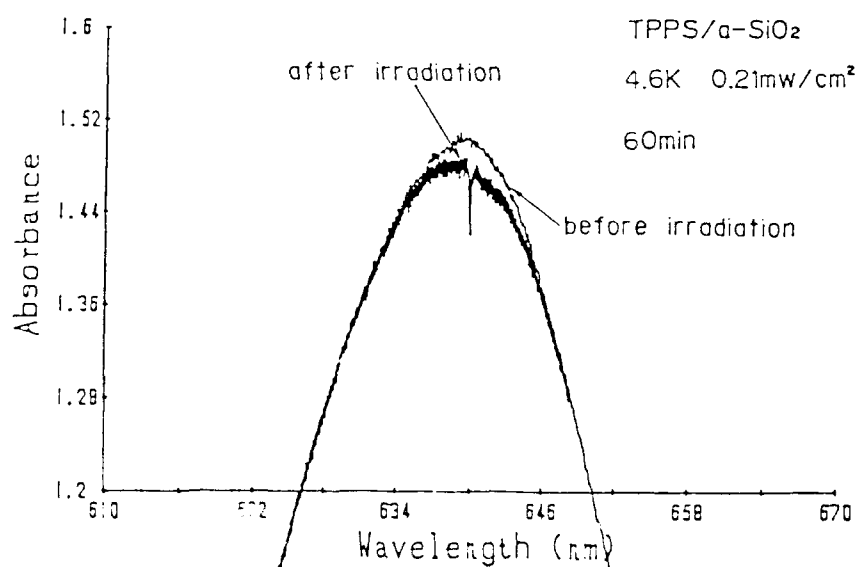


Fig.6. The observed photochemical hole burning of TPPS/a-SiO<sub>2</sub> in Fig.5.

Though the present process was carried out in the neutral condition, further study is needed to clarify the reasons why doping of organic compounds into amorphous silica was unsuccessful for the process of hydrolysis with  $\text{NH}_4\text{OH}$  solution.

#### 4.ACKNOWLEDGMENTS

The authors express their thanks to Y.Sakakibara, T.Hayakawa and K.Konoshi for their cooperation in the experiments and informative discussions.

#### 5.REFERENCES

1. H.Dislich, "Glassy and Crystalline Systems from Gels : Chemical Basis and Technical Application, "J.Non-Cryst.Solids, 57, pp.371-88, 1983.
2. B.E.Yoldas, "Preparation of Glasses and Ceramics from Metal-Organic Compounds, "J.Mater.Sci., 12, pp.1203-1208, 1977.
3. S.Sakka and K.Kamiya, "Glasses from Metal Alcoholates, "J.Non-Cryst.Solids, 42, pp.403-422, 1980.
4. A.R.Gutierrez, J.Friedrich, D.Haarer and H.Wolfrum, "Multiple Photochemical Hole Burning in Organic Glasses and Polymers:Spectroscopy and Storage Aspects, "IBM J.Res.Dev., 26[2] pp.198-208, 1982.
5. A.Makishima and T.Tani, "Preparation of Amorphous Silicas Doped with Organic Molecules by the Sol-Gel Process," J.American Ceramic Soc. 69, 4, pp.c72-74, 1986.
6. A.Makishima and T.Tani, "Functional Organic-Inorganic Composite Amorphous Materials and Process for its Production", U.S.P., 46393229(Jan.27, 1987).
7. T.Tani, A.Makishima, H.Namikawa, and K.Arai, "Photochemical Hole Burning Study of 1,4-dihydroxyanthraquinone in Amorphous Silica" J.Appl.Phys.58(9), 1 November, pp.3559-3565, 1985.
8. M.Nogami and Y.Moriya, "Glass Formation Through Hydrolysis of  $\text{Si}(\text{OC}_2\text{H}_5)_4$  with  $\text{NH}_4\text{OH}$  and  $\text{HCL}$ , "J.Non-Cryst.Solids, 37, pp.191-201, 1980.



SOL-GEL OPTICS

Volume 1328

**SESSION 5**

**Films and Coatings I**

*Chair*

**David A. Payne**

University of Illinois/Urbana-Champaign



92-11428



## SOL GEL SYNTHESIS OF OPTICAL THIN FILMS AND COATINGS

D.R. Uhlmann, J.M. Boulton, G. Teowee,  
L. Weisenbach and B.J.J. Zelinski  
Department of Materials Science and Engineering  
Arizona Materials Laboratory  
University of Arizona  
Tucson, Arizona 85721

ABSTRACT

Sol-gel methods offer a number of notable advantages for the synthesis of optical films and coatings. Areas of potential or actual application of this technology range from single layer and multilayer antireflection coatings to embossed planar waveguides and organic-modified oxide materials. The most notable advantages of these wet chemical methods will be surveyed, as will progress achieved to date in a number of the most attractive representative areas. The technical bases for the success/failure in each case will be considered. Also to be discussed will be the prospects - in both the near-term and long-term - of future developments in the sol-gel synthesis of optical films, as well as the principal technical hurdles which must be overcome in order that such synthesis methods may achieve more widespread use in the future. Finally, a comparison will be made between the microstructures and characteristics of films and coatings deposited using sol-gel methods with those deposited from the vapor phase. In all cases, use will be made of recent advances in our laboratory in the subject area.

I. INTRODUCTION

Wet chemical deposition of optical films is a rapidly advancing technology. Coatings can be formed from solution by a number of methods, including spin, dip, spray and roller coating; a wide range of compositions can be synthesized; doping can readily be effected; and the inherently high raw material cost of wet chemical processing is relatively unimportant in the case of coatings because competitive optical coating techniques, such as CVD or sputtering, are highly capital intensive and thus are also expensive.

The characteristics of wet chemical processing proves particular opportunities for synthesizing films for optical applications. These include: (1) The solutions employed can be vehicles for incorporating specific active constituents, such as colloidal particles for colored coatings or luminescent rare earth ions; (2) The highly porous intermediate state can be used to good advantage, as in preparing graded index antireflection coatings, in infiltrating optically-active dyes, and in providing contrast in properties between densified and non-densified regions; (3) The

92 4 28 046

ease of changing composition makes available a wide range of indices of refraction; (4) The range of properties between the just deposited gel and final glass opens a useful window in mechanical properties which permit procedures such as embossing to be applied to coatings; (5) In the case of multicomponent coatings, problems with vapor phase deposition methods (use of multiple targets, preferential deposition of specific components, etc.) are substantially reduced or eliminated; and (6) The ability to coat large areas and non-flat geometries with economic efficiency.

The present paper will review the principal developments to date in the wet chemical synthesis of optical coatings. Attention will first be directed to passive coatings and subsequently to active coatings. Looks will be taken into an admittedly hazy crystal ball to project some courses of future development and to identify present outstanding problems.

## II. PASSIVE COATINGS

### A. Antireflection Coatings

Antireflection (AR) coatings provide a good example of the exploitation of the versatility of the sol-gel process to solve technological challenges. To reduce reflection losses at the surface of an optical medium, two principal approaches have been employed. In the first approach, an AR film, whose optical path length is  $1/4 \lambda$  of the incident radiation, is deposited on the surface. The refractive index,  $n$ , of the AR coating is intermediate between the indices of the body and the external medium. This condition often requires the use of materials with  $n$  values less than 1.3, and hence directs attention to the use of porous coatings. When films with  $n$  values of 1.4 - 2.3 are required, a binary silicate system such as  $\text{SiO}_2\text{-TiO}_2$  is generally used.

Despite the replacement of one interface with two, the reflection losses are reduced in this single layer antireflection (SLAR) configuration. Reflection at the top surface is lower than the original interface reflectivity because the indices are more closely matched, and the reflection at the coating-substrate interface is reduced to zero because the coating is at the quarterwave condition.

The SLAR approach is effective only at one  $\lambda$  because of the quarterwave condition, but by using several layers, properly adjusted to have reflectance minima at close but not identical  $\lambda$ 's, it is possible to increase significantly the band in  $\lambda$  over which low reflection losses can be achieved.

The second approach for obtaining low reflection losses over a range of  $\lambda$  is based on the fact that reflection is caused by the

sharp index discontinuity at the interface. In this approach, the sharp interface is essentially eliminated by depositing a film whose  $n$  varies smoothly between the original interface  $n$ 's. The gradient in the  $n$  of the film is achieved by controllably modifying the pore structure and composition of the film.

Sol-gel methods have been used to exploit both approaches for preparing AR coatings<sup>1</sup>. Single-layer, double-layer, multi-layer and gradient index coatings have been deposited on a variety of materials. These coatings utilize the inherent flexibility of wet chemical methods to manipulate the chemical composition and film microstructure to make coatings for specific applications. As examples, porosity can be controlled by altering the size and structure of the condensed species prior to deposition, dip-coating gives generally denser films than spin-coating, after deposition, the  $n$  of the coating can be decreased by etching or increased by thermal treatment (densification and/or crystallization). Sol-gel routes also have potential economic advantages. It has been estimated that coating solar cells by sol-gel methods is 5% of the cost per watt required to coat using conventional methods.<sup>2</sup>

Various SLAR sol-gel coatings have been studied including  $Ta_2O_5$ <sup>2,3</sup>,  $SiO_2-TiO_2$ <sup>2,4</sup> and  $SiO_2-B_2O_3-Al_2O_3-BaO$ <sup>1,5</sup>. Single layer  $SiO_2-B_2O_3-Al_2O_3-BaO$  coatings have been deposited on glass and plastics for solar thermal and photovoltaic applications<sup>1,5</sup>. These coatings provided a quarter-wave, single layer interference surface with a reflectance minimum of <1% at 600 nm. Pettit et al.<sup>1</sup> investigated the use of this system for AR coatings on Pyrex, and found that aging of the solution prior to deposition was a key factor in the development of the desired microstructure. When fired to 500C coatings made from unaged solutions did not etch because the films were dense. Coatings made from aged solutions contained a large fraction of porosity after firing which permitted the acid treatment to modify the pore structure and obtain optimum AR behavior. Modification of the process enabled plastics (acrylic and polycarbonate) to be coated successfully without heating or etching.

With respect to performance, SLAR  $SiO_2-TiO_2$  coatings have increased the efficiency of Si solar cells (up to 48%)<sup>2</sup>. Compared to plasma  $SiN_x$  coatings, however, sol-gel derived  $SiO_2-TiO_2$  films have a narrower range of reflectance<sup>6</sup>. Double layers of  $SiO_2$  and  $TiO_2$  have also been deposited on Si solar cells increasing efficiency by 44%<sup>6</sup>, and double layers of  $TiO_2$  and 90%  $SiO_2$ -10%  $TiO_2$  increased efficiency by 49%<sup>2</sup>. Triple interference layers ( $TiO_2/SiO_2-TiO_2/SiO_2$ ) have been deposited by sol-gel dip-coating on both sides of plate glass. These coatings reduce reflection by 90% and are used in the manufacture of front covers for computer terminals<sup>7,8</sup>. Three layer coatings ( $SiO_2-TiO_2/ZrO_2/SiO_2$ ) on optical glass have been prepared from alkoxides for AR use in near infra-

red applications. These films gave ~99.6% transmission in the wavelength range 1.1-1.3  $\mu\text{m}$ <sup>9</sup>.

The conventional approach to making graded index AR coatings is to vapor deposit onto the interface a glass coating which phase separates when heat treated. One of the phases is then chemically etched or leached to produce a porous structure with a graded index. The disadvantages with this method include substrate deformation and a limited number of suitable glass compositions<sup>1</sup>.

In the wet chemical approach to graded index AR coatings a porous layer is first deposited and exposed to a chemical etching treatment. The etchant not only increases the scale of the pore structure but also preferentially etches one or more of the glass cations to produce a gradient in composition (and hence  $n$ ) through the film. Since the pore structure dominates the etchant interaction, and not the requirement for phase separation, many more glass compositions are available for different applications than with the conventional approach.

Chemical leaching of multicomponent silicate gel coatings ( $\text{SiO}_2\text{-BaO}$ ,  $\text{SiO}_2\text{-B}_2\text{O}_3\text{-Na}_2\text{O}$ ) can produce films for high power laser applications with reflectivities in the range 0.15-0.7% at 1.06 $\mu\text{m}$ . These films have up to four times greater threshold damage than conventional AR coatings.<sup>10-12</sup> Porous silica coatings deposited by wet chemical routes have also been investigated as high threshold damage coatings<sup>13-15</sup>.  $\text{SiO}_2\text{-TiO}_2$  sol-gel derived coatings, deposited under clean conditions, also show higher laser damage resistance than similar coatings prepared by vacuum deposition<sup>7</sup>.

An alternative approach to gradient-index AR coatings is to coat a series of  $\text{SiO}_2$  sols of differing particle sizes (TMOS-based sols aged for differing time periods). This method has the potential to overcome problems associated with chemical etching and leaching to produce a coating with graded porosity<sup>16,17</sup>.

Finally, taking advantage of the use of sol-gel solutions as vehicles for colloidal particles, AR light-scattering coatings have been prepared by spray-coating alcoholic solution of colloidal  $\text{SiO}_2$  particles suspended in a partially condensed Si alkoxide. The optical quality of the coatings are comparable with that of acid-etched glass surfaces<sup>8</sup>.

## B. Planar Waveguides

Planar waveguides are used in integrated optical circuits to route signals between different input, output and processing components of a chip. Since light is guided in the plane of these coatings, these films must be of reasonably high optical quality. Index uniformity must be sufficient to achieve losses on the order

of 1 dB/cm or less and compatability requirements indicate that processing should permit n reproduciblity to at least 1%.

The first reported use of wet chemical techniques for synthesizing planar waveguide synthesis was by Ulrich and Weber in 1972.<sup>18</sup> These authors dip coated commercially available PbO-SiO<sub>2</sub> solutions onto glass slides and synthesized waveguides with index 1.6 and losses of 0.5 dB/cm at 632 nm. In 1983, Tiefenthaler et al.<sup>19</sup> dip-coated LiNbO<sub>3</sub> from commercially available solutions to make waveguides of index 2.1. They also made SiO<sub>2</sub>-TiO<sub>2</sub> waveguides of compositions 1:1, 1:2 and 1:3. Losses at HeNe and Ar λ's were determined to be < 1 dB/cm. The SiO<sub>2</sub>-TiO<sub>2</sub> system is often utilized for such waveguide applications because the n can be tailored between the two end member values of 1.46 for SiO<sub>2</sub> and about 2.6 for TiO<sub>2</sub>.

La Serra et al.<sup>20</sup> and Aegerter et al.<sup>21</sup> have synthesized PbO-TiO<sub>2</sub> waveguides by dip coating glass slides. Their dipping solution was prepared by reacting Ti(O<sup>i</sup>Pr)<sub>4</sub> with 2,4-pentanedione and then mixing with Pb acetate. By applying as many as 15 coatings these authors produced 1 micron thick films which guided several orders of the TE mode. The films exhibited good optical quality and no apparent scattering was caused by the many interfaces in the films.

Research conducted by our group<sup>22,23</sup> on the synthesis and properties of SiO<sub>2</sub>-TiO<sub>2</sub> waveguides has shown that index reproducibility is a sensitive function of processing. Fig.1 shows n versus temperature for two sets of 50:50 SiO<sub>2</sub>-TiO<sub>2</sub> waveguides. These waveguides were synthesized from Si and Ti alkoxides using 2,4-pentanedione as a complexing agent. One set of films was prebaked at 100C for 1.5 mins. and then heated to the indicated temperature and the other was immediately immersed into the furnace after spin coating. This variation in thermal processing produces about a 3% variation in the observed film index after heating at 400C. These results support earlier observations on the effects of thermal processing on SiO<sub>2</sub>-TiO<sub>2</sub> films used as AR coatings.<sup>1</sup> These effects are most likely caused by variations in the film viscosity due to thermally induced differences in the crosslink density of the films. Films which experience a prebake or a slow heating rate are more crosslinked by the time they reach elevated temperatures, and hence they flow and densify at a slower rate.

Fig. 2 shows the relationship between n and shrinkage for films fired at the indicated temperatures for one hour. In this figure shrinkage has been normalized using the film thickness after a 100C, 1.5 minute prebake. The results indicate a processing window between 500 and 600C where stable values of both n and thickness can be achieved. Losses in these waveguides are about 1-2 dB/cm. The index increases upon firing at temperatures above 600C due to the crystallization of TiO<sub>2</sub>.<sup>23</sup>

Despite the wide range of available compositions, only a limited number of systems have been investigated to date for planar waveguide applications. In addition, the origin of loss in these films remains to be identified. Losses in these waveguides are all around 1 dB/cm. Computer simulations performed by Weller-Brophy et al.<sup>24</sup> have indicated that the losses cannot be caused by surface scattering at the interfaces. This suggests that volume fluctuations in the  $n$  limit the loss. Density fluctuations in the form of porosity and/or chemical inhomogeneity are possible sources for these fluctuations.

### C. Surface Patterning in Sol-Gel Films

Many optical applications are based on the use of surface relief features or gratings in or on thin films. Specific grating geometries are used to create a wide range of optical components including input/output couplers, focusing grating couplers, distributed feedback gratings, filter, lenses, beam splitters and mirrors. Two creative approaches have been used to generate these types of surface relief structures in wet chemical films. In the first, embossing or pressing of a pattern is used to create a negative of the master in the film. The technique is based on the malleability of sol-gel films at suitable stages of processing. The process has been used for some time to form surface relief structures in polymer films. However, the sol-gel process now provides the opportunity to manufacture these gratings in dense, hard dielectric materials.

Tiefenthaler<sup>19,25</sup>, Heuberger et al.<sup>26</sup> and Lukosz<sup>27</sup> have reported extensive work on embossed  $\text{SiO}_2$ - $\text{TiO}_2$  waveguide structures. They produced embossed grating couplers with 1200 lines/mm in dip-coated waveguides made from commercially available organometallic solutions. After a densifying heat treatment the gratings were found to have retained their periodicity and spatial frequency. The resulting profiles were, however, quite shallow, having a depth much less than the film thickness of 120 nm. The impressed grating structure produced an input coupling efficiencies of 50%. Attempts to make gratings with 2400 and 3600 lines/mm were not so successful.

Roncone et al.,<sup>28,29</sup> have successfully embossed deep grating structures into sol-gel derived films. In this work 50:50  $\text{SiO}_2$ - $\text{TiO}_2$  solutions were spin coated onto microscope slides and then pre-baked by heating at 70C for 0 to 80 minutes. After prebaking, the films were embossed and fired at 400C for 30 mins. The master was a photoresist grating coated with Au-Pd prior to use.

Fig. 3 shows SEM micrographs of the grating structure which resulted for films prebaked for 15 mins. The resulting gratings are "negatives" of the master. Although the exact (negative) profile is not replicated, the negative duty cycle and period (0.52

$\mu\text{m}$ ) are. The embossed grating depths are 0.1-0.2  $\mu\text{m}$ , compared with the 0.4  $\mu\text{m}$  depth of the master grating. It is likely that they represent the depths achievable with a master grating depth of 0.4  $\mu\text{m}$  because the films exhibit a 60-70% shrinkage during the post-emboss baking. The exact relationship between master grating shape and the resulting embossed grating shape has, however, yet to be determined.

Roncone et al. also documented the changes occurring in the embossing mechanism as a function of the pre-emboss bake. At early prebake times adhesion of the film to the master was a problem, at intermediate times, the films were quite moldable and flowed under the influence of the master, and at long times, the grating structure was not replicated but periodic stress cracks were produced. At the last stage, the film is sufficiently crosslinked to prevent significant plastic deformation.

In related work, Tohge et al.<sup>30</sup> have been successful at embossing deep features into sol-gel films by modifying the film viscosity through addition of an organic species to the coating solution. These researchers investigated the effects of polyvinyl alcohol, cellulose, polytetramethylene glycol and polyethylene glycol (PEG) on patterning. Only PEG was found to improve significantly the surface replication properties of the coating. Using PEG in a  $\text{SiO}_2\text{-B}_2\text{O}_3$  solution, Toghe et al. successfully embossed surface structures onto glass disks. PEG additions produced films that were much softer, and therefore more moldable, than films with no PEG. After embossing, the PEG was burned out of the sample.

Matsuno et al.<sup>31</sup> synthesized pregrooved glass disks by embossing  $\text{SiO}_2\text{-TiO}_2\text{-PEG}$  solutions which had been coated onto glass substrates. This produced films which replicated the 1.6  $\mu\text{m}$  pitch of the master. The final groove depth was a function of the PEG content of the film and as large as 122 nm. The  $n$  of samples containing PEG was observed to be lower than the same compositons formed without PEG.

Much of this work demonstrates the importance of thermal treatment in establishing conditions for embossing sol-gel coatings. Very little is known, however, about the evolution of the mechanical properties of thin films during the sol-gel-oxide transitions, or about the impact of precursor chemistry and additives on the evolution of mechanical properties during heat treatment.

In addition to the applications cited above for surface relief gratings, several specialized applications are being pursued. Lukosz et al.<sup>32</sup> observed directional switching in  $\text{SiO}_2\text{-TiO}_2$  planar waveguides as a function of the adsorption and desorption of water and other molecules. Tiefenthaler et al.<sup>33,34</sup> demonstrated that



input grating couplers on planar  $\text{SiO}_2\text{-TiO}_2$  could be used as a sensitive humidity sensor, and using the sensing effect could be made into a switch (utilizing the induced change in  $n$ ). Tiefenthaler and Lukosz<sup>35</sup> suggested that the sensitivity of the thin films to humidity and other molecules was caused by two factors: adsorption and desorption of vapor phase molecules from (1) the external surface of the film, and (2) the internal surfaces associated with the porosity in the film.

In addition to the potential practical applications, this phenomena has important implications with respect to reproducibility in  $n$ . Lukosz, et al., observed a  $\Delta n$  of 0.04 between films that had adsorbed water vapor versus dry films. This large index change, while useful for sensing applications, would be devastating in applications which require extremely stable values of  $n$ . Further work needs to be done to establish the relationship between the atmosphere sensitivity of  $n$  and the film microstructure.

Lukosz et al.<sup>36</sup> dip-coated  $\text{SiO}_2\text{-TiO}_2$  waveguides onto a commercial thin film electrode and made an integrated thermo-optic switch. They measured a change in the  $n$  with temperature as a voltage was applied across the electrode. Lukosz et al. also observed optical bistability and self-pulsing in  $\text{SiO}_2\text{-TiO}_2$  planar waveguides coupling with prisms and grating couplers.<sup>37-43</sup> The optical bistability is due to a photo-thermal mechanism, the interaction of the evanescent wave with the metal layer causes a local change in temperature which causes the film to expand. The expansion of the film decreases the optical gap between the film and the external grating used for coupling into the film. The optical bistability was measured by measuring the output power vs. the input power.

Lukosz et al.<sup>44</sup> and Nellen et al.<sup>45</sup> demonstrated the use of  $\text{SiO}_2\text{-TiO}_2$  waveguides with and without embossed gratings as biochemical sensors, used to detect specific proteins of the human and rabbit immune systems. A change in  $n$  as small as  $1 \times 10^{-6}$  could be detected.

Another approach for patterning sol-gel films is based on the use of laser light to densify local regions of the film. The undensified regions can then be etched away to produce surface features. Krchnavcek et al.<sup>46</sup> used an argon laser to do maskless writing of  $\text{SiO}_2$  onto Si substrates. The heat source was the Si substrate beneath the film which absorbed the laser light. The authors argued that heating in this manner will avoid any cracking, and provides a way of controlling densification in the  $z$ -direction. This method was also used to place patterns onto GaAs, CdS and  $\text{SiO}_2$  substrates.

Shaw et al.<sup>47</sup> used a CO<sub>2</sub> laser to densify a thin surface of a silica disk. Density and hardness changes with heating were measured, and used to determine a "densification threshold", above which bloating and the formation of bubbles was noted. The penetration depth of the CO<sub>2</sub> laser was 40  $\mu$ m. In this technique the laser light is coupled into the metal-oxygen bonds of the film to provide heating. As a result, the technique is not substrate specific.

In recent work, reported at this Conference, Fabes et al.<sup>48</sup> have used laser densification to generate channel waveguide structures in SiO<sub>2</sub>, SiO<sub>2</sub>-TiO<sub>2</sub> and Ta<sub>2</sub>O<sub>5</sub> coatings. SiO<sub>2</sub> slides were first coated, covered with a thin metal layer, and then translated across a Nd:YAG laser beam. The laser energy was absorbed by the metal film, which heated the underlying sol-gel coating causing local densification. Ridged waveguide structures were formed by etching away the undensified portion of the waveguide.

These workers have also shown that photolithographic techniques can be used to define waveguide structures on a coating. A photoresist masking process was used to define an array of metal lines on the sol-gel coatings. Rastering the laser beam over the sample caused consolidation only over those portions of the coating which had been delineated by the masking process.

The use of laser techniques to generate surface relief structures in optical films is in its infancy. With the exception of the work by Fabes et al., only SiO<sub>2</sub> coatings have been investigated.<sup>49-51</sup> A variety of different laser  $\lambda$ 's have been exploited. Each of them has advantages and disadvantages. The CO<sub>2</sub> laser is convenient in that it will couple into any oxide film, but the interaction volume is large (about 40 microns). While this may be acceptable for single layer systems, if multilayer sequential processing is required, such lasers may lead to undesirable inter-layer interactions. Densification using Ar or Nd:YAG laser both require the presence of a metallic layer to absorb the laser light. At high powers, implantation or melting of the metal layer may cause problems with metallic impurities. However, the interaction volume is much smaller for these systems and photolithography can be used to mask and then densify fine features rapidly and repeatably.

Other issues remain to be addressed including the potential for carbon and other gas entrapment due to the rapid thermal processing. Also the impact of this rapid thermal processing on microstructure development, including crystallization, remains to be established.

#### D. Colored Coatings

Sol-gel routes to coating substrates have allowed a number of novel colored compositions to be developed. Because these films are typically quite thin, imparting color to the film is achieved via scattering effects and not absorption. Yellow coatings of  $\text{CeO}_2\text{-TiO}_2$  have been deposited on soda-lime-silica,  $\text{PbO}$ -containing glass and Al foil by dip-coating a solution of  $\text{CeCl}_3$  and  $\text{Ti}(\text{O}^i\text{Pr})_4$  and firing to  $500^\circ\text{C}$ <sup>52,53</sup>. These films had good chemical durability and adhesive properties. Coatings of  $\text{SiO}_2$  and transition metal oxides have been extensively studied, using transition metals such as Fe, Co, Ni, Mn, Cr and Cu<sup>54-59</sup>. With mixtures of transition metal oxides, the order of depositing different layers influenced the final color, although no redox reactions occurred between the different transition metals<sup>55</sup>. Other work<sup>59</sup> has also demonstrated that thin films can have strong colors due to the presence of colloidal particles.

An alternative approach to colored coatings involves incorporating inorganic pigments into alkoxide coating solutions.<sup>60</sup> For example, white  $\text{ZnO}$  films have been prepared from a dispersion of  $\text{ZnO}$  in an iso-propanol solution of Zn iso-propoxide.

#### E. Reflective Coatings

$\text{TiO}_2\text{-Pd}$  (IROX) coatings are produced commercially by Schott Glaswerke<sup>7</sup>. Double-sided, single layer coatings are applied to large plates of float glass from solution using a dip coating process. The glass plates are coated with an alkoxide based solution containing colloidal Pd particles. As the plates are pulled from the coating solution they are exposed to an atmosphere containing water vapor to set the film. The plates are then fired at  $400\text{-}500^\circ\text{C}$  to densify the coatings. The coatings are used for solar control applications. Various ratios of transmission to reflection can be obtained by modifying the Pd content. Similar  $\text{TiO}_2\text{-Au}$  coatings are produced commercially by the Asahi Glass Company.

Transparent IR reflecting coatings have also been produced by wet chemical methods. These include ITO<sup>61</sup> and Sb-doped  $\text{SnO}_2$ .<sup>62</sup> To the best of the present authors' knowledge, such coatings are not produced commercially.

$\text{TiO}_2\text{-SiO}_2$  sol-gel derived coatings on soda-lime-silica glass are used for head up display purposes in automobiles.<sup>63</sup> In this application, which has been commercialized on Nissan cars, alkoxide-based solutions are coated onto the desired area of a glass plate. After patterning, resist coating and etching, the coated area is densified and the glass bent and laminated to produce a windshield having an abrasion-resistant area with high reflectivity. This area permits heads-up observation of the

vehicle's speed projected from a high brightness vacuum fluorescent display.

### III. ACTIVE COATINGS

#### A. Electrooptic Materials

Electrooptic (EO) thin film materials are increasingly important in the development of optical device technology. Examples include optical phase retarders, optical and electrooptic switches, spatial light modulators, and devices based on optical phase conjugation. EO materials also have potential for optical data storage and computing by exploiting their inherent field induced birefringence to create a two-state optical system. Typical EO materials are ferroelectric (FE) with crystal structures which lack a center of symmetry. Notable examples include  $\text{Pb}(\text{Zr},\text{Ti})\text{O}_3$  (PZT),  $\text{PbLaZr}$  titanate (PLZT),  $\text{SrBa}$  niobate (SBN),  $\text{PbMg}$  niobate (PMN) and  $\text{LiNbO}_3$ .

EO thin films can be single crystal or polycrystalline. For signal processing in the plane of the film (e.g., waveguides) inhomogeneity in  $n$  must be minimized to reduce losses. This is best achieved by using single crystals since grain boundaries present in polycrystalline materials are regions of either compositional or structural discontinuities which produce undesirable variation in  $n$ . This requirement does not, however, preclude the use of oriented epitaxial films. These films may be sufficiently uniform to exhibit losses of less than 10 dB/cm.

For in-plane application which rely on second or higher order harmonic generation the film must be phase matched. In this case only selectively oriented single crystal films are acceptable. Unfortunately, single crystal thin film materials are difficult to synthesize. This difficulty arises from the requirement that the crystal layer be grown in a desired orientation on a substrate that provides the proper epitaxial relationship for growth.

For through plane applications the optical path length is small so polycrystalline materials can be utilized without significant losses. For many applications, the polycrystalline nature of the film offers many advantages compared to single crystal films. Poling is often utilized to orient the domain structure and/or the optic axes. In single crystals, the optic axis is constrained by the crystal orientation. Also, the grain boundaries in polycrystalline films exert a clamping effect on the domain structure and make possible localized switching within a small volume. This phenomena increases the resolution achievable in optical memory systems. Detrimental film-substrate chemical interaction are often more extensive in polycrystalline films due to preferential segregation and favorable diffusion sites along grain or domain boundaries.

The composition of the film is also application specific. In applications where domain reversals are used PLZT's are the favored material because they possess faster switching times and lower coercive fields than other FE materials. To optimize the quadratic electrooptic coefficient (R), PLZT compositions are chosen which possess the near-cubic crystal structure. Due to the near-cubic symmetry, there is either little or no permanent polarization; and the birefringence exists as long as the electric field is applied.

Optimization of the linear electrooptic coefficient ( $r_c$ ) and coercive field is achieved in samples having compositions with a pronounced tetragonal character. There is a close relationship between induced birefringence and strain. Because these materials are tetragonal, the differences in expansion coefficient along different crystallographic axes induce strains in the film. Also, the linear EO effect is an intrinsic material characteristic, not due to any domain reorientation process. Hence the high coercive field will not mask this effect.

The ability to tailor EO coefficients through compositional and subsequently structural variations is found in other ferroelectric materials as well. As an example, the composition-driven electrooptic properties for PLZT are shown in Table 1.

Table 1: Electrooptic Coefficient of Bulk Ceramics

COMPOSITION (x,y,z)	LINEAR COEFFICIENT, $r_c$ $\times 10^{-10} \text{m/V}$	QUADRATIC COEFFICIENT, R $\times 10^{-16} \text{m}^2/\text{V}^2$	REFERENCE
PLZT <sup>a</sup> 8.5/65/35		38.60	64
PLZT 9/65/35		3.80	64
PLZT 9.5/65/35		1.50	64
PLZT 10/65/35		0.80	64
PLZT 12/65/35		0.16	64
PLZT 8/40/60	1.02		64
PLZT 12/40/60	1.20		64
PLZT 14/30/70	1.12		64
KTN <sup>b</sup> 65/35		0.17	64
SBN <sup>c</sup> 50/50		2.10	64
SBN 75/25		14.00	64
LiNbO <sub>3</sub>	0.16		64
LiTaO <sub>3</sub>	0.22		64
Ba <sub>2</sub> NaNb <sub>5</sub> O <sub>15</sub>	0.38		65
KDP	0.52		64

<sup>a</sup> For PLZT's x,y,z refers to the formula  $\text{Pb}_{1-x}\text{La}_y(\text{Zr}_{1-x}\text{Ti}_x)_{1-x/4}\text{O}_3$

<sup>b</sup> For KTN x,y refers to the formula  $\text{KTa}_x\text{Nb}_{1-x}\text{O}_3$

<sup>c</sup> For SBN x,y refers to the formula  $\text{Sr}_x\text{Ba}_{1-x}\text{Nb}_2\text{O}_6$

A major problem in the synthesis of SBN, PZT, and PLZT films by all techniques is the undesirable formation of metastable pyrochlore phases during post-deposition annealing processing. This paraelectric material is detrimental to optical film performance because, as a second phase, it contributes to scattering losses and reduces the volume percent of FE phase in the films. Conversion of the pyrochlore phase to the stable perovskite phase can be difficult and typically requires post-deposition annealing under special atmospheres at elevated temperature. Such annealing can cause deleterious film-substrate reactions.

The pyrochlore phase is a defect structure having the basic formula of  $A_2B_2O_7$ . It can be either oxygen or lead deficient. The basic structural unit for both the pyrochlore and perovskite structure is a corner shared  $BO_6$  octahedron. In the pyrochlore structure the octahedra are joined in a zig-zag fashion along the (110) direction while in the perovskite structure they form linear chains along the (100) direction. This similarity in structure most likely accounts for the early formation of the metastable pyrochlore phase as well as its sluggish conversion to the stable perovskite phase. Unfortunately, there exists no comprehensive investigation of the chemical and kinetic factors which influence phase evolution in such systems.

The pyrochlore phase does not form when PLZT is deposited on a fully crystallized  $PbTiO_3$  layer.<sup>66</sup> This does not represent a universal cure, however, because the  $PbTiO_3$  layer may be detrimental to EO performance due to losses from multiple reflection at interfaces or a lowering of the composite EO coefficients.

Many PLZT films have been made by sputtering. Sputtered epitaxial PLZT films, including single crystalline films, have been obtained on substrates such as MgO and sapphire. For example, 28/0/100 PLZT films exhibited epitaxial (111) and (211) on (0001) and (1010) sapphire respectively<sup>66,67</sup> while the preferred orientation is (100) when (100) single crystal  $SrTiO_3$  or spinel is utilized.<sup>68</sup> The crystallinity of such films increases when an intermediate layer of  $PbTiO_3$  is used. Attempts to spray-pyrolyze PLZT on sapphire led to the formation of a non-perovskite, non-pyrochlore phase.<sup>69</sup> Second harmonic generation in ion-sputtered PLZT films with compositions between 7/0/100 and 28/0/100 has been reported<sup>70</sup> with the signal decreasing with increasing La content.

Various EO thin films have been prepared using wet chemical processing. These include PZT<sup>71</sup>, PLZT<sup>72</sup>, SBN<sup>73</sup> and  $LiNbO_3$ <sup>74-78</sup>. Wet chemical synthesis of PLZT films is usually based on the use of Pb and La salts, such as acetates, in combination with Zr and Ti alkoxides. These precursors are often reacted in methoxyethanol<sup>71</sup> to form complex alkoxides. The solvent is, however, teratogenic

and can cause neurological and hematological damage even at the ppm level.

For sol-gel derived 8/65/35 PLZT films on sapphire, preferred orientation was observed in the (001) plane parallel to substrate when annealed at 750C. The degree of preferred orientation decreased with further heating to 850C.<sup>72</sup> Schwartz et. al.<sup>66</sup> reported (111) orientation for chemically derived PLZT films on platinized silicon.

The linear and quadratic EO coefficients of both sol-gel and sputtered PLZT films are tabulated in Table 2. The data on sol-gel derived PLZT films are very limited. The results in the table indicate, however, that the properties of sol-gel derived films compare very favorably with those of sputtered films.

Table 2: Electrooptic Coefficient of PLZT Thin Films

COMPOSITION (x/y/z) <sup>a</sup>	LINEAR COEFFICIENT, $r_c$ $10^{-11}$ m/V	QUADRATIC COEFFICIENT, R $\times 10^{-16}$ (m/V) <sup>2</sup>	REFERENCE
8/65/35	3.0	0.5	72, Sol-gel
0/60/40 (PZT)	2.4	0.01	79, Sol-gel
28/0/100		0.8	67, Sputtering
9/65/35		1.0	80, Sputtering
28/0/100		0.6	
14/0/100	2.8		80, Sputtering
21/0/100	8.1		80, Sputtering
9/65/35		0.6	70, Sputtering

<sup>a</sup> Here x/y/z refers to the formula  $Pb_{1-x}La_y(Zr,Ti_z)_{1-x/4}O_3$ .

It is interesting to compare these thin film properties with those of bulk material in the same systems. The EO coefficients of bulk materials are shown in Table 1. It is apparent that the values for the films are consistently lower than those for bulk samples. Possible reasons for this include film-substrate chemical interaction leading to the formation of deleterious intermediate layers, differences in the amount and distribution of pyrochlore phases in thin film and bulk samples, and differences in porosity. Porosity differences are expected because traditional bulk

synthesis techniques often include hot-pressing to enhance densification. Further, the effects of substrate clamping on the film samples could limit the development of optimum values of the quadratic coefficient in a fashion similar to that of the well-known thickness dependence of dielectric properties of FE thin films.

$\text{LiNbO}_3$  is a versatile EO material used widely for its piezoelectric, pyroelectric, birefringent, photoelastic and photorefractive properties. Sputtering has been used to make  $\text{LiNbO}_3$  films but liquid phase epitaxy (LPE) is the favored technique, specially to obtain single crystal  $\text{LiNbO}_3$  films.

Sol-gel derived  $\text{LiNbO}_3$  film have been prepared, some exhibiting c-axis preferred orientation on (0001) sapphire.<sup>74-78</sup> No such behavior is observed, however, for films deposited on Si.<sup>77,78</sup> The presence of an amorphous layer of native oxide on Si can negate any possible epitaxial effect. Interestingly, sputtered  $\text{LiNbO}_3$  films on Si shows c-axis preferred orientation if the substrate is Si(111) but many preferred orientations if Si(100) is used instead.<sup>81</sup> This could be due to the varying degree of lattice mismatch.

$\text{LiNbO}_3$  films can crystallize at temperature as low as 250C if an underlying fully crystallized film is first deposited. When single crystal  $\text{LiNbO}_3$  is used as a substrate, epitaxial films are obtained.<sup>82</sup> The refractive index of sol-gel  $\text{LiNbO}_3$  films is 2.10 - 2.25<sup>83</sup> comparable to that of sputtered film but less than the single crystal value, presumably due to residual porosity.

Hirano has reported making a successful waveguide using a sol-gel derived Ti-doped  $\text{LiNbO}_3$  film.<sup>78</sup> No data on attenuation were reported. The losses are expected to be high due to grain boundary scattering. There are no reports on EO coefficients on these films. The dielectric constant has been measured as about 22; and the value of  $\tan \delta$  is highly dependent on the choice of metal contacts used.

The attenuation losses for various PLZT and  $\text{LiNbO}_3$  films are tabulated in Table 3. It can be seen that eiptaxial films have higher losses than single crystal films. This likely reflects scattering from grain boundaries in the epitaxial films. Within the single crystal films, domain boundaries also exist which can cause scattering losses. Note that SBN and most PLZT compositions used in EO applications are relaxor FE's. In such materials, microheterogeneous regions such as microdomains lead to scattering losses. The effects of FE domains, whether "normal," microdomains or compositional inhomogeneities on scattering losses have received scant attention in the literature. Poling may be utilized to effect a monodomain single crystal FE film.



Table 3: Waveguide Loss in Sputtered Films

FILM	SUBSTRATE	LOSS dB/cm	REFERENCE
PLZT 28/0/100	sapphire	26	67 epitaxial
PLZT 9/65/35	sapphire	10	68 single
PLZT 28/0/100	sapphire	14	crystal
LiNbO <sub>3</sub>	LiTaO <sub>3</sub>	8	84 epitaxial
			85 single
			crystal

For obtaining high quality epitaxial single crystal LiNbO<sub>3</sub> films, non sol-gel techniques, namely LPE<sup>86,87,88</sup> and sputtering<sup>85,89</sup>, still dominate. Dopants such as Na, Ag, Ti, etc. have been successfully introduced via LPE.<sup>88</sup> The crystallinity of sputtered films can be enhanced by post-deposition annealing. This is one area where sol-gel processing has yet to compete - i.e. the fabrication of single crystal thin film materials.

In LiNbO<sub>3</sub>, polycrystalline films (obtained without much difficulty via sol-gel methods) introduce too much loss due to grain boundary scattering for optimum usage in EO application. This contrasts with PLZT where grains can be exploited for certain EO phenomena.

In viewing sol-gel and sputtered EO films, one particular advantage of sol-gel method stands out, namely the greater potential reproducibility of chemically derived films. With sputtered films, the film properties depend on a large number of parameters including the process used (diode, rf, or magnetron), the Ar pressure, Ar/O<sub>2</sub> ratio, substrate to target distance and substrate temperature. It is likely that sol-gel derived films will prove to be less sensitive to variation in process parameters.

## B. Dyes in Gels

The low temperatures associated with sol-gel processing offer an attractive route for incorporating thermally unstable organic molecules into inorganic matrices, either in bulk form or thin film form. It is impossible to prepare similar materials by conventional glass-forming methods unless extremely low melting glasses are used.<sup>90</sup> An alternative approach that has been considered is the adsorption of dye molecules in a porous glass.<sup>91</sup> Chemically derived oxide or organically modified oxide networks are far superior as host materials compared to organic polymers due to their higher thermal and photochemical stability. Potential applications of these novel materials investigated to date include solid-state dye lasers, solar light guides and optical memory devices.<sup>90,92,93</sup> Additionally, the incorporation of dyes and organometallic molecules in gels can provide useful insight into

sol-gel chemistry and gel structure by functioning as molecular probes.<sup>94,95</sup>

Fluorescent thin films have been prepared by incorporating fluorescent dyes into alkoxide-derived  $\text{SiO}_2$  and  $\text{SiO}_2\text{-TiO}_2$  films with the aid of a surfactant.<sup>96</sup> The dyes, such as rhodamine 6G, rhodamine B and oxazine-4-perchlorate were either encapsulated in the gel coatings as they formed or adsorbed onto the pore walls of pre-formed films. Dyes in the former coatings exhibited good resistance to leaching by water, in comparison to the adsorbed versions. Photophysical properties of the films indicated that the dye molecules were trapped within closed cages of  $\text{SiO}_2$  or  $\text{SiO}_2\text{-TiO}_2$  and that dye aggregation was considerably reduced compared to aqueous solutions.

The spectroscopic behavior of rhodamine 6G in solution, PMMA films and alkoxide-derived  $\text{SiO}_2$  have been compared.<sup>97</sup> The inorganic matrix gave the best performance with stable emission and absorption maxima and no change in emission intensity over a period of weeks. Addition of  $\beta$ -cyclodextrin (a cyclic polysugar) to the starting alkoxide solution gave the maximum amount of monomers in the film. The monomer is highly luminescent while the dimer is non-fluorescent. Rhodamine 6G has also been incorporated into alkoxide derived  $\text{SiO}_2$  coatings containing silver aggregates prepared in situ.<sup>98</sup> The aggregates gave an overall increase in absorption and emission of the dye due to energy transfer between the fluorescent dye molecules and the silver particles (interaction between the electric dipole of the dye and the localized electron clouds on each of the silver islands).

Many dyes have been incorporated into free standing  $\text{Al}_2\text{O}_3$  films (10-100 $\mu\text{m}$ ) prepared from colloidal sols.<sup>99-102</sup> The dyes, such as rhodamine 6G, showed lower degrees of aggregation in the films than in aqueous solutions. The incorporation of surfactants in the starting sol enabled a monomeric dispersion of the dye to be formed in the film. When a film containing a monomeric dispersion of rhodamine 6G was irradiated with a  $\text{N}_2$  laser, the film gave a laser emission with a beam divergence of  $\sim 0.1$  rad, which is typical of a dye laser. The calculated conversion efficiency was 2.1% which is close to the value obtained with a plastic host. However, continued irradiation resulted in bleaching - the power decrease was linearly proportional to the shot number indicating a one-photon process. In  $\text{Al}_2\text{O}_3$  films the laser emission of rhodamine  $\beta$  by  $\text{N}_2$  laser pumping could be increased by the addition of rhodamine 6G, which increases pumping efficiency.<sup>101</sup> Dyes active in photochemical hole burning and non-photochemical hole burning, such as sodium resorufin, 5,8-dihydroxy-1,4-naphthoquinone and  $\alpha, \beta, \gamma, \delta$ -tetrakis(4-sulphophenyl)porphine have also been incorporated into  $\text{Al}_2\text{O}_3$  films.<sup>102</sup>

With respect to non-linear optics, sol-gel derived composites of  $\text{SiO}_2$  and poly-p-phenylenevinylene have been prepared.<sup>103</sup> The value of  $\chi^3$  was dependent on composition and was  $\geq 5 \times 10^{-11}$  esu. This material formed promising waveguiding films. Recent results in our laboratory have shown that significant second harmonic generation can be obtained on incorporating non-linear organic dyes, such as 2-methyl-4-nitroaniline into organic-modified inorganic films.<sup>104</sup> The films were prepared by the hydrolysis and co-condensation of tetraethoxysilane and a trimethoxysilylpropyl substituted polyethyleneimine. Sol-gel approaches to  $\text{SiO}_2$ -based fluorescent paints<sup>105</sup> and  $\text{Al}_2\text{O}_3$ -based marking materials<sup>106</sup> have also been successful.

### C. Luminescent Coatings

Highly luminescent films have been prepared by incorporating  $\text{Tb}^{3+}$  and  $\text{Eu}^{3+}$  cryptates into sol-gel derived  $\text{SiO}_2$ .<sup>107</sup> Processing was performed at room temperature and no further thermal treatment was used. Encapsulation of the lanthanides in cryptate cages overcame the problem of quenching due to the effect of O-H oscillators on the excited states. Similar films based on  $\text{TiO}_2$ , have also been investigated as sensors.<sup>108</sup> In this application the luminescence of the  $\text{Eu}^{3+}$  cryptate is activated by the molecule to be sensed. The porous films gave absorption-energy-transfer-emission when exposed to salts of light harvesting 4-tert-butylbenzoic acid.

Cathodoluminescent films of  $\text{Tb}^{3+}$  doped  $\text{Y}_2\text{SiO}_5$  have been prepared from  $\text{Si}(\text{OEt})_4$  and nitrates.<sup>109,110</sup> The internal conversion of these films was about 40% of that of single crystal material.  $\text{Zn}_2\text{SiO}_4:\text{Mn}$  phosphor films have also been prepared.<sup>111</sup> Films up to 15  $\mu\text{m}$  thick could be obtained by using intermediate firing steps. The resultant film exhibited green luminescence on UV and cathode ray irradiation.

### D. Electrochromic Films

The classical electrochromic (EC) materials are W and Mo oxides. Films of these materials are typically prepared by vacuum methods such as evaporation and sputtering<sup>112,113</sup> but sol-gel routes are very amenable for producing EC coatings.<sup>114-123</sup>  $\text{WO}_3$  coatings have been prepared from tungstic acid<sup>114-117</sup> and tungsten oxyalkoxides.<sup>118</sup>  $\text{WO}_3 \cdot n\text{H}_2\text{O}$  coatings deposited from colloidal tungstic acid had a layer structure leading to anisotropic properties.<sup>115</sup> Chemical intercalation of long-chain alkylammonium ions and electrochemical intercalation of  $\text{Li}^+$  was possible. The intercalation of  $\text{Li}^+$  caused a blue coloration. The coloring efficiency of  $\text{WO}_3$  gels has been shown to be comparable to coatings prepared by other procedures<sup>116</sup>.  $\text{WO}_3\text{-MoO}_3$  gels have been cathodically deposited from a colloidal solution of  $\text{H}_2\text{WO}_4$  and  $\text{H}_2\text{MoO}_4$ .<sup>119</sup>

The electrochemical insertion of  $\text{Li}^+$  in  $\text{V}_2\text{O}_5$  gel coatings gave rise to anisotropic layers which turned from yellow to green.<sup>120</sup> Thicker (10  $\mu\text{m}$ ) layers gave a three-color device of red-yellow-green. Similar treatment of  $\text{TiO}_2$  gel coatings derived from  $\text{Ti}(\text{O}^n\text{Bu})_4$  gave a transparent to grey color change. Acetate chelation of the Ti alkoxide precursor, prior to coating, gave rise to similar electrochemical and EC properties (similar cyclic voltammogram and optical switching), but yielded a blue coloration instead of grey due to different ligand field environments.<sup>120</sup>

While wet chemical routes to transition metal oxide films for EC applications are attractive, they remain relatively unexplored. Process advantages over conventional vacuum deposition include the use of inexpensive coating equipment and the ability to coat large areas easily. Chemical advantages include the ability to form organically modified electrodes by using chelating agents to alter the ligand field environments of transition metal ions. Use of chemical methods to make a viable multilayer device would, however, be complicated by the interdiffusion of cations using several dip-and-fire steps as sharp inter-layer profiles are necessary for good EC behavior.

#### IV. CONCLUDING DISCUSSION

Wet chemical processing of ceramics offers many notable advantages, which have been summarized in previous publications. The issues of precursor cost and drying stresses seem, however, to limit appreciably the application of such methods to the formation of bulk objects. It seems clear that the areas of greatest opportunity are those of forming specialty powders (as ferrites) where the ability to achieve high purity and tailored chemistry are important, and the formation of coatings for a variety of applications.

In a previous paper<sup>124</sup>, many of the areas of potential application for wet chemical methods in the production of coatings have been considered, as have some of the obstacles to the effective implementation of such methods. The present paper has focused attention on the use of such methods in the fabrication of optical thin films and coatings.

Many of the critical issues identified previously for coatings in general are important for optical coatings. These include the need for coatings with a high degree of uniformity in thickness, often over large areas, sometimes on curved surfaces, with minimal/negligible edge effects; chemical homogeneity in complex multicomponent systems; thick coatings provided in a single operation (0.5  $\mu\text{m}$  remains an effective limiting thickness for ceramic coatings, for reasons which are poorly understood); shelf life of coating solutions; pinholes; and structural inhomogeneity.

For many optical applications, it is clearly desirable: (a) to explore a wider range of chemistry, including far more extensive exploration of non-oxide systems and systems containing non-oxides; (b) to investigate a wider range of organically modified ceramic systems, as a route to avoiding the 0.5 $\mu$ m barrier in coating thickness as well as to developing new functionalities; (c) to understand better the role of complexing agents in film development and post-deposition processing; (d) to develop improved methods of carbon and hydroxyl removal; (e) to improve the reproducibility and reliability of coating solutions and coatings made therefrom; (f) to establish the effects of processing treatments on the mechanical properties of films, and the role of additives in modifying these properties; (g) to develop useful models of stress development in chemically derived films, and its effect on n, EO coefficients, etc.; (h) to develop greatly improved ability to control the crystallization behavior of films, particularly oriented crystallization and the development of single crystal layers; (i) to provide expanded and more detailed characterization of the optical properties of chemically derived films; (j) to develop the ability to control the grain size and domain characteristics of polycrystalline films and to bypass formation of the pyrochlore phase; and (k) to expand greatly the range of dye-matrix systems and provide more detailed characterization of the optical properties of such systems.

Taken in toto, notable progress has been made during the past few years in the area of optical coatings by wet chemical methods. Much, however, remains to be done, and not alone in the technical areas cited above. One needs effective collaboration - not only between chemists, ceramic scientists and optical scientists, but also and perhaps now more importantly between wet chemical technologists and creative device engineers who can understand and utilize the attractive and sometimes unique opportunities offered by wet chemical processing.

Beyond this, we have seen a number of areas where wet chemical methods provide viable alternatives to conventional processing for fabricating optical films; yet the new methods have failed to supplant the old in the world of commerce. One needs therefore to appreciate the long delay times involved in introducing any new technology to the marketplace, and the myriad of nitty-gritty problems which must be solved in translating advances in the laboratory into products. Beyond this, one needs to develop a new paradigm to render more efficient this translation from invention to innovation, and hence to make our research more effective.

#### ACKNOWLEDGMENTS

Financial support for the present work was provided by the Air Force Office of Scientific Research. This support is gratefully acknowledged.

## REFERENCES

1. R.B. Pettit, C.S. Ashley, S.T. Reed, and C.J. Brinker, pp. 80-109 in Sol-gel Technology for Thin Films, Fibers, Preforms, Electronics and Specialty Shapes, ed. L.C. Klein, Noyes, Park Ridge, NJ, 1988.
2. B.E. Yoldas, U.S. Patent 4 346 131, Aug. 24, 1982.
3. T.J. Rehg, J.A. Ochoa-Tapia, A. Knoesen, and B.G. Miggins, Appl. Optics, 28(1989)5215.
4. C.J. Brinker and M.S. Harrington, Sol. Energy Mat., 5(1981)159.
5. C.S. Ashley and S.T. Reed, MRS Symp. Proc., 73(1986)671.
6. R.B. Pettit, C.J. Brinker, and C.S. Ashley, Solar Cells, 15(1985)267.
7. H. Dislich pp. 50-79 in Sol-Gel Technology for Thin Films, Fibers, Preforms, Electronics and Specialty Shapes, ed. L.C. Klein, Noyes, Park Ridge, NJ, 1988.
8. P. Hinz and H. Dislich, J. Non-Cryst. Solids, 82(1986)411.
9. P.K. Biswas, D. Kundu, and D. Ganguli, J. Mat. Sci. Lett., 8(1989)1436.
10. S.P. Mukherjee and W.H. Lowdermilk, J. Non-Cryst. Solids, 48(1982)177.
11. S.P. Mukherjee, pp. 178-88 in Ultrastructure Processing of Ceramics, Glasses and Composites, eds. L.L. Hench and D.R. Ulrich, Wiley, New York, NY, 1984.
12. W.H. Lowdermilk and S.P. Mukherjee, NBS Spec. Pub. (US), 638(1984)432.
13. B.E. Yoldas and D.P. Partlow, Eur. Pat. Appl. 13081, Jan. 9, 1985.
14. B.E. Yoldas and D.P. Partlow, Thin Solid Films, 124(1985)1.
15. M.C. Staggs, D. Milam, I.M. Thomas, and J.G. Wilder, NBS Spec. Pub. (US), 746(1988)404.
16. J.C. Debsikdar, J. Non-Cryst. Solids, 91(1987)262.
17. J.C. Debsikdar, U.S. Patent 4 830 879, May 16, 1989.
18. R. Ulrich and H.P. Weber, Applied Optics, 11(1972)428-434.
19. K. Tiefenthaler, V. Brigue, E. Buser, M. Horisberger, and W. Lukosz, Proc. SPIE. 401(1983)165.
20. E.R. La Serra, Y. Charbouillot, P. Baudry, and M.A. Aegerter, accepted by the J. Non-Cryst. Solids for publication, 1990.
21. M.A. Aegerter, Y. Charbouillot, N. Mohallem, A.A. da Silva, and L.H. de Godoy, presented at the Feb. 1989 Ultrastructures Conference in Tucson, AZ, to be published.
22. G.W. Dale, H.H. Fox, B.J.J. Zelinski, and L.A. Weller-Brophy, to be published in Better Ceramics Through Chemistry IV.
23. L. Weisenbach, T. Davis, B.J.J. Zelinski, R.L. Roncone, L.A. Weller-Brophy, to be published in Better Ceramics Through Chemistry IV.
24. L.A. Weller-Brophy, R.L. Roncone, L. Weisenbach and B.J.J. Zelinski, Optical Data Storage Center Quarterly Report, September 15, 1989, Optical Science Center, University of Arizona, Tucson, AZ, p. 51.
25. K. Tiefenthaler and W. Lukosz, IEE Conf. Pub 227(1983)108.

26. K. Heuberger and W. Lukosz, *Applied Optics*, 25(1986)1499.
27. W. Lukosz and K. Tiefenthaler, *Optics Letters*, 8(1983)537.
28. R.L. Roncone, L.A. Weller-Brophy, and B.J.J. Zelinski, presented at Feb. 1989 Ultrastructure Conference in Tucson, AZ, to be published.
29. R.L. Roncone, L.A. Weller-Brophy, L. Weisenbach and B.J.J. Zelinski, submitted to the *J. Non-Cryst. Solids* for publication, July, 1990.
30. N. Toghe, A. Matsuda and T. Minami, *J. Non-Cryst. Solids*, 100(1988)501.
31. Y. Matsuno, A. Matsuda, S. Kataoko, S. Katayama, T.T. Suno, presented at July 1990 Meeting of Soc. Photo-Opt. Instrum. Eng. in San Diego, CA, to be published.
32. W. Lukosz and K. Tiefenthaler, *IEE Conf. Pub.* 227 (1983)152.
33. K. Tiefenthaler and W. Lukosz, *Proc. SPIE*, 514(1984)215.
34. K. Tiefenthaler and W. Lukosz, *Optics Lett.*, 10(1984)137.
35. K. Tiefenthaler and W. Lukosz, *J. Opt. Soc. Am. B*, 6(1989)209.
36. W. Lukosz and V. Briguët, *Thin Solid Films*, 119(1985)197.
37. V. Briguët, P. Pirani and W. Lukosz, *Proc. SPIE* 813 (1987)535-536.
38. V. Briguët, J. Kramer and W. Lukosz, *J. de Phys. Colloq. C2* Supp no. 6, 49(1988)325.
39. W. Lukosz and V. Briguët, *Optical Bistability III*, Springer Proceedings in Physics, 8(1986)87.
40. W. Lukosz, P. Pirani, V. Briguët, *Optical Bistability III*, Springer Proceedings in Physics, 8(1986)109.
41. W. Lukosz P. Pirani and V. Briguët, *Optics Lett.* 12(1987)263.
42. P. Pirani, V. Briguët, and W. Lukosz, *Proc. SPIE*, 813 (1987) 191.
43. V. Briguët, P. Pirani and W. Lukosz, *Optics Letters*, 12(1987)525.
44. W. Lukosz, and K. Tiefenthaler, *Sensors and Actuators*, 15(1988) 273-284.
45. P.M. Nellen, K. Tiefenthaler and W. Lukosz, *Sensors and Actuators*, 15(1988)285-295.
46. R.R. Krchnavek, H.H Gilgen and R.M. Osgood, Jr., *J. Vac. Sci. Tech. B2*, 4(1984)641.
47. D.J. Shaw, A.J. Berry and T.A. King, *Inst. Phys. Conf. Ser. no 103: Part I*, p. 85.
48. B.D. Fabes, private communication.
49. D.J. Taylor, B.D. Fabes and M.G. Steinthal, to be published in *Better Ceramics Through Chemistry IV*.
50. R.V. Ramaswamy, T. Chia, R. Srivastava, A. Miliou and J. West, *Proc. SPIE*, 878(1988)86.
51. A. Miliou, R. Srivastava, R.V. Ramaswamy, R.W. Slocumb, T. Chia and J. West, private communication.
52. A. Makishima, M. Asami and K. Wada, *J. Non-Cryst. Solids*, 100(1988)321.
53. A. Makishima, H. Kubu, K. Wada, V. Kitami and T. Shimohira, *J. Am. Cer. Soc.*, 64(1986)C127.

54. N.D.S. Mohallem and M.A. Aegerter, J. Non-Cryst. Solids, 100(1988)526.
55. A. Duran, J.M.F. Navarro, P. Mazon and A. Joglar, J. Non-Cryst. Solids, 100(1988)494.
56. A. Duran, P. Mazon, A. Joglar and J.M.F. Navarro, Riv. Stn. Sper. Vetro, 16(1986)59.
57. A. Duran, J.M.F. Navarro, P. Casariego, and A. Joglar, J. Non-Cryst. Solids, 82(1986)391.
58. Y. Yamamoto, K. Kensuke, K. Kamiya, and S. Sakka, Yogyo Kyokaishi, 91(1983)222.
59. F. Orgaz and H. Rawson, J. Non-Cryst. Solids, 82(1986)378.
60. T. Kojima, Jpn. Kokai Tokkyo Koho JP 62/32153, Feb. 12, 1987.
61. N.J. Arfsten, J. Non-Cryst. Solids, 63(1984)243.
62. G. Gowda and D. Nguyen, Thin Solid Films, 136(1986)L39.
63. S. Sakka, pp. 346-374 in Sol-Gel Science and Technology, eds. M.A. Aegerter, M. Jafellicci Jr., D.F. Souza and E.D. Zanotto, World Scientific, Singapore, 1989.
64. G.H. Haertling pp. 371-491 in Electronic Ceramics, eds. L.M. Levinson, Marcel Dekker, New York, NY, 1987.
65. C.E. Land, P.D. Thatcher and G.H. Maertling, Appl. Sol. State Sci., 4 (1974) 137.
66. S.L. Swartz, S.J. Bright, J.R. Busch, and T.R. Shrout, paper presented at 1st Int'l Cer. Sci. and Tech. Cong., Anaheim 1989.
67. H. Adachi, T. Kawaguchi, M. Kitabatake and K. Wasa, Jpn. J. Appl. Phys., 22(Suppl. 2)(1983)11.
68. H. Matsunami, K. Kimura, M. Ishida, and T. Tanaka, J. Phys. Soc. Jpn., 49(Suppl. B)(1980)194.
69. A. Kavanaugh and J.O. Williams, Brit. Cer. Soc. Proc., 41(1989)59.
70. S. Krishnakumar, S.C. Esener, V. Ozguz, M.a. Title and S.H. Lee, presented at Sym. Y, MRS Spring Meeting, San Francisco, CA 1990.
71. K.D. Budd, S.K. Dey, and D.A. Payne, Brit. Cer. Proc., 36(1986)107.
72. R.W. Vest and J. Xu, Ferroelectrics, 93(1984)21.
73. C.J. Chen, Y. Xu, R. Xu and J.D. MacKenzie, paper presented at 1st Int'l Cer. Sci. and Tech. Cong., Anaheim, 1989.
74. S. Hirano and K. Kato, J. Non-Cryst. Solids, 100(1988)538.
75. S. Hirano and K. Kato, Adv. Cer. Materials, 3(1988)503.
76. S. Hirano and K. Kato, Solid State Ionics, 32/33(1989)765.
77. S. Hirano and K. Kato, Bull. Chem. Soc. Jpn., 62(1989)429.
78. S. Hirano and K. Kato, MRS Symp. Proc., 155(1989)181.
79. G. Yi, Z. Wu, and M. Sayer, J. Appl. Phys. 64(1988)2717.
80. H. Adachi, T. Mitsuyu, O. Yamazaki, and K. Wasa, J. Appl. Phys., 60(1986)736.
81. T.A. Rabson, R.C. Baumann and T.A. Rost, paper presented at Colorado Microelectronics Conference with the 1st Symp. Integrated Ferroelectrics 1989.
82. D.P. Partlow and J. Gregg, J. Mat. Res., 2(1987)595.
83. D.J. Eichorst and D.A. Payne, MRS Symp. Proc. 121(1988)773.



84. H. Higgshino, T. Kawaguchi, H. Adachi, T. Makino and O. Yamazaki, *Jpn. J. Appl. Phys.*, 24(Suppl. 2)(1985)284.
85. A. Okada, *Ferroelectrics*, 14(1976)739.
86. T. Fukuda and H. Hirano, *Appl. Phys. Lett.*, 28(1976)575.
87. R.R. Neurgaonkar, M.H. Kalisher, E.J. Staples, and T.C. Lim, *Appl. Phys. Lett.*, 35(1979)606.
88. R.R. Neurgaonkar, J.R. Oliver, and E.T. Wu, *J. Cryst. Growth*, 84(1987)409.
89. T. Kanata, Y. Kabayashi, and K. Kubota, *J. Appl. Phys.*, 62(1987)2989.
90. R. Reisfeld, pp. 322-345 in *Sol-Gel Science and Technology*, eds. M.A. Aegerter, M. Jafelizzi Jr., D.F. Souza and E.D. Zanotto, World Scientific, Singapore, 1989.
91. D.I. Santos, M.A. Aegerter, C.H. Brito Cruz, M. Scarparo, and J. Zarzycki, *J. Non-Cryst. Solids*, 82(1986)165.
92. D. Levy, S. Einhorn, and D. Avnir, *J. Non-Cryst. Solids*, 113(1989)137.
93. A. Makishima and T. Tani, *J. Am. Cer. Soc.*, 69(1986)C72.
94. B. Dunn, E. Knobba, J.M. McKiernan, J.C. Pouxviel, and J.I. Zink, *MRS Symp. Proc.*, 121(1988)331.
95. D. Avnir, D. Levy, and R. Reisfeld, *J. Phys. Chem.*, 88(1984)5956.
96. V.R. Kaufman, D. Levy, and D. Avnir, *J. Non-Cryst. Solids*, 82(1986)103.
97. R. Reisfeld, R. Zusman, Y. Cohen, and M. Eyal, *Chem. Phys. Lett.*, 147(1988)142.
98. R. Reisfeld, M. Eyal, and D. Brusilovskyy, *Chem. Phys. Lett.*, 153(1988)210.
99. Y. Kobayashi, Y. Kurokawa, Y. Imai, and S. Muto, *J. Non-Cryst. Solids*, 105(1988)198.
100. Y. Kobayashi, Y. Imai, and Y. Kurokawa, *J. Mat. Sci. Lett.*, 7(1988)1148.
101. H. Sasaki, Y. Kobayashi, S. Muto, and Y. Kurokawa, *J. Am. Cer. Soc.*, 73(1990)453.
102. H. Tanaka, J. Takahashi, J. Tsuchiya, Y. Kobayashi, and Y. Kurokawa, *J. Non-Cryst. Solids*, 109(1989)164.
103. P.N. Prasad, presented at Feb. 1989 Ultrastructure Conference. Tucson, AZ, to be published.
104. J. M. Boulton, J. Thompson, H.H. Fox, I. Gorodisher, G. Teowee, P.D. Calvert, and D.R. Uhlmann, to be published in *Better Ceramics Through Chemistry IV*.
105. S. Oka and H. Mizuguchi, *Jpn. Kokai Tokkyo Koho JP 62/15268* Jan. 23, 1987.
106. K. Yoshizaki, *Jpn. Kokai Tokkyo Koho JP 57/52237*, Nov. 6, 1982.
107. R.B. Lessard, K.A. Berglund, and D.G. Nocera, *MRS Symp. Proc.*, 155(1989)119.
108. J.I. Dulebohn, S. Van Vlierberge, K.A. Berglund, R.B. Lessard, J. Yu, and D.G. Nocera, to be published in *Better Ceramics Through Chemistry IV*.
109. E.M. Rabinovich, J. Shmulovich, and V.J. Fratello, *Am. Cer. Soc. Bull.*, 66(1987)1505.

110. V.J. Fratello, E.M. Rabinovich, and J. Shmulovich, Eur. Pat. Appl. 310308, Apr. 5, 1989.
111. D.M. DeLeeuw, W.K. Zwickler, and R. Bhargava, Eur. Pat. Appl. 232941, Aug. 19, 1987.
112. S. Sun and P.H. Holloway, J. Vac. Sci. Tech., A1(1983)529.
113. K. Miyake, H. Kaneko, N. Suedomi, and S. Nishimoto, J. Appl. Phys., 54(1983)5256.
114. J. Covino and G.E. McManis, MRS Symp. Proc., 121(1988)553.
115. A. Chemseddine, F. Babonneau, and J. Livage, J. Non-Cryst. Solids, 91(1987)271.
116. A. Chemseddine, R. Morineau, and J. Livage, Solid-State Ionics, 9-10(1983)357.
117. A. Chemseddine, M. Henry, and J. Livage, Rev. Chim. Miner., 21(1984)487.
118. I. Kato, A. Ariizumi, and N. Kimura, Jpn. Kokai Tokkyo Koho JP 61/36292, Feb. 20, 1986.
119. T. Yoshino, N. Baba, and K. Yasuda, Nippon Kagaku Kaishi, 9(1988)1525.
120. M. Navabi, S. Doeuff, C. Sanchez, and J. Livage, Mat. Sci. Eng., B3(1989)203.
121. R. Morineau, Vide Couches Minces, 40(1985)281.
122. N.R. Lynam, F.H. Moser, and B.P. Hichwa, Proc. SPIE, 823(1987)130.
123. S. Dieuff and C. Sanchez, C.R. Acad. Sci., Ser. 2, 309(1989)531.
124. D.R. Uhlmann and G.P. Rajendran, pp. 241-254 in Ultrastructure Processing of Advanced Ceramics, eds. J.D. Mackenzie and D.R. Ulrich, Wiley, New York, NY, 1988.

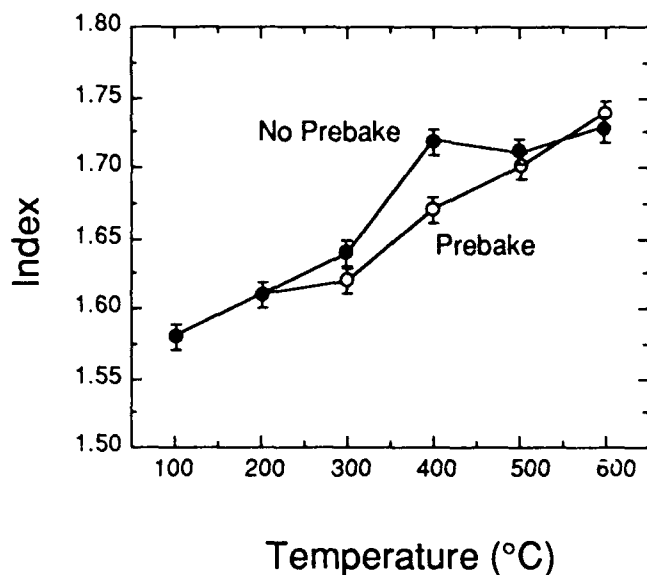


**Figure 1:** Index vs. temperature for SiO<sub>2</sub>-TiO<sub>2</sub> waveguides fired to 400 °C for 15 minutes. Prebaked samples were heated to 100 °C for 1.5 minutes prior to being plunged into furnace at isothermal temperature [Reference 23].

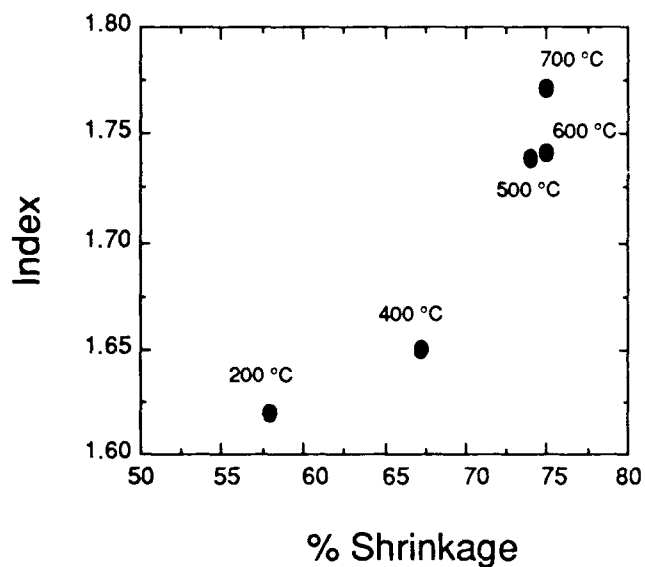


**Figure 2:** Index vs. shrinkage measured for SiO<sub>2</sub>-TiO<sub>2</sub> waveguides prebaked 1.5 minutes at 100 °C and then heated isothermally for an hour at the indicated temperatures [Reference 23].

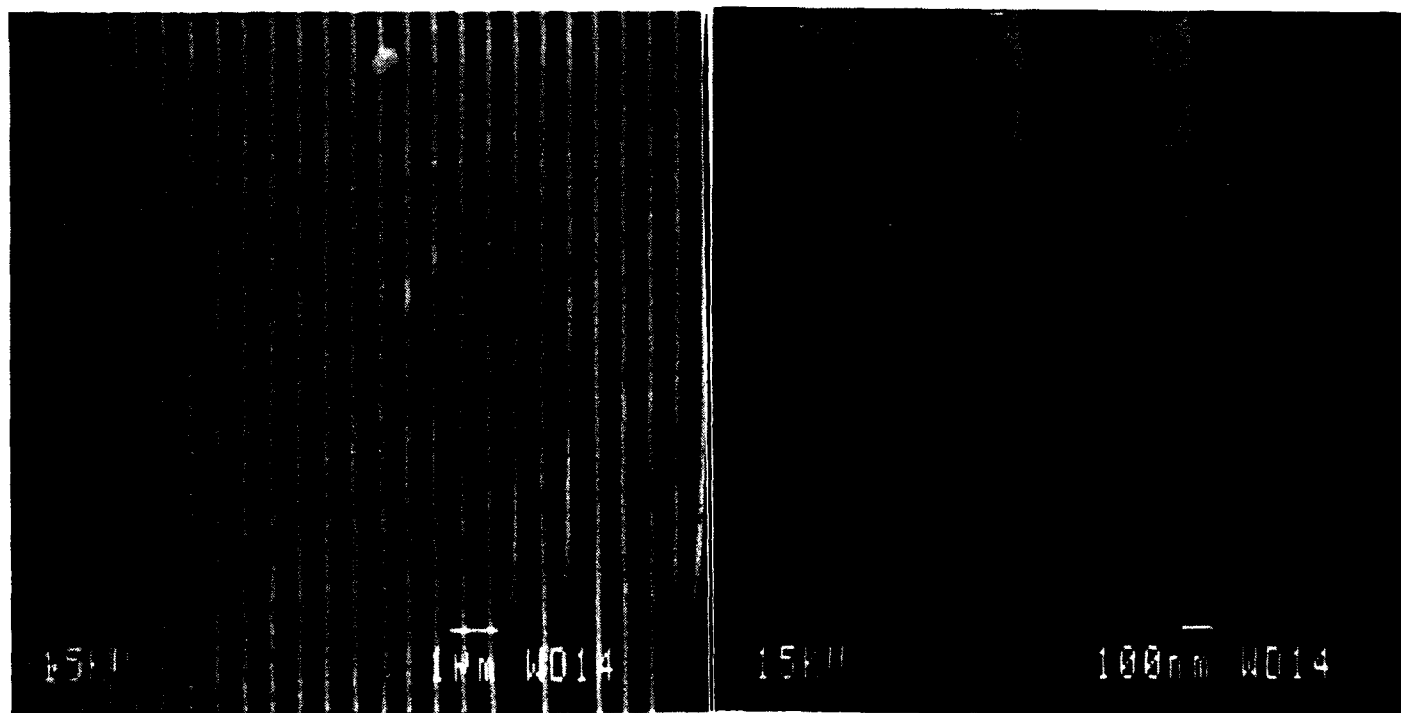


**Figure 3:** (a) SEM micrograph showing a top view of an embossed grating in SiO<sub>2</sub>-TiO<sub>2</sub> waveguide. The light regions are the grating ridges, the dark stripes are troughs. The grating period is 0.52 μm. (b) High magnification cross-sectional micrograph of the embossed grating features [Reference 29].



## Process induced variations in sol-gel derived oxide coatings

Bulent E. Yoldas

PPG Industries, Inc., Advanced Research Division  
P.O. Box 11472, Pittsburgh, Pennsylvania 15238

### ABSTRACT

Process parameters introduce a wide range of property and behavior variations in inorganic coatings deposited from metal-organic derived solutions. The modifications occur in the molecular, morphological, and the stoichiometric states and present some unique design opportunities for applications in the optical and electronic fields. The nature of the modifications and the processing parameters that introduce the modifications are discussed for the metal-organic derived oxide coatings.

### 2. INTRODUCTION

Sol-gel derived oxide films may be deposited either from colloidal suspensions or clear polymer solutions prepared from metal-organic compounds<sup>1-5</sup>. The latter solutions contain oxide constituents in chemical association with solvating organic groups, and upon application deposit a glass-like film on substrates. A bake temperature of ~300-500°C is required to drive off the organic components. Sol-gel derived films are finding ever-increasing applications in various technologies due to some unique characteristics and design advantages<sup>5-8</sup>.

Typical characteristics of films deposited from polymeric solutions are:

- porous ( $\approx 30-70\%$  porosity,  $\approx 10-100\text{\AA}$  pore size)
- contains organic and hydroxyl groups ( $\approx 5-10\%$  wt.)
- amorphous
- thickness is limited ( $t < \approx 1\mu\text{m}$ )
- properties are variable.

These and other properties are very sensitive to processing parameters. The modifications can occur at various levels in molecular structure, in stoichiometry, in morphology and porosity. Physical constraints, such as film thickness, are also found to have substantial effect in film properties.

One characteristic that singularly differentiates sol-gel derived films is its pore morphology. This porosity presents some unique opportunities in a number of fields, including membrane technology, catalysis, composites, etc. The best opportunity created by this characteristic appears to occur in the optical field. For this reason, pore morphology in relation to optics is briefly discussed prior to the presentation of the effects of process parameters.

92 4 28 047

92-11429



### 3. POROSITY OF SOL-GEL FILMS AND ITS IMPLICATIONS IN OPTICS

There is a significant technological and economic need for antireflective (AR) coatings. For example, operation of high power laser systems without AR coating not only can cause considerable damage to the optics but also the reduced energy transmission through reflective surfaces would represent millions of dollars for a relatively small (20 KJ) laser fusion system. Most glasses reflect ~4% of incident light from each surface. Elimination of this reflection would represent a corresponding increase in the efficiency of devices that use transmitted radiation<sup>7,8</sup>.

The coating of a surface with a nonabsorbing film is one way of eliminating the reflectance. For a coated surface, the minimum reflection is given by

$$R_m = (n_c^2 - n_1 n_2)^2 / (n_c^2 + n_1 n_2)^2, \quad (1)$$

where  $n_c$  is index of coating,  $n_1$  is index of medium and  $n_2$  is index of substrate.

From Equation (1) it is obvious that, in air ( $n_1 = 1$ ) for the minimum reflectivity to be zero, i.e.,  $R_m = 0$ , the numerator in Equation (1) must be zero, therefore, the relation between the indices of the substrate and coating must be

$$n_c = \sqrt{n_2}, \quad (2)$$

The thickness of the film  $t$  must also meet the quarterwave optical thickness requirement

$$t = \lambda_m / (4n_c), \quad (3)$$

where  $\lambda_m$  is the wavelength of minimum reflectivity.

This means that an antireflective (AR) film on a glass having an index of refraction of 1.52, must have an index of ~1.23 from Equation (2). This low-index requirement makes it practically impossible to design a dense single-layer AR film for glass. The lowest index inorganic material  $\text{MgF}_2$  has an index of 1.38, which would only reduce the minimum reflection to ~1.2% from Equation (1).

Figure 1 shows how the reflectivity varies as the index of refraction and thickness of coating deviate from the ideal values indicated by Equations (2) and (3).

The index of refraction of a material is related to its density, which can be lowered by introducing porosity. It is required that the pore size be substantially smaller than the wavelength of the light, and the pore distribution must be homogeneous in order not to cause scattering. These are the conditions that naturally exist in sol-gel derived materials.

The density and index of refraction in this type of material are related by<sup>9</sup>

$$(n_p^2 - 1) / (n_d^2 - 1) = d_p / d_d \quad (4)$$

where  $n_d$  and  $d_d$  are index and density of the dense material, and  $n_p$  and  $d_p$  are index and density of the porous material.

Equation (4) can be written in terms of porosity:

$$n_p^2 = (n^2 - 1) (1 - P/100) + 1, \quad (5)$$

where  $P$  is percent porosity.

Listed in Table 1 are the amounts of porosity required to lower these indices to 1.21, the square root of the refractive index of the  $\text{SiO}_2$  substrate.

Table 1. Reduction of Refractive Index  
by Inclusion of Nonscattering Porosity for AR Coating on Silica

Oxide	Refractive Index	~% Porosity required for $n = 1.21^a$
$\text{SiO}_2$	~1.46	53
$\text{Al}_2\text{O}_3$	~1.6	73
$\text{La}_2\text{O}_3$	~1.8	80
$\text{ThO}_2$	~1.9	83
$\text{HfO}_2$	~2.0	85

<sup>a</sup> Square root of the refractive index of  $\text{SiO}_2$ .

The porosities indicated in Table 1 are readily obtainable in sol-gel derived oxides. Fifty to 70 percent porosity is routinely obtained for bulk  $\text{SiO}_2$  and  $\text{Al}_2\text{O}_3$  produced by sol-gel methods. Still, a porous coating whose refractive index is the square root of that of the substrate and whose thickness is tuned to suppress reflection at a particular wavelength will not do so across the entire spectrum. Broadband antireflection with a single layer requires a coating with a graded index of refraction. Introduction of graded porosity within the coating will accomplish this. Such a graded porous coating can be formed by grading the porosity by chemical leaching of a sol-gel deposited oxide film<sup>10-11</sup>. Figure 2 shows the spectral transmission curve on a fused silica substrate coated with graded porosity  $\text{SiO}_2$  film<sup>11</sup>.

As will be further discussed in the following sections, the formation of this graded porosity, its thermal behavior and its density are strongly dependent on process parameters.

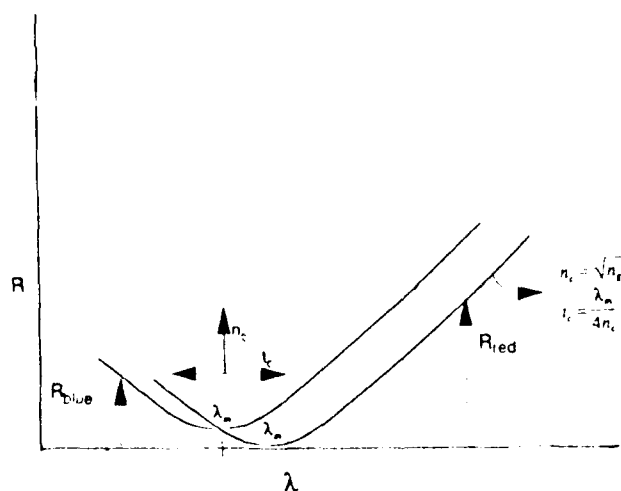


Fig. 1. Antireflectivity produced by a single layer coating, as a function of its index and thickness.

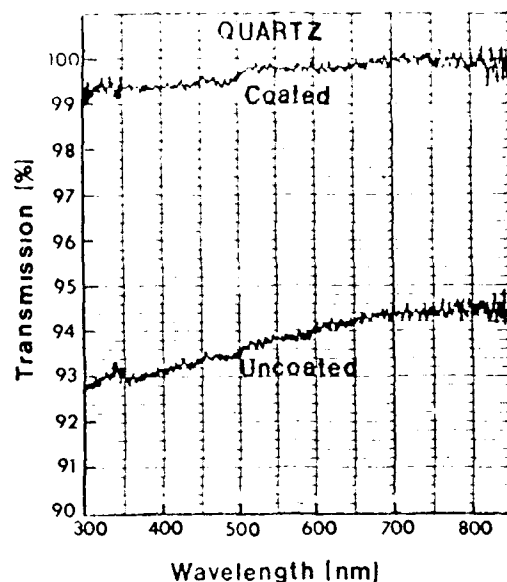


Fig. 2. Broad band antireflectivity of a graded porosity sol-gel  $\text{SiO}_2$  coating on quartz.

#### 4. PROCESS PARAMETERS AND THEIR EFFECTS

The entire sol-gel coating process is normally carried out in three sub-stages. These are (a) solution preparation, (b) solution application, and (c) heat treatment. In the first stage, chemical parameters predominate. In the second stage, physical and mechanical parameters play predominant roles. In the last stage, both chemical as well as physical parameters come into play.

##### 4.1 Solution preparation parameters

In most metal alkoxide systems, hydrolysis reactions rapidly lead to condensation of insoluble oxide and hydroxide particles, making the solution unsuitable for optical coating applications. These difficulties have been circumvented by Schroeder and others<sup>12,13</sup> by using unhydrolyzed metal alkoxide solutions as coating precursors and allowing the air humidity or surface OH groups present on surfaces to hydrolyze the alkoxides. A wide variety of oxides has been deposited by this technique.

Recently, techniques have been developed which allow clear polymerized solutions of almost any oxide to be made<sup>14-17</sup>. These solutions are prepared by controlled reactions of metal alkoxides with water in a mutual solvent such as alcohols. These hydrolysis reactions result in the formation of soluble polymeric species whose skeleton in an oxide network are framed by hydroxyl and ester groups.

Deposition of oxide films from these solutions does not depend on external supply of  $\text{H}_2\text{O}$  or OH groups to complete the oxide forming reactions. The terminal groups not only keep the species in soluble form, they also enable the system to polymerize into an extended oxide network, thus permitting continuous film formation; for example:



The parameters that introduce molecular and chemical variations in these solutions may be listed as follows<sup>18</sup>

- Selection of starting compounds and host medium.
- Water/alkoxide ratio.
- Molecular separation by dilution.
- Catalytic effects, pH.
- Reaction temperatures.

By affecting the kinetics of condensation reactions, these parameters determine the molecular size, network topology, the nature of terminal groups of the condensation product, e.g.,:



where "n" is the number of silicons polymerized in the polymer molecule, "k" and "p" are the number of terminal groups "OR" and "OH". The oxide content of the polymer becomes a function of size, n, topology and type of terminal groups. The oxide content of gel film is related to the extent of polymerization and the nature of the terminal groups. This property is very sensitive to water/alkoxide ratio. By manipulation of this parameter, one can deposit  $\text{SiO}_2$  and  $\text{TiO}_2$  films whose oxide content is as low as 70% or as high as 95% by weight<sup>19</sup>.

During the hydrolytic condensation the alkoxides of lower alkyl groups generally produce polymers having a higher oxide content. The host medium also affects this. Hydrolysis products produced in lower alcohols have a higher equivalent oxide content. For example, when  $\text{Ti}(\text{OC}_2\text{H}_5)_4$  is hydrolyzed in ethanol ( $\text{C}_2\text{H}_5\text{OH}$ ) and dried at  $100^\circ\text{C}$ , the oxide content of the gel by weight is ~83-84%. This figure drops to about 73% when the hydrolysis is performed in butanol,  $\text{C}_4\text{H}_9\text{OH}$ <sup>5</sup>. Consequently,  $\text{TiO}_2$  films deposited from the latter solution have a lower index of refraction and are generally inferior due to their lower density after heat treatment.

The effect of water/alkoxide ratio on sintering is also dramatic<sup>19</sup>. The terminal groups affect the densification behavior of the resultant films and eventually determine its pore morphology. In a recent study, it was observed that only when  $\text{Si}(\text{OC}_2\text{H}_5)_4$  was hydrolyzed with 2.0 to 2.8 moles water, it deposited  $\text{SiO}_2$  films which produced suitable porosity for broad band AR coating under the specific conditions<sup>8</sup> (see Table 1 in Reference 8).

Finally, Table 2 shows the effect of the dispersion medium on the pore morphology and surface area of  $\text{Al}_2\text{O}_3$  fired at  $600^\circ\text{C}$ .



Table 2. Effect of Dispersion Medium on Alumina Gel Porosity

Dispersion Medium	Average Pore Radius (Å)	Total Pore Volume (mlg <sup>-1</sup> )	Surface Area (m <sup>2</sup> g <sup>-1</sup> )
Methyl alcohol	47	0.27	230
Ethyl alcohol	50	0.37	294
Water	55	0.57	423
Propylene glycol	71	0.52	293
Triethylene glycol	96	0.82	367

\*Fired at 600°C.

#### 4.2 Solution deposition parameters

The precursor solution is applied on substrates by any liquid application methods including dipping, spinning and spraying, depending on the substrate geometry, etc. For optical applications, preferred methods are dipping the substrate into the liquid followed by a controlled rate of pulling the substrate out (or draining the solution) or spinning the solution on substrate.

These two processes involve drastically different speeds and shear rates under which the polymer molecules are aligned and deposited on the substrate. Spin coating dries the film in a few seconds in a dynamic condition. Drain coatings, typically at several cm/min, allows for polymer alignment into a denser configuration<sup>11</sup>. Surface roughness of spin coated films is found to be significantly higher than dip or drain coated films<sup>20,21</sup>. Thus, morphology created by the application of a given polymeric solution is significantly different for the drain process than for the spin process.

Figure 3 shows coating thickness as a function of the application rate in spin coating of 5-cm diameter fused silica disks with a solution in silica system<sup>8</sup>. Under these conditions, films thicker than 1000-1100 nm tend to craze.

Figure 4 shows coating thickness as a function of pull or drain rate in the drain coating process. As shown in this case, film morphology is such that the coating starts to craze at 600 nm.

Densification of these films, as shown in Figure 5, indicates the fundamental differences between the films deposited by spin coating and dip coating as well as it elucidates the nature of the crazing in these films. When 1  $\mu$ m thick spin coated film is densified its thickness is reduced by ~50%, indicating it was initially ~50% porous. The thickness reduction of drain coated films upon densification is approximately half as much as this, indicates that the initial porosity was half as much.

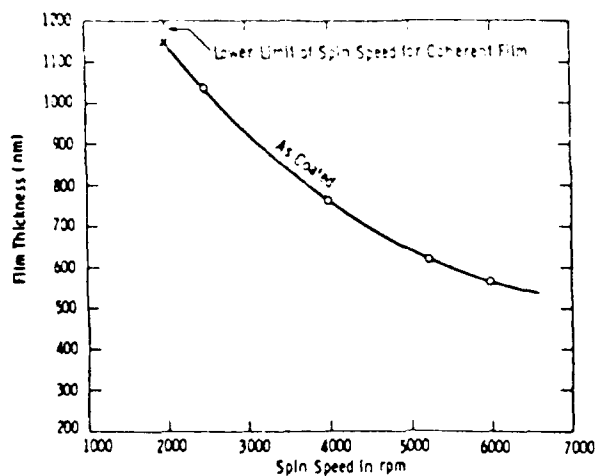


Fig. 3. Coating thickness as a function of spin speed on 5-cm diameter optically polished silica disks.

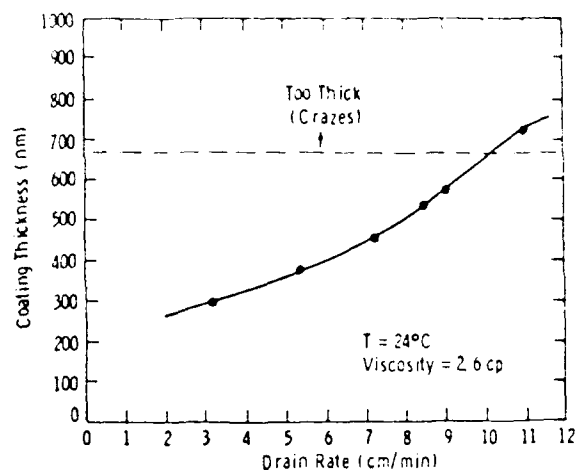


Fig. 4. Coating thickness as a function of solution drain rate on optically polished silica.

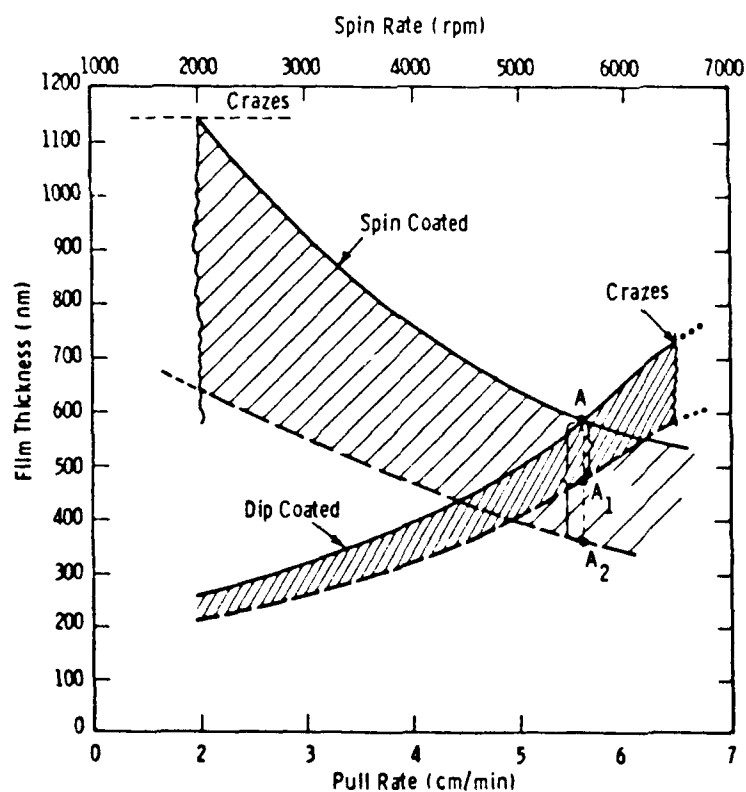


Fig. 5. Thickness of  $\text{SiO}_2$  films as a function of application rate by spin and dip coating before (solid lines) and after (dash lines) the densification. Note that after densification crazing thickness becomes about the same. Also compare the film shrinkages at point "A" where the as-deposited thickness is the same.

Figure 5 indicates two other significant events. The first one is that when densified, the crazing thickness, i.e., 1100 nm for spin coating, 600 nm for dip coating, becomes about the same for both types of films, ~600 nm. This indicates that the crazing phenomenon in this film is directly related to the density, i.e.,  $t_c \propto 1/d$ . The second indication, which is somewhat more

surprising, is that as the films get thinner they are deposited denser. This means that a degree of density and refractive index gradient normally occurs in sol-gel deposited films.

#### 4.3 Heat treatment parameters

Sintering and densification of sol-gel films are not smooth functions of temperature. There are temperature regimes where there are selective chemical bond cleavages, and certain chemical components are released. Since intermolecular atmosphere within the film is diffusion dependent, the heat rate becomes important, especially as the film gets thicker.

Atmospheric effects are extremely important in certain systems. A 100%  $\text{TiO}_2$  film baked in air to  $500^\circ\text{C}$  has an index of refraction of  $\sim 2.1$ . The same film gives an index of  $\sim 2.4$  if the baking is performed in vacuum. Figure 6 shows this effect of heat treatment atmosphere which diminishes as the composition changes from  $\text{TiO}_2$  to  $\text{SiO}_2$  in  $\text{TiO}_2$  -  $\text{SiO}_2$  binary<sup>5</sup>.

However, atmospheric humidity has a significant effect on the densification of silica films. Silica films that are normally densified at around  $900$ - $1000^\circ\text{C}$  are found to densify around  $450$  -  $500^\circ\text{C}$  when exposed to humid atmosphere.

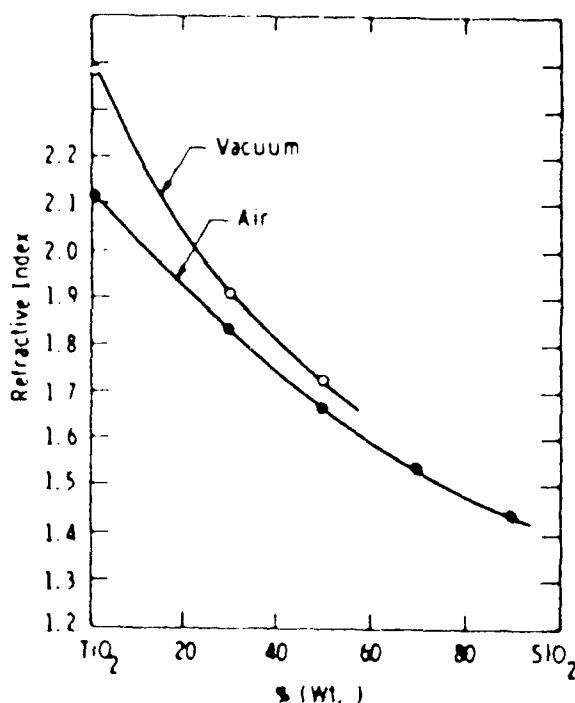


Fig. 6. Effect of heat treatment atmosphere on the index of refraction of coating as a function of its composition in the  $\text{TiO}_2$ - $\text{SiO}_2$  binary.

#### 5. FILM THICKNESS EFFECT

One of the more interesting aspects of sol-gel deposited films is the naturally occurring density gradient<sup>2</sup>. As was seen in Figure 5, the relative thickness differences between the as-deposited state and the densified state diminishes as the films are deposited thinner and thinner.

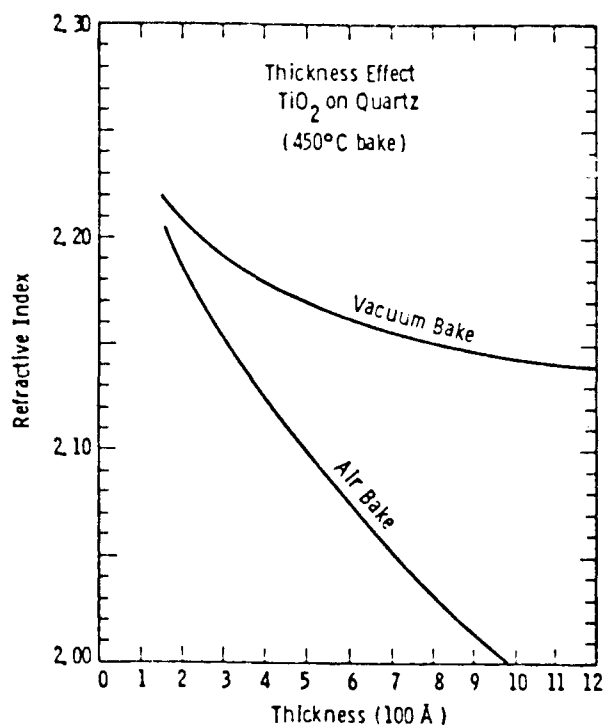


Fig. 7. Effect of film thickness on refractive index of  $\text{TiO}_2$  films deposited on quartz (from Reference 2).

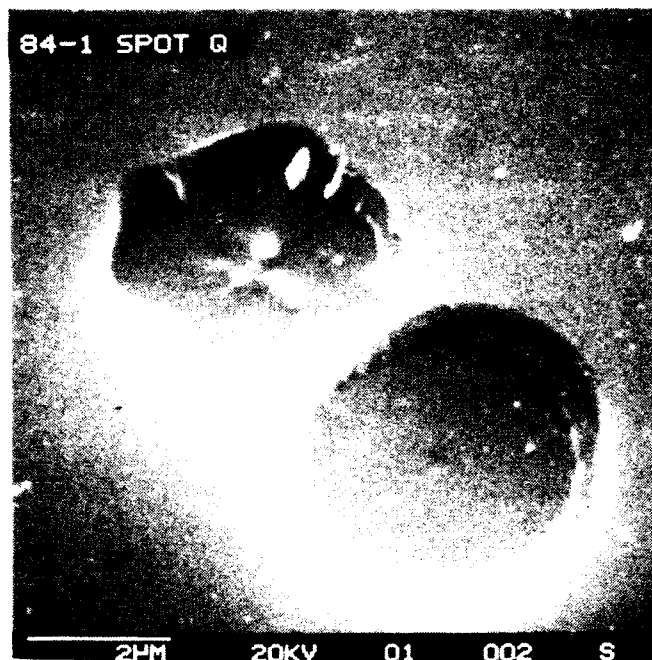


Fig. 8. Scanning electron micrograph of a laser damage site in a sol-gel deposited  $\text{SiO}_2$  AR coating on quartz. Note the layered morphology.

Figure 7 brings this aspect of sol-gel deposited films into sharper focus. Here the refractive index indicates that the density of  $\text{TiO}_2$  films increases with decreasing thickness. It is even more revealing that the differences between the air bake and vacuum bake films also diminish with decreasing thickness and completely disappears around  $\sim 100\text{-}150\text{\AA}$ . A reasonable interpretation of this is that at around  $\sim 100\text{\AA}$  thickness the  $\text{TiO}_2$  films become completely dense; a case under which the effect of the bake atmosphere on densification becomes inoperative. The impervious nature of very thin  $\text{TiO}_2$  films has also been demonstrated chemically (for example, see Figure 8 in Reference 2).

It is thought that in thinner films, the polymer alignment attained by the spinning or dipping motion is less likely to become disoriented by fast drying and geometrical constraints. This effect of thickness on the index of refraction appears to be operative in all thin films deposited from polymerized solutions. For example, a  $\text{Ta}_2\text{O}_5$  film similarly deposited and baked at  $500^\circ\text{C}$  in air had a refractive index of 1.938 when the film was  $475\text{\AA}$  thick and 1.917 when the thickness was  $675\text{\AA}$ . The same effect was found for  $\text{SiO}_2$  films<sup>2</sup>.

In Figure 8, the scanning electron micrograph of a laser damage site ( $4\text{ }\mu\text{m}$  in diameter) of an  $\text{SiO}_2$  antireflective film deposited on quartz clearly shows the density layers of this film<sup>22</sup>.

## 6. SUMMARY

Properties of sol-gel derived oxide coatings are significantly modified by process parameters. Main effects are summarized below.

**Precursor Effects:** Alkoxides of lower alkyls produce denser films with higher initial oxide content. The same applies to solvent. Porosity, pore size and surface area are strongly affected by the dispersion medium.

**Condensation Effects:** Hydrolytic condensation under diluted conditions result in smaller molecular size, finer texture, generally higher porosity. Hydrolysis with higher water/alkoxide ratio gives solutions depositing denser films, with enhanced sinterability.

**Method of Deposition Effects:** Spin coating gives significantly higher porosity, and surface roughness than dip coated films.

**Thickness Effect:** There are significant density gradient in the first several hundred angstrom of sol-gel deposited films. The first  $\sim 100$ - $150$  Å layer appears to be substantially dense.

**Heat Treatment Effects:** There are significant atmospheric effects in some oxide systems. There are thermal conditions which lead to selective cleavage of bonds with significant consequences.

## 7. REFERENCES

1. C. J. Brinker and G. W. Scherer, The Physics and Chemistry of Sol-Gel Processing, Chpt. 13, Academic Press, Inc., San Diego, 1990.
2. B. E. Yoldas, "Deposition and Properties of Optical Oxide Coatings from Polymerized Solutions," *Appl. Opt.*, vol. 21, no. 16, pp. 2960-2964, 1982.
3. J. D. Mackenzie, "Applications of the Sol-Gel Process," *J. Non-Cryst. Solids*, vol. 100, no. 1-3, pp. 162-168, 1988.
4. D. R. Uhlmann, B. J. J. Zelinski and G. E. Wnek, *Mat. Res. Soc. Symp. Proc.*, vol. 32, pp. 59-70, Elsevier Science Publishing Company, Inc., New York, NY, 1984.
5. K. D. Budd, S. K. Dey and D. A. Payne, "The effect of hydrolysis conditions on the characteristics of  $\text{PbTiO}_3$  gels and thin films," in Better Ceramics Through Chemistry II, vol. 73, Pittsburgh: Materials Research Society, pp. 711-716, 1986.
6. B. E. Yoldas and T. O'Keefe, "Deposition of Optically Transparent IR Reflective Coating on Glass," *Appl. Opt.*, vol. 23, no. 20, pp. 3638-3643, 1984.
7. I. M. Thomas, "Single Layer  $\text{Al}_2\text{O}_3 \cdot \text{H}_2\text{O-SiO}_2$  Optical Coatings Prepared from Colloidal Suspensions," *Appl. Opt.*, vol 28, no. 18, pp. 4013-4016, 1989.

8. B. E. Yoldas and D. P. Partlow, "Formation of Broad Band Antireflective Coatings on Fused Silica for High Power Laser Applications," *Thin Solid Films*, vol. 129, no. 1, pp. 1-14, 1985.
9. B. E. Yoldas, "Investigation of Porous Oxides as an Antireflective Coating for Glass Surfaces," *Appl. Opt.*, vol. 19, no. 9, pp. 1425-1429, 1980.
10. S. P. Mukherjee, "Gel-Derived Single-Layer Antireflection Films with a Refractive Index Gradient," *Thin Solid Films*, vol. 81, no. 1, L89-90, 1981.
11. B. E. Yoldas and D. P. Partlow, "Wide Spectrum Antireflection Coating for Fused Silica and Other Glasses," *Appl. Opt.* vol. 23, no. 9, pp. 1418-1424, 1984.
12. H. Schroeder, "Oxide Layers Deposited from Organic Solutions," *Phys. Thin Films*, vol. 5, pp. 87-141, 1969.
13. H. Dislich in Sol-Gel Technology for Thin Films, Fibers, Preforms, Electronics and Special Shapes, Chpt. 4, Ed. L. C. Klein, Noyes, Park Ridge, NJ, 1988.
14. B. E. Yoldas, U.S. Patent 4,251,185, Dec. 17, 1981.
15. B. E. Yoldas, U.S. Patent 4,361,598, Nov. 30, 1983.
16. B. E. Yoldas, "Hydrolysis of Titanium Alkoxides and Effects of Hydrolytic Polycondensation Parameters," *J. Mater. Sci.*, vol. 21, pp. 1087-1092, 1987.
17. P. Papet, et al., "Transparent Monolithic Zirconia Gels: Effects of Acetylacetone Content on Gellation," *J. Mater. Sci.*, vol. 24, pp. 3850-3854, 1989.
18. B. E. Yoldas, "Modification of Polymer-Gel Structures," *J. Non-Cryst. Solids*, vol. 63, pp. 145-154, 1984.
19. B. E. Yoldas, "Effect of Variations in Polymerized Oxides on Sintering and Crystalline Transformations," *J. Am. Ceram. Soc.*, vol. 49, no. 5, pp. 387-393, 1982.
20. W. D. Partlow, et al., "Characterization of Plasma-Deposited and Dip-Coated Films for Critical Optical Applications," *Appl. Opt.*, vol. 26, no. 8, pp. 1537-1545, 1987.
21. B. E. Yoldas, "Surface Roughness of Optical Oxide Coatings Deposited from Solutions and the Morphological Effect of Different Deposition Methods," *Mat. Res. Soc. Symp. Proc.*, vol. 47, pp. 107-111, 1985.
22. B. E. Yoldas, et al., "Laser Damage Studies of Polymer Oxide Coated Silica Optics at 350 nm," *J. Appl. Phys.*, vol 57, no. 7, pp. 2455-2459, 1985.



**$\text{Al}_2\text{O}_3 \cdot \text{H}_2\text{O} \cdot \text{SiO}_2$  Sol-Gel HR-Coatings  
for High-Power Laser Applications**

---

H.G. Floch & J.J. Priotton  
CEA Centre d'Etudes de Limeil-Valenton  
94 195 Villeneuve Saint Georges Cedex  
FRANCE.

and

I.M. Thomas  
Lawrence Livermore National Laboratory  
University of California, P.O. Box 5508  
94 550 Livermore (CA).  
USA.

---

**92-11430**



ABSTRACT.

Pursuing our official collaborative ICF-laser search and development program at Limeil National Laboratory (LNL) with the Lawrence Livermore National Laboratory (LLNL) for high damage threshold optical coatings, we have now formally established that Sol-Gel highly reflective coatings prepared from colloids are superior to those prepared from solutions of precursor materials. Thus, single layer coatings of bohemite  $\text{Al}_2\text{O}_3 \cdot \text{H}_2\text{O}$  have been prepared on fused silica and BK-7 substrates from aqueous colloidal suspensions of hydrated alumina at room temperature. Such coatings were porous and therefore revealed a measured refractive index of about 1.44, lower than the relevant dense material. These single coats when laser damage tested, have exhibited thresholds, under S-on-1 irradiation mode (S shots at the same fluence onto a selected site) of respectively 12-14 J/cm<sup>2</sup> with 3-ns pulses and 35-50 J/cm<sup>2</sup> with 16 ns pulses at 30-Hz. Multilayer, high reflectivity, dielectric coatings were also prepared at room temperature by laying down quarterwave-thick, alternating coats of this alumina with silica also prepared from colloidal sol, and having a refractive index of 1.22. To achieve 99 % reflectivity 32 to 36 total layers were required. Such HR-coatings revealed damage thresholds as good as those of single layers of the constituting oxides in the same laser conditions.

1. INTRODUCTION.

Since the first incidental observation in 1846<sup>1</sup> of the "Sol-Gel" process, and which covered the hydrolysis and polycondensation of silicic acid under humidity until a silicate glass formation occurred, it is reasonable to state that a well-marked revival of such a method started with the works of Dislich<sup>2</sup> and Roy<sup>3</sup> about 20 years ago. Many results have been published since then, but the future of this technology depends mainly on whether it will be able to make better materials or even completely brand new materials. Therefore, a real process mastery is required from both a scientific and technologic point of view.

Nowadays an increasing interest, from both academic and industrial laboratories, is devoted to this new technology. Indeed, it is to date well-recognized that the sol-gel process is a very attractive versatile

route for the preparation of porous or dense films and monolithic bodies of high purity glasses and ceramics. Since the advent of such a chemical method many "exotic" new composite systems with unusual microstructures and physico-chemical properties have been obtained. Most of these sol-gel innovations have been regrouped through excellent books of papers submitted in basic symposia<sup>4-10</sup> and also through a recent book describing the principles, developments, techniques and applications of sol-gel processing<sup>11</sup>.

The uniqueness of the so-called "*Sol-Gel*" process is to go all the way from the precursor to the product, allowing better control of the whole process and the synthesis of "tailor-made" ultrapure materials. Such an approach is basically articulated in three steps :

1. Preparation of a solution or colloidal suspension of the suitable(s) component(s). This step gives the *SOL*.
2. Gelation of the *SOL* by polymerization or coagulation. This step gives the *GEL*.
3. Conversion of the wet *GEL* to a useful product, generally through a thermal treatment

Products vary from films to fine homogeneous powder to monolithic bodies. This is illustrated in Figure 1.

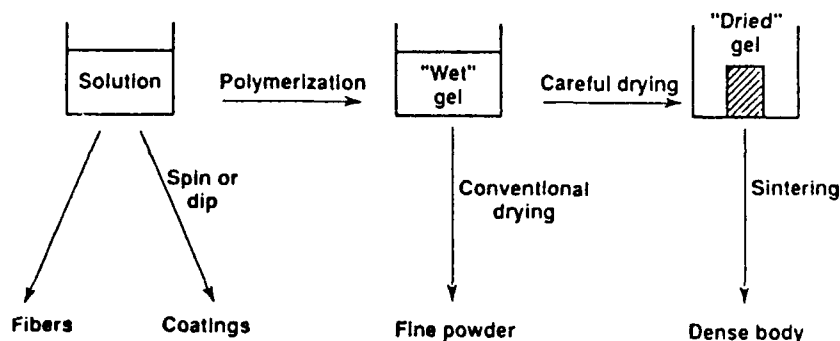
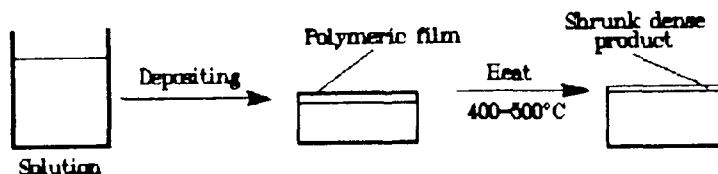


Figure 1. Several and various products can be prepared by the sol-gel process.

Coatings appear to be one of the most promising applications of the sol-gel process. Optical films for architectural uses deposited onto glass windows by dip-coating are already commercially available from Schott since the 1960s<sup>12</sup>.

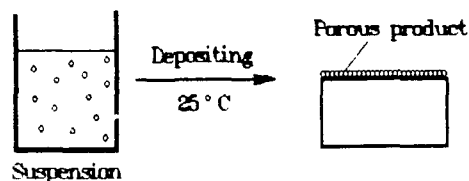
Two methods are commonly used for the preparation of coatings by the sol-gel process :

a) Application of a precursor solution to a substrate with a subsequent conversion of the precursor to an oxide or an other product family on the substrate surface. This normally requires the combination of water and heat.





b) Application of a colloidal suspension of an oxide or other material followed by an evaporation of the suspending medium. This can usually be accomplished at room temperature.



It is very important to differentiate clearly each of these coating routes. The precursor-solution approach has been already investigated in 1962 at Schott-Germany for protective coatings onto architectural glass windows of poor chemical resistance<sup>13</sup>, then in Soviet Union in 1967 for durable laser-coatings<sup>14</sup> and more recently at LLNL (University of California) for the preparation of laser damage resistant highly reflective dielectric multilayer stacks<sup>15</sup>.

The work described in this paper is part of a continuing effort we maintain at Limeil National Laboratory and in synergy with our colleagues of the Lawrence Livermore National Laboratory on the preparation of high damage threshold coatings suitable for use on the optical components of current and future high-power lasers devoted to laser-fusion experiments (ICF-program).

Previous works, with the same objective to develop highly damage resistant optical thin-films on, porous silica antireflective (AR) coatings<sup>16,17</sup>, porous fluoride AR coatings<sup>18</sup>,  $\text{ThO}_2$  and  $\text{ThO}_2\text{-SiO}_2$  HR coatings<sup>19</sup>,  $\text{TiO}_2$  and  $\text{TiO}_2\text{-SiO}_2$  HR coatings<sup>20,21</sup>, and more recently on  $\text{ZrO}_2$  and  $\text{ZrO}_2\text{-SiO}_2$  HR coatings<sup>22</sup> and on  $\text{Ta}_2\text{O}_5$  and  $\text{Nb}_2\text{O}_5$  reflective coatings<sup>23</sup> have been essentially reported over these last five years by Thomas and Floch. For details of experimental procedures and product performances referal to the given literature is recommended. At this juncture, it is clear to precise that doctor Ian M. Thomas is likely the pioneer as for the development and promotion of highly damage resistant sol-gel coatings presently used in the most powerful laser-systems operating at Livermore (Nova 100 KJ - 1 ns) and Limeil (Phebus 20 KJ - 1 ns) laboratories and elsewhere<sup>24</sup>.

Our investigation is based on the use of colloidal suspensions as coating media. Indeed, it is now clearly established that dielectric multilayered mirrors must be built up from colloidal media (Sols) and not from solutions (Gels) as summarized and illustrated, in a recent survey<sup>25</sup>, and not even more by the use of chelated-solutions<sup>26</sup>. The main practical advantage of the colloidal route over other systems, especially when large optics are considered is probably the room temperature processing, because only solvent evaporation is required after application of the coating suspension. There is also the advantage of the low capital cost of equipment and the low cost of processing. Finally, such an approach allows the elaboration of stress-free coatings, that is beneficial because strain is suspected to be prejudicial to high laser damage threshold achievement.

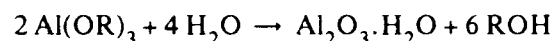
More precisely, the aim of this paper, in continuation of recent works<sup>27</sup>, is to present and evaluate properties of single-layer  $\text{Al}_2\text{O}_3\cdot\text{H}_2\text{O}$  coatings deposited from a specific alumina suspension. By associating these coatings with coatings of silica also obtained from colloids<sup>16,17</sup>, we have been able to produce multilayered HR dielectric films. All coatings were optimized in optical response for use at 1064-nm wavelength, this being the current wavelength of interest in Nd : doped solid state lasers.

## 2. COLLOIDAL ALUMINA SUSPENSIONS.

Since Gay Lussac's pioneering Work in 1810<sup>27</sup>, numerous studies have been addressed for obtaining colloidal alumina sols and gels. Basically, we can distinguish three categories of chemical synthesis, all of which have been widely used for the production of a variety of ceramics. The first method concerns the forced-hydrolysis of aluminum salts and has been patented by Bugosh<sup>28</sup>. The second one provides a process

for the preparation of a stable sol which comprises contacting an aluminum salt with an epoxy compound leading to hydrated oxide formation. This synthesis by partial neutralization has been patented by Lane<sup>29</sup>. The third access to alumina colloids deals with the ability of freshly precipitated aluminum hydroxide from homoleptic trialkoxides to redisperse progressively by adding suitable acid electrolytes<sup>30</sup>. The references mentioned are by no means complete, and should be considered exemplary only.

Although aluminum salts are very convenient precursors for colloidal alumina preparation, we have preferred to start with molecular-precursors as alkoxides, because many of them are volatile liquids that can therefore be readily purified by fractional distillation. As impurities can contribute to laser damage, this latter factor is of significant importance. Accordingly, the digestion in acidic medium of freshly precipitated hydroxide to a clear sol was retained as the preparative method, because metal alkoxide compounds are very sensitive to hydrolysis. Indeed, most of the metal alkoxides are extremely reactive species which may be due to the presence of electronegative alkoxy groups making the metal atoms highly prone to nucleophilic attack. We specifically selected for our purpose an adoption of the Yoldas method<sup>29</sup>. Such a method involved the hydrolysis of an adequate aluminum trialkoxide in hot water followed by the addition of a critical amount of certain organic or inorganic acids, to resuspend the precipitated aluminum hydroxide. The overall reaction can be represented as follows :



We chose the aluminum sec-butoxide,  $\text{Al(OC}_4\text{H}_9)_3$ , as alkoxide starting material, because it is a suitable liquid that boils roughly at 150°C under 0.25 mmHg, and hydrochloric acid rather than nitric acid as the electrolytic stabilizer because the major absorption band of likely residual chloride anion in the coating is at about 180 nm (UV-cut off) and therefore is far away from the wavelength of our interest 1064-nm. The use of organic dispersing agents such as acetic or trichloroacetic acids has been precluded because these acids require a mild heat treatment for efficient removal and in addition they tend to favorize the presence of carbonaceous residues inside the final coating. This last point is suspected as detrimental for laser-resistance<sup>31</sup>.

Hydrolysis of aluminum sec-butoxide was performed by introducing rapidly the alkoxide into excess hot water under vigorous stirring ; the sec-butanol by-product being removed by distillation. Adding the inorganic acid to the slurry induced a gentle redispersion (peptization) of it into a fluid translucent suspension within a few hours at reflux temperature, but the mixture was kept in these operating conditions for an additional 15 hours, to guarantee the peptization as completed. Then, the resulting aqueous suspension was concentrated under vacuum by rotative evaporation. This mixture was subsequently filtered through a 1.0- $\mu\text{m}$  Millipore fiber-glass membrane prior to coating use. Yoldas<sup>30</sup> reports that the suspension contains irregular and rectangular plates averaging  $\sim 400 \text{ \AA}$  long by  $200 \text{ \AA}$  wide and  $50 \text{ \AA}$  or less in thickness. He also reports that X-ray diffraction of these colloids revealed a crystallinity closely corresponding to gamma aluminum oxide hydrate as bohemite allotropic variety and not as bayerite<sup>32</sup>.

A typical alumina suspension was prepared as follows : Aluminum sec-butoxide,  $\text{Al(OC}_4\text{H}_9)_3$  was bought (Alfa supplier) rather than lab-made because it is a relatively cheap starting material and meticulously distilled twice to ensure a high purity-grade. The purified alkoxide was stored in a carefully cleaned and dried stoppered inactinic glass flask containing a molecular sieve dehydrating bed. Double-distilled aluminum sec-butoxide (246 g : 1 mole) was rapidly added into vigorously magnetic stirred deionized water (3 kg) at roughly 70° C. The generated sec-butanol by-product was then eliminated by simple distillation (98° C at 760 mmHg). Concentrated hydrochloric acid (7.0 g : 0.07 mole,  $d = 1.18$ ) in deionized water (100 g) was added to the briskly stirred slurry, and reflux was kept to allow peptization. The agglomerated hydrated alumina dispersed slowly and an opalescent fluid colloidal suspension was obtained after about 5-7 hours refluxing. Peptization was maintained overnight to complete it. Acid additions are generally specified in term of pH for peptization operation. However, in this case it was noticed that the

nature of the digesting acid was much more critical than the pH of the mixture. By subsequently distilling off water under reduced pressure using a rotoevaporator device we concentrated the aqueous bohemite alumina sol until the equivalent of 5 %  $\text{Al}_2\text{O}_3$  by weight (1020 g). Because of the presence of an excess of acid stabilizer in such a final suspension that tends to prevent multicoat operation by washing off all or part of the first coat, we have been faced to the necessity to reduce the acidity of the suspension by proceeding to a dialysis or an ion-exchange step. We selected the ion-exchange alternative to deacidify because it is a much more convenient and rapid mean compared to the membrane-dialysis when attempt is made to treat quite voluminous sol quantities. In this way, we utilized an anion-exchange resin as Amberlite IRA-93 SP that corresponds to a secondary amine free-base, to partially neutralize the suspension from an initial pH value of 3-4 to about 6-5 with no decrease in colloidal stability. Before use, the granular resin was abundantly washed with a solution of diluted hydrogen peroxide in deionized water until the washing liquor came out limpid. As low as pH 5, there was no more problem with wash off and many coatings could be applied successively at room temperature with only a few minutes drying time between each coat. At this stage the deacidified alumina sol remained very fluid, but with a tendency to thicken progressively until complete gelation after a few day storage. However, by carrying out a simple strenuously agitation the gelly-product was easily refluidized until recovering its original viscosity. Finally, this partially neutralized sol was then concentrated by distillation until obtaining a translucent paste containing the equivalent of 12 %  $\text{Al}_2\text{O}_3$  by weight (425 g). Such a viscous gel-like alumina network was readily refluidized when the addition of suitable aliphatic alcohols was performed. Methanol was the preferred diluting-solvent because it allows the preparation of sufficiently stable sols over roughly one week storage. The use of ethanol, isopropanol or 2-methoxy ethanol was precluded because all of these alcohols induced a quick gelation of the alumina-suspension therefore useless for coating-application. The aqueous methanolic coating sol was readily filtered through a 1.0- $\mu\text{m}$  fiber-glass membrane, without any clogging up trouble as encountered with the use of teflon filters.

### 3. COLLOIDAL SILICA SUSPENSION.

A typical amorphous silica sol was prepared by the base catalyzed hydrolysis of distilled tetraethylsilicate in pure ethanol by the method previously described<sup>16,17</sup>. In basic medium, hydrolysis of the silicate precursor into nucleated spheres is preferred over condensation to soluble organosiloxane polymers<sup>33</sup>. The material was prepared at 3.0 % silica content, and consisted of monodispersed roughly spherical particles with a diameter of about 20-nm. Such a silica sol was easily filtered through a 0.2- $\mu\text{m}$  teflon membrane.

### 4. COATING PROCEDURE.

Before use, all coating suspensions were carefully filtered as precised above. We have preferred to spin-coat rather to dip-coat because it uses much less material. Coatings were deposited on 20-cm diameter and 2.5-cm thick fused silica or BK-7 glass or even plexiglass substrates using a spin-coater in a 0.2- $\mu\text{m}$  filtered, forced air, clean hood. All coatings were prepared at an optical thickness of 266-nm, corresponding to quarterwave at the use wavelength of 1064-nm. All coating suspensions were applied at room temperature with a relative humidity in the range 50-60 %. Before coating-operation all substrates, except plexiglass, were  $\text{UV}/\text{O}_2/\text{H}_2\text{O}_2$  cleaned using an ozone-photoreactor (PR-100 ; UVP.Inc), achieving hydrophilic surfaces.

Alumina coatings were applied at room temperature, from an aqueous methanolic suspension containing 4 %  $\text{Al}_2\text{O}_3$  and prepared by diluting the 12 %  $\text{Al}_2\text{O}_3$  stock paste with twice an equal weight of methanol. The redispersion of the gelatinous paste was carried out with an ultrasonic treatment giving a fluid opalescent coating-sol. One coat at 1000 rpm was necessary to give coatings of the required thickness. After about 5-min air-drying a second coating-operation could be run without wash off nuisance. This step could be substancially shortened by exposing the freshly deposited coat to a mild heat treatment (IR-lamp).

Silica coatings were applied from the 3.0 %  $\text{SiO}_2$  stock solution. One application at 1000 rpm gave a coating of the desired thickness. Such a coating was easily water-wetted in contrast to n-propanol diluted silica sols which were water-repellent. In the preparation of multilayered films, both silica and alumina coatings were normally air-dried for 5-min prior to the application of the next coat. As mentioned above a slight heating could accelerate the coating-process. Looking at the reflected color of the coated parts, we could appreciate with unaided eyes the uniformity of the films. Except a weak edge-effect of about 2-mm wide, the majority of our coatings had no discernible color variations.

## 5. LASER DAMAGE MEASUREMENTS.

Damage threshold measurements were carried out at 1064-nm wavelength either at Limeil National Laboratory on the  $\omega_0$ -laser system delivering single shots of 3-ns pulse duration and at Lawrence Livermore National Laboratory on the *Reptile*-laser system delivering multishots of 16-ns pulse duration each in a 30 Hz repetition rate. In both cases, spatio-temporally, the laser beam was gaussian with a spot size of about 2.0-mm diameter for the  $\omega_0$ -facility and 0.6-mm for the *Reptile*-facility. The respective pulse durations and beam diameters were the widths at half maximum of, respectively, the temporal and spatial profiles. The incidence angle was roughly  $10^\circ$ . Both, we conducted "S-on-1" (S shots of known fluence onto a selected site) damage tests. We defined as representative for damage measurements cumulative-shot values as  $S=5$  at LNL and  $S=1000$  at LLNL. Each sample site was inspected under a microscope and video-memorized before and after laser irradiation to allow a simple and performant photographic comparison. In like manner, we could attest if the sample damaged yes or no. Damage was defined to be any evolutive 5-10 micron size range alteration observable by our technique. From a sequence of irradiations, the damage threshold was defined as the average of the highest fluence which caused no damage and the lowest fluence which did. While in general, we do not wish to discount the significance of minute damage spots at low fluence levels, we feel that it is important and logical to differentiate the notion of very minor and nonevolutive damage from one of consistent and growing damage. Such an interpretation of damage threshold seemed to us more adequate to judge the suitability of a particular coating for practical application.

## 6. DISCUSSION OF RESULTS.

### A. Single Layer $\text{Al}_2\text{O}_3\text{-H}_2\text{O}$ coatings

The transmission spectrum of a typical sample of a BK-7 substrate, both uncoated and coated on both sides with hydrated alumina, is shown in Fig.2. The coating is antireflective, meaning it has a lower index than the substrate. The spectrum is typical of that for a homogeneous, quarterwave AR coating with a maximum transmission (i.e. minimum reflection) of about 95 % at about 1060 nm and a minimum transmission at the halfwave point ; this being the same as that of the bare substrate. Standard optics calculations indicate that the refractive index of the coating is therefore 1.44, assuming an index of 1.51 for the substrate. This index is considerably higher than the index reported by Yoldas for the same material deposited from water suspension ; his figure being 1.32. He doesn't, however, report that the index increases when the water is partially replaced by lower alcohols but gives no details. We found that when we dip-coated a BK-7 sample in an aqueous methanol suspension of hydrated alumina, our index was 1.41. The highest index is, of course, preferred for HR coatings and, as we prefer to spin rather than dip anyway, the causes of this difference were not investigated. It could be that improved packing of the alumina platelets is obtained when they are subject to the high shear forces present in spin coating as compared to the much lower shear during dip coating.

The optical properties of this coating were unchanged on heating to  $100^\circ\text{C}$ , and there was no difference when an ion exchange resin neutralized coating suspension was used rather than the as-prepared material. There were also no change in the optical spectrum when coatings were exposed to varying relative

humidity. If alumina was deposited first onto the bare substrate, we had no wetting problems with our aqueous methanolic mixtures because as mentioned before the UV-ozone treated surfaces remained very hydrophilic and this within about 20-min. So, such a coating procedure allowed us to avoid the use of a nonionic surfactant and therefore eliminated a risk of potential carbonaceous contamination leading to laser damage.

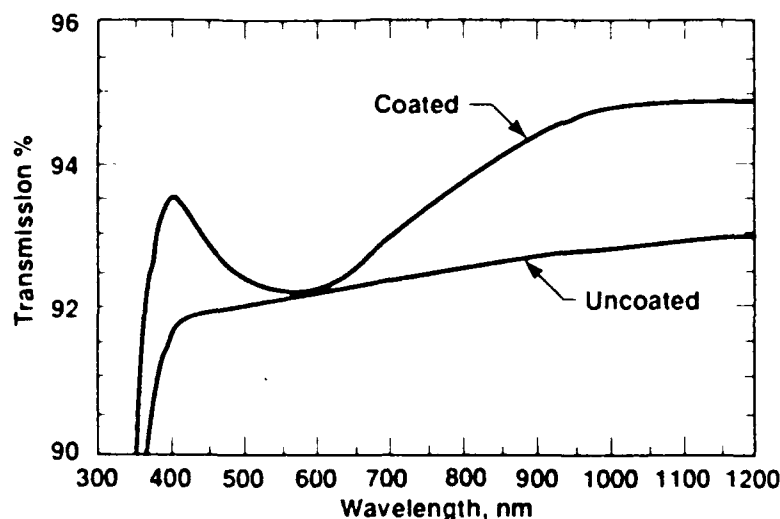


Fig. 2. Transmission of  $\text{Al}_2\text{O}_3\text{-H}_2\text{O}$  coating on BK-7 substrate.

Laser damage threshold measurements, with 3-ns pulses at LNL and 16-ns pulses at LLNL, revealed values ranging respectively from a low of  $10.2 \text{ J/cm}^2$  to a high of  $14.6 \text{ J/cm}^2$  and from 25 to  $45 \text{ J/cm}^2$ . Such figures corresponded to single-layer bohemite alumina deposited onto UV-ozone precleaned Herasil-I fused silica 200-mm diameter discs, and in both cases for a total of 10 samples. We think the wide range of damage thresholds is probably attributed to local coating-contamination inherent to the process itself and consequently favoring laser-induced damage. Samples with low thresholds generally showed only few microscopic pits with diameter of  $10 \mu\text{m}$ , in the beam area. Massive damage over the whole laser spot did not occur until fluences in the range  $15\text{-}16 \text{ J/cm}^2$  at LNL and  $45\text{-}50 \text{ J/cm}^2$  at LLNL were reached and the observed damage resulted in uniform removal of coating-material. After fine visual analysis under Reichert-stereomicroscope, we noticed that in almost all cases damage originated at visible artifacts present in coating or at substrate - interface. So, clean areas appeared really stronger to laser irradiation than those busy. In contrast to the previously investigated  $\text{TiO}_2$  material<sup>20,21</sup> that failed at relatively low fluences with severe damage when exposed to a high repetition rate, the  $\text{Al}_2\text{O}_3$  component has proved to be a stoutly refractory material enduring efficiently quite high fluences in a high repetition rate.

When laser-annealing was directed onto such sol-gel crystalline alumina single-layer coatings, we didn't observed, as for previous works onto zirconia<sup>22</sup>, a significant enhancement of the laser-strength. The laser-annealing post-treatment consisting in a progressive increase of the laser fluence onto the exposed surface sample has been experimentally confirmed as effective for alumina coatings prepared from aluminum sec-butoxide only distilled once. In this latter case, we measured at LNL alumina quarterwave thick coating with a damage threshold figure averaging  $9.2 \text{ J/cm}^2$  and that moved up to  $13.8 \text{ J/cm}^2$  when laser-conditioned. Regarding such alumina sol-gel coatings, that must be in good thermodynamic-equilibrium as conferred by the chemical nature of the sol-gel process itself, we actually think that the observed raising in laser-resistance, by a factor of about 1.5, might be likely due to a gentle desorption of volatile absorbing impurities through coating-porosity, and not to electronic rearrangements as already advanced by Kozlowski et al for condensed dielectric materials<sup>34</sup>. Therefore, the reason that double-distilled aluminum alkoxide precursor gave alumina coatings with laser damage threshold was surely the result of a high purity-grade of synthesized alumina.

## B. Multilayer coatings.

Multilayer coatings were readily prepared at room temperature by applying alternating coats of silica and alumina. The silica coating was preferentially applied first and the outside coating-layer was always alumina. Therefore, most of our prepared samples contained a similar number of layers, in contrast to the more conventional samples using dense silica as the low index component. These coatings have an odd number of layers because the high index component is applied first. Layers were applied with approximately 5-min drying time between applications and with the substrate remaining in the spin coater. Occasional samples would contain comets as a result of coating over small artifacts on the surface of the previous layer. In multilayer applications the cleanliness criterion becomes drastically critical, so, stringently tidy conditions during coating deposition must be required.

The transmission spectrum of an HR-coating consisting of 16 pairs of  $\text{SiO}_2\text{-Al}_2\text{O}_3$  quarterwave thick layers is shown in Fig.3. It has 99% reflectivity at the assigned wavelength. Of particular significance was the ease of preparing this 32-total layer sample. The mirror was stress-free and devoid of peeling or crazing except maybe on the rim where a slight edge-effect induced a dawning flaking phenomenon.

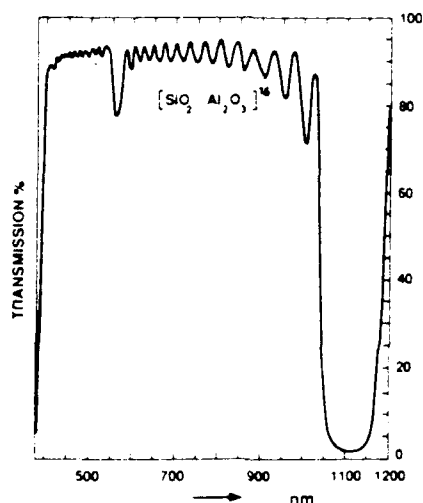


Figure 3 : Transmission spectrum of  $\text{SiO}_2\text{-Al}_2\text{O}_3$  HR-coating on fused silica substrate.

The weak reflection peak at roughly 550-nm wavelength discloses a certain thickness-inhomogeneity in coating stack. Such a reflection peak could be suppressed by better adjusting the quarterwave-thickness condition the low- and high-index materials must fulfill to fit the theory. Calculations using Fresnel laws indicated that, with refractive indices of 1.22 for silica and 1.44 for hydrated alumina, about 34-36 layers would be required to achieve reflectance greater than 99 % on BK-7 glass substrate, and this was experimentally confirmed. After about 10-15 successive layers were deposited onto well-polished substrates, coating surface aspect evidenced fine radial-lines testifying likely of an apparent inhomogeneous flow motion of coating solution. Subsequent interferometric measurements with a Zygo-device showed that the radial lines didn't have any prejudicial impact towards the reflected wave quality. We conducted too on several sol-gel coated pieces some relative-roughness measurements, using a Reicher apparatus, and that gave quite good figures in the range 15-20 Å RMS.

Figure 4 illustrates our present knowing-how with this colloidal sol-gel route and for instance shows a 300-mm diameter polished plexiglass substrate coated with a 32 total layer silica-alumina HR-coatings. In order to minimize or even hinder the flaking effect on the rim of thick HR-films, we have observed that using curved-edge substrate improved consistently the situation. Indeed, in this case, the coating-solution motion after deposition flows until the edges and therefore gives a much more homogeneous and flaking-free coating.



Figure 4 : A 300-mm diameter dielectric sol-gel mirror realized onto a polished plexiglass substrate.

The laser damage thresholds in different repetition rate and pulse conditions are shown in Fig.5. These threshold values vary at LNL (3-ns pulse ; 5 pulses at 0.03-Hz) from a low of  $10.1 \text{ J/cm}^2$  to a high of  $15.2 \text{ J/cm}^2$  with an average of  $12.4 \text{ J/cm}^2$  and at LLNL (16-ns pulse ; 1000 pulses at 30-Hz) from a low of  $21 \text{ J/cm}^2$  to a high of  $50 \text{ J/cm}^2$  with on average of  $35.5 \text{ J/cm}^2$ . To explain the dispersion of these threshold figures, we think the artifact problem, discussed earlier, also applied here, even maybe with a more pronounced significance because of the large number of layers required in HR-stacks. As for single layer coatings coming from double-distilled precursor, the use of laser-annealing has been ineffective on multilayered coatings to boost more the laser-strength. The threshold values presented here are higher than those of conventional electron-beam evaporated coatings on large optics (typically in the range  $5\text{-}8 \text{ J/cm}^2$  under 3-ns shot). There may, therefore, be some strong advantage to the use of solution-deposited coatings on large optics due to the relative ease of their fabrication and also if the damage threshold can be retained on scale-up.

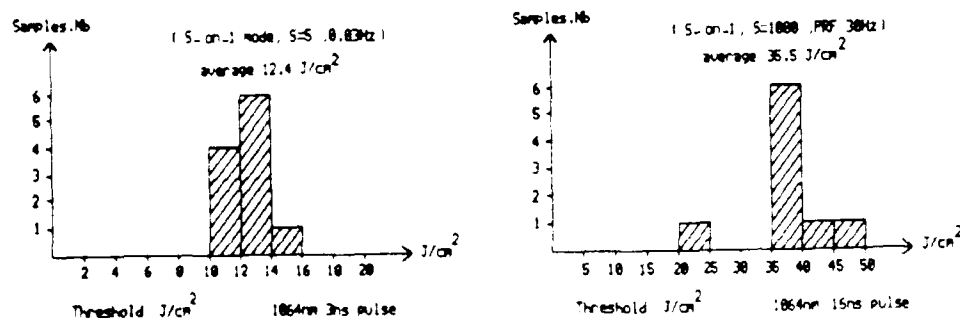


Fig. 5 : Laser damage thresholds in different conditions of  $\text{SiO}_2\text{-Al}_2\text{O}_3$  sol-gel mirrors.

The nature of any colloidal coating consists of layers of discrete material particles stacked on a substrate and is such that it is kept intact only by point contact forces between the individual particles and the abrasion resistance is therefore quite low. This is of no concern in our current applications at LNL and LLNL and in fact is an advantage as it allows easy removal of the coating without damage to the optical form of the substrate beneath, and furthermore affords a beneficial cost saving by avoiding the tricky and onerous polishing step. If cleaning operation of the coating is required, no physical contact procedure can be tolerated and consequently only the use of a suitable solvent-spray must be carried out.

## 7. CONCLUSION.

We have prepared using the sol-gel process, porous crystalline bohemine  $\text{Al}_2\text{O}_3 \cdot \text{H}_2\text{O}$  coatings on fused silica, borosilicate glasses and even plexiglass substrates from aqueous methanolic colloidal suspensions. These coatings were easily spin-applied at room temperature and required no subsequent processing after solvent evaporation. This single-layer alumina coating had a refractive index of about 1.44 with multishot damage thresholds ranging 10.5-14.6 J/cm<sup>2</sup> at 3-ns pulse duration and 25-45 J/cm<sup>2</sup> at 16-ns pulse duration at the assigned wavelength of 1064-nm.

Multilayer HR-coatings were also elaborated by stacking alternate quarterwave coatings of this hydrated alumina with amorphous silica also prepared from a colloidal suspension. This operation was readily run at room temperature, with about 5-min air drying time between each coat. About 32-total layers were needed to achieve reflectivity close to 99 %. Such mirrors exhibited in the same laser conditions than previously, median thresholds of respectively 12.5 J/cm<sup>2</sup> at 3-ns and 35.5 J/cm<sup>2</sup> at 16-ns pulse length.

In the future, we intend to significantly improve the general aspect of our HR-coatings (less artifacts, better homogeneity), by acquiring a novel spin-coater specially conceived for our needs and following from the technology used currently in microelectronic to coat silicon wafers. Our short-term goal at Limeil National Laboratory is actually to demonstrate the possible realization of a 420-mm diameter dielectric sol-gel mirror useful for laser-system projects now in progress. This interest is shared with our partner from Lawrence Livermore National Laboratory alike involved in similar projects.

## 8. ACKNOWLEDGEMENTS.

The authors are very grateful to C. Cordillot for damage threshold measurements performed at LNL and to A. Morgan and F. Rainer for damage tests performed at LLNL.



## 9. REFERENCES.

1. Ebelmen, Annales de Chimie et de Physique, Ser. 3, Bd 57 : 319-55 (1846).
2. H. Dislich, Angew. Chem. Int. Ed. Engl. 10, 363 (1971).
3. R. Roy, J. Am. Ceram. Soc., 52, 344 (1969).
4. Better Ceramics Through Chemistry I, Edited by C.J. Brinker, D.E. Clark and D.R. Ulrich, (Mater. Res. Soc. Proc. 32, Albuquerque, New Mexico, 1984).
5. Better Ceramics Through Chemistry II, Edited by C.J. Brinker, D.E. Clark and D.R. Ulrich, (Mater. Res. Soc. Proc. 73, Palo Alto, California, 1986).
6. Better Ceramics Through Chemistry III, Edited by C.J. Brinker, D.E. Clark and D.R. Ulrich, (Mater. Res. Soc. Proc. 121, Reno, Nevada, 1988).
7. Ultrastructure Processing of Ceramics, Glasses and Composites, Edited by L. Hench and D.R. Ulrich (John Wiley and Sons, Inc., 1984).
8. Science of Ceramic Chemical Processing, Edited by L. Hench and D.R. Ulrich (John Wiley and Sons, Inc., 1986).
9. Ceramic Powder Science, vol 21, Edited by G.L. Messing, K.S. Mazdiasni, J.W. McCauley and R.A. Haber (American Ceramic Society Inc., 1987).
10. Ceramic Powder Science, vol II A and II B, Edited by G.L. Messing, E.R. Fuller, Jr., H. Hausner (American Ceramic Society Inc., 1987).
11. Sol-Gel Technology, Edited by L. Klein (Noyes Publications, 1988).
12. Prospect Calorex (trade mark), Jaener Glaswerk Schott and Gen. Mainz (1978).
13. H. Schroeder, "Properties and Applications of Oxide Layers Deposited on Glass from Organic Solutions", Opt. Acta 9, 249 (1962).
14. T.N. Krylova, R.S. Sokolova and I.F. Bokhonskaya, "Interference Coatings with a Large Number of Layers and Prepared by a Chemical Method", Sov. J. Opt. Techn., 34, 664 (1967).
15. I.M. Thomas, J. Wilder, R. Gonzales and D. Georges, "1064-nm and 350-nm Laser Damage Thresholds of High-Index Oxide Films Deposited from Organic Solutions and Sols", 18 th Boulder Damage Symposium, Boulder, CO, (1986), NIST Special Publication.
16. I.M. Thomas, "High Laser Damage Threshold Porous Silica Antireflective Coating", Appl. Opt., 25, 1481 (1986).
17. H.G. Floch, J.J. Priotton, "Porous Silica Sol-Gel Coatings for Nd : Glass High-Power Pulsed Laser Uses", The Physics and Technology of Amorphous SiO<sub>2</sub>, Edited by R.A. Devine, Plenum press, 561 (1988).
18. I.M. Thomas, "Porous fluoride Antireflective Coatings", Appl. Opt., 27, 3356 (1988).

19. H.G. Floch, J.J. Priotton, J.F. Mengue and C. Cordillot, "1064-nm and 350-nm Radiation Stability of Low Density  $\text{ThO}_2\text{-SiO}_2$  High-Reflective Coatings Deposited from Sols", 19 th Boulder Damage Symposium Proc., 290 (1987), NIST Special Publication.
20. I.M. Thomas, "Single-Layer  $\text{TiO}_2$  and Multilayer  $\text{TiO}_2\text{-SiO}_2$  Optical Coatings Prepared from Colloidal Suspensions", Appl. Opt., 26, 4688 (1987).
21. H.G. Floch, J.J. Priotton and I.M. Thomas, " $\text{TiO}_2\text{-SiO}_2$  colloidal HR-films for High Power Lasers", Le vide, Les Couches Minces, vol 44, 245, 33 (1989).
22. H.G. Floch and J.J. Priotton, "1-on-1 and N-on-1 Laser Strength of Binder Aided  $\text{ZrO}_2$  and  $\text{ZrO}_2\text{-SiO}_2$  Reflective Sol-Gel Coatings", 21 st Boulder Damage Symposium, Boulder, CO, (1989), NIST Special Publication.
23. S. Parraud, L.G. Hubert-Pfalzgraf and H.G. Floch, "Stabilization, Characterization and Optical Applications of Niobium and Tantalum Oxide Sols Prepared Via Alkoxide Routes", Proc. Mater. Res. Soc., Symposium, San Fransisco, April 90.
24. F. O'Neill, I.N. Ross, D. Evans, J.U.D. Langridge, B.S. Bilan and S. Bond, "Colloidal Silica Coatings for KrF and Nd : Glass Laser Applications", Appl. Opt. 26, 828, (1987).
25. H.G. Floch, J.P. Priotton and I.M. Thomas, "Optical Coatings Prepared from Colloidal Media", Thin Solid Films, 175, 173 - 178 (1989).
26. K. Yamada, T.Y. Chow, T. Horiata and M. Nagata, "A Low Temperature Synthesis of Zirconium Oxide Coating Using Chelating Agents", J. of Non-Cryst. Solids, 100, 316 (1988).
27. I.M. Thomas, "Single-Layer  $\text{Al}_2\text{O}_3\cdot\text{H}_2\text{O}$  and Multilayer  $\text{Al}_2\text{O}_3\cdot\text{H}_2\text{O-SiO}_2$  Optical Coatings Prepared from Colloidal Suspensions", Appl. Opt., 28, 4013 (1989).
28. Gay-Lussac, Ann. Chim. Phys., 74, 193 (1810).
29. J. Bugosh, "Fibrous Alumina Monohydrate and Its Production", US Patent, 2, 915,475 (1959), assigned to E.I. du Pont de Nemours and Compagny.
30. E.S. Lane, "Preparation of Sols and Gels", U.K. Patent, 2, 111, 966 (1983).
31. B.E. Yoldas, "Alumina Sol Preparation from Alkoxides" Am. Chem. Soc. Bull. 54, 289 (1975).
32. I.M. Thomas, J. wilder, A. Lee and D. George, "Influence of Post-Deposition Treatment by UV-Light and Oxygen (Ozone) on 350 nm Damage Thresholds of  $\text{SiO}_2$  Films Deposited from Sols", in Proceedings of the 18 th Boulder Damage Symposium, Boulder, CO (1986), NIST Special Publication.
33. B.E. Yoldas, "Hydrolysis of Aluminum Alkoxides and Bayerite Conversion", J. Appl. Chem. Biotechnol., 23, 803 (1973).
34. B.E. Yoldas and D.P. Partlow, "Wide Spectrum Antireflective Coating for Fused Silica and Other Glasses", Appl. Opt., 23, 1418 (1984).
35. M.R. Kozlowski, M. Staggs, C.R. Wolfe and J.H. Campbell, "Large Area Laser Conditioning of Dielectric Thin Film Mirrors", 21 st Boulder Damage Symposium, Boulder, CO (1989), NIST Special Publication.



## Laser processing of channel waveguide structures in sol-gel coatings

B. D. Fabes, D. J. Taylor, L. Weisenbach, M. M. Stuppi, D. L. Klein, L. J. Raymond,  
B. J. J. Zelinski, and D. P. Birnie III

University of Arizona, Department of Materials Science and Engineering, Tucson, AZ 85721

ABSTRACT

Sol-gel derived silica, silica-titania, and tantala coatings were covered with a thin metal film and translated across a Nd:YAG laser beam (1.06  $\mu\text{m}$ ). The laser energy was absorbed by the metal film, which heated the underlying sol-gel coating. This heating densified the sol-gel coatings, thereby increasing the index of refraction of the laser heated region, and forming channel waveguide structures in all three systems. The channels formed by this technique were etched, to remove the undensified regions, which resulted in ridged waveguide structures. The structures were also produced by depositing a metal pattern using photolithographic techniques, and rastering the laser across the entire sample. The refractive indices of laser densified and furnace densified silica coatings were similar. Large differences were observed in the indices of laser and furnace densified coatings for the silica-titania and tantala systems.

1. INTRODUCTION

One of the basic components in integrated optical circuits is the channel waveguide. The channel waveguide provides two-dimensional confinement of the optical signal, which permits the routing of signals between various input, output, and processing components on a chip. While most often used as a passive component, channel waveguides can also be fabricated in electro-optic and semiconducting materials such as  $\text{LiNbO}_3$  and GaAs, where they actively participate in signal processing. Various geometries (e.g., ridged and imbedded channel guides and strip-loaded planar guides) can be used to synthesize channel waveguides (For a detailed discussion see Reference 1). However, the basis for all of these geometries is the formation of a channel which guides light when it is surrounded on all sides by lower index material.

The modal properties of the channel waveguide are determined by the index difference between the waveguide and its surroundings, and by the waveguide dimensions. When the index differences are small, on the order of 1 to 2%, the single mode operation requires channel dimensions on the order of one to several operating wavelengths. For index differences of 10 to 30% these dimensions are reduced to 1/4 to 1/3 the operating wavelength. When the channel dimensions exceed these minimum values, multi-mode operation is possible. For most applications minimum operating efficiencies require that channel waveguide losses be no larger than about 1 dB/cm. However, losses approaching 0.1 dB/cm are much more desirable.

A wide range of techniques have been used to synthesize both active and passive channel waveguides. These include radio frequency sputtering,<sup>2</sup> chemical vapor deposition,<sup>3,4</sup> liquid phase epitaxy,<sup>5</sup> vapor phase epitaxy,<sup>6,7</sup> and organo-metallic chemical vapor deposition.<sup>8</sup> All of these techniques require the use of a mask-and-etch process to define the channels and extensive high vacuum equipment to deposit the desired film structure.

While high vacuum techniques are a necessity for defining channel structures in active materials such as GaAs, no such inherent constraints exist for synthesizing channel structures in oxides. For this reason, the majority of channel waveguide synthesis in oxides is performed using diffusion and ion-exchange techniques. In the diffusion technique high temperatures are used to cause the diffusion of some doping species into local regions of a planar waveguide that has been previously masked and coated with the dopant. Channel waveguides synthesized via the ion exchange process closely resemble those made by the diffusion technique, the difference being that the chemical exchange process occurs in a bath where one ionic species is substituted in the substrate for another. This process produces the composition and index changes



required to form the channel.

In both techniques, the resulting change in chemistry typically causes an index change of about 1%. These small index changes necessitate the formation of channel dimensions on the order of microns by diffusional processes. In many cases the use of elevated temperatures or exposure to the ion exchange solution causes stresses which lead to degradation of the substrate material and subsequently high losses in the waveguides. Despite these complications, diffusional doping using Ti is the most popular way to form channel structures in  $\text{LiNbO}_3$ ,<sup>9</sup> while ion exchange is extensively utilized to form passive channel waveguides in oxide glasses.<sup>10</sup>

Sol-gel processing provides a non-vacuum technique to deposit waveguiding coatings.<sup>11,12</sup> The flexibility of the sol-gel process also provides the potential for creating index differences which are far greater than those created using the diffusion or ion exchange techniques. For example, the index of a  $\text{SiO}_2$ - $\text{TiO}_2$  coating can be varied from 1.63 to 1.77 simply by heating.<sup>20</sup> During heating, changes occur in both the chemistry (organics are burned out, and metal-oxygen-metal bonds are formed) and the density of sol-gel coatings. If these changes can be confined to a small strip of material, channel waveguides could easily be formed in sol-gel coatings. Translating a laser across the sample should be a convenient way to do this.

Shaw et al<sup>13</sup> and Ramaswamy et al<sup>14</sup> used a  $\text{CO}_2$  laser ( $10.6\text{ }\mu\text{m}$ ) to densify channels on the surface of gel-derived silica monoliths. In both cases, the  $\text{CO}_2$  laser was absorbed by the monolith. An increase in hardness of the laser-heated area<sup>13</sup> indicated that densification occurred in the laser irradiated region. Krchnavek et al<sup>15</sup> partially densified organosilicate-deposited silica coatings on silicon substrates using a Nd:YAG laser ( $1.06\text{ }\mu\text{m}$ ). The coating in this case was transparent to the laser. Heating came from the substrate, which absorbed the laser energy.

For forming channel waveguides, an optimal process would densify the sol-gel coating, while leaving the underlying substrate unaffected. This probably precludes the use of a  $\text{CO}_2$  laser, which would be absorbed by most substrates of interest in integrated optics. A Nd:YAG laser, on the other hand, would not be absorbed by most substrates, although a way to couple the energy into the coating would have to be developed. One possibility would be to dope the coating with a material that absorbs at  $1.06\text{ }\mu\text{m}$ . This would be

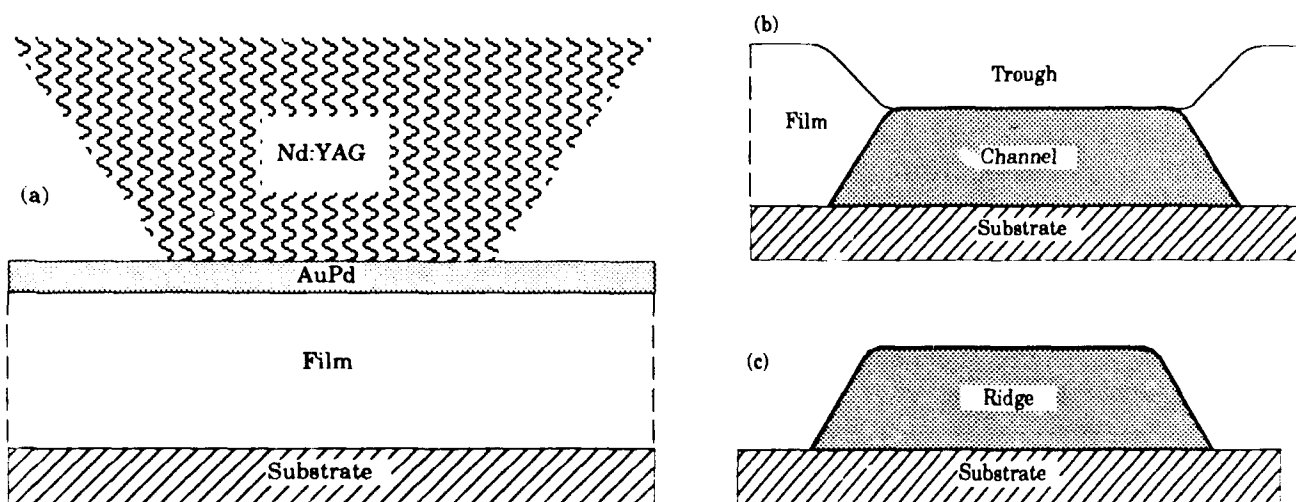


**Figure 1:** (a) Schematic drawing of heating a metal-coated sol-gel coating using a Nd:YAG laser; (b) Channel produced after metal film is washed off; and (c) Ridge produced after etching undensified region.

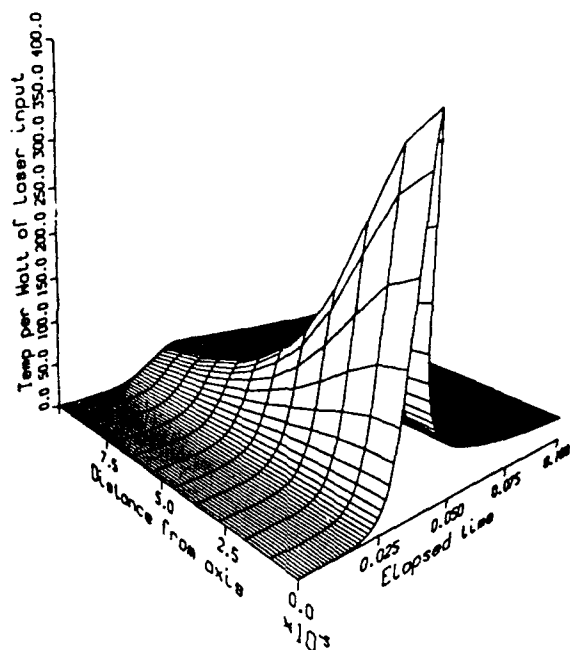


**Figure 2:** Computer simulation of the temperature ( $^{\circ}\text{C}$ ) about a point on the surface of a metal-coated sol-gel coating as a Nd:YAG laser traveling at 10 mm/s passes the spot (distance in m, time in s). The large decrease in temperature within  $25\text{ }\mu\text{m}$  of the laser indicates that channels should be formed by the laser. (From Reference 16.)

effective, so long as the dopant did not adversely affect the desired properties of the coating. Alternatively, the "dopant" could be applied as a film on top of the coating (Figure 1a). A computer model of the laser heating of sol-gel coatings suggested that high temperatures would be produced by scanning a Nd:YAG laser across a sol-gel coating covered with a thin absorbing layer (Figure 2).<sup>16</sup> Further, these temperatures should be confined – both laterally and vertically – so that channels with notably higher indices than the surrounding material would be produced. After heating, the metal film could be washed off, leaving a channel with increased index (Figure 1b). Finally, if desired, the undensified regions might be etched away, leaving ridged channels (Figure 1c).

An advantage of using radiation of a wavelength that is absorbed by an overlayer, but not by the coating, is the ability to preselect the areas to be densified. This may be done by depositing the absorbing (metal) film in a pattern using lithographic writing techniques. Here, one would not have to define patterns with the laser, but could instead irradiate the entire sample, heating only the areas covered by the metal film. Further, since the size of the features produced using a photolithographical mask can be less than a micron, the channels need not be limited by the size of the laser beam.

In this paper we report on using the metal film/Nd:YAG method to produce channel waveguide structures in  $\text{SiO}_2$ , 1:1  $\text{SiO}_2\text{-TiO}_2$ , and  $\text{Ta}_2\text{O}_5$  sol-gel coatings. First, we describe the coating fabrication and characterization techniques. Next, we describe direct writing of channels in these coatings, forming ridged structures from these channels, and using a patterned metal film to defined the channel patterns. We conclude with a brief discussion of some interesting mechanistic questions concerning laser densification of sol-gel coatings.

## **2. EXPERIMENTAL PROCEDURES**

### **2.1 Coating Fabrication**

Silica, 1:1 mole ratio silica-titania, and tantalum coatings were investigated. Silica was chosen because it has been shown that laser heating can be used to increase the index of sol-gel derived silica coatings.<sup>17</sup> Silica-titania was chosen because previous work has shown that this system can be used to make planar waveguides on silica glass.<sup>12</sup> Tantalum was chosen because it is a single component oxide with a high index

and should be suitable for planar waveguide applications.

The silica coatings were made by mixing tetraethoxysilane (TEOS) in a 1:4 volume ratio with ethanol. Two moles of water per mole of TEOS were added to the TEOS/ethanol solution, resulting in a solution with 5 weight percent solids. Dilute HCl was added to give the solution a final pH of 2. The solutions were allowed to react for at least three days prior to coating.

A silica-titania solution containing 50 mole percent titania and 50 mole percent silica was made using a procedure similar to Dale et al.<sup>12</sup> TEOS (21.4 ml) was mixed with 18 ml of isopropanol, 3.5 ml of water, and enough HCl to bring the solution pH to 2. In a separate container, 32.8 ml of titanium butoxide was mixed with 19.5 ml of acetylacetone (AcAc). The titanium butoxide/AcAc solution was allowed to react for twenty minutes, after which the solutions were mixed together. Then 6 ml of isopropanol was added to bring the final solution to 20 weight percent solids. This mixture was allowed to react for four days before being used for coating.

The tantala films were made using a process similar to that developed by Silverman et al.<sup>19</sup> However, the solutions were made less sensitive to the atmosphere by adding a complexing agent (AcAc) to slow the hydrolysis reactions. Specifically, 5.7 ml of tantalum ethoxide was added to 20 ml of ethanol in a dry box. Then 3 ml of this solution was mixed with 0.3 ml of AcAc. A solution which contained 0.05 ml of water and 8.6 ml of ethanol was then added dropwise to the tantalum ethoxide/ethanol/AcAc solution while stirring. The final solution contained 5 weight percent solids.

Coatings were made by either dip- or spin-coating the solutions onto fused silica substrates. Prior to laser firing, the silica coatings were prebaked at 100 °C for 15 minutes, the silica-titania films were prebaked at 200 °C for 15 minutes, and the tantala films were prebaked at 230 °C for 30 minutes.

## 2.2 Laser Heating

Laser heating was done using a single mode Nd:YAG laser beam (1.06  $\mu\text{m}$ ) with a width of approximately 75  $\mu\text{m}$  at half maximum intensity. The laser energy was absorbed by a 400 Å 60Au/40Pd sputtered film, which was washed off after laser heating using aqua regia (3:1 HCl:HNO<sub>3</sub>).

## 2.3 Etching

To form ridged waveguides, silica and silica-titania films were etched using a buffered HF (1HF:6NH<sub>3</sub>F) solution. Etch rates were determined for the different coating materials by coating silicon substrates and firing the coatings in air at various temperatures between 100 and 1000 °C. Steps were formed on the coatings by masking half of the coating with positive photoresist and removing the unmasked coating with a buffered HF solution. Next, the photoresist was removed with ethanol, exposing a sharp step over which thickness measurements were made using a mechanical surface profilometer. Since the etch rates of the various coatings were found to vary by over four orders of magnitude, the HF solution was diluted in water so that the etch rate of each of the coatings was approximately 5-10 Å/s. The coatings were then etched for 15 second intervals, after which the change in coating thickness was measured. Standardized etch rates were then calculated by dividing the measured etch rates by the dilution.

# 3. FABRICATION OF CHANNEL PATTERNS

## 3.1 Direct Writing Approach

In the direct writing approach, an absorbing film is sputtered onto the coating, and the sample is then

translated across the laser to make a densified line or area (Figure 1a). After washing off the metal film, a densified channel is observed in the coating (Figure 1c). The surface profile trace which resulted from scanning the Nd:YAG laser (0.75 Watt, 8 mm/s) across a 2150 Å silica-titania coating is shown in Figure 3. With a single pass of the laser, the trough formed is roughly gaussian, with dimensions corresponding roughly to the width of the laser beam.

As the power of the beam was increased, the film shrunk further, leading to a corresponding increase in the depth of the trough. The shrinkage of the coatings as a function of laser power for a constant scan speed is shown in Figure 4. In this figure, the percent shrinkage is defined as the relative change between coating thickness after laser firing and coating thickness after prebaking. The index also increased with laser power, as shown in Figure 5. This indicates that the coatings are densifying, and not simply being ablated by the laser.

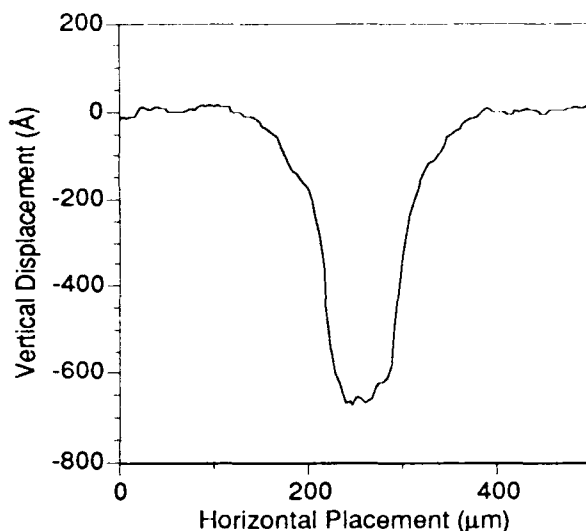


**Figure 3:** Surface profile of a channel formed by laser heating (0.75 W, 8 mm/s) a 2150 Å silica-titania sol-gel coating.

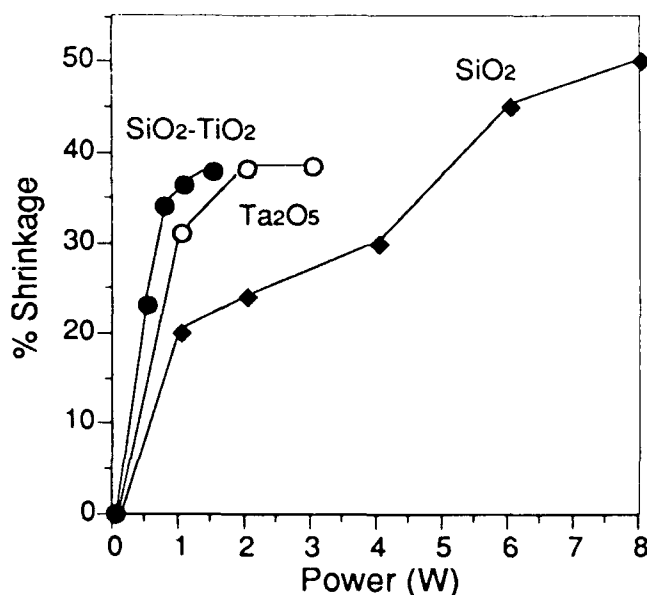


**Figure 4:** Shrinkage of silica, silica-titania, and tantala coatings vs. laser power.

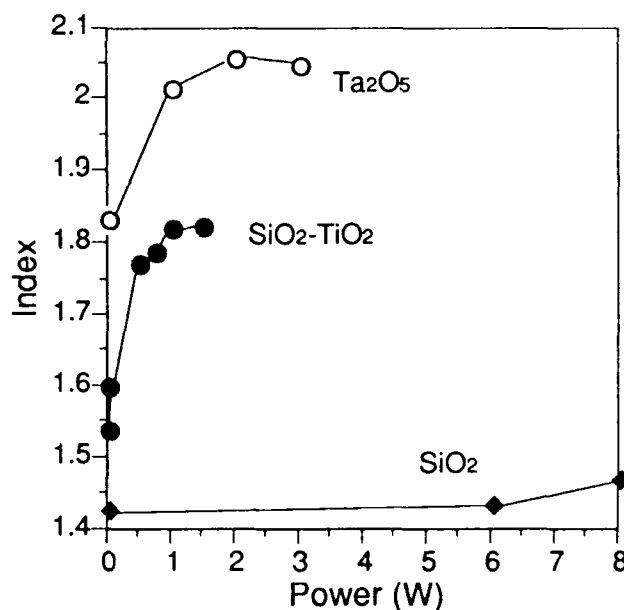


**Figure 5:** Index of silica, silica-titania, and tantala coatings vs laser power.

### 3.2 Direct Writing and Etching

Densification changes not only the index, but also the etch rate of sol-gel coatings. As shown in Figure 6, the change in etch rate can be dramatic. For silica coatings, the etch rate varies by over two orders of magnitude – from approximately 1000 Å/s for an as-deposited coating to less than 10 Å/s for a fully densi-

fired coating.

For the silica-titania coatings, the change in etch rate is even more pronounced. When heated in a furnace, densification takes place up to 600 °C in these coatings.<sup>20</sup> As shown in Figure 6, the etch rate changes by a factor of almost 40 when the coatings are fired to this temperature. Silica titania coatings fired to 800 °C are crystalline.<sup>18</sup> This crystallization leads to a decrease in the etch rate by an additional factor of almost 1000.

The large difference between the etch rates of densified and undensified coatings can be used to produce ridged waveguides in sol-gel coatings. After forming a channel by laser irradiation, etching the coating in a dilute HF solution can leave the densified regions unperturbed, while the undensified portions are removed (Figure 1c). For example, a channel was formed in a 2150 Å silica-titania coating by laser irradiation. After removing the absorbing coating, the trough was 600 Å deep and 150 μm wide (Figure 7a). This sample was then etched in a buffered HF solution, diluted 1:5 with water, for 20 s. This resulted in ridges, with nearly vertical sides, which were 1500 Å tall and 150 μm wide (Figure 7b). (Since the sum of the trough depth and the ridge height is equal to the initial coating thickness, this experiment also verified that the laser treatment does not ablate the coating.)

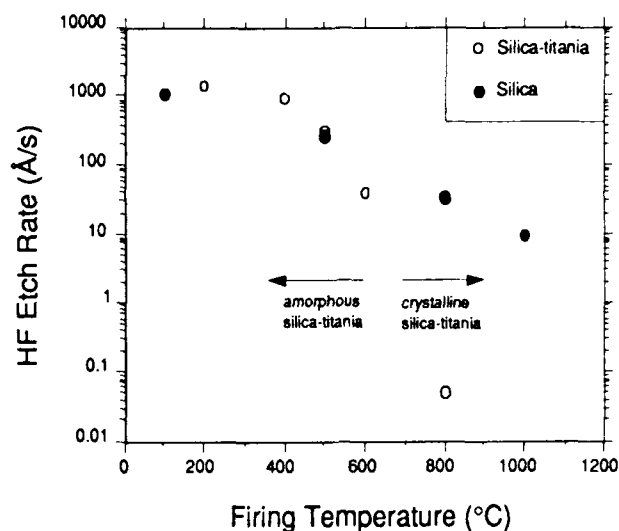


Figure 6: Etch rates for silica and silica-titania coatings vs. firing temperatures.

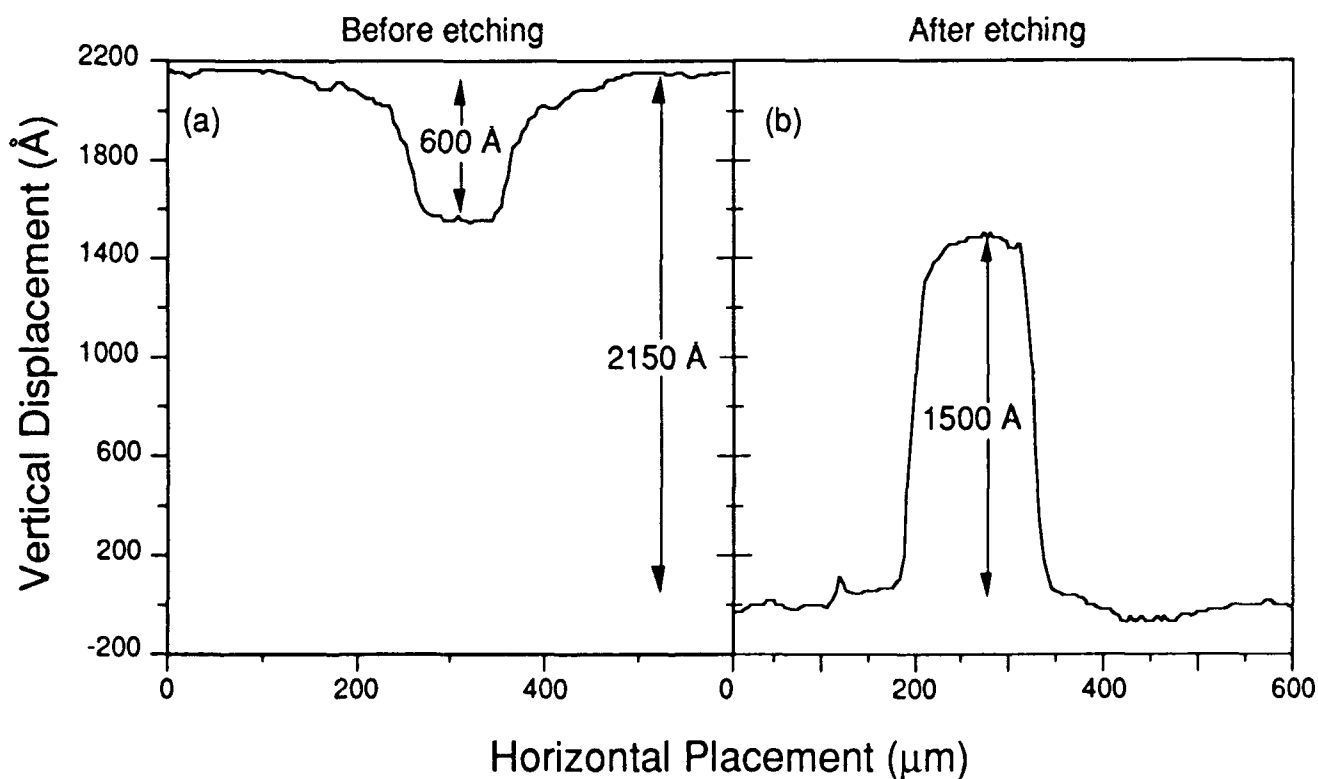


Figure 7: Profilometer traces of (a) trough produced in silica-titania coating after laser densification, and (b) corresponding ridge produced in the same coating after HF etching.



### 3.3 Masking

To test the ability to reproduce lithographically produced patterns by laser densification, 50  $\mu\text{m}$  stripes of the Au/Pd alloy, separated by 100  $\mu\text{m}$  spaces, were deposited onto a silica-titania coating using photolithographic methods. A transmitted light micrograph of the metal pattern is shown in Figure 8a. This sample was then rastered across the laser beam (perpendicular to the direction of the stripes) at 5 mm/s, with 50  $\mu\text{m}$  spacings between passes. After removing the metal coating, a surface profile perpendicular to the stripes showed that 50  $\mu\text{m}$  wide troughs, separated by approximately 100  $\mu\text{m}$  wide hills were produced in the coating (Figure 8b). This result shows that lithographic masking can be used to predefine areas to be densified by laser heating.

After etching the sample in buffered HF, 50  $\mu\text{m}$  ridges, separated by 100  $\mu\text{m}$  spaces were produced (Figures 8c and 8d). The spots where the laser passed over the sample are easily seen in the micrograph. These spots, which resulted from the coarseness of the raster, produced a roughness of approximately 400  $\text{\AA}$  over the top of the ridges. Interestingly, the regions between the ridges are better defined after etching than before. Apparently, the large difference in etch rate between the densified and undensified regions has cleaned up the pattern, and produced a sharper ridge than the corresponding channel.

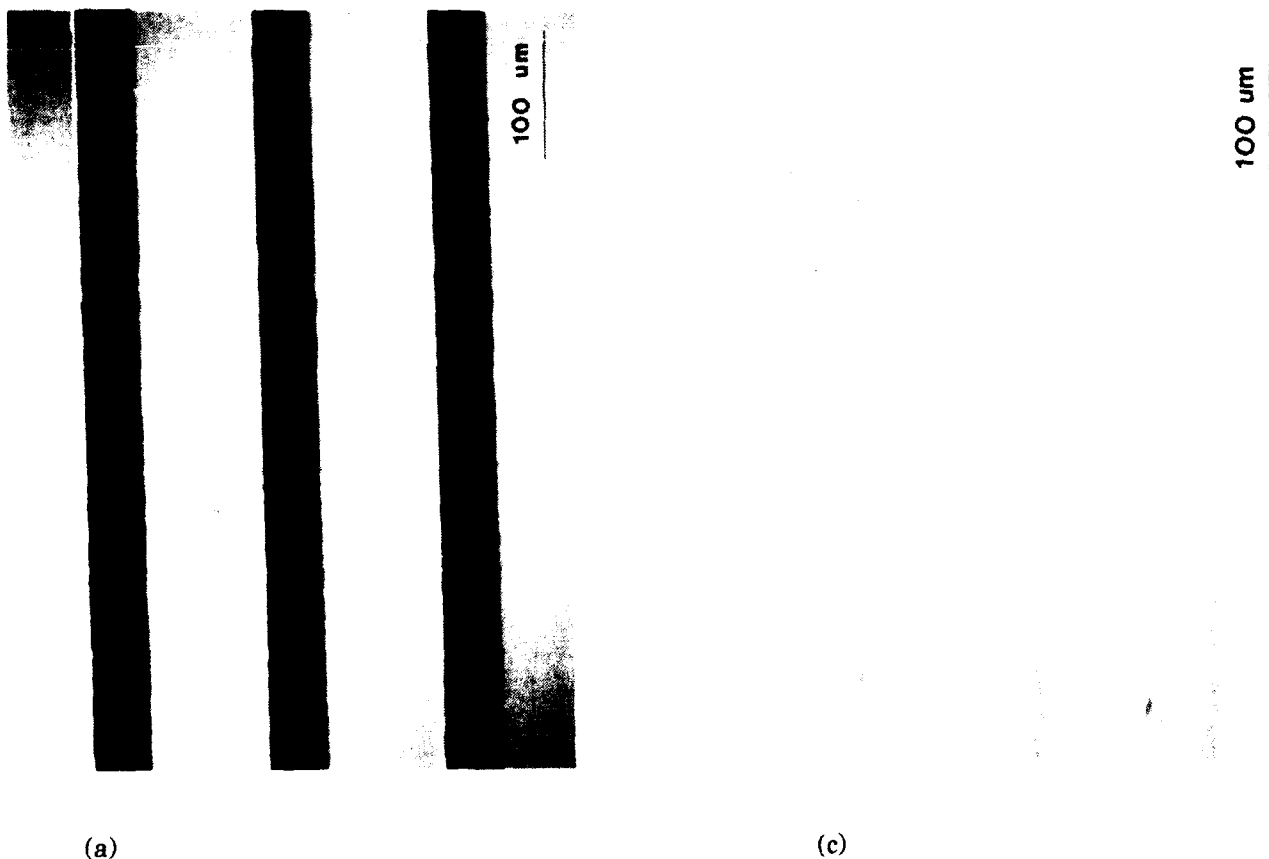


**Figure 8:** (a) Transmitted light micrograph of lithographically patterned AuPd stripes (dark areas) on a silica-titania coating (light areas). (b - next page) Profilometry traces of troughs produced after rastering laser across patterned area. (c) Optical micrograph of ridges produced after etching the rastered area. and (d - next page) Profilometry trace across etched ridges.

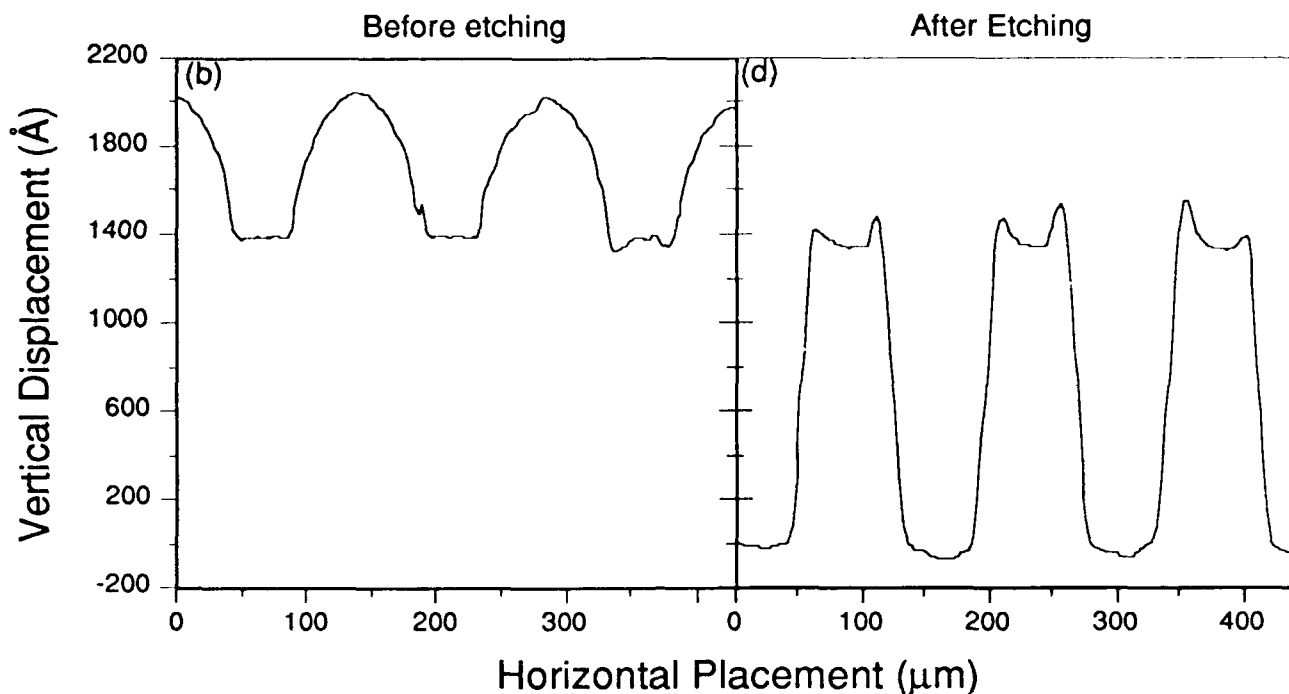


Figure 8: Continued

#### 4. MECHANISTIC ISSUES

It is well established that the structure and properties of sol-gel coatings depend strongly not only on the coating solution chemistry, but also on the subsequent firing. During firing, organics are burned out, condensation reactions are driven to completion, and densification occurs, in some systems, with crystallization. In conventional furnace firing of sol-gel coatings, the competition between burn-out, densification, and crystallization usually requires that the organics be eliminated before pores are closed off, and that porosity is eliminated before crystallization takes place if a dense ceramic film is desired as the end product. Because the competition between these processes can be affected by the heating rate, firing history can have a noticeable impact on the properties of sol-gel coatings.<sup>20</sup>

The most apparent difference between laser firing and conventional heating of sol-gel coatings is the extremely rapid heating rate ( $10^5$  °C/s).<sup>17</sup> We might expect, therefore, that organic residue would be trapped inside of laser densified coatings. It is also possible that metal atoms from the absorbing layer are driven into the coating, volatile constituents from the substrate are sublimed, or crystallization is suppressed because of the short time at elevated temperature.

The shrinkage of a TEOS coating as a function of laser power and as a function of furnace firing temperature is shown in Figure 9. Except at the

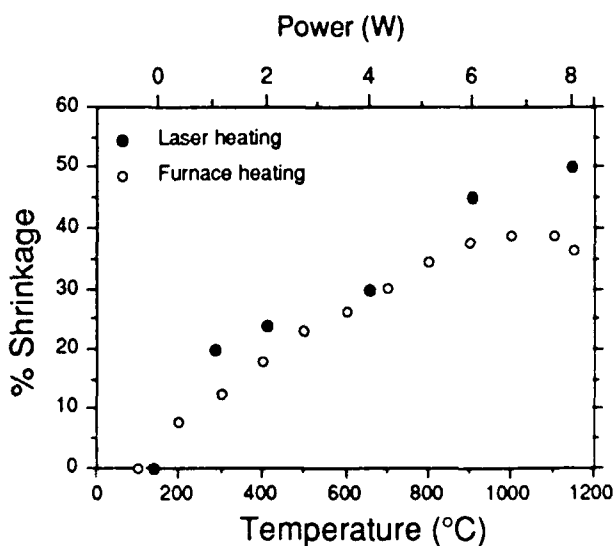


Figure 9: Shrinkage vs. laser power and firing temperature for a TEOS coating.

highest powers, where it is possible that the coatings are ablated, the shrinkage is similar for both furnace and laser heating. The indices after firing are also quite similar – 1.456 for coatings densified in the furnace and 1.466 for laser densified coatings.

In the silica-titania and tantala systems, however, significant differences are observed between furnace and laser firing. For a given shrinkage, the index of the silica-titania coatings is much lower for furnace fired coatings than for laser densified coatings (Figure 10). The same trend is observed in the tantala system (Figure 11). Presently, the source of these differences is unknown. It is interesting that the differences between furnace and laser firing are less pronounced in the silica system, which does not crystallize upon heating. Whether the absence of crystallization in the silica system is the source of these differences is not known. It is also possible that the larger volume of organics in the silica-titania and tantala systems plays a role, or that the higher firing temperature of the silica system makes a difference.

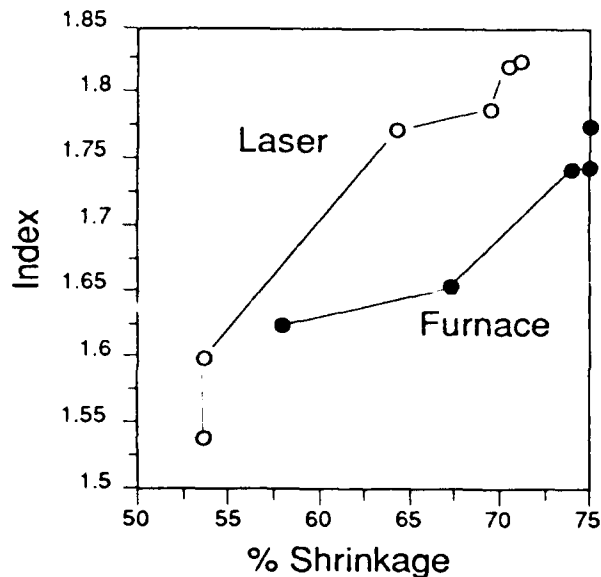


Figure 10: Index vs. % shrinkage for laser fired and furnace fired silica-titania coatings.

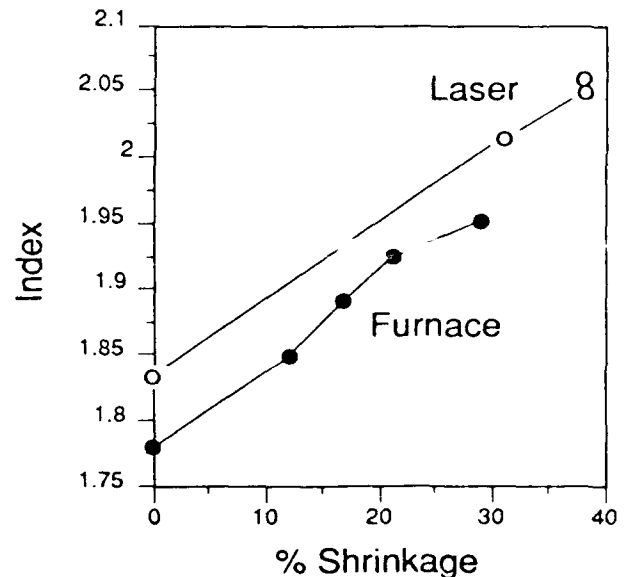


Figure 11: Index vs. % shrinkage for laser fired and furnace fired tantala coatings.

## 5. SUMMARY

We have shown that channel structures suitable for channel waveguides can be fabricated in sol-gel derived silica, silica-titania, and tantala coatings using a laser that is transparent to both the film and substrate, but is absorbed by a thin metal film on top of the sol-gel coating. The large difference between the etch rates of densified and undensified coatings allows ridged structures to be produced. Channels and ridges can also be formed by patterning the metal layer using photolithographic techniques, and rastering the laser across the entire sample. The index of the laser densified silica coatings is similar to the index of furnace densified silica coatings. The index of laser densified coatings is significantly higher than that of furnace densified coatings in the silica-titania and tantala systems.

## 6. ACKNOWLEDGEMENTS

This research was supported by the Donnelly Corporation. Their support is gratefully acknowledged. The authors also wish to thank Teri Davis, Ray Zanoni, Tian-Hoe Lim, Gil MacLaughlin, and Ron Roncone for assistance with optical measurements, and Ken Jackson for many helpful suggestions.

## 7. REFERENCES

1. E. Garmire, "Semiconductor Components for Monolithic Applications by E. Garmire," in Topics in Applied Physics, Vol 7, Integrated Optics, T. Tamir, ed. Springer-Verlag, NY, NY (1979).
2. N. Imoto, N. Shimizu, H. Mori, and M. Ikeda, "Sputtered silica waveguides with an embedded three dimensional structure," *IEEE J. Lightwave Technol.*, **LT-1**, 298 (1983).
3. Y. Murakami, M. Ikeda, and I. Izawa, "Optical directional coupler using deposited silica waveguides (DS guides)," *IEEE J. Quantum Electron.*, **QE-17**, 1982 (1981).
4. H. Mori and N. Shimizu, "Multimode deposited silica waveguide and its application to an optical branching circuit," *IEEE J. Quantum Electron.*, **QE-18**, 776 (1982).
5. J. Shelton, F. Reinhart, and R. Logan, "Rib waveguide switches with MOS electro-optic control for monolithic integrated optics in GaAs-Al<sub>x</sub>Ga<sub>1-x</sub>As," *Appl. Opt.*, **17**, 2548 (1978).
6. F. Leonberger, C. Bozler, R. McClelland, and I. Melngailis, "Low loss GaAs optical waveguide formed by lateral epitaxial growth over oxide," *Appl. Phys. Lett.*, **38**, 313 (1981).
7. E. Erman, N. Vodjdani, J. Theeten, and J. Cabanie, "Low loss waveguides grown on GaAs using localized vapor phase epitaxy," *Appl. Phys. Lett.*, **43**, 894 (1983).
8. H. Inoue, K. Hiruma, Ishida, T. Asai, and H. Matsumura, "Low Loss GaAs optical waveguides," *IEEE J. Lightwave Technol.*, **LT-3**, 1270 (1985).
9. A.M. Glass, I.P. Kaminow, A.A. Ballman, and D.H. Olsson, "Absorption loss and photorefractive-index changes in Ti:LiNbO<sub>3</sub> crystals and waveguides," *Appl. Opt.*, **19**, 276 (1980).
10. T. Findakly, "Glass waveguides by ion-exchange a review," *Opt. Eng.*, **24**, 244 (1985).
11. K. Tiefenthaler, V. Brigue, E. Buser, M. Morisberger, and W. Lukoz, "Preparation of Planar Optical SiO<sub>2</sub>-TiO<sub>2</sub> and LiNbO<sub>3</sub> Waveguides with Dip Coating Method and an Embossing Technique for Fabricating Grating Couplers and Channel Waveguides," in Thin Film Technologies, Proceedings of the SPIE, Vol. 401, Geneva, Switzerland, April 20-22, 1983, pp. 165-173.
12. G. W. Dale, H. H. Fox, Brian J. J. Zelinski, and Laura Weller-Brophy, "Sol-Gel Synthesis of Thin Films for use as Planar Waveguides," to be published in *Mat. Res. Soc. Symp. Proc.*, Better Ceramics Through Chemistry IV (1990).
13. D. J. Shaw, A. J. Berry and T. A. King, "Laser Densification of Sol-Gel Silica Glass," *Inst. Phys. Conf. Ser. No. 103: Part 1*, pp. 85-90 (1989).
14. R. V. Ramaswamy, T. Chia, R. Srivastava et. al., "Gel Silica Waveguides," in Multifunctional Materials, SPIE Proceedings Vol. 878, pp. 86-93 (1988).
15. R. R. Krchnavek, H. H. Gilgen and R. M. Osgood, "Maskless Laser Writing of Silicon Dioxide," *J. Vac. Sci. Technol.*, **B2**(4): 641-644, (1984).
16. T. C. Zaugg, J. Mai and B. D. Fabes, "Laser Heating of Sol-Gel Coatings: Thermal Modeling," to be published.
17. D. J. Taylor, B. D. Fabes and M. G. Steinthal, "Laser Densification of Sol-Gel Coatings," to be published in *Mat. Res. Soc. Symp. Proc.*, Better Ceramics Through Chemistry IV (1990).
18. L. Weisenbach, D. L. Klein, B. J. J. Zelinski, and B. D. Fabes, "TEM Investigation of Sol-Gel Coatings," to be published in *Mat. Res. Soc. Symp. Proc.*, Better Ceramics Through Chemistry IV (1990).
19. L. A. Silverman, G. Teowee, and D. R. Uhlmann, "Characterization of Sol-Gel Derived Tantalum Oxide Films," *MRS Symp. Proc.*, **73**, 725 (1986).
20. L. Weisenbach, T. Davis, B. J. J. Zelinski, R. Roncone, and L. A. Weller-Brophy, "Shrinkage Behavior of SiO<sub>2</sub>-TiO<sub>2</sub> Thin Film Waveguides," to be published in *Mat. Res. Soc. Symp. Proc.*, Better Ceramics Through Chemistry IV (1990).



## Vibrational spectra and structure of silica gel films spun on c-Si substrates

Rui M. Almeida

Centro de Física Molecular/I.N.E.S.C., Instituto Superior Técnico  
Av. Rovisco Pais, 1000 Lisboa, PORTUGAL

Carlo G. Pantano

Department of Materials Science and Engineering, The Pennsylvania State  
University, University Park, PA 16802

ABSTRACT

A series of silica gel films were spin-coated on single crystal silicon (c-Si) substrates and their structure was characterized by vibrational spectroscopy. The films were either dried at room temperature or partially densified at 450 °C. Fourier transform infrared absorption spectra have been obtained for each film and they are compared to the spectrum of thermal SiO<sub>2</sub> films. The gel films (ca. 150 nm thick) show the presence of residual OH groups, but very little molecular water or organic species and the fundamental Si-O-Si vibrations exhibit shifts toward lower frequencies, compared to the thermal oxide. The Si-O-Si antisymmetric stretch near 1070 cm<sup>-1</sup> was narrower for the gels and the shoulder on the high frequency side was stronger. The nature of this feature is discussed based also on oblique incidence transmission and reflection-absorption spectra taken with polarized infrared light.

1. INTRODUCTION

The structure and properties of amorphous silica films on c-Si substrates are highly relevant to the electronics industry, for example in metal-oxide-semiconductor (MOS) devices which include thermal SiO<sub>2</sub> layers and also in the integrated optics area. Besides thermal oxidation, silica films may be deposited by sputtering, e-beam evaporation, CVD, thermal decomposition of alkoxysilanes or by the sol-gel method using spin-on solutions.

At present there is still substantial disagreement concerning the structure of thermal silica films and that of the SiO<sub>2</sub>/Si interface. Namely, Hubner et al.<sup>1</sup> used IR transmission at oblique incidence (55° off-normal) to show that the high frequency shoulder at ca. 1260 cm<sup>-1</sup> was the longitudinal optic (LO) component of the antisymmetric stretch of bridging oxygens parallel to the Si-Si direction, whose transverse optic (TO) component coincided with the transmission minimum at 1091 cm<sup>-1</sup>, in agreement with the assignments of Galeener<sup>2</sup> for bulk v-SiO<sub>2</sub>. Kirk,<sup>3</sup> on the other hand, interpreted the transmission spectra of 10-100 nm thick thermal SiO<sub>2</sub> films at oblique incidence (60° off-normal) in terms of an in-phase antisymmetric stretch (AS<sub>1</sub>) TO-LO pair at 1076-1256 cm<sup>-1</sup> and an out-of-phase (AS<sub>2</sub>) TO-LO pair at 1200-1160 cm<sup>-1</sup>. Therefore, the conventional normal incidence transmission spectra revealed only the TO peaks, with the high frequency shoulder corresponding to AS<sub>2</sub>. However, Olsen and Shimura<sup>4</sup> used multiple internal reflectance at 60° off-normal incidence with linearly polarized light and they were able to detect, in 3 nm thick thermal SiO<sub>2</sub> films, the TO and LO components at 1080 cm<sup>-1</sup>

92-11432

92 4 28 050



and  $1240\text{ cm}^{-1}$ , using parallel polarized (**P**) light, whereas perpendicular polarized (**S**) light detected essentially only the TO mode. These authors apparently observed also the TO and LO components of the antisymmetric stretch in 10 nm thick CVD silica films, near  $1060\text{ cm}^{-1}$  and  $1200\text{ cm}^{-1}$ , respectively, but they failed to detect the LO component for uncured 6 nm thick spin-on  $\text{SiO}_2$  films, presumably because a continuous network structure had not developed yet. Apparently, there are no additional studies of the fundamental IR spectra of silica gel films in the literature.

The observation of LO components in oblique incidence transmission spectra is based on Berreman's rationale. Berreman argued that crystalline films which are thin compared to the IR wavelengths will have TO vibrations (those for which the atomic motions are perpendicular to the phonon wave vector) parallel to the film surface and LO vibrations (for which the motions are parallel to the wave vector) perpendicular to the surface. (The phonon wave vector is perpendicular to the surface). In conventional IR transmission spectroscopy, because electromagnetic waves are transverse, only TO modes are excited, but the **P** polarized component of radiation incident obliquely to the surface will have electric field components both parallel and normal to the surface, thus interacting with both TO and LO modes, respectively.

## 2. EXPERIMENTAL

The spin-on solutions were prepared by mixing 20 ml of tetraethoxysilane (TEOS, Morthon Thiokol, 99%), 40 ml of ethanol (200 proof) and 20 drops of 1N HCl solution at room temperature, adding 25 ml of distilled water and heating up to  $\sim 70^\circ\text{C}$  with continuous stirring. These solutions were cooled to room temperature and finally diluted 1:1 in ethanol. Thin films of silica gel were spun on single crystal silicon wafers from 5 drops of solution, with a Headway Research photoresist spinner mod. 1-EC101D at 2500 rpm, for 15 seconds. The wafers were polished on one side and they were chemically cleaned with  $\text{H}_2\text{O}_2$ ,  $\text{H}_2\text{SO}_4$  and HF. A free standing silica gel foil was prepared on the walls of a glass test tube. The films were either dried at room temperature in a dessicator or they were heat-treated in air for 3 hours at  $450^\circ\text{C}$ , in a tube furnace. The thickness and refractive index of some of the films were measured with a Rudolph Research Automatic Ellipsometer (AutoEL-III), with  $\lambda=632.8\text{ nm}$ .

Fourier transform IR transmission spectra were recorded at normal incidence with an IBM IR/98 FTIR spectrometer or with a Nicolet 5DXC FTIR instrument, both equipped with a Ge/KBr beamsplitter and a DTGS detector, using natural light. Reflection-absorption spectra were collected with polarized IR light, at  $55^\circ$  off-normal, with a Spectra-Tech variable angle reflectance accessory. Some transmission spectra were collected at  $45^\circ$  off-normal incidence by approximately positioning the sample holder at this angle. All spectra were taken at room temperature.

## 3. RESULTS AND DISCUSSION

Fig. 1 shows the transmission spectrum (at normal incidence) of a silica gel film which was dried at room temperature only. It had a thickness of 167 nm and a refractive index of 1.427, compared with 1.462 as measured for the thermal oxide or 1.458 for bulk vitreous silica. Fig. 2 shows the corresponding spectrum for the thermal oxide, in the case of two films grown on opposite

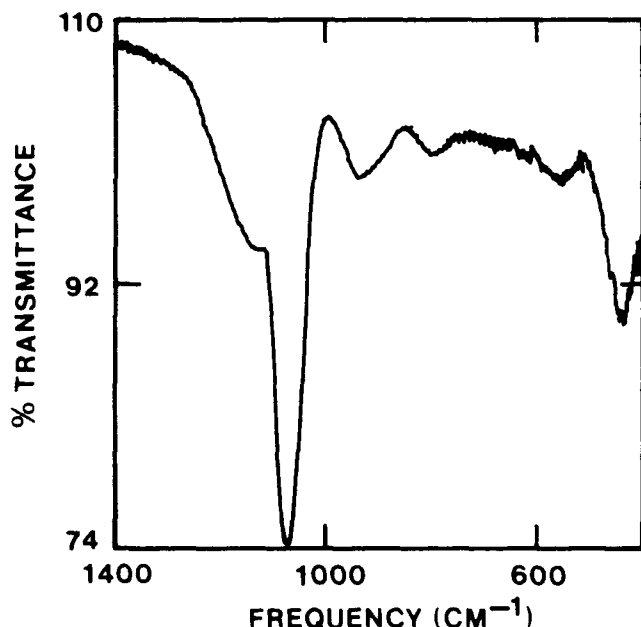


Fig. 1. FTIR spectrum of silica gel film dried at room temperature, referenced to a bare c-Si wafer.

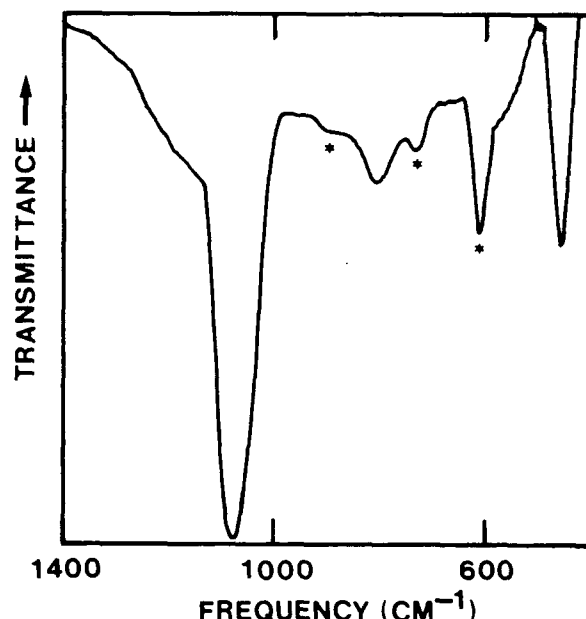


Fig. 2. FTIR spectrum of thermal oxide films grown on c-Si. (Peaks marked with \* are due to incomplete subtraction of the substrate spectrum).

sides of the same Si wafer, having thicknesses of 110 nm and 127 nm, respectively. The gel film exhibits a peak at  $934\text{ cm}^{-1}$ , which is absent in the thermal oxide and may be attributed to stretching of Si-OH or Si-O groups. The shoulder on the high frequency side of the dominant peak at  $1070\text{--}1079\text{ cm}^{-1}$  was much more pronounced in the gel sample than in the thermal oxide.

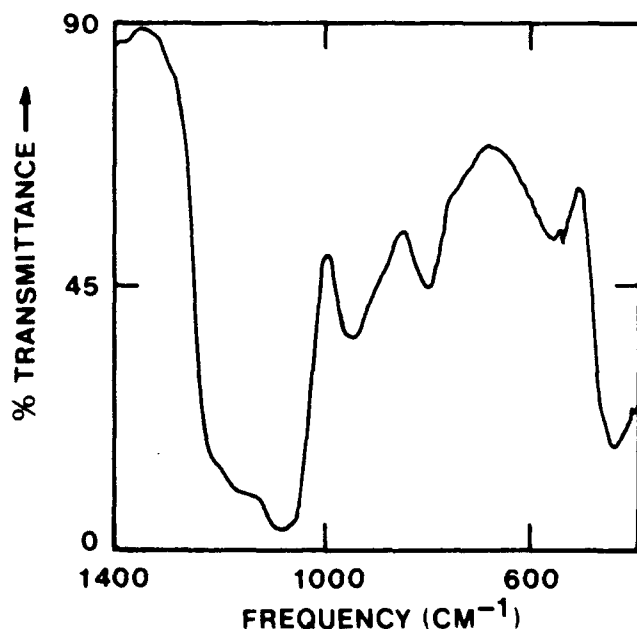


Fig. 3. FTIR spectrum of free standing silica gel foil dried at room temperature.

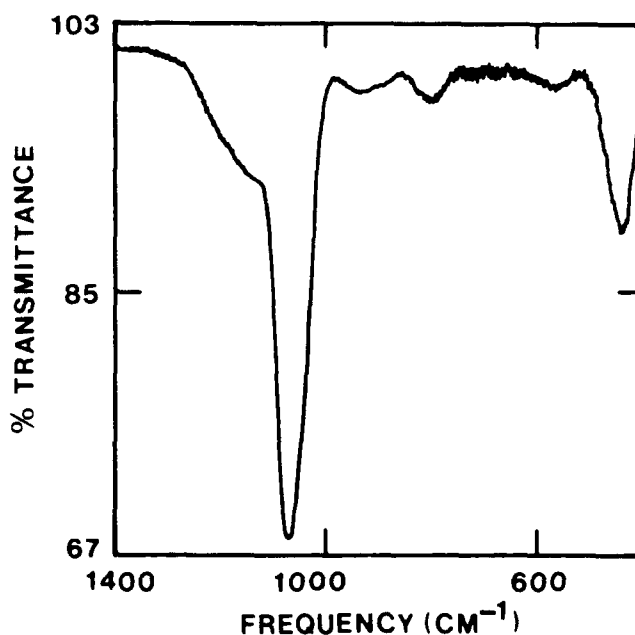


Fig. 4. FTIR spectrum of silica gel film dried at  $450^\circ\text{C}$ , referenced to a bare c-Si wafer.

In order to further illustrate this point, fig. 3 shows the fundamental IR spectrum of a gel foil whose thickness was estimated at roughly  $\sim 1 \mu\text{m}$ , where the shoulder was even stronger and the peak at  $950 \text{ cm}^{-1}$  was also stronger than the corresponding peak of the gel film at  $934 \text{ cm}^{-1}$ . The gel foil, which was dried only at room temperature, was considerably thicker than the film and it had more residual water, mostly in the form of silanol (Si-OH) groups. Very little molecular water or organic species were found in the gel films.

Fig. 4 shows the spectrum of a silica gel film which was dried at  $450^\circ\text{C}$  for 3 hours, having a thickness of 150 nm and a refractive index of 1.438. The intensity of the main vibrational features of this partially densified film is found to lie between those corresponding to the wet film of fig. 1 and the thermal oxide of fig. 2. Namely, the band at  $936 \text{ cm}^{-1}$  and the high frequency shoulder are not as strong as in the wet gel film.

Fig. 5 shows a comparison of the IR spectra of a silica gel film dried at room temperature only, but for a longer time than the film of fig. 1, for normal incidence and  $45^\circ$  oblique incidence. The vibrational features at normal incidence are intermediate between those of fig. 1 and fig. 4, as one might expect. For the  $45^\circ$  incidence transmission spectrum, a dramatic change was observed in the high frequency shoulder, which grew into a well defined peak at  $1233 \text{ cm}^{-1}$ . The same behavior is perhaps even more clearly demonstrated in the spectra of the thermal oxide of silica in fig. 6. Again the shoulder transforms into a peak at oblique incidence, now at  $1256 \text{ cm}^{-1}$ .

In addition to the peak near  $935 \text{ cm}^{-1}$ , characteristic of Si-OH groups present in the gels (or perhaps some Si-O<sup>-</sup> as well), the remaining features in

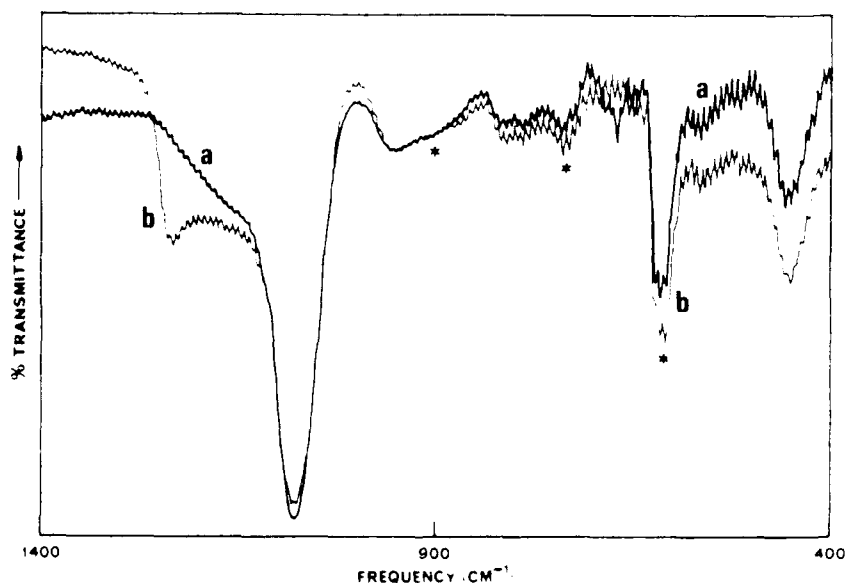


Fig. 5. FTIR spectra of silica gel film dried at room temperature: (a) transmission at normal incidence; (b) transmission at  $45^\circ$  off-normal incidence. (Bands marked with \* are due to the c-Si substrate).



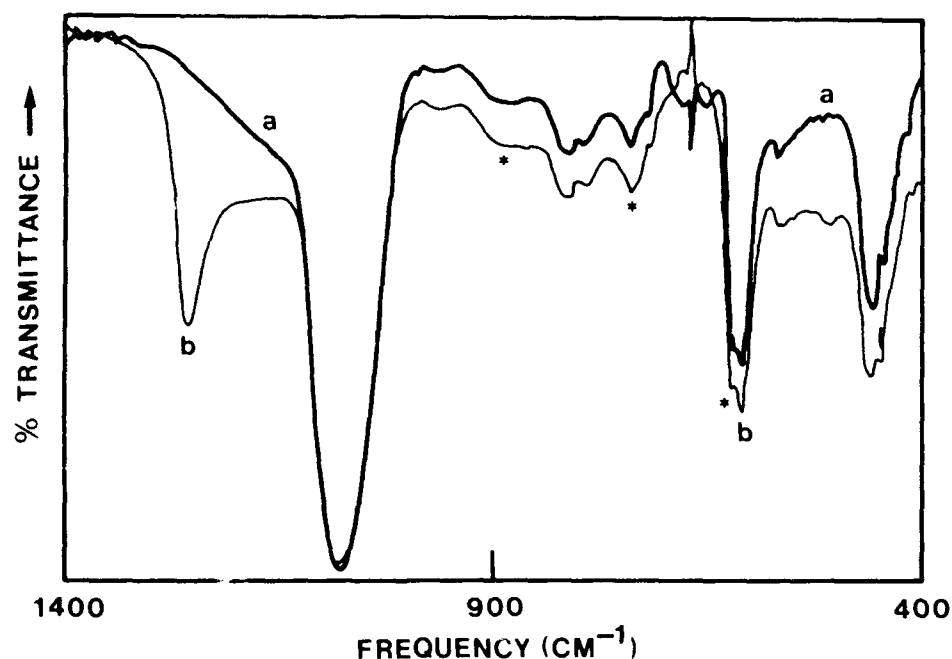


Fig. 6. FTIR spectra of thermal  $\text{SiO}_2$  films: (a) transmission at normal incidence; (b) transmission at  $45^\circ$  off-normal incidence. (Bands marked with \* are due to the c-Si substrate).

the silica gel spectra may be assigned as in bulk  $\text{v-SiO}_2$ <sup>2</sup>. The low frequency peak near  $450 \text{ cm}^{-1}$  is due to rocking motions of the oxygens perpendicular to the Si-O-Si plane plus some Si cation motion; the weak peak near  $800 \text{ cm}^{-1}$  is due to symmetric stretching of the oxygens along the bisector of the Si-O-Si bridging angle, with some Si motion as well; the strong peak near  $1070 \text{ cm}^{-1}$  may be attributed to antisymmetric stretching of the oxygens along the Si-Si direction, accompanied by a substantial amount of Si cation motion. In this framework, the shoulder on the high frequency side of the dominant peak in the normal incidence spectrum may be interpreted as an incipient LO component of the antisymmetric stretch (the dominant peak being the TO component), which appears at normal incidence because there may be no pure LO and TO modes in glass, due to the absence of long range order. The possible alternative assignment of Kirk<sup>3</sup> will not be considered here.

The major differences found between the spectra of the gel and the thermal oxide films lie in the  $935 \text{ cm}^{-1}$  peak and the high frequency shoulder. The assignment of the former to silanol groups is in agreement with the presence of a significant concentration of these species in the gels, especially those which were not submitted to partial densification at higher temperatures. The high frequency shoulder is related to the LO component of the antisymmetric stretch of the oxygens, which becomes fully activated at oblique incidence, in agreement with Berreman's rationale<sup>5</sup> and with the results of Hubner et al.<sup>1</sup> (LO at  $1260 \text{ cm}^{-1}$ , for  $55^\circ$  off-normal incidence). It should be noted that the other minor LO-TO splittings reported by Hubner et al.<sup>1</sup> are hardly noticeable in the spectra of figures 5 and 6. In the present work, the high frequency LO peaks were found at  $1233 \text{ cm}^{-1}$  and  $1256 \text{ cm}^{-1}$ , for the room temperature dried gel film and the thermal silica film, respectively. Therefore, the LO position in the thermal oxide at  $45^\circ$  off-normal incidence is in good agreement with the thermal oxide results of Hubner et al.<sup>1</sup> at  $55^\circ$ . The LO frequency of the gel

film, on the other hand, is in very good agreement with the LO frequency of  $1237\text{ cm}^{-1}$  determined in bulk  $\text{SiO}_2$  gel by Kramers-Kronig analysis of near-normal reflectivity<sup>6</sup>.

As argued by Almeida et al.<sup>6</sup>, the reason why the frequency of the LO component of the antisymmetric stretch, which is probably closer to the bare mode, is considerably lower than that of the corresponding LO mode in vitreous silica may be due to the Si-O-Si bridging sequences being strained near the surface of the gel pores, with larger bridging angles and slightly longer Si-O bonds than v- $\text{SiO}_2$ , the latter effect being predominant. In terms of the central force network model of Sen and Thorpe<sup>8</sup>, this will in fact lead to a larger vibrational frequency for the antisymmetric stretching.

The fact that the high frequency shoulder, related to the high frequency LO mode, is stronger in a wet gel than in the thermal oxide may be an indication that the porous gel scatters the  $10\text{ }\mu\text{m}$  wavelength IR light to some extent, sending it in all directions, even for light originally at normal incidence. The fraction of light which becomes effectively off-normal incident in this way will further activate the LO mode and the effect will increase with porosity, as observed.

The oblique incidence data for the gel film and the thermal oxide show that the Berreman argument<sup>5</sup> for thin crystal films clearly applies to glassy films as well. It is not clear at this point, however, why the LO mode in the thermal oxide is apparently stronger, compared to the TO component, than in the porous gel film. Although the difference is not too large, one would rather expect the opposite to happen, from the previous argument concerning the normal incidence transmission data.

Another difference which is noticed between the gel and the thermal oxide film spectra concerns the width of the dominant TO peak, which was highest for the thermal oxide ( $\sim 77\text{ cm}^{-1}$ ) and smallest for the room temperature dried gel films ( $\sim 58\text{ cm}^{-1}$ ), with intermediate values for the partially densified gel films ( $\sim 65\text{ cm}^{-1}$ ). This indicates that the spread in the intertetrahedral angles is largest in the thermal oxide and narrowest in the room temperature dried gels, in agreement with the suggestion that the Si-O-Si bridges are strained near the surface of the gel pores. The porosity will be larger in the untreated gels, compared to partially densified films.

Fig. 7 shows IR reflection-absorption spectra of a silica gel film on a Si substrate, dried at room temperature only, referenced to a bare Si wafer. The behavior for an incidence angle of  $55^\circ$  off-normal was quite different for the two polarizations **S** and **P**. For the former, the spectrum had the appearance of a specular reflectance spectrum (or inverted transmittance), where the dominant peak at  $1075\text{ cm}^{-1}$  virtually coincided with the position of the TO mode at  $1070\text{ cm}^{-1}$  (fig. 1) and the shoulder coincided with the high frequency shoulder of the transmission spectra of the gels. This behavior was similar to that observed by Wong and Yen<sup>7</sup> for 30 nm thick thermal silica films. For **P** polarization, on the other hand, the spectra had a completely different appearance. At  $1075\text{ cm}^{-1}$ , precisely the same TO frequency as the peak in the **S**-polarized spectrum, there was a peak with a specular reflectance appearance, similar to that in the **S**-polarized spectrum, but much more intense (50 % reflectance with reference to the bare wafer, compared to 16 % for **S**-polari-

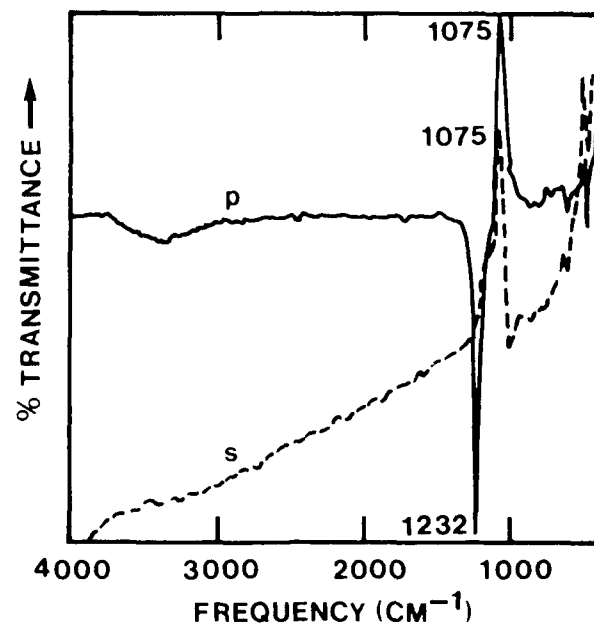


Fig. 7. FTIR reflection-absorption spectra at  $55^\circ$  off-normal incidence of silica gel film dried at room temperature, taken with: (s) - perpendicular polarized radiation; (p) - parallel polarized radiation.

zation) and without a clear shoulder on the high frequency side. In addition to this, at  $1232\text{ cm}^{-1}$  (precisely the LO frequency of the gel film of fig. 5), there was an inverted peak, i.e., transmission-like or IRRAS-like and very intense, corresponding to a 80 % drop in transmittance. Again this was similar to the behavior observed by Wong and Yen<sup>9</sup> for  $30\text{-nm}$  thick thermal silica films, who recorded an inverted peak at  $1260\text{ cm}^{-1}$  with **P**-polarized radiation (approximately the LO frequency of the thermal oxide of fig. 6 at  $1256\text{ cm}^{-1}$ ), in addition to a reflectance peak at  $1078\text{ cm}^{-1}$ .

Wong and Yen<sup>9</sup> called their spectra IRRAS, but, according to the commonly accepted terminology<sup>10</sup>, the acronym IRRAS (IR Reflection-Absorption Spectroscopy) refers to transmission-like spectra, whereas inverted transmittance should preferably be called reflectance. In fact, out of the three peaks of fig. 7, only the  $1232\text{ cm}^{-1}$  transmission minimum is IRRAS-like and this was found to become reflectance-like (pointing upward) for incidence angles above  $\sim 72^\circ$  off-normal (the Brewster angle of silicon  $\theta_B$  is ca.  $73.7^\circ$ ). For such large incidence angles, the electric vector of the **P**-polarized radiation is almost perpendicular to the film surface and the reflectance of the film at the LO frequency is very strong; therefore, the penetration depth of the radiation is small and the Si wafer is not reached by it, leading to a specular reflectance spectrum (even at the Brewster angle, when the **P** radiation would not be reflected off the wafer) and not to an IRRAS spectrum. For incidence angles below  $72^\circ$ , the interaction of the **P**-polarized radiation with the film becomes progressively weaker, leading to an IRRAS-like peak at the LO frequency. At the TO frequency, on the other hand, for **S**-polarized radiation, there is strong reflection interaction at any incidence angle (only with this mode); for **P**-polarized radiation, as the incidence angle becomes larger, the component of the incident electric vector perpendicular to the film becomes also

larger and that parallel to the film becomes increasingly smaller, leading to a decrease in specular reflectance at the TO frequency, becoming an IRRAS peak at very large incidence angles away from the normal. Near  $\theta_B$ , however, the TO peak has a specular reflectance maximum, due to the fact that the p-polarized light is not reflected off the Si wafer surface and any weak reflectance peak will become very strong when referenced to the bare Si wafer.

The reflection spectra of the silica films taken with p-polarized light at oblique incidence ( $55^\circ$  off-normal) and referenced to the bare Si wafer are especially interesting. In fact, there is a tremendous intensification of the signal, with an amplitude of 130 % (in transmittance units) for the case shown in fig. 7, compared to 35 % only for a similar sample in normal incidence transmission (fig. 1). Therefore, this reflection-absorption technique appears quite attractive for quick, non-destructive analysis of thin films on Si wafers in the industrial processing of semiconductor devices and circuits. From a structural viewpoint, it is also a good method to quickly determine the position of the TO and LO components of the high frequency vibrations of glassy films such as silica.

#### 4. CONCLUSIONS

A series of silica gel films, spin-coated on c-Si substrates, was analyzed by FTIR in transmission, at both normal and oblique incidence and also by reflection-absorption at  $55^\circ$  off-normal. Compared to a dense thermal oxide, the gel films had a peak characteristic of Si-OH groups, whose intensity decreased with heat treatment and they also had a stronger high frequency shoulder, related to the LO component of the oxygen antisymmetric stretch. This was shown to become a fully activated peak at the exact LO frequency in oblique incidence transmission spectra. The LO frequency in the gels was lower than in the thermal oxide, in agreement with strained Si-O-Si bridges at the surface of the gel pores. The reflection-absorption spectra showed a large intensification of the signal (IRRAS-like for the LO mode and reflection-like for the TO component of the high frequency response), which may be useful for industrial analysis of thin films on silicon wafers and also for structural analysis of the films.

#### 5. ACKNOWLEDGMENTS

The authors wish to acknowledge the Office of Naval Research (N00014-86-K-0191) for their support of this research. RMA also wishes to thank the support of INESC, INIC and the Fundação Calouste Gulbenkian, in Portugal.

#### 6. REFERENCES

1. K. Hubner, L. Schumann, A. Lehmann, H.H. Vajen and G. Zuther, "Detection of LO and TO Phonons in Amorphous  $\text{SiO}_2$  Films by Oblique Incidence of IR Light", Phys. Stat. Sol. (b), Vol. 104, pp. K1-K5, 1981.
2. F.L. Galeener, "Band limits and the vibrational spectra of tetrahedral glasses", Phys. Rev. B, Vol. 19, pp. 4292-4297, 1979.
3. C.T. Kirk, "Quantitative analysis of the effect of disorder-induced mode coupling on infrared absorption in silica", Phys. Rev. B, Vol. 38, pp. 1255-1273, 1988.
4. J.E. Olsen and F. Shimura, "Infrared reflection spectroscopy of the

SiO<sub>2</sub>-silicon interface", J. Appl. Phys., Vol. 66, pp. 1353-1358, 1989.

5. D.W. Berreman, "Infrared Absorption at Longitudinal Optic Frequency in Cubic Crystal Films", Phys. Rev., Vol. 130, pp. 2193-2198, 1963.

6. R.M. Almeida, T.A. Guiton and C.G. Pantano, "Characterization of Silica Gels by Infrared Reflection Spectroscopy", J. Non-Crystalline Solids (in press).

7. R.M. Almeida, T.A. Guiton and C.G. Pantano, "Detection of LO Mode in  $\nu$ -SiO<sub>2</sub> by Infrared Diffuse Reflectance Spectroscopy", J. Non-Crystalline Solids (letter to the editor, in press).

8. P.N. Sen and M.F. Thorpe, "Phonons in AX<sub>2</sub> glasses: From molecular to band-like modes", Phys. Rev. B, Vol. 15, 4030-4038, 1977.

9. J.S. Wong and Y-S Yen, "Intriguing Absorption Band Behavior of IR Reflectance Spectra of Silicon Dioxide on Silicon", Appl. Spectroscopy, Vol. 42, pp. 598-604, 1988.

10. P.R. Griffiths and J.A. de Haseth, Fourier Transform Infrared Spectrometry, pp. 549-553, Wiley-Interscience, New York, 1986.



# OPTICAL AND MECHANICAL CHARACTERIZATION OF SPIN-ON DEPOSITED SILICON AND TITANIUM DIOXIDE FILMS

P.Shen, M.J.Li, S.I.Najafi, J.F.Currie and R.Leonelli\*

Integrated Optics Laboratory, and Thin Films Group (GCM)

Ecole Polytechnique, P.O. Box 6079, Station A, Montreal (Quebec) H3C 3A7, Canada

\*Physics Department, University of Montreal, Box 6128, Sta. A., Montreal (Quebec), H3C 3J7, Canada

## Abstract

Spin-on deposited SiO<sub>2</sub>-TiO<sub>2</sub> thin films (pure and doped with dyes) are produced. Their optical and mechanical properties are determined and their use for a number of applications is investigated. The spin-on deposited SiO<sub>2</sub> film has been successfully doped with coumarin as a colour center and characterized as a waveguide overlay.

Solution deposited thin films of silicon and titanium dioxide, and their mixtures, are suitable for a number of applications such as antireflection coating and waveguides for integrated optics. Both dipping and spinning methods can be used to obtain good quality films [1] [2]. For the dipping process, processing standardization ensures good reproducibility of refractive index and thickness [1]. In this paper, we use a spin-on and baking process to produce pure and doped SiO<sub>2</sub> and TiO<sub>2</sub> films and we study some of their optical and mechanical properties. The solution we used is commercially available E.Merck liquicoat solutions [3]. They are metal alkoxide colloidal solutions containing 7% and 9% SiO<sub>2</sub> and TiO<sub>2</sub> respectively. By varying the volume ratio of the two component solutions, films of various thickness (80-250 nm) and refractive index (1.4-2.0) can be obtained. We used 0.02 inch thick P-doped [100] silicon, Corning 0211 glass, and 1 mm thick Fisher microscope slides as three substrate materials. We use standard silicon and glass cleaning procedures and carried out the film deposition in a class 100 clean room. The solution were mixed immediately before coating to ensure reproducibility. After spin-on coating we baked the substrate in an air atmosphere for 10 min at 105°C +/- 5°C. The spin on films were then heated in a dry oxygen atmosphere. The glass substrates were heated to the range of 300-500 °C while the silicon substrates were heated to the range of 300-800 °C.

The reflection minimum method is used to determine, at the same time, the refractive index and the thickness of the film on silicon substrates. For glass substrates, the effective reflective index method is used to obtain these results. The normalized reflectivity of the film on silicon is measured by a Leitz spectrophotometer. Fig.1 gives the relationship between spinning speed and thickness for 500 °C baked silicon dioxide and titanium dioxide films and their mixtures. As the volume ratio of the titanium solution increases, the resulting films show cracking and crazing after a baking in the 300-500 °C range. To obtain crack-free titanium rich films, the solution must be diluted with solvent two three times.

To study the relationship of refractive index to the processing conditions, we made a series of samples of different thicknesses and measured the refractive index in the wavelength range of 400 to 800 nm. The results are compared with the data of thermally grown silicon dioxide on the same silicon substrate. Fig.2 is the refractive index of SiO<sub>2</sub> obtained at different baking temperatures. Also shown in this figure is the calculated dispersion curve of fused silica according to Ref.[4]:

$$n(\lambda) = \sqrt{c_0 \frac{\lambda^2}{\lambda^2 - c_1^2} + c_2 \frac{\lambda^2}{\lambda^2 - c_3^2} + c_4 \frac{\lambda^2}{\lambda^2 - c_5^2} + 1}$$

, where

92 4 28 051

92-11433



$$c = \begin{bmatrix} 0.6961663 \\ 0.0684043 \\ 0.4079426 \\ 0.1162414 \\ 0.8974794 \\ 9.8961610 \end{bmatrix}$$

We note that the experimental curves of Fig. 2 can all be obtained from the theoretical expression by a simple shift of the index of refraction by a constant,  $\Delta n$ , which for the three experimental curves of 800 °C, 500 °C and 300 °C baked solution deposited silicon dioxide are 0.018, 0.028 and 0.045 respectively. The  $\Delta n$  for thermally grown native oxide is 0.003. We conclude that the higher the heating temperature, the denser and more like the thermal oxide the spin on film becomes. We tested the reproducibility of the film thickness and of the index of refraction by building up a thick film of SiO<sub>2</sub> by making three successive spinning and heating operations. Fig 3. shows a comparison of the measured normalised reflectivity and one calculated by assuming the constants of Fig.2 appropriate for a film three times as thick. Agreement is excellent. Mechanically, if at any of the heating steps in a multiple deposition are incomplete, cracking occurs due to partial dissolution of the underlying layer.

It is noted that to get multi-layer films of good quality, complete cycling for each layer is necessary. Otherwise the last applied layer will partially dissolve the first applied layer and after baking the result thicker film will show crack. If each layer is completely cycled, we find the first layer and the later layer have same thickness and processing condition relationship. These layers will have same refractive index and the results can transfer to glass or other semiconductor substrate.

Spatially, the film is uniform. For a two inch wafer, the uniformity is about 1.2%. Fig.4 shows a film thickness map of a 2 inch wafer spin coated with SiO<sub>2</sub> and baked at 300 °C. Both pure TiO<sub>2</sub> and mixed SiO<sub>2</sub>-TiO<sub>2</sub> solution deposited films on silicon have essentially the same large area uniformity as the pure SiO<sub>2</sub> spin-on film. However pure and TiO<sub>2</sub> rich films have a tendency to crack. Generally, for TiO<sub>2</sub> volume ratios greater than 50%, solvent dilution is essential to avoid cracking.

The tensile stress of the solution deposited SiO<sub>2</sub> film and the TiO<sub>2</sub>-SiO<sub>2</sub> film on silicon wafer are quite different. For example, at 300 °C and for a thickness of 166 nm the tensile stress of pure SiO<sub>2</sub> films is  $2 \times 10^9$  dynes/cm<sup>2</sup>; but for the 1:1 SiO<sub>2</sub>-TiO<sub>2</sub> films it is as great as  $13 \times 10^9$  dynes/cm<sup>2</sup>. If we increase the heating temperature to 500 °C, the tensile stress of pure SiO<sub>2</sub> film increases to  $6 \times 10^9$  dynes/cm<sup>2</sup>, while for 1:1 SiO<sub>2</sub>-TiO<sub>2</sub> films it is  $17 \times 10^9$  dynes/cm<sup>2</sup>. The TiO<sub>2</sub> concentration influence on the tensile stress is stronger than that of the processing temperature. This is in agreement with the experiment that to get crack free films we must use low TiO<sub>2</sub> concentration as well as the low temperature processing.

For integrated optics applications, it is useful to incorporate a colour center into a thin film such as SiO<sub>2</sub>. We have used coumarin 504 as a colour center in the spin-on SiO<sub>2</sub> film and have studied the absorption and fluorescence spectra. The coumarin doped thin films are made by directly dissolving the coumarin in SiO<sub>2</sub> liquicoat solution and applied on the potassium ion exchanged glass waveguide and then processed as the ordinary SiO<sub>2</sub> coating. The coumarin doped thin film is transparent and show the characteristic yellowish color and the color begin to fade at 200 to 300 °C baking. But the film always keep transparent. Fig.5 is the waveguide absorption spectrum of a coumarin doped SiO<sub>2</sub> film covered 10 µm potassium ion extranged glass waveguide. The film is baked at 150 °C. The coumarin concentration in the Liquicoat solution is 0.02 mole and the film thickness is 180 nm. In the wavelength range of 370-490 nm it shows absorption.

We use a He-Cd laser of 5 mW output and a 40 X objective to couple the laser beam into the waveguide with a coumarin doped solution deposited SiO<sub>2</sub> overlayer. The excited photoluminescence is shown in Fig.6.

It is concluded that for spin-on  $\text{SiO}_2$ ,  $\text{TiO}_2$  and their mixtures, the refractive index and thickness can be strictly controlled by selecting suitable processing conditions. The films obtained are uniform and suitable for applications such as antireflection coatings and doped waveguide overlay. Coumarin 504 is a useful colour center for the spin-on  $\text{SiO}_2$  film showing characteristic fluorescence in the wavelength range of 520-570 nm.

This work is funded in part by research grants from NSERC, FCAR and Ecole Polytechnique.

### References

- [1] D.W. Hewak, J.W.Y. Lit, "Standardization and control of a dip-coating procedure for optical thin films prepared from solution," *Can.J. Phys.* 66, 861-867, (1988).
- [2] R.W. Phillips, J.W. Dodds, "Optical interference coatings prepared from solution," *Appl. Opt.* 20, 40-47, (1981).
- [3] E. Merck Liquicoat Si ZLI 2123 and Liquicoat Ti ZLI 1857, product data sheets.
- [4] I.H. Maltson, "Inter-specimen comparison of the refractive index of fused silica," *J. Optical Soc. of America* 55, 1205-1209, (1965). J. Gower, "Optical communication systems," Prentice/Hall international, 44, (1984).
- [5] L.J. Fried and H.A. Froot, "Thickness measurement of silicon dioxide films over small geometries," *J. Appl. Phys.* 39, 5732-5735, (1968).

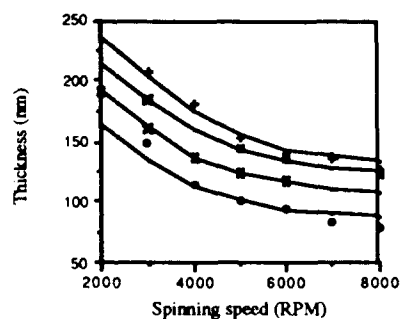


Fig.1 Thickness-RPM relation of solution deposited films.

+--  $\text{SiO}_2$  \* --  $\text{SiO}_2:\text{TiO}_2=1:1$   
 x--  $\text{SiO}_2:\text{TiO}_2=3:7$  o--  $\text{TiO}_2$

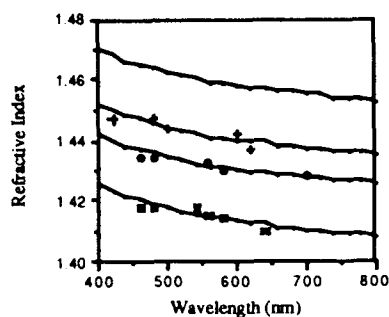


Fig.2 Refractive index of solution deposited silicon dioxide.

-- Calculated +--800°C baking  
 o--500°C baking x--300°C baking



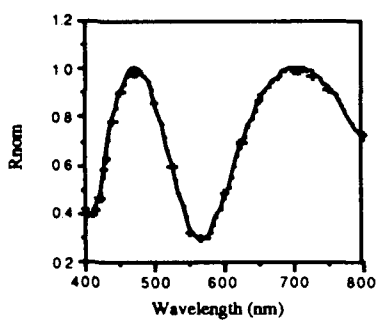


Fig.3 Normalized reflectivity of solution deposited  $\text{SiO}_2$  on Si.  
-- Calculated    +---Experimental

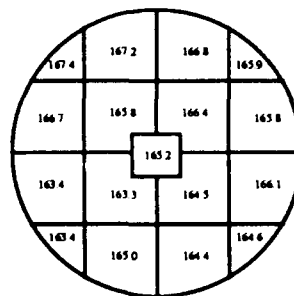


Fig.4 Flatness of solution deposited silicon dioxide film.

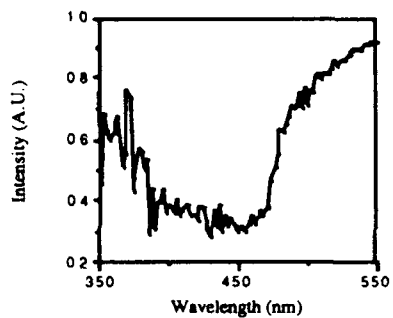


Fig.5 Absorption spectrum of a waveguide with Coumarin doped  $\text{SiO}_2$  overlay.

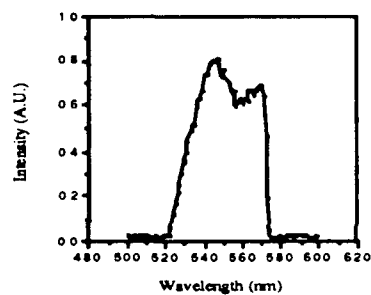


Fig.6 Fluorescence spectrum of a waveguide with coumarin doped  $\text{SiO}_2$  overlay.

SOL-GEL OPTICS

Volume 1328

**SESSION 6**

**Films and Coatings II**

*Chair*

**Masayuki Yamane**

Tokyo Institute of Technology (Japan)



## ELECTROCHROMIC PROPERTIES OF SOL-GEL DERIVED WO<sub>3</sub> COATINGS

P. Judeinstein\* and J. Livage

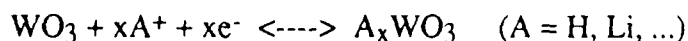
Laboratoire de Chimie de la Matière Condensée (UA 302),  
Université Pierre et Marie Curie, 4 place Jussieu, 75252 Paris - France.

### ABSTRACT

Amorphous tungsten oxide layers are deposited via the sol-gel route. Aqueous solutions of tungstate salts (Na<sub>2</sub>WO<sub>4</sub>) or chloroalkoxides (WOCl<sub>2</sub>(OPri)<sub>2</sub>) provide cheap and suitable precursors for the synthesis of WO<sub>3</sub>, nH<sub>2</sub>O colloidal solutions. Layers of large area can be deposited by spray or dip-coating. They exhibit electrochromic properties and could be used for making display devices or smart windows. Their electrochromic properties depend on the structure of the oxide network and the amount of water of the WO<sub>3</sub>, nH<sub>2</sub>O layers. Switching time and stability decrease when n increases due to faster ion diffusion. Optical absorption arising from electron delocalization varies with the crystalline structure of the oxide network. Both the structure and the hydration state of the layers depend on the experimental procedure. It is therefore possible to optimize the electrochromic properties of sol-gel derived layers.

### 1. INTRODUCTION

Electrochromic properties of amorphous tungsten oxide thin films have been extensively studied during the last decade<sup>1</sup>. Optical absorption arises from an electron hopping process between tungsten ions in different valence states, namely W<sup>6+</sup> and W<sup>5+</sup>. Coloration and bleaching can be reversibly obtained via electrochemical reactions as follows :



Charge compensation leads to the formation of tungsten ions in a reduced valence state (W<sup>5+</sup>). Electron and ions are simultaneously injected into the oxide layers that turns from white to blue upon reduction. Optical switching is not very fast. It is limited by ion diffusion rates through the oxide network. However coloration remains stable for a long time even in the absence of any applied voltage. Electrochromic materials find applications as display devices<sup>2</sup>, smart windows<sup>3</sup> or rear-view mirrors<sup>4</sup>.

Amorphous tungsten oxide thin films are usually deposited by vacuum evaporation<sup>5</sup>, sputtering<sup>6</sup> or anodic oxydation<sup>7</sup>. They can also be made via the sol-gel process from inorganic<sup>8</sup> or alkoxide<sup>9,10</sup> precursors. In both cases hydrolysis and condensation of these precursors leads to the formation of an hydrated tungsten oxide network giving rise to sols or gels. Thin films of large area can then be easily deposited under ambient conditions by such techniques as dip-coating, spin-coating, spray deposition or even screen-printing. Crystalline tungsten hydrates can also be obtained at room temperature.

92 4 28 052

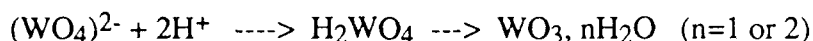
92-11434



This paper describes the synthesis of tungsten oxide sols and their deposition as thin films onto transparent conducting electrodes. Their electrochromic properties are discussed. They mainly depend on the structure and the water content of the oxide network.

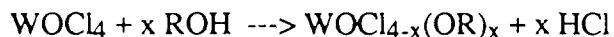
## 2. SOL-GEL SYNTHESIS OF WO<sub>3</sub> THIN FILMS

Tungsten oxide sols are formed upon acidification of sodium tungstate aqueous solutions. Protonation of such solutions (0.3 M) can be conveniently performed through a proton exchange resin (Dowex 50WX2). A clear transparent colloidal solution is first obtained. However it is not stable. Condensation keeps on going so that gelation occurs after some hours followed by the precipitation of tungstic hydrates :



Colloidal species can be stabilized for several months by adding organic solvents such as ethanol or acetone. These solutions can be easily deposited onto a transparent conducting electrode by spray and dried around 80°C. Transparent layers about 0.5µm thick are thus obtained.

Tungsten alkoxides have already been used for the sol-gel synthesis of tungsten oxide<sup>9,10</sup>. However, such precursors are very reactive towards hydrolysis. They are not commercially available and rather difficult to handle. Oxochloroalkoxides appear to be more suitable precursors. They can be made by reacting tungsten chloride or oxochloride with alcohols<sup>11</sup>. 6 g of anhydrous WOC1<sub>4</sub> are dissolved into 100cm<sup>3</sup> of alcohol under a dry atmosphere. A violent exothermic reaction occurs while gaseous HCl evolves leading to a yellow solution. According to similar experiments performed on MoCl<sub>4</sub>, the overall reaction can be described as follows<sup>12</sup> :



Chemical analysis and spectroscopic characterization (infra-red, N.M.R, EXAFS) show that under ambient conditions oligomeric species [WOC1<sub>2</sub>(OR)<sub>2</sub>]<sub>n</sub> are formed (x=2 and n <4) with ROH = iso-propanol. Such molecular solutions remain stable for months when kept in a closed vessel. Thin films about 0.1µm thick can be made by dip-coating. Hydrolysis and condensation are promoted by ambient moisture while most of the organic solvent rapidly evaporates. Chemical analysis gives a chlorine content smaller than 0.2% in weight. Thicker films can be obtained with several dip-coating procedures.

Tungsten oxide films WO<sub>3</sub>·nH<sub>2</sub>O, prepared from both inorganic and metal-organic precursors, appear to be amorphous by X-ray diffraction. Infra-red spectroscopy and X-ray absorption experiments show that tungsten is surrounded by six oxygen atoms with a short W=O double bond. (WO<sub>6</sub>) octahedra are linked via corners as in crystalline WO<sub>3</sub> or edges as in polyanions leading to an amorphous oxide network. The water content is close to n = 1.8 when the xerogel is dried under ambient conditions. Most of the water can be removed upon heating at 120°C. More tightly bonded water molecules or OH groups (n=0.3) are removed at higher temperature around 320°C. Crystallization then occurs at 400°C giving rise to orthorhombic WO<sub>3</sub>. Crystallization of the amorphous oxide is also observed at room temperature when the film is left in the presence of a humid atmosphere. The film remains transparent but the well known WO<sub>3</sub>·2H<sub>2</sub>O crystalline hydrate is obtained. It exhibits a layered structure with water molecules intercalated between tungsten oxide planes. Dehydration occurs when these films are heated at 120°C giving rise to transparent crystalline WO<sub>3</sub>·H<sub>2</sub>O. Anisotropic WO<sub>3</sub>·nH<sub>2</sub>O layers are thus obtained as evidenced by X-ray diffraction and infra-red dichroism. They exhibit interesting intercalation properties<sup>13</sup>.

The sol-gel process then appears to be very convenient for the preparation of tungsten oxide thin film having different structures and hydration states.

### 3. ELECTROCHROMIC PROPERTIES OF $\text{WO}_3 \cdot n\text{H}_2\text{O}$ THIN FILMS

Electrochemical properties of  $\text{WO}_3 \cdot n\text{H}_2\text{O}$  thin films were studied using a classical three electrodes potentiostatic cell. The electrochromic electrode is placed into a  $\text{LiClO}_4$ /propylene carbonate solution (1M). A platinum plate is used as a counter electrode and  $\text{Ag}/\text{AgClO}_4$  ( $10^{-2}$  M) as a reference electrode. Optical absorption at 633nm and electrochemical measurements are carried out simultaneously according to an experimental procedure already described in a previous paper<sup>14</sup>.

#### 3a. Role of the hydration state.

Cyclic voltammograms of amorphous  $\text{WO}_3 \cdot n\text{H}_2\text{O}$  layers are shown in figure 1. Experiments were performed at scan rates of 100mV/s in the range +1 V to -1.5 V (vs.  $\text{Ag}/\text{Ag}^+$ ). Cathodic potentials lead to the coloration of the film arising from the electrochemical insertion of lithium and the reduction of tungsten ions. The reverse process is observed for anodic potentials leading to the bleaching of the layer. Continuous curves are observed for both reduction and oxidation processes. They are typical of amorphous compounds where no phase transition occurs. Figure 1 however shows that the electrochemical behavior of  $\text{WO}_3 \cdot n\text{H}_2\text{O}$  layers upon cycling depend on the amount of water. The number of  $\text{Li}^+$  ions injected into the more hydrated sample ( $n=1.8$ ) decreases as the number of cycles increases while it increases in the other sample ( $n=0.5$ ). The reversibility of the electrochemical process can be measured as the ratio  $R$  of  $\text{Li}^+$  ions exchanged during the reduction and oxidation steps. It is almost complete ( $R=1$ ) with the hydrated sample, even for the first cycle, while it is rather small ( $R=0.5$ ) during the first cycles with the less hydrated sample. It then increases as more cycling experiments are performed. These variations are related to a modification of the layers.

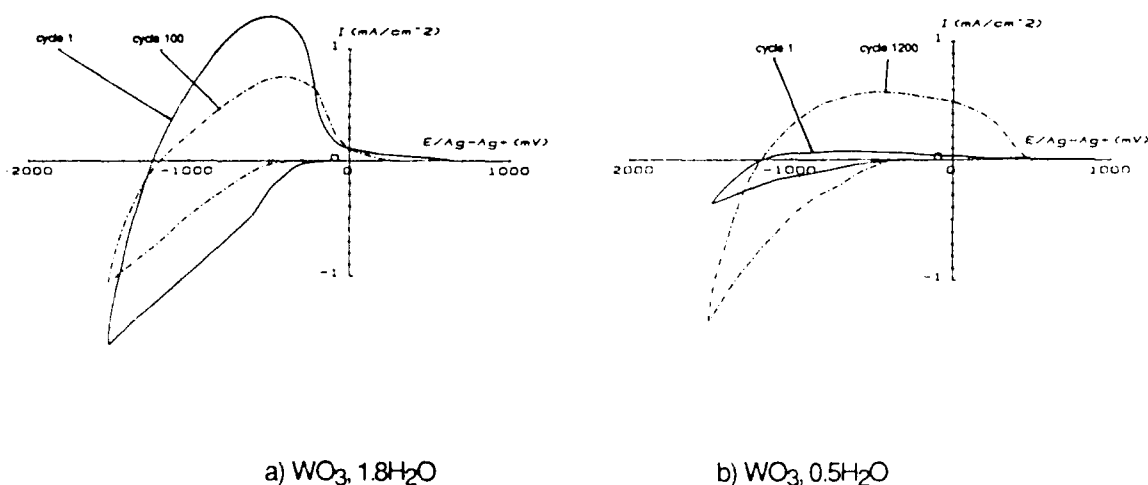


Figure 1: Cyclic voltammograms of amorphous  $\text{WO}_3 \cdot n\text{H}_2\text{O}$  thin films  
Evolution with cycling. Scan rate : 100mV/s

The amount of  $\text{Li}^+$  ions inside the tungsten oxide layer was measured by Secondary Ion Mass Spectroscopy (SIMS). These experiments show that the electrochemical lithium insertion is not completely reversible during the first cycles, when the amount of water is small ( $n < 1.5$ ). All  $\text{Li}^+$  ions are not removed from the layer even after complete bleaching. About 0.05 Li per W remain trapped inside the oxide network. This is not the case for hydrated samples ( $n = 1.5$ ). However spontaneous lithium insertion occurs, even in the absence of any applied voltage, when the layer is dipped into the  $\text{LiClO}_4/\text{PC}$  electrolyte. Such exchange properties are not observed when the amount of water decreases ( $n < 0.8$ ).

Cycling experiments show a modification of the electrochromic properties of the layers as the number of coloring-bleaching cycles increases. They suggest some structural evolution of the amorphous oxide network. Figure 2 shows that the charge  $Q$  reversibly exchanged during each cycle progressively decreases in the hydrated layers. This could be related to the poor stability of these layers towards dissolution or to a shift of the starting cathodic potential towards more negative values. A reverse phenomenon is observed when the amount of water is small ( $n < 0.5$ ). The injected charge increases during the first hundred cycles and the lithium insertion process becomes more reversible. This could be related to irreversibly trapped lithium ions increasing ionic conductivity.

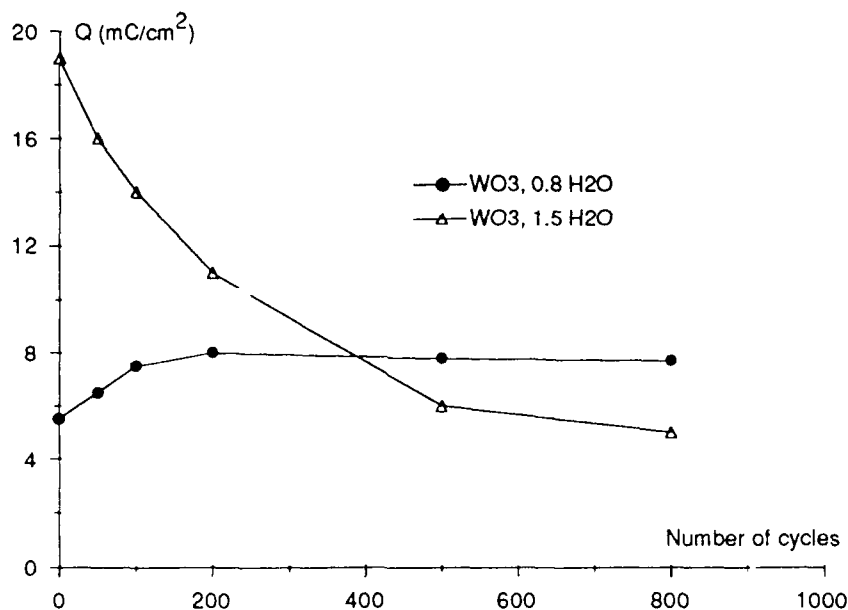


Figure 2 : Evolution of injected charge ( $Q$ ) versus number of cycles  
cyclic voltammetry; scan rate : 100 mV/s  
 $V_{\text{coloration}}$  : -1500 mV vs  $\text{Ag}/\text{Ag}^+$   
 $V_{\text{bleaching}}$  : 200 mV vs  $\text{Ag}/\text{Ag}^+$

### 3b. Role of the structure.

Cyclic voltammograms of amorphous ( $n=0.8$ ) and crystalline ( $n=1$ )  $\text{WO}_3 \cdot n\text{H}_2\text{O}$  layers are shown in figure 3. They are recorded at scan rates of  $10\text{mV/s}$  with materials having already been cycled  $10^3$  times.

The variation of the optical density of the layer as a function of the number of inserted  $\text{Li}^+$  is shown in figure 2 ( $x=\text{Li}/\text{W}$ ). An optical density of about 0.5 corresponds to the insertion of about  $0.4 \text{ Li}^+$  per W. A quasi linear variation is observed up to  $x=0.35$ . The slope of the curve then decreases showing that the coloration yield decreases.

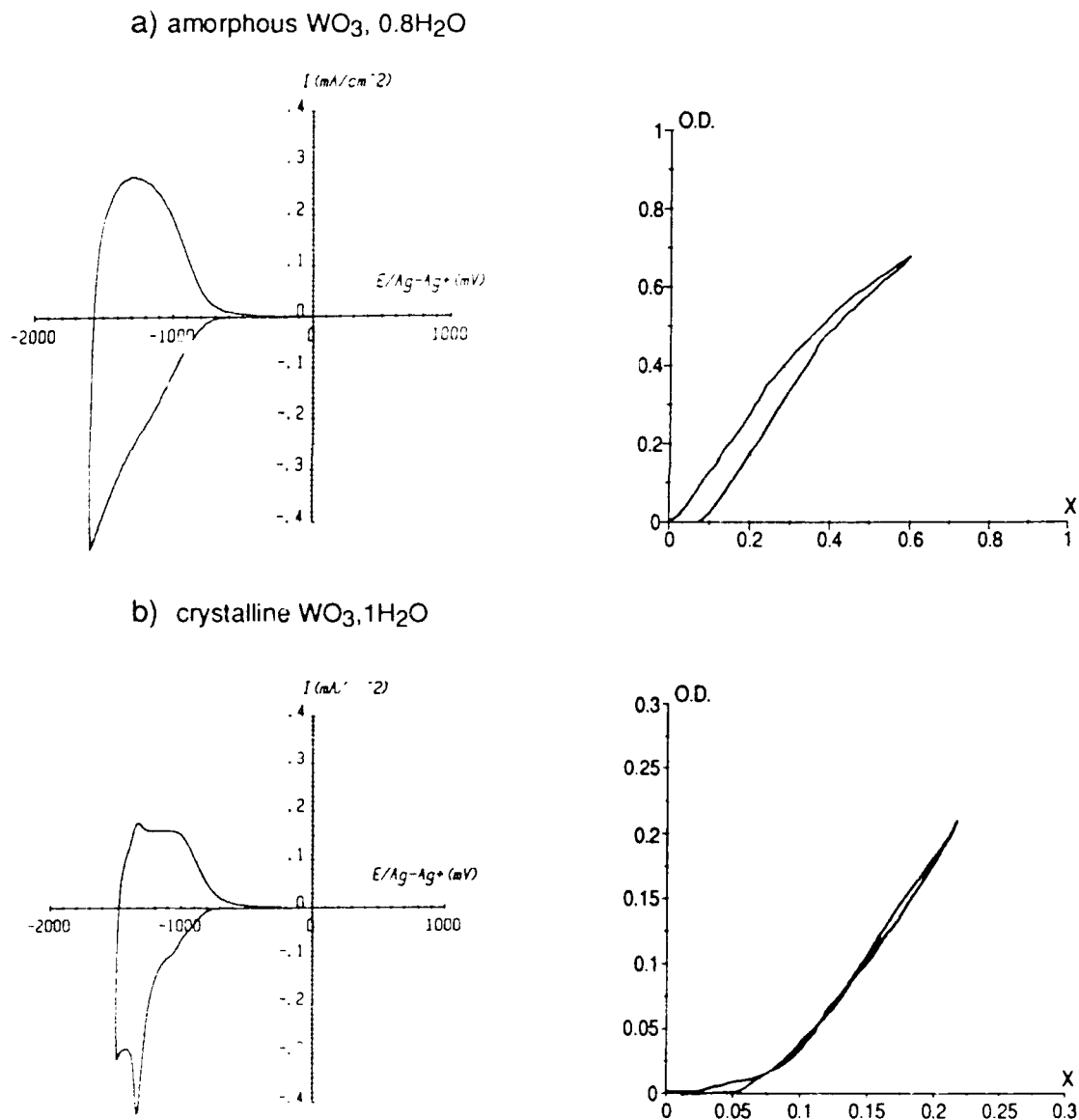


Figure 3 : Cyclic voltammograms ( $10 \text{ mV/s}$ ) of  $\text{WO}_3$  thin films after  $1000$  cycles and corresponding variations of the optical density (OD) versus injected charge ( $x=\text{Li}/\text{W}$ )

The cyclic voltammogram of crystalline  $\text{WO}_3 \cdot \text{H}_2\text{O}$  exhibits several bumps and one sharp peak during the reduction process. This corresponds to the insertion of  $\text{Li}^+$  ions into well defined sites followed by phase transitions. The optical density variation is no more linear. Coloration yields are first very small, up to  $x=0.06$ . Lithium insertion and tungsten reduction do not lead to strong optical absorption at 633nm. They then increase faster up to  $x=0.25$ , leading to an optical density of 0.25. The process is fully reversible.

Optical spectra of amorphous and crystalline layers are reported in figure 4. Amorphous  $\text{WO}_3 \cdot 0.8\text{H}_2\text{O}$  exhibits a broad absorption band between 500nm and 1500nm with a maximum around 900nm (0.75eV). It increases in intensity with the amount of  $\text{Li}^+$  into the layer. Such a spectrum is typical of an intervalence transition in a mixed valence compound arising from the optically activated hopping of localized electrons between  $\text{W}^{5+}$  and  $\text{W}^{6+}$  sites<sup>15</sup>. This is confirmed by electron spin resonance. ESR spectra of amorphous blue layers show two signals around  $g=1.83$  and  $g=1.68$  typical of paramagnetic  $\text{W}^{5+}$  ions.

Optical spectra of crystalline  $\text{WO}_3 \cdot \text{H}_2\text{O}$  blue layers exhibit an absorption edge with a maximum around 1300nm (1.1eV) and a slow decrease in the infra-red part of the spectrum. Such a behavior can be described in terms of band theory<sup>16</sup>. It could be assigned to delocalized electrons. This is confirmed by ESR, no signal being observed even at liquid helium temperature.

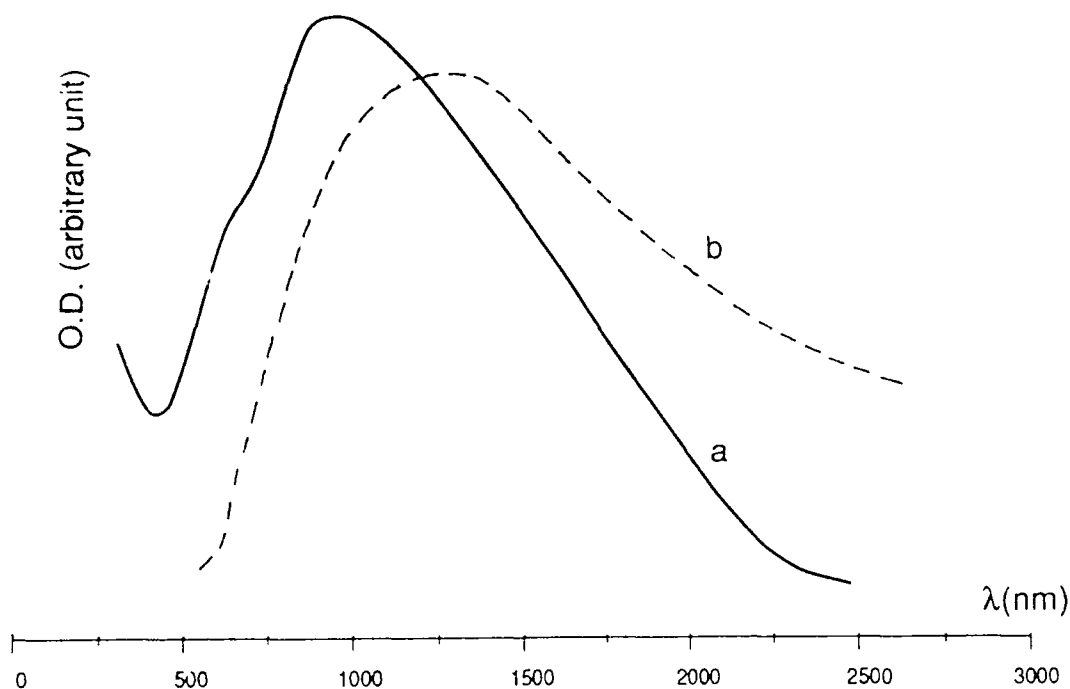


Figure 4 : visible spectra of :  
a : amorphous  $\text{WO}_3 \cdot 0.8\text{H}_2\text{O}$   
b: crystalline  $\text{WO}_3 \cdot \text{H}_2\text{O}$



## 4. CONCLUSION

The sol gel synthesis of amorphous tungsten oxides offers a versatile way for making electrochromic devices. Layers of large area can be deposited by spray or dip-coating onto glasses or even polymeric substrates. An hydrated amorphous oxide network  $\text{WO}_3 \cdot n\text{H}_2\text{O}$  is obtained. However both the structure and the hydration state of the layers can be modified via low temperature treatments. Electrochromic properties (optical absorption, switching time, memory) can then be conveniently tailored depending on the desired application.

The response time depends on the amount of water. This is related to the diffusion coefficient of  $\text{Li}^+$  ions through the layer. Impedance spectroscopy measurements and solid state NMR<sup>14</sup> show that  $\text{Li}^+$  diffusion is much faster in the hydrated samples. Optical response depends on the localization of electrons, i.e. on the structure of the oxide network. A metal-like behavior is observed in crystalline layers (tungsten bronzes) while the random disorder of the amorphous oxide leads to a localization of the charge carriers.

Moreover "all gel" electrochromic devices<sup>17</sup> have been made in which all active layers (transparent conducting electrode, electrochromic coating, electrolyte, counter electrode) are deposited from gels or colloidal solutions.

## 5. REFERENCES

1. T. Oi, Ann. Rev. Mater. Sci., "Electrochromic Materials", 16, pp. 185, (1986).
2. S. A. Agnihotry, K. K. Saini, S. Chandra, "Physics & Technology of Thin Films Electrochromic Displays; Device Technology", Indian J. Pure Appl. Phys., 24, pp. 34-45, (1986).
3. J. S. E. M. Svensson, C. G. Granquist, "Electrochromic Materials For Smart Windows", Solar Energy Mater., 11, pp. 29-34, (1984).
4. F. G. K. Baucke, J. A. Duffy, "Darkening Glass By Electricity", Chem. Brit., 21, pp. 643-646, (1985).
5. S. K. Deb, "Optical and Photoelectric Properties of Colour Centres in Thin Films of Tungsten Oxide", Phil. Mag., 27, pp. 801-822, (1973).
6. G. Deneuville, P. Gerard, R. Billat, "Principles and Operation of an All Solid State Electrochromic Display Based on  $\alpha\text{-WO}_3$ ", Thin Solid Films, 70, pp. 203-225, (1980).
7. A. Dipaola, F. Diqarto, C. Sunseri, "Electrochromism in Anodically Formed Tungsten Oxide", J. Electrochem. Soc., 125, pp. 1344-1347, (1978).
8. A. Chemseddine, R. Morineau, J. Livage, "Electrochromism of Colloidal Tungsten Oxide", Solid State Ionics, 9&10, pp. 357-362, (1983).
9. H. Unuma, K. Tonooka, Y. Suzuki, T. Furusaki, K. Kodaira, T. Matsushita, "Preparation of Transparent Amorphous Tungsten Trioxide Thin Films by a Dip Coating Method", J. Mat. Sci. Letters, 5, pp. 1248-1251, (1986).
10. I.E. Obvintseva, M. I. Yanovskaya, S. I. Kucheiko, N. Ya. Turova, R. R. Shifrina, V. I. Kukuev, E. N. Lubnin, Yu. N. Venevtsev,

- "Formation of Powders and Films of  $\text{WO}_3$  Obtained by Alkoxide Technology", *Izv. Akad. Nauk. SSSR, Neorg. Mater.*, 24, pp. 790-794, (1988).
11. O. J. Klejnot, "Chloride Alkoxides of Pentavalent Tungsten", *Inorg. Chem.*, 4, pp. 1668-1670, (1965).
  12. S. K. Anand, R. K. Multani, B. D. Jain, "Reactivity of Molybdenum Chloride with Alcohols", *J. Indian Chem. Soc.*, 45, pp. 1130-1135, (1968).
  13. A. Chemseddine, F. Babonneau, J. Livage, "Anisotropic  $\text{WO}_3 \cdot n\text{H}_2\text{O}$  Layers Deposited from Gels", *J. Non Cryst. Solids*, 91, pp. 271-278, (1987).
  14. P. Judeinstein, J. Livage, "Role of the Water Content on the Electrochromic Properties of  $\text{WO}_3 \cdot n\text{H}_2\text{O}$  Thin Films", *Mat. Sci. Engineer.*, B3, pp. 129-132, (1989).
  15. R.B. Goldner, D.H. Mendelsohn, J. Alexander, W.R. Henderson, D. Fitzpatrick, T.E. Haas, H.H. Sample, R.D. Rauh, M.A. Parker, T.L. Rose, "High Near-Infrared Reflectivity Modulation with Polycrystalline Electrochromic  $\text{WO}_3$  Films", *Appl. Phys. Rev.*, 43, pp. 1093-1095, (1983).
  16. W. C. Dautremont-Smith, M. Green, K. S. Kang, "Optical and Electrical Properties of  $\text{WO}_3$  Electrochemically Coloured", *Electrochimica Acta*, 22, pp. 751-759, (1977).
  17. P. Judeinstein, J. Livage, A. Zarudiansky, R. Rose, "An 'All Gel' Electrochromic Device", *Solid State Ionics*, 28-30, pp. 1722-1725, (1988).



## Sol-gel nano-porous silica-titania thin films with liquid fill for optical interferometric sensors

Andrew J. Martin and Mino Green

Electrical Engineering Department  
Imperial College  
London SW7 2BT, U.K.

### ABSTRACT

The production of thin films whose refractive index is measurand specific, for use in an interferometric fiber optic chemical sensor, is discussed. The problem of making such coatings has been tackled by a system we have termed the "guest-host" approach, in which an active liquid whose index varies with measurand, is contained within a porous glass host of fixed index. Suitable porous silica-titania glass films have been produced via the sol-gel process. The use of this system enables the index of the glass to be varied, so that the composite index of the liquid filled film can be tailored to that required by the optical system. The sol-gel method developed is based upon the hydrolysis and polymerisation of metal alkoxides, in an acidic aqueous/alcoholic solution. Thin film slab waveguides were deposited in order to measure the light scattering losses, which were found to be typically  $\sim 1\text{dB/cm}$ . The porosity of films was studied using a new technique developed in which water adsorption isotherms are plotted using ellipsometry. The pore size was found to be very small of pore diameter in the nanometer range, and the total porosity  $\sim 10\%$ . Both of these factors were increased by the removal of residual organic material, using hydrogen peroxide. Finally the use of pH indicator dyes as a liquid fill is discussed, to produce a pH sensor.

### 1. INTRODUCTION

Various chemical sensors have been proposed based upon the principle of a thin film whose refractive index is measurand specific, varying the optical characteristics of some device via interaction with the evanescent field<sup>1,2</sup>. Whilst devices have been demonstrated to work in principle, there has been little progress on the production of suitable films whose response is both reproducible and reversible. One particular device requiring such a coating is a Mach Zehnder interferometer constructed from a single twin core fiber optic, previously developed in our group<sup>3</sup>.

The monochromatic light transmission of this fiber varies with the refractive index of a thin film coated onto the fiber, which acts as a phase modulator in one arm of the interferometer. As an example, one fiber cycled through 24 fringes for a change in the coating index from 1.512 to 1.522. In the case of white light transmission in the fiber, the output is a dispersion in wavelength, which is a function of the coating index. This mode of operation has the advantage of no ambiguity with respect to fringe number. Thus it can be seen that with a suitable coating a sensor could be constructed.

The coating material should have the following characteristics:

- a reproducible and reversible response to measurand,
- a rapid response ( $\sim$ seconds),
- an index suitable for the fiber (about 1.52 in the above case),
- a reasonably large change in index (typically at least 0.001),
- transmit light with low losses (i.e.  $< 3\text{dB/cm}$ ).

92 4 28 053

92-11435



Other factors which may be of importance, depending upon the particular application, are long term stability, selectivity, and durability. Of particular importance is the required change of index. A reasonably large change implies that the electronic configuration of the material must be changed in some way, i.e. chemical reactions must occur (reversibly) between the material and the measurand species. Simple thermodynamic and kinetic considerations indicate that inorganic materials are unlikely to be suitable, but organic solids (i.e. polymers) may be. After further considerations however a more promising scheme was developed: the use of aqueous solutions.

Obviously the liquid must be retained on the fiber in some way, for water we propose the use of a porous matrix. Thus we have a composite material where the liquid is an active component, (i.e. changing its index with measurand), contained within an inert matrix. We have termed this the guest-host approach; the liquid being the guest and the matrix the host. This approach has many advantages over the use of a single phase material, the principal one being that a suitable reaction between measurand and material is more likely to occur in the liquid phase than the solid phase. Another major advantage is that the composite index of the film can be tailored to that required, by variation of the index of the matrix material, irrespective of the liquid phase index. The problem of producing a suitable material is thus split into two parts: the guest and the host.

The host material must satisfy the following conditions:

- it must be chemically inert,
- be porous,
- have low scattering losses (and thus the pore size must be small),
- be non-absorbing,
- be producible with a large range of refractive indices,
- have the capability to be deposited in thin film form.

One way to satisfy all the above criteria, is the production of silica-titania glass using the sol-gel process. The sol-gel method gives intrinsically porous glasses, is ideal for the production of thin films, and the index can, in this case, be varied from that of silica (~1.46) to that of titania (~2.3).

## 2. PRODUCTION OF SILICA-TITANIA THIN FILMS

### 2.1 Sol production

The sol-gel method based upon the hydrolysis and polycondensation of metal alkoxides was chosen, since this method gives great flexibility. The use of this sol-gel technique for the production of thin oxide films, for optical applications, is well documented<sup>4</sup>. The majority of these applications are concerned with situations where light transmission is perpendicular to the film surface, e.g. antireflective coatings. Films are also usually sintered in order to achieve full or near full density. For this application however light propagation is along the film (which is part of a waveguide) and so low attenuation is important, as is the retention of porosity. Since it was not obvious from the literature what was the optimum sol composition for this application, a scheme was developed whereby sols of differing compositions could be produced for the deposition of films. Subsequent examination of these films was used to reveal the optimum sol chemistry.

The principle process variables were: water to alkoxide ratio (termed the 'R' value), type and concentration of catalyst (i.e. sol pH), the ratio of silicon to titanium alkoxides, and the concentration of the sol. It was necessary to make sols of composition ranging from pure silica to 50 mol.% silica/50 mol.% titania, (or 100S to 50T50S in the commonly used notation), thus giving products with a range of refractive indices from approximately 1.46 to 1.84. Both hydrochloric acid

and ammonium hydroxide were used to give acid and base catalysed conditions for comparison, with R values of 2, 4, and 10 (i.e. below, equal to, and above the stoichiometric ratio). The metal alkoxides used were tetraethylorthosilicate (TEOS), and titanium isopropoxide (TPOT - tetrapropylorthotitanate), in an ethyl alcohol solvent.

After much experimentation a scheme was developed which allowed for the deposition of films from sols ranging from 100S to 50T50S, with R values of 2, 4, and 10. Of the many different methods tried, it was always found that the use of the ammonium hydroxide catalyst lead to precipitation in solution. The method developed involves the partial hydrolysis of the TEOS before the addition of the TPOT, this allows for the difference in reaction rates of the two alkoxides. Dilution was found to be important in that if the sol was too concentrated, it would rapidly gel, hence dilute solutions were used to give stable sols.

Practically the sols were produced as shown in figure 1. The TEOS and TPOT were obtained as 98% pure (Aldrich chemical company), and further purified by double distillation (under vacuum in the case of TPOT). All other chemicals were obtained as high purity reagents (BDH Chemical Company). The TEOS is first hydrolysed with a quarter the stoichiometric ratio of water/HCl, by refluxing the solution at 70°C for 2 hours.

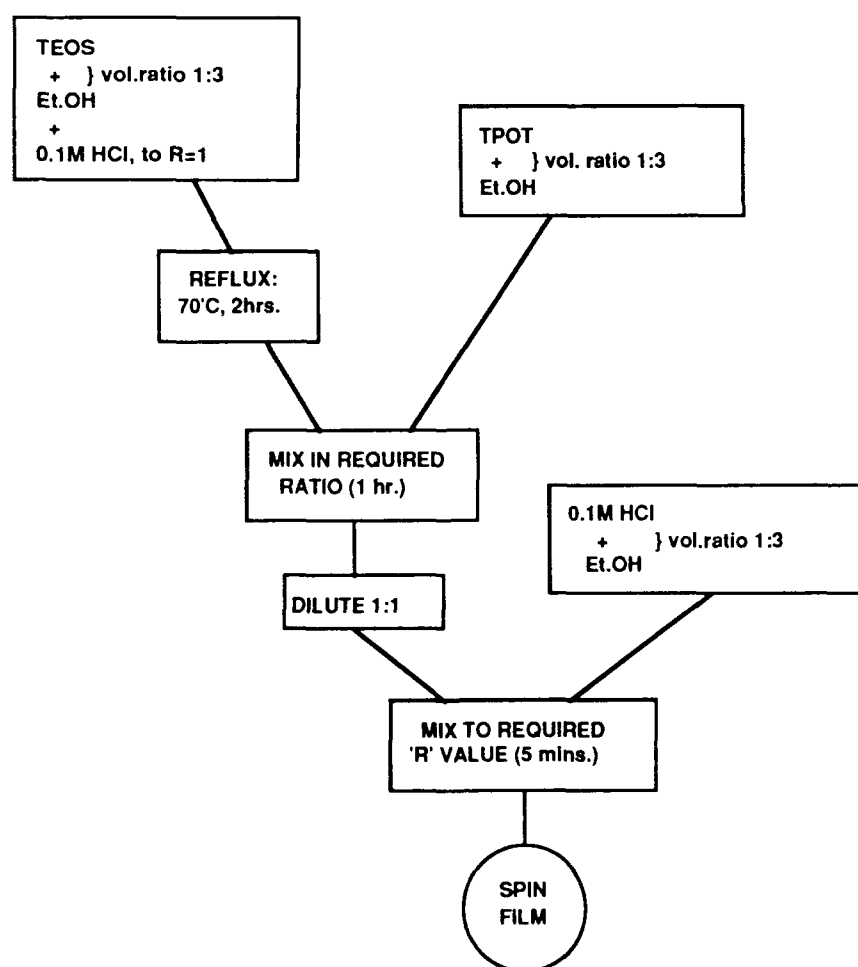
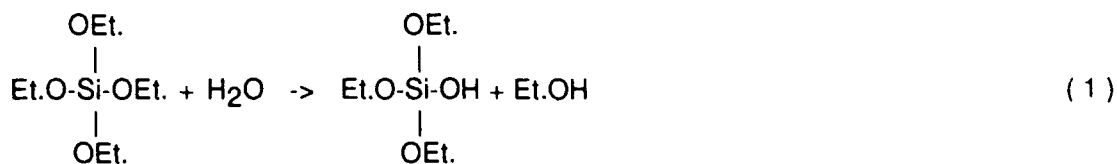
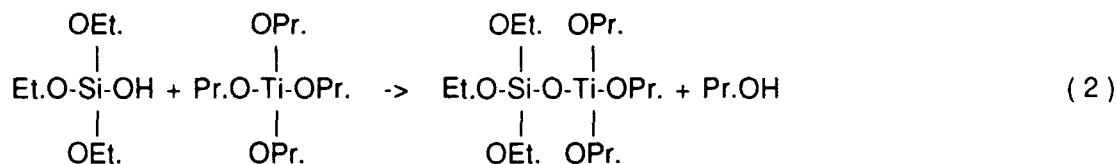


Fig. 1: Sol production scheme

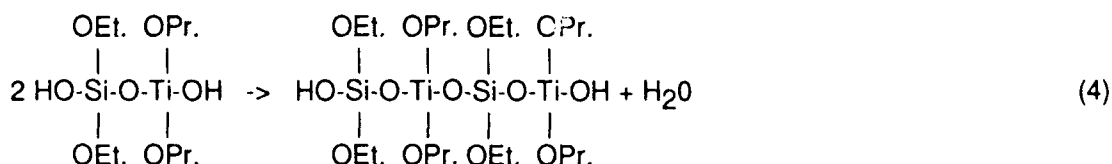
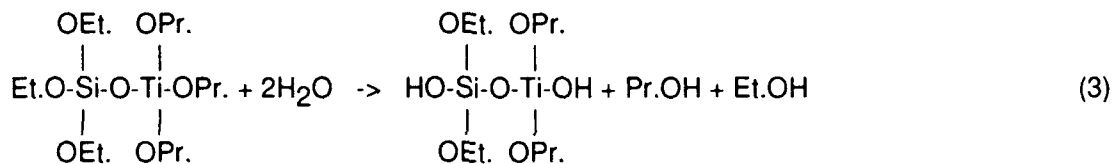
Thus on average one ligand on each of the TEOS molecules will be hydrolysed:



The TPOT is next added (in the required ratio) which forms a double alkoxide by reaction with the partially hydrolysed TEOS:



These intermediates cannot polymerise since there is no remaining water for hydrolysis, and so the sol is stable for these conditions. Upon the addition of further water and HCl (to the required R value), hydrolysis and polymerisation takes place between the intermediates, one possible route being:



In this way a gel network, homogeneous on a molecular scale, is built in a controlled manner. Before gellation occurs however, (only about 30 minutes for the R=10 sols), the sol is coated onto the substrate.

## 2.2 Film deposition

The film deposition technique used was spin coating, onto polished silicon and glass substrates. An excess of the sol was filtered through a 0.2 micron millipore filter onto the substrate in clean room conditions. The substrate was then rapidly accelerated to the spinning speed, held for 30 seconds, and decelerated. The films were then left to gel/dry for 24 hours in covered petri dishes, followed by baking at 100°C in air for 30 minutes. Films coated onto polished silicon wafers were used for index and thickness measurement by ellipsometry, (Rudolph Research AutoEL), and those onto cleaned glass slides to form slab waveguides. A total of 18 different sols were produced: 100S, 10T90S, 20T80S, 30T70S, 40T60S, 50T40S, each at R values of 2, 4, and 10. All were spun onto the substrates at various thicknesses.

### 2.3 Selection of optimum film

Selection of the optimum film is essentially the selection of the optimum R value to give the best film, (over the range 100S to 50T50S), in terms of maximum porosity and minimum light scattering. Attenuation of light due to factors other than scattering is negligible in comparison.

The porosity of the films was calculated from index measurements under dry and water saturated nitrogen, i.e. with pores empty and full of water (see later for more detailed explanation). Assuming the composite index of a film to be additive and the index of water in the pores to be 1.333, the porosity could be calculated. The results however were not very accurate due to the limited accuracy of the ellipsometer. For films of R=2 and 4 the porosity was approximately 10%, and for R=10 slightly greater at about 15%.

Films coated onto glass however indicated an R value of 10 to be unsuitable, as the films with higher titania content had a slight haze. Furthermore microscopic examination of these films revealed them to contain particles, as opposed to those with R values of 2 and 4 which appeared smooth and featureless. Film selection was thus reduced to those with R=2 and R=4, and since porosity is similar, selection is dependent only upon scattering losses.

The scattering losses were measured from a He-Ne laser source (633nm) propergating along slab waveguides, coupled in via a rutile prism<sup>5</sup>. Due to the high dilution of the sols, films deposited tended to be rather thin, typically 0.1 microns. This is too thin to form asymmetric slab waveguides with the glass substrate index of 1.512, and air the other side, even for the 50T50S films (measured index approximately 1.72). Thicker waveguides were thus produced by spinning five successive layers of the 50T50S sol on top of each other, allowing each layer to gel before the deposition of the next, giving a total thickness of about 0.5 micron. Microscopic examination of these films revealed those with R values of 4 to contain fine hairline cracks, as those with R=2 were featureless. The scattered light intensity as a function of distance for these waveguides is shown in figure 2, together with the calculated losses. Clearly, the higher losses of the R=4 sample are due to the cracks in the film.

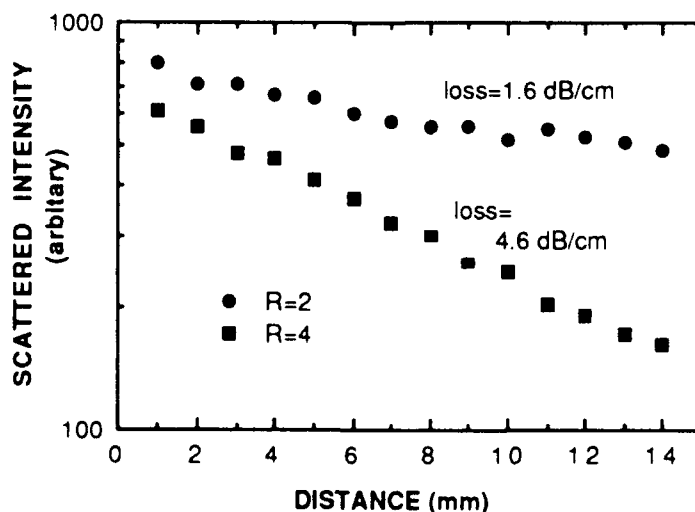


Fig. 2: Scattering losses for multilayer 50T50S slab waveguides

The final application of the film (i.e. coated onto a fiber) requires a thickness in the region of half a micron, and hence an R value of 2 becomes the only option since the losses of the cracked film are

too great. With this sub-stoichiometric water content however, the sol concentration can be increased and still remain stable over long periods. This enables a film of the required thickness to be deposited in one layer. The sol production scheme was thus accordingly modified.

#### 2.4 Final film production scheme

The finalised sol production scheme is essentially as shown in figure 1, except that the overall concentration is greater. This was achieved by mixing the TPOT and TEOS with ethanol in a volume ratio of 1:1, all other factors remaining unchanged. It was now found that 50T50S sols gelled very rapidly, however 45T55S sols were stable and this was considered to be a suitable maximum for the titania content.

Another problem was that spinning these more concentrated sols tended to give films with a slight mottled appearance to the surface, particularly at higher titania concentrations. It was found that ageing the sols in a closed flask for 24 hours prior to spinning greatly improved the surface quality. This also had the effect of slightly increasing the film thickness, by about 10%, presumably due to an increase in sol viscosity caused by polymerisation in solution.

Finally, in an attempt to increase the porosity of the films, samples were immersed in a 7 mole% solution of hydrogen peroxide at 100°C, to remove residual organic matter.

### 3. ANALYSIS OF THE FILMS

#### 3.1 Microscopic examination

Examination by both optical and scanning electron microscopes showed the films to be featureless with a smooth surface, with no indication of particulate matter or cracks. Films treated with hydrogen peroxide on the other hand were degraded, with discontinuous cracks and defects appearing in the film.

#### 3.2 Refractive index and thickness measurements

The film thickness variation with spin speed for the 100S film is shown in figure 3, the other films being comparable. The hydrogen peroxide treatment of samples had no effect on thickness.

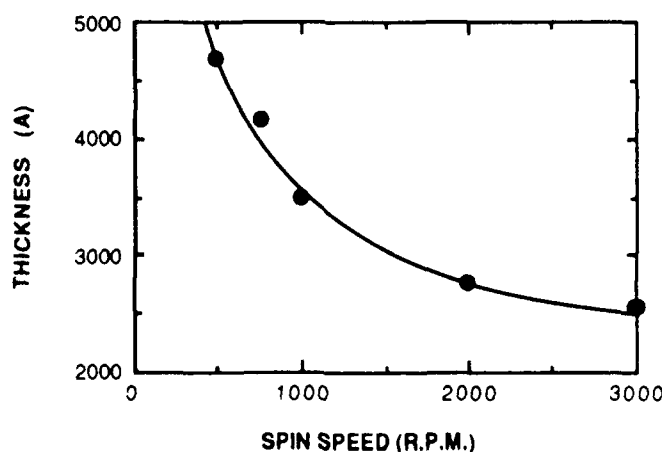


Fig. 3: Thickness variation with spin speed



Variation in thickness and indices as the films were gradually sintered down, in air, to full density are shown in figures 4 and 5. The samples were heated to the required temperature, held for 30 minutes, cooled, the thickness and index measured, and so on.

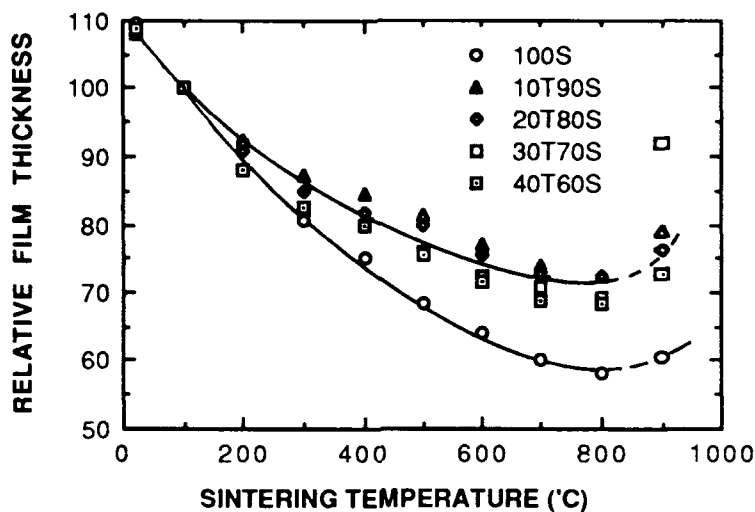


Fig. 4: Variation of film thickness with sintering temperature

For most of the films the reduction in thickness is about 30%, for the 100S samples however it is greater at 40%. This reduction in thickness is due to the removal of water (100 to 250°C), the combustion of residual organic matter (250-300°C), and the reduction of porosity (over 300°C)<sup>6</sup>. The increase in thickness above 800°C is due to the thermal growth of silica on the silicon wafer, this also indicates that the film porosity is still continuous.

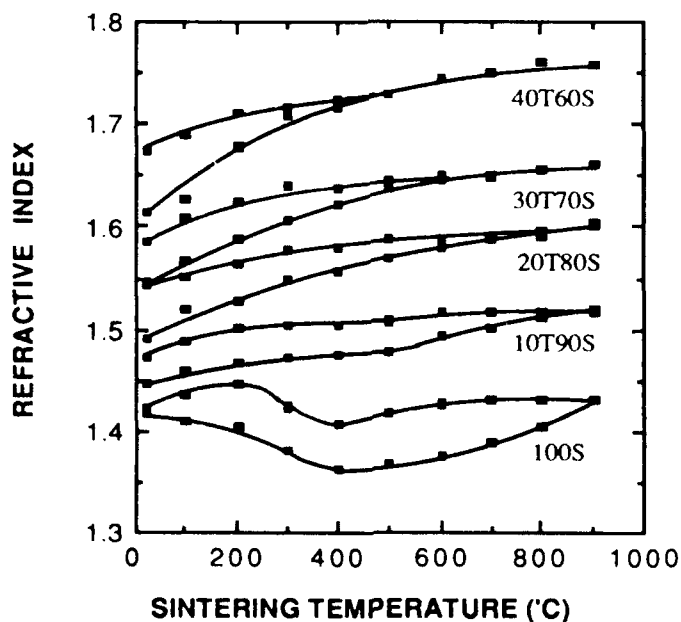


Fig. 5: Index variation with sintering temperature

In the index variation of samples with sintering temperature, (figure 5), two curves are shown for each film, the lower one for pores empty of water and the upper for pores full. The general trend is a decrease in porosity and an increase in index with temperature, although again the 100S samples behave slightly differently. Surprisingly, the films with higher titania content sinter at lower temperatures. One possible explanation is that these films have a smaller pore size.

Figure 6 shows the above data plotted to show the index variation with silica-titania ratio. Also shown is the theoretical fully dense index, assuming silica and titania indices to be 1.456 and 2.3 respectively. This is not reached in practice, probably due to residual porosity and OH groups, as well as the effect of the thermally grown silica affecting index measurement.

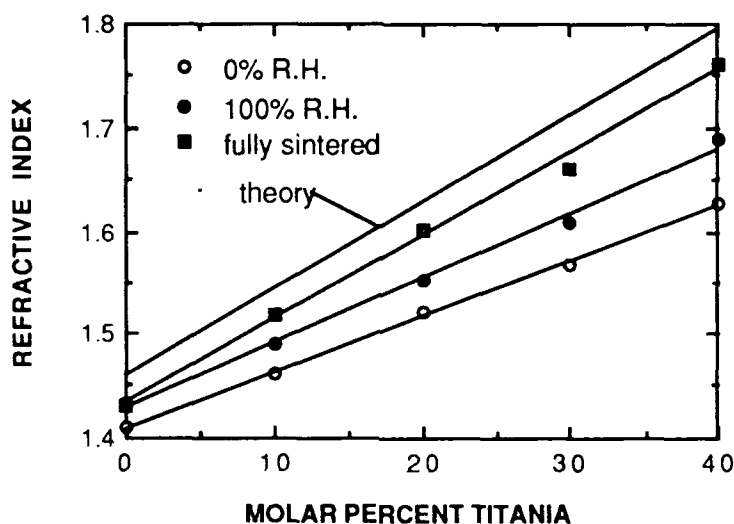


Fig. 6: Index variation with sol composition

The effect of the hydrogen peroxide treatment of the films is to dramatically reduce the index, to such an extent that with the pores empty of water the ellipsometer will not measure the resultant low indices. With the pores full of water the indices of all samples are surprisingly similar:  $1.401 \pm 0.005$ . A 10 minute treatment was found to be sufficient, after which no further change in index was observed. This reduction in index is due to two factors, removal of the high index organic material and the associated increase in porosity.

### 3.3 Pore morphology

To study the pore morphology of the films in terms of pore size and pore size distribution, as well as total porosity, a technique was developed to plot water vapour adsorption isotherms due to capillary condensation in the films. An environmental chamber was fitted to the ellipsometer sample stage, and nitrogen whose relative humidity could be varied from 0 to 100%, (by means of a bubbler/flowmeter/humidity meter arrangement), was flowed into this chamber. The relationship could thus be obtained between refractive index and humidity, which is effectively an isotherm of mass of water adsorbed with partial pressure of water vapour. Figure 7 shows the isotherm for the 30T70S film.

No hysteresis was observed as might be expected, this was probably due to limitations in accuracy. Isotherms were also obtained for the other films, which were very similar to the above.

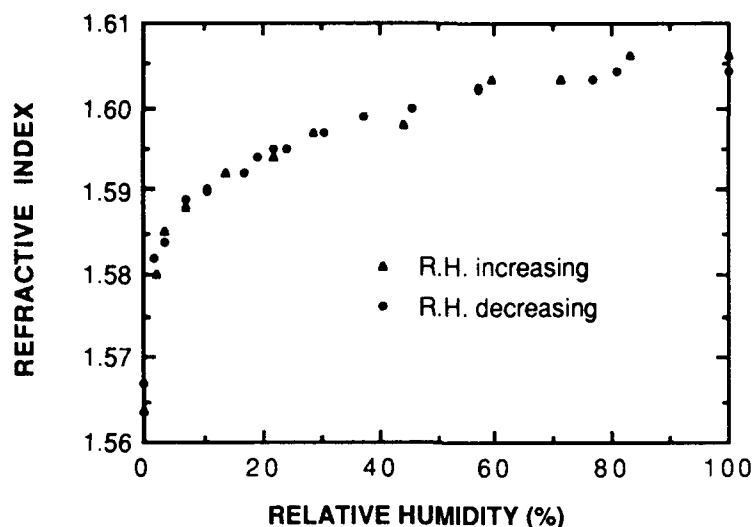


Fig. 7: Water adsorption isotherm for 30T70S film

From these isotherms the pore size distribution can be calculated using the Kelvin equation<sup>7</sup>:

$$r = \frac{-2\gamma V_m}{RT \ln (p/p_0)} \quad (5)$$

where:  $r$  = pore radius  
 $\gamma$  = surface tension of water  
 $V_m$  = molar volume of water  
 $R$  = gas constant  
 $T$  = absolute temperature  
 $p/p_0$  = partial pressure of water vapour

Pore size distributions calculated using the above equation, are shown in figure 8. As can be seen the pore size of the untreated samples is very small, the 100S film having a slightly larger pore size than the others. The 10T90S was only treated with hydrogen peroxide for 5 minutes, so as not to decrease the index to such an extent that measurements could not be made at low humidity. For this film not only is the total porosity increased to about 30%, but also the mean pore size and the width of the distribution. Presumably the full 10 minutes treatment would further increase porosity and pore size.

These results are however only approximate, since factors such as surface tension fail to be valid for such small pore sizes. Also, this technique only takes into account the free water, there may be water molecules adsorbed onto the pore surface which does not desorb at zero humidity. The thickness of this layer should be added to the above values for pore radius. The size of a water molecule is  $\sim 1.3 \text{ \AA}$  (somewhat dependent upon orientation), and so it seems likely that the total pore diameter is in the region of a nanometer.

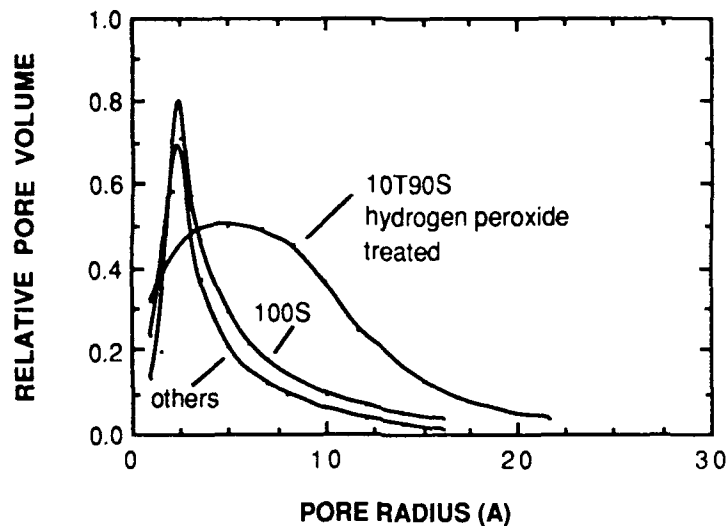


Fig. 8: Pore size distributions

### 3.4 Scattering losses

The waveguiding scattering losses for these single layer slab waveguides were measured as previous. The experimental results are shown in figure 9, together with the calculated losses in dB/cm. Unfortunately, slab waveguides could not be made from the hydrogen peroxide treated films due to their low indices. It was thus not possible to judge the extent to which the surface damage would cause scattering.

○

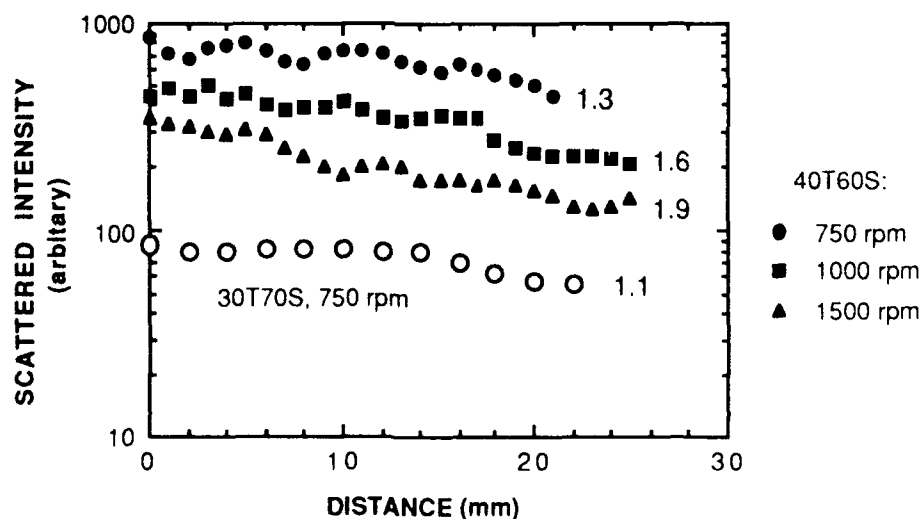


Fig. 9: Scattering losses for single layer waveguides

The scattering losses decrease with increasing film thickness, which tends to indicate that scattering is associated with imperfections in the surface region. To test this hypothesis, oil of the same index as the substrate (1.512) was coated onto the surface. The result was a dramatic decrease in scattered intensity, typically less than 25% of the original loss. Unfortunately reliable curves of intensity variation with distance could not be obtained due to the low intensity of scattered light, and contamination of the oil with dust causing excess scattering at singularities. However it seems likely that in the final application, i.e. only the evanescent field penetrating the film, losses will be very low.

### 3.5 Conclusions

Whilst some of the data is not of high accuracy, the following conclusions can be drawn:

- (i) The films are porous with a porosity in the region of 10%. The pore size is in the region of a nanometer in diameter. Both of these factors can be increased by removing the organic content with hydrogen peroxide.
- (ii) The films are transparent, and when applied as a cladding material to an optical fiber the losses are likely to be <1 dB/cm.
- (iii) The films can be produced with a range of indices, and at the required thickness.

## 4. CONSTRUCTION OF A SENSOR

The next step in producing a practical device is to fill the pores with a suitable liquid. For a gas sensor operating in ambient conditions (i.e. R.H. > few %) with an aqueous based liquid fill, no membrane is required for the retention of an aqueous solution in the pores, as it is maintained by atmospheric moisture (see figure 7). This obviously greatly simplifies the construction of a practical sensor. For non-aqueous based solutions, or for sensors to be used in liquid environments, some kind of semi-permeable membrane is required for the retention of the liquid.

One possibility for the construction of a sensor is the use of pH indicating dyes in aqueous solutions. The molecular structure is typically based upon two or three benzene rings, which are about 2.8Å in diameter, and so the dye molecules should fit into the pores of the glass host. The change in optical absorption (i.e. colour) of such dyes has an associated change in refractive index, for example changes of the order of 0.01 have been reported<sup>8</sup> using phenol red at 633nm<sup>8</sup>.

Such a dye could be used for the detection of ammonia vapour in air, based upon the change in pH of solution with the concentration of ammonia<sup>9</sup>. A more useful device would be a sensor for the detection of solution pH. Such a device would however require a membrane to retain the (large) dye molecules, but allow through the (much smaller) H<sup>+</sup> ions. Polymers should be capable of performing this function, e.g. cellulose acetate.

The construction of a sensor for the measurement of blood pH, *in vivo*, over the physiological range of pH 7.0 to 7.5 is currently under investigation, based upon phenol red.

## 5. ACKNOWLEDGMENTS

The authors wish to thank John Cozens, Yi Gu, and Gerasimos Pagiatakis for many useful discussions regarding practical and theoretical aspects of the Mach Zehnder fiber. The SERC (UK) and Alcan International are also gratefully acknowledged for their financial support.

## 6. REFERENCES

1. A. M. Smith, "Materials Interactions in Optical Fiber Sensors", Optical Fiber Sensors, J. Dakin and B. Culshaw (eds.), chapt. 6, Artech House, 1988.
2. R. J. Black, F. Gonthier, S. Lacroix, J. Lapierre, J. Burnes, "Abruptly tapered fibers: index response for sensor application", 4th int. conf. optical fiber sensors, pp Pd-3-1 to PD-3-4, Tokyo, 1986.
3. J. R. Cozens, M. Green, Y. Gu, "Special fibers for sensing", SPIE 1011, pp 62-66, 1988.
4. R. B. Pettit, C. S. Ashley, S. T. Reed, C. J. Brinke, "Antireflective films from the sol-gel process", Sol-gel technology for thin films, fibers, preforms, electronics and specialty shapes, L. C. Klein (ed.), pp 80-109, Noyes, New Jersey, 1988.
5. P. K. Tien, R. Ulrich, "Theory of prism film coupler and thin-film light guides", J. Op. Soc. Am., 60, pp 1325-1337, 1970.
6. J. Zarzycki, "Sol-gel preparative methods", Glass...current issues, A. F. Wright and J. Dupuy (eds.), NATO ASI series, series E: no. 92, pp 203-223, Martinus Nijhoff, 1985.
7. J. Oscik, Adsorption, chapter 3, Ellis Horwood Ltd, Chichester (UK), 1982.
8. J. W. Attridge, K. D. Leaver, J. R. Cozens, "Design of a fibre-optic sensor with rapid response", J. Phys. E: Sci. Instrum., 20, pp 548-553, 1987.
9. J. F. Giuliani, H. Wohltjen, N. L. Jarvis, "Reversible optical waveguide sensor for ammonia vapours", Op. Lett. 8, pp 54-56, 1983.



Optical switches based on semiconducting vanadium dioxide  
films prepared by the sol-gel process

Richard S. Potember and Kenneth R. Speck

The Johns Hopkins University Applied Physics Laboratory  
Laurel, Maryland 20723, USA

ABSTRACT

Vanadium dioxide thin films have been grown from vanadium tetrakis (t-butoxide) by the sol-gel process. A new method for the synthesis of the vanadium precursor was also developed. Films were deposited by dipcoating glass slides from an isopropanol solution, followed by post-deposition annealing of the films at 600°C under nitrogen. The properties of these films, to a high degree, were a function of crystalline boundaries and crystalline grain size. These gel-derived VO<sub>2</sub> films undergo a reversible semiconductor-to-metal phase transition near 72°C, exhibiting characteristic resistive and spectral switching comparable with near stoichiometric VO<sub>2</sub> films prepared on non-crystalline substrates by other techniques. Paralleling the investigation of pure VO<sub>2</sub>, films were doped with hexavalent transition metal oxides to demonstrate lowering of the transition of the transition temperature.

2. INTRODUCTION

2.1. Vanadium dioxide

Several transition metal oxides are known to undergo a sudden metal-to-nonmetal transition over a discrete temperature range<sup>1,2</sup>. Materials which exhibit this behavior are metal oxides or sulfides. Pronounced and reversible changes in the optical, electrical conductivity, and magnetic properties of these materials make them an interesting subject from both a theoretical and applications perspective. Among the materials discovered to exhibit this behavior is vanadium dioxide.

Vanadium dioxide is known to undergo a reversible thermally-induced semiconductor-to-metal phase transition at 68°C<sup>1,2</sup>. Associated with this transition, the material exhibits large changes in its optical, electrical, and magnetic characteristics with respect to temperature<sup>3,4</sup>. This anomalous behavior has prompted considerable interest in the fabrication of vanadium dioxide thin films for scientific investigation and for use in various technological applications<sup>5,6</sup>.

In the metallic state of VO<sub>2</sub>, the vanadium atoms are arranged in a body-centered, tetragonal structure<sup>7,8</sup>. Each vanadium atom is surrounded by six oxygen atoms in a distorted octahedral arrangement. The metallic phase is sometimes called the "rutile" crystal structure

92 4 28 054

92-11436



since the symmetry is the same as the naturally occurring structure of  $\text{TiO}_2$ . Below the transition temperature,  $\text{VO}_2$  is a semiconductor with a monoclinic crystal structure. In the transition from the metallic to semiconducting state, the vanadium atoms shift in directions both parallel and perpendicular to the tetragonal c-axis, which now becomes the monoclinic a-axis, thus doubling the unit cell size<sup>7</sup>. As a result, there is a nonhomogeneous one percent volume change in the material.

J. B. Goodenough performed much of the early work on the band structure of  $\text{VO}_2$  in the semiconductive and metallic state<sup>7</sup>. He developed a model which gives a rapidly disappearing band gap as a result of the crystalline structure distortion and attributed the change in the band structure to a change of chemical bonding. In the metallic state, the uppermost (3d) bands overlap, resulting in partial occupation. As the temperature of the system is lowered, it becomes energetically favorable for the crystal to change its structure and for the energy gap to appear. The perpendicular displacement of the vanadium cations shortens the vanadium-oxygen distance, raising the energy of the  $\pi^*$  band above the Fermi level. The parallel displacement results in the splitting of the d-band. Below  $T_t$  a band gap of approximately 0.7 eV opens up within the 3d bands of the vanadium, separating a filled band from the higher-lying empty bands.

Abrupt changes in the physical properties of  $\text{VO}_2$  are seen as it is cycled through the transition temperature. A discontinuous change in the electrical resistivity, as large as  $10^5 \Omega\text{-cm}$  in single crystals<sup>9</sup>, has been reported as the material goes from semiconducting to the metallic state. For thin films of vanadium dioxide, the resistivity ratio ( $\rho_{T < T_t} / \rho_{T > T_t}$ ) is on the order of  $10^3 \Omega\text{-cm}$ <sup>10</sup>. Metallic conduction is not reached in thin films, still being semiconducting above  $T_t$ .

A heating-cooling hysteresis effect is also connected with this first-order transition. The largest and sharpest transition with the minimum hysteresis is seen in stoichiometric single crystals with few structural defects<sup>9</sup>. The size of the hysteresis is as small as  $1^\circ\text{C}$  for single crystals, and is typically between 5 to  $10^\circ\text{C}$  for high quality thin films.

The optical properties of vanadium dioxide also change abruptly at  $T_t$ , which is attributed to the change in the band structure. Optical and infrared reflection and transmission spectra of  $\text{VO}_2$  have been taken on both bulk single crystals and thin films<sup>3,11</sup>. The optical properties of high quality thin films were found to be quite similar to bulk crystals. An absorption edge, seen only in the semiconducting phase, occurs at approximately 0.8 eV and can be taken as the energy gap<sup>11</sup>. When heated above  $T_t$ , the infrared spectra show a sudden increase in reflectivity and a decrease in transmission. Both properties are indicative of a metallic state. There is again a heating-cooling hysteresis associated with the transition, causing the transmission to begin increasing and the reflectivity to begin decreasing  $10^\circ\text{C}$  lower than  $T_t$  when the sample was cooled.



Changes in the optical properties of vanadium dioxide are extremely broadband, occurring not only in the visible and infrared regions, but also at microwave wavelengths. Vanadium dioxide exhibits a low temperature transmitting and a high temperature reflecting behavior in this region.

Vanadium dioxide has been studied extensively over the past 30 years because the transition temperature ( $T_t$ ) is the most convenient to attain, and because its optical properties change appreciably in the visible and near-IR range of the spectrum. Recently,  $\text{VO}_2$  has been studied for use as an energy-conserving coating for windows and walls. Other applications include electro- and photo-chromic devices, thermal sensors and transparent electrical conductors.

There have also been numerous studies involving the incorporation of various transition metal ions into the  $\text{VO}_2$  lattice. It was observed that the transition temperature may be raised or lowered, depending on the valence of the dopant ion. The direction of the change in the transition temperature can be correlated with the relative size of the impurity ion compared to that of the  $\text{V}^{+4}$  ion<sup>12</sup>, which has an ionic radius of 0.63 Å. Impurity ions with ionic radii smaller than  $\text{V}^{+4}$  raise the transition temperature. Conversely, impurity ions which have larger radii reduce  $T_t$ . Tungsten, molybdenum, and tantalum ions are known to decrease  $T_t$  with increasing concentration, with tungsten having the largest effect per atomic percent added<sup>6,7,13</sup>. In each case, the resistance ratio before and after the transformation decreases quickly for low dopant levels. However, large changes in the infrared transmission are observed even when the resistance ratio is small<sup>13</sup>.

## 2.2. Sol-gel processing

In the past two decades there has been considerable interest in the sol-gel deposition of single and multicomponent metal oxide coatings. The sol-gel method involves the formation of oxides from solutions of metal organic precursors, primarily alkoxides. The alkoxide precursors are converted to oxides by hydrolysis and condensations reactions. The main objective of this work was to simplify the deposition process of oxide films by exploring the use of the sol-gel method for the deposition of vanadium dioxide films. High optical quality thin films were prepared by the hydrolysis and condensation of vanadium tetraalkoxides.

Geffcken and Berger first used the sol-gel method to prepare thin metal oxide coatings in 1939<sup>14</sup>. They showed that it is possible to convert simple hydrolyzable metal compounds into layers of metal oxides. The first commercial products for optical applications, made by the sol-gel method, appeared in 1953. However, little interest was shown in sol-gel process over the following years, owing to advancements in the more popular technique of vacuum deposition of metal oxide coatings. In the sixties, Schroeder developed a further understanding of the parameters involved in sol-gel coatings<sup>15,16</sup>. In recent years, the sol-gel process has been seen as an economic alternative to vacuum coating.

The sol-gel method first involves the preparation of a colloidal suspension of metal oxide particles dispersed in a volatile solvent, known as a sol. The sol can be spread out across the substrate by a number of techniques, which will be described later. These sols readily wet clean glass, ceramic or metal substrates, and show a tendency to solidify into a rigid gel when sufficiently concentrated by solvent evaporation. The gel is then heated to give a highly pure metal oxide coating.

Sol-gel coatings have been deposited by four techniques. The techniques differ in how a thin layer of the sol is applied to the substrate. The most popular technique is dipcoating, where a substrate is submerged into the sol and slowly withdrawn. In the second process, called lowering, the substrate remains stationary while the liquid level is lowered. The third process is spincoating, in which the sol is applied to the substrate, then spun at high velocities to spread a liquid film across the surface. Spincoating is often most suitable for circular substrates. The final process is spray coating. A fine mist of the sol is sprayed onto a substrate.

The sol-gel method offers some distinct advantages over the vacuum deposition of thin metal oxide films<sup>17</sup>. The most obvious advantage is that the sol-gel process does not require a sophisticated high vacuum chamber, and the instrumentation that is required is rather simple. There is no great difference between coating small or large substrates by the sol-gel method. Coating large plates by a vacuum deposition process is extremely difficult, and requires a large expensive system. Also, the deposition rate is much higher in the sol-gel process. The sol-gel process offers flexibility in film composition in multicomponent films by adjusting the concentration of the starting compounds in solution.

This paper describes the synthesis and characterization of sol-gel grown vanadium dioxide using vanadium tetrakis(t-butoxide) as the precursor. The sol-gel method offers an attractive alternative to the vapor deposition of vanadium dioxide thin films, and to the conventional processing of powders. With this process, we also show that it is possible to make doped vanadium dioxide ( $V_{1-x}M_xO_2$  where  $M = W, Mo$ ) films easily, quickly, and inexpensively.

### 3. EXPERIMENTAL

Sol-gel processing of  $VO_2$  films is shown schematically in Figure 1. Thin films of  $VO_2$  were deposited by dipcoating glass slides from an isopropanol solution. Approximately 200 to 300 mg of  $V(Ot-Bu)_4$  were dissolved in 10 mL of isopropanol (Aldrich, HPLC Grade). Dopant ions were placed into the crystal structure of the vanadium dioxide by combining isopropanolic solutions of the vanadium tetrakis (t-butoxide) with those of tungsten or molybdenum (VI) oxytetrachloride (Alfa). Tungsten and molybdenum were chosen as dopants because of the very large effects they have on the transition temperature<sup>7,12,13</sup>. For example, in making  $VO_{0.98}Mo_{0.02}O_2$  films,  $MoOCl_4$  (11 mg) was dissolved in isopropanol (10 mL). This solution (2.7 mL) was then added to a solution (10 mL) of

$V(\text{Ot-Bu})_4$  (200 mg). Hydrolysis of the vanadium compound was catalyzed by  $\text{HCl}$ , the by-product.

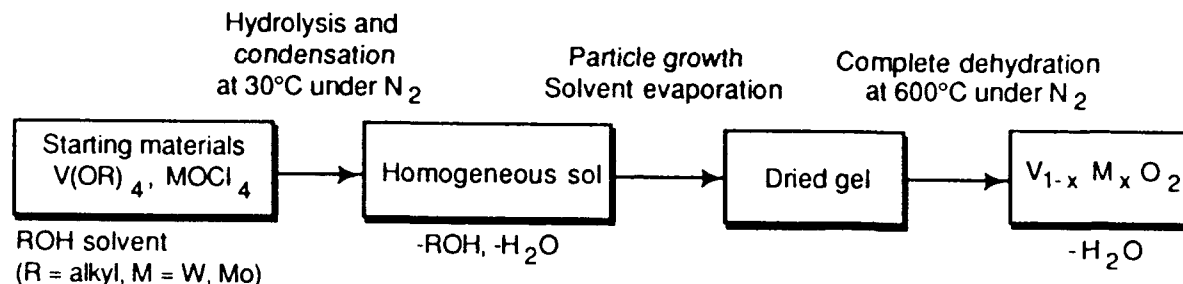
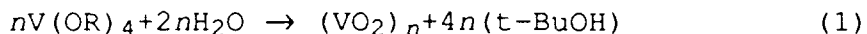


Figure 1: Preparation of  $V_{1-x}M_xO_2$  thin films by the sol-gel method.

Deposition of the films was performed under nitrogen to vent oxidation of the vanadium compound. Corning 7059 barium borosilicate glass slides were withdrawn from the solution at a typical withdrawal rate of 1 mm/sec. The overall reaction leading to  $\text{VO}_2$  formation is



where  $M = \text{MoO}$ ,  $\text{WO}$ . The molar ratio of metal ions in the film is assumed to be the same as the molar ratio of metal ions in solution from which the films were grown<sup>13</sup>. An olive green film immediately formed on both sides of the slide as it was withdrawn from the sol. Slides were often coated more than one time to build up the desired thickness. To convert the films into the  $\text{VO}_2$  phase, they were annealed at  $600^\circ\text{C}$  for 30 min under nitrogen to achieve complete dehydration, residual solvent removal, and crystallization. It was necessary to heat the films under nitrogen to prevent oxidation of the film to  $\text{V}_2\text{O}_5$ .

A pressure versus temperature equilibrium diagram for the V-O system is plotted in Figure 2<sup>18</sup>. Vanadium dioxide is easily oxidized by heating near  $600^\circ\text{C}$  in air. Conversely, it is known that  $\text{V}_2\text{O}_5$  loses oxygen on heating in high vacuum at  $600^\circ\text{C}$ <sup>19</sup>. It is clear from this figure that isobaric heating at  $10^{-19}$  torr near  $600^\circ\text{C}$  transforms  $\text{V}_2\text{O}_5 \rightarrow \text{V}_6\text{O}_{13} \rightarrow \text{VO}_2$ . Isothermal decompression at  $600^\circ\text{C}$  and lower oxygen partial pressures causes the same transformation. Note that  $\text{V}_2\text{O}_5$  melts at  $660^\circ\text{C}$ . Heating at temperatures over  $600^\circ\text{C}$  forms liquid droplets on the surface of films.

The partial pressure of oxygen required for the reduction of  $\text{V}_2\text{O}_5$  to  $\text{VO}_2$  is not as low as indicated in Figure 2. A eutectic point exists in the vanadium-oxygen system at  $600^\circ\text{C}$ . At  $600^\circ\text{C}$ , the equilibrium oxygen pressure for  $\text{VO}_2$  is  $10^{-20}$  torr. Lowering the oxygen pressure, isothermally, is necessary to reduce  $\text{VO}_2$ . The partial pressure required to do this is orders of magnitude higher than can be achieved in the best vacuum systems available. Therefore, at  $600^\circ\text{C}$  and 1 mtorr,  $\text{V}_2\text{O}_5$  is reduced while  $\text{VO}_2$  is not<sup>18</sup>. This type of reduction can also be achieved in a nitrogen atmosphere.

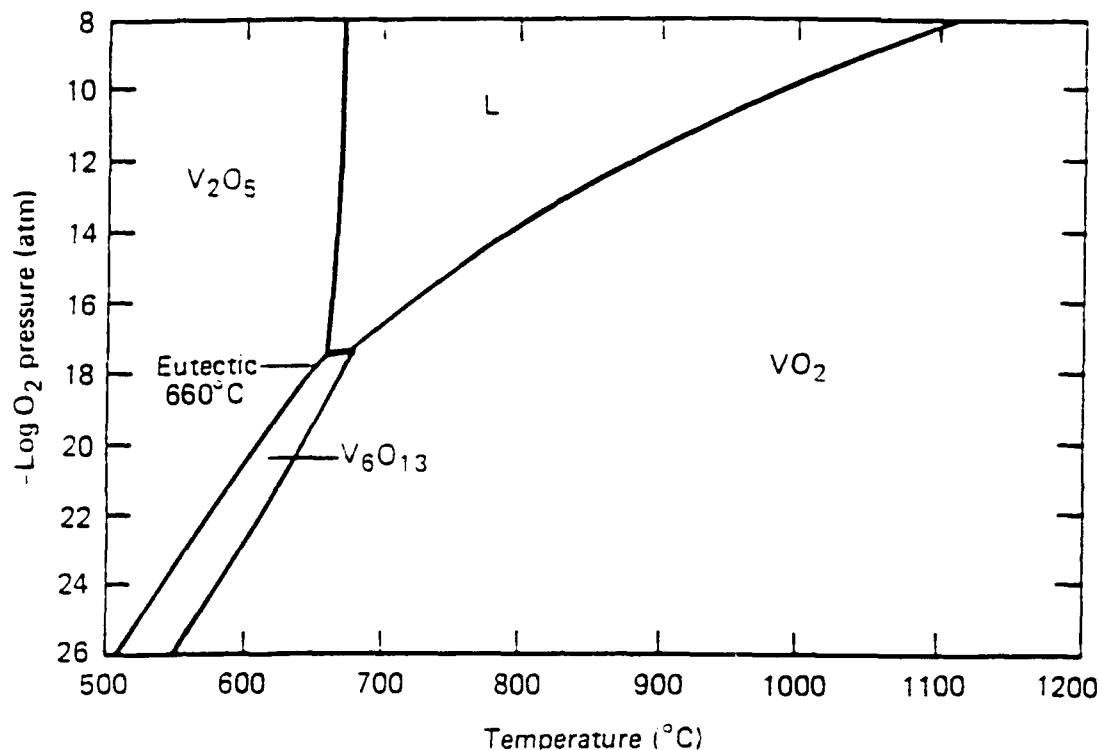


Figure 2: Pressure versus temperature phase diagram, Ref. 18.

The electrical and optical properties of the gel-derived  $\text{VO}_2$  films were measured when heated through the transition temperature. The experimental setup was the same as previously described<sup>20,21</sup>. The arrangement allowed for the concurrent measurement of the electrical resistance and optical transmission at 2400 nm of the film as a function of temperature. The data was collected and recorded by an Apple II computer interfaced to the experimental setup. Spectral transmission of these films was also scanned above and below the transition temperature. The scan range was 400 to 2600 nm. A Sloan Dektak 3030 profilometer was used to determine the film thickness. It was necessary to etch a sharp step to measure the film thickness. Samples were masked with wax, then etched with nitric acid or aqua regia. The wax was then removed with hot hexanes. Films were always etched after all electrical and optical measurements were made.

#### 4. RESULTS

Several factors influence the electrical, optical, and magnetic properties of vanadium dioxide. Maintaining the stoichiometry of vanadium dioxide is extremely important. The sharpest transition occurs in films closest to stoichiometric  $\text{VO}_2$ . Shifts in the transition temperature also occur with variations in stoichiometry<sup>22</sup>. A decrease in oxygen concentration reduces  $T_t$ , while an increase in oxygen increases  $T_t$ . Samples with mixed stoichiometric compositions exhibit much smaller changes in electrical and optical properties. This inhomogeneity also leads to an increase in the hysteresis width.

Film thickness has a similar effect on transition. A decrease in the film thickness decreases the resistance ratio, increases the width of the hysteresis loop, and causes the transition temperature to become less distinct<sup>22,23</sup>. The decrease in the resistance ratio comes entirely from an increase in the resistance of the high temperature phase, the semiconductor resistivity remaining mostly unchanged. No discontinuous step in the resistance is seen when the film thickness is between 100 to 200 Å.

The substrate on which the VO<sub>2</sub> films are deposited also has a large influence on the switching parameters. These effects are related to substrate-film interactions<sup>23,24</sup>. The largest resistance changes have been seen in films grown on sapphire, with resistance ratios of  $\sim 10^4 \Omega\text{-cm}$ . The resistance changes are somewhat less in films on glass and ceramic substrates, typically on the order of  $\sim 10^3 \Omega\text{-cm}$ .

Crystal orientation influences the phase transition in VO<sub>2</sub> films. Anomalous behavior in optical transmission has been seen in highly textured films<sup>25</sup>. Films containing crystallites with a (210) orientation in the tetragonal phase have two phase transitions for the cooling branch. This behavior is due to an overlap of two types of hysteresis with different widths. Transition curves with the sharpest transitions and narrowest hysteresis have (110) crystal orientation in the tetragonal phase.

The near-IR transmittance at 2400 nm of 1000 Å thick film on glass is plotted in Figure 3A. There was an abrupt decrease in transmission near 65°C, beginning slightly before the change in resistance occurs as expected. Large spectral switching occurred when the resistive switching was between two to three orders of magnitude. The usual hysteresis effect caused the transmission to increase 10 degrees lower on cooling. The cooling portion of the curve shows an anomalous hysteresis due to a (210) texturing of the film<sup>25</sup>.

The switched and unswitched transmittance spectra shown in Figure 3B is typical for these gel-derived vanadium dioxide films. The observed transmission changes between 400 to 2500 nm are consistent with that reported for VO<sub>2</sub><sup>8</sup>. Above  $T_t$ , the transmission is low at wavelengths longer than 1000 nm. The film thickness was measured to be 1000 Å for Figure 3B.

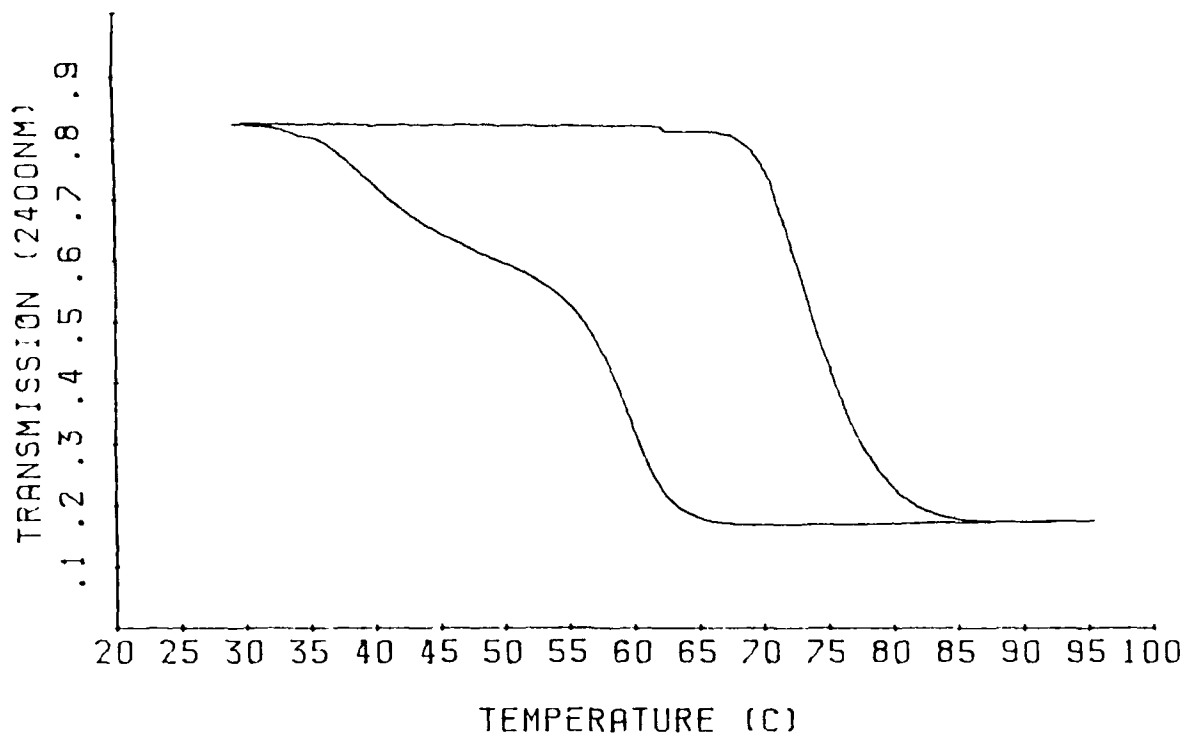


Figure 3A: Temperature dependence of optical transmission at 2400 nm for a vanadium dioxide film 1000 Å thick on glass.

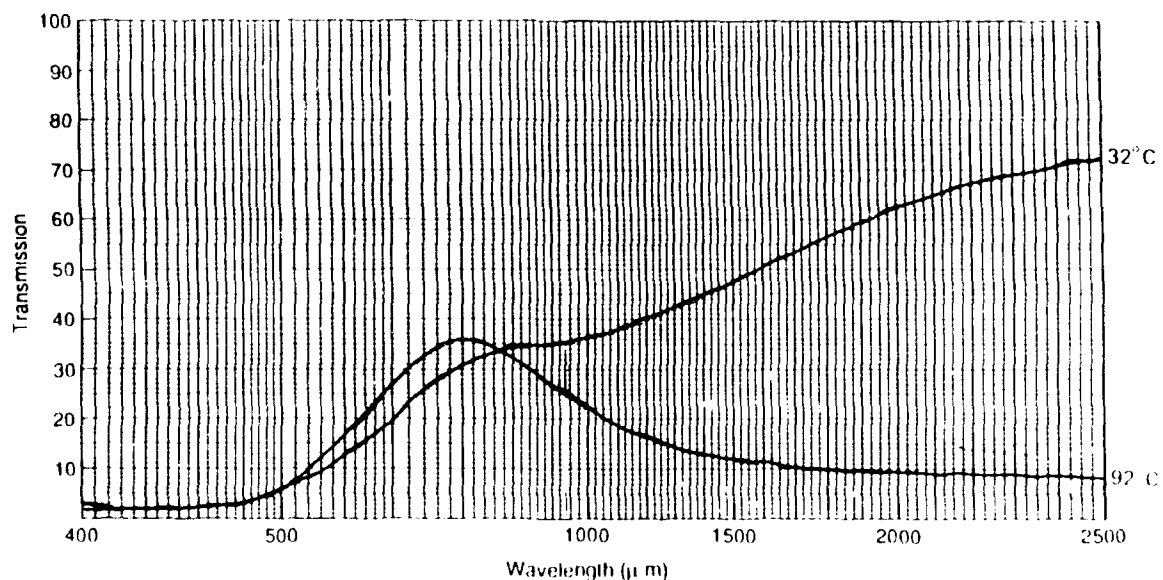


Figure 3B: Spectral transmission of a 1000 Å thick VO<sub>2</sub> film above and below the transition temperature on glass.

The optical transmission of a 250 Å thick  $V_{0.98}Mo_{0.02}O_2$  film at 2400 nm is shown in Figure 4(a). It was assumed that the concentration of the dopant in the film was the same as that in solution. The transition temperature, taken as the inflection point of the heating curve, is near 56°C. Resistance changes from pure  $VO_2$  were minimal, and therefore not included here.

The results obtained for a 500 Å thick  $V_{0.99}W_{0.01}O_2$  film are shown in Figure 4(b). The phase transition occurred over a larger range of temperatures, but the transition temperature ( $T_t = 35^\circ C$ ) was significantly lower than the undoped or molybdenum doped films. Although the dopant ions greatly influenced the transition temperature of vanadium dioxide, they had little effect on the observed spectral transmission<sup>3,13</sup>. The results were similar to other work involving doping vanadium dioxide.

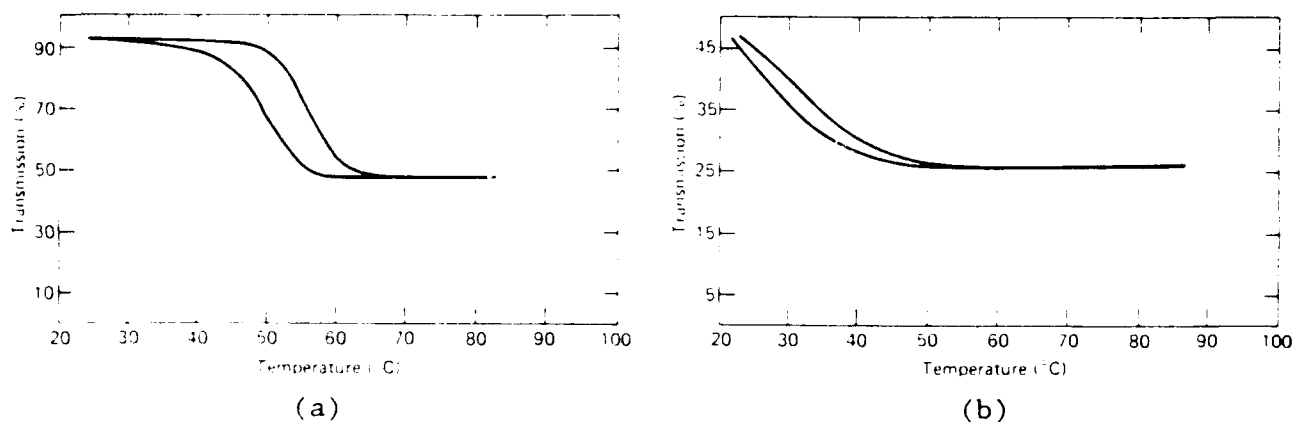


Figure 4: (a) Temperature dependence of the transmission at 2400 nm for 250 Å thick  $V_{0.98}Mo_{0.02}O_2$  film and for (b) 500 Å thick  $V_{0.99}W_{0.01}O_2$  film.

## 5. APPLICATIONS OF VANADIUM DIOXIDE

Most applications involve  $VO_2$  in thin film form. Threshold electrical switching devices have been designed which are based on the conductivity increase at the transition temperature. The phase transformation is induced by the Joule heating of the film when an external voltage is applied. The phase transition can be induced by heating vanadium dioxide with visible light, infrared and microwave radiation, or an electron beam<sup>26</sup>. The optical properties of  $VO_2$  provide a high-resolution, two-dimensional format for switching, recording and processing of optical signals, or for use as an infrared protective device against laser radiation.

A great deal of interest has also arisen concerning applications using the thermochromic properties of vanadium dioxide<sup>27,28</sup>. The

material passively switches between a heat-transmitting and a heat-reflecting state. Tungsten doping vanadium dioxide at a level of two percent produces a material that switches at the optimum temperature for energy control in certain buildings ( $\sim 15^{\circ}\text{C}$  or  $60^{\circ}\text{F}$ ). W-doped films have been shown to reject  $\sim 70\%$  of the total solar and  $50\%$  of the visible radiation when it switches. This material is currently being developed for coating building windows and as pigments for wall coatings.

Other applications of vanadium dioxide include electro- and photochromic devices, and thermal sensors. The relationship between electrical resistivity and strain in thin vanadium dioxide films has been investigated for use as high-sensitivity strain gauges<sup>29</sup>.

## 6. CONCLUSION

Doped and undoped vanadium dioxide thin films were deposited on glass slides by dipcoating from an isopropanol solution of vanadium tetrakis (t-butoxide). A new method was discovered for the synthesis of the vanadium precursor. The starting materials were purified by standard chemical procedures which helped to improve the quality of the final product. The electrical and optical behavior of these gel-derived films proved to be comparable to that observed in other thin film deposition techniques.

The sol-gel process provides a versatile way of making doped vanadium dioxide devices. Doping was achieved by mixing metal oxychlorides with the vanadium precursor in solution. This technique permits mixing of the constituents at the molecular level, which leads to a more homogeneous product. It has been demonstrated that the addition of tungsten and molybdenum depresses the switching temperature with increasing concentration.

Potential advantages of this new approach for producing vanadium dioxide thin films via the sol-gel process are numerous. The process does not require an expensive vacuum system to grow films, and the instrumentation that is required is rather simple. Large surface area may be coated with a homogeneous thickness, and in some cases both sides may be coated at the same time. The sol-gel process affords the possibility of coating substrates which have a variety of sizes, shapes, and thicknesses. In many areas, the sol-gel method is an attractive alternative to the vapor deposition of vanadium dioxide.

## 7. ACKNOWLEDGMENT

This work was supported by the U.S. Navy under Contract No. N00039-87-C-5301.



## 8. REFERENCES

1. F. J. Morin, Phys. Rev. Lett., **3** (1959) 34.
2. D. Adler, Rev. Mod. Phys., **40** (1968) 714.
3. H. W. Verleur, A. S. Barker, Jr., and C. N. Berglund, Phys. Rev. Lett., **172** (1968) 788.
4. C. N. Berglund and H. J. Guggenheim, Phys. Rev., **185** (1969) 1022.
5. F. A. Chudnovskii, Sov. Phys. Tech. Phys., **20** (1976) 999.
6. G. V. Jorgenson and J. C. Lee, Solar Energy Materials, **14** (1986) 205.
7. J. B. Goodenough, J. Solid State Chem., **3** (1971) 490.
8. C. H. Griffiths and H. K. Eastwood, J. Appl. Phys., **45** (1974) 2201.
9. L. A. Ladd and W. Paul, Solid State Commun., **7** (1969) 425.
10. G. A. Rozgonyi and D. H. Hensler, J. Vac. Sci. Tech., **5** (1968) 194.
11. A. S. Barker, Jr., H. W. Verleur, and H. J. Guggenheim, Phys. Rev. Lett., **17** (1966) 1286.
12. J. B. MacChesney and H. J. Guggenheim, J. Phys. Chem. Solids, **30** (1969) 225.
13. C. B. Greenberg, Thin Solid Films, **110** (1983) 73.
14. W. Geffcken and E. Baerger, Jenaer Glaswerk Schott and Gen., Jena, G.D.R., G.D.R. Patent 736,411 (1939).
15. H. Schroeder, Opt. Acta, **9** (1962) 249.
16. H. Schroeder, Phys. Thin Films, **5** (1969) 87.
17. H. Dislich and E. Hussmann, Thin Solid Films, **77** (1981) 129.
18. G. A. Nyberg, Ph.D Thesis, Cornell Univ., (1985).
19. J. B. MacChesney, J. F. Potter, and H. J. Guggenheim, J. Am. Ceram. Soc., **51** (1968) 176.
20. T. E. Phillips, R. A. Murphy, and T. O. Poehler, Mat. Res. Bull., **22** (1987) 1113.
21. K. R. Speck, H. S-W. Hu, M. E. Sherwin, and R. S. Potember, Thin Solid Films, **165** (1988) 317-322.
22. A. R. Begishev, A. S. Ignat'ev, V. V. Kapaev, and V. G. Mokerov, Sov. Phys. Tech. Phys., **24** (1979) 1263.
23. R. L. Remke, R. M. Walser, and R. W. Bene, Thin Solid Films, **61** (1979) 73.
24. E. V. Babkin, A. A. Charyev, A. P. Dolgarev and H. O. Urinov, Thin Solid Films, **150** (1987) 11.
25. W. Haidinger and D. Gross, Thin Solid Films, **12** (1972) 433.
26. L. A. Beresneva, L. L. Vasil'eva, S. F. Devyatova, V. G. Pan'kin, K. K. Svitashv, and N. L. Shvarts, Sov. Tech. Phys. Lett., **3** (1977) 170.
27. G. V. Jorgenson and J. C. Lee, Solar Energy Materials, **14** (1986) 205.
28. S. M. Babalanam, T. S. Eriksson, G. A. Niklasson, and C. G. Granquist, Solar Energy Materials, **16** (1987) 347.
29. M. O. Hakim, S. M. Babalanam, and C. G. Granquist, Thin Solid Films, **158** (1988) 149.



## Characterization of an all solid-state electrochromic window

Juan Carlos López Tonazzi  
Bruno Valla  
Marcelo A. Macedo  
Paul Baudry\*  
Michel A. Aegerter

University of São Paulo, Instituto de Física e Química  
de São Carlos, 13560 São Carlos, SP, Brazil

Ana C. Martins Rodrigues

Federal University of São Carlos, Departamento de  
Materiais, 13560 São Carlos, SP, Brazil

Luis O. Bulhões

Federal University of São Carlos, Departamento de  
Química, 13560 São Carlos, SP, Brazil

92-11437

ABSTRACT

Sol-gel cerium - titanium oxide layers present potential application as transparent counter-electrode (ion storage layer) in electrochromic windows and mirrors using lithium conducting electrolyte and  $\text{WO}_3$  electrochromic coating. The precursor sol, prepared by mixing  $\text{Ti}(\text{OPr}^1)_4$  and  $\text{Ce}(\text{NO}_3)_6 \cdot (\text{NH}_4)_2$  in ethanol, is initially dark red and becomes transparent after a few days aging indicating the presence of  $\text{Ce}^{3+}$  complexes. The layers have been obtained by dip coating technique and heat treated at  $450^\circ\text{C}$  during 15 minutes. They have been characterized by XRD, SIMS, optical absorption and electrochemical techniques; it is shown that the electrochemical reaction corresponds to a reversible insertion-extraction of lithium ions within a  $\text{TiO}_2$  amorphous film containing small  $\text{CeO}_2$  crystallites. At low sweep frequencies the process is controlled by a diffusion mechanism ( $\tilde{D}_{\text{Li}} \approx 6.4 \cdot 10^{-12} \text{cm}^2/\text{s}$  at  $25^\circ\text{C}$ ). Characterizations of an all solid state electrochromic window/glass/ITO/ $\text{WO}_3$ /POE-Li N  $(\text{SO}_2 \text{CF}_3)_2$  /  $\text{TiO}_2$  -  $\text{CeO}_2$  / ITO / glass / are also presented.

1. INTRODUCTION

Considerable attention is being directed to use sol-gel methods for the production of single, multilayer coatings as these techniques offer outstanding opportunities over other methods of deposition such as CVD, sputtering or vacuum evaporation<sup>1</sup>. Investigations have also been very active in the field of chromogenics to develop and particularly improve electrochromic devices such as all solid state energy efficient windows (smart windows) and reflecting mirrors<sup>2</sup>. These devices have the properties to alter their transmissive or reflective properties by application of an electric field or current and can therefore regulate the heat transfer and the luminous radiation.

Figure 1 shows a typical cross-section of a transmissive device (smart window). It is made of five layers sandwiched between two glass substrates. There are two transparent electrical conductors required for setting up a distributed electric field, an electrochromic layer, an ionic conductor (electrolyte) and an ion storage layer (counter electrode). When a small current is passed through the cell the active electrochromic layer changes its transmittance continuously over a wide range

\*Present address : Electricité de France EDF - Paris

(typically 70 - 10%). The electrochromic coating typically switches in a time period of seconds to less than a minute and can maintain its properties when the power is turned off (memory effect). The process is fully reversible and the original bleached state is obtained by reversing the applied voltage.

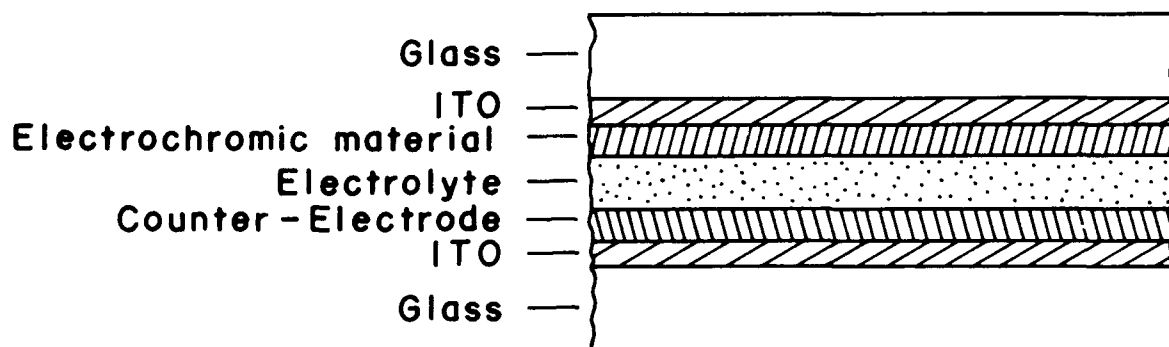
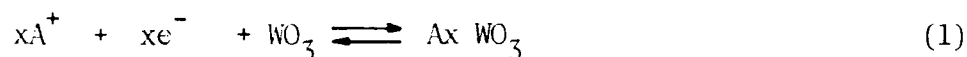


Fig. 1 - Schematic cross-section of a solid state transmissive electrochromic window.

The glass conducting substrates do not present any problem and are readily available on the market. The best electronic conductors are  $\text{In}_2\text{O}_3 - \text{SnO}_2$  (ITO) coatings on glass substrates which present today satisfactory electronic conduction (down to  $10 \Omega/\text{sq}$ ) and optical transparency for the realization of small devices<sup>3</sup>. However, sheet resistance of about  $1 \Omega/\text{sq}$  will be needed for large scale electrodes ( $1 \times 1 \text{ m}^2$ ).

Several materials exhibit electrochromic properties. Among them the metal transition oxides such as tungsten and molybdenum trioxides ( $\text{WO}_3$ ,  $\text{MoO}_3$ ) are modified by the electrochemical insertion of alkali ions or protons. The corresponding reaction is written below for  $\text{WO}_3$ :



where  $\text{A}^+ = \text{H}^+, \text{Li}^+$

The net result of the insertion reaction is the reduction of the transparent  $\text{WO}_3$  host material and its transformation into a blue colored tungsten bronze ( $\text{Ax WO}_3$  or  $\text{W}_{1-x}^{6+}\text{O}_{3-x}\text{W}_x^{5+}(\text{O})_x$ ); its coloration is due to the presence of a large absorption band in the visible and near infrared region ( $E_{\text{max}} \approx 1.4 \text{ eV}$ ) attributed to electronic transitions from the reduced tungsten ions states  $\text{W}^{5+}$  toward the conduction band<sup>4,5</sup>. Both proton and lithium insertion are possible. Although the chemical diffusion coefficient of  $\text{H}^+$  in  $\text{WO}_3$  is higher than that of  $\text{Li}^+$ ,<sup>6</sup> a complete transmissive or reflective device is easier to realize with lithium conductors than with protonic ones as hydrogen gassing and layer corrosion in acid media limit the life of the protonic based devices.

Many electrolytes have been proposed and tested for the realization of these devices. The advantages of polymeric ion conductor over liquid ones have been recently recognized<sup>7,8</sup>. Due to their elastomeric properties they provide a good electrolyte/electrode contact, do not present problems of leakage and are easily elaborated in thin film forms. Among them PEO (polyethylene oxide) or PPO (polypropylene oxide) complexed with alkali salts ( $\text{Li ClO}_4$ ,  $\text{Li CF}_3\text{SO}_3$  or  $\text{Li N}(\text{SO}_2\text{CF}_3)_2$ ) exhibit

$\text{Li}^+$  conductivities in the range  $10^{-5}$  -  $10^{-7}$   $\text{Scm}^{-1}$  at room temperature suitable for fast switching time.

The electrochromic devices also require the presence of a counter electrode or ion storage layer. Several oxide materials have been proposed recently but none of them exhibit ideal properties of transparency, reversibility and high kinetics of the electrochemical reaction for lithium ions.  $\text{V}_2\text{O}_5$  is fast enough and reversible but its transmission in the bleached state is too low<sup>9,10</sup>.  $\text{Ir}_2\text{O}_3$  retains a good transparency but the insertion of lithium is poor and the reaction is partially irreversible<sup>11,12</sup>.  $\text{CeO}_2$  exhibits a good reversibility, is colourless in both oxidized and reduced states but shows a low reaction kinetics<sup>13</sup>. Recently we have proposed<sup>10</sup> the use of  $\text{TiO}_2$  -  $\text{CeO}_2$  layers and shown<sup>14</sup> that this new structure allows a better  $\text{Li}^+$  insertion kinetics than pure  $\text{CeO}_2$ . These films were deposited on ITO coated glasses by sol-gel dip coating technique.

In this paper we first describe in section 2 the techniques used to prepare the electrochromic, electrolyte and ion storage layers. In section 3 we discuss essentially the properties of the precursor sol and the sol-gel  $\text{TiO}_2$  -  $\text{CeO}_2$  coating which have been characterized by X-ray diffraction (XRD), secondary ions mass spectroscopy (SIMS), optical transmission and electrochemical techniques. In section 4 the basic properties of an all solid state smart window/glass/ $\text{WO}_3$ /POE-Li N( $\text{SO}_2\text{CF}_3$ )<sub>2</sub>/ $\text{TiO}_2$  -  $\text{CeO}_2$  /ITO/glass are reported and finally the conclusions are given in section 5.

## 2. MATERIALS

We describe in this section the procedures used for making thin coatings based on  $\text{WO}_3$  and  $\text{TiO}_2$  -  $\text{CeO}_2$ . These layers were backed by a 1.1mm thick glass substrates precoated with transparent and conducting ITO (Baltracon 220 Balzers). We also report on the procedure used for the preparation and deposition of the polymer electrolyte.

### 2.1. Electrochromic Coating

$\text{WO}_3$  layers were deposited from the corresponding oxide powder by vacuum evaporation onto 400nm thick indium tin oxide (ITO) coated glasses. The  $\text{WO}_3$  films were amorphous to X-ray diffraction and their thickness, measured by a Talystep, was of the order of 200 - 300nm. The films have been characterized electrochemically as deposited without any heat treatment<sup>10</sup>. The determination of the chemical diffusion coefficient for lithium  $\bar{D} = 2.5 \cdot 10^{-11}$   $\text{cm}^2/\text{s}$  at 25°C has been determined by analysing the low frequency response of the impedance data.

### 2.2. Electrolyte

The polymer electrolyte was polyethylene oxide- LiX complex with  $X = \text{ClO}_4$  or  $\text{N}(\text{SO}_2\text{CF}_3)_2$ . They were prepared by dissolving the PEO powder (M.W. =  $5 \cdot 10^6$ ) and the lithium salt in acetonitrile with an O:Li atomic ratio of 8:1 giving rise to the highest ionic conductivity in these systems<sup>15,16</sup>. The viscous and transparent complex was doctor-bladed on a teflon substrate; the solvent was then evaporated at 70°C during 24 hours. The films having a thickness of 50 to 200 nm were kept in a dry box ( $< 1\text{ppm H}_2\text{O}$ ) in order to eliminate any residual solvent or moisture.

### 2.3. Sol-Gel storage coating (counter-electrode)

$\text{TiO}_2$  -  $\text{CeO}_2$  films with various Ti/Ce ratios have been synthesized by the sol-gel

process. The precursor sol was prepared by dissolving  $\text{Ce}(\text{NH}_4)_2(\text{NO}_3)_6$  in ethanol to which was added tetraisopropyl orthotitanate  $\text{Ti}(\text{O-iso-C}_3\text{H}_7)_4$ . The concentration of the cerium salt in ethanol never exceeded 0,25M (limit of solubility). No special care was taken to limit the presence of water in the solution so that the cerium salt acts as an acid which reduces the pH and prevents the  $\text{Ti}(\text{OPr})_4$  precipitation. The layers were deposited by dip coating technique on carefully cleaned and dried ITO coated glasses (Baltracon 220) at a withdrawn speed of the order of 10cm/min. The films were let to dry at room temperature for 15 minutes and then have been partially densified by heat treatment in air at 450°C for 15min. Their thickness was typically 60 to 80nm. The whole procedure was repeated to obtain thicker layers.

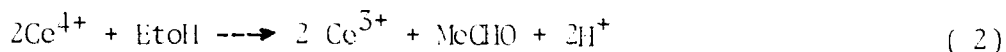
### 5. PROPERTIES OF THE $\text{TiO}_2$ - $\text{CeO}_2$ ION STORAGE LAYER

The characterization of the  $\text{WO}_3$  electrochromic layer and of the polymer electrolyte has been already published elsewhere<sup>10,17</sup>. In this chapter we shall therefore only report on the characterization of the new  $\text{TiO}_2$  -  $\text{CeO}_2$  sol-gel ion storage layer using techniques such as optical spectroscopy, X-ray diffraction (XRD), secondary ion mass spectrometry (SIMS), cyclic voltammetry and impedance spectroscopy.

#### 5.1. Physico-Chemical Study of the Sol

The cerium-titanium layers which give the best Li insertion-extraction behavior are those prepared from an aged sol with a ratio  $\text{Ce}/\text{Ti} = 1$ . These sols are initially clear and dark redish and turn to pale yellow after 6 - 7 days. The gelification that occurs 1 or 2 days after this change of color begins with a phenomenon of flocculation already observed by Kamiya et al<sup>18</sup>. The solution is then milky white. In a parallel study, we observed that the solution Ce salt/ $\text{EtOH}$  is initially clear and dark redish and becomes colorless in about 6 days. This period of time depends on the presence of water which accelerates the clarification. Figure 2 shows the change in optical transmission in the visible region of a 1mm thick Ce salt - ethanol solution 0,25 M as a function of aging time.

E.M.F. measurement of the electrochemical cell  $\text{Pt}/0,25\text{M Ce}(\text{NO}_3)_6(\text{NH}_4)_2 - \text{EtOH} // \text{H}^+ - \text{Cl}^- // \text{AgCl}/\text{Ag}$  shows also a decrease of about 700mV during this evolution. The results are in agreement with Ardon<sup>19</sup> who showed that this behavior corresponds to a reduction reaction of  $\text{Ce}^{4+}$  into  $\text{Ce}^{3+}$  according to :



The reduction of the  $\text{Ce}^{4+}$  is preceded by the formation of a dark redish complex  $\text{Ce}^{4+}/\text{EtOH}$ <sup>20</sup>. We can therefore consider that the color change of the sol prepared for the dip process is due to the reduction of Ce. Thus, the starting solution contains  $\text{Ce}^{3+}$  instead of  $\text{Ce}^{4+}$  as initially presumed. However the use of  $\text{CeCl}_3$  instead of  $\text{Ce}(\text{NO}_3)_6(\text{NH}_4)_2$  gives coatings with bad electrochemical characteristics<sup>14</sup>. This different behavior is presently not understood.

#### 5.2. X-Ray Diffraction

X-ray were carried out on powders obtained from  $\text{TiO}_2$  -  $\text{CeO}_2$  gels and thin oxide films. The powder was prepared by letting the sol to gel slowly at room temperature until solidification, and followed by a heat treatment in open furnace at different temperatures (230 - 550°C). In this temperature range no difference was observed in the X-ray spectra. Although the gel has been obtained with a sol containing  $\text{Ce}^{3+}$  complexes the X-ray patterns show the presence of crystalline  $\text{CeO}_2$  and small

peaks belonging to the  $\text{TiO}_2$  anatase structure (Figure 3).

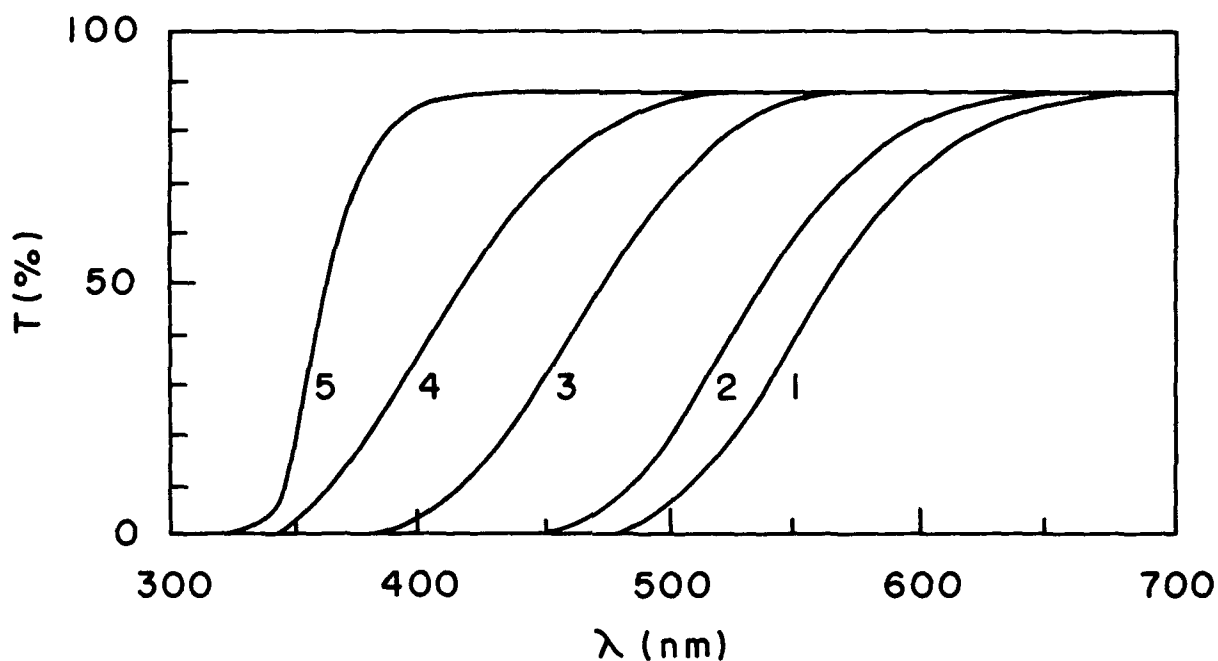
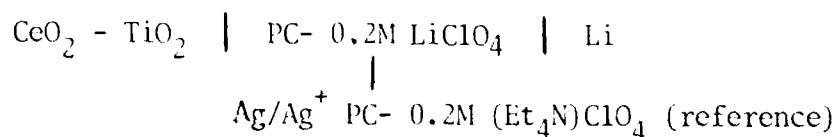


Fig. 2 - Optical transmission of a 1mm thick 0,25M  $\text{Ce}(\text{NH}_4)_2(\text{NO}_3)_6$ - ethanol sol as a function of aging time 1, 2, 3, 4 and 5 days.

The thin films obtained after three dips and heat treated at  $450^\circ\text{C}$  during 15 minutes have a thickness of about 300nm. They are essentially amorphous under X-ray. Nevertheless, the observation of the main peaks of  $\text{CeO}_2$  (Fig. 3b) indicates the presence of very small crystallites. It is worthwhile to mention that the presence of  $\text{CeO}_2$  proves that the cerium has been reoxidized during the thermal treatment.

### 3.3. Electrochemical Characterization

Cyclic voltammetry was employed for surveying the redox process at the  $\text{TiO}_2$ - $\text{CeO}_2$  film. The automated impedance system consisted of a potentiostat/galvanostat EG&G model 273, and a lock-in analyzer which were both controlled by a computer. Impedance spectra were generated over the frequency range of 10kHz to 0.01Hz using a 10mV peak to peak a.c. excitation. a.c. impedance and voltammetry measurements were made at room temperature and performed in a dry box using a three electrodes cell



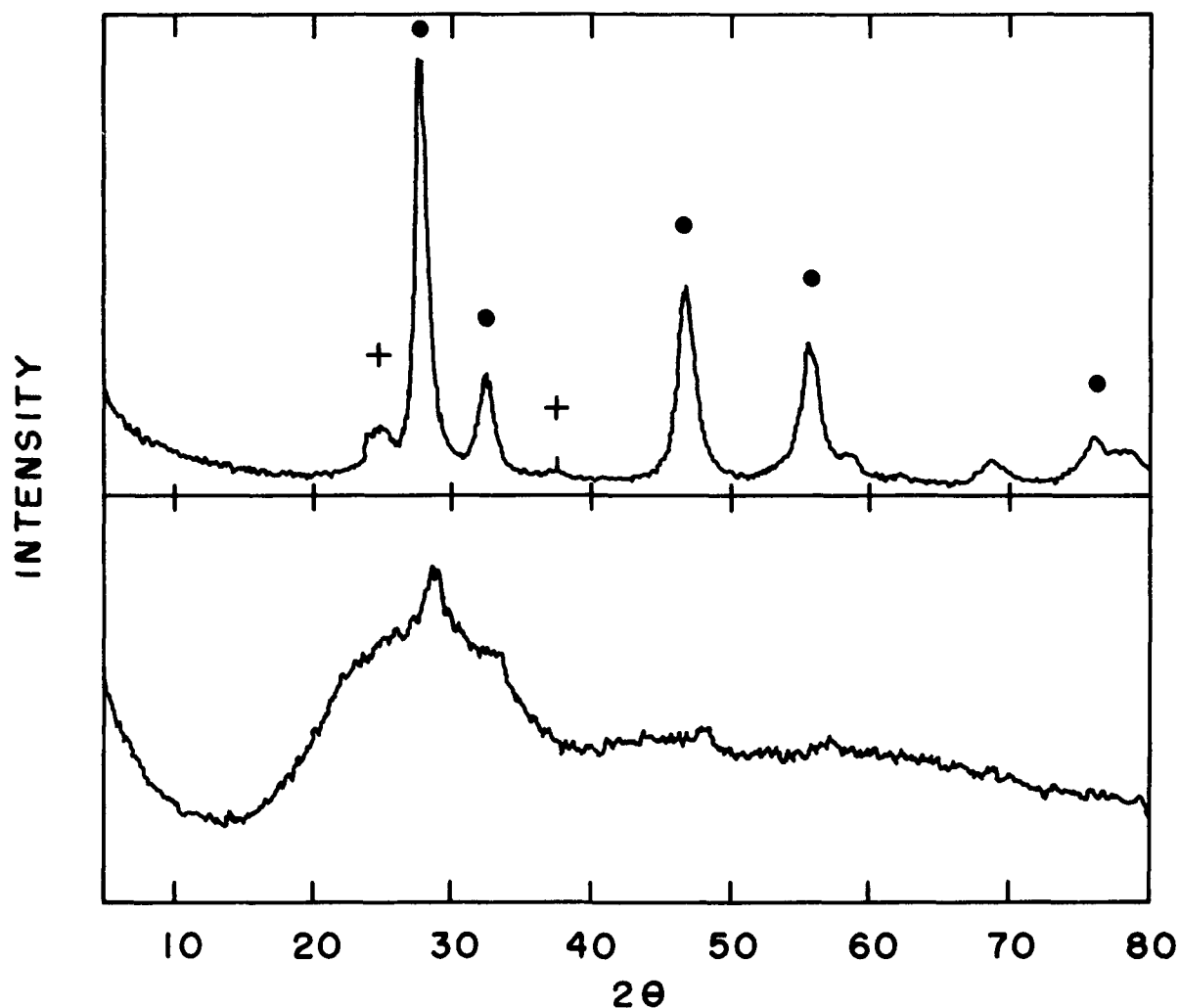


Fig. 3 - X-ray diffractogram of a)  $\text{TiO}_2$  -  $\text{CeO}_2$  powder heat at  $230^\circ\text{C}$  during 14 h. The peaks marked (o) corresponds to  $\text{CeO}_2$  and those marked (+) to the  $\text{TiO}_2$  anatase structure. b)  $\text{TiO}_2$ - $\text{CeO}_2$  thin film of about 300nm thickness treated at  $450^\circ\text{C}$  during 15 minutes.

All reagents used were of analytical grade. Anhydrous lithium perchlorate was dried under vacuum at  $150^\circ\text{C}$  for 24h before use. Propylene carbonate (PC) was purified by distillation. Figure 4 shows typical voltammogram of  $\text{TiO}_2$  -  $\text{CeO}_2$  electrode heat treated at  $450^\circ\text{C}$  during 15 minutes. No difference has been observed for coatings obtained with one or three dips. The cathodic and anodic peaks are characteristics of a reversible insertion process of lithium ions in the electrode material. The stability of these electrodes under repeated charge and discharge conditions has been tested up to 100 cycles and no modification has been observed.

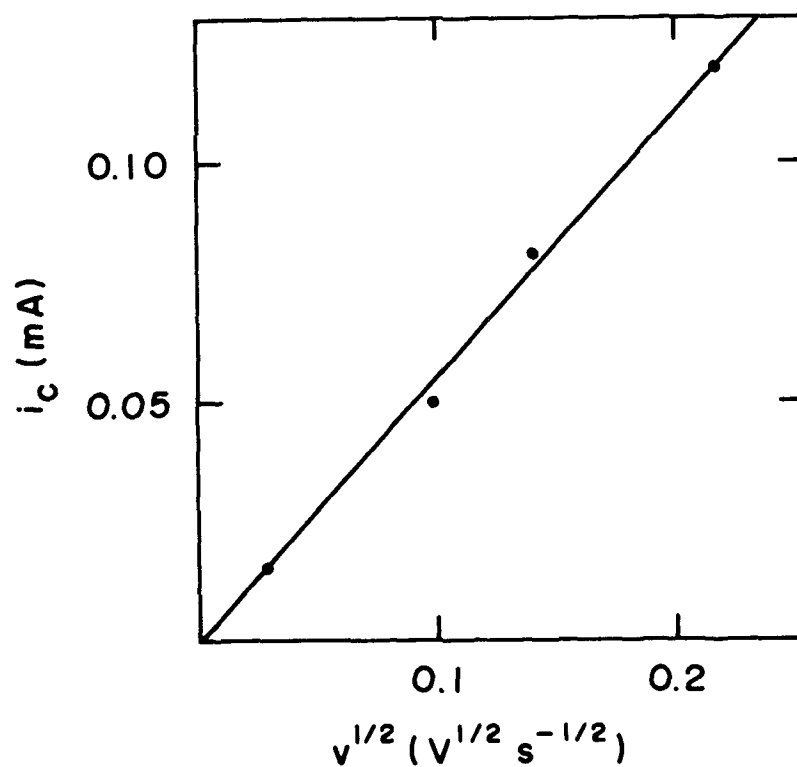
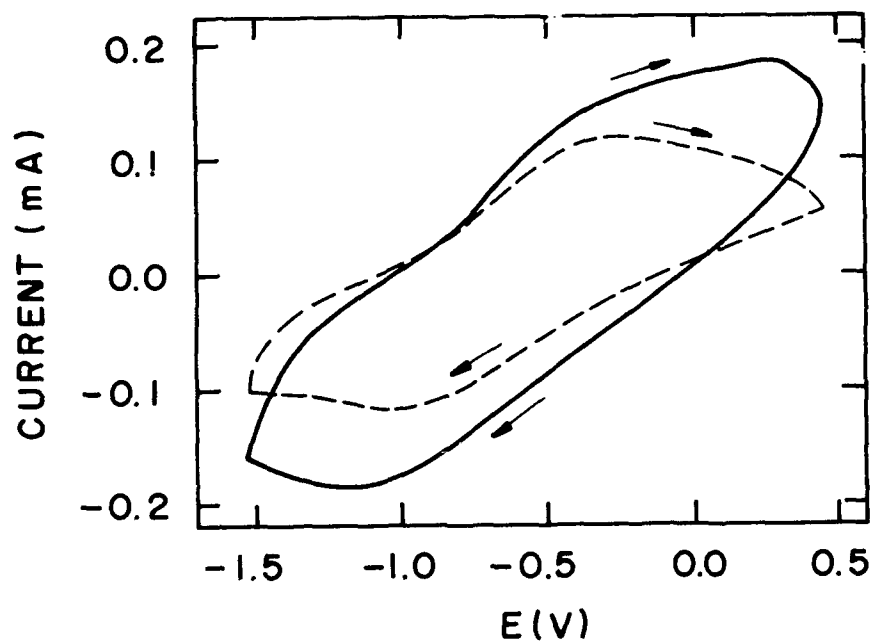


Fig. 4 - a) Cyclic voltammogram of a  $\text{TiO}_2$  -  $\text{CeO}_2$  electrode in PC - 0,2M  $\text{LiClO}_4$  measured at 50mV/s (----) and 100mV/s (—) sweep rate.  
 b) Variation of the cathodic peak current  $i_c$  of the same electrode as a function of the square root of the sweep rate.



Fig. 4b shows the variation of the cathodic peak current as a function of the square root of the sweep rate. The variation was found linear, characteristic of a process which is controlled by the solid state diffusion of  $\text{Li}^+$  ions through the film<sup>21</sup>. Impedance data are shown in figure 5. The straight line observed below 10Hz and at equilibrium potential indicate that the rate of lithium injection is diffusion controlled.

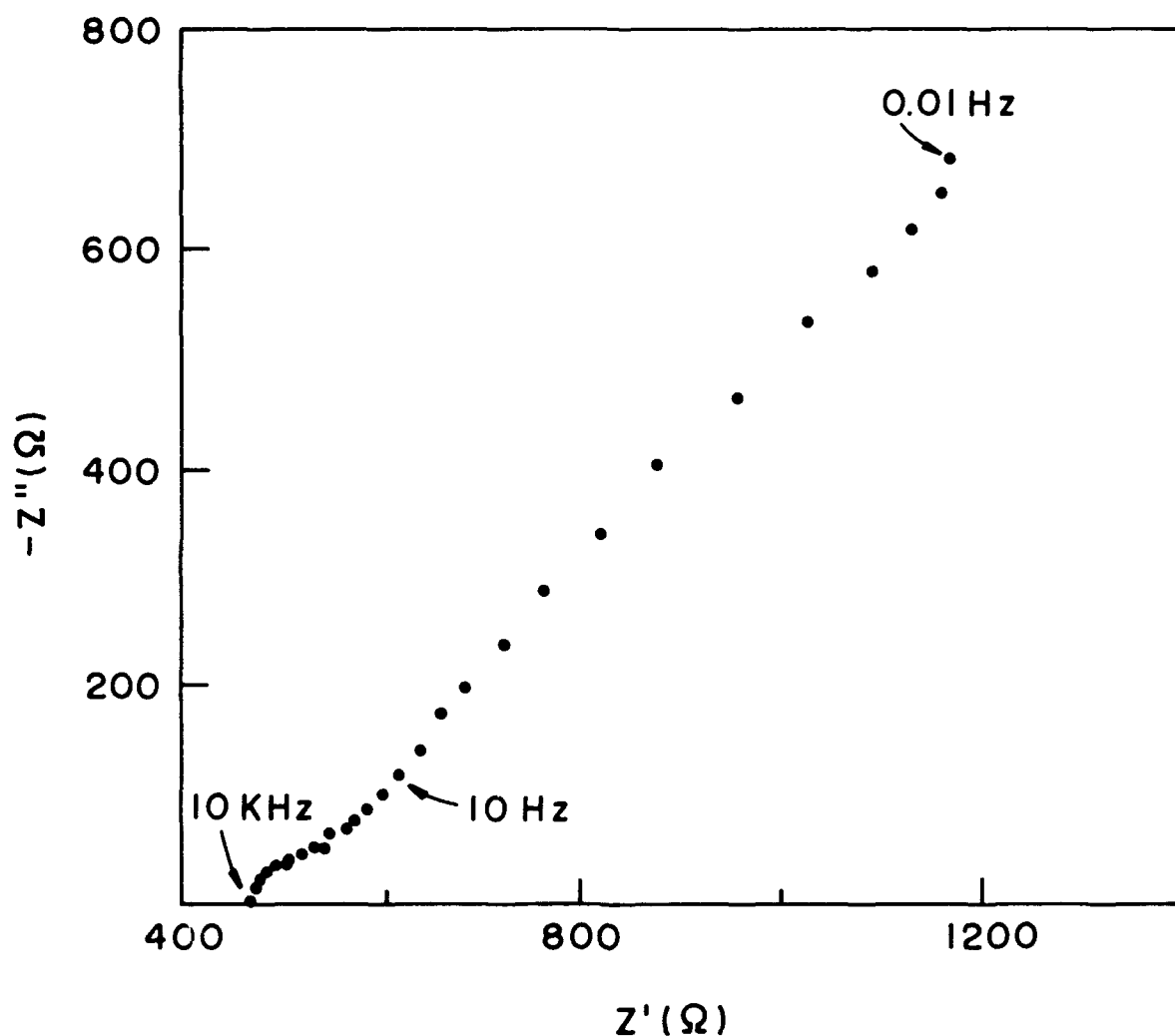


Fig. 5 - Complex impedance representation of a  $\text{TiO}_2 - \text{CeO}_2$  electrode in PC - 0.2M  $\text{LiClO}_4$ ,  $E = 0.5\text{V}$  vs  $\text{Ag}/\text{Ag}^+$ .

The ac response has been analysed by the Randles equivalent circuit<sup>22</sup> shown on the left side of figure 6. The circuit elements are the charge transfer resistance  $\theta$ , the double layer capacitance  $C_{DL}$ , the electrolyte resistance  $R_l$  and a Warburg

element  $Z_w$ . The left side of the figure shows the frequency response of the circuit and is to be compared with the experimental results of figure 5.

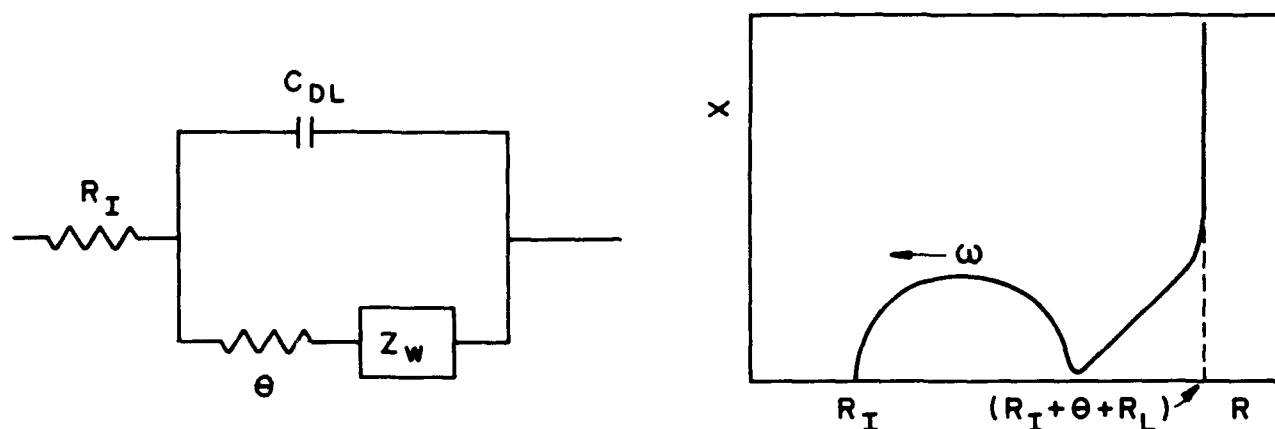


Fig. 6 - a) Equivalent circuit  
b) Frequency response of the equivalent circuit (from 22)

The value of the Li diffusion coefficient were obtained either from the straight line region or from the low frequency limiting behavior (vertical line in complex plane not shown in the figure). Both real and imaginary parts of the impedance are proportional to  $\omega^{1/2}$  between 10Hz and 1 Hz. The diffusion coefficient was calculated using equation<sup>23</sup> :

$$\tilde{D} = (V_m/2FS)^2 (dE/dy)^2 (1/2A^2) \quad (3)$$

where  $V_m$  is the molar volume,  $S$  the surface area of the electrode,  $A$  the slope of  $Z''$  vs  $\omega^{1/2}$ ,  $F$  is the Faraday constant and  $dE/dy$  is the slope of the coulometric titration curve at a given insertion rate. This value can also be determined from the imaginary part of the impedance diagram at very low frequency (see figure 6b) where

$$R_L = \frac{V_m}{2FS} \left( \frac{dE}{dy} \right) \frac{1}{5\tilde{D}} \quad (4)$$

The value of the molar volume used was that of crystalline  $\text{CeO}_2$ . For the experimental conditions represented in figure 6, for a film with a thickness  $l = 60\text{nm}$  and for  $E = 0.5\text{V}$  vs  $\text{Ag}/\text{Ag}^+$ , we obtain :

$$\tilde{D} = 6.4 \cdot 10^{-12} \text{cm}^2/\text{s} \quad (5)$$

This value is comparable with those already obtained in  $\text{WO}_3$  film<sup>23</sup>.

Figure 7 shows a potentiostatic cycling performed on the  $\text{TiO}_2$  -  $\text{CeO}_2$  electrode between  $-1.8 \text{ V/Ag}$  and  $+0.5 \text{ V/Ag}$ . After 30 cycles we see that the loss in the charge passing through the cell is extremely low. This result confirms the voltammetric measurements.

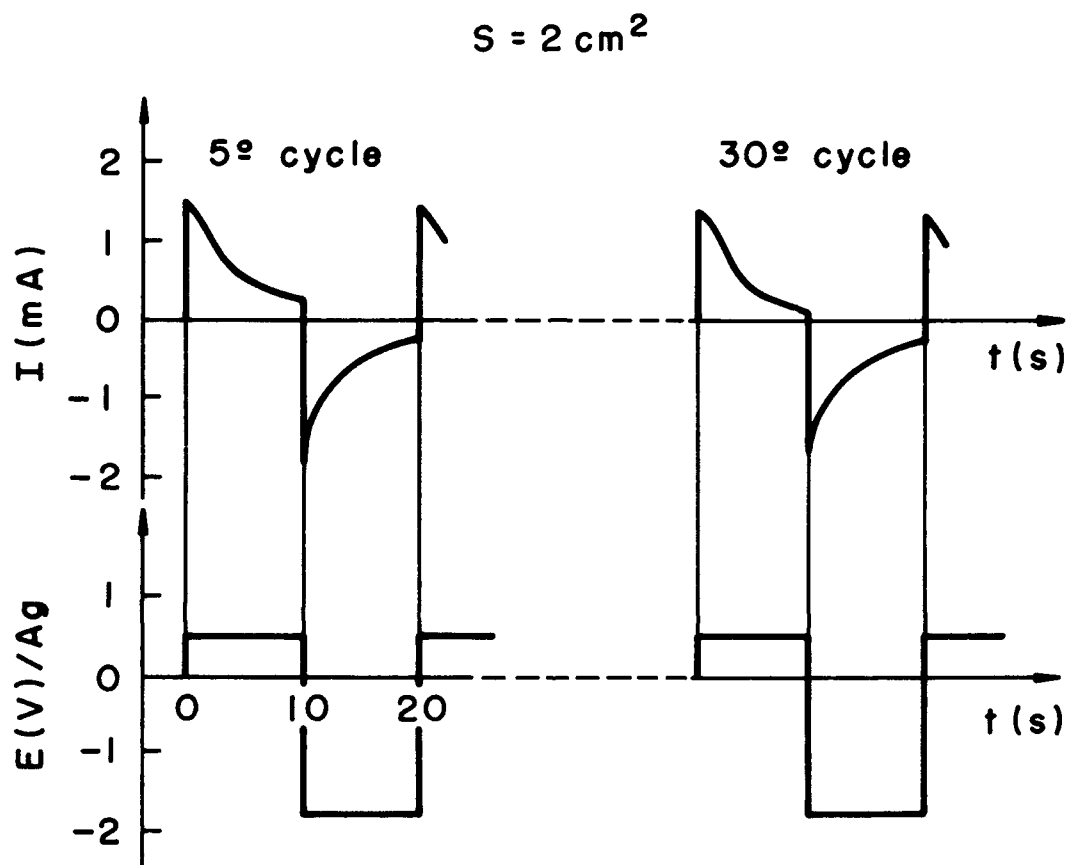


Fig.7 - Potentiostatic cycling of a three dip  $\text{TiO}_2$  -  $\text{CeO}_2$  electrode ( $\text{Ti/Ce} = 1$ ) in a  $0.2\text{M}$  propylene carbonate -  $\text{LiClO}_4$ .

#### 3.4. SIMS Characterization

SIMS profiles have been obtained at the Center for Microanalysis of Materials, University of Illinois at Urbana Champaign using a Camera IMS 3f instrument<sup>24</sup>. Figure 8 shows the profiles of Ti, Ce, Li, Na, K, O, Si, Sn<sup>118</sup> and In for a two dip layer  $\text{TiO}_2$  -  $\text{CeO}_2$  film deposited on an ITO coating and heat treated at  $450^\circ \text{C}$  for 15 minutes. Lithium was electrochemically inserted into the oxide film. A thin gold layer was also deposited on the top surface to eliminate the ion beam charging

effects. As no standard was available the height of each curve cannot be related to the elements concentration. We see that the concentration of these elements is constant throughout the layer and that diffusion of Sn and In of the ITO coating does not affect the composition of the ion storage layer. The figure 8 also proves that  $\text{Li}^+$  ions have been inserted into the layer and that its concentration is homogeneously distributed.

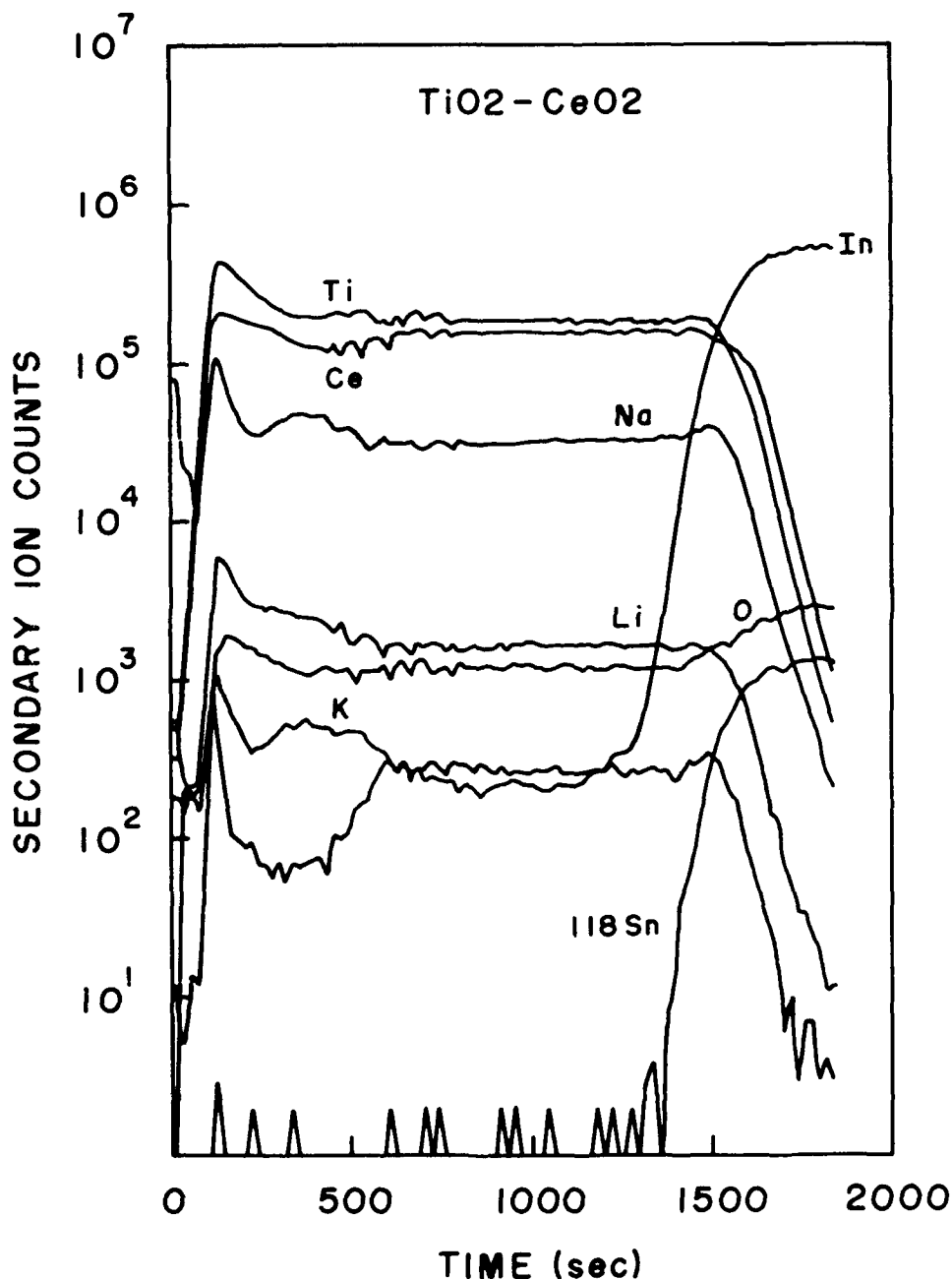


Fig. 8 - SIMS profiles of Ti, Ce, Li, Na, K, O, Si, In and  $^{118}\text{Sn}$  of a 2 dip layer  $\text{TiO}_2$  -  $\text{CeO}_2$  film deposited on ITO coated glass and heat treated at 450°C for 15 minutes measured after  $\text{Li}^+$  ions insertion.

### 3.5. Optical Characteristics

Figure 9 shows the transmission spectrum of a  $\sim 300\text{nm}$  thick  $\text{TiO}_2\text{-CeO}_2$  oxide prepared with a sol aged 3 days and subsequently heat treated at  $450^\circ\text{C}$  for 15 minutes and measured before and after  $\text{Li}^+$  ions insertion. The optical transmission remains practically unaltered. This exceptional behavior is technologically of great importance as no coloration will appear at this electrode during the cycles.

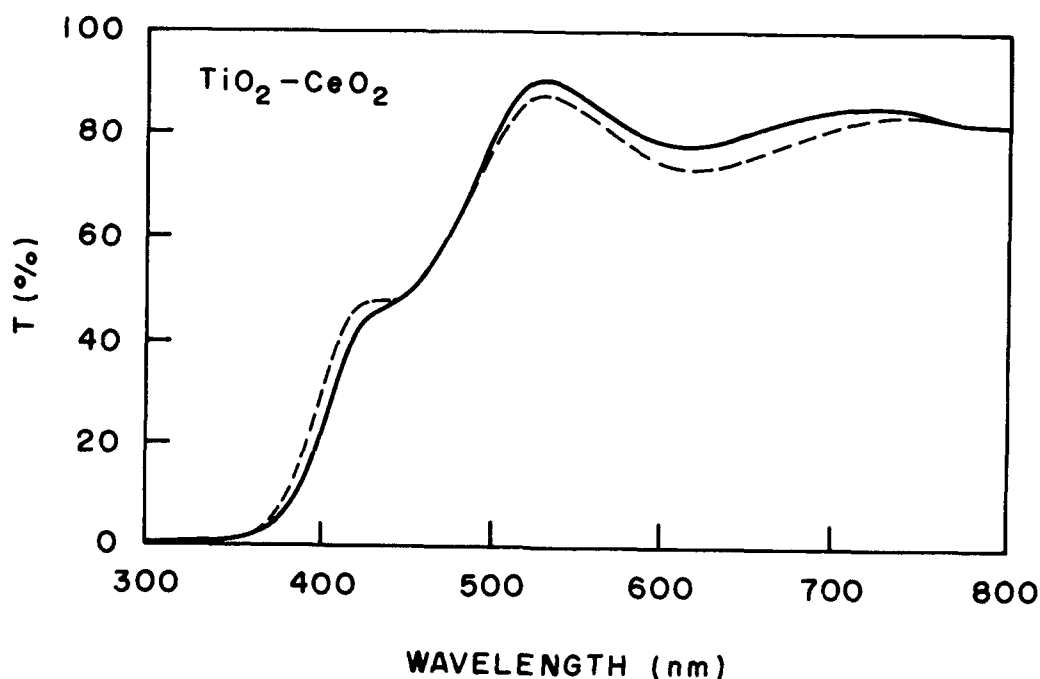


Fig.9 - Optical transmission of a  $\text{nm}$  thick  $\text{TiO}_2 - \text{CeO}_2$  (3 dips) deposited on ITO coating and heat treated at  $450^\circ\text{C}$  during 15 minutes measured before (—) and after (-----)  $\text{Li}^+$  ions insertion.

The contrast of a complete cell will be less sensible to any thickness variation of the layer, as in the case of a rocking chair configuration. Moreover the higher transmittivity obtainable with this ion storage coating is not dependent of the counter electrode layer thickness. The coloration of an electrochromic device (window or mirror) will only arise from the optical properties of the electrochromic layer ( $\text{WO}_3$  for instance).

### 4. PROPERTIES OF THE ELECTROCHROMIC LAYER AND THE WINDOW

As discussed in the previous section, the coloration of a complete device which uses a  $\text{TiO}_2 - \text{CeO}_2$  ion storage layer is only governed by the properties of the

electrochromic layer. The window which is presently tested has the configuration shown in figure 1. The sandwich is composed of the following elements :

/glass/ITO/ $\text{WO}_3$ /POE-Li N ( $\text{SO}_2$   $\text{CF}_3$ ) $_2$ / $\text{TiO}_2$  -  $\text{CeO}_2$ / ITO / glass / (6)

Figure 10 shows the optical response of the electrochromic layer  $\text{WO}_3$  250nm thick deposited by evaporation technique on an ITO coated glass substrate before and after a partial  $\text{Li}^+$  ions insertion corresponding to a charge of  $10.5\text{mC}/\text{cm}^2$ . It shows a reduction of the optical transmission already reaching 50% at 600nm. A complete window is presently under test. It is built by assembling three separate components : glass / ITO /  $\text{WO}_3$ , electrolyte and  $\text{TiO}_2$  -  $\text{CeO}_2$  / ITO / glass. After their assembling the complete cell is hot pressed at  $80^\circ\text{C}$  in a dry box and sealed with a low vapor pressure resin (Varian Torr - seal ).

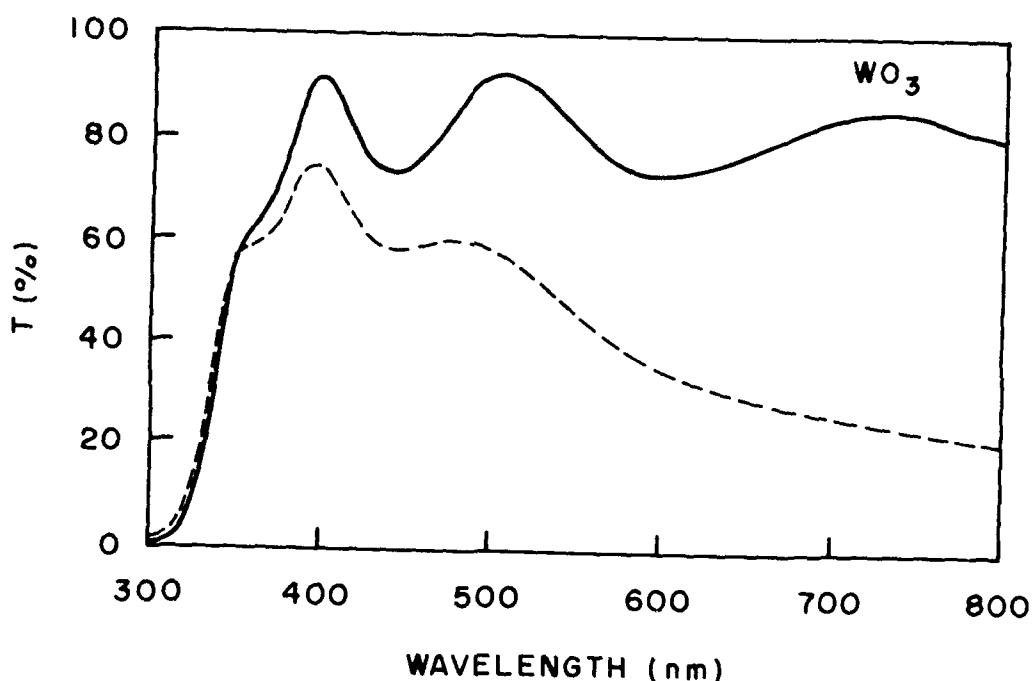


Fig. 10 - Optical transmission of an 250nm thick  $\text{WO}_3$  deposited by evaporation technique on ITO coated glass substrate measured before (—) and after (---)  $\text{Li}^+$  ions insertion.

Fig. 11 shows the cyclic voltammetry of such a device. The  $\text{TiO}_2$  -  $\text{CeO}_2$  counter electrode is used as a reference electrode. The coloration of this cell changes reversibly by applying a suitable voltage between the two electronic electrodes. It is blue when  $\text{WO}_3$  is reduced and transparent and colourless when it is oxidized. Complete optical characterizations are underway.

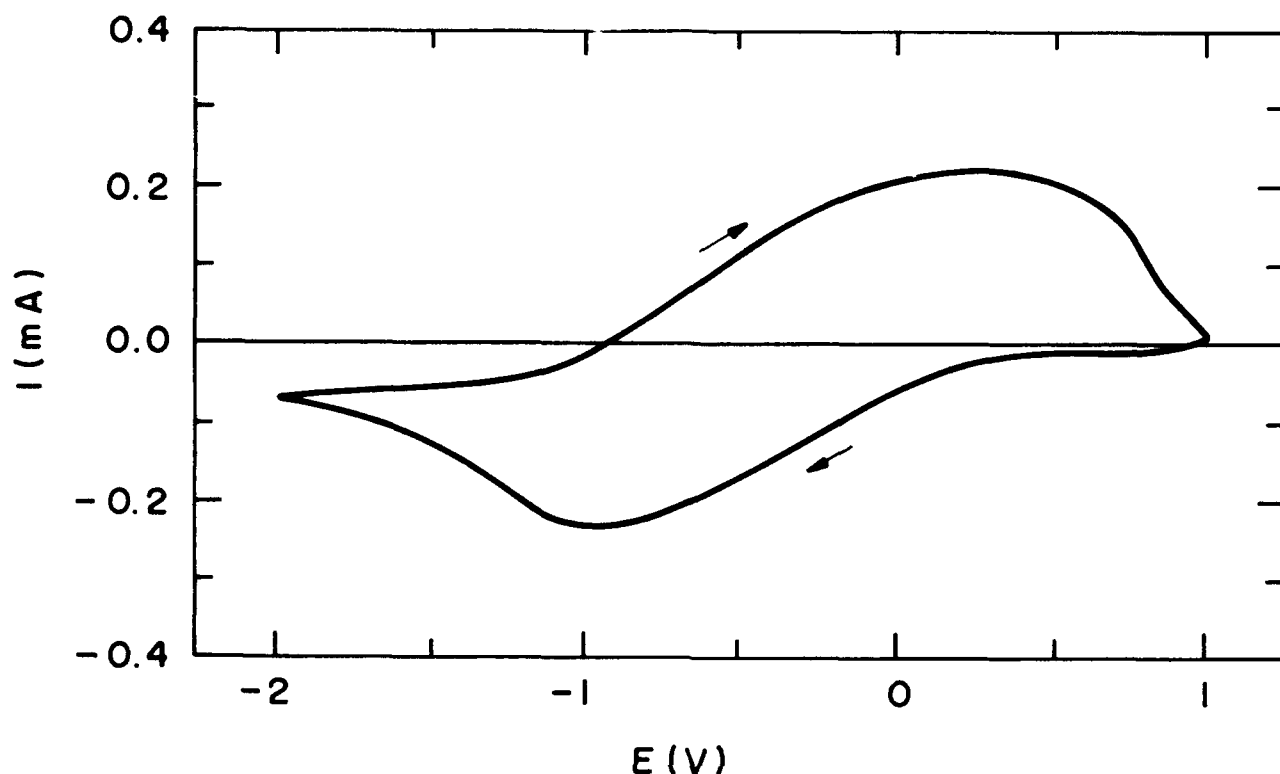


Fig. 11 - Cyclic voltammetry of a complete transmission window glass / ITO/  $\text{WO}_3$  / PEO- Li N  $(\text{SO}_2 \text{ C F}_3)_2$  /  $\text{TiO}_2$  -  $\text{CeO}_2$  / ITO /glass.

## 5. CONCLUSIONS

This paper presents an investigation of the physical properties of  $\text{TiO}_2$  -  $\text{CeO}_2$  thin films prepared by the sol-gel process using the dip coating technique. This material presents an outstanding behavior as  $\text{Li}^+$  ion storage electrode and its use is quite promising for electrochromic devices such as smart windows or mirrors<sup>25</sup>. The lithium insertion is reversible and the electrode kinetics is acceptable. The process is controlled by solid state diffusion. No coloration is observed during the electrochemical cycles which should improve the uniformity of the optical contrast of such devices. The chemical diffusion of Li at room temperature is  $\bar{D} = 6.4 \cdot 10^{-12} \text{ cm}^2/\text{s}$  ( $E = 0.5 \text{ V}$  vs  $\text{Ag}/\text{Ag}^+$ ). This value is comparable to those obtained in  $\text{WO}_3$  electrochromic film. The detailed mechanism of the lithium insertion is still not very well understood.

The best electrochemical results have been obtained with a 5 to 7 days aged sol. Physico chemical studies show that in such a sol the cerium is present almost as  $\text{Ce}^{3+}$ . It is however oxidized into  $\text{Ce}^{4+}$  during the heat treatment of densification and very small crystallites of  $\text{CeO}_2$  are observed in a still amorphous  $\text{TiO}_2$ .

matrix. The presence of these crystallites seems to be fundamental as well as the choice of the cerium precursor. The use of  $\text{CeCl}_3$  for instance, which is also found as  $\text{Ce}^{3+}$  in the precursor sol, gives poor electrochemical reaction.

Complete transmissive and reflective devices are presently under extensive tests in order to determine their optical properties, long term reversibility and general performances under different ambient conditions. The feasibility of preparing other components by the sol-gel process such as the electrochromic coating ( $\text{WO}_3$ ) and a solid state electrolyte is also underway.

#### ACKNOWLEDGMENTS

This research was financially supported by CNPq, FAPESP and FINEP(Brazil). P.B. and B.V. acknowledge the Ministère des Affaires Étrangères (France) for a scholarship to realize this research.

#### REFERENCES

1. D.R. Uhlmann and G.P. Rajendran, "Coatings : the Land of Opportunity for Sol-Gel Technology", Ultrastructure Processing of Advanced Ceramics, J.D. Mackenzie and D.R. Ulrich ed, pp 241 - 253, Wiley Interscience (1988).
2. C.M. Lampert and C.G. Granqvist, ed. "Large-Area Chromogenics : Materials and Devices for Transmittance Control", SPIE Institute for Advanced Optical Technologies, vol. IS4, SPIE, Bellingham 1990.
3. M. Misonon and H. Kawahara, "Transparent Electronic Conductors in electrochromic devices", see ref. 2 pp 402 - 412.
4. B.W. Fanghnan, R.S. Crandall and P.M. Heyman, RCA Rev., 36 pp 177 1975.
5. T.E. Haas and R.B. Goldner, "Fundamentals of Electrochromism in metal oxide bronzes", see reference 2 pp 170 - 180.
6. J.P. Randin and R. Viennet, "Proton diffusion in Tungsten Trioxide Thin Films", J. Electrochem. Soc. 129, pp 2349 - 2354 1982.
7. M. Armand, "Polymer Electrolytes Reviews I" Ch I: "Current state of PEO-Based Electrolytes", pp 1 - 22, J.R. Mac Callum Editor - Elsevier 1987.
8. J. Nagai, M. Mizuhashi and T. Kamimori, "Polymeric ion Conductors", see reference 2, pp 378 - 385.
9. R.D. Rauh and S.F. Logan, "Counter Electrodes in Transmissive Electrochromic Light Modulators", Solid State Ionics 28 - 30, pp 1707 - 1714, 1988.
10. P. Baudry, M.A. Aegerter, D. Deroo and B. Valla, "Electrochromic window with lithium conductive polymer electrolyte", Proc. 176<sup>th</sup> Symposium of the Electrochemical Society, Hollywood, FL, October 14 - 20, 1989.
11. R.B. Goldner, T.E. Haas, G.Seward, K.K. Wong, P. Norton, G. Foley, G. Berera, G. Wei, S.Schulz and R. Chapman, "The film solid state ionic materials for electrochromic smart window TM glass", Solid State Ionics 28 - 30, pp 1715 - 1721, 1988.
12. S.F. Logan and R.D. Rank, "The  $\alpha\text{-WO}_3$  /  $\alpha\text{-IrO}_2$  electrochromic system" see ref. 2, pp 482 - 493.
13. D.Deroo, P.Baudry and H. Arribart, French Patent No. 88 08 809.
14. P. Baudry, A.C.M. Rodrigues, M.A. Aegerter and L.O. Bulhões, "Dip-Coated  $\text{TiO}_2\text{-CeO}_2$  films as transparent counter-electrode for transmissive electrochromic devices, Proc. 7<sup>th</sup> International Workshop on Glasses and Ceramics from Gels, Rio de Janeiro, August 1989 M.A. Aegerter ed, to be published in J.Non-Crystalline Solids, May issue 1990.
15. M.B. Armand, "Polymer Solid Electrolytes- An Over View", Solid State Ionics 9 - 10, pp 745 - 754 1983.
16. M.B. Armand, W.Gorecki and A. Andreani, 2<sup>nd</sup> International Conference on Poly-



mer Electrolytes Siena, Italy, June 14 - 16, 1989.

17. P. Baudry, PhD Thesis, Etude de Vitrages électrochromes à électrolyte polymère, Institut National Polytechnique de Grenoble, 27.1.1989.

18. K. Maniya, K. Tanimoto, T. Yoko, "Preparation of  $\text{TiO}_2$  fibres by hydrolysis and polycondensation of  $\text{Ti}(\text{O}-i-\text{C}_3\text{H}_7)_4$ ", J. Materials Science Letters, 5, pp 402 - 404 1986.

19. M. Ardon, "Oxidation of Ethanol by Ceric Perchlorate", J.Chem. Soc. pp 1811-1815 1957.

20. R.J. Meyer and R. Jacoby, Zeit. Anorg. Chem. 27, 359/89, 369 1901.

21. M. Armand, F. Dalard, D.Deroo and C.Moulion, "Modelling the Voltammetric study of intercalation in host structure. Application to Lithium intercalation in  $\text{RuO}_2$ ", Sol. State Ionics, 15 pp 205 - 210 1985.

22. J.E.B. Randles, "Kinetics of rapid electrode reactions", Disc. Faraday Soc. I pp 11 - 19 1977.

23. C. Ho, I.D. Raistrich and R.A. Huggins, "Application of A-C Techniques to the study of Lithium Diffusion in Tungsten Trioxide Thin Films, J. Electrochem.Soc. 127 pp 343 - 350 1980.

24. J.C.L. Tonazzi, B.Valla, M. Macedo, P. Baudry, M.A. Aegerter, A.C.M. Rodrigues and L.O. Bulhões, "Characterization of an all solid state electrochromic window" SPIE Proceedings, Vol 1328, Paper 1328 - 37, Sol-Gel Optics, this volume.



Characterization of Sol-Gel Thin Films of  
 $\text{TiO}_2\text{-PbO}$ ,  $\text{TiO}_2\text{-Bi}_2\text{O}_3$  and  $\text{TiO}_2\text{-CeO}_2$  Compositions.

Michel A. Aegerter, Eliane R. La Serra

University of São Paulo, Instituto de Física e  
 Química de São Carlos, 13.560 - São Carlos, SP, Brazil

Ana Candida Martins Rodrigues

Federal University of São Carlos  
 13.560- São Carlos, SP, Brazil

George Kordas, Glenn Moore

University of Illinois at Urbana/Champaign  
 Department of Science and Engineering-Ceramics Division  
 Urbana, Illinois, 61801, USA

ABSTRACT

Single and multilayer sol-gel thin films of  $\text{TiO}_2\text{-PbO}$ ,  $\text{TiO}_2\text{-Bi}_2\text{O}_3$  and  $\text{TiO}_2\text{-CeO}_2$  composition were deposited on glasses using the dip coating technique. The precursors included  $\text{Ti}(\text{OPr}^i)_4$  chemically modified by acetyl acetone and diluted in  $\text{Pr}^i\text{OH}$  and sols of  $\text{Pb}(\text{OAc})_2$ ,  $\text{Bi}(\text{NO}_3)_3 \cdot 5\text{H}_2\text{O}$  diluted in acetic acid. The  $\text{TiO}_2\text{-CeO}_2$  sol was prepared by mixing  $\text{Ce}(\text{NH}_4)_2(\text{NO}_3)_6$  in ethanol and then adding  $\text{Ti}(\text{O-iso-C}_3\text{H}_7)_4$ . Structure texture and homogeneity of their main constituents was established by XRD, XPS, SIMS and SEM-EDX techniques as a function of heat treatments.

1. INTRODUCTION

The utility of sol-gel methods for producing glass and ceramic materials with high chemical homogeneity at relatively low temperatures is now well recognized. Recently considerable attention has been directed to the use of these methods for the production of thin, thick, single and multilayers coatings as these techniques offer outstanding opportunities, including low cost of precursors, rapid drying, uniform shrinkage and easy elimination of volatiles. The possibility to obtain coatings with microscopic structures which can be tailored by heat treatment from highly porous to fully dense is also an asset for several interesting applications. Furthermore, rather simple and commercially viable processing methods are available to coat substrates of nearly any size and geometry<sup>1</sup>.

We have shown in earlier publications that Sol-Gel coatings of  $\text{TiO}_2\text{-PbO}$ ,

92 4 28 056

92-11438



TiO<sub>2</sub>-Bi<sub>2</sub>O<sub>3</sub> and TiO<sub>2</sub>-CeO<sub>2</sub> compositions obtained by dip-coating, have a high optical quality; almost flat spectral transmission and reflection characteristics can be obtained in the visible by adjusting their thickness. These properties suggest their use for the preparation of achromatic beam splitters and neutral-colored solar-energy-reflecting windows<sup>2,3</sup>. We have also demonstrated that thick films of TiO<sub>2</sub>-PbO composition can be successfully used for the realization of passive planar wave guides where up to 4 effective modes have been optically coupled<sup>2,3</sup>. More recently we discovered that TiO<sub>2</sub>-CeO<sub>2</sub> films exhibit reversible electrochemical insertion for Li<sup>+</sup> ions while maintaining high optical transmissivity; these outstanding properties turn these films natural candidates for the realization of transparent counter electrode in all solid state electrochromic transmissive or reflective devices<sup>4,5</sup>.

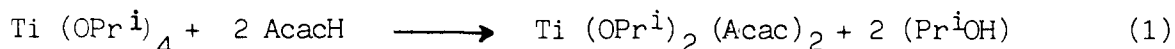
These various applications prompted therefore a more thorough investigation of the film structure, texture, and (2D, 3D) homogeneity of their elemental constituents during the densification process. This paper presents original and recent data obtained with sol-gel of TiO<sub>2</sub>-PbO, TiO<sub>2</sub>-Bi<sub>2</sub>O<sub>3</sub> and TiO<sub>2</sub>-CeO<sub>2</sub> thin films compositions using techniques such as X-ray photoelectron spectroscopy (XPS), secondary ion mass spectroscopy (SIMS), scanning electron microscopy (SEM), electron diffraction spectroscopy (SEM-EDX) and X-ray diffraction (XRD).

## 2. EXPERIMENTAL PROCEDURES

### 2.1. Precursor and sol preparations of TiO<sub>2</sub>-PbO composition

The method used to prepare the precursor sols is based on the chemical modification of titanium isopropoxide Ti(OPr<sup>i</sup>)<sub>4</sub> by the rather strong chelating ligand and stabilizing agent acetylacetone AcacH<sup>6,7</sup>.

The preparation of the complex alkoxide is described by the exothermic reaction<sup>9</sup>.



The yellow and homogeneous solution is then mixed for 30 minutes until its temperature lowers to 25°C. A solution of lead acetate Pb(OAc)<sub>2</sub> in acetic acid (concentration 720 g/l) is then added and stirred for 30 minutes. This sol is quite stable and does not present gelation or precipitation for several months. Both precursor sols can be mixed in any proportion. The typical volumes used for films of composition TiO<sub>2</sub>- 0,25 PbO (PbTi<sub>4</sub>O<sub>9</sub>) are given below:

Pr <sup>i</sup> OH	Acac H	Ti(OPr <sup>i</sup> ) <sub>4</sub>	Pb acetate sol	pH
40 ml	3 ml	4 ml	1,81 ml	5,7

## 2.2. Precursor and sol preparation of $\text{TiO}_2\text{-Bi}_2\text{O}_3$ composition

Similar procedures were also used for the preparation of precursors and sols of  $\text{TiO}_2\text{-Bi}_2\text{O}_3$  composition. However, the bismuth sol was prepared by mixing  $\text{Bi}(\text{NO}_3)_3 \cdot 5\text{H}_2\text{O}$  in acetic acid with a concentration of 665 g/l. The typical volumes used for films of  $\text{TiO}_2\text{-}0,12\text{Bi}_2\text{O}_3$  composition are given below:

$\text{Pr}^i\text{OH}$	Acac H	$\text{Ti}(\text{OPr}^i)_4$	Bi nitrate sol	pH
30 ml	1,8 ml	2,5 ml	1,9 ml	0,86

## 2.3 Precursors and sol preparation of $\text{TiO}_2\text{-CeO}_2$ composition

The starting solution was prepared by dissolving  $\text{Ce}(\text{NH}_4)_2(\text{NO}_3)_6$  in ethanol, adding then tetraisopropyl orthotitanate  $\text{Ti}(\text{O-iso-C}_3\text{H}_7)_4$ . The concentration of  $\text{Ce}(\text{NH}_4)_2(\text{NO}_3)_6$  cannot exceed 0,25 M because of the solubility limit of the salt in ethanol at room temperature. The presence of the cerium-ammonium nitrate stabilizes the solution.

## 2.4. Films preparation and characterization

The thin films have been obtained by dip-coating on common glass substrate except those of  $\text{TiO}_2\text{-CeO}_2$  which have been coated on ITO Baltracon substrates. The withdrawal speed was of the order of 4-15 cm/min. After each coating procedure the films were dried and heat treated in air at a specified temperature (up to 500° C) for different period of time (up to 1 h). The whole process was repeated to obtain thicker films.

The films have been characterized by XPS, SIMS, SEM, SEM-EDX and XRD techniques in order to study the evolution of their structure, texture, 2D and in depth profile composition during the densification treatment.

- a) XPS was performed on a PHI model 5900 instrument\* equipped with a hemispherical analyser and unmonochromatized Mg X-ray source. The samples were sputtered depth profiled with Ar ions ( 2 KV, ~ 7nA). XPS recording was performed with the ion beam off at the pressure lower than  $10^{-9}$  Torr. The angle between the surface sample and the analyser was 70°. The chemical analysis was obtained by using the PHI software routines, version 3 modification B. The concentration of each element is given in atomic percent and represents the total atomic concentration regardless the chemical state.
- b) SIMS was performed on a Cameca IMS 3 f instrument\*. A 8 Kev mass analysed cesium ion beam with approximately 500  $\mu\text{m}$  diameter was used for all analyses and depth

profiles. All samples were coated with a thin gold layer and covered with a grid in order to avoid charging effects.

- c) SEM was performed on a Hitachi s-800 instrument\*.
- d) SEM-EDX was performed on a Jeol/Tracor instrument\*\*
- e) XRD was performed on a Rigaku Rotaflex RU200B instrument\*\*\*

## RESULTS AND DISCUSSION

### 3.1. Films of $\text{TiO}_2$ -PbO composition

The basic composition of these films was  $\text{TiO}_2 - 0,25 \text{ PbO}$  ( $\text{PbTi}_4\text{O}_9$ ) equivalent to an atomic concentration of 7,7% Pb, 28,6% Ti and 64,2% O. All the films heat treated in air up to a temperature of 500°C for up to 60 minutes were found amorphous to X-ray. Figure 1 shows SEM micrograph of films heat treated at 190°C and 60 min. They appear uniform except for small amount of dust, possibly precipitations and small inhomogeneities. The coatings fired at 500°C for 60 minutes are practically densified with an overall smooth continuous surface. Figure 2 indicates a micrograph of a layer with pox marks and possibly precipitates and cracking near the lower edge of the substrate (end of the dip process) were also observed.

XPS analysis was performed on two similar samples. Figure 3 shows three typical survey scans for a  $\text{TiO}_2 - 0,25 \text{ PbO}$  film heat treated at 190°C for 60 minutes: a) spectrum recorded at the surface (as received). b) spectrum recorded after 20 minutes Ar sputtering (at  $\sim 1/6$  of the depth). c) spectrum recorded after 125 minutes Ar sputtering near the glass-film interface. All the peaks have been identified and the spectra shows the presence of O, Ti, Pb, C, Na and Ca. A detailed analysis<sup>8</sup> shows that the O and Ti peaks are hardly affected by the sputtering while features appear on the lower binding energies (BE) side of the Pb 4f peaks already after 4 or 8 minutes of sputtering; these features grow into a doublet of equal intensity of the original doublet after 75 minutes of sputtering. After 125 minutes (near the interface) the doublet of lower BE has a higher intensity. This behavior is due to ion-induced chemical damage leading to a reduction of lead. The fact that the Ti 2p peaks are not affected is not clear and will be discussed later.

Figure 4 shows the relative concentration in atomic percent of the elements O, C, Ti, Na, Pb and Ca determined as a function of the sputtering time (depth). The concentration of carbon is still high and goes high deep into the layer but decreases with distance from the film surface. The elimination of the organic group is not yet complete at this temperature and the fact that lead was introduced as an acetate

\* Center for Microanalysis of Materials, University of Illinois at Urbana Champaign(USA) sponsored by the US DOE under DE-AC62-76ER01198.

\*\* School of Civil Engineering, Purdue University, West Lafayette (USA)

\*\*\* IFQSC/University of São Paulo, São Carlos (Brazil)



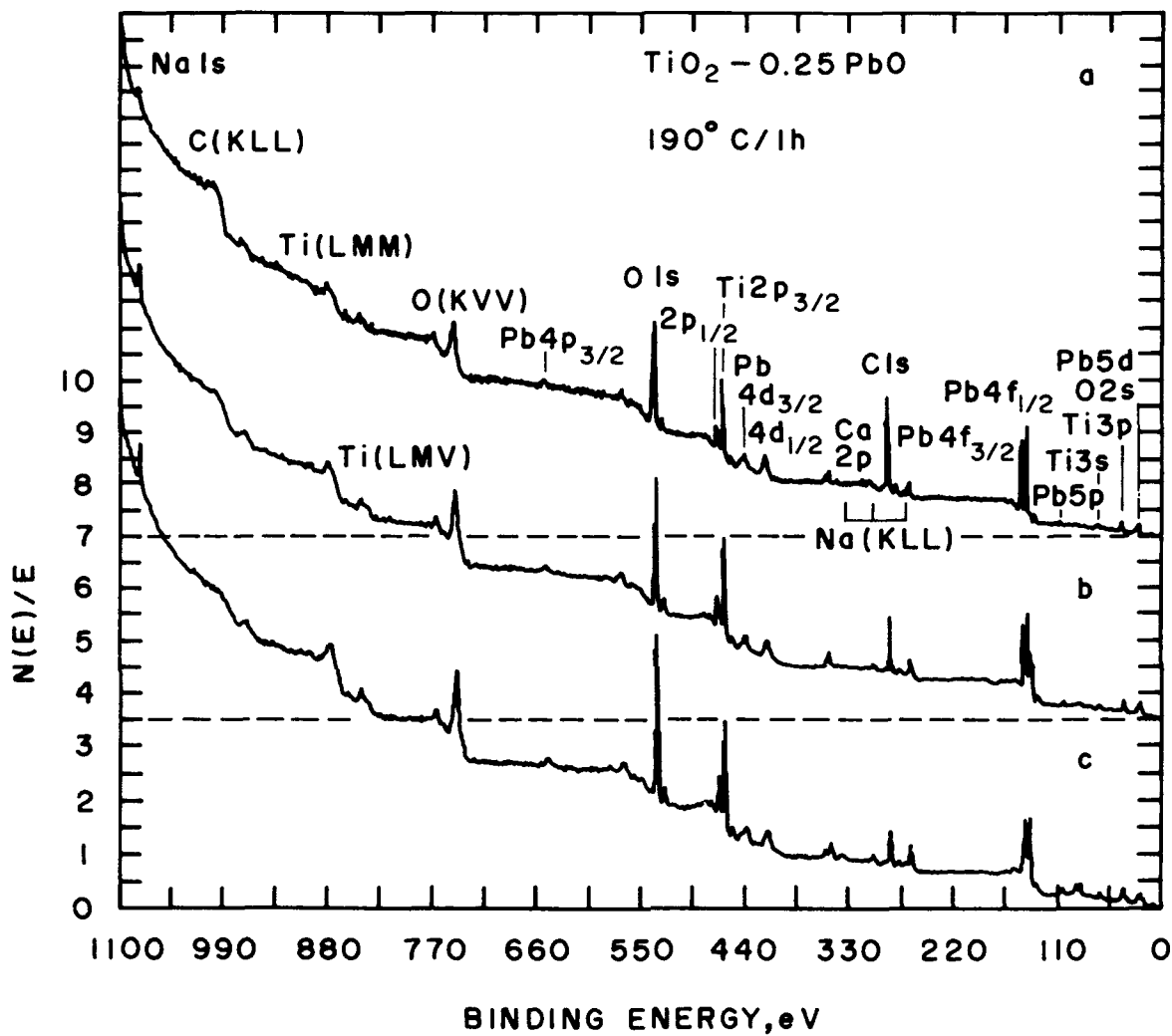


Fig.3. XPS survey of a one layer  $\text{TiO}_2 - 0.25 \text{PbO}$  film heat treated in air at 190°C during 60 minutes and recorded a) at the surface as received, b) after 20 minutes sputtering ( $\sim 1/6$  of the depth), c) after 125 minutes of sputtering (near the glass-film interface)

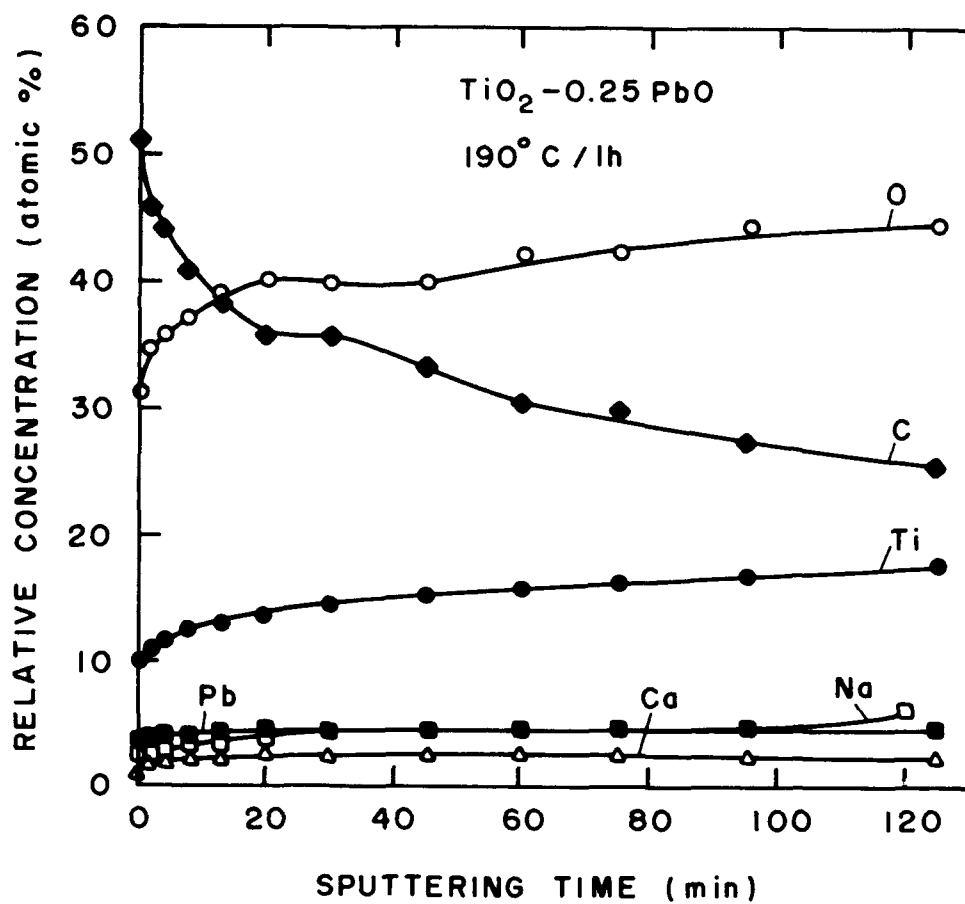


Fig. 4 XPS profile of  $\text{TiO}_2-0.25 \text{ PbO}$  film heat treated in air at  $190^\circ \text{C}$  during 60 minutes.



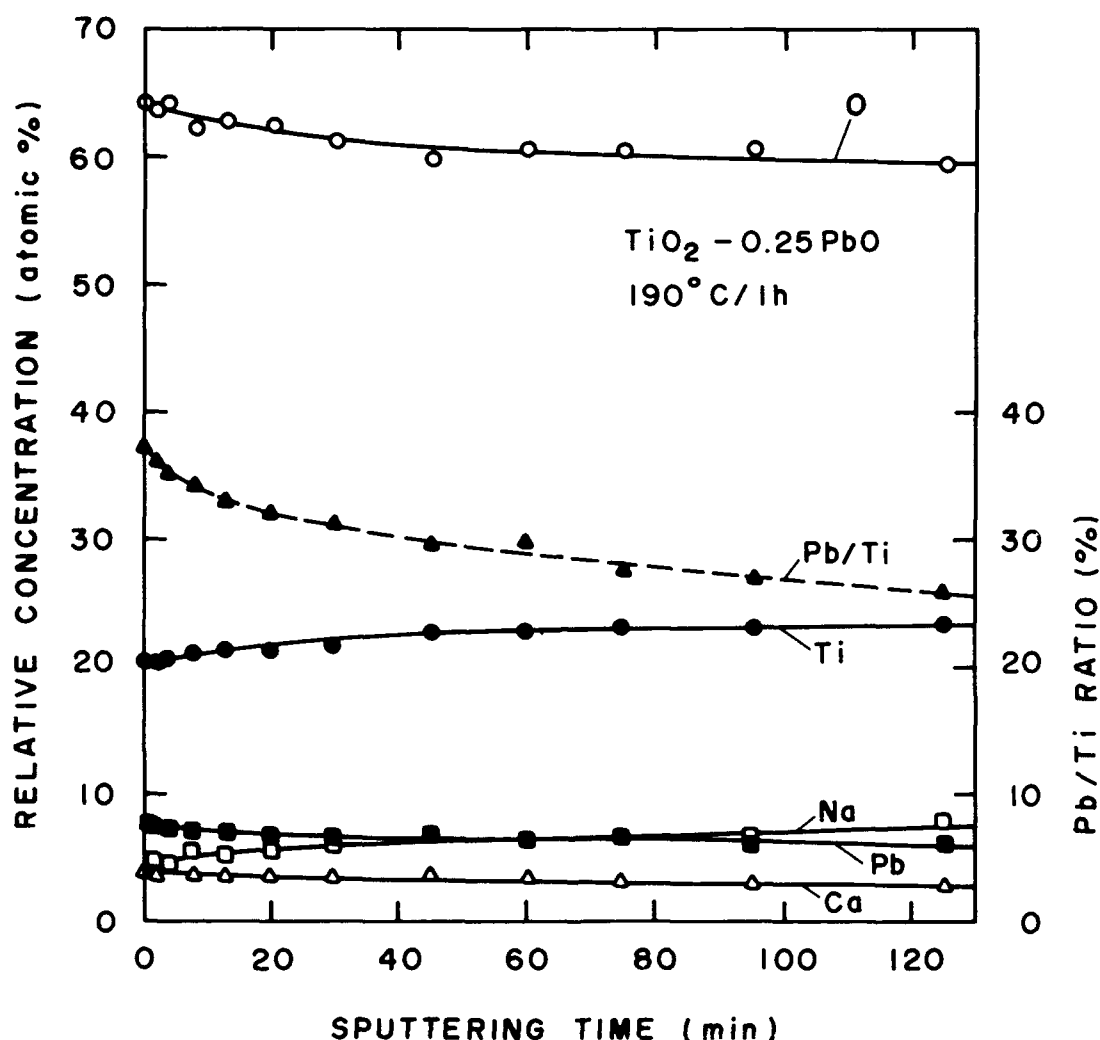


Fig. 5 Same as figure 4 after elimination of the carbon contribution and recormalization of the atomic concentration (left scale). The depth profile of the ratio Pb/Ti is also shown (right scale).

received) b) after 20 minutes of sputtering (~ 1/3 of the depth) c) after 80 minutes of sputtering (beginning of the glass-film interface).

A detailed analysis<sup>8</sup> shows that sputtering has little effect on the O 1s peak; however a small shoulder appears at lower BE when the interface is reached due probably to oxygen in the glass substrate. On the other hand the sputtering has now a stronger effect on the Pb 4f peaks; a low BE doublet already appears after 3 minutes sputtering indicating lower oxidation states and its intensity grows rapidly as we penetrate into the layer and becomes even higher than the original doublet. The

high BE doublet tends to decrease and becomes finally a shoulder near the interface. Ti 2p doublet peaks are now also affected by the sputtering. A shoulder starts to develop already after 5 minutes and is present throughout the layer indicating the transformation of  $\text{Ti}^{4+}$  to lower oxydation states. The carbon peak is only present in the upper 3 nm and practically disappears after 5 minutes sputtering. Ca concentration has also dropped below the detection limit. The profile of the elements is

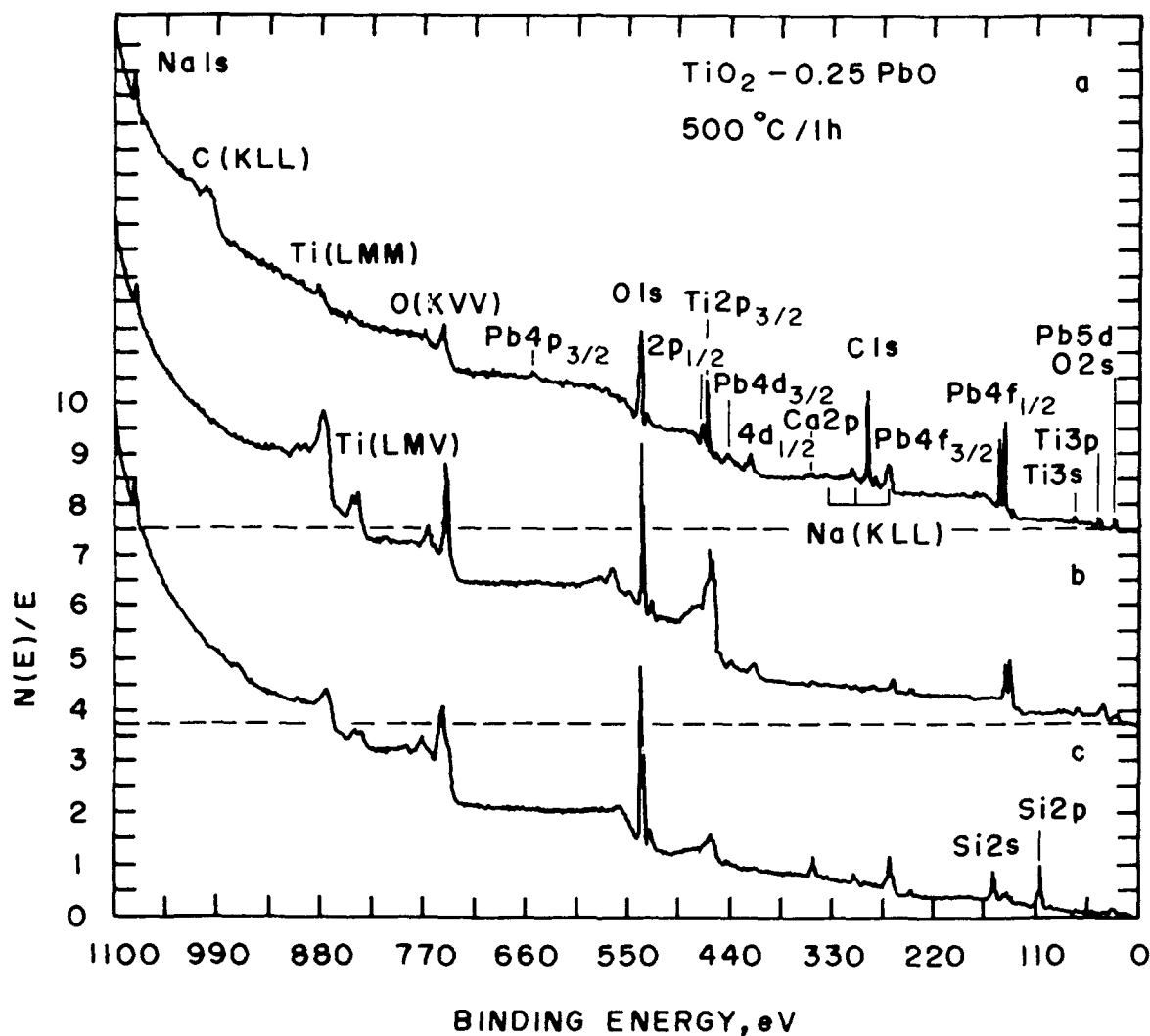


Fig.6 XPS survey of a one layer  $\text{TiO}_2 - 0.25 \text{ PbO}$  film heat treated in air at  $500^\circ\text{C}$  during 60 minutes and recorded a) at the surface (as received), b) after 20 minutes of sputtering ( $\sim 1/3$  of the depth), c) after 80 minutes of sputtering (beginning of the glass-film interface).

shown in Figure 7. The ordinate gives the relative concentration of O, Ti, Pb and Na only. The carbon contribution has been eliminated and its profile, shown in the figure as a dotted line is only given for information.

The most important result of this figure is the depth variation of the ratio Pb/Ti (originally equal to 0,25). This ratio is high near the surface because of the segregation of Pb and the strong depletion of Ti; it rapidly decreases below

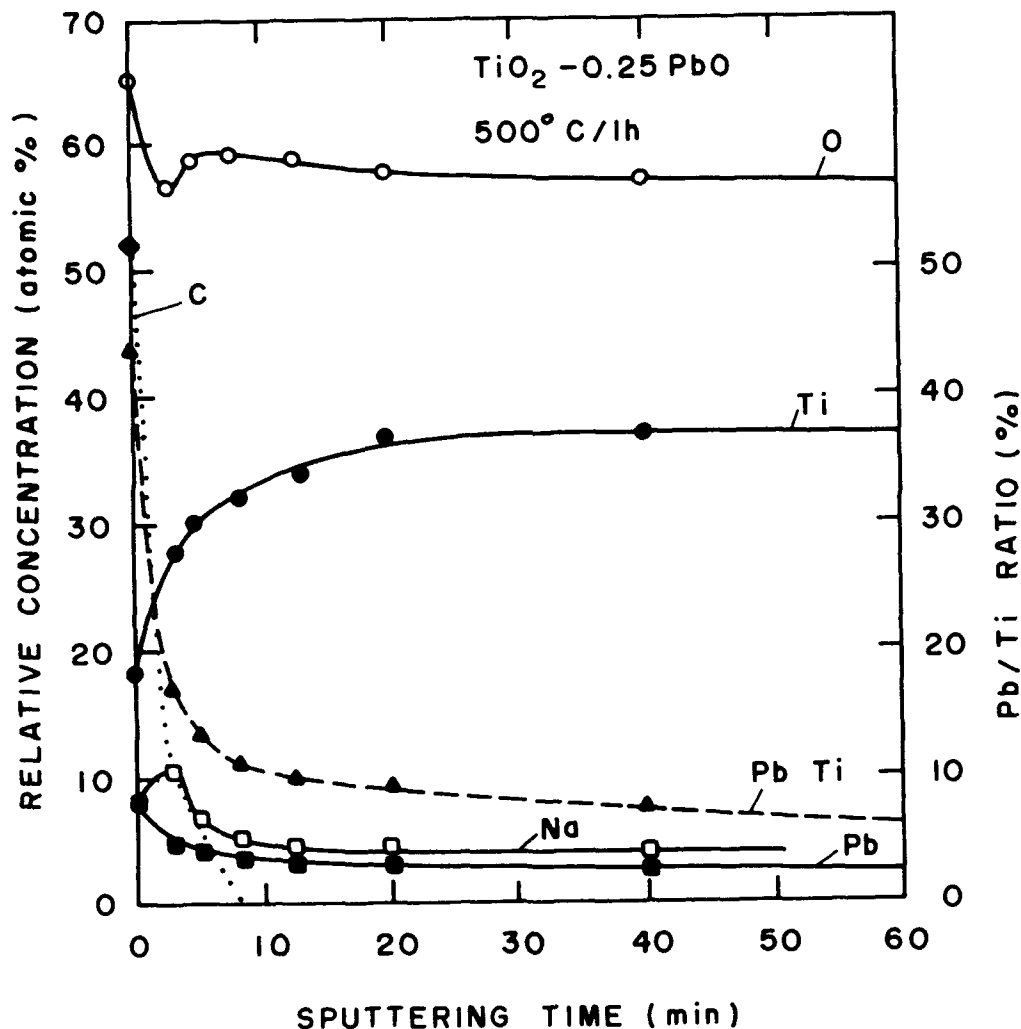


Fig. 7 XPS profile of a one layer  $\text{TiO}_2 - 0.25 \text{ PbO}$  film heat treated in air at  $500^\circ \text{C}$  during 60 minutes. The C contribution (shown as a dotted line) has been eliminated and the left ordinate scale refers to the relative concentration of O, Ti, Pb, Na only. The ratio Pb/Ti is also shown (right scale)

the original values, because the lead concentration beyond the subsurface is low (3% instead of 7.2%).

These results indicate that lead (or lead oxide) volatilizes easily even at this low temperature (500°C). It may be therefore difficult to obtain in film form compound materials of technical interest with definite stoichiometry in the

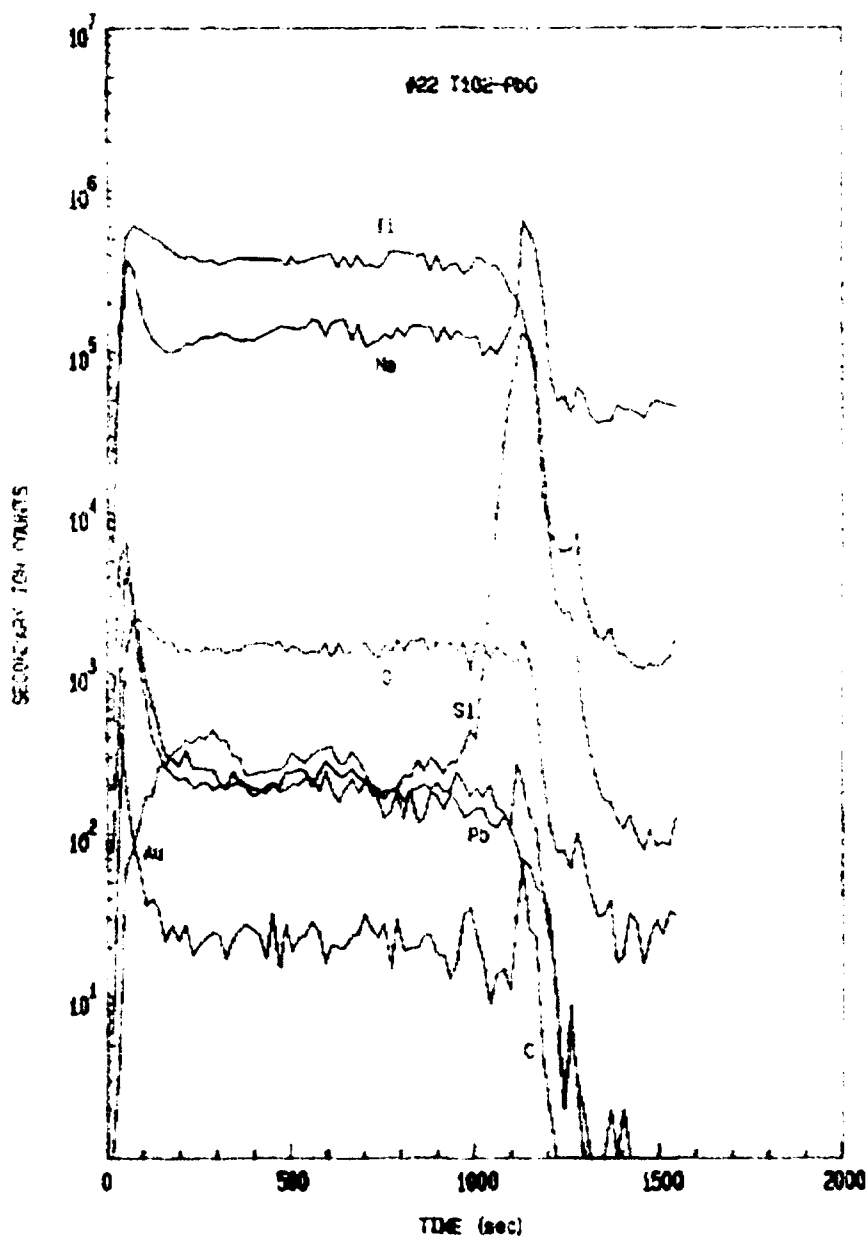


Fig. 8 SIMS profiles on a 3 layers  $\text{TiO}_2$ -0.25 PbO film heat treated at 500°C during 15 minutes after each dip.

TiO<sub>2</sub>-PbO system using the sol-gel process. This (expected) behavior confirms recent XRD results<sup>10,11</sup> on the observation of significant phase formation of lower lead content such as PbTi<sub>3</sub>O<sub>4</sub> in sol-gel prepared PbTiO<sub>3</sub> after 570°C firing.

SIMS profiles obtained with a 3 layers TiO<sub>2</sub>-0,25 PbO coating heat treated, after each dip, at 500°C during 15 minutes are shown in figure 8 and confirmed the XPS results. We must however recall that comparison of the ordinate (count values) of each element has no significance as no standard was available. Moreover the sharp variations observed at the outer surface (gold coating) and at the interface glass-film are consequences of the secondary ionization process (variation of the sensibility in different matrices) and are therefore not indicative of the relative concentration of the elements within these layers.

We clearly observe a decrease of Pb concentration with the distance from the film surface. The carbon profile presents an interesting behaviour: although its concentration is extremely low within the layer (see figure 7) its profile is similar to three inverted U shape function and clearly indicates the position of the three deposited layers. Moreover the large atmospheric peak observed on the surface

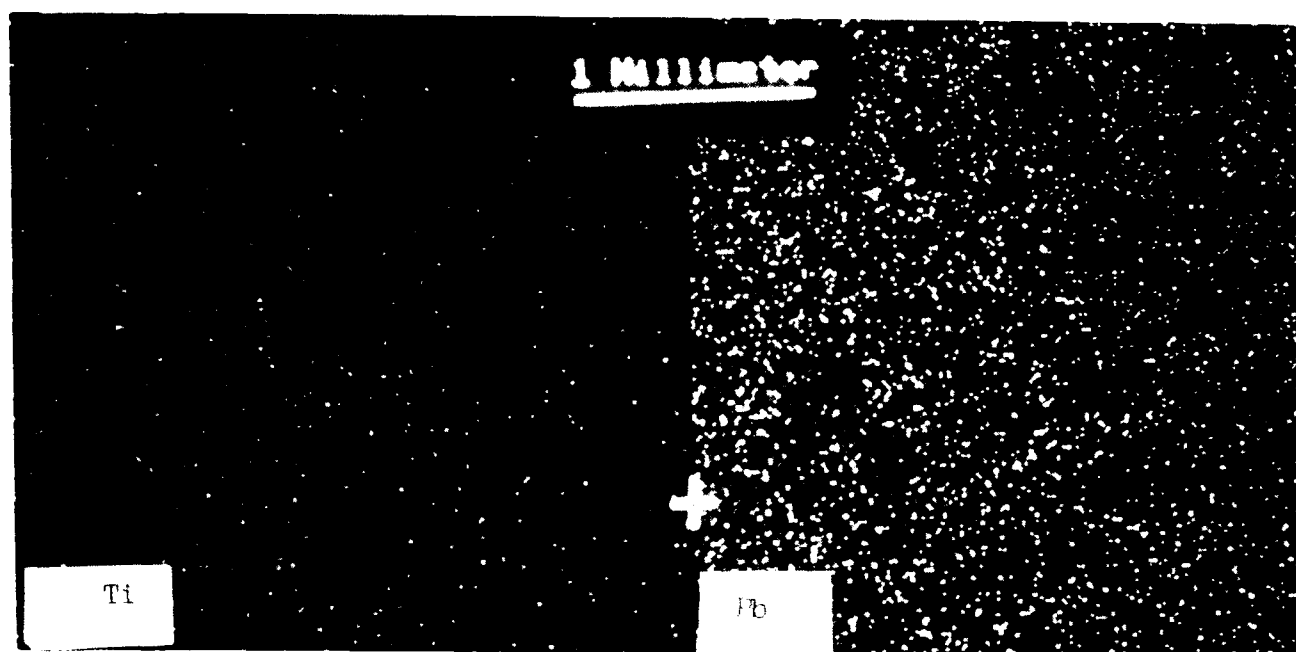


Fig. 9 2-D repartition of Ti and Pb measured by SEM-EDX with a TiO<sub>2</sub> - 0,25 PbO sample fixed at 500°C during 60 minutes.

layer by XPS and which we would expect at each layer interface (around  $t = 450$  s and 750 s respectively) are not present.

Finally figure 9 shows that the 2-D repartition of Ti and Pb measured by SEM-EDX with a  $\text{TiO}_2\text{-}0,25 \text{ PbO}$  sample fired at  $500^\circ\text{C}$  is quite homogeneous and uniform. Similar results have been obtained for the other elements up to very high magnification of 56000x.

### 3.2. Films of $\text{TiO}_2\text{-Bi}_2\text{O}_3$ composition

The basic composition of these films was  $\text{TiO}_2\text{-}0,125\text{Bi}_2\text{O}_3(\text{Ti}_4\text{BiO}_{9,5})$  giving an atomic concentration of 6,9% Bi, 27,6% Ti, 65,5% O. All the films heat treated in air up to a temperature of  $500^\circ\text{C}$  for the period of time up to 60 minutes were found amorphous to X-ray. The films heat treated at  $190^\circ\text{C}$  for 60 minutes have a very good surface quality (Fig.10). The surface of samples heat treated at  $480^\circ\text{C}$  presents however

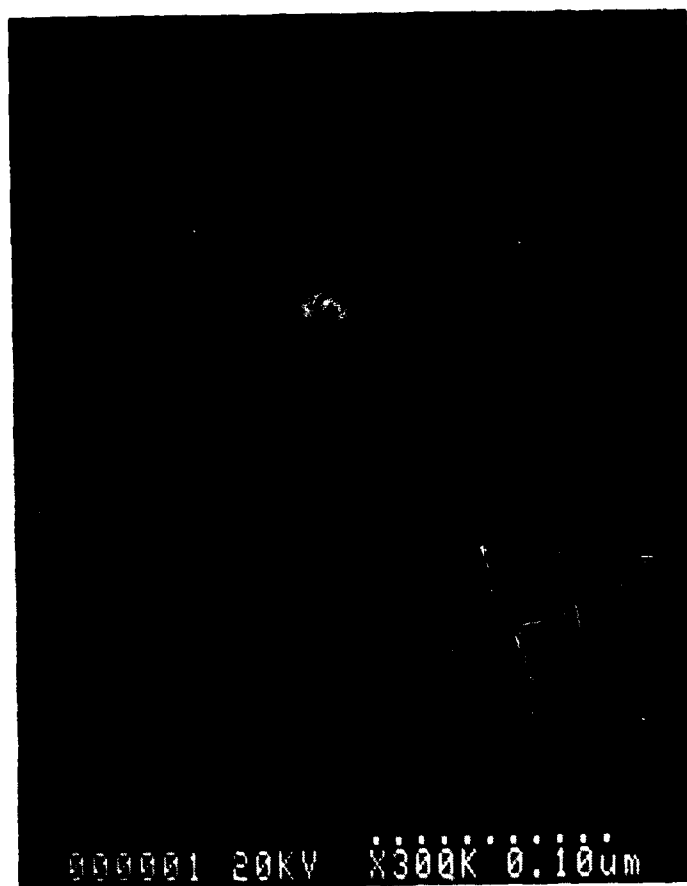


Fig. 10 SEM micrograph of a one layer  $\text{TiO}_2\text{-Bi}_2\text{O}_3$  film heat treated at  $190^\circ\text{C}$  during 60 minutes.

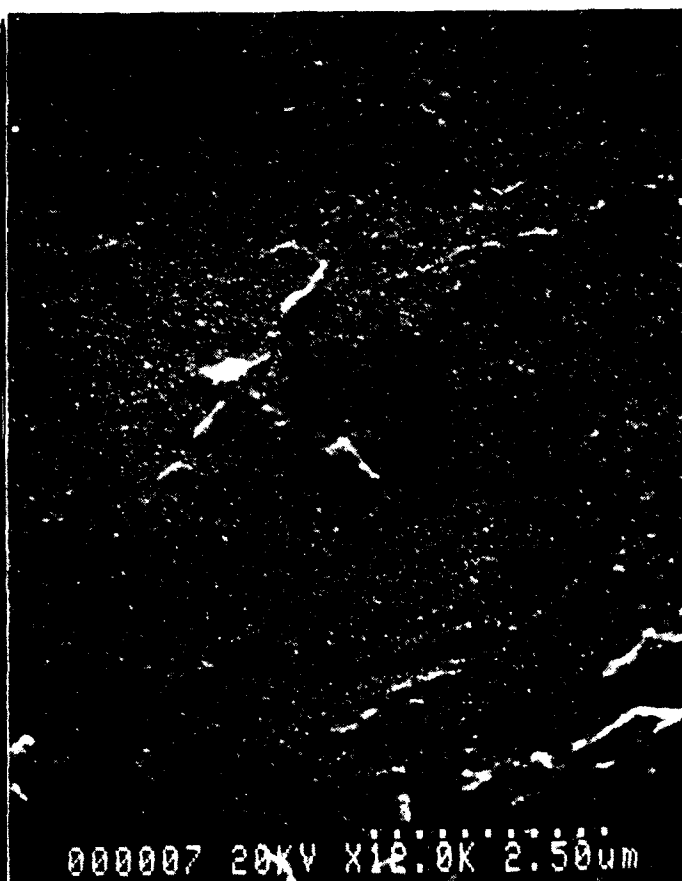


Fig. 11 SEM micrograph of a one layer  $\text{TiO}_2\text{-Bi}_2\text{O}_3$  film heat treated at  $480^\circ\text{C}$  during 60 min showing inhomogeneities and precipitates on the surface.

some inhomogeneities with cracks near the edge of the film (Figure 11).

XPS analysis was performed on two similar samples. Figure 12 shows three typical survey scans obtained with a film heat treated at 190°C during 60 minutes. (a) at the surface (as received). (b) after 32 minutes Ar sputtering ( $\sim 1/6$  of the depth) (c) after 180 minutes Ar sputtering at the beginning of the interface. All the peaks have been identified and the recorded spectra show the presence of O, Ti, Bi, C, Na and Si (in the interface). Detailed analysis<sup>8</sup> shows that the sputtering does not

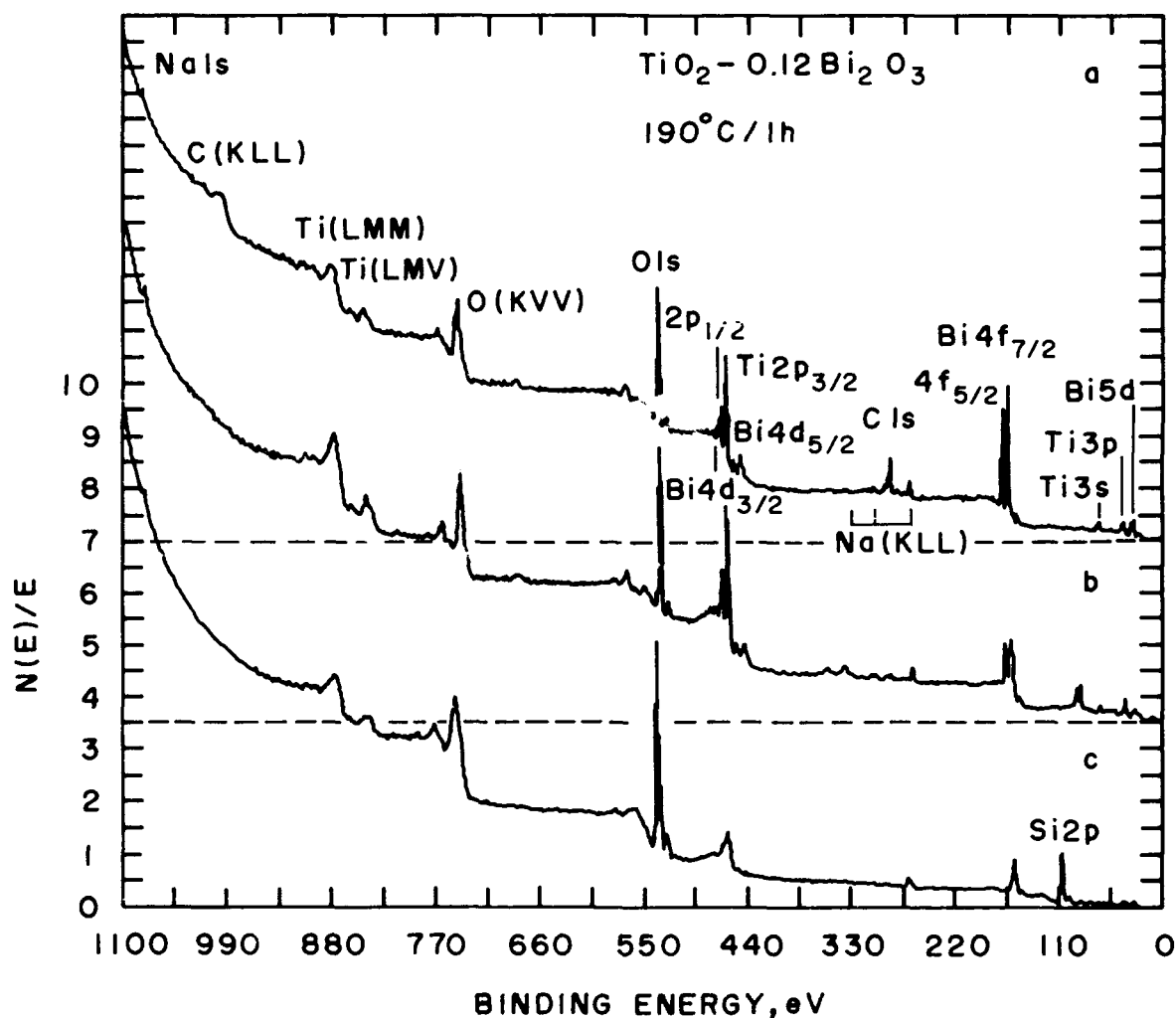


Fig. 12 XPS survey scans of a one layer  $\text{TiO}_2\text{-Bi}_2\text{O}_3$  film heat treated in air at 190°C during 60 minutes and recorded a) at the surface (as received), b) after 32 minutes Ar sputtering ( $\sim 1/6$  of the depth), c) after 180 minutes sputtering (beginning of the glass-layer interface).

affect the O 1s peak. However contrary to the  $\text{TiO}_2\text{-PbO}$  composition, the Ti 2p doublet is affected by the ions and reduced Ti features are observed after 40 min sputtering. The Bi 4f doublet is also strongly affected; a shoulder appears already after two minutes sputtering indicating that bismuth has been reduced. As we proceed two doublets are observed and after 40 minutes sputtering the reduced form is the dominant one. Na and C are only observed in the first half of the layer.

Figure 13 shows the relative concentration of the observed elements determined as a function of the sputtering time (depth). Contrary to what has been observed with the  $\text{TiO}_2\text{-PbO}$  composition, C and Na appear only in the subsurface of the film together

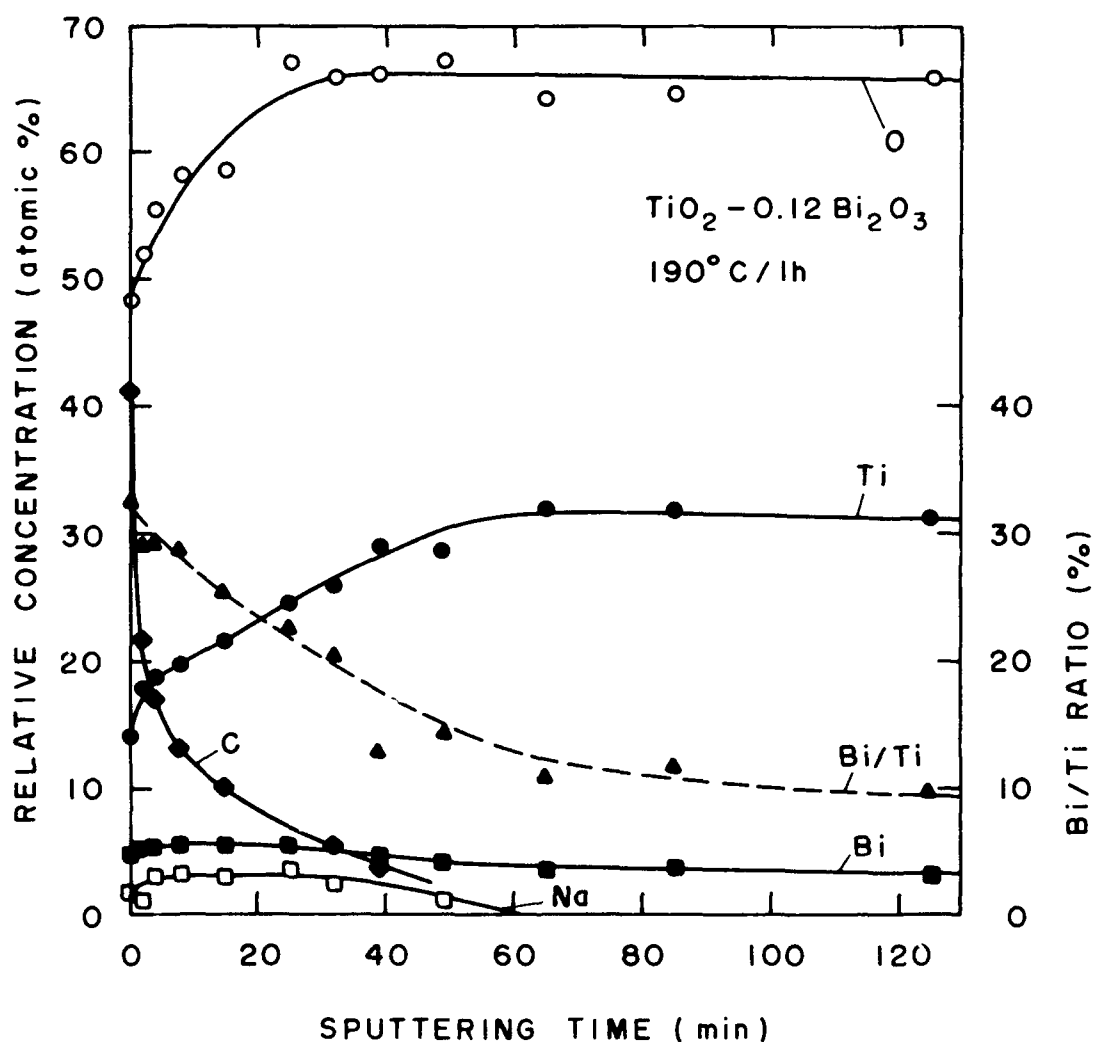


Fig. 13 XPS profiles of a one layer  $\text{TiO}_2\text{-Bi}_2\text{O}_3$  film heat treated in air at  $190^\circ\text{C}$  during 60 minutes.



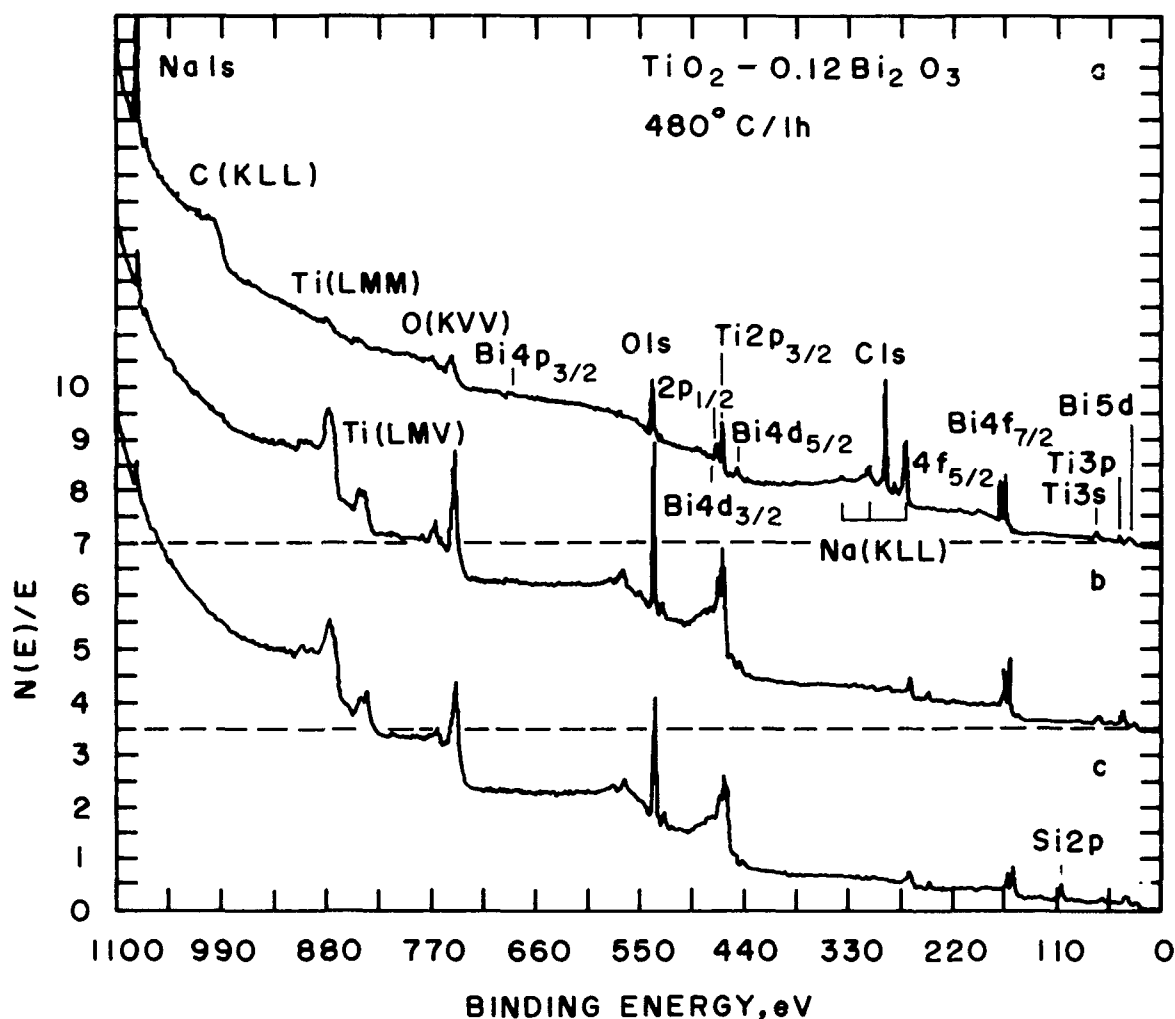


Fig. 14 XPS survey scan of a one alyer  $\text{TiO}_2\text{-Bi}_2\text{O}_3$  heat treated in air at  $480^\circ\text{C}$  during 60 minutes a) surface as received, b) after 12 minutes Ar sputtering ( $\sim 1/4$  of the depth), c) after 65,5 minutes sputtering (beginning of a glass-layer interface).

with a relatively large depletion of Ti. Beyond 60 minutes sputtering ( $\sim 1/3$  of the depth) the titanium concentration is constant but much higher than expected. The concentration of bismuth is relatively constant through the layer but is much lower than expected (4% instead of 6,9%). Both effects strongly affect the Bi/Ti ratio profile which is not constant through the layer and much lower than expected (originally 0,25). The reason for the low incorporation of Bi is not clear as we do not have data on dried sample at room temperature without heat treatment. However as we shall see below, Bi like Pb (or their oxides) volatilizes during the heat treatment and

this effect is already well pronounced for bismuth at 190°C.

Figure 14 shows three typical XPS scans of a similar sample heat treated at 480°C during 60 minutes and recorded a) at the surface (as received), b) after 12,5 Ar sputtering ( $\sim 1/4$  of the depth), c) after 65,5 minutes sputtering (in the interface glass-layer). The behavior of the O 1s peak is similar to what has been observed in the  $\text{TiO}_2$ -PbO compositions. The peak is not affected throughout the layer but a small shoulder appears toward higher BE when the interface is reached. This

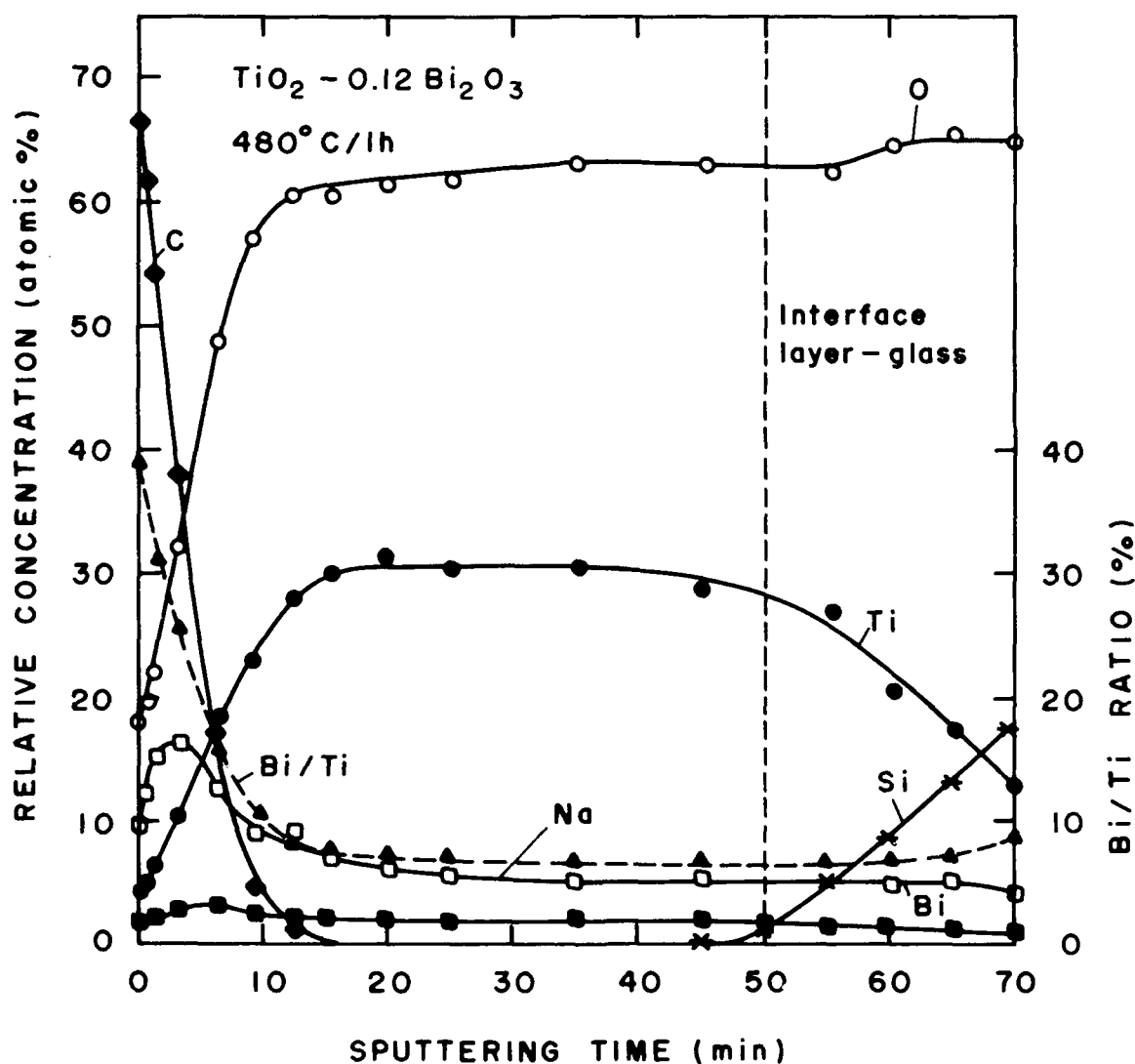


Fig. 15 XPS profiles of a one layer  $\text{TiO}_2$ - $\text{Bi}_2\text{O}_3$  film heat treated in air at 480°C during 60 minutes (left scale). The ratio Bi/Ti is shown as a broken line (right scale).

feature is attributed to oxygen in the glass substrate.

The results on Ti are also similar. We observe a broadening of the 2 p peaks and the appearance of a shoulder. A new doublet was never observed. The Bi behaviour is interesting. A shoulder at lower BE values of the 4 f doublet is already seen at the surface. It indicates the presence of a lower oxidation state even without sputtering. Sputtering enhances this feature. After 3,5 minutes sputtering the high and low BE doublet are of almost equal intensity and after 6,5 minutes the lower BE doublet become dominant. At the interface we observe Si 2 p and Si 2s as a shoulder of the Bi 4 f 7/2 peak. C is only observed at the surface while a low concentration of Na appears now throughout the layer.

Figure 15 shows the profile of all the elements. The most important result of this figure is the depth variation of the Bi/Ti ratio which clearly indicates that Ti is strongly depleted at the surface and that Bi has continued to evaporate. Its overall concentration is now of the order of  $\sim 2\%$  (originally 6,9%). The preparation of stoichiometric thin film compound in the  $\text{TiO}_2\text{-Bi}_2\text{O}_3$  system may therefore be very difficult.

The SIMS measurements performed in the same condition as that of figure 8 are shown in figure 16 and confirm these results. The intensity of Ti, Na and O curves are practically identical to those obtained for films of  $\text{TiO}_2\text{-PbO}$  composition but the carbon concentration (not shown in the figure) is a factor 2 to 5 smaller. The concentration of the elements is constant beyond the subsurface. The interface glass-layer appears however thinner.

SEM-EDX measurements indicate that the 2-d repartition of Ti, O, Bi, Na is uniform and homogeneous.

### 3.3. Films of $\text{TiO}_2\text{-CeO}_2$ composition

$\text{TiO}_2\text{-CeO}_2$  composition is particularly important for the realization of counter electrode for electrochromic devices and their optical and electrochemical behaviour have been reported<sup>4,5,6</sup>. Figure 17 shows XRD characterization of a three layer  $\text{Ce}_{0,5}\text{Ti}_{0,5}\text{O}_2$  film heat treated at 520°C during 30 minutes. The film is essentially amorphous to X-ray but broad peaks are superimposed. The identification of this structure is difficult; the position of the peaks seems however compatible with the presence of a small ceria crystallites.

Figure 18 shows SIMS profiles for Ti, Ce, Na, O,  $\text{Sn}^{118}$  and In for a two layer  $\text{Ti}_{0,5}\text{Ce}_{0,5}\text{O}_2$  film deposited on an ITO coating and heat treated at 420°C during 15 minutes. Comparing the intensity of the curves with those obtained previously under identical experimental conditions we see that the oxygen level is identical and that the titanium counts are smaller indicating that cerium has substituted these ions in

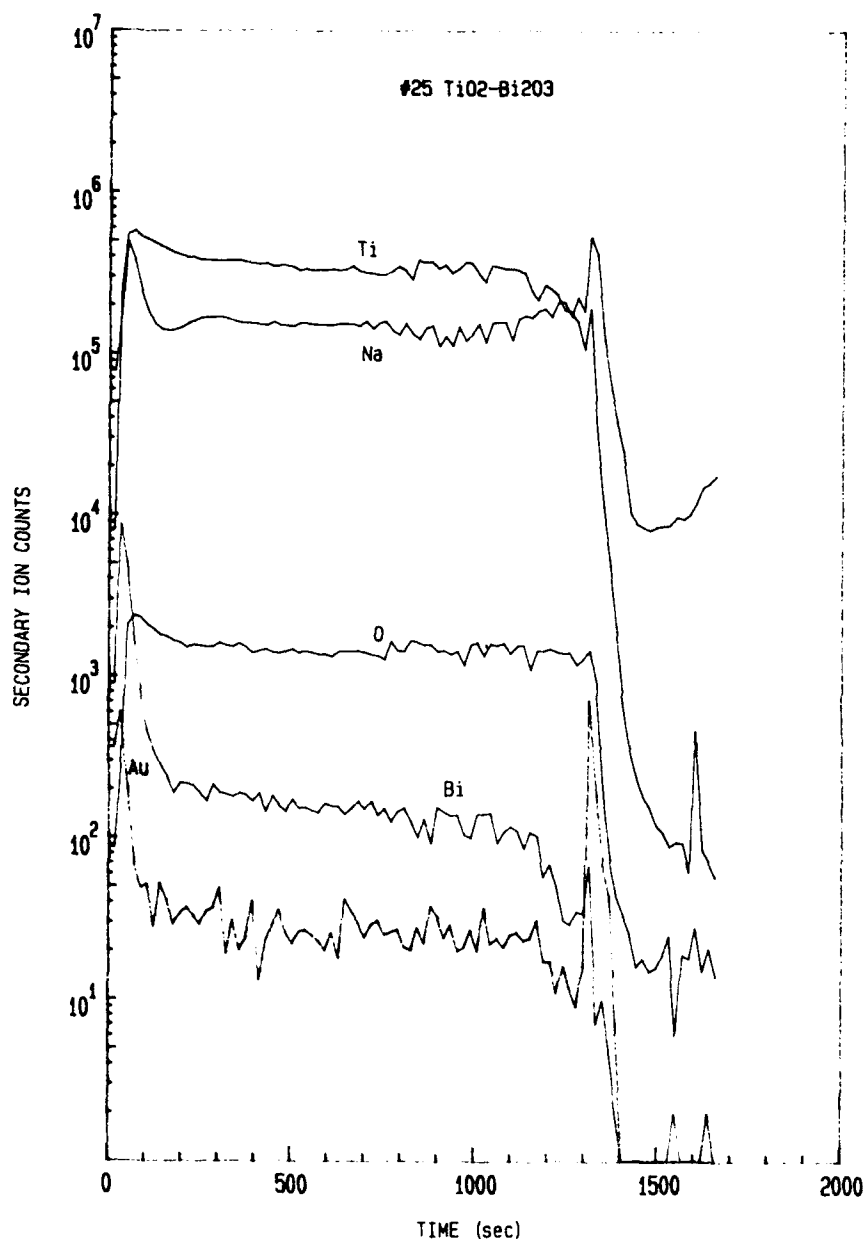


Fig. 16 SIMS profiles of a 3 layer  $\text{TiO}_2\text{-Bi}_2\text{O}_3$  film heat treated in air at  $480^\circ\text{C}$  during 60 minutes.

higher amount than bismuth and lead and probably has not suffered volatilization effect. Sodium counts are a factor four lower indicating that the ITO barrier has impeded its diffusion from the substrate. It appears in this film as an atmospheric contamination brought about during the manipulation and heat treatment. XPS measurements have not yet being done.

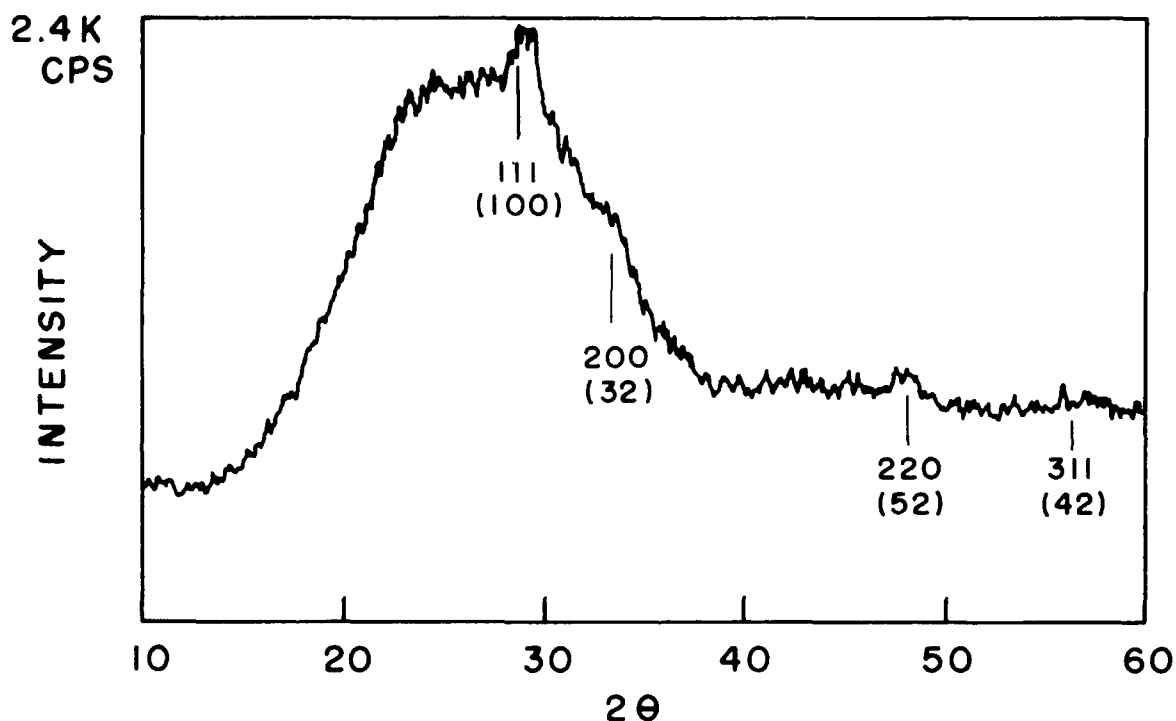


Fig. 17 XRD diffractogram of  $\text{TiO}_2\text{-CeO}_2$  film heat treated at  $520^\circ\text{C}$  during 30 minutes. The vertical marks indicate the position of the first four lines of crystalline  $\text{CeO}_2$  as well as their hkl and relative intensity values.

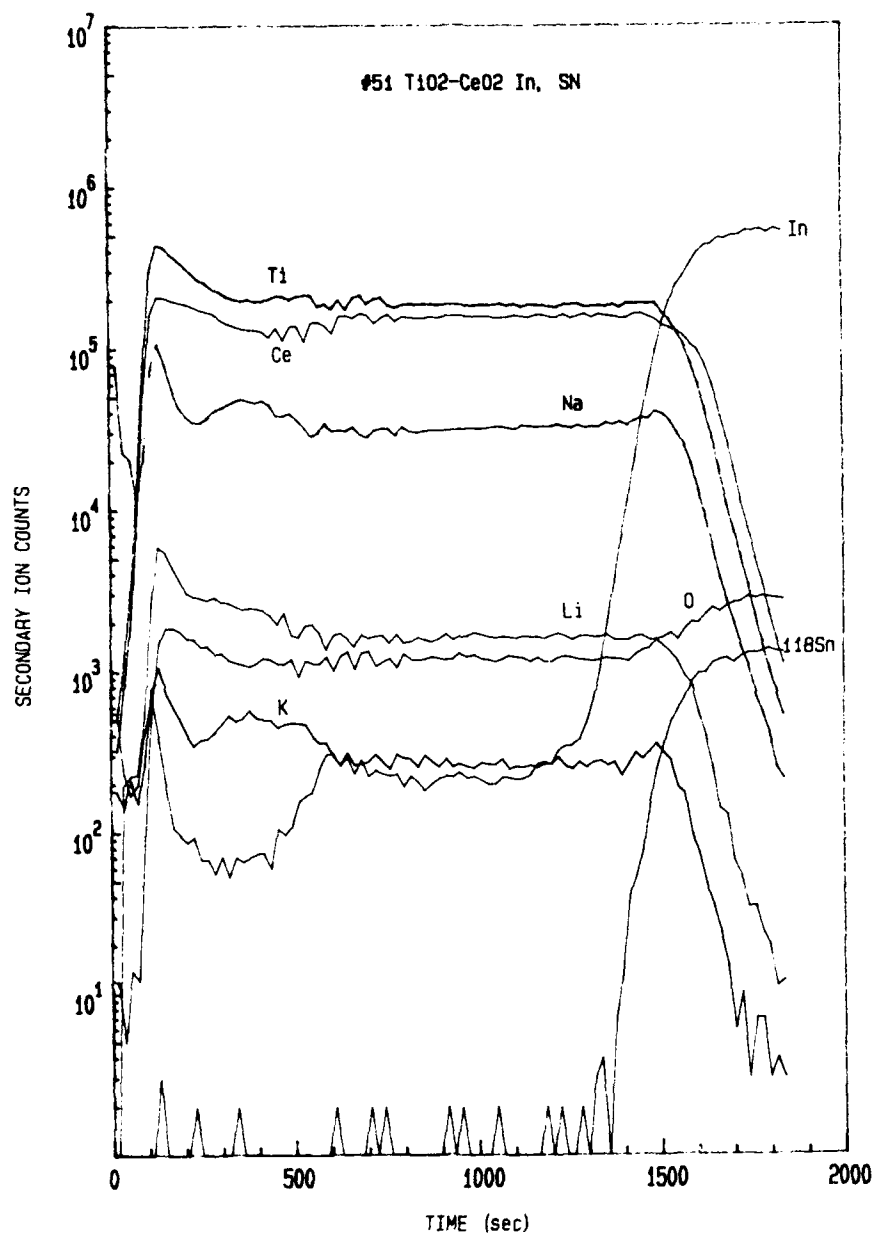


Fig. 18 SIMS profiles of Ti, Ce, Na, O, In and 118 Sn of a 2 layer  $\text{Ti}_{0.5}\text{Ce}_{0.5}\text{O}_2$  film deposited on ITO coated glass substrate and heat treated at  $420^\circ\text{C}$  during 15 minutes.

#### 4. CONCLUSIONS

The structure, texture and 2 d and depth profile chemical composition of thin films of  $\text{TiO}_2\text{-PbO}$ ,  $\text{TiO}_2\text{-Bi}_2\text{O}_3$  and  $\text{TiO}_2\text{-CeO}_2$  compositions prepared by sol-gel methods and deposited by dip coating process have been examined by XRD, SEM, DEM-EDX, XPS and SIMS techniques. For heat treatment up to  $500^\circ\text{C}$  during 60 minutes the films were found amorphous to X-ray except those of  $\text{TiO}_2\text{-CeO}_2$  composition which show the presence of very small crystallites of Ceria ( $\text{CeO}_2$ ). Their texture observed by SEM was found uniform except on the edge of the coatings where cracks and pores appeared. 2 D SEM-EDX analyse indicate a homogeneous repartition of all the main elements even under high magnification ( $560000\times$ ). The depth profiles measured by XPS in  $\text{TiO}_2\text{-PbO}$  and  $\text{TiO}_2\text{-Bi}_2\text{O}_3$  films show that the subsurface ( $\sim 10$  to  $15$  nm) has a different composition of that of the bulk layer. We observe a depletion of Ti and a segregation of Pb and Bi so that the ratios Pb/Ti and Bi/Ti decrease with the distance from the film surface.

Moreover the concentration of Pb and Bi beyond the subsurface is lower than expected indicating that these elements evaporate during the heat treatment of densification. This behaviour is already observed for treatment at  $200^\circ\text{C}/60$  minutes but is more pronounced at  $500^\circ\text{C}/60$  minutes. The subsurface is also strongly contaminated by carbon. These important results show that the realization of multicomponent thin film of definite stoichiometric composition in the  $\text{TiO}_2\text{-PbO}$  and  $\text{TiO}_2\text{-Bi}_2\text{O}_3$  may be difficult. Other compositions involving low vapor pressure oxide like BaO, etc are likely to present the same phenomena; this may explain in part the low ferroelectric performance obtained on  $\text{BaTiO}_3$  films<sup>12,13</sup>. Multilayer films present homogeneous composition beyond the subsurface and no subsurface effects are observed at the layers interfaces. In particular no atmospheric carbon is detected at these interfaces although each layer has been densified separately.

Interesting results have also been found relatively to the interaction of Ar ion beam with these solid surfaces. It is known that ion beam treatment may change the chemical nature of the surface to be examined. Reduction of lead, bismuth and titanium have been observed in all densified samples heat treated at  $500^\circ\text{C}$ . In partly densified samples heat treated at  $190^\circ\text{C}$  the effect is only observed for lead and bismuth but the 2p titanium peaks were not affected by the beam.

It is accepted that the ion-induced chemical damage is due to preferential sputtering of the oxygen from the oxide matrix and atomic rearrangement. Models based on a Sigmund's classification of sputtering events and sputtering yield equation have been developed by Malherbe<sup>14</sup> using a collisional approach in which both mass and bonding effects of the binary components are incorporated and by Kelly<sup>15</sup> using a thermal approach in which chemical binding is presumed to be the dominant factor. A more detailed analysis of these porous and densified samples<sup>8</sup> may therefore bring valuable indications on the viability of these models.

## 5. ACKNOWLEDGEMENTS

We would like to acknowledge J. Woodhouse, M. Kaufherr and J. Baker of the Material Research Laboratory, University of Illinois for the realization of the SEM, XPS and SIMS measurements and helpful discussion as well as J. Olek of Purdue University for performing the SEM-EDX measurements. M.A.A. would also like to thank Prof. Dr. D. Uhlmann, Arizona Materials Laboratories for his hospitality and discussions when writing this paper. The work was financially supported by the Program USP - BID CNPq, FAPESP and FINEP (Brazil).

## 6. REFERENCES

1. D.R. Uhlmann and G.P. Rajendran, "Coatings: the Land of Opportunity for Sol-Gel Technology" *Ultrastructure Processing of Advanced Ceramics*, J.D. Mackenzie and D.R. Ulrich ed, pp.241-253, Wiley-Interscience (1988)
2. M. A. Aegerter, Y. Charbouillot, N. D. S. Mohallem, A. A. Silva and L. H. Godoy "Synthesis, Characterization and Applications of Lead and Barium-Titanate Materials Prepared by the Sol-Gel Method", *Proceedings Ultrastructure Processing of Ceramics Glasses and Composites*, Tucson 1989, D. Uhlmann and D. Ulrich ed. (in press).
3. E. R. La Serra, Y. Charbouillot, P. Baudry and M. A. Aegerter "Preparation and Characterization of Thin Films of  $\text{TiO}_2$ -PbO and  $\text{TiO}_2$ - $\text{Bi}_2\text{O}_3$  Compositions", *Proceedings of the V<sup>th</sup> International Workshop Glasses and Ceramics from Gels*, Rio de Janeiro 1989, M. A. Aegerter ed. To be published in the *J. Non Cryst. Solids*, May issue 1990.
4. P. Baudry, A. C. M. Rodrigues, M. A. Aegerter and L. O. Bulhões "Dip-Coated  $\text{TiO}_2$ - $\text{CeO}_2$  films as transparent counter electrode for transmissive electrochromic devices", *Proceedings of the V<sup>th</sup> International Workshop - Glasses and Ceramics from Gels*, Rio de Janeiro 1989, M. A. Aegerter ed. To be published in *J. Non Cryst. Solids* May issue 1990.
5. J. C. L. Tonazzi, B. Valla, M. Macedo, P. Baudry, M. A. Aegerter, A. C. M. Rodrigues and L. O. Bulhões, "Characterization of an all solid state electrochromic window" *SPIE Proceedings*, Vol 1328, Paper 1328-37, *Sol-Gel Optics*, this volume.
6. C. Sanchez, "Précurseurs Moléculaires de Matériaux Inorganiques", *Procédés Sol-Gel*, Greco 93 CNRS (France), 1987.
7. C. Sanchez, F. Babonneau, S. Doeff and A. Léaustic, "Chemical Modifications of Titanium Alkoxide Precursors", *Ultrastructure Processing of Advanced Ceramics* J.D. Mackenzie and D. R. Ulrich ed. pp. 77-78, Wiley-Interscience (1988).
8. M. A. Aegerter, G. Kordas, to be published
9. A. Yamamoto and S. Kambara, *J. Am. Chem. Soc.* 79, p. 4344, 1957.
10. K. Iijima, Y. Tomita, R. Takaqama and I. Ueda, "Preparation of c-Axis Oriented  $\text{PbTiO}_3$  Thin Films and their Crystallographic Dielectric and Pyroelectric Properties" *J. Appl. Phys.* 60, pp. 361-367 (1986).
11. C. Chan, D. F. Ryder Jr., W. A. Spurgeon, "Synthesis and Microstructure of highly oriented Lead Titanate Thin Films prepared by a Sol-Gel Method", *J. Am. Cer. Soc.* 72, pp. 1495-1498 (1989).



12. N. D. S. Mohallem, "Preparação de pós e filmes finos de BaTiO<sub>3</sub> pelo método Sol-Gel" PhD Thesis, University of São Paulo, São Carlos (SP), Brazil (1990).

13. N. D. S. Mohallem and M. A. Aegerter, "Preparation and characterization of bulk and thin film BaTiO<sub>3</sub> Ceramics", Extended Abstract Electronics Division, Paper I-90, 92<sup>nd</sup> Annual Meeting, American Ceramic Society Meeting, Dallas 22-26 April 1990.

14. J. B. Malherhe, S. Hofmann and J. Sanz "Preferential Sputtering of oxides: a comparison of model predictions with experimental data". Appl. Surf. Sci, 27, pp. 355-365, 1986.

15. R. Kelly "On the Problem of whether Mass or Chemical Bonding is more important to Bombardment-induced Compositional Changes in Alloys and Oxides", Surf. Sci. 100, pp. 85-107, 1980.

SOL-GEL OPTICS

Volume 1328

**SESSION 7**

**Films and Coatings III**

*Chair*

**Jane A. Alexander**  
DARPA/DSO



## Preparation of $\text{Li}_2\text{B}_4\text{O}_7$ thin films by sol-gel method and their characterization

Toshinobu YOKO, Hiroya YAMASHITA and Sumio SAKKA

Institute for Chemical Research, Kyoto University, Uji, Kyoto-Fu 611, Japan

### ABSTRACT

The sol-gel method using lithium and boron-n-tributoxide as starting materials has been applied to prepare  $\text{Li}_2\text{B}_4\text{O}_7$  coating films on silica glass, silicon and sapphire single crystal substrates. The effects of the amounts of water and acid added to coating solutions, and the kinds of substrate on the crystallization of  $\text{Li}_2\text{B}_4\text{O}_7$  coating films were fully investigated. It was found that a sufficient amount of water is required for obtaining well-crystallized  $\text{Li}_2\text{B}_4\text{O}_7$  films of single phase, the addition of acids such as hydrochloric and acetic acids to the coating solution suppresses crystallization up to 600°C and gives highly oriented  $\text{Li}_2\text{B}_4\text{O}_7$  single phase films on further heating at 800°C.

### 1. INTRODUCTION

Recently, there have been increasing applications of the sol-gel method to the preparation of various functional thin coating films.<sup>1,2</sup> This is probably due to the facts that this method has several advantages over other ones such as CVD, sputtering and spray pyrolysis:

- 1) Any special apparatuses are not required for film formation.
- 2) Homogeneous multicomponent oxide films, even with exactly stoichiometric, can be obtained, because an intimate mixing is achieved in a liquid state.
- 3) A large size of coating films can be easily obtained by dip- or spin-coating technique.
- 4) Films with highly porous structure inherent in a gel can be obtained. The porous structure may disappear on heating. In some cases, it remains after heat-treatment if an appropriate heating condition is adopted.
- 5) Films of a metastable phase may be obtained, since low temperature synthesis is possible.

In the present study, the sol-gel method has been applied to the preparation of  $\text{Li}_2\text{B}_4\text{O}_7$  films which are promising materials for surface acoustic (SAW) devices<sup>3-5</sup>, and thermally stimulated exoelectron emission dosimeter (TSEED) and thermally stimulated luminescence dosimeter (TLD)<sup>6-9</sup>. The present paper deals with the effects of the addition of water<sup>10</sup> and acid<sup>11,12</sup> to the coating solution, and the kinds of substrate on the nature of the sol-gel derived  $\text{Li}_2\text{B}_4\text{O}_7$  coating films.

### 2. EXPERIMENTAL

Coating solutions were prepared by hydrolyzing lithium methoxide,  $\text{LiOCH}_3$  and boron tri-n-butoxide,  $\text{B}(\text{OC}_4\text{H}_9)_3$ . Lithium methoxide was synthesized by dissolving lithium metal in methanol at temperature of 0 to 20°C.  $\text{B}(\text{OC}_4\text{H}_9)_3$  was added to the resultant transparent  $\text{LiOCH}_3$  methanol solution with a syringe at a rate of 10ml/min at 20°C. The solution was stirred at 40°C until it became transparent, and then diluted to a concentration of 0.4M  $\text{LiOCH}_3$  and 0.8M  $\text{B}(\text{OC}_4\text{H}_9)_3$  with methanol. All the procedures were carried out in a dry nitrogen atmosphere. Then, various amounts of water for hydrolysis were added to the solution in air to form a coating solution.

In some cases, an acid was added to the solution.

Silica glass, Si (100), (110) and (111) single crystal and sapphire ( $\bar{1}\bar{1}02$ ) single crystal plates were used as substrates.  $\text{Li}_2\text{B}_4\text{O}_7$  thin gel films were formed on substrates by dip-coating. The substrates were immersed in a coating solution, withdrawn at a fixed speed and dried at 200°C for 10min. This procedure was repeated until the desired film thickness was attained. The films thus obtained were subjected to post-heat treatment at a given temperature between 450 to 800°C for 30 and 60min. In order to check the effect of film thickness on the crystallization, thick films of about 0.5 mm in thickness were prepared by spreading a drop of coating solution on the commercial slide glasses and heat-treated at temperatures between 200 and 550°C for 30 min.

The crystallization behavior of the as-prepared gel films was monitored by an X-ray thin film diffractometer of Rigaku Denki model RINT-1400. Transmission spectra were recorded using a UV-visible spectrophotometer of Hitachi model 624. Surface structure was observed with a scanning electron microscope of Hitachi model S-450.

### 3.RESULTS

#### 3.1.Effects of water

Fig.1 a-d show the X-ray diffraction patterns of  $\text{Li}_2\text{B}_4\text{O}_7$  coating films, 3.5 $\mu\text{m}$  thick, formed on silica glass substrates from the coating solutions with different amounts of water and post-heated at 450, 500, 550 and 600°C, respectively, for 30min.  $R_w$  in the figures represents the molar ratio of water to the total alkoxides. It can be said from these figures that for  $R_w=0$  gel films do not crystallize below 500°C, but for  $R_w=1.6$  they do even at 450°C, and for smaller amounts of water than  $R_w=1.2$  the side-products such as  $\text{LiCOOH}\cdot\text{H}_2\text{O}$  and  $\alpha\text{-Li}_4\text{B}_2\text{O}_5$  are formed in addition to  $\text{Li}_2\text{B}_4\text{O}_7$  phase.

Fig.2 a-d show the SEM photographs of some of the samples shown in Fig.1. For  $R_w=0$  the films which were not well crystallized have a relatively smooth and glassy surface. On the contrary, for  $R_w=1.6$  they have a well developed particulate and very porous surface structure.

#### 3.2.Effects of film thickness

In order to check the effects of film thickness on the crystallization behavior, thicker films of about 0.5mm in thickness were prepared by spreading a drop of coating solution with  $R_w=0.2$  on the slide glasses and heat-treated at temperatures of 200 to 500°C for 30min. Their X-ray diffraction patterns are shown in Fig.3. In this case, crystallization begins at 250°C, which is much lower compared with the case for the thin films shown in Fig.1. Therefore, one can say that thin films have a higher resistance against crystallization than thick films do.

#### 3.3.Effect of acid

Fig.4 shows the optical transmission spectra of  $\text{Li}_2\text{B}_4\text{O}_7$  films formed on the silica glass substrates from the coating solutions with  $R_w=2.4$ , and different amounts and kinds of acid. The  $\text{Li}_2\text{B}_4\text{O}_7$  film prepared from the coating solution without acid has a very low transmittance less than 20%. On the other hand, when an acid such as acetic, hydrochloric and nitric acids is added to the coating solution, the transmittance of  $\text{Li}_2\text{B}_4\text{O}_7$  films is markedly improved up to more than 80%.  $R_A$ ,  $R_H$  and  $R_N$  in the figure represent the molar ratios of acetic, hydrochloric and nitric acids, respectively, to the sum of  $\text{LiOCH}_3$  and  $\text{B}(\text{OC}_4\text{H}_9)_3$ .

The SEM photographs of  $\text{Li}_2\text{B}_4\text{O}_7$  films which were formed on Si(100) single crystal

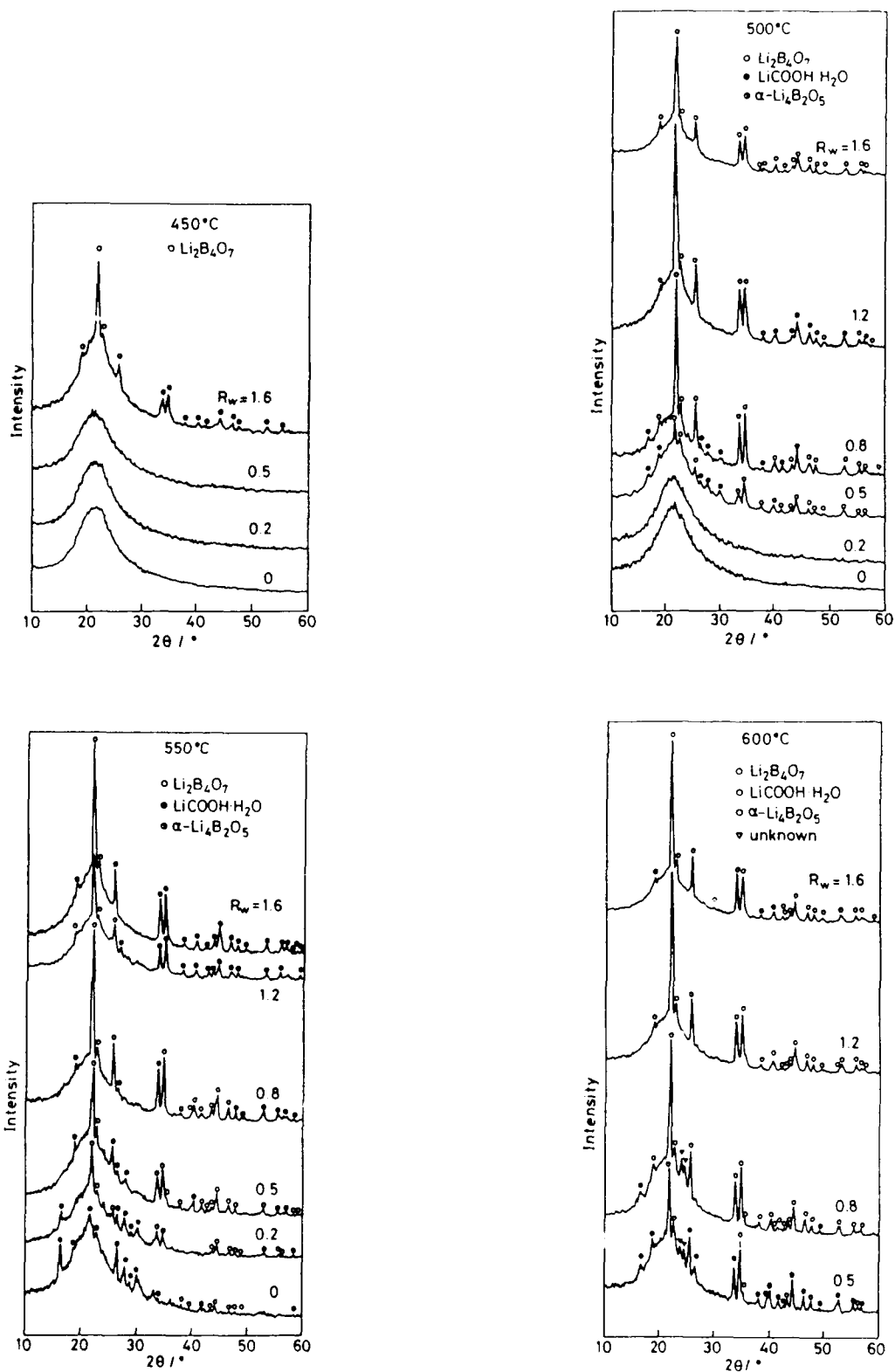


Fig.1. X-ray diffraction patterns of  $\text{Li}_2\text{B}_4\text{O}_7$  thin films of  $3.5\mu\text{m}$  in thickness on the silica glasses heated at (a) 450°C, (b) 500°C, (c) 550°C and (d) 600°C for 30 min for  $R_w$  ranging from 0 to 1.6.

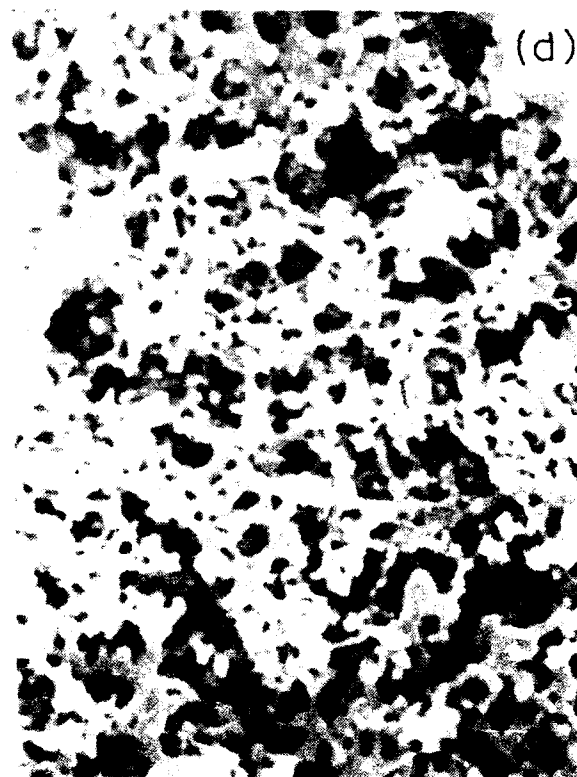
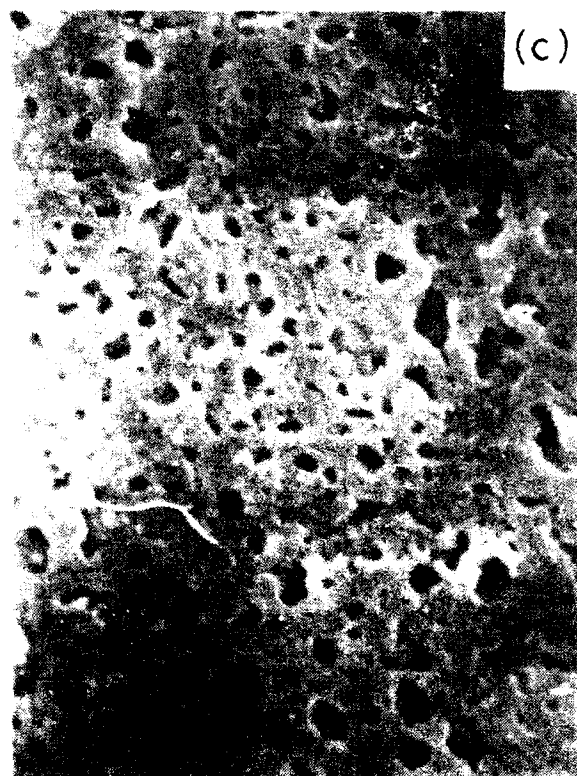


Fig.2. Scanning electron microphotographs of the surface of  $\text{Li}_2\text{B}_4\text{O}_7$  thin films prepared from solutions with different water content under different heating temperatures: (a)  $R_w=0$ ,  $500^\circ\text{C}$ , (b)  $R_w=1.6$ ,  $500^\circ\text{C}$  (c)  $R_w=0$ ,  $550^\circ\text{C}$  and (d)  $R_w=1.6$ ,  $550^\circ\text{C}$ .

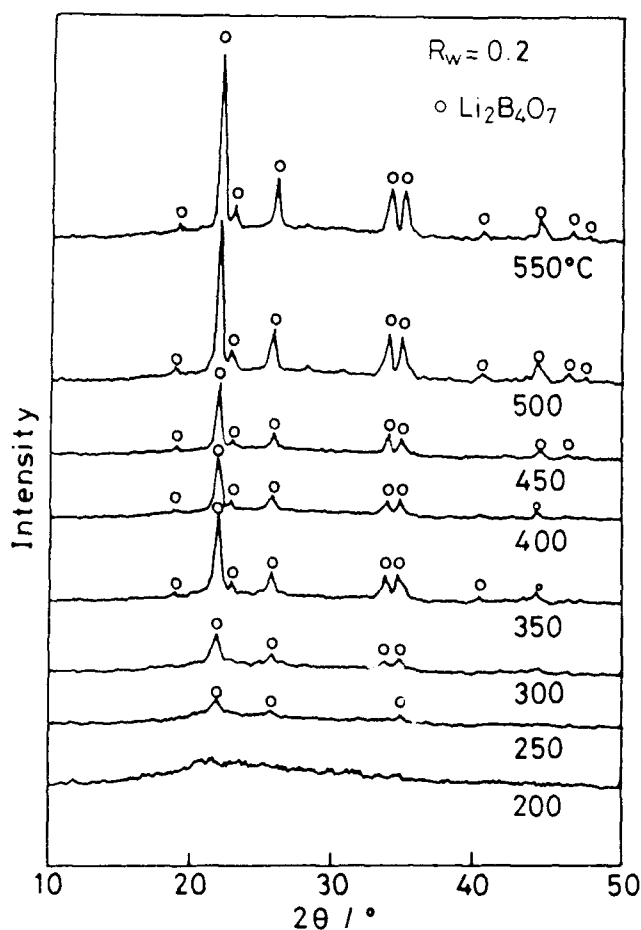


Fig.3. X-ray diffraction patterns of  $\text{Li}_2\text{B}_4\text{O}_7$  thick films of 0.5mm in thickness on the slide glasses heated at various temperatures from 200°C to 550 °C.  $R_w$  defined as the mole ratio of  $[\text{H}_2\text{O}]/([\text{LiOCH}_3]+3[\text{B}(\text{OC}_4\text{H}_9)_3])$  is fixed at 0.2.

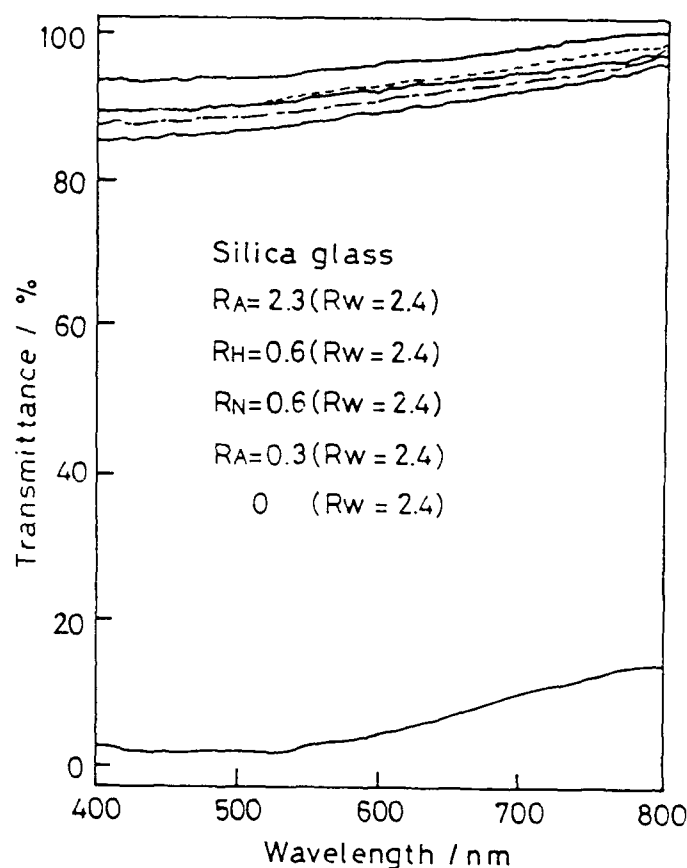


Fig.4. Optical transmission spectra of  $\text{Li}_2\text{B}_4\text{O}_7$  films on silica glasses which were heated at 550°C. The number of applications is 8 except the bottom curve for which it is 4, the speed of withdrawing 10 cm/min and  $R_w$  2.4. From the top to downward, the acid contents in the solution are as follows; silica glass only,  $R_A=2.3$ ,  $R_H=0.6$ ,  $R_N=0.6$ ,  $R_A=0.3$ , and without acid.

substrates and post-heated at 550°C for 30min are shown in Fig.5 and 6. In the films prepared from the coating solution without acid, particles of about 1μm in diameter can be seen as shown in Fig.5a. The addition of a small amount of acetic acid of  $R_A=0.02$  inhibits the formation of particles, and for  $R_A=2.3$  no such particulate structure can be seen and the surface is very smooth. This is also the case for the  $\text{Li}_2\text{B}_4\text{O}_7$  films from the coating solutions containing other acids as shown in Fig.6.

Fig.7 shows X-ray diffraction patterns of the  $\text{Li}_2\text{B}_4\text{O}_7$  films whose SEM photographs are shown in Fig.5 a-c. For  $R_A=0$  and 0.02 the diffraction peaks due to  $\text{Li}_2\text{B}_4\text{O}_7$  can be seen, while for  $R_A=2.3$  no peaks are found, indicating that the films from the coating solution with  $R_A=2.3$  are amorphous. Similarly, the addition of hydrochloric acid of  $R_A$  more than 0.3 to the coating solution results in the formation of amorphous films.

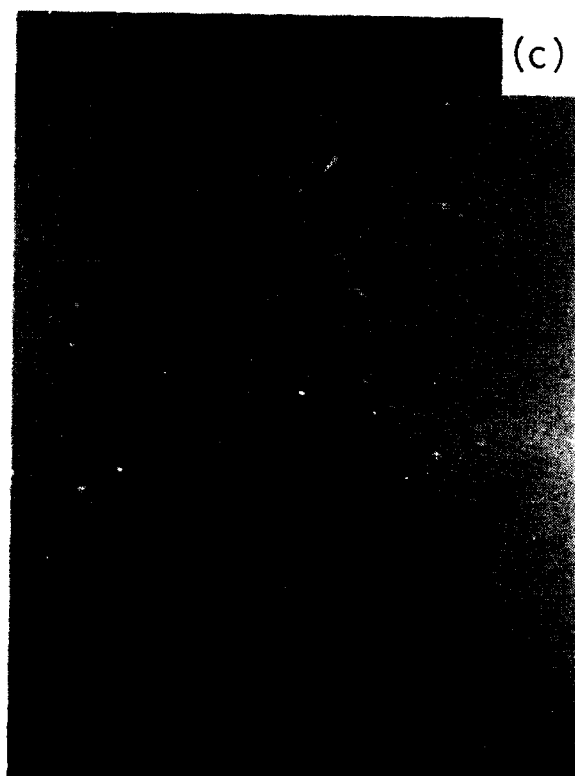
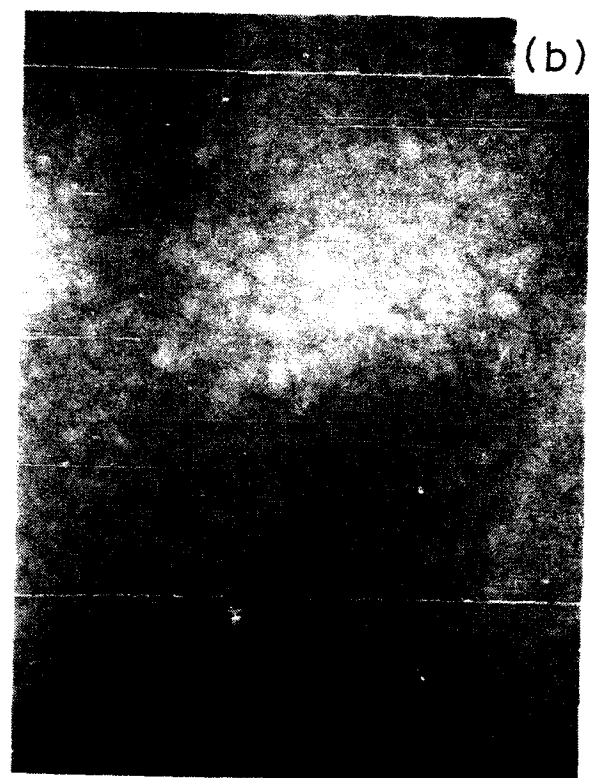


Fig. 5. Scanning electron micrographs of coating films on silicon (100) substrates heated at 550°C. The number of applications is 8, the speed of withdrawing 10 cm/min and  $R_w$  2.4. The acid contents in the solutions are as follows: (a) without acid, (b)  $R_A=2.0 \times 10^{-3}$  and (c)  $R_A=2.4$ .



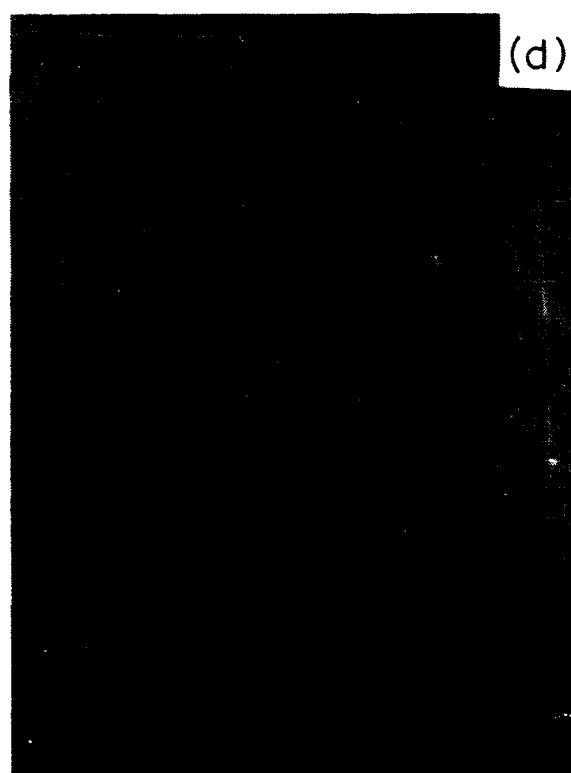
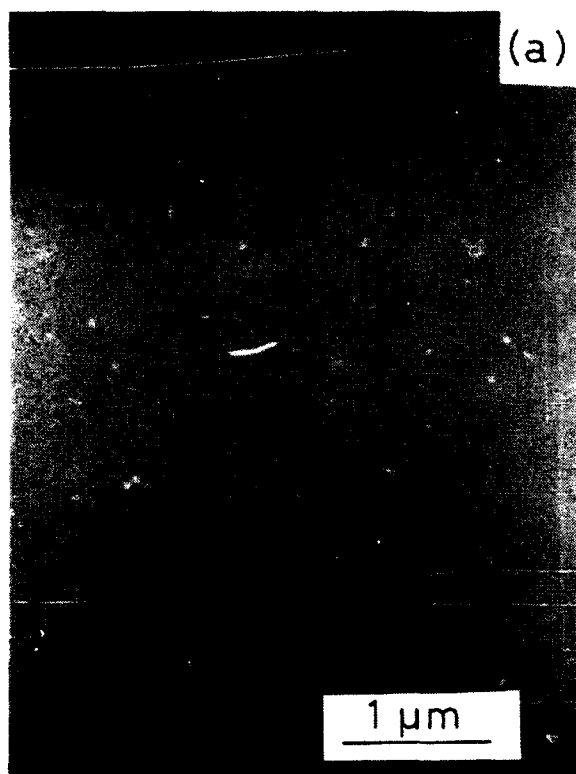


Fig.6. Scanning electron micrographs of coating films on silicon (100) substrates heated at 550°C. The number of applications is 8, the speed of withdrawing 10 cm/min and  $R_w$  2.4. The acid contents in the solutions are as follows: (a)  $R_H=0.3$ , (b)  $R_H=0.6$ , (c)  $R_H=1.3$  and (d)  $R_H=0.6$ .

### 3.4. Highly oriented coating films

Next, crystallization behavior of the amorphous films was investigated. Fig. 8 shows the variation of X-ray diffraction patterns, when  $\text{Li}_2\text{B}_4\text{O}_7$  films formed on Si (100) from the coating solutions with  $R_w=2.4$  and  $R_A=2.3$  and heated at  $600^\circ\text{C}$  for 30 min were further heated at  $800^\circ\text{C}$  for 60 min in nitrogen atmosphere. It is interesting to note that a strong peak due to (244) and a small one due to (235) planes of  $\text{Li}_2\text{B}_4\text{O}_7$  appear although the formation  $\alpha$ -quartz takes place due to the oxidation of silicon substrate. This clearly indicates that the  $\text{Li}_2\text{B}_4\text{O}_7$  crystals are highly oriented in the films. The degree of orientation along (122) plane estimated by the method of Lotgering<sup>13</sup> is 0.81.

Fig. 9 shows the X-ray diffraction patterns of the  $\text{Li}_2\text{B}_4\text{O}_7$  films formed on Si (100) from the coating solutions containing hydrochloric acid of  $R_H=1.3$ . In this case, only a peak due to (244) plane can be seen, although the peak intensity is slightly lower compared with the case where acetic acid is added. The degree of orientation along (122) plane is 0.80.

Much higher degrees of orientation were observed for the films from the coating solutions containing acetic and hydrochloric acids as shown in Fig. 9 a and b, when Si(111) substrates were used. For both cases, the degree of orientation along (122) plane is as high as 0.98. However, the formation of  $\alpha$ -quartz is observed at the same time.

In Fig. 10 the X-ray diffraction patterns of the  $\text{Li}_2\text{B}_4\text{O}_7$  films which were prepared from the coating solutions with  $R_H=0.3$  and post-heated at  $600^\circ\text{C}$  are shown. In this case any other peaks than (244) plane cannot be observed and the degree of orientation is 0.99. That is, lowering heating temperature and acid content of the coating solution effectively suppresses the formation of  $\alpha$ -quartz and at the same time improves the degree of orientation.

A similar behavior was also observed when Si(100) substrates were used. In this case, however, the preferentially oriented plane is not (244) but (235). The results for sapphire (1102) substrate is shown in Fig. 11. Both (244) and (235) planes are preferentially oriented. Their degrees of orientation are 0.74 and 0.25, respectively, which are not so good as the case for Si.

## 4. DISCUSSION

### 4.1. Role of water

It has been found that the addition of a sufficient amount of water to the coating solution for hydrolysis promotes the crystallization of  $\text{Li}_2\text{B}_4\text{O}_7$  gel films without the formation of the side-products such as  $\text{LiCOOH}\cdot\text{H}_2\text{O}$  and  $\alpha\text{-Li}_4\text{B}_2\text{O}_5$  phases.  $\text{Li}_2\text{B}_4\text{O}_7$  crystal is known to consist of three-dimensionally linked diborate groups.<sup>14</sup> Therefore, it is reasonable to assume that the addition of a sufficient amount of water to

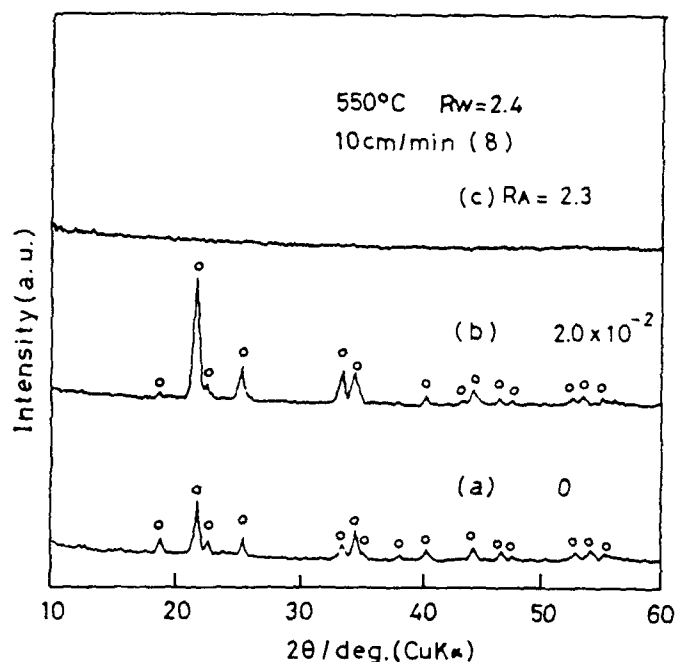


Fig. 7. X-ray diffraction patterns of the coating films heated at  $550^\circ\text{C}$ . The content of acetic acid in the solutions are as follows: (a) 0, (b)  $R_A=2.0\times 10^{-2}$  and (c)  $R_A=2.3$ .

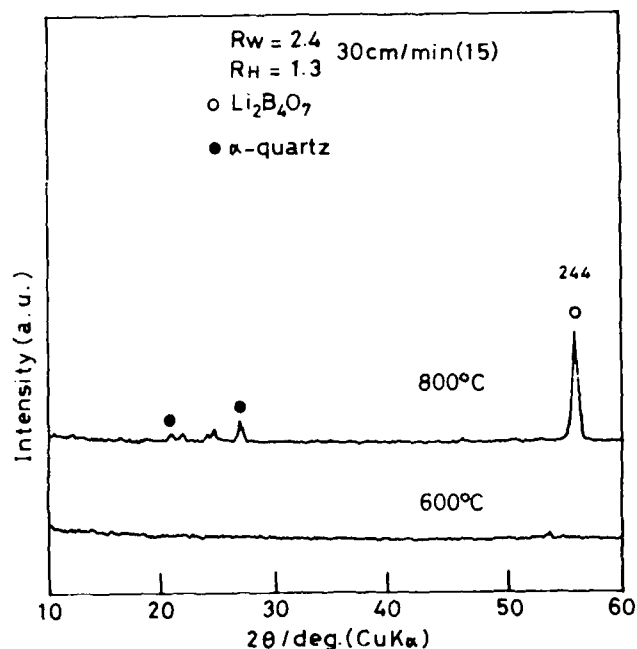
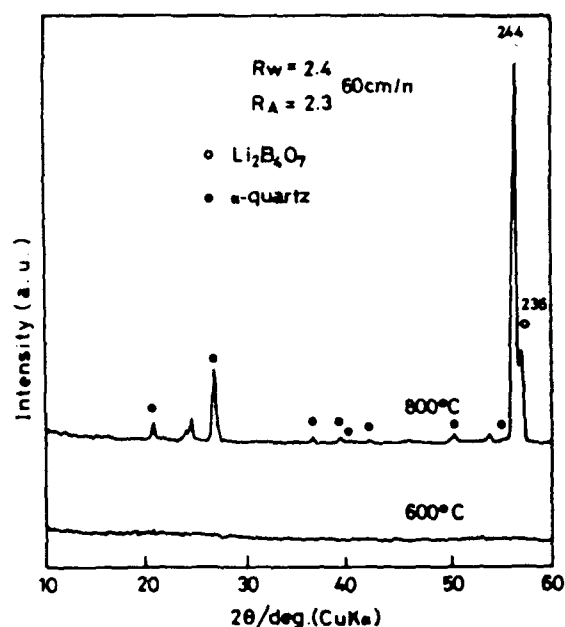


Fig.8. X-ray diffraction patterns of  $\text{Li}_2\text{B}_4\text{O}_7$  films on silicon (100) heat-treated at 600°C and 800°C. The number of applications is 15 and the speed of withdrawing is 60 cm/min.  $R_w$  is fixed at 2.4 and (a)  $R_A = [\text{CH}_3\text{COOH}]/([\text{LiOCH}_3] + [\text{B}(\text{OC}_4\text{H}_9)_3])$  is fixed at 2.3 and (b)  $R_H = [\text{HCl}]/([\text{LiOCH}_3] + [\text{B}(\text{OC}_4\text{H}_9)_3])$  at 1.3.

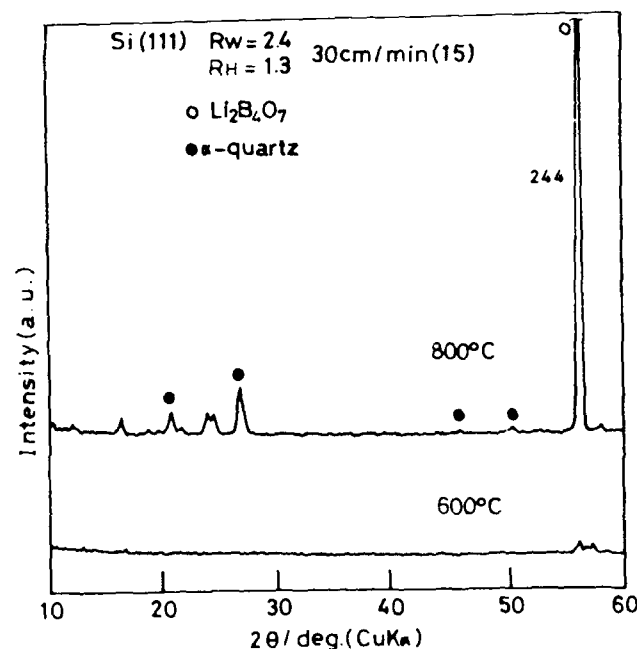
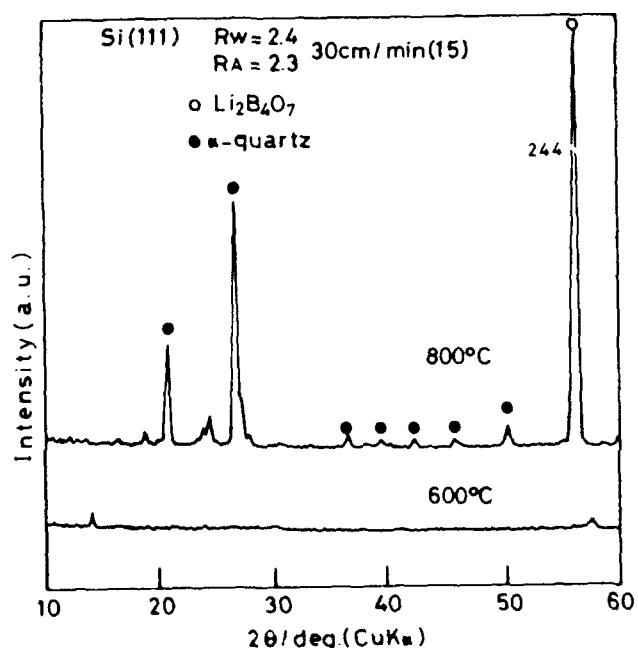


Fig.9. X-ray diffraction patterns of  $\text{Li}_2\text{B}_4\text{O}_7$  films on silicon (111) heat-treated at 600°C and 800°C. The number of applications is 15 and the speed of withdrawing is 30 cm/min. (a) acetic acid and (b) hydrochloric acid.  $R_w$ ,  $R_A$  and  $R_H$  are fixed at 2.4, 2.3 and 1.3, respectively.

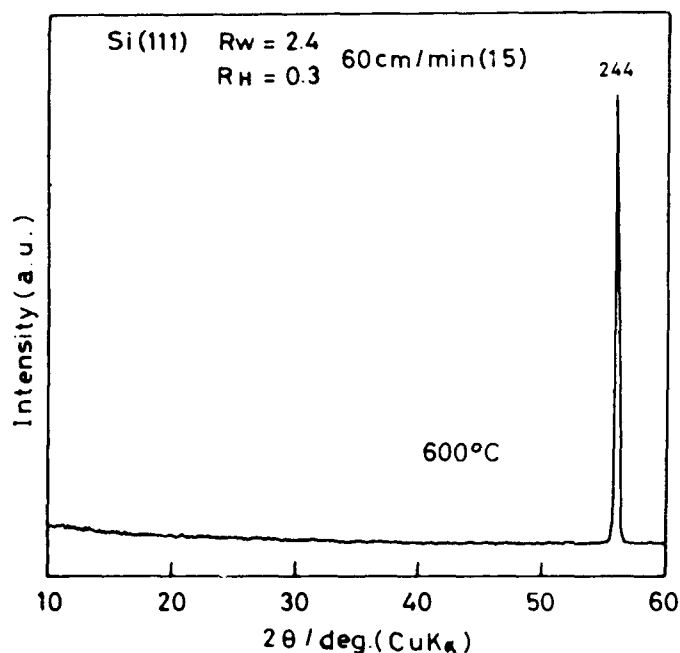


Fig.10. X-ray diffraction patterns of  $\text{Li}_2\text{B}_4\text{O}_7$  films on silicon (111) heat-treated at  $600^\circ\text{C}$ . The number of applications is 15 and the speed of withdrawing is 60 cm/min.  $R_w$  and  $R_H$  are fixed at 2.4 and 0.3, respectively.

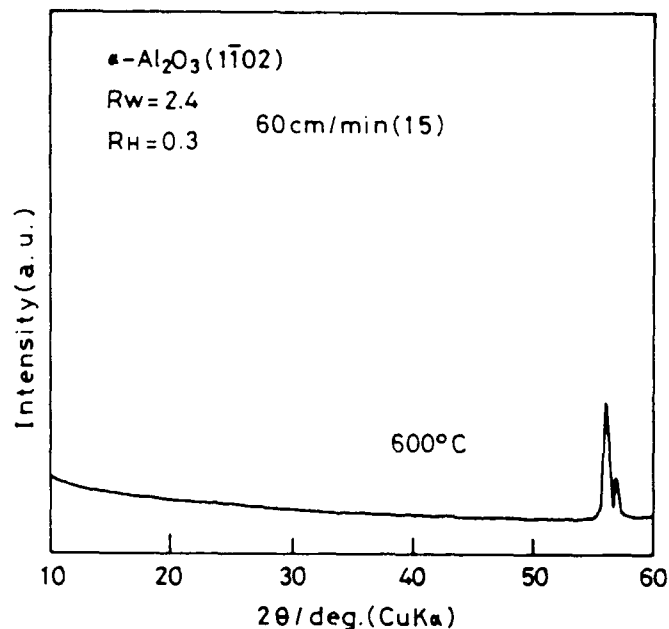
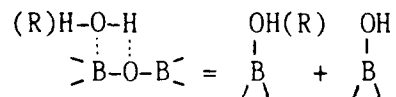


Fig.11. X-ray diffraction patterns of  $\text{Li}_2\text{B}_4\text{O}_7$  films on sapphire (1102) heat-treated at  $600^\circ\text{C}$ . The number of applications is 15 and the speed of withdrawing is 60 cm/min.  $R_w$  and  $R_H$  are fixed at 2.4 and 0.3, respectively.

the alkoxide solution may result in the formation of diborate groups whose negative charges are compensated by  $\text{Li}^+$  ions. The presence of 4-coordinated boron in a sol was confirmed by means of  $^{11}\text{B}$  NMR by Brinker et al.<sup>15</sup> Although they claimed that water/alkoxide ratios greater than 0.4 often resulted in precipitation of boric acid, in the present study water in the ratios up to 1.6 and 2.4 without and with the addition of acid, respectively, could be successfully introduced in sols. Weinberg et al.<sup>16</sup> reported that lithium borate gels heated at  $450^\circ\text{C}$  are still amorphous. This can be explicable by insufficient amounts of water added for hydrolysis.

$\text{B}(\text{OC}_4\text{H}_9)_3$  is a very volatile substance. Therefore, unless a sufficient amount of water is added to the alkoxide solution for hydrolysis, unhydrolyzed  $\text{B}(\text{OC}_4\text{H}_9)_3$  may evaporate on drying and heating, causing the deficiency of  $\text{B}(\text{OC}_4\text{H}_9)_3$  component in the gel film. This, in turn, may lead to the formation of the side-products such as  $\text{LiCOOH}\cdot\text{H}_2\text{O}$  and  $\alpha\text{-Li}_2\text{B}_2\text{O}_5$  phases due to the lack of boron content.

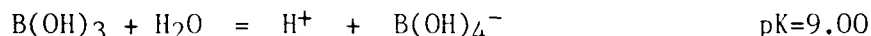
Brinker et al.<sup>15</sup> also pointed out that excess alcohol or water breaks  $=\text{B}-\text{O}-\text{B}=$  bonds and prevents gelation according to the reaction,



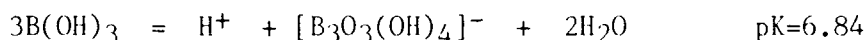
However, as found in the present study, the addition of water of more than 1.6 in the molar ratio to the total alkoxides is required to avoid the vaporization loss of boron alkoxide and the precipitation of the side-products.

#### 4.2. Role of acid

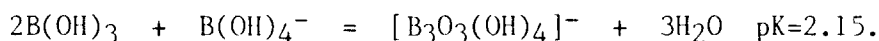
The addition of acid to the coating solution has been found to suppress the crystallization of  $\text{Li}_2\text{B}_4\text{O}_7$  gel films to a considerable extent, the effect of which is completely different from water. As is well-known, boric acid is in equilibrium with tetrahedral  $\text{B}(\text{OH})_4^-$  in aqueous solution as follows,<sup>17</sup>



At boron concentrations greater than about 0.025M and pH values between 8 and 10, polyborate species become important, for example,



and



The former two equations suggest that the addition of acid to the solution shifts the equilibrium of the last equation towards the left, leading to the depolymerization of polyborate species containing tetrahedral boron species. Therefore, the crystallization of  $\text{Li}_2\text{B}_4\text{O}_7$  gel films is suppressed and the films remain amorphous up to a higher temperature of 600°C.

### **4.3. Crystal growth with preferred orientation**

It is very interesting to note that the suppression of the crystallization of  $\text{Li}_2\text{B}_4\text{O}_7$  gel films is rather favorable for crystal growth with preferred orientation. The epitaxial crystal growth of  $\text{Li}_2\text{B}_4\text{O}_7$  gel films on the silicon and sapphire single crystal substrates becomes possible since the crystal growth proceeds very slowly via amorphous state.

In the separate paper<sup>12</sup>, the reason for the preferential crystal growth along  $\text{Li}_2\text{B}_4\text{O}_7$  (122) plane both on the Si (100) and (111) substrates is discussed in detail based on the lattice mismatch between the  $\text{Li}_2\text{B}_4\text{O}_7$  (100), (001) and (122), and the Si (100) and (111) planes. Since there is not significant difference in the lattice mismatch between them, it is concluded that the preferred orientation along  $\text{Li}_2\text{B}_4\text{O}_7$  (122) plane without respect to the plane of the substrate is possibly ascribed to the smaller number of oxygen atoms in the (122) plane of  $\text{Li}_2\text{B}_4\text{O}_7$  involved in the lattice matching to minimize the lattice distortion energy between the  $\text{Li}_2\text{B}_4\text{O}_7$  film and the Si substrate. The crystal growth along  $\text{Li}_2\text{B}_4\text{O}_7$  (122) plane is also observed for the sapphire (1102) substrate in the present study as shown in Fig.11, the oxygen atom arrangement of which is very different from that of Si (100) and (111). This experimental fact also supports the previous conclusion.

On the other hand, Hirano and Kato<sup>18</sup> reported that the sol-gel derived  $\text{LiNbO}_3$  films with preferred orientation are formed on sapphire single crystals, but not on Si. In this case, the preferential crystal growth takes place along the oxygen closest packing differing from the present result for the  $\text{Li}_2\text{B}_4\text{O}_7$  films.

### **5. ACKNOWLEDGMENTS**

One of the authors (T.Y.) would like to express his appreciation to the Iwatani Naoji Foundation for the financial support of this work.

## 6. REFERENCES

- 1.S. Sakka, Science of Sol-Gel Methods, pp.85-103, AGNE Shoufusha, Tokyo, 1988.  
[in Japanese]
- 2.S. Sakka, "Sol-Gel Fibers and Coating Films", Sol-Gel - Science and Technology, eds. by M.A. Aegerter et al., pp.346-374, World Scientific, Singapore, 1989.
- 3.R.W.Whatmore, N.M.Shorrocks, C.O'hara, F.W.Ainger and I.M.Yuung, "Lithium Tetraborate: A New Temperature-Compensated SAW Substrate Material", Electron. Lett., **17**, 11-12, 1981.
- 4.T.Shiosaki, M.Adachi, H.Kobayashi, K.Araki and A.Kawabata, "Elastic, Piezoelectric, Acousto-Optic and Electro-Optic Properties of  $\text{Li}_2\text{B}_4\text{O}_7$ ", Jpn. J. Appl. Phys., **24**, 25-27(1985).
- 5.K.Fukuta, J.Ushizawa, H.Suzuki, Y.Ebata and S.Matsumura, "Growth and Properties of  $\text{Li}_2\text{B}_4\text{O}_7$  Single Crystal for SAW Device Applications", ibid., **22-2** (supplement), 140-142(1983).
- 6.T.Kawamoto, R.Kikuchi, M.Sato, H.Yanagisawa and M.Kawanishi, "Exoelectron Emission from Surface Layer of  $\text{Li}_2\text{B}_4\text{O}_7$  Glass Ceramics", J.Ceram.Soc.Jpn., **92**, 268-73, 1984. [in Japanese]
- 7.T. Kawamoto, R. Kikuchi, M. Sato, H. Yanagisawa and M.Kawanishi, "Thermally Stimulated Exoelectron Emission and Thermoluminescence from Ion Implanted  $\text{Li}_2\text{B}_4\text{O}_7$  Glass Ceramics and LiF", ibid., **92**, 575-78, 1984. (in Japanese)
- 8.A. Tomiya and N. Takeuchi, "Thermally Stimulated Exoelectron Emission Observed in Mixed  $\text{Li}_2\text{B}_4\text{O}_7$ -LiCl Ceramics", J. Mater. Sci. Lett., **7** 1157-59, 1988.
- 9.Y.Kutomi and N. Takeuchi, "Thermoluminescence in Lithium Tetraborate Doped with Activators", ibid., **5**, 51-53, 1986; Y. Kutomi, T. Ariyasu and N. Takeuchi, "Thermoluminescence of Crystallized Glasses  $\text{Li}_2\text{B}_4\text{O}_7$ ", J. Ceram. Soc. Jpn., **95**, 686-92, 1987. [in Japanese]
- 10.H.Yamashita, T.Yoko and S.Sakka, "Preparation of  $\text{Li}_2\text{B}_4\text{O}_7$  Thin Films by Sol-Gel Method", J.Mater.Sci.Lett., in press.
- 11.Idem., "Sol-Gel Preparation of Amorphous  $\text{Li}_2\text{B}_4\text{O}_7$  Coating Films", in press.
- 12.Idem., "Preparation of  $\text{Li}_2\text{B}_4\text{O}_7$  Films with Preferential Orientation by Sol-Gel Method", submitted to J.Am.Ceram.Soc.
- 13.F. K. Lotgering, "Topotactical Reactions with Ferrimagnetic Oxides Having Hexagonal Crystal Structures-I", J. Inorg. Nucl. Chem., **9**, 113-123, 1959.
- 14.J.Krogh-Moe, "The Crystal Structure of Lithium Diborate,  $\text{Li}_2\text{O} \cdot 2\text{B}_2\text{O}_3$ ", Acta Cryst., **15**, 190-3, 1962; "Refinement of the Crystal Structure of Lithium Diborate,  $\text{Li}_2\text{O} \cdot 2\text{B}_2\text{O}_3$ ", **B24**, 179-81, 1968.
- 15.C.J.Brinker, K.J.Ward, K.D.Keefer, E.Holupka, P.J.Bray and R.K.Pearson, "Synthesis and Structure of Borate Based Aerogels", Aerogels, ed. by J.Fricke, pp.57-67, Springer Verlag, Berlin, 1986.
- 16.M.C.Weinberg, G.F.Neilson, G.L.Smith, B.Dunn, G.S.Moore and J.D.Mackenzie, "The Preparation and Characterization of a Lithium Borate Glass Prepared by the Gel Technique", J.Mater.Sci., **20**, 1501-08, 1985.
- 17.W.L.Jolly, Modern Inorganic Chemistry, pp.198, McGraw-Hill, New York, 1985.
- 18.S.Hirano and K.Kato, "Preparation of Crystalline  $\text{LiNbO}_3$  Films with Preferred Orientation by Hydrolysis of Metal Alkoxides", Adv. Ceram., **3**, 503-6, 1988.



## **PHOTOVOLTAIC EFFECT AND OPTICAL PROPERTIES OF FERROELECTRIC THIN FILMS MADE BY SOL-GEL PROCESSING**

Yuhuan Xu, Ching Jih Chen, N. Desimone and John D. Mackenzie

Department of Materials Science and Engineering,  
University of California, Los Angeles, CA 90024, USA

### **ABSTRACT**

Ferroelectric thin films including undoped and doped PZT (lead zirconate titanate),  $\text{BaTiO}_3$  (barium titanate), SBN (strontium barium niobate),  $\text{KNbO}_3$  (potassium niobate), PBN (lead barium niobate), KNSBN (potassium sodium strontium barium niobate), and  $\text{LiNbO}_3$  (lithium niobate) were made on silicon and fused silica substrates by a sol-gel process. A heterojunction effect was observed in ferroelectric thin films on both n-silicon and p-silicon through measurement of  $I$ - $V$  characteristics, and by the demonstration of a photocurrent effect. Transparent and preferentially orientated SBN thin films on fused silica substrates can be obtained by applying a d.c. electric field during heat treatment. The films have structural and optical anisotropies as well as photorefractive properties. Two-wave mixing experiment was demonstrated by using these films and a maximum holographic efficiency of near 1 % was obtained.

### **1. INTRODUCTION**

In the past twenty years ferroelectric thin films have been extensively studied. Many applications, including piezoelectric or electro-acoustic transducers,<sup>1,2</sup> high frequency surface acoustic wave devices,<sup>3</sup> pyroelectric infrared detectors,<sup>4-6</sup> ferroelectric memory cells,<sup>7,8</sup> ferroelectric-photoconductive displays,<sup>9-12</sup> optical modulators,<sup>13</sup> ferroelectric gate (field effect transistor's), and "MIST" (metal/insulator/semiconductor transistor) devices,<sup>14,15</sup> etc. have been studied in the past.

Many thin film fabrication techniques, such as evaporation, sputtering, epitaxial deposition, chemical vapor deposition (CVD) and sol-gel processing, have been used to make ferroelectric thin films on various substrates.<sup>16,17</sup>

The ferroelectric thin films studied in this work were made by a sol-gel process. The advantages of the sol-gel processing technique are good homogeneity, ease of composition control, low sintering temperature (about 50% of that of corresponding ceramics) and the ability to fabricate thin films of large areas.<sup>18-24</sup> In our laboratory, ferroelectric thin films ( $\text{PZT}$ ,  $\text{BaTiO}_3$ , SBN,  $\text{KNbO}_3$ , PBN, KNSBN, and  $\text{LiNbO}_3$ ) on fused silica, single crystal silicon and GaAs substrates were fabricated by the sol-gel technique and studied.

92 4 28 058

92-11440



## 2.FABRICATION OF FERROELECTRIC THIN FILMS

Ferroelectric thin films studied were fabricated by the sol-gel method. Homogeneous solutions were prepared by mixing the metal alkoxides in appropriate compositions. After evaporation and hydrolysis accompanied with polycondensation, when the solution viscosity reaches a desired value, direct dipping and spin-on techniques were used to form thin films of gel on fused silica plates, silicon wafers [n-type (111) wafer with a resistivity of 0.005 - 0.025 ohm-cm and p-type (111) wafer with a resistivity of 0.010 - 0.020 ohm-cm] or GaAs wafers. The films were then dried and heat treated in air. Heat treatment temperatures and times employed for these ferroelectric thin films were 500 °C to 850 °C and 0.5 to 1 hour, respectively. When final heat treatment was finished, the average film thickness for one single dipping was estimated to be around 1000 Å. Thicker films may be obtained by multiple dipping and heat treatment. Films used in electrical conduction measurements were from 0.17 to 1.1 μm in thickness. The thickness of the film was determined from SEM micrograph of the polished cross section of the film.

For electrical measurements, electrodes on ferroelectric films were made by sputtering gold or evaporating aluminum thin films onto the corresponding surface. The other electrode was the silicon substrate. A metal / ferroelectric film / Si sandwich structure was thus formed.

Transparent ferroelectric films (SBN, KNSBN, and LiNbO<sub>3</sub>) were also deposited on fused silica substrates for studying microstructure and optical properties. Symmetric ferroelectric hysteresis loops were observed in these thin films by using a pair of parallel Au-electrodes sputtered on the surface of the film. Microstructures of these thin films were observed by microscopy and X-ray diffraction. For example, the SEM micrograph of the surface of a Sr<sub>0.60</sub>Ba<sub>0.40</sub>Nb<sub>2</sub>O<sub>6</sub> thin films (0.8 μm thickness, heat treatment at 750 °C/ 1 hr.) with the dimensions of the grains are from 0.3 to 0.8 μm was obtained. By using polarized light, ferroelectric domain patterns were revealed and the regions of uniform and homogeneous spontaneous electrical polarization between several grains can be observed.<sup>27</sup>

A preferentially orientated SBN thin film on a fused silica substrate can be formed by applying a d.c. electric field (about 1 kV/mm) parallel to the surface of the film during heat treatment. Diffractive intensity of lines which have low Miller indices on c-axis, such as (130), (620), (121), (131), etc., are strongly enhanced as shown in Fig.1. This result indicates that lattice planes (130), (620), (121), (131), etc. were parallel to the surface of the substrate and the c-axes in the grains have preferred orientation parallel (or nearly parallel) to the direction of the applied d.c. field.

The optical anisotropy of the preferentially orientated SBN film on fused silica substrate was measured by putting the SBN film between a detector and a rotatable polarizer which was in the front of a He-Ne laser. The measured result by using a laser beam with beam diameter of 2 mm is shown in Fig. 2.



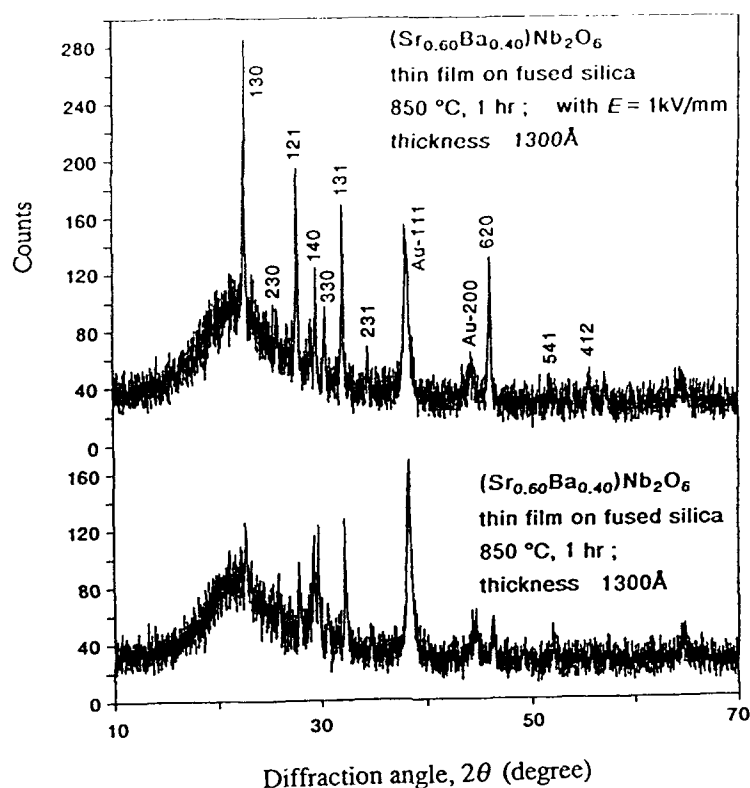


Fig.1. X-ray diffraction patterns of SBN thin films with (upper) and without (lower) applying d.c. field during heat treatment.

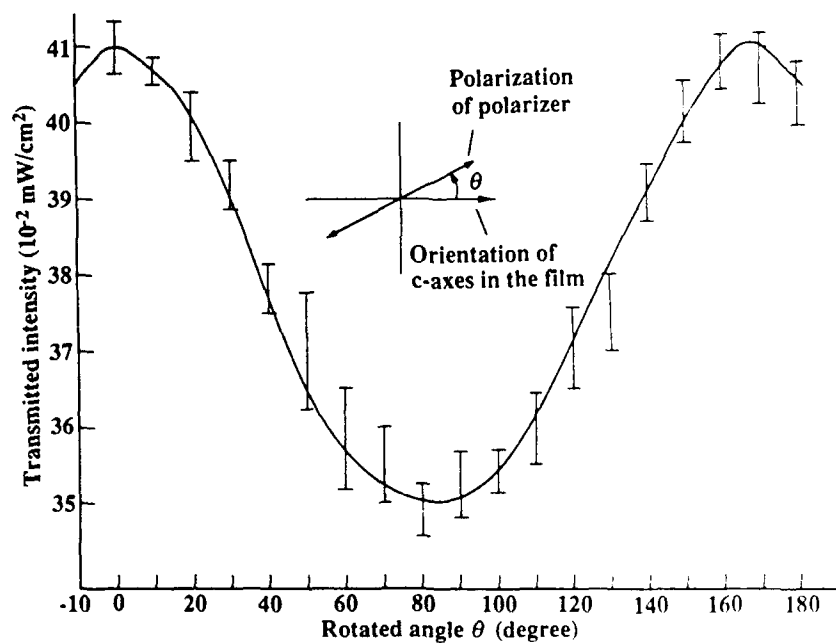
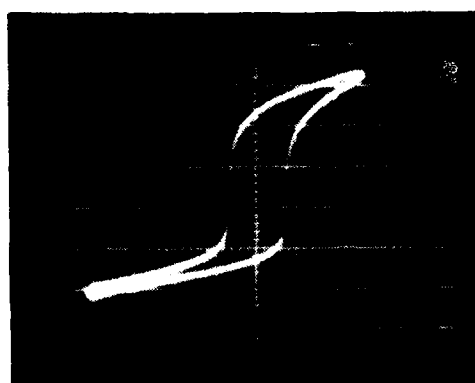


Fig.2. Optical anisotropy of the preferentially orientated SBN thin film with the thickness of 0.6  $\mu\text{m}$ .

Table 1 Optical Refractive Indices of films

SBN		LiNbO <sub>3</sub>	
single crystal	thin film (by sol-gel)	single crystal	thin film (by sol-gel)
$n_o = 2.3123$	$n = 2.31$	$n_o = 2.296$	$n = 2.23$
$n_e = 2.2734$	$\pm 0.01$	$n_e = 2.208$	$\pm 0.01$

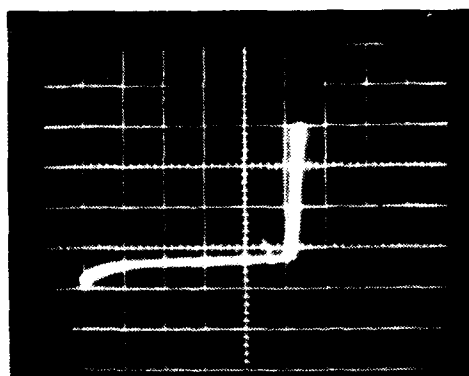


(a)

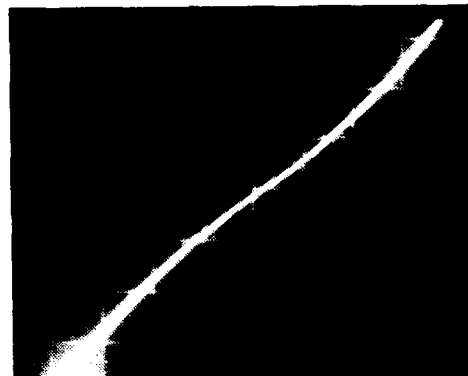


(b)

Fig.3. Ferroelectric  $P$ - $E$  hysteresis loops of PZT thin films ( $0.8 \mu\text{m}$ ) on n-Si (a) and p-Si (b). Scale of X-axis is  $22 \text{ kV/cm/div.}$  and scale of Y-axis is  $18 \mu\text{C/cm}^2/\text{div.}$  in (a). Those of  $24 \text{ kV/cm/div.}$  and of  $13 \mu\text{C/cm}^2/\text{div.}$  in (b).



(a)



(b)

Fig.4.  $J$ - $V$  characteristics (at  $50 \text{ Hz}$ ) of PZT thin films ( $0.8 \mu\text{m}$ ) on n-Si (a) and p-Si (b). Scale of X-axis is  $1.5 \text{ V/div.}$  and scale of Y-axis is  $12 \mu\text{A/cm}^2/\text{div.}$  in (a). Those of  $0.43 \text{ V/div.}$  and of  $4.6 \mu\text{A/cm}^2/\text{div.}$  in (b).

The optical transmission of transparent films was measured in the wavelength range of 0.2 to 2.5  $\mu\text{m}$  by a Perkin Elmer 330 UV spectrometer.<sup>27</sup> Table I lists refractive indices of  $2.31 \pm 0.01$  and  $2.23 \pm 0.01$ , which were measured on SBN and  $\text{LiNbO}_3$  films, respectively, at the wavelength of 6328 Å by an Automatic Ellipsometer (Auto E1-11).

Pyroelectric coefficient was measured by using a dynamic method<sup>25</sup>, on a Au/ ferroelectric film/ Si sandwich structure. Before the measurement, the sample of SBN film was poled at 100 °C with a d.c. electric field of about 2.5 kV/mm. The pyroelectric coefficient of  $2 \times 10^{-8} \text{ C/ cm}^2\text{K}$  was obtained at room temperature, which is of the same order of magnitude of that of SBN single crystal.<sup>25</sup>

### **3.HETEROJUNCTION, PHOTOVOLTAIC AND PHOTOCURRENT EFFECTS**

Ferroelectric hysteresis loops of thin films were observed by a modified Sawyer-Tower bridge. In general, hysteresis loops of metal/ ferroelectric films/ Si-substrate are asymmetric, and the  $P$ - $E$  loops of films with the same composition on silicon wafers with different conduction type are very different. Fig.3(a) and (b) shows the loops generated at 50 Hz for PZT films with 0.8  $\mu\text{m}$  thickness on n- and p- Si, respectively.

$I$ - $V$  characteristics of samples with metal/ ferroelectric PZT film/ silicon sandwich structure are shown in Fig.4(a) and (b).  $I$ - $V$  curves of  $\text{BaTiO}_3$ ,  $\text{KNbO}_3$ , SBN, PBN, and KNSBN films on silicon were also observed.<sup>26</sup>

In order to understand the  $I$ - $V$  characteristic of ferroelectric films on silicon, we have proposed a physical model of ferroelectrics/ semiconductor heterojunction effects (see Fig.5) and obtained current

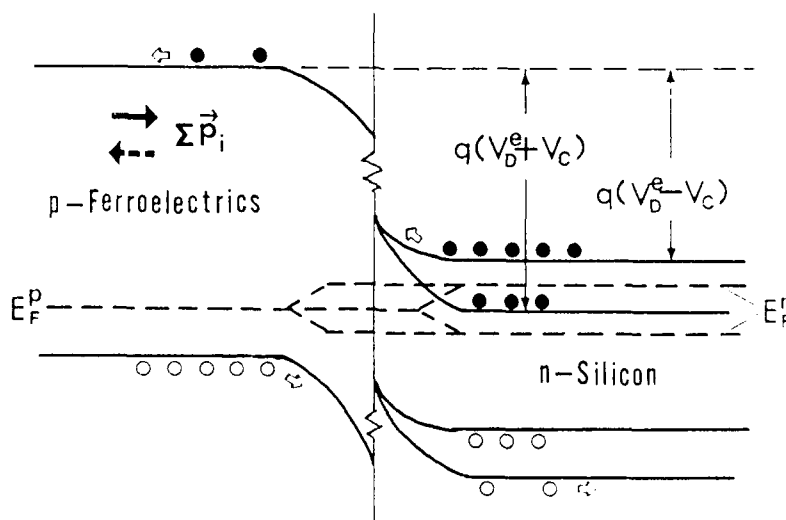


Fig.5. The energy band diagram at the ferroelectrics-silicon interface of the proposed physical model for the self-biased heterojunction effect.

density  $J$  as a function of the applied voltage  $V$  as following:<sup>26</sup>

$$J = J_0 [1 - (V - V_c) / V_D^e] \exp[q(V - V_c) / kT - 1], \quad (1)$$

where

$$J_0 = (qA^*TV_D^e/k) \exp(-qV_D^e/kT), \quad (2)$$

and  $A^*$  and  $k$  are the effective Richardson constant and Boltzmann constant respectively.

Photocurrent and photovoltaic effects were demonstrated by using a transparent ITO (indium tin oxide) electrode/ ferroelectric film/ silicon structure (as shown in Fig.6). The measured results of stable photocurrent density and stable photovoltage in PZT and SBN thin films on silicon substrate are shown in Fig.7 to Fig.12, respectively. These effects were caused by neither pyroelectric effect (because pyroelectric current density is in the order of  $10^{-8}$  A/cm<sup>2</sup>) nor photovoltaic effect in a ferroelectric monodomain crystal (because the ferroelectric thin films were not poled before, i.e., the films have a polydomain structure with randomly orientated grains). This result strongly supports the presently photovoltaic and photocurrent effects were caused by the heterojunction effect at the interface between the ferroelectric thin film and the silicon substrate. The photovoltaic effect of the ferroelectric film/silicon heterjunction can be utilized as detector devices and moreover as solar cell devices.

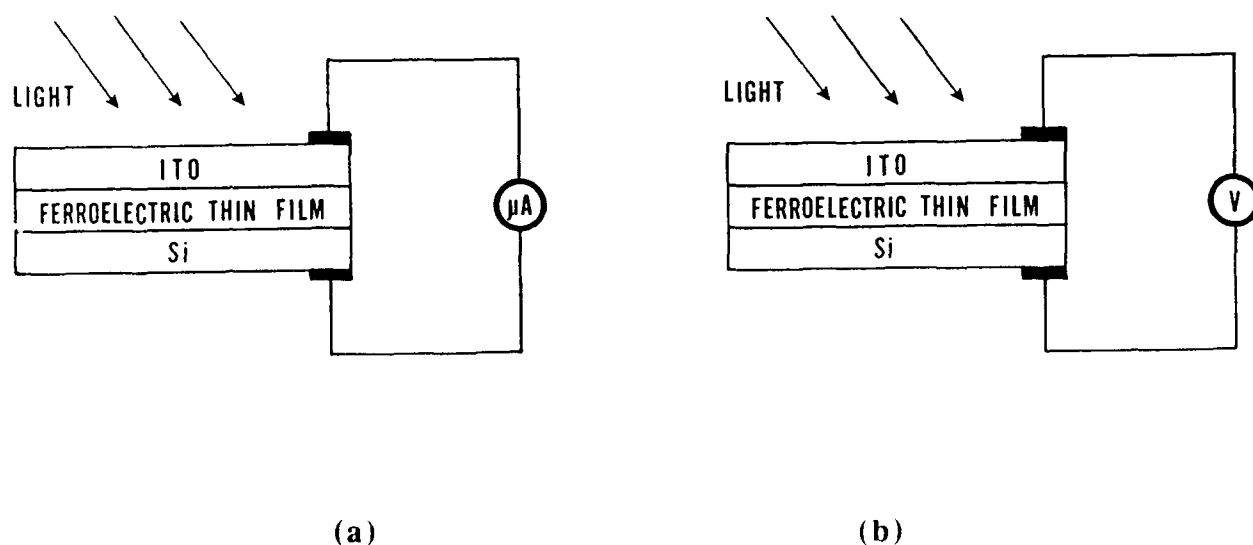


Fig.6. Transparent ITO (indium tin oxide) electrode / ferroelectric film / silicon structure for measuring photocurrent (a) and photovoltaic (b) effects.

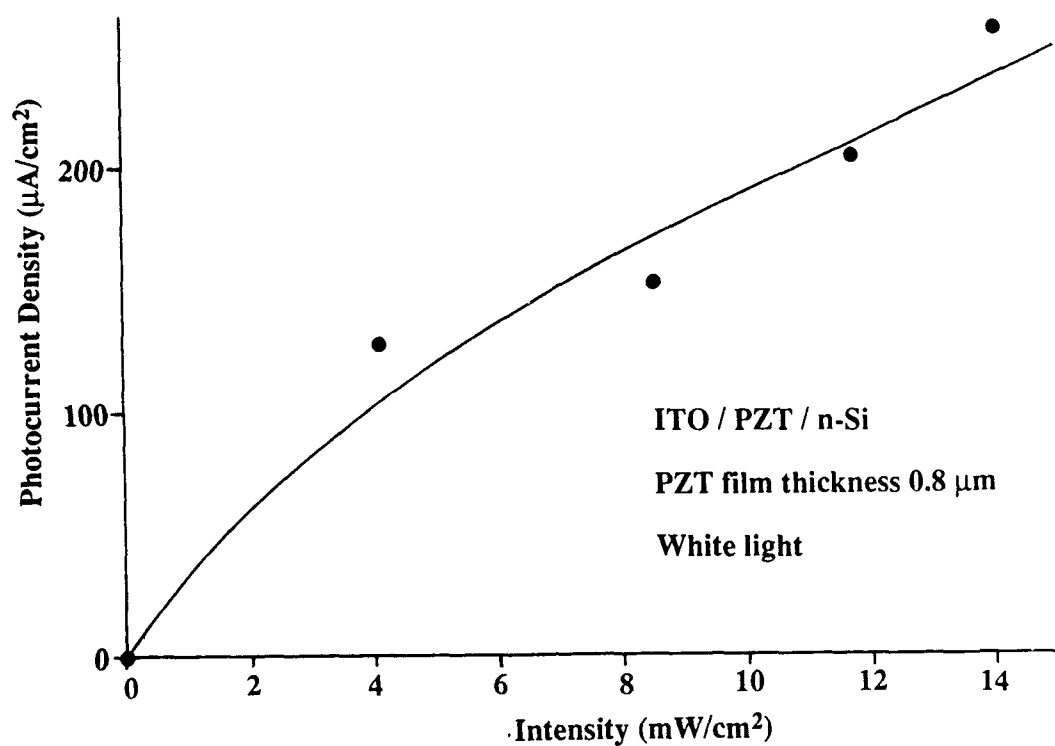


Fig.7. Stable photocurrent density in PZT thin film vs. light intensity (white light).

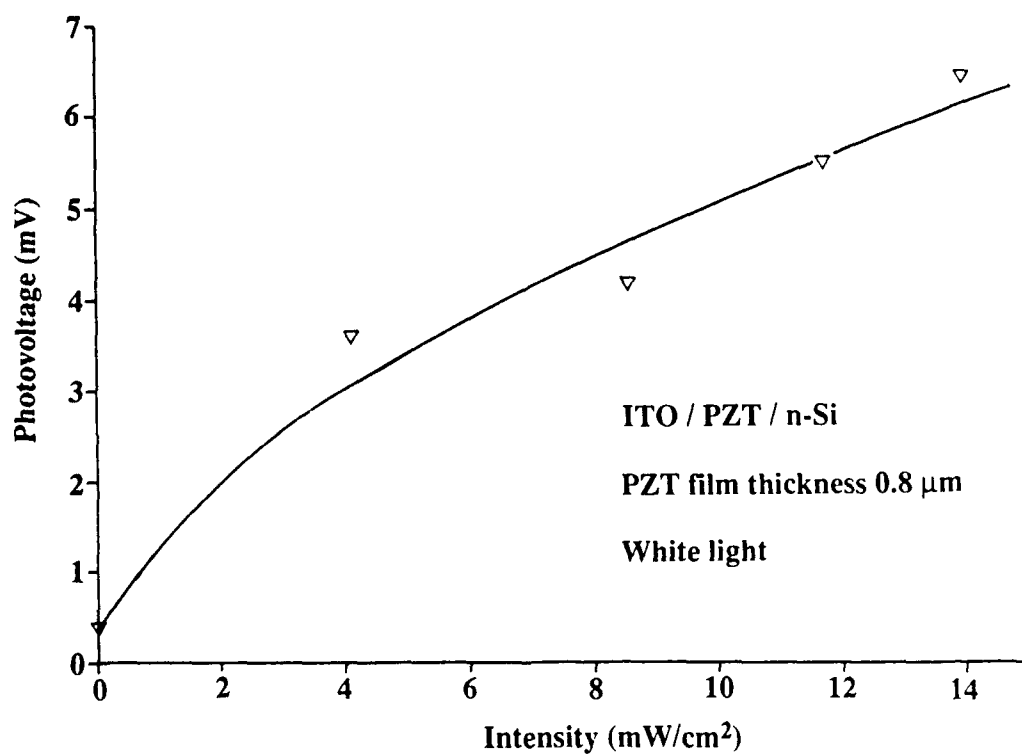


Fig.8. Stable photovoltage in PZT thin film vs. light intensity (white light).

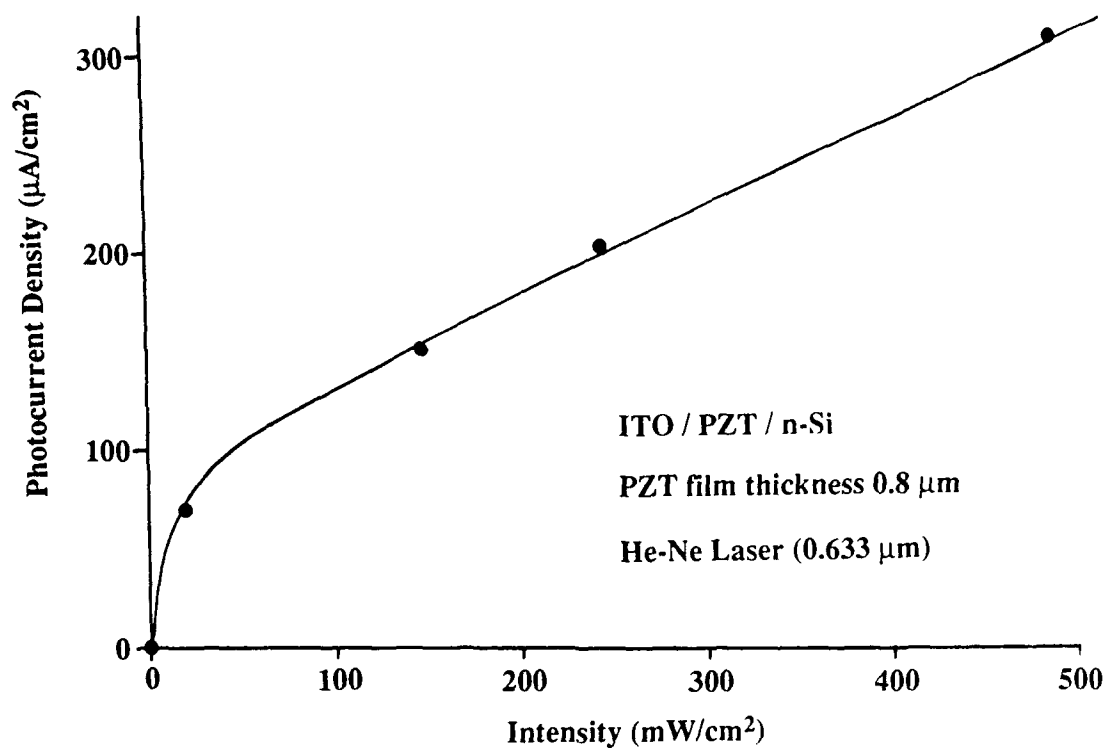


Fig.9. Stable photocurrent density in PZT thin film vs. light intensity ( $6328 \text{ \AA}$ ).

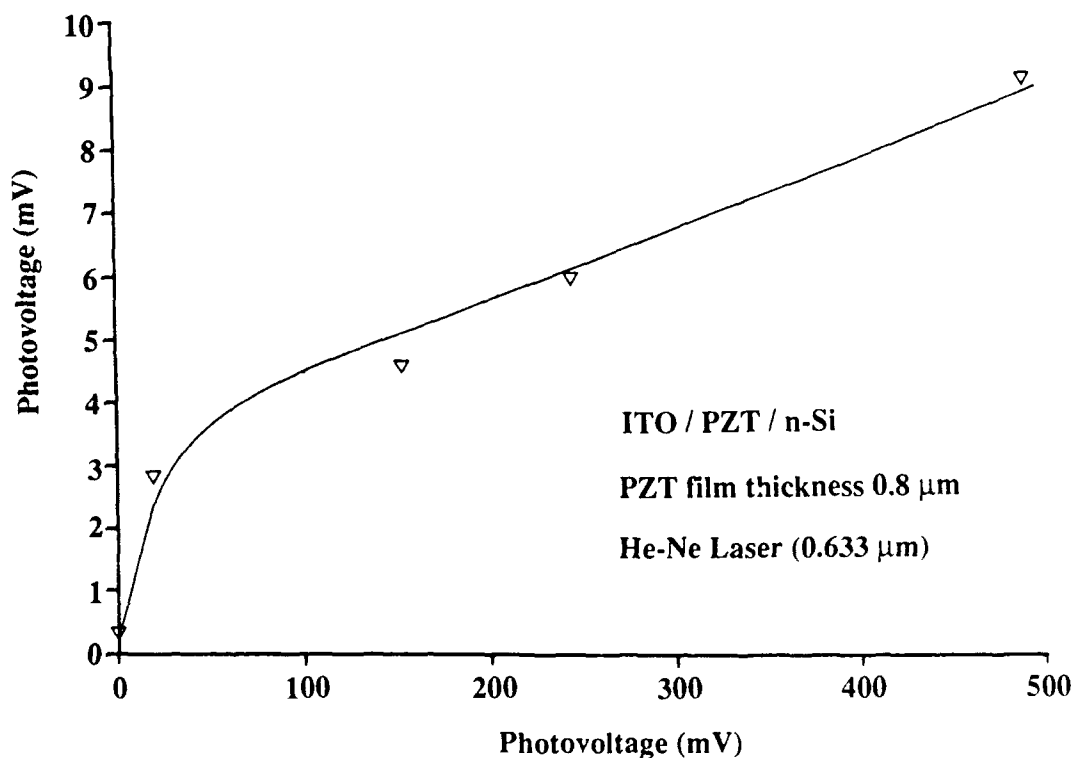


Fig.10. Stable photovoltage in PZT thin film vs. light intensity ( $6328 \text{ \AA}$ ).

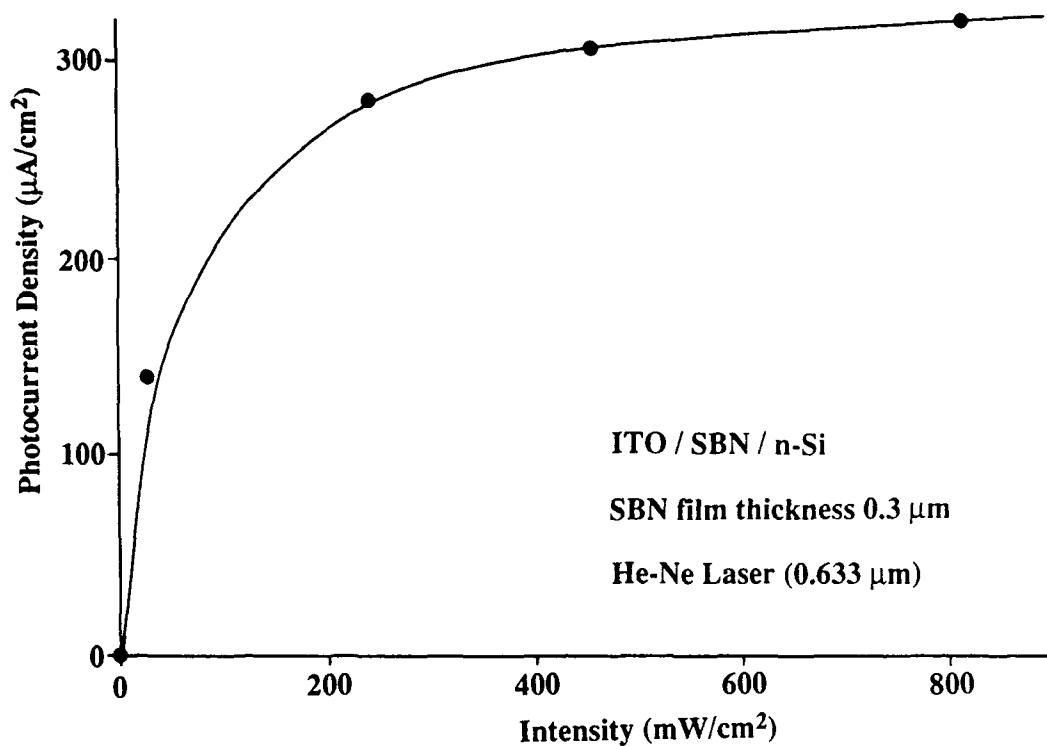


Fig.11. Stable photocurrent density in SBN thin film vs. light intensity ( $6328 \text{ \AA}$ ).

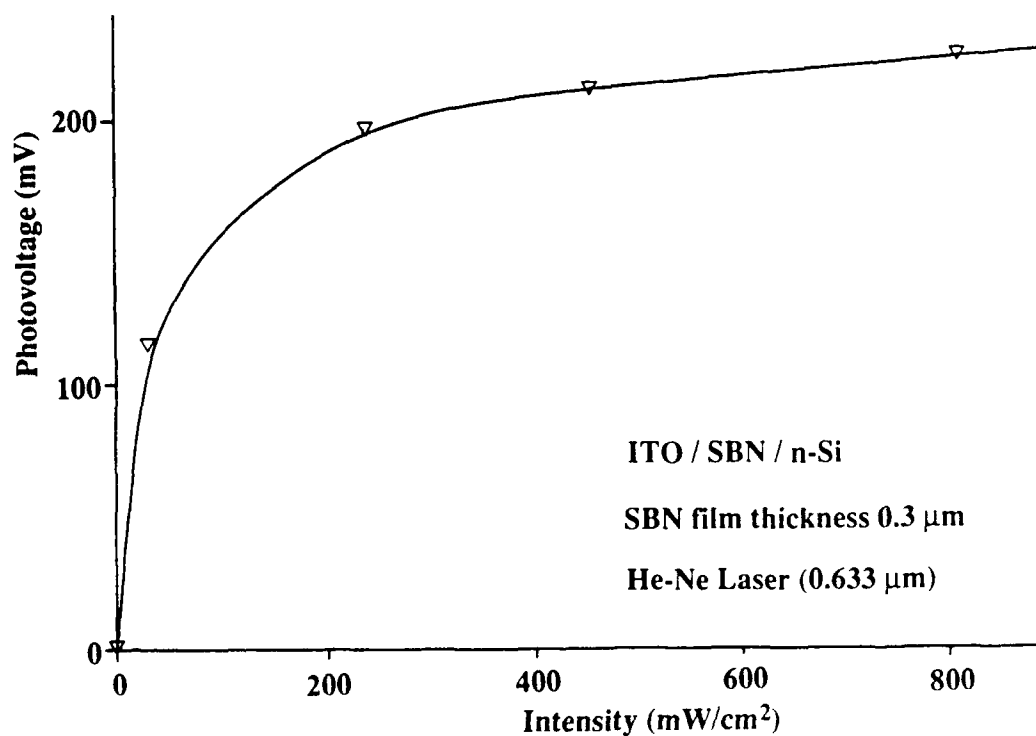


Fig.12. Stable photovoltage in SBN thin film vs. light intensity ( $6328 \text{ \AA}$ ).

#### 4. HOLOGRAPHIC GRATING RECORDED IN SBN THIN FILM

By using the SBN thin films two-wave mixing has been demonstrated in our laboratory. The equipment for the recording of holograms is schematically shown in Fig.13. Two polarized beams  $I_1$  and  $I_2$  (with the intensity ratio 1 : 9) generated by a beam splitter, which is located at the output of a He-Ne laser, are incident on a SBN thin film. Incident angles of the two beams are kept equal, i.e.,  $2\theta = 16^\circ$ . In this configuration the direction of preferential orientation of the  $c$ -axes in the film is parallel to the plane of incidence. In order to filter out scattered light, a polarizer with the polarization-direction parallel to that of the  $I_1$  and  $I_2$  beams was set on the front of the detector. By using a unpoled sample, two wave mixing could not be observed. However, when a d.c. field of 20 kV/cm was applied on the unpoled sample, the intensity of signal beam was amplified. An interference pattern of light intensity was formed by the two coherent beams  $I_1$  and  $I_2$ . Fig.14 is a plot of light intensity distribution in the film. Thus, a holographic grating was formed in the thin film through the photorefractive effect. Therefore, the beam  $I_1$  was amplified owing to the energy exchange from  $I_2$  to  $I_1$  (i.e., the Bragg

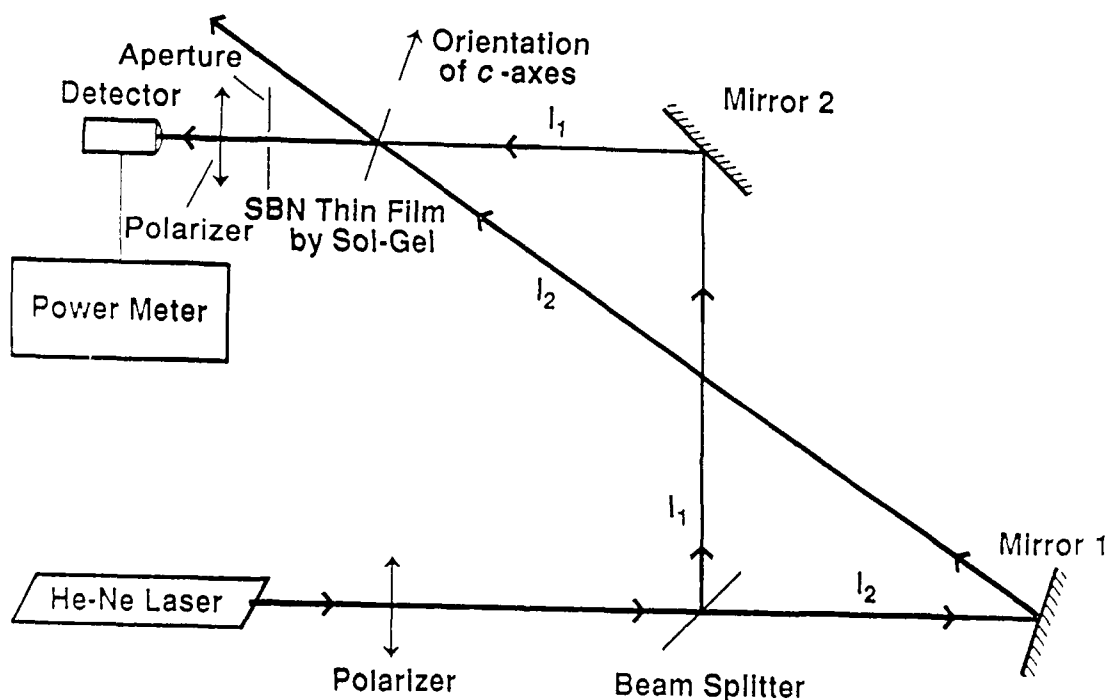


Fig.13 Experimental set-up for two-wave mixing experiments in SBN thin films.



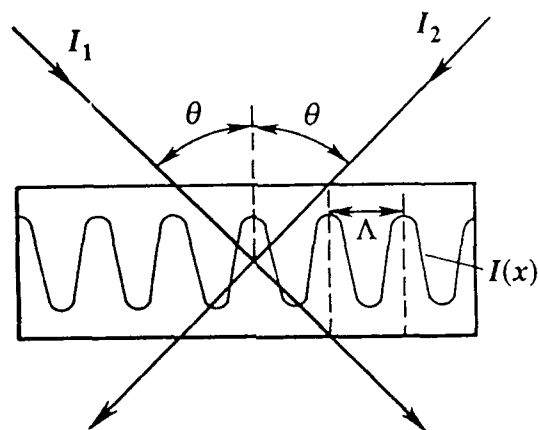


Fig.14. A plot of light intensity distribution formed by interference of two coherent beams.

diffraction). In our experiment we measured the Bragg diffraction efficiency  $\eta$  defined as follows:<sup>28</sup>

$$\eta = \frac{(\text{diffracted intensity})}{(\text{diffracted intensity} + \text{transmitted intensity})}, \quad (3)$$

Without any applied field on the poled sample a maximum  $\eta$  of near 1% at the wavelength of 6328 Å and the intensity of 12 mW/mm<sup>2</sup> was obtained. Owing to the thickness of our sample is very thin this value of  $\eta$  appears to be unusually large as compared with those of single crystals in published work.<sup>29-32</sup> One of possible explanations is that some diffuse lights, which were formed by the scattering of the grain boundaries of the film, contributed to the diffraction beam. It should be mentioned that theoretical calculation for the holographic recording in transparent PLZT ceramics with applied field suggests that the gain  $\Gamma$  could reach values larger than 1200 cm<sup>-1</sup> at an applied field of 25 kV/cm.<sup>33</sup>

## 5. CONCLUSION

1) Transparent, crack-free, polycrystalline and ferroelectric thin films (PZT, BaTiO<sub>3</sub>, SBN, KNbO<sub>3</sub>, PBN, KNSBN, and LiNbO<sub>3</sub>) on fused silica substrate have been fabricated by the sol-gel process.

2) A heterojunction effect in the sandwich structure of metal / ferroelectric film / silicon has been observed by the measurement of  $I$ - $V$  curve and confirmed by the demonstration of photovoltaic effect.

3) Preferentially orientated SBN thin films on fused silica substrate can be formed by applying a d.c. electric field (about 1 kV/mm) parallel to the surface of the substrate during heat treatment. The films have optical anisotropy and photorefractive properties. By using the SBN films two-wave mixing effect was observed.

4) We are optimistic that ferroelectric thin films made by the sol-gel process have potential in various device applications, such as holographic memory, infrared detector, optical bistable and/or electrical bistable devices, non-volatile semiconductor memory devices, etc..

## **6. ACKNOWLEDGEMENTS**

This work was supported by the Air Force Office of Scientific Research, Directorate of Chemical and Atmosphere Sciences under Grant No. AFOSR-88-0066. The authors also wish to thank Mr. Ren Xu and C. Cheng for their help in part of the experiments in this work.

## **7. REFERENCES**

1. Mfakoto Minakata et. al., *J. Appl. Phys.*, **50**, 7898 (1979).
2. N. F. Foster, *J. Appl. Phys.*, **40**, 420 (1969).
3. R. N. Castellans and L. G. Feinstein, *J. Appl. Phys.*, **50**, 4406 (1979).
4. A. M. Glass, *Phys. Rev.*, **172**, 564 (1968).
5. H. P. Beerman, *Ferroelectrics*, **2**, 123 (1971).
6. A. M. Glass and R. L. Abrams, *J. Appl. Phys.*, **41**, 4455 (1970).
7. D. W. Chapman, *J. Vac. Sci. Technol.*, **9**, 425 (1972).
8. R. B. Atkin, *Ferroelectrics*, **3**, 213 (1971).
9. S. Y. Wu, W. J. Takei, M. N. Francombe, and S. E. Cummins, *Ferroelectrics*, **3**, 217 (1972).
10. D. W. Chapman, In "*Proc. IEEE. Comp. Gp. Conf.*" Washington (1970).
11. D. W. Chapman and P. R. Mehta, *Ferroelectrics*, **3**, 101 (1972).
12. P. R. Mehta, *Ferroelectrics*, **4**, 5 (1972).
13. J. C. Webster and F. Zernike, *Ferroelectrics*, **10**, 249 (1976).
14. S. Y. Wu, *Ferroelectrics*, **11**, 379, (1976).
15. Shu-Yau Wu, *IEEE Trans. on Electron. Devices*, **ED-21**[8], 499, (1974).

16. J. C. Burfoot, "Pyroelectric and Ferroelectric Thin film Devices" (T. J. Coutts Ed.: «*Active and Passive Thin Film Devices* ») 697-741, Academic Press, 1978.
17. M. H. Francombe: "Ferroelectric Film and Their Device Applications", *Thin Solid Films*, **13**, 413-433, 1972.
18. C. J. Chen et. al. *Proc. of 1st symp. on Integrated Ferroelectrics*, CMC-89, Colorado, March, 1989 (to be published in *Ferroelectrics* ).
19. A. Mosset, et. al., *J. Non-Crystalline Solids*, **100**, 339 (1988).
20. K. D. Budd, S. K. Dey and D. A. Payne, *Mat. Res. Soc. symp. Proc.*, **73**, 711 (1986).
21. S. K. Dey, K. D. Budd and D. A. Payne, *IEEE Trans. on Ultrasonics Ferroelectrics and Frequency Control*, **35**(1), 80 (1988).
22. K. D. Budd, S. K. Dey and D. A. Payne, *Brit. Cer. Soc. Proc.*, **36**, 107 (1985).
23. S. Hirano, and K. Kato, *J. Non-Crystalline Solids*, **100**, 538 (1988).
24. R. W. Vest, and J. Xu, *Ferroelectrics*, **23**, 21 (1989).
25. M. E. Lines, and A. M. Glass, « *Principles and Applications of Ferroelectrics and Related Materials* », Clarendon Press, Oxford, 1977.
26. Yuhuan Xu, Ching-Jih Chen, Ren Xu and J. D. Mackenzie, *J. Appl. Phys.*, **67**, 2985 (1990).
27. Yuhuan Xu, Ching-Jih Chen, Ren Xu and J. D. Mackenzie, *Proc. of MRS '90 Spring Meeting*, Symposium Section **Y.1.2**, San Francisco, April (1990).
28. R. A. Rupp, A. E. Krumins, K. Kerperin and R. Matull, *Phys. Rev. B*, **39**, 9541 (1989).
29. C. Medrano, E. Voit, P. Amrhein and P. Gunter, *Ferroelectrics*, **22**, 289 (1989).
30. D. Rytz, M. B. Klein, R. A. Mullen, R. N. Schwartz, G. C. Valley, B. A. Wechsler, *Appl. Phys. Lett.*, **52**, 1759 (1988).
31. D. Rytz and Shen De Zhong, *Appl. Phys. Lett.*, **54**, 2625 (1989).
32. D. Rytz, B. A. Wechsler, R. N. Schwartz, C. C. Nelson, C. C. Brandle, A. J. Valentino and G. W. Berkstresser, *J. Appl. Phys.*, **66**, 1920 (1989).
33. R. A. Rupp, K. Kerperin and A. Krumins, *Ferroelectrics*, **20**, 75 (1989).



## Properties of Undoped, Copper-doped Strontium Barium Niobate Thin Films by Sol-gel Method

Ching Jih Chen, Yuhuan Xu, and John D. Mackenzie

Materials science and Engineering Department  
University of California, Los Angeles, CA 90024, USA

**92-11441**



### ABSTRACT

Transparent strontium-barium niobate (SBN) thin films, 0.3-1.0  $\mu\text{m}$ , have been made by the sol-gel method. Alkoxide solutions were used as starting materials. Polycrystalline SBN thin films were grown on fused silica, single crystals silicon, and GaAs substrates after firing at 700°C. Dielectric, ferroelectric, and pyroelectric properties of SBN films were observed. Absorption spectra of SBN and SBN doped with 0.3 % Cu (SBN:Cu) were measured. The photorefractive effect of SBN was demonstrated by a two-wave mixing experiment.

### 1. INTRODUCTION

Strontium barium niobate ( $\text{Sr}_x\text{Ba}_{1-x}\text{Nb}_2\text{O}_6$ , SBN) is photorefractive material which has been investigated in a number of studies on phase conjugation<sup>1</sup>, two-wave mixing<sup>2</sup>, and holographic storage<sup>3</sup>. For such applications, it is necessary that materials possess three important features: high optical quality, high coupling coefficient, and low response time. SBN crystals have been found to satisfy these requirements.

Sol-gel technique has been used to grow ferroelectric thin films, such as PZT<sup>4</sup>, PLZT<sup>5</sup>,  $\text{BaTiO}_3$ <sup>6</sup>,  $\text{LiNbO}_3$ <sup>7</sup>, and SBN<sup>8</sup>. The advantages of the sol-gel method are low processing temperature and excellent homogeneity, which make it possible for the films to be integrated on various substrates for device applications.

The films of  $\text{Sr}_{0.6}\text{Ba}_{0.4}\text{Nb}_2\text{O}_6$  (SBN) and copper-doped  $\text{Sr}_{0.6}\text{Ba}_{0.4}\text{Nb}_2\text{O}_6$  (SBN:Cu) on fused silica, single crystals Si, and GaAs, have now been prepared by the sol-gel method. The processing and characteristic of the films will be described. The dielectric, ferroelectric, and pyroelectric properties of SBN films on various substrates were measured. Photorefractive effect of SBN and SBN:Cu is discussed. A two-wave mixing experiment of SBN film has also been studied, and demonstrated the photorefractive effect.

### 2. SOL-GEL PROCESS

In the sol-gel process, a non-aqueous solution of metal-organic precursors is first prepared with metal cations in the desired ratios. Alkoxide solutions of  $\text{Ba}(\text{OC}_2\text{H}_5)_2$ ,  $\text{Sr}(\text{OC}_2\text{H}_5)_2$ , and  $\text{Nb}(\text{OC}_2\text{H}_5)_5$  were the starting materials, with ethanol as solvent. They were mixed and refluxed for 24 hours in an  $\text{N}_2$  atmosphere and had a concentration of 0.05 mole/l. The preparation of the solutions in an  $\text{N}_2$  atmosphere can minimize the formation of carbonates during heat-treatment. The formation of crystalline carbonates would reduce the chemical homogeneity of film and thus negates the advantage of the sol-gel process.

The homogeneous alkoxide solution of SBN was used for dip-coating or spin-coating on single crystals Si, and GaAs, and fused silica substrates. The film was then exposed to wet air for hydrolysis

and subsequent polymerization. The gels were dried in air at 100° C for 1 hour, and then heated to 700° C for 2 hours, finally cooled down to room temperature slowly. A crack-free SBN film was thus formed by repeating the coating-firing process. During drying, large shrinkage can occur, which may result in cracking. However, a strong bond between the film and the substrate will prevent lateral shrinkage and thus promote densification in the vertical direction.

### 3. RESULTS AND DISCUSSIONS

#### 3.1. Characteristic of Films

From the phase diagram, the films with a composition of  $\text{Sr}_{0.6}\text{Ba}_{0.4}\text{Nb}_2\text{O}_6$  should have the tungsten bronze structure. The x-ray diffraction patterns showed that the films were crystallized, as the firing temperature was raised to above 700° C. The thickness of the films, 0.3-1.0  $\mu\text{m}$ , was determined by the scanning electron micrography. Figure 1 shows the microstructure of SBN doped with 0.3% Cu on silicon where random domains were observed. As a SBN film was poled at 1 kV/mm at 800° C, the x-ray diffraction peaks of (130), (121), (131), and (620) were enhanced, indicating that the domains were oriented and the film had a preferred orientation along the c-axis<sup>9</sup>.

Polycrystalline SBN films can be oriented along c-axis by applying an electric field higher than the coercive field. It is necessary that the films have preferred orientation for pyroelectric property and the photorefractive effect. Hirano<sup>10</sup> has prepared a single crystal-like  $\text{LiNbO}_3$  thin film by controlling the hydrolysis of the solution. Therefore, it should be possible to grow a ferroelectric thin film of good optical quality for optical applications.

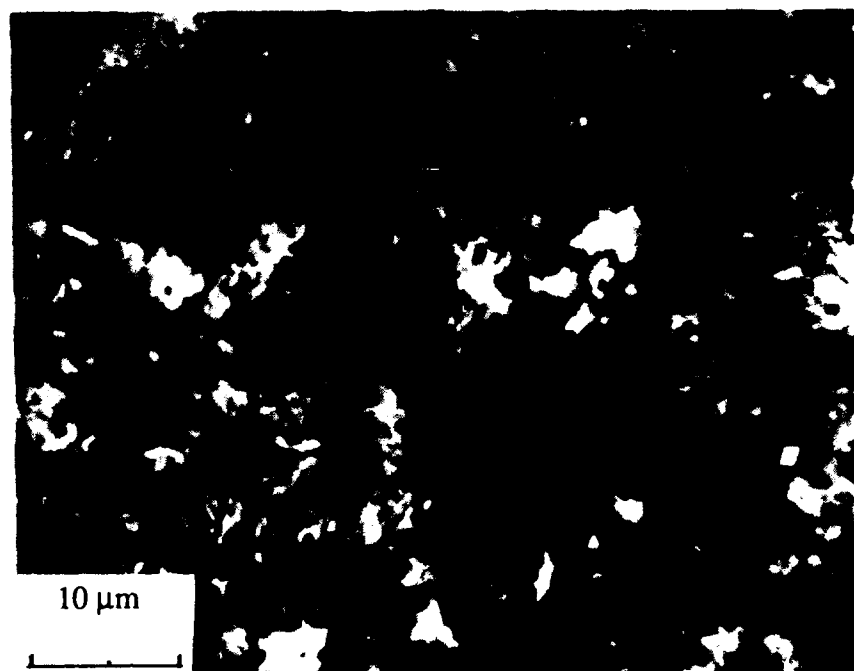


Figure 1 Microstructure of SBN film, doped with 0.3% Cu, grown on silicon (111) substrate after firing at 700° C. Random ferroelectric domains were observed without poling.

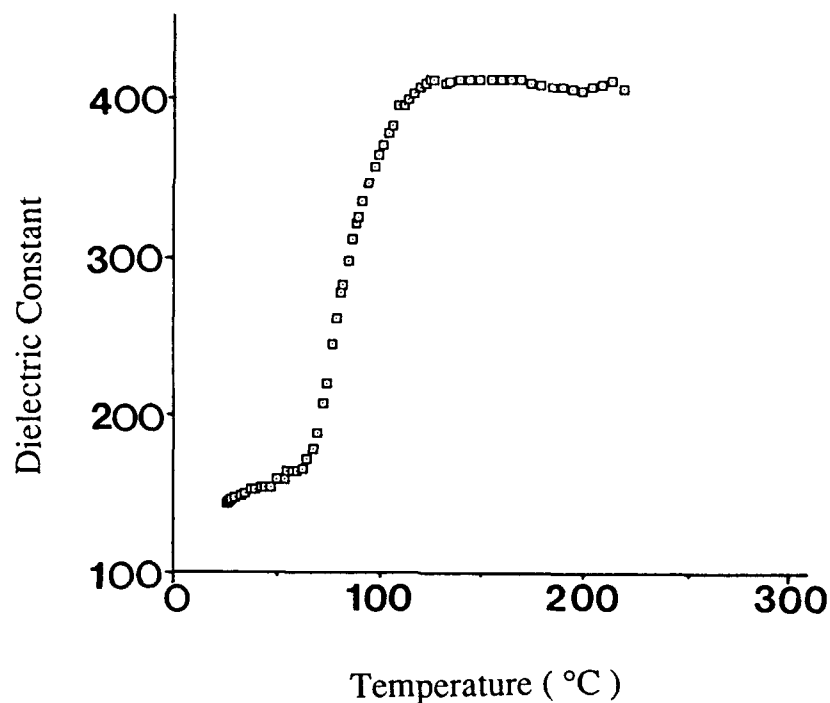


Figure 2 Dielectric constant versus ambient temperature for  $\text{Sr}_{0.6}\text{Ba}_{0.4}\text{Nb}_2\text{O}_6$  thin film (thickness = 3000 Å) on silicon substrate.

### 3.2. Dielectric Property

The temperature variation of the dielectric constant of a film was measured between 30°C and 240°C and shown in Figure 2. The dielectric constant ( $\epsilon$ ) was calculated from the capacitance measured by an LCR meter at 1 kHz. Gold (area = 4.03 cm<sup>2</sup>) was sputtered on SBN film as electrode. The film (thickness = 3000 Å) was deposited on a silicon substrate, and thus a Au/SBN/Si configuration was formed. The relative dielectric constant increased by a factor of 3.3 as the temperature was increased from 30°C to 110°C. There was no maximum peak obvious in the  $\epsilon$  vs.  $T$  curve, although a maximum should be observable at  $T_c$ . This smearing of the transition temperature has been observed by Okazaki and Nagata<sup>11</sup> and attributed to the small grain size of the film.

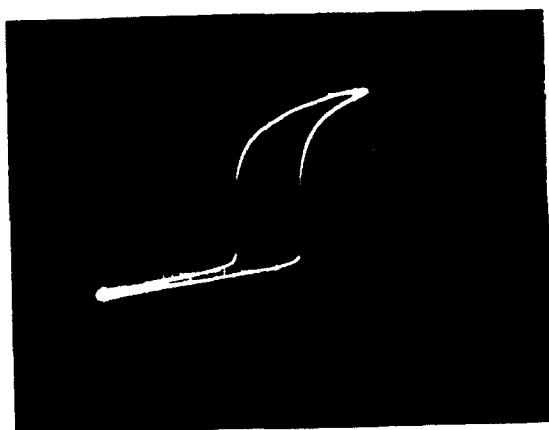
### 3.3. Ferroelectric Properties

Ferroelectric properties of the films were confirmed by P-E hysteresis loops. Ferroelectric hysteresis loop measurement was made using a modified Sawyer-Tower circuit at a frequency of 50 Hz, the dielectric loss being compensated in each measurement. To study the ferroelectric properties, gold electrodes were deposited on the SBN films by sputtering. Figure 3 shows the ferroelectric hysteresis loops observed in the  $\text{Sr}_{0.6}\text{Ba}_{0.4}\text{Nb}_2\text{O}_6$  films on silicon (resistivity = 2 ohm-cm), GaAs (resistivity =  $6 \times 10^{-3}$  ohm-cm), and fused silica. The ferroelectric hysteresis loop for SBN film on fused silica substrate (measured from Au/SBN/Au configuration, where Au are both electrodes) was symmetric, but asymmetric hysteresis loops were observed for SBN films on Si (Au/SBN/Si) and GaAs (

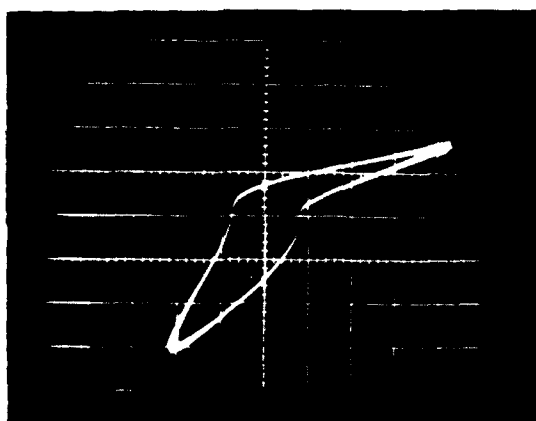
Au/SBN/GaAs) substrates. This may be due to a heterojunction effect<sup>12</sup>. The remanent polarization  $P_r$  was  $34 \mu\text{C}/\text{cm}^2$ , and the coercive field  $E_c$  was  $51 \text{ kV}/\text{cm}$  as measured from the Au/SBN/Si configuration. Because of the uncertainty of the area of the electrodes,  $P_r$  and  $E_c$  were not determined for the Au/SBN/Au and Au/SBN/GaAs configurations.

### 3.4. Pyroelectric Property

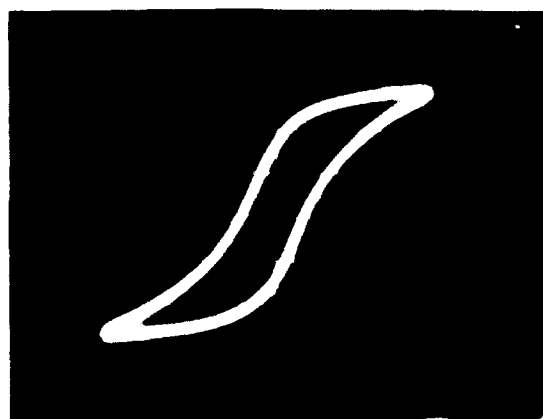
(A)



(B)



(C)



(D)

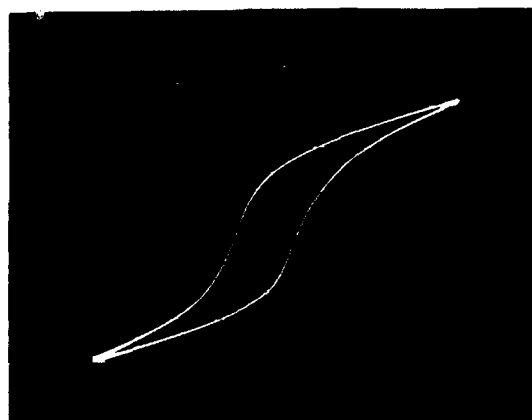


Figure 3 P-E hysteresis loop of SBN film on (a) n-type Si substrate, scale of x axis of loop field  $E$  is  $66 \text{ kV}/\text{cm}/\text{div}$ , and scale of y axis of loop polarization  $P$  is  $14 \mu\text{C}/\text{cm}^2/\text{div}$ , (b) p-type Si, scale of x axis of loop field  $E$  is  $88 \text{ kV}/\text{cm}/\text{div}$ , and scale of y axis of loop polarization  $P$  is  $17 \mu\text{C}/\text{cm}^2/\text{div}$ , (c) fused silica, (d) p-type GaAs.

The pyroelectric coefficient was measured using a dynamic technique<sup>13</sup>, in which the samples were heated and measured in the temperature range of 20° C to 140° C, and the pyroelectric current  $i_p$  was measured by a picoammeter ( 417 Keithley Instruments ) connected in series to the sample. Prior to the measurement, the film was poled at 100° C with a d.c. electric field of 25 kV/cm. The pyroelectric coefficients were about  $2 \times 10^{-8}$  C/cm<sup>2</sup> K and  $80 \times 10^{-8}$  C/cm<sup>2</sup> K at 27° C and 100° C respectively. This suggests that the domains on the SBN polycrystalline film by the sol-gel method were preferentially oriented after electric poling.

#### 4. PHOTOREFRACTIVE EFFECT

Polycrystalline SBN films were studied using a two-wave mixing experiment to determine their photorefractive effect. An experimental arrangement is shown in Figure 4. Coherent beams  $I_1$  and  $I_2$  intersect in the film and thus forms an intensity interference pattern. Charge is excited by this periodic intensity distribution into the conduction band, where it migrates under the influence of the internal electric field and then recombines with traps in the region of low irradiance. A periodic space charge is thus created that modulates the refractive index by means of the electro-optic effect. This index grating, being out of phase with intensity distribution, introduces an asymmetry that allows one beam to be amplified by constructive interference with light scattered by the grating while the other beam is attenuated by destructive interference with diffraction light. The photorefractive mechanism is shown in Figure 5.

The gain coefficient of two-wave mixing is dependent on the concentration of free carriers<sup>14</sup>. Photorefractive SBN has the tungsten bronze structure. The schemes of (a) SBN, and (b) SBN:Cu are shown in Figure 6. SBN crystals studied typically had bandgap of 3-4 eV<sup>15</sup>. SBN crystals were not intentionally doped, but oxygen vacancies or defects may associate with the nonstoichiometric composition of SBN crystals, and introduce an energy level ( Figure 6 (a) ) in the band gap as the origin of free carrier excitation in the visible region of the spectrum. In SBN crystal, oxygen vacancies seem to contribute to the photorefractive effect. The formation of oxygen vacancies can be described

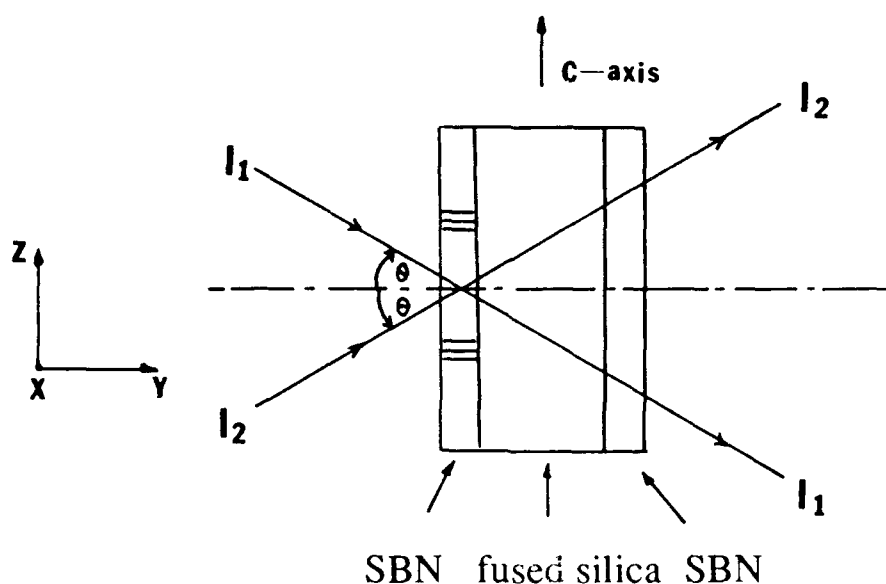
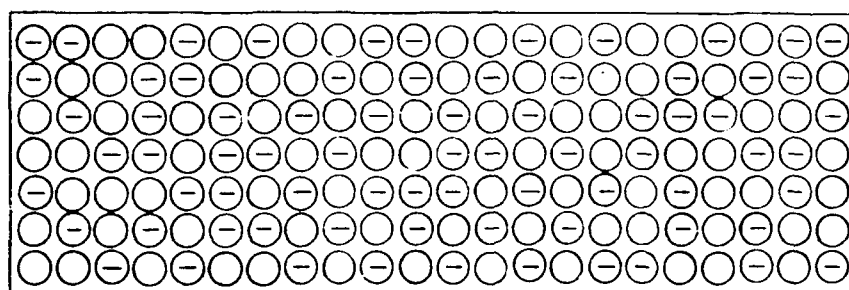
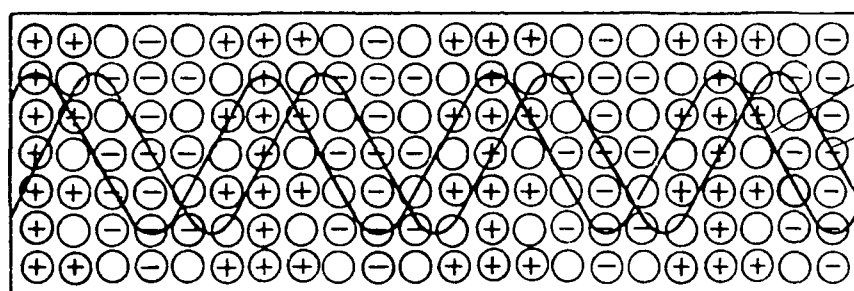


Figure 4 Experimental arrangement for two-wave mixing experiments.





a. Crystalline medium before illumination



b. The same medium after illumination

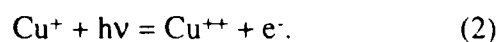
Figure 5 The photorefractive mechanism. Two laser beams intersect, forming an interference pattern. Charge is excited where the intensity is large and migrates to regions of low intensity. The electric field associated with the resultant space charge operates through the electro-optic coefficients to produce a refractive index grating. ( Ref. 17 )

as

$$O_o = V_o^{\cdot\cdot} + 1/2 O_2 + 2 e^- \quad (1)$$

where  $O_o$  is an oxygen ion in the normal site,  $V_o^{\cdot\cdot}$  is a double ionized oxygen vancancy , and  $e^-$  is an electron.

Free carriers can also be controlled by introducing impurities into the crystal. Because vacancies are present in the SBN crystal, this permits the addition of a wide range of dopants into the lattice<sup>14</sup>. Copper doped into the crystal, filling the unoccupied sites, will create an energy level in the band gap ( Figure 6 (b) ). The valence state can be varied from  $Cu^+$  to  $Cu^{++}$  by oxidation and reduction of the crystals. The mechanism leading to the photorefractive effect is the reaction



Oxygen vacancy defect in SBN and copper impurity in SBN:Cu are absorption centers which provide free electrons to the conduction band under visible light. It is suggested that the photorefractive effect can be modulated by controlling defects or impurities.

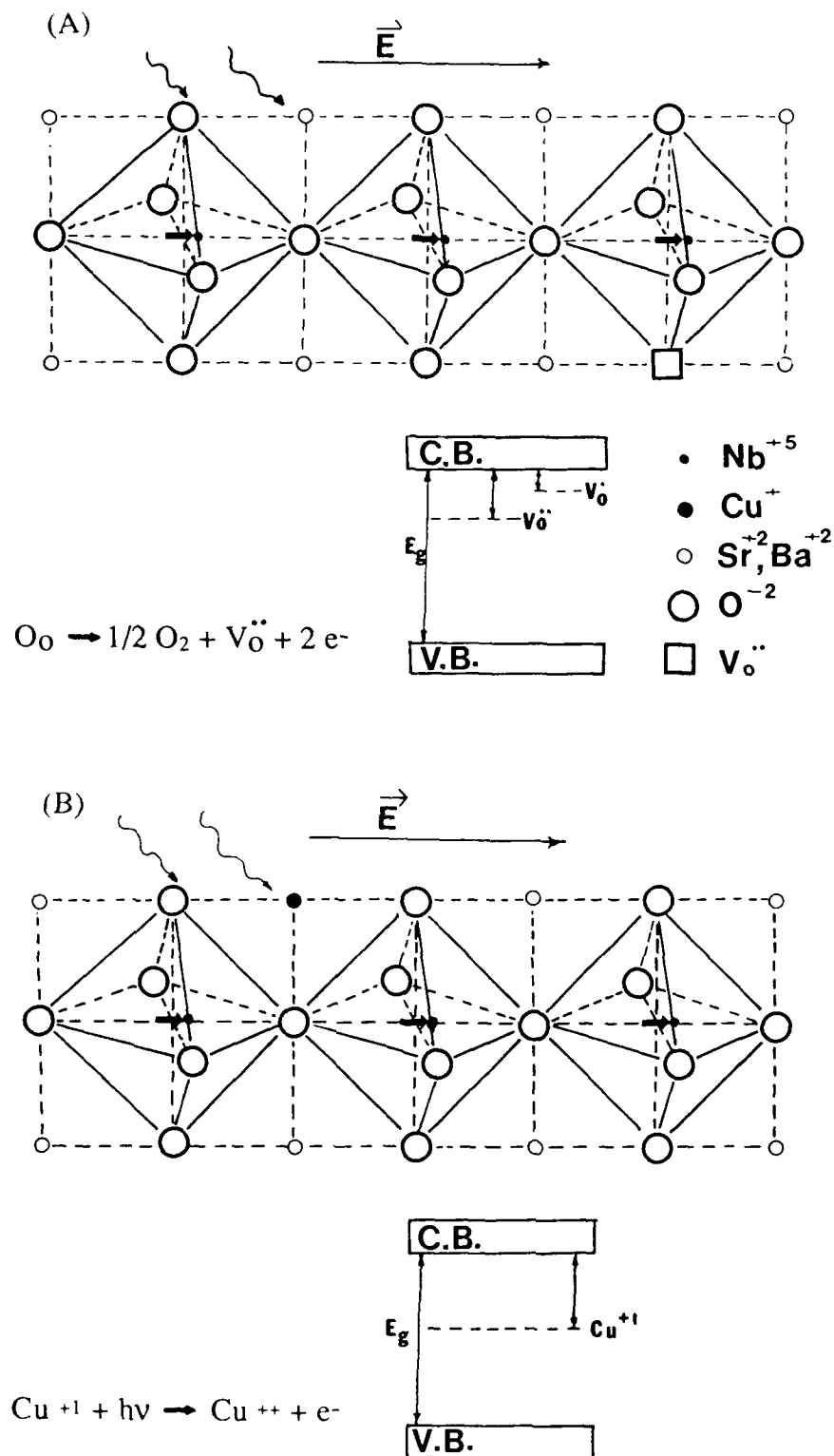


Figure 6 The molecular mechanism of photorefractive effect in SBN is shown in (a), where oxygen vacancy is the absorption center, and in SBN:Cu, (b), where  $\text{Cu}^+$  is the absorption center.

Maximum coupling will result in a crystal with large gain coefficient  $\Gamma$  but small absorption coefficient  $\alpha$ . However, gain and absorption coefficients are not independent. In fact, since charge must be excited into a conduction band by intensity interference pattern in order to start the photorefractive process, some absorption is necessary. If defects or impurities are introduced, donor or acceptor sites are created and become absorption centers as mentioned above.

Figure 7 shows the absorption spectra of doped and undoped SBN. The effect of copper impurities on the absorption spectrum of undoped SBN film was revealed. The absorption edge shifts from 300 nm in SBN to 320 nm in SBN:Cu. The effect of Cu impurity in SBN seems to be significant. However, it is undesirable that the absorption does not contribute to the photorefractive mechanism. Future study of the absorption is necessary to indicate whether they contribute to the photorefractive effect or not.

A two-wave mixing experiment of SBN film has been studied. A gain coefficient  $\Gamma$  under illumination of He-Ne laser (  $2\theta = 18^\circ$  in Figure 4 ) was observed. The detail will be discussed elsewhere<sup>16</sup>. However, the photorefractive effect of a transparent SBN film by sol-gel method has been demonstrated.

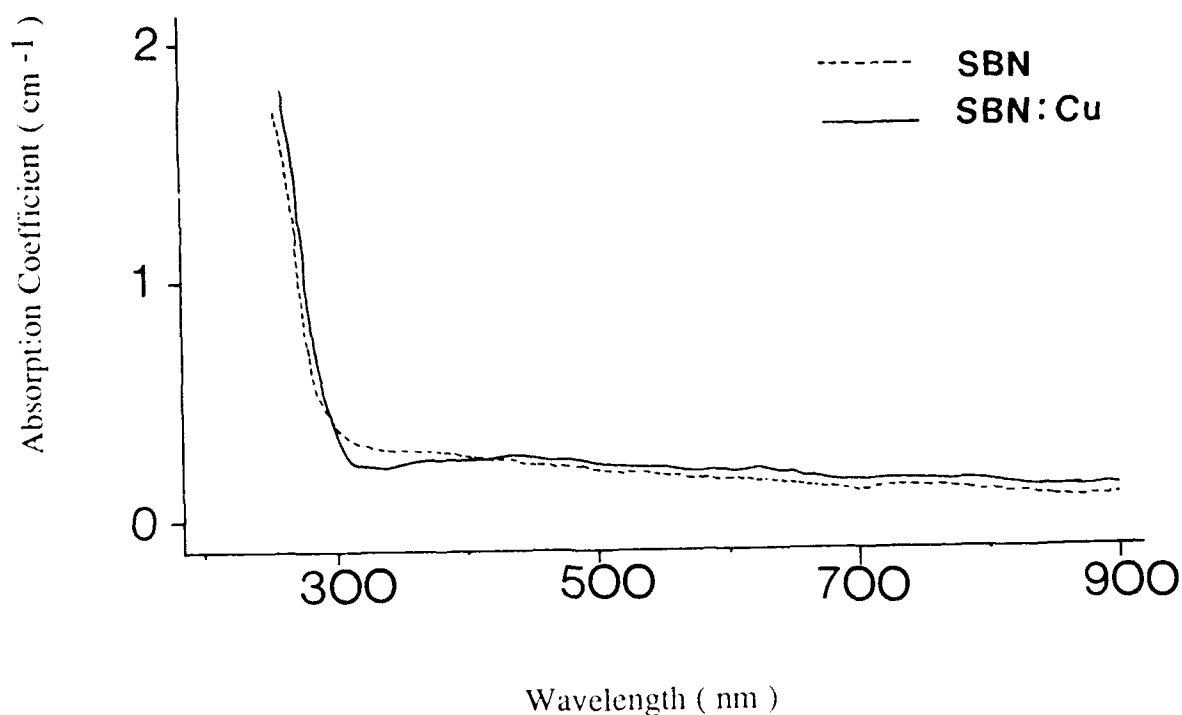


Figure 7 Absorption spectrum of SBN and SBN:Cu. The thickness of the films is about 1000 Å.

## 5. SUMMARY

Transparent ferroelectric SBN thin films have been made by the sol-gel method. Alkoxide solutions are the desirable starting materials for ferroelectric thin films, because of the homogeneity of the gels and the formation of strong M-O-M bond at low temperatures. The temperature variation of the dielectric constant of the films was measured. There was no obvious maximum peak in the  $\epsilon$  vs.  $T$  curve at the ferroelectric transition temperature. The smearing of the transition temperature observed may be attributed to the small grain size of the film. The films grown on fused silica, single crystal silicon, and GaAs possess ferroelectric properties. Asymmetrical P-E hysteresis loops have been found with Au/SBN/Si and Au/SBN/GaAs configurations. It appears that the heterojunction effect influences ferroelectric properties. The pyroelectric coefficient was measured to be about  $2 \times 10^{-8}$  C/cm<sup>2</sup> K at 27°C. This suggests that domains on the polycrystalline SBN films are preferentially oriented after electric poling. High optical quality undoped and copper-doped polycrystalline SBN films have been shown to be photorefractive by a two-wave mixing experiment. The results of this work indicate that ferroelectric thin film derived by the sol-gel method has potential for optical applications.

## 6. ACKNOWLEDGEMENT

This work was supported by the Air Force Office of Scientific Research, Directorate of Chemical and Atmosphere Sciences under Grant No. AFOSR-88-0066.

## 7. REFERENCES

1. G.A. Rakuljic, A. Yariv, and R. Neurgaonkar, *Optical Engineering*, **25** (11), 1212 (1986).
2. D. Rytz, B.A. Wechsler, R.N. Schwartz, and C.C. Nelson, *J. Appl. Phys.*, **66** (5), 1920 (1989).
3. R.A. Rupp, and A.E. Krumins, *Ferroelectrics*, **90**, 75 (1989).
4. K.D. Budd, S.K. Dey, and D.A. Payne, *Mat. Res. Soc. Symp. Proc.*, **72**, 317 (1986).
5. J. Fukushima, *J. Mat. Sci.*, **19**, 595 (1984).
6. S.K. Muralidhar, *Ceram. Bull.*, **63**, 486 (1984).
7. S. Hirano, K. Kato, *J. Non-Crystalline Solids*, **100**, 538 (1988).
8. C.J. Chen, Y. Xu, R. Xu, and J.D. Mackenzie, "Ferroelectric  $\text{Sr}_{1-x}\text{Ba}_x\text{Nb}_2\text{O}_6$  (SBN) thin film derived by sol-gel technique", *Am. Cera. Soc. Symp. Proc.*, Anaheim, Oct., (1989), accepted for publication.
9. Y. Xu, C.J. Chen, R. Xu, and J.D. Mackenzie, "Ferroelectric thin films on silicon and fused silica substrates by sol-gel process", *Mat. Res. Soc. Symp. Proc.*, San Francisco, April (1990), accepted for publication.
10. S. Hirano, K. Kato, *Adv. Ceram. Mat.*, **2** (2), 142 (1987).
11. K. Okazaki, and K. Hagata, *J. Am. Ceram. Soc.*, **56**, 82 (1973).
12. Y. Xu, C.J. Chen, R. Xu, and J.D. Mackenzie, *J. Appl. Phys.*, **67** (6), 2985 (1990).
13. A.M. Glass, *J. Appl. Phys.*, **40**, 4699 (1969).
14. R.A. Rupp, and A.E. Krumins, *Phys. Rev. B*, **39** (13), 9541 (1989).
15. A.M. Glass, *Optical Engineering*, **17** (5), 470 (1978).
16. Y. Xu, C.J. Chen, N. Desimone, and J.D. Mackenzie, "Photovoltaic effect and optical properties of ferroelectric thin films by sol-gel processing", *SPIE Symp. Proc.*, San Diego, July (1990), to be published.
17. I. Bunget, and M. Popescu, *Physics of Solid Dielectrics*, Elsevier, New York, (1984).

Optical Properties and Densification of Sol-Gel Derived PbTiO<sub>3</sub> Thin-LayersK. D. Budd<sup>†</sup> and D. A. Payne

Department of Materials Science and Engineering, Materials Research Laboratory and  
The Beckman Institute for Advanced Science and Technology,  
University of Illinois at Urbana-Champaign, Urbana, IL 61801.

**ABSTRACT**

Refractive index values are reported for sol-gel derived PbTiO<sub>3</sub> thin-layers as a function of thermal processing conditions. Dense amorphous layers were formed at 350°C ( $n = 2.35$ ) with crystallization at 450°C ( $\bar{n} = 2.65$ ). A spin-casting method is described for the deposition of coatings. Ellipsometry was used to monitor optical properties as a function of heat-treatment conditions.

**1. INTRODUCTION**

In this paper we report on the sol-gel processing of lead titanate (PbTiO<sub>3</sub>) in thin-layer (<1.0μm) form for optical applications. Lead titanate is an acentric polar material (4mm,  $P_s = 0.8\text{C/m}^2$ ) well suited for second harmonic generation (SHG). The high degree of tetragonality ( $c/a = 1.06$ ) can be reduced and modulated by zirconium (Zr) and lanthanum (La) substitutions. This gives rise to the well known families of Pb(Zr,Ti)O<sub>3</sub> (i.e., PZT) piezoelectrics and PbLa(Zr,Ti)O<sub>3</sub> (i.e., PLZT) electrooptic materials. Potential devices which may make use of the electrooptic and acoustooptic properties, include, displays, storage media, optical connectors and modulators.

We previously demonstrated a non-linear ferroelectric memory<sup>1</sup> for sol-gel PZT and an optical shutter<sup>2</sup> in PLZT. In this paper we report on the optical properties of PbTiO<sub>3</sub> thin-layers, with particular emphasis on the densification process which take place on heat-treatment, for pore-free coatings. Refractive index measurements are reported as a function of thermal processing conditions.

Ramamurthi and Payne<sup>3,4</sup> recently reviewed the chemical processing of PbTiO<sub>3</sub> from lead acetate trihydrate (Pb(00CCH<sub>3</sub>)<sub>2</sub>·3H<sub>2</sub>O) and titanium isopropoxide (Ti(OiPr)<sub>4</sub>) in methoxyethanol (CH<sub>3</sub>OCH<sub>2</sub>CH<sub>2</sub>OH). Budd et al.<sup>5</sup> reported on the sol-gel processing of PZT and PLZT in 1985. Since that time there have been several articles on the effects of hydrolysis and condensation reactions on polymeric structures which develop in sol-gel derived PbTiO<sub>3</sub>-based materials<sup>6,7</sup>. The effects of acid and base additions on the free-volume in dense amorphous coatings, and subsequent crystallization behavior, were reported<sup>8,9</sup>. This has led to the sol-gel processing of PbTiO<sub>3</sub>-based materials at sufficiently reduced temperatures (~500°C) which are compatible for the integration of devices with semiconductors (e.g., Si, GaAs)<sup>10,11</sup>.

**2. EXPERIMENTAL**

Thin-layers were cast on a variety of substrate materials, including, glass, silicon and platinum, at 1000-4000 rpm using a photoresist spinner<sup>a</sup>. The processing method was similar to that reviewed above<sup>1-11</sup>. The spin time was approximately thirty seconds, which was slightly longer than the time required to obtain a constant interference color from the coating. Prior to spin-casting, the substrates were de-greased with trichloroethylene and/or acetone, and rinsed with isopropanol and methoxyethanol. Silicon wafers were etched prior to cleaning with hydrogen peroxide and a buffered HF solution. Platinum substrates were polished through the use of a series of decreasing sized diamond pastes, followed by 0.3 micron and

<sup>†</sup> Present address: 3M, St. Paul, MN

<sup>a</sup> Headway model EC101-D, Headway Research Inc.; Garland, Texas

92 4 28 060

92-11445



Table 1. Color Chart for the Deposition of Thin -Layers

Thickness (microns) for a given refractive index						
color	1.25	1.50	1.75	2.00	2.25	2.50
brown	0.08	0.07	0.06	0.05	0.05	0.04
violet	0.12	0.10	0.08	0.07	0.06	0.06
blue	0.16	0.13	0.11	0.10	0.09	0.08
green	0.19	0.16	0.14	0.12	0.11	0.10
gold	0.23	0.20	0.17	0.15	0.13	0.12
orange	0.28	0.24	0.20	0.17	0.15	0.13
violet	0.33	0.28	0.23	0.20	0.18	0.16
blue	0.36	0.31	0.26	0.23	0.20	0.18
yellow	0.46	0.39	0.33	0.28	0.25	0.23
red	0.51	0.44	0.37	0.32	0.28	0.26
blue	0.57	0.49	0.41	0.36	0.31	0.28
yellow	0.66	0.57	0.48	0.42	0.37	0.33
pink	0.72	0.62	0.53	0.46	0.41	0.36
blue	0.82	0.70	0.59	0.52	0.46	0.41
orange	0.93	0.80	0.67	0.58	0.52	0.47
violet	0.99	0.85	0.71	0.62	0.55	0.50

0.05 micron alumina on microcloths. Precursor solutions were syringed through in-line filters directly onto the substrates in clean-room conditions.

The as-deposited layers were dried at 70°C for five minutes and stored in unsealed plastic boxes prior to heat treatment. A microprocessor-controlled molybdenum disilicide box furnace <sup>b</sup>, and sometimes a hot plate, were used for thermal processing. Initially, the layer thickness was estimated from weight and interference color characteristics. The apparent color of a coating is known to depend on the phase difference between the light reflected from the surface and the light reflected from the substrate beneath the coating. The wavelength,  $\lambda$ , for constructive interference, is given by

$$\lambda = \frac{4nt}{2k-1}, \quad (1)$$

where  $k = 0, 1, 2, \dots$ ,  $t$  is the layer thickness, and  $n$ , the refractive index. A color chart, based upon experimental observations, is summarized, above, in Table 1. This method was used initially as a guide for the preparation of layers of a desired thickness. For partially densified layers, neither the refractive indices nor densities were known with enough certainty to estimate the thicknesses reliably. SEM, and mechanical measurements with a step-gauge, were used to supplement the above techniques. Finally, for precise measurements, an ellipsometer <sup>c</sup> was used for the determination of refractive index and thickness.

Ellipsometry is a useful method for determining the optical properties of flat surfaces, and transparent coatings up to a few microns thick. The technique is essentially based upon the fact that the state of polarization of a light beam is altered on reflection from a bare or coated surface. Both the angular

<sup>b</sup> Teresco Inc., Champaign, IL

<sup>c</sup> Gaertner model L-117, Chicago, IL

position of the ellipse (azimuth), and the shape (ellipticity), are affected. Two independent parameters,  $\psi$  and  $\Delta$ , describe the polarization state. They are determined by finding local intensity minima for an elliptical polarizer and analyzer, allowing independent determination of thickness and refractive index, according to,

$$\tan \psi e^{i\Delta} = \frac{(r_1 + r_2 e^{-2ix})(1 + r_3 r_4 e^{-2ix})}{(1 + r_1 r_2 e^{-2ix})(r_3 + r_4 e^{-2ix})}, \quad (2)$$

$$x = \frac{2\pi}{\lambda} t (n^2 - n_0^2 \sin^2 \phi)^{1/2}, \quad (3)$$

where  $r_i$  are various Fresnel reflection coefficients,  $n_0$  is the refractive index of the ambient, and  $\phi$ , the angle of incidence. Good agreement with the expected interference colors was observed. Film thicknesses were measured with a precision of better than  $5\text{\AA}$ .

The density of a thin-layer was calculated from the weight, thickness, and area of the coating on a two-inch diameter silicon wafer. The use of larger sized samples allowed for a precision of nearly three significant figures in the weight of the coating. Figure 1 gives a calibration curve between density and average refractive index ( $\bar{n}$ ) for sol-gel derived coatings. Densification studies were carried out by successive heat treatments on a hot-plate followed by ellipsometer measurements. Film temperatures were determined by a thermocouple, which was pressure-contacted to a similar substrate. Isothermal heat treatments were accomplished by placing a coated substrate directly onto a pre-heated hot plate. Little or no difference was detected between layers given a single continuous heat treatment, or between layers which had been heated for the same total amount of time, but via a sequence of shorter heat treatment schedules.

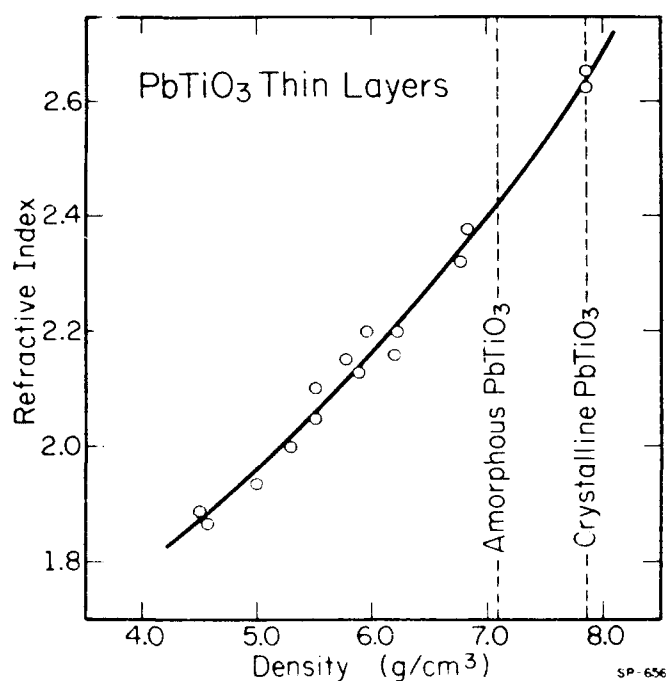


Fig. 1. Density dependence of refractive index.

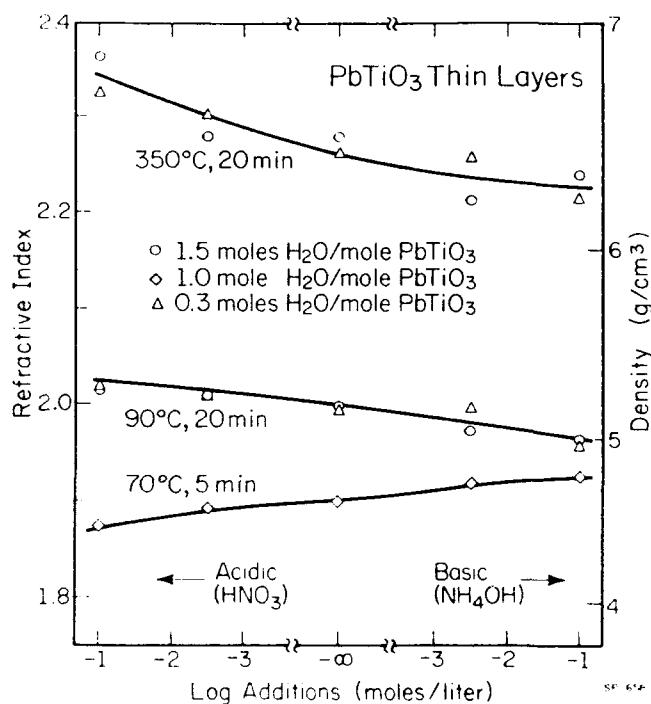


Fig. 2. Effect of acid and base additions on the refractive index of amorphous coatings.

Continuous-heating studies were approximated by a series of short heat treatments at steadily increasing temperatures. Satisfactory agreement was found between these data, and data obtained by ramping and quenching experiments.

### 3. RESULTS AND DISCUSSION

Figure 2 gives information for refractive index as a function of acid or base additions, for thin-layers heat-treated at 70°C, 90°C, and 350°C in air. It was found that the refractive index (and density) of coatings heated at 350°C increased monotonically with acid content in the precursor solution. Under acidic conditions, pore free amorphous coatings developed with densities up to 6.8 g/cm<sup>3</sup> (i.e., 92% of the theoretical density for crystalline lead titanate). That is, the dense amorphous materials had up to 8% free volume, and was formed at relatively low temperatures of 350°C, and with refractive indices up to 2.35.

Interestingly, air-dried or mildly-dried (70°C, five minutes) thin-layers exhibited the opposite trend in refractive index with additive content (Figure 2). It was found that acidic films contained excess organic content, probably in the form of adsorbed solvent, which was trapped in the finer nanostructure. Longer heat treatments, at slightly higher temperatures, were sufficient to remove the excess organic matter, and reverse the trend. Apparently, rearrangement and shrinkage in the gel structures was dependent on the removal of organic species in the system. This is further illustrated in Figures 3 and 4 which indicate a progressive increase in density and refractive index, with heat treatment temperature, after short periods of time at temperature. The effective heating rates were 10°C/min and 30°C/min, respectively. For each case, coatings which contained acid additions were initially less dense than basic ones (attributable to excess organic content) but later became more dense after heat treatment. Careful examination of the data indicate coatings became more dense at lower temperatures with faster heating rates.

Gels used in this work had characteristics consistent with polymeric structures. There was no evidence for colloidal particles. Polymeric gels shrink more gradually, and over a broader temperature range, than colloidal gels. Additional mechanisms of shrinkage can occur for polymeric gels over colloidal gels, which include, structural relaxation, condensation polymerization, and network rearrangement. By contrast, amorphous colloids, usually density by viscous flow, in a much more narrow temperature

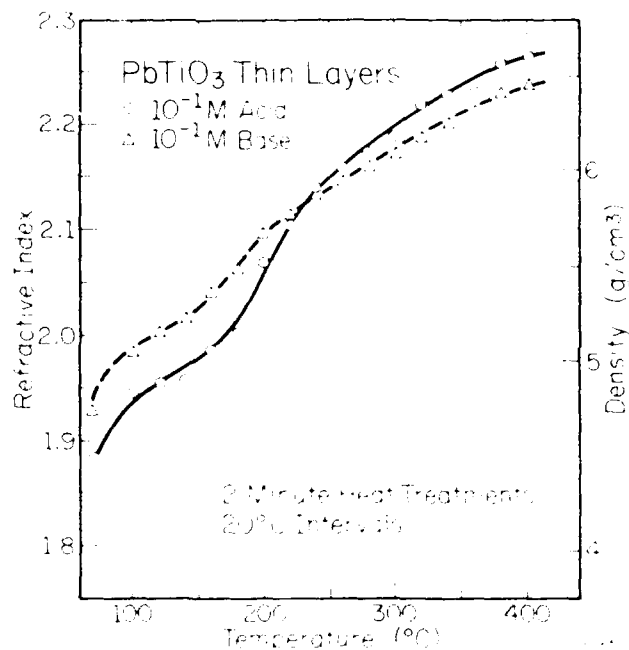


Fig. 3. Density and refractive index as a function of heat treatment (10°C/min).

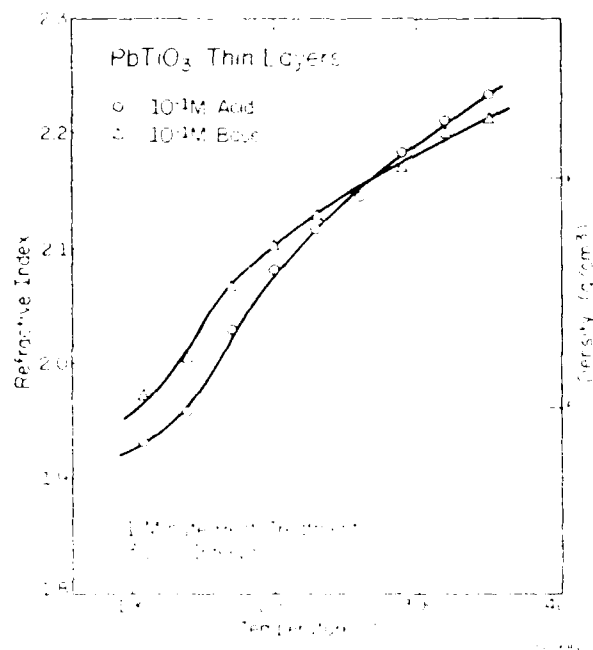


Fig. 4. Density and refractive index as a function of heat treatment (30°C/min).



range. The shrinkage behavior of acidic and basic thin-layers is given in Figure 5. A continuous shrinkage was observed from room temperature to 400°C, consistent with the expected behavior for polymeric gels. This was accompanied by a weight loss of organic matter.

Semi-quantitative analysis of polymeric gel shrinkage is possible by comparison with competing viscous flow mechanisms for amorphous particles. Shrinkage equations can be derived by equating the energy dissipated in viscous flow with the decrease in surface energy that drives densification. Isothermal shrinkage data can then be compared with model particulate systems. Little change in shrinkage rate is expected over much of the densification range if shrinkage does occur by viscous flow. By contrast, a large decrease in shrinkage rate was observed during isothermal heat treatments of  $\text{PbTiO}_3$  thin-layers. Figure 6 illustrates isothermal shrinkage data at 150°C, 250°C, and 350°C for both acid and base additions. These data suggest that other mechanisms (in addition to viscous flow) occurred and contributed to the shrinkage, and suggest that the coatings were quite polymeric in nature, rather than colloidal. These data have been analyzed elsewhere<sup>12</sup>.

#### 4. SUMMARY

Sol-gel processing was used for the integration of  $\text{PbTiO}_3$  thin layers ( $<1\mu\text{m}$ ) on a variety of substrate materials. A spin-casting method was used. Precursor solutions were formed by reflux and distillation of lead acetate trihydrate and titanium isopropoxide in methoxyethanol; and prehydrolyzed solutions were spin-cast at 1000-4000 rpm. The effects of acid and base additions on densification behavior and optical properties were investigated by ellipsometric methods. In general, acid additions (e.g., 0.1M  $\text{HNO}_3$ ) resulted in denser amorphous coatings after heat treatment, and which crystallized at lower temperatures. The pathways by which structure evolved were consistent with polymeric gel networks. Typical values for refractive index were 2.35 in amorphous coatings, and 2.65 in crystalline material.

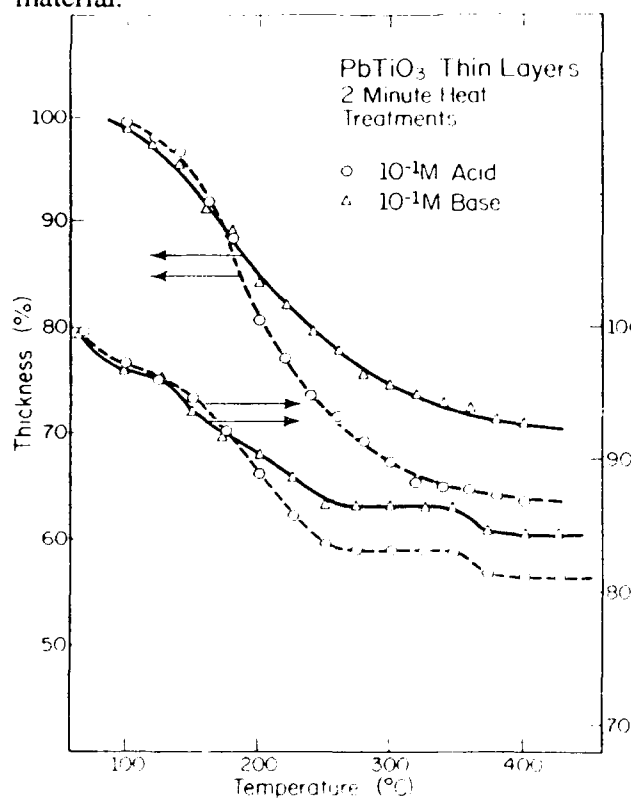


Fig. 5. Shrinkage and weight loss for  $\text{PbTiO}_3$  thin-layers.

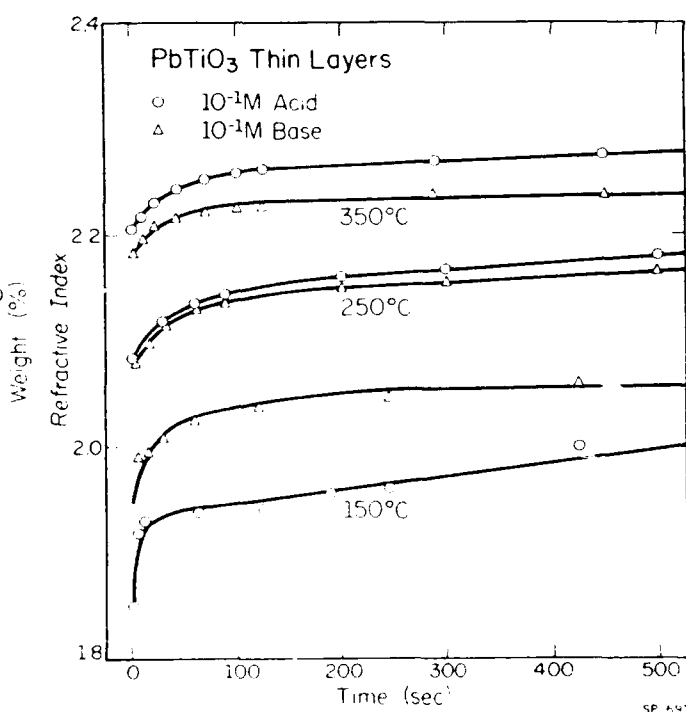


Fig. 6. Isothermal shrinkage curves for  $\text{PbTiO}_3$  thin-layers.

## 5. ACKNOWLEDGEMENTS

The authors acknowledge support from an ONR-ASEE Fellowship (KDB) and from US DOE DMR-DE-ACO2-76ER01198 (DAP). Technical assistance from G. Manuel and A. Yu is recognized. Continued interaction with S. K. Dey, R. W. Schwartz, S. D. Ramamurthi and C. D. E. Lakeman is gratefully acknowledged.

## 6. REFERENCES

1. S. K. Dey, D. A. Payne, K. D. Budd, "Thin Film Ferroelectrics of PZT by Sol-Gel Processing," *IEEE UFFC*, 35, No. 1, 80-81, 1988.
2. K. D. Budd and D. A. Payne, "Sol-Gel Processing of Thin-Layer Dielectrics in Lead Titanate-Based Systems," *Inst. Phys. Conf. Ser.* 103 (1) 13-22, 1989.
3. S. D. Ramamurthi and D. A. Payne, "Structural Investigations of Prehydrolyzed Precursors Used in the Sol-Gel Processing of  $\text{PbTiO}_3$ ," *J. Am. Ceram. Soc.* 73 (7), in press, 1990.
4. S. D. Ramamurthi and D. A. Payne, "NMR Spectroscopic Investigations of  $\text{PbTiO}_3$  Sol-Gel Processing" Better Ceramics Through Chemistry IV, eds. C. J. Brinker, B. J. J. Zelinski, D. F. Clark and D. R. Ulrich, Mat. Res. Soc. Symp. 180, in press, 1990.
5. K. D. Budd, S. K. Dey and D. A. Payne, "Sol-Gel Processing of  $\text{PbTiO}_3$ - $\text{PbZrO}_3$  and PLZT Thin Films," *Brit. Cer. Proc.* 36: 107-121, 1985.
6. K. D. Budd, S. K. Dey and D. A. Payne, "The Effect of Hydrolysis Conditions on the Characteristics of  $\text{PbTiO}_3$  Gels and Thin Films," in Better Ceramics Through Chemistry II, Mat. Res. Soc. Symp. Proc. 73:711-716, C. J. Brinker et al. (eds.), 1986.
7. S. K. Dey, K. D. Budd and D. A. Payne, "Structure of Polymeric  $\text{PbTiO}_3$  Gels," *J. Am. Ceram. Soc.* 70: (10) 295-296, October 1987.
8. R. J. Schwartz and D. A. Payne, "Crystallization Behavior of Chemically Prepared and Rapidly Solidified  $\text{PbTiO}_3$ ," Better Ceramics Through Chemistry III C. J. Brinker et al (eds.) Mat. Res. Soc. Proc. 121: 199-206, 1988.
9. R.W. Schwartz, D. A. Payne and A. J. Holland, "The Effects of Hydrolysis and Catalysis Conditions on the Surface Area and Decomposition of Polymeric Sol-Gel Derived  $\text{PbTiO}_3$  Powders," Ceramic Powder Processing Science, eds. H. Hausner, G. R. Messing and S-I Hirano, Deutsche Keramische Gesellschaft, 165-172, 1989.
10. R. W. Schwartz, C. D. E. Lakeman and D. A. Payne, "The Effects of Hydrolysis Conditions, and Acid and Base Additions, on the Gel-to-Ceramic Conversion in Sol-Gel Derived  $\text{PbTiO}_3$ ," Better Ceramics Through Chemistry IV, eds. C. J. Brinker, B. J. J. Zelinski, D. F. Clark and D. R. Ulrich, Mat. Res. Soc. Symp. 180, in press, 1990.
11. R. W. Schwartz, Z. Xu, D. A. Payne, T. A. DeTemple and M. A. Bradley, "Preparation and Characterization of Sol-Gel Derived  $\text{PbTiO}_3$  Thin Layers on GaAs," Ferroelectric Thin Films eds. A. I. Kingon and E. R. Myers, Mat. Res. Soc. Symp. 200, in press, 1990.
12. K. D. Budd, "Structure Evolution in Sol-Gel Derived Lead Titanate-Based Materials, and Application to the Processing of Thin Dielectric Layers," Ph.D. Thesis, University of Illinois, 1986.

**Sol-gel processing of lithium niobate thin-layers for optical applications****Dennis J. Eichorst and David A. Payne**

Department of Materials Science and Engineering, Materials Research  
Laboratory, and The Beckman Institute for Advanced Science and Technology  
University of Illinois at Urbana-Champaign, Urbana, IL 61801

**ABSTRACT**

The sol-gel processing of lithium niobate thin-layers on silicon from heterometallic alkoxide solutions is described. Advantages of sol-gel processing for low-temperature formation of stoichiometric lithium niobate are discussed. A recrystallization procedure, involving a bimetallic alkoxide, was developed for the purification of alkoxide solutions. The alkoxide complex contained the appropriate cation ratio for the preparation of stoichiometric lithium niobate. Solvent selection, addition of nitric acid or ammonium hydroxide, and thermal processing conditions were shown to affect the ceramic microstructures. In particular, the solvent system and additives influenced grain growth and porosity in the crystallized layers. Methoxyethanol-derived layers had a grain size approximately twice that observed for the ethanol system. Use of a rapid heating process produced dense layers at 650 °C, whereas oxygen treatments allowed for crystallization at 400 °C.

**1. INTRODUCTION**

Lithium niobate single crystals have been widely investigated for their optical properties and information processing capabilities. However, single crystal growth of stoichiometric lithium niobate remains a difficult task due to incongruent melting and the presence of a lithium-deficient solid solution. As a result, lithium niobate crystals prepared from stoichiometric melts have compositional fluctuations which affect optical properties (e.g., birefringence).<sup>1</sup> So as to minimize compositional fluctuations and produce homogeneous crystals, a congruently melting but non-stoichiometric composition (48.6% Li<sub>2</sub>O) is commonly used. A major drawback to the use of lithium niobate in optical circuits is optical damage, where a change in refractive index occurs on exposure to high intensity light (i.e., photorefractive effect). The effect appears more severe for material prepared from the congruently melting composition required for the preparation of homogeneous material.<sup>2</sup> Thus, there is a need for low temperature processing methods, which allow for the preparation of homogeneous lithium niobate of the stoichiometric composition.

Thin-films of lithium niobate have also received considerable interest for integrated optical circuits. Epitaxial (single crystal) lithium niobate films have been prepared by epitaxial growth by melting (EGM) and liquid phase epitaxy.<sup>3,4</sup> However, the methods are susceptible to incongruent melting, as previously discussed, and require substrate materials (i.e., lithium tantalate) which can withstand the high melt temperatures. Therefore, alternate processing methods, which are amenable to a wider variety of substrate materials (e.g., silicon, sapphire) and which offer greater compositional control, are required. Polycrystalline films prepared by rf sputtering and melt techniques have demonstrated optical waveguiding,<sup>3,5-7</sup> but, optical attenuation has been a significant problem.

Optical loss has generally been attributed to grain-boundary scattering (and surface roughness), indicating a need for single crystal smooth films. However, a review of the literature indicates limited microstructural characterization of polycrystalline specimens. In particular, grain size, the presence of porosity, microcracking and secondary phases, have not been reported which would influence the degradation of optical quality. Madayan showed attenuation was primarily a function of surface roughness with losses of 17 dB/cm, which could be reduced to 1 dB/cm by polishing.<sup>7</sup> Many polycrystalline films can contain secondary phases (i.e., LiNb<sub>3</sub>O<sub>8</sub> or Li<sub>3</sub>NbO<sub>4</sub>) which act as scattering centers. Compositional inhomogeneities have been attributed to differential sputtering rates and sticking coefficients for lithium and

**92 4 28 061****92-11442**

niobium during vapor phase deposition. Furthermore, lithium niobate prepared from a melt of lithium and niobium oxides, or by sputtering with an oxide target, typically have transition metal impurities (i.e., Fe) which lead to optical damage. The results to date indicate the major obstacles for the preparation of high optical quality lithium niobate layers are control of composition, homogeneity, and the development of dense fine ceramic microstructures.

Typically, wet-chemical forming methods offer reduced temperature processing, control of stoichiometry, and a high degree of purity. Therefore, chemical processing methods may be of considerable advantage to the formation of optical materials. In the sol-gel processing method, alkoxide precursors undergo hydrolysis and condensation reactions, resulting in a polymeric network which can subsequently be converted to an amorphous oxide on heat-treatment. Additional heat-treatment results in the crystallization of the amorphous material. The process avoids both incongruent melting and the formation of powders which can be detrimental to compositional homogeneity. A "homogeneous" polymeric network is developed. Relative homogeneity is offered through molecular mixing in solution prior to deposition. However, preferential hydrolysis (i.e., of niobium ethoxide) could result in a distribution of niobium-rich and lithium-rich regions. Potential problems may be avoided by i) pre-hydrolysis of less-reactive species, to give similar hydrolysis rates for all components, or ii) preparation of a heterometallic alkoxide which would hydrolyze without dissociation. In this paper, we report on the use of bimetallic alkoxides,  $\text{LiNb}(\text{OR})_6$ , for the sol-gel processing of lithium niobate thin-layers on silicon. Advantages of the sol-gel method were investigated with respect to specific processing problems observed for lithium niobate. Furthermore, the effects of solution chemistry and thermal processing conditions on microstructure development were explored. The results indicate processing routes which allow for the preparation of dense layers with controlled grain sizes required for high quality optical layers.

## **2. EXPERIMENTAL METHODOLOGY**

### **2.1. Solution preparation**

Alkoxide solutions of lithium niobium ethoxide,  $\text{LiNb}(\text{OCH}_2\text{CH}_3)_6$ , and lithium niobium methoxyethoxide,  $\text{LiNb}(\text{OCH}_2\text{CH}_2\text{OCH}_3)_6$ , were prepared in ethanol or methoxyethanol, respectively, as indicated in Figure 1. Alkoxide solutions were prepared in their parent alcohols (i.e., niobium ethoxide in ethanol), thereby avoiding partial alcohol exchange reactions, which could give differences in hydrolysis and condensation behavior for varying degrees of exchange.<sup>8</sup> The reactions were carried out under a dry nitrogen atmosphere using standard Schlenk procedures.<sup>9</sup> Lithium alkoxides were prepared by direct addition of lithium metal to alcohol causing evolution of hydrogen. Niobium ethoxide was either obtained commercially or synthesized and subsequently purified according to the method of Bradley.<sup>10</sup> Niobium methoxyethoxide was prepared by alcohol exchange; distillation of a solution of niobium ethoxide in 2-methoxyethanol. Complete reaction was indicated by a boiling point of 125 °C (b.p. of 2-methoxyethanol) and confirmed by  $^1\text{H}$  and  $^{13}\text{C}$  NMR spectroscopy. Lithium and niobium alkoxide solutions were reacted and subsequently concentrated by distillation to yield 0.8 M lithium niobium ethoxide or 1.0 M lithium niobium methoxyethoxide solutions. Previous NMR results indicated immediate reaction of the alkoxides at room temperature, forming bimetallic alkoxide species.<sup>11</sup> Further concentration of the ethoxide, but not the methoxyethoxide, resulted in crystallization of  $\text{LiNb}(\text{OEt})_6$ .

Stock solutions were diluted with alcoholic additions of water, nitric acid or ammonium hydroxide to give either 0.25 M or 0.5 M precursor solutions. Water additions of 0-2 moles/Nb, and acid or base additions of 0.1 mole/Nb were investigated. Ethanol solutions with greater than 1 mole  $\text{H}_2\text{O}$ /Nb tended to precipitate, whereas up to 3 moles  $\text{H}_2\text{O}$ /Nb could successfully be added to the methoxyethanol system without immediate gelation or precipitation. The solutions were stable for several months and were used for the deposition of lithium niobate layers on silicon by spin-casting methods.

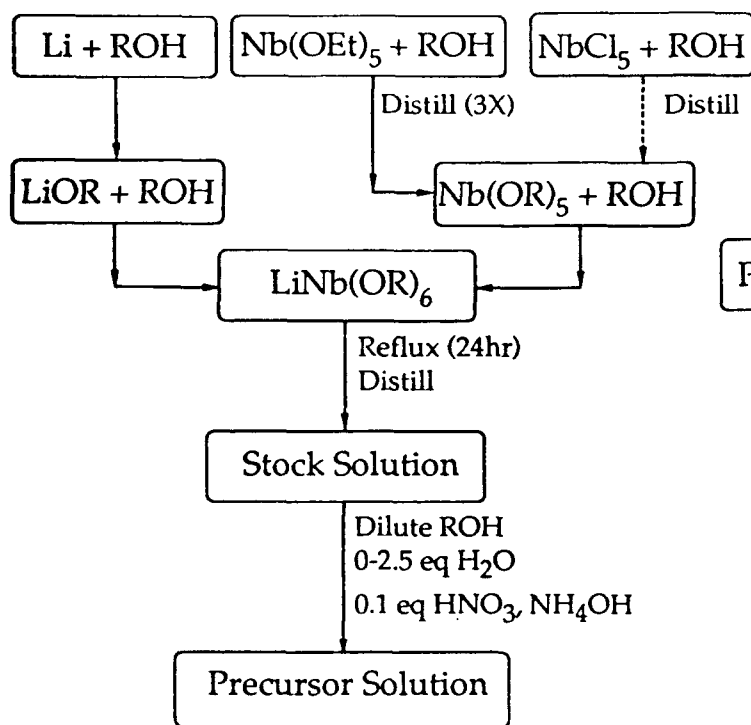


Figure 1. Flow diagram for the synthesis of lithium-niobium alkoxide solutions.

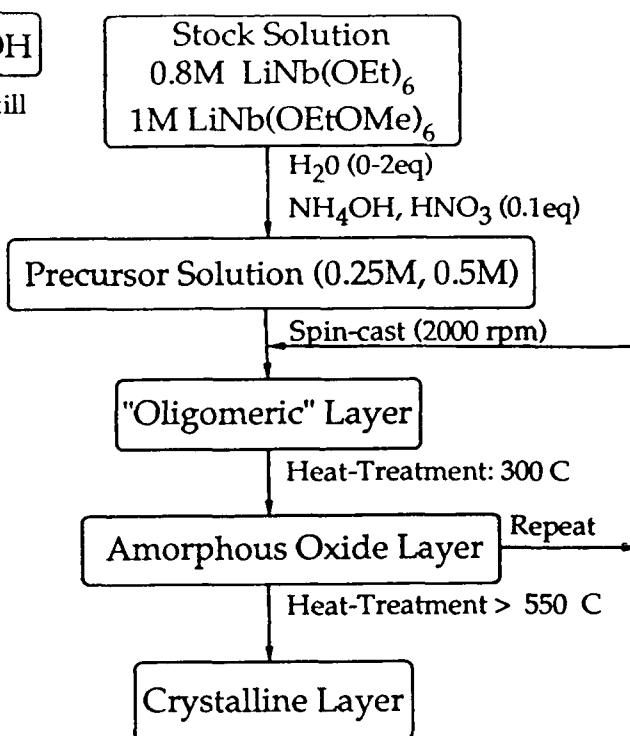


Figure 2. Deposition procedure for the formation of lithium niobate layers on silicon substrates.

## 2.2. Thin-layer processing

Thin-layers of lithium niobate were deposited on silicon by spin-casting at 2000 rpm for 45 seconds. Silicon substrates were ultrasonically treated in: deionized water (2x), trichloroethylene, acetone, and isopropanol. The silicon wafers had a final ultrasonic treatment in either ethanol or 2-methoxyethanol for the appropriate system. Solutions were filtered with a 0.2  $\mu\text{m}$  filter prior to deposition. As-deposited layers were approximately 1500 Å thick (for 0.5M methoxyethanol). A 30 second heat-treatment at ~300 °C (on a hot-plate) facilitated removal of entrapped solvent and residual organic material, resulting in an amorphous lithium niobate layer. The thickness was increased by a multiple deposition technique, outlined in Figure 2, in which subsequent layers were deposited on an amorphous layer. Layer thicknesses of 0.75  $\mu\text{m}$  could be obtained without noticeable cracking.

Amorphous samples were converted to crystalline lithium niobate by heat-treatment after the desired thickness had been obtained. Samples were heat-treated between 400 and 800 °C for 5 minutes to 8 hours using either a 10 °C/min heating rate or by inserting the samples into a pre-heated furnace (i.e., arapid heating process, RHP). Heat-treatments were carried out either in ambient atmosphere or in flowing oxygen.

### 3. RESULTS AND DISCUSSION

#### 3.1. Advantages of sol-gel processing

It has been widely stated that sol-gel processing offers (i) preparation of high-purity materials, (ii) control of stoichiometry, (iii) better homogeneity and (iv) reduced processing temperatures, with respect to conventional oxide routes.<sup>12</sup> Use of the alkoxide precursor materials, through the above advantages, may alleviate many of the processing problems associated with lithium niobate. Molecular level mixing may occur for a solution of alkoxide species in a mutual solvent, allowing preparation of a homogeneous solution which can be converted to the oxide. We would like further to explore these possible advantages with respect to the specific processing of lithium niobate ceramics.

Bradley investigated the boiling points of niobium alkoxides as a possible method for separating niobium and tantalum.<sup>13</sup> Boiling points of niobium ethoxide (156 °C/0.05 mm Hg) and tantalum ethoxide (146 °C/0.015mm Hg) were significantly different and could allow separation of the two compounds. Distillation of niobium alkoxides produced from ferrous niobium (via chloride) has been investigated for the preparation of high-purity niobium oxide powders.<sup>14</sup> Powders prepared from hydrolysis of the alkoxides had iron contents less than 10 ppm; whereas powders prepared from sublimed niobium chloride (used for alkoxide preparation) had 700 ppm of iron. The results indicate distillation of niobium alkoxides can successfully be used as a purification technique which could prove invaluable in improving the optical quality (i.e., reducing optical damage) of lithium niobate.

We have previously reported on the crystal structure of the double metal alkoxide,  $\text{LiNb}(\text{OCH}_2\text{CH}_3)_6$ , shown in Figure 3.<sup>15</sup> The complex forms infinite helical polymers comprised of niobium ethoxide,  $\text{Nb}(\text{OEt})_6$ , octahedral units linked by lithium, in a distorted tetrahedral environment, with bridging alkoxy ligands. The alkoxide molecule fixes the cation ratio required for the preparation of

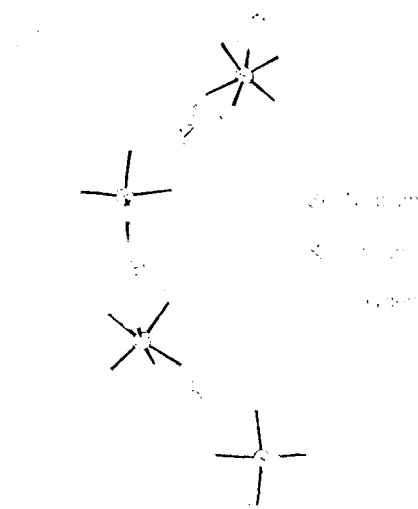


Figure 3. Solid-state crystal structure of  $\text{LiNb}(\text{OEt})_6$ .

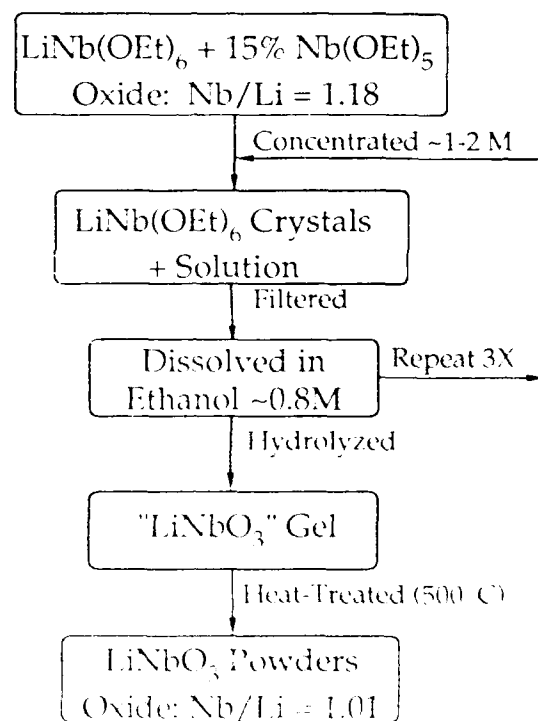


Figure 4. Flow diagram for the successive crystallization of ethoxide solutions.

stoichiometric lithium niobate. Furthermore, the Nb-O-Li bonds within the material suggest molecular level homogeneity and perhaps low temperature processing. The utility of the crystals has been demonstrated for compositional control from non-stoichiometric alkoxide solutions. Figure 4 shows a successive crystallization technique devised to purify an alkoxide solution with a nominal addition of 15% excess niobium ethoxide. Crystals of the bimetallic alkoxide were obtained by concentration at room temperature, and any remaining solvent was removed by filtration, and the crystals redissolved in dry ethanol. After three crystallizations, the material was gelled and subsequently crystallized. Chemical analysis of the crystalline powder indicated a 1:1.01 lithium:niobium ratio, stoichiometric within experimental accuracy. Furthermore, ICPE analyses of stoichiometric solutions and crystalline powders prepared from the solution detected no transition metal impurities (levels below detection limits, i.e.,  $\text{Fe} < 50$  ppm). The results indicate isolation of the alkoxide crystals can allow purification and compositional control during the sol-gel processing of lithium niobate.

### 3.2. Microstructure dependence on processing conditions

Figure 5 shows ceramic microstructures obtained for lithium niobate multilayer samples (5 depositions) prepared using ethanol and 2-methoxyethanol solvent systems with the addition of 1 mole  $\text{H}_2\text{O}/\text{Nb}$ . Dense crystalline layers were obtained after heat-treatment at  $650^\circ\text{C}$  for 1 hour using the rapid heating process. The layers were crack-free and had no apparent porosity. However, selection of the solvent system did have an effect on grain size. Lithium niobium ethoxide resulted in an average grain size of  $0.1\text{--}0.2\ \mu\text{m}$ , whereas the methoxyethoxide gave a grain size of approximately  $0.5\ \mu\text{m}$ . Differences in grain size may be due to different polymeric structures produced during hydrolysis and condensation. Structural differences of the precursor alkoxides may be indicated by the inability to crystallize lithium niobium methoxyethoxide from solution.

The evolution of microstructure after 1 hour heat-treatments (RHP) is illustrated in Figure 6. At  $500^\circ\text{C}$ , the material appeared dense with no discernable structure (i.e., amorphous). X-ray diffraction indicated only a slight degree of crystallization at  $500^\circ\text{C}$  in thin-layers. For samples heat-treated at  $600^\circ\text{C}$ , the grains were evident but with a breakdown in film continuity. Significant grain growth and densification have occurred by  $650^\circ\text{C}$ . There was little increase by  $700^\circ\text{C}$ . Heat-treatment of lithium niobate powders in

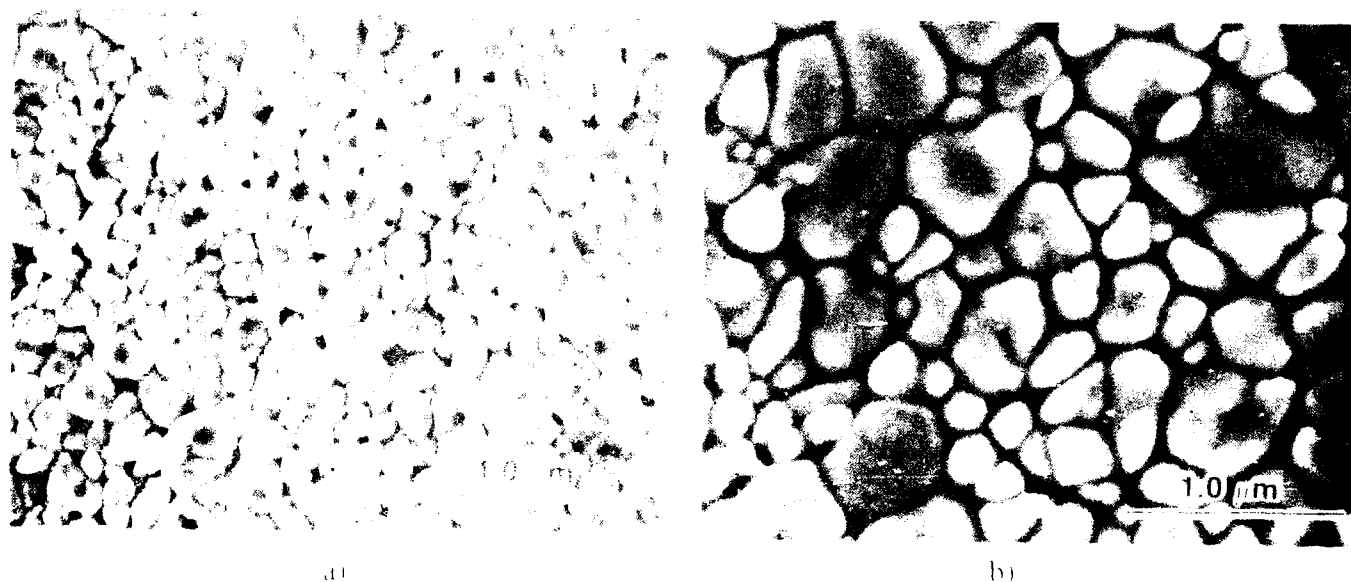


Figure 5 Microstructures of lithium niobate layers prepared using a) ethanol and b) methoxyethanol solvent systems, after one hour at  $650^\circ\text{C}$  (RHP).

excess of 700 °C indicated the formation of  $\text{LiNb}_3\text{O}_8$ , which was associated with the volatilization and loss of lithium oxide. The results indicate the importance of reduced temperature processing so as to maintain the chemical stoichiometry offered through the use of the synthesized bimetallic alkoxide. Similar results were observed for increasing time at temperature. For heat-treatment at 650 °C, no observable structure was resolved after 10 minutes. After 30 minutes the formation of a porous microstructure with fine grains was observed. With increasing time, considerable grain growth (0.1  $\mu\text{m}$ -0.5 $\mu\text{m}$ ) and densification had occurred. The results indicate a rapid nucleation event giving rise to a large number of nuclei which grow at the expense of other grains to eventually produce a dense microstructure.

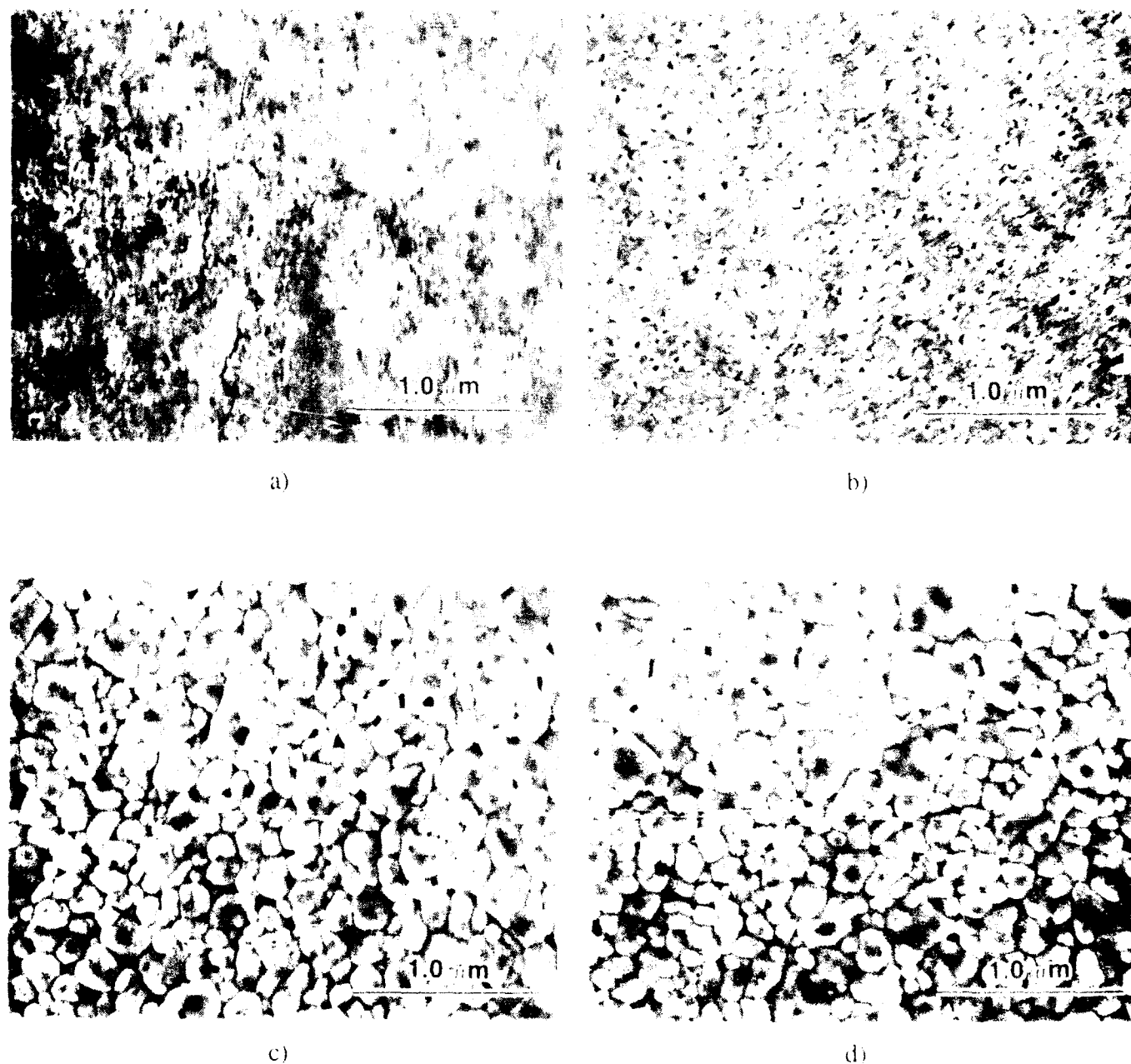


Figure 6. Evolution of microstructure (from 0.5M methoxyethanol) for 1 hour heat treatments (RHP) at a) 550 °C, b) 600 °C, c) 650 °C, and d) 700 °C.



Additions of nitric acid or ammonium hydroxide had an effect on the development of ceramic microstructure for material heat-treated at 10 °C/min (to 800 °C for 1 hour), as shown in Figure 7. Base additions resulted in dense structures similar to those obtained without additives (Figure 5), whereas acid additions yielded porous structures. It should be pointed out that lithium alkoxides can be viewed as base additions to niobium systems, and as such could be "neutralized" through the additions of acids. For similar samples, but through the use of RHP, differences in the development of ceramic microstructure were not as severe. However, acid systems remained more porous than neutral or base systems.

Heating rate had a dramatic effect on microstructure development as indicated in Figure 8. RHP gave dense layers with an average grain size of approximately 0.5  $\mu\text{m}$  after 1 hour at 650 °C. However, at 10 °C/min to the same temperature, and for the same hold time, the microstructure was finer (0.1-0.2  $\mu\text{m}$ ) and had a high degree of porosity. Heat-treatment in oxygen produced crystalline layers with a grain size of ~0.25  $\mu\text{m}$  and with residual porosity. However, the layers were crystalline at a lower temperature of 400 °C, indicating an oxygen assisted crystallization process. Results for differential thermal analysis and X-ray diffraction are given in Figure 9 for gel specimens heat-treated to 250 °C in air and oxygen. A typical decomposition exotherm was observed for the air-fired material, and XRD indicated an amorphous structure. Heat-treatment in oxygen gave a very strong exotherm, due to decomposition of residual organic material, and produced crystalline lithium niobate at a furnace temperature of 250 °C. The decomposition exotherm indicates a temperature difference between the sample and the reference material ( $\text{Al}_2\text{O}_3$ ) of ~40-50 °C. Furthermore, the heat of combustion was greater than the programmed heating rate, resulting in a displacement of the exotherm from the vertical. This indicates the sample temperature was increased to 375-400 °C, i.e., above the furnace temperature of 250 °C. Therefore, the lithium niobate gel was heated to the crystallization point in an oxygen atmosphere. In effect, in-situ rapid thermal processing can lead to crystallization at reduced furnace temperatures (250 °C) if oxygen atmospheres are used. However, this is an apparent effect, since the true temperature of the sample is really above 400 °C. A similar process is

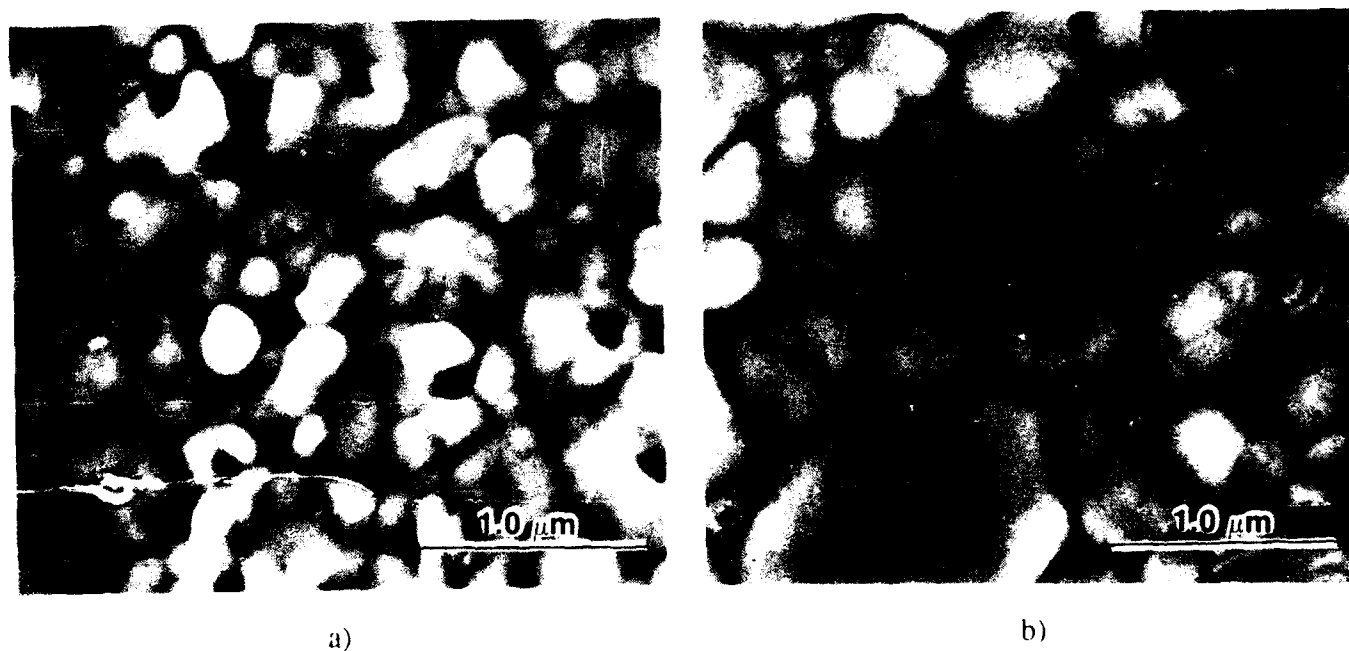
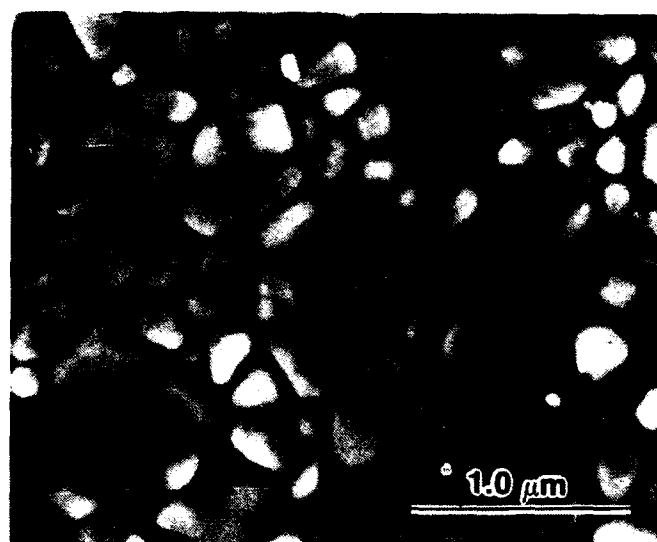
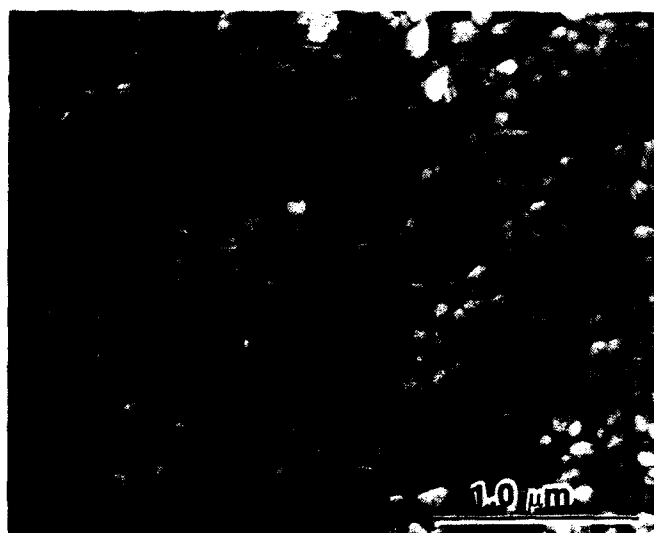


Figure 7. Microstructures of lithium niobate layers (from 0.5 M methoxyethanol) with the addition (0.1 mole/Nb) of a) nitric acid and b) ammonium hydroxide, after 30 minutes at 800 °C with a heating rate of 10 °C/min.

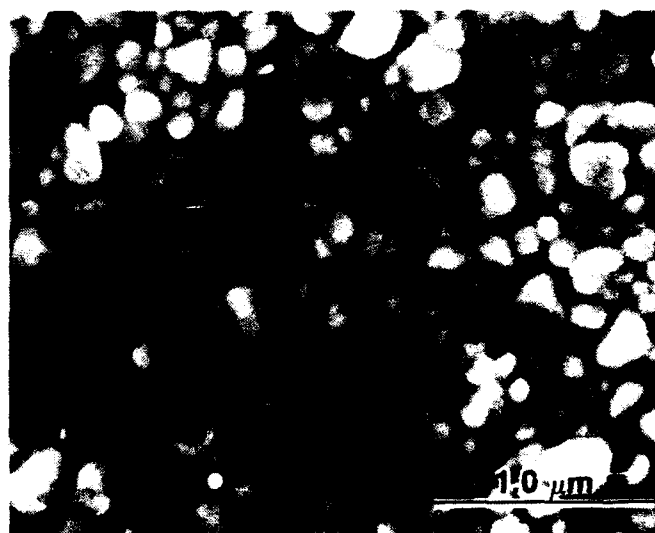
believed to occur for heat-treatment of the lithium niobate layers crystallized at 400 °C in oxygen. Oxygen heat-treatments may be beneficial for integrated optical or microelectronic applications, if the substrate temperature can be maintained below 400 °C, as the layer is crystallized by in-situ rapid thermal processing.



a)



b)



c)

Figure 8. Microstructures for lithium niobate layers (from 0.5 M methoxyethanol) heat-treated using a) RHP (650 °C for 1 hour), b) 10 °C/min heating rate (650 °C for 1 hour) and c) 10 °C/min in oxygen (400 °C for 1 hour).

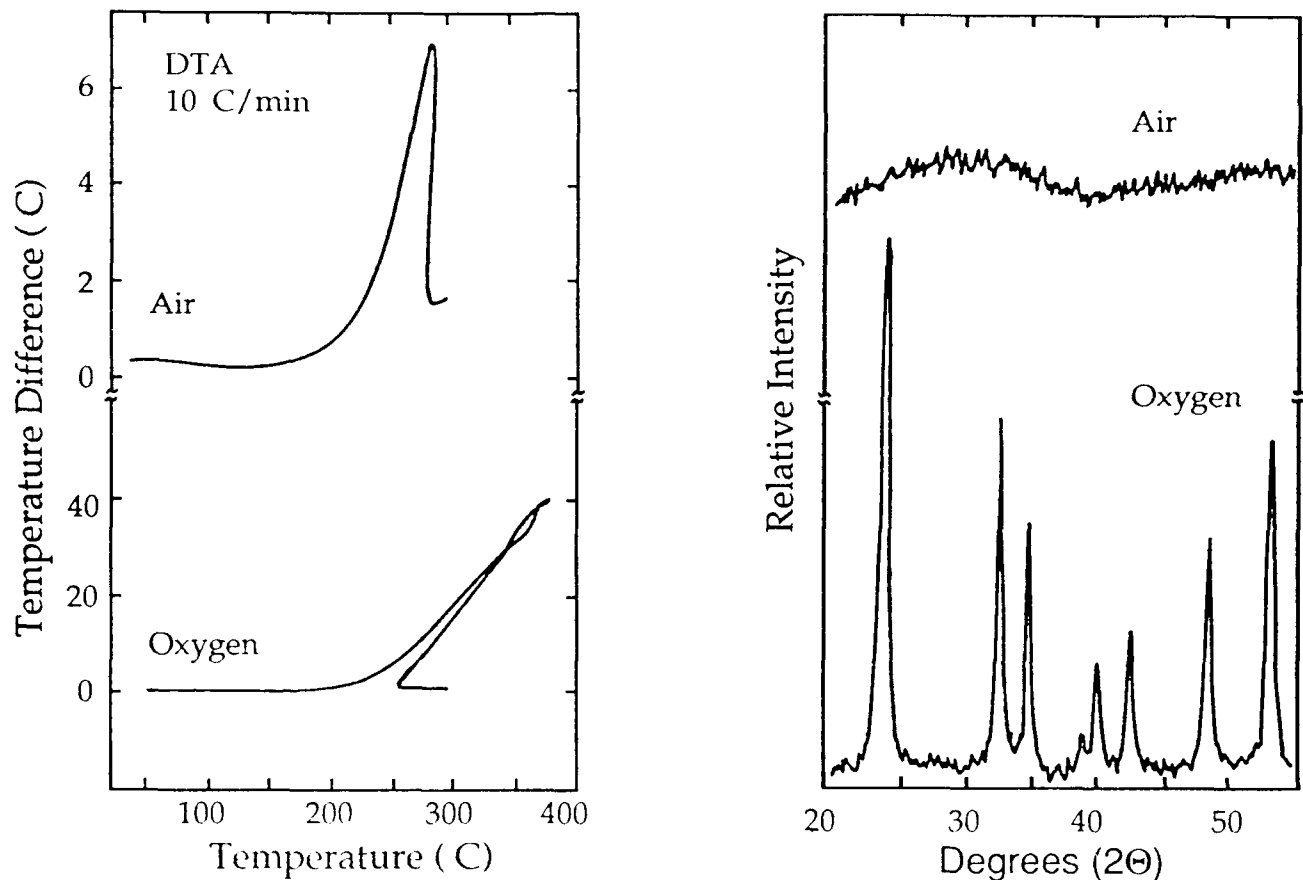


Figure 9. Differential thermal analysis and X-ray diffraction results for lithium niobate gels heat-treated in air and oxygen atmospheres.

#### 4. SUMMARY

Sol-gel processing of lithium niobate was investigated using ethanol and methoxyethanol-based systems. Distillation of niobium alkoxides was an effective method in developing enhanced purity. Furthermore, lithium niobium ethoxide could be crystallized, allowing further purification of alkoxide solutions. The processes indicate an enhanced method of purity and stoichiometry control in addition to the mixing of known quantities of pure precursor compounds.

The sol-gel method was used for the preparation of lithium niobate layers on silicon substrates. Rapid heating gave dense lithium niobate layers after one hour at 650 °C. Slower heating rates produced more porous microstructures and of a fine grain size. Rapid heating methods, with possible additions of ammonium hydroxide were necessary for the formation of dense crack-free layers suitable for optical applications (elimination of scattering centers). Furthermore, the layers were single phase  $\text{LiNbO}_3$  at temperatures below 750 °C. Finally, the use of oxygen assisted heat-treatments indicated further reductions in processing temperatures were possible, approaching furnace temperatures of 400 °C.

The sol-gel processing method was shown to allow preparation of high-purity stoichiometric lithium niobate. The purification and compositional control potentially offered by the bimetallic alkoxide precursor could lead to a reduction in optical damage which has been a significant problem in melt-grown materials. Furthermore, stoichiometric lithium niobate layers appeared homogeneous, without the presence

of secondary phases, which has been difficult to accomplish by vapor deposition techniques. Furthermore, the reduced processing temperatures may allow for the integration of LiNbO<sub>3</sub> on a variety of substrate materials for practical applications.

## **5. ACKNOWLEDGEMENTS**

The authors would like to thank Mr. Daniel Hagberg for helpful discussions. Support of an IBM Fellowship on Materials and Processing Sciences, and the U.S. Department of Energy under contract DE-AC02-76ER01198 are greatly appreciated. The use of facilities in the School of Chemical Sciences at the University of Illinois is also acknowledged.

## **6. REFERENCES**

1. J. G. Bergman, A. Ashkin, A. A. Ballman, J. M. Dziedzic, H. J. Levinstein, and R. G. Smith, "Curie Temperature, Birefringence, and Phase-Matching Temperature Variations in LiNbO<sub>3</sub> as a Function of Melt Stoichiometry," *Appl. Phys. Lett.*, vol. 12, pp. 92-94, 1968.
2. A. Räuber, "Chemistry and Physics of Lithium Niobate," in *Current Topics in Materials Science*, vol. 1 ed. E. Kaldis, pp. 481-601, North-Holland Publishing, Amsterdam, 1978.
3. S. Miyazawa, "Growth of LiNbO<sub>3</sub> Single-crystal Film for Optical Waveguides," *Appl. Phys. Lett.*, vol. 23, pp. 198-200, 1973.
4. A. Baudrant, H. Vial, and J. Daval, "Liquid Phase Epitaxy of LiNbO<sub>3</sub> Thin Films for Integrated Optics," *Mat. Res. Bull.*, vol. 10, pp. 1373-1378, 1975.
5. S. Miyazawa, "Optical Waveguiding in LiNbO<sub>3</sub> Single-crystal Film Grown by the EGM Technique," *J. Appl. Phys.*, vol. 46, pp. 2223-2228, 1975.
6. G. H. Hewig, K. Jain, F. O. Sequeda, R. Tom, and P. W. Wang, "RF Sputtering of LiNbO<sub>3</sub> Thin Films," *Thin Solid Films*, vol. 88, pp. 67-74, 1982.
7. R. S. Madoyan, G. N. Sarkisyan, and O. A. Khachaturyan, "Growth, X-ray Structure and Optical Investigations of Epitaxial Films of Solid-Solutions of Lithium Niobate-Tantalate," *Cryst. Res. Technol.*, vol. 20, pp. 1031-1040, 1985.
8. K. D. Budd, PhD Thesis, University of Illinois, 1986.
9. D. F. Shriver, *Manipulation of Air-sensitive Compounds*, Robert E. Krieger Publishing Company, Malabar, FL, 1982.
10. D. C. Bradley, B. N. Chakravarti, and W. Wardlaw, "Normal Alkoxides of Quinquevalent Niobium," *J. Chem. Soc.*, pp. 2381-2384, 1956.
11. D. J. Eichorst, K. E. Howard, and D. A. Payne, "NMR Investigations of Lithium Niobium Alkoxide Solutions," in *Ultrastructure Processing of Ceramics, Glasses and Composites*, eds., D. R. Uhlmann, M. C. Weinberg, S. H. Risbud, and D. R. Ulrich, J. Wiley & Sons, New York, (in press, 1990).
12. see for example, D. W. Johnson, Jr. "Sol-Gel Processing of Ceramics and Glass," *Am. Ceram. Soc. Bull.*, vol. 64, pp. 1597-1602, 1985.
13. D. C. Bradley, R. C. Mehrotra, and D. P. Gaur, *Metal Alkoxides*, Academic Press, New York, 1978.
14. N. Sato and M. Nanjo, "Formation of Ultrafine Niobium Pentoxide Powder from Ferroniobium via Alkoxide," *Shigen to Sozai*, vol. 105, pp. 745-50, 1989. (English Abstract in *Chem. Abstracts*, vol. 112, #9409d, 1990).
15. D. J. Eichorst, D. A. Payne, S. R. Wilson, and K. E. Howard, "The Crystal Structure of LiNb(OCH<sub>2</sub>CH<sub>3</sub>)<sub>6</sub>: A Precursor for Lithium Niobate Ceramics," *Inorg. Chem.*, vol. 29, pp. 1458-1459, 1990.



## Electrical and optical properties of alkoxide-derived lithium niobate thin-layers

Daniel S. Hagberg, Dennis J. Eichorst, and David A. Payne

Department of Materials Science and Engineering, and The Beckman Institute for Advanced Science and Technology, University of Illinois at Urbana-Champaign, Urbana, IL 61801

**ABSTRACT**

Sol-gel processing methods were investigated for the preparation of lithium niobate optical layers. Two alkoxide systems, ethanol and 2-methoxyethanol, were studied. The methods resulted in either randomly oriented polycrystalline layers on silicon or grain-oriented layers on sapphire and platinum substrates. Data are reported for the electrical and optical properties of the layers. In addition to stoichiometric lithium niobate layers,  $\text{Ti:LiNbO}_3$  was prepared by the addition of titanium alkoxides to the solutions. Optical data are presented for the  $\text{Ti:LiNbO}_3$  layers as a function of titanium content.

**1. INTRODUCTION**

Lithium niobate has received considerable attention for optical or microelectronic applications because of its field-responsive characteristics. Device applications have focussed on optic and acoustic properties. Typically, devices are fabricated from single crystals of lithium niobate grown from the melt. Lithium niobate exists in a continuous solid solution range between 45-50 %  $\text{Li}_2\text{O}$  (i.e., lithium deficient) at elevated temperatures. However, due to incongruent melting of the stoichiometric material, compositional inhomogeneities can result, resulting in property variations throughout melt-grown crystals. In order to prepare more uniform samples, a lithium deficient (48.6 %  $\text{Li}_2\text{O}$ ), but congruently melting composition is commonly used. Furthermore, it has been shown that many properties are strongly dependent on lithium content. For example, the maximum negative birefringence (important for phase matching) is obtained from stoichiometric lithium niobate (50 %  $\text{Li}_2\text{O}$ ).<sup>1</sup> Thus, so as to allow for device optimization, a processing method suitable for a range of lithium contents at reduced temperatures would be desirable.

Optical waveguides have typically been fabricated from lithium niobate, using: (i) titanium in-diffusion, (ii) lithium out-diffusion, or (iii) proton exchange to increase the refractive index in a channel pattern or surface layer. A common feature of these methods is a standard diffusion profile for the waveguiding region. Enhanced optical containment can be achieved by a refractive index step-profile, if the step is large. Titanium in-diffusion is the most used and well characterized method. In this process, a strip of titanium is evaporated and then heated ( $\sim 1000^\circ\text{C}$ ) to facilitate diffusion into lithium niobate. A typical problem, however, is concurrent out-diffusion of lithium which can create a planar waveguide in addition to the desired channel guide.<sup>2,3</sup> Furthermore, the elevated processing temperatures are not compatible with integrated optical technologies. Therefore, a reduction in processing temperatures and alternate methods of forming a waveguide region are needed.

Recently, lithium niobate thin films have received interest for integrated optical applications in which a waveguide can be formed by depositing lithium niobate on a substrate of a lower refractive index.  $\text{LiNbO}_3$ ,  $\text{LiTaO}_3$ , and sapphire have been the substrates most widely investigated<sup>4-8</sup> based on their transparency and crystallographic similarity to  $\text{LiNbO}_3$ . Liquid phase epitaxy<sup>3</sup> and epitaxial growth by melting<sup>2</sup> have been reported for the preparation of lithium niobate films from the melt. These methods were shown to produce optical waveguides; however, the congruently melting, nonstoichiometric composition was required, as discussed previously. Furthermore, substrate selection was limited to those materials which could withstand the melt temperatures. Rf sputtering<sup>5,9</sup> and molecular beam epitaxy<sup>10</sup> have also been used for the deposition of lithium niobate layers. Unfortunately, compositional control was difficult due to preferential sputtering rates and sticking coefficients. Samples prepared by these methods also had secondary phases (e.g.,  $\text{LiNb}_3\text{O}_8$  and  $\text{Li}_3\text{NbO}_4$ ) which degraded the optical properties.

92 4 28 062

92-11443



A key issue in film formation is epitaxial growth which can control the film properties. Lithium niobate is an acentric material, therefore, properties depend on the crystallographic orientation. For example, the dielectric constant in the a-direction ( $\sim 78$ ) is greater than in the c-direction ( $\sim 28$ )<sup>11</sup>, furthermore, the largest electrooptic coefficient is  $r_{33}$ , corresponding to the c-axis of lithium niobate. To make use of the optimum properties for a specific application, preferential orientation of the film would be desired. Proper selection of the substrate material is known to influence the growth of deposited layers. Therefore, crystallographic relations between lithium niobate and a potential substrate material are of interest.

Sol-gel processing may allow stoichiometry control through additions of lithium and niobium alkoxides of known concentration. Furthermore, liquid mixing can also facilitate the preparation of homogeneous materials. As-deposited layers may be crystallized at temperatures greatly reduced from melt temperatures, thereby, avoiding evaporation and incongruent melting problems. In addition, grain-orientation has been reported to occur in sol-gel derived layers that have been deposited on sapphire and platinum.<sup>12-14</sup> We report now on a sol-gel processing method for the preparation of homogeneous, single-phase lithium niobate layers deposited on a variety of substrate materials. The process has been demonstrated to allow purification and stoichiometry control through use of a precursor alkoxide containing a fixed lithium:niobium cation ratio.<sup>15</sup> Furthermore, a solution-based process has been developed for the formation of titanium-doped lithium niobate layers.

## **2. EXPERIMENTAL METHODOLOGY**

### **2.1 Solutions**

Alkoxide solutions of lithium niobium ethoxide,  $\text{LiNb}(\text{OCH}_2\text{CH}_3)_6$ , and lithium niobium methoxyethoxide,  $\text{LiNb}(\text{OCH}_2\text{CH}_2\text{OCH}_3)_6$ , were prepared in ethanol\* or 2-methoxyethanol,<sup>†</sup> respectively, as indicated in Figure 1. Lithium alkoxides were synthesized by direct addition of lithium metal to alcohol. Niobium ethoxide\*\* was obtained commercially. Niobium methoxyethoxide was formed by an alcohol exchange reaction by distillation of a solution of niobium ethoxide in 2-methoxyethanol. Lithium and niobium alkoxide solutions were mixed and concentrated, through distillation, to give 1.0 M lithium niobium methoxyethoxide or 0.8 M lithium niobium ethoxide stock solutions.

Stock solutions were subsequently diluted with alcoholic solutions of water and titanium alkoxide to give either 0.25 M or 0.5 M precursor solutions with 1 mole  $\text{H}_2\text{O}$ /mole Nb. Titanium ethoxide<sup>†</sup> was obtained commercially and, as in the case of niobium alkoxides, converted to titanium methoxyethoxide by solvent exchange. Titanium dopant concentrations of 0-1 mole %/mole Nb were investigated. Solutions so prepared were stable over a period of several months and were used for the deposition of lithium niobate layers by spin-casting methods.

### **2.2 Deposition of layers**

Layers were deposited on (100) silicon, (001) sapphire or polycrystalline platinum substrates as outlined in Figure 2. Multiple depositions allowed for an increase in overall thickness. The substrates were first cleaned ultrasonically in deionized water, trichloroethylene, acetone, and isopropyl alcohol. They also received a final wash in ethanol or 2-methoxyethanol, as appropriate, prior to deposition. Solutions were deposited onto the substrates using a photo-resist spinner<sup>++</sup> at 2000 rpm. After deposition on silicon, each layer received a 300 °C heat-treatment to yield an amorphous oxide. The amorphous material was then crystallized by a single heat-treatment, after the final thickness was obtained. Samples were heat-treated in

\* Midwest Grain Products, Pekin, IL.

† Aldrich Chemical Company, Inc., Milwaukee, WI.

\*\* Alfa Products, Ward Hill, MA.

++ Headway Research, Inc., Model EC101-D, Garland, TX.

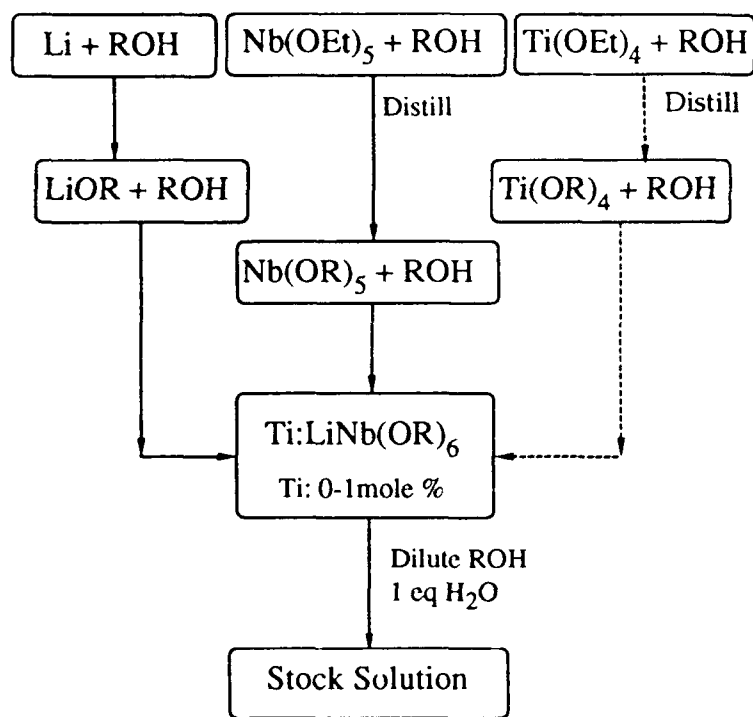


Figure 1. Synthesis of  $\text{LiNbO}_3$  and  $\text{Ti:LiNbO}_3$  alkoxide solutions.

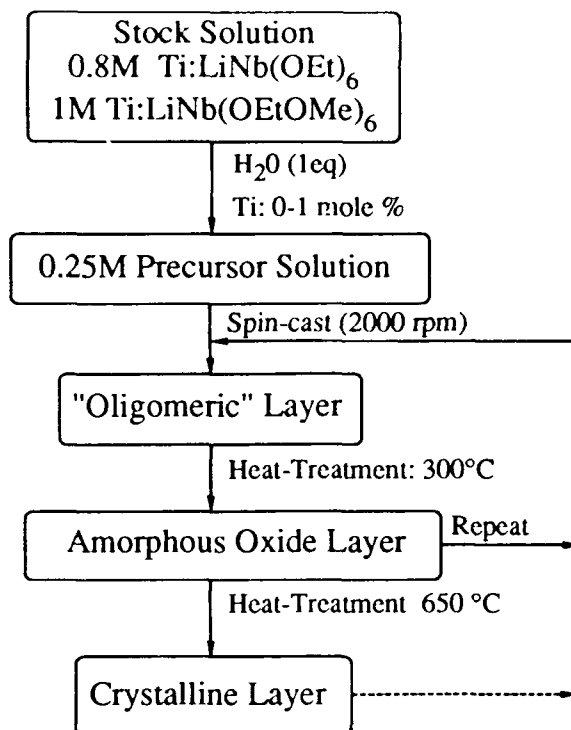


Figure 2. Deposition procedure for the formation of lithium niobate thin-layers.

air at 650 °C for 1 hour using either (i) a rapid heating process (RHP), i.e., insertion into a preheated box furnace or (ii) a 10 °C/min heating rate.

A modified heat-treatment procedure, i.e., an alternate pathway, is indicated in Figure 2 for the enhanced adhesion of layers on platinum or sapphire. Based on the results for microstructure development on silicon, RHP was used to densify layers on platinum and sapphire. After the initial deposition, the layer was heat-treated at 300 °C, as in the silicon case. However, the amorphous layer was then crystallized in air at 650 °C using RHP for 1 hour. After crystallization, two additional layers were deposited with 300 °C heat-treatments. Crystallization was then carried out at 650 °C, and the process repeated for successive depositions. The cycle, crystallization after every second deposition, was continued until the desired thickness was reached.

### 2.3 Characterization techniques

The refractive index of the layers was investigated by ellipsometric\* methods. The effects of various titanium dopant levels, final heat-treatment temperatures, and number of depositions were studied. Fourier transform infrared (FTIR) spectra were obtained for layers deposited on platinum using an IBM IR/32 in a diffuse reflectance mode.†

Electrical property measurements (dielectric constant, loss tangent) were obtained for ethanol-derived (0.25 M with 1 mole  $\text{H}_2\text{O}/\text{Nb}$ ) lithium niobate layers deposited on platinum substrates. Platinum served as both a support and a bottom electrode. Counter electrodes were deposited by evaporation of aluminum through a shadow mask (0.02 × 0.02 cm). Ag, Pt and Au electrode materials were also investigated. Dielectric measurements were made from 1kHz-1MHz on a Hewlett-Packard 4192A low frequency impedance analyzer.

\* Gaertner Scientific Corporation, Model L-117, Chicago, IL.

† Spectra-Tech Inc., Diffuse Reflectance Accessory Model 6106640, Stamford, CT.

### 3. RESULTS AND DISCUSSION

#### 3.1 Microstructure evolution and x-ray analysis

Microstructures for lithium niobate samples prepared by (i) RHP or by (ii)  $10\text{ }^{\circ}\text{C}/\text{min}$  are compared in Figure 3. For identical temperatures and time, the faster heating rate gave denser layers with a larger average grain size ( $\sim 0.5\text{ }\mu\text{m}$  compared with  $0.1\text{--}0.2\text{ }\mu\text{m}$ ). This effect was attributed to RHP rapidly heating the samples through the nucleation zone, and directly into the growth regime. Thus, fewer nuclei were produced which could grow larger before impinging on neighboring grains.

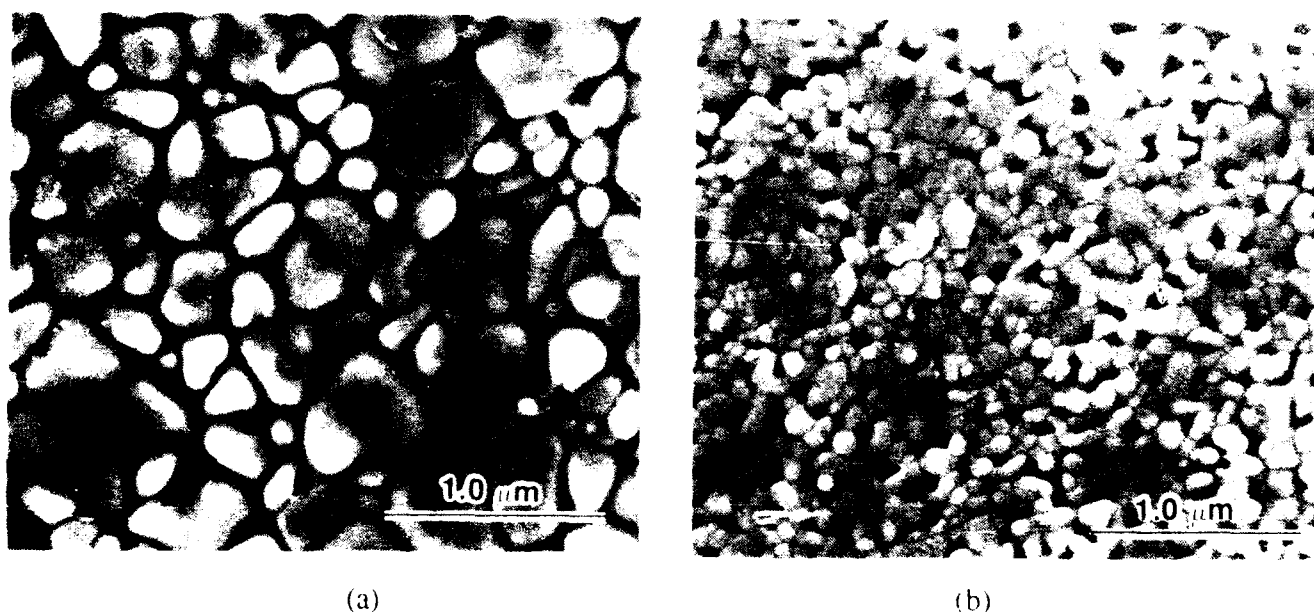


Figure 3. Microstructure of lithium niobate thin-layers heat-treated by (a) RHP or (b) at  $10\text{ }^{\circ}\text{C}/\text{min}$ .

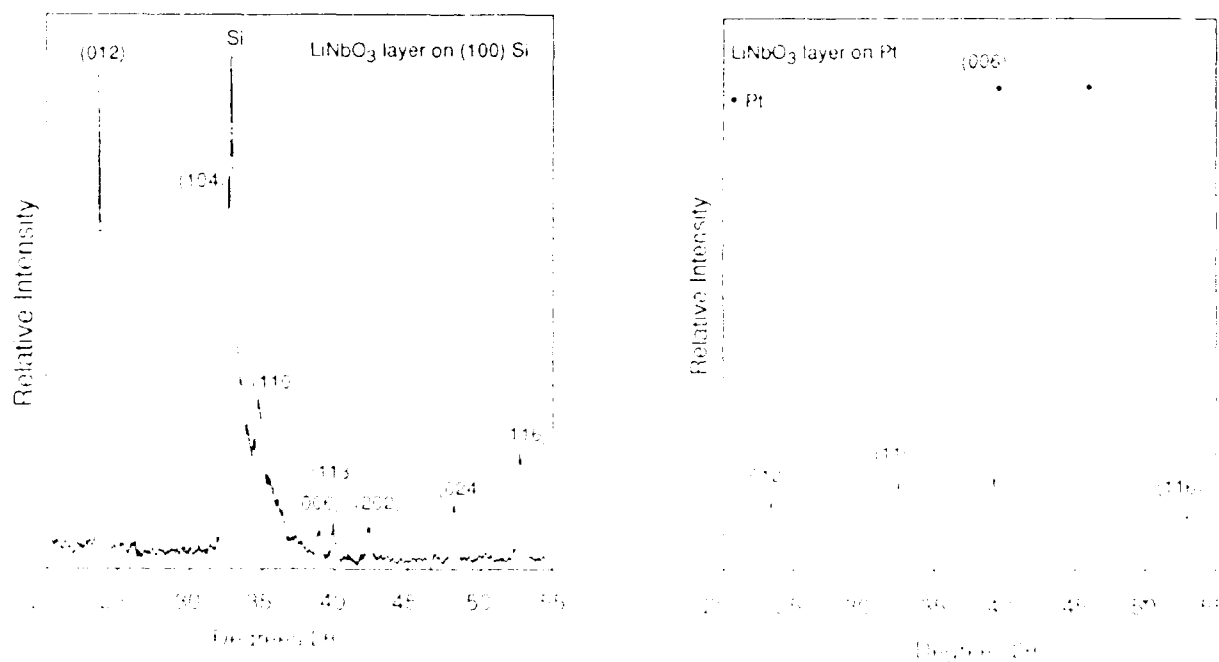


Figure 4. X-ray diffraction patterns for  $\text{LiNbO}_3$  layers deposited on silicon and platinum.



X-ray diffraction patterns for lithium niobate layers deposited on silicon and platinum are given in Figure 4. It should be noted that in powder patterns, the (006) diffraction peak is of minor intensity (4%), and the major diffraction peak is from (012).<sup>16</sup> Thus, the grains appear to be randomly oriented on the silicon substrate. By contrast, formation of  $\text{LiNbO}_3$  with a preferred alignment (006) was noted on platinum.

The preferred alignment was investigated further by x-ray rocking curve measurements. Although the platinum substrate was polycrystalline, the alignment of (006)  $\text{LiNbO}_3$  was consistent with (111)

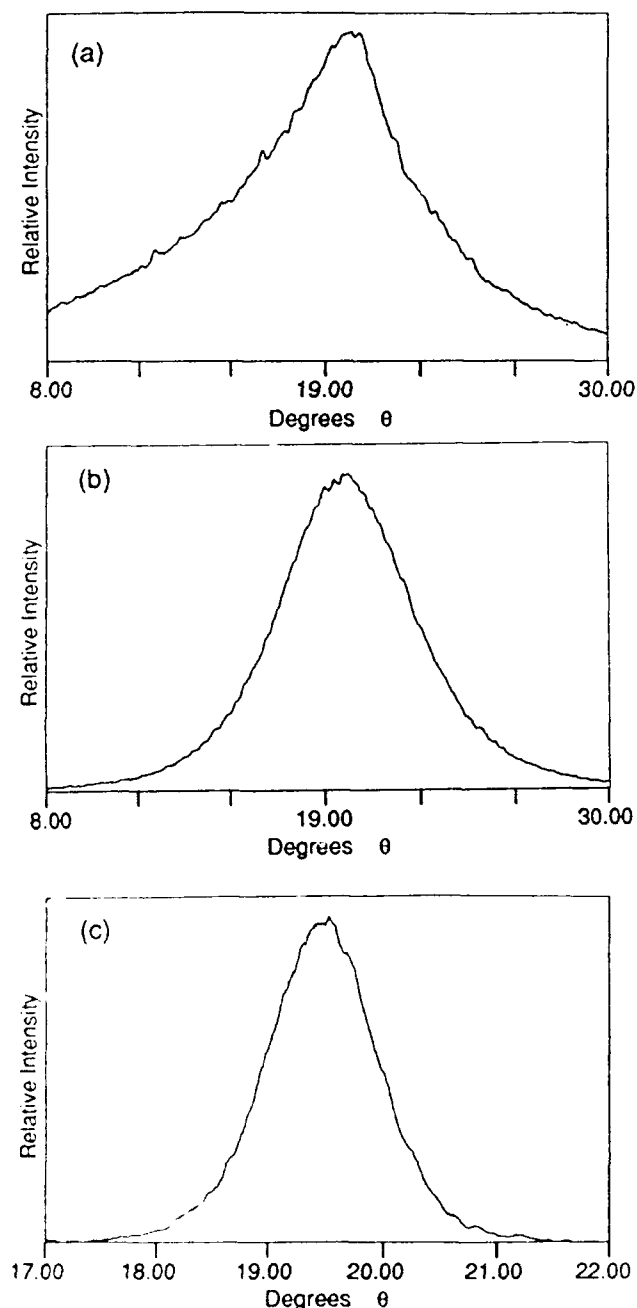


Figure 5. X-ray rocking curves for (a) Pt(111), (b)  $\text{LiNbO}_3$  (006) on platinum, and (c)  $\text{LiNbO}_3$  on sapphire.

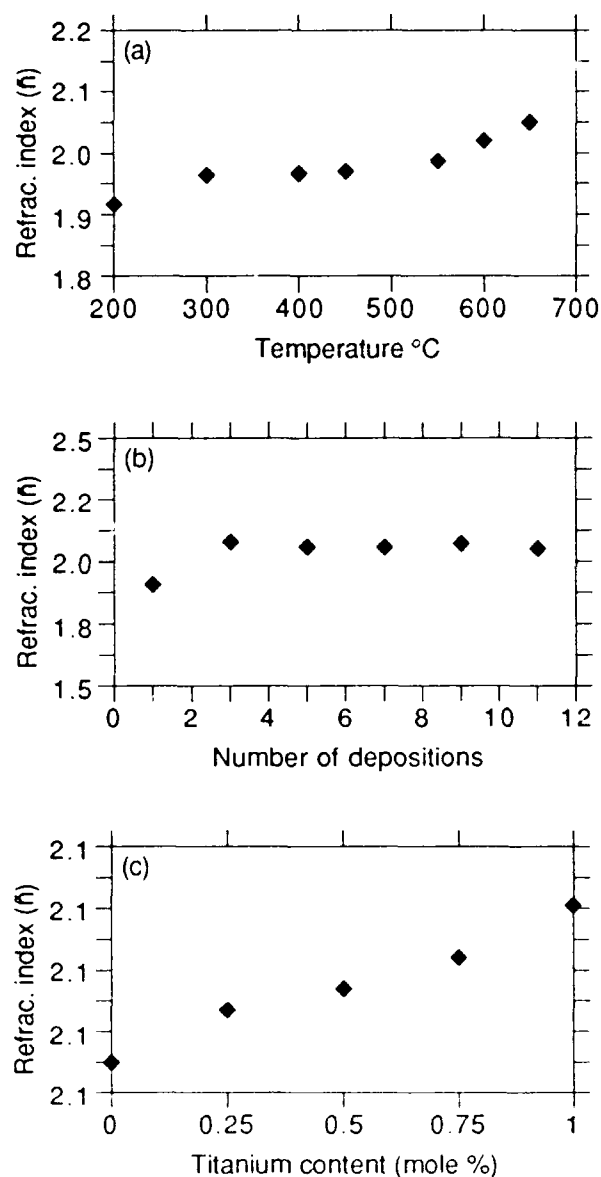


Figure 6. Refractive index for lithium niobate layers as a function of (a) RHP heat-treatment temperature, (b) number of depositions, and (c) Ti concentration.

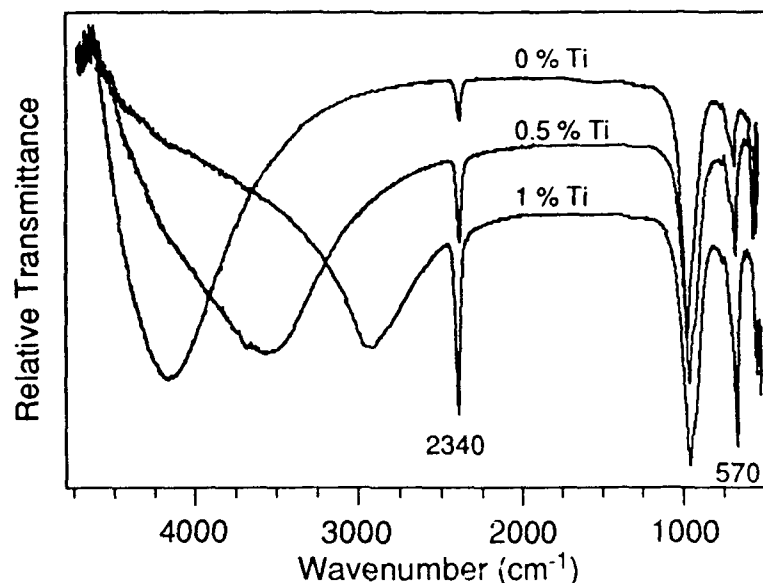


Figure 7. FTIR-diffuse reflectance spectra of lithium niobate layers on platinum.

platinum. A rocking curve for (111) Pt is given in Figure 5a. The curve indicates there was some alignment, but the relatively high intensity levels at the extreme values through which  $\theta$  was scanned suggests that (111) Pt alignment was limited. However, for LiNbO<sub>3</sub> deposited on Pt there was considerably more alignment of (006) LiNbO<sub>3</sub>. Figure 5b indicates a peak width at half peak height of  $5.5^\circ \theta$  for LiNbO<sub>3</sub> on Pt. Therefore, most of the grains were aligned with their c-axes within  $3^\circ$  to the normal of the Pt substrate.

An even higher degree of preferred orientation was obtained for (006) LiNbO<sub>3</sub> on (001) sapphire. A rocking curve is given in Figure 5c, where the peak width at half peak height was  $1^\circ \theta$  for LiNbO<sub>3</sub> on single crystal Al<sub>2</sub>O<sub>3</sub>. The beam width was collimated with a  $0.05^\circ$  aperture.

### 3.2 Optical properties

Figure 6a shows the refractive index for layers deposited on silicon as a function of final heat-treatment temperature. A refractive index of approximately 1.95 was obtained for amorphous material (heat-treated at  $\leq 400^\circ\text{C}$ ) which increased to 2.05 upon crystallization at  $650^\circ\text{C}$ . The values of refractive index for single crystal lithium niobate are  $n_o = 2.29$  and  $n_e = 2.20$  at  $\lambda = 0.6328 \mu\text{m}$ .<sup>12</sup> The lower values measured ( $\sim 2.05$ ) were attributed residual porosity and dilution effects. A refractive index as high as 2.22 could be achieved by RHP at  $650^\circ\text{C}$  and through use of ammonium hydroxide additions for some samples (Note: nitric acid additions resulted in porous microstructures<sup>15</sup> and had a measured refractive index of 1.90). It can be seen from Figure 6b that the refractive index was effectively independent of the number of depositions (after the first one), indicating no interfacial scattering between layers. Layers formed by only one deposition were found to be more difficult to crystallize, requiring longer time at similar temperatures. Since all samples received identical heat-treatments, the lower values of refractive index for a one deposition coating was attributed to a lower degree of crystallinity.

A typical advantage touted for chemical processing is the ability to uniformly distribute dopants at the molecular level. Figure 6c indicates the effect of titanium concentration on refractive index. The refractive index increased with titanium content, as expected from in-diffused Ti:LiNbO<sub>3</sub>. Note, the refractive index increase was accomplished without the need of a high temperature diffusion step. Furthermore, the process may allow tailoring of more complex profiles.

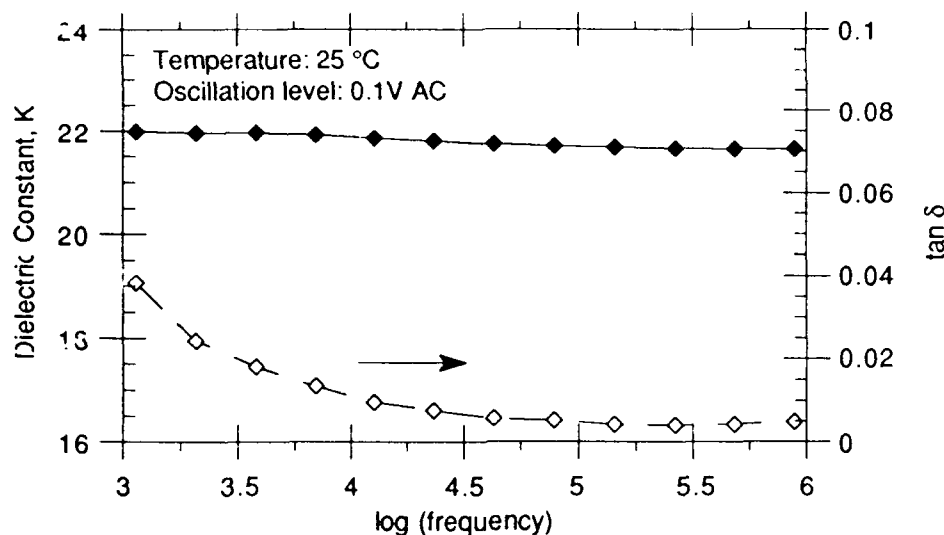


Figure 8. Dielectric data for a lithium niobate layer on platinum.

Infrared spectra for layers on platinum are shown in Figure 7. Undoped, stoichiometric  $\text{LiNbO}_3$  had an IR window of approximately 100 % transmittance between  $1000$  and  $3200\text{ cm}^{-1}$ . The absorption band at  $2340\text{ cm}^{-1}$  was associated with  $\text{CO}_2$ , (probably from the atmosphere). The band at  $577\text{ cm}^{-1}$  increased in intensity with titanium content and may allow for the calibration of titanium distribution. In addition, the hydroxyl band at  $\sim 4200\text{ cm}^{-1}$  shifted to lower wavenumbers with increasing titanium additions. This shift is thought to be an artifact of the analytical technique and may result from specular reflectance in addition to diffuse reflectance.<sup>17</sup> Diffuse reflectance is primarily a scattering technique, and hence, sensitive to the topography of the specimen surface. Specular reflectance, on the other hand, occurs from a flat reflective surface. Infrared radiation transmitted through the sample may be specularly reflected from the platinum substrate. Therefore, specular reflectance will depend on the sample's refractive index (i.e., optical pathlength) which is altered by titanium additions. Specular reflectance is manifested primarily for high energy radiation and observed at higher wavenumbers.

### 3.3 Electrical properties

Dielectric data are given in Figure 8 for  $\text{LiNbO}_3$  on polycrystalline Pt. The calculated value of dielectric constant (K) was approximately 22 between 1kHz and 1MHz, with  $\tan \delta = 0.005$  at 1MHz. Single crystal values for  $K_{33}$  are 27-28. The lower than expected value in grain-oriented  $\text{LiNbO}_3$  can be attributed to incomplete crystallization and some residual nano-porosity. Additional measurements indicated no thickness dependence on dielectric constant for layers between  $0.15$  and  $0.70\text{ }\mu\text{m}$ . Use of electrodes other than aluminum tended to give higher values of  $\tan \delta$  at lower frequencies.  $\tan \delta$  also increased at temperatures above  $200\text{ }^\circ\text{C}$  which was attributed to conductivity effects. The dielectric constant at  $200\text{ }^\circ\text{C}$  and 1MHz was 26. Several samples were also prepared on platinum using a shorter heat-treatment schedule and were found to be minimally grain-oriented. A dielectric constant of approximately 38 at 1MHz was determined, indicating a greater contribution from  $K_{11}$  (78) in the less aligned material.

## 4. SUMMARY

Alkoxide processing was used for the synthesis of lithium niobate thin-layers for possible optical applications. Solutions of stoichiometric lithium niobate and titanium-doped lithium niobate were prepared. Ethanol and 2-methoxyethanol solvent systems were found suitable for the deposition of layers. Grain oriented (006) lithium niobate was obtained on sapphire (001) and polycrystalline platinum. Layers

on platinum exhibited grain orientation with values of dielectric constant and loss tangent of 22 and 0.005, respectively at 25 °C and 1 MHz. Refractive index was observed to increase with degree of crystallinity (1.93-2.05) and increasing Ti content (2.05-2.12). Essentially no variation in refractive index was observed as a function of multiple depositions (i.e., increasing thickness). Infrared spectra showed an absorbance band at  $\sim 570\text{ cm}^{-1}$  which increased with increasing titanium content. Lithium niobate layers were found to be highly transmitting from 1000 to  $3200\text{ cm}^{-1}$ . Finally, a solution-based, reduced temperature processing method was developed for the preparation of Ti:LiNbO<sub>3</sub> layers on a variety of substrate materials.

## **5. ACKNOWLEDGEMENTS**

The authors gratefully acknowledge support from an Office of Naval Research Graduate Fellowship (D.S.H.) and an IBM Fellowship on Materials and Processing Sciences (D.J.E.). The use of x-ray facilities in the Materials Research Laboratory is gratefully acknowledged. The Center for Microanalysis of Materials is supported by the U.S. Department of Energy under contract DE-AC-02-76ER01198. The authors also thank Prof. David Brady for helpful discussions.

## **6. REFERENCES**

1. J. G. Bergman, A. Ashkin, A. A. Ballman, J. M. Dziedzic, H. J. Levinstein, and R. G. Smith, "Curie Temperature, Birefringence, and Phase-Matching Temperature Variations in LiNbO<sub>3</sub> as a Function of Melt Stoichiometry," *Appl. Phys. Lett.*, vol. 12, pp. 92-94, 1968.
2. J. L. Jackel, "Suppression of Outdiffusion in Titanium Diffused LiNbO<sub>3</sub>: A Review," *J. Opt. Commun.*, vol. 3, pp. 82-85, 1982.
3. A. Rasch, M. Rottschalk, and W. Karthe, "Suppression of Outdiffusion in Ti: LiNbO<sub>3</sub>," *J. Opt. Commun.*, vol. 6, pp. 14-17, 1985.
4. S. Miyazawa, "Growth of LiNbO<sub>3</sub> Single-crystal Film for Optical Waveguides," *Appl. Phys. Lett.*, vol. 23, pp. 198-200, 1973.
5. A. Baudrant, H. Vial, and J. Daval, "Liquid Phase Epitaxy of LiNbO<sub>3</sub> Thin Films for Integrated Optics," *Mat. Res. Bull.*, vol. 10, pp. 1373-1378, 1975.
6. S. Miyazawa, "Optical Waveguiding in LiNbO<sub>3</sub> Single-crystal Film Grown by the EGM Technique," *J. Appl. Phys.*, vol. 46, pp. 2223-2228, 1975.
7. G. H. Hewig, K. Jain, F. O. Sequeda, R. Tom, and P. W. Wang, "RF Sputtering of LiNbO<sub>3</sub> Thin Films," *Thin Solid Films*, vol. 88, pp. 67-74, 1982.
8. R. S. Madoyan, G. N. Sarkisyan, and O. A. Khachatryan, "Growth, X-ray Structure and Optical Investigations of Epitaxial Films of Solid-Solutions of Lithium Niobate-Tantalate," *Cryst. Res. Technol.*, vol. 20, pp. 1031-1040, 1985.
9. P. R. Meek, L. Holland, and P. D. Townsend, "Sputter Deposition of LiNbO<sub>3</sub> Films," *Thin Film Solids*, vol. 141, pp. 251-259, 1986.
10. R. A. Betts and C. W. Pitt, "Growth of Thin-film Lithium Niobate by Molecular Beam Epitaxy," *Electronics Letters*, vol. 21, pp. 960-962, 1985.
11. R. S. Wei, and T. K. Gaylord, "Lithium Niobate: Summary of Physical Properties and Crystal Structure," *Applied Physics A*, vol. 37, pp. 191-203, 1985.
12. D. P. Partlow and J. Gregg, "Properties and Microstructure of Thin LiNbO<sub>3</sub> Films Prepared by a Sol-Gel Process," *J. Mater. Res.*, vol. 2, pp. 595-605, 1987.
13. S. I. Hirano and K. Kato, "Formation of Crystalline LiNbO<sub>3</sub> Films with Preferred Orientation by Hydrolysis of Metal Alkoxides," *Adv. Ceram. Mater.*, vol. 3, pp. 503-506, 1988.
14. D. S. Hagberg and D. A. Payne, "Grain-Oriented Lithium Niobate Thin-Layers Prepared by Sol-Gel Methods," to appear in *Ferroelectric Thin Films*, eds. A. I. Kingon and E. R. Myers, Mat. Res. Soc. Symp., vol. 200, 1990.
15. D. J. Eichorst and D. A. Payne, "Sol-gel Processing of Lithium Niobate Thin Layers for Optical Applications," *Sol-Gel Optics*, SPIE Proc. No. 1328, 1990.
16. ASTM card number 20-631.
17. K. E. Howard (private discussion, 1990).